THE DEVELOPMENT AND MECHANISTIC INVESTIGATION OF NI(0)/SILANE CATALYTIC SYSTEMS FOR THE TRANSFORMATION OF ALKENES

by

KIANA EMILY KAWAMURA

A DISSERTATION

Presented to the Department of Chemistry and Biochemistry
and the Division of Graduate Studies of the University of Oregon
in partial fulfillment of the requirements
for the degree of
Doctor of Philosophy

June 2022

DISSERTATION APPROVAL PAGE

Student: Kiana Emily Kawamura

Title: The Development and Mechanistic Investigation of Ni(0)/Silane Catalytic System for the Transformation of Alkenes

This dissertation has been accepted and approved in partial fulfillment of the requirements for the Doctor of Philosophy degree in the Department of Chemistry and Biochemistry by:

Darren W. Johnson	Chairperson
Amanda K. Cook	Advisor
Ramesh R. Jasti	Core Member
Benjamin McMorran	Institutional Representative

and

Krista Chronister	Vice Provost for Graduate Studies

Original approval signatures are on file with the University of Oregon Division of Graduate Studies.

Degree awarded June 2022

DISSERTATION ABSTRACT

Kiana Emily Kawamura

Doctor of Philosophy

Department of Chemistry and Biochemistry

June 2022

Title: The Development and Mechanistic Investigation of Ni(0)/Silane Catalytic Systems for the Transformation of Alkenes

The transformation of alkenes plays an important role in chemical transformations from a scale that spans fine chemical, natural product synthesis up to the industrial scale synthesis of materials. The development of new catalytic methods that broaden substrate scopes, provide mechanistic understanding, and contribute fundamental knowledge of reactivity is critical to continually improve chemical synthesis. The focus of this thesis is centered on investigating the feasibility of using molecular silanes as mild and modular hydride sources in Ni catalysis. Reaction development of a Ni(0)/silane catalytic system for alkene isomerization, mechanistic elucidation of the catalytic system, and preliminary application of this knowledge toward the rational design of more complex tandem catalytic systems for the remote functionalization of alkenes are reported. Chapter I motivates the development of Ni-based catalytic systems for the transformation of alkenes and explains our inspiration and approach to developing the catalytic system described in Chapter II.

Chapter II outlines the development of a Ni(0)/silane catalytic system for alkene isomerization. The substrate scope and initial mechanistic information is included.

Chapter III describes the deeper mechanistic investigation of the Ni(0)/silane catalytic system developed in Chapter II. The focus of this chapter is on elucidating the

impact of substrate structure on the observed mechanism.

Chapter IV builds on the mechanistic work explored in Chapters II and III by expanding the library of ligands used, showing the feasibility of using steric modulation to enhance catalytic activity. Chapter IV also presents preliminary work toward developing an *in situ* approach to make this Ni(0)/silane catalytic system more practical and easily modified for different synthetic goals.

Chapter V outlines our approach and initial efforts to develop a catalytic system for the remote hydroboration of alkenes.

This dissertation includes previously published and unpublished coauthored material.

CURRICULUM VITAE

NAME OF AUTHOR: Kiana Emily Kawamura

GRADUATE AND UNDERGRADUATE SCHOOLS ATTENDED:

University of Oregon, Eugene
Colby College, Waterville

DEGREES AWARDED:

Doctor of Philosophy, Chemistry, 2022, University of Oregon
Master of Science, Chemistry, 2019, University of Oregon
Bachelor of Arts, Chemistry and Spanish, 2017, Colby College

AREAS OF SPECIAL INTEREST:

Organometallic chemistry
Transition metal catalysis
Mechanism elucidation

PROFESSIONAL EXPERIENCE:

President, A Community for Minorities in STEM, 2019-2021

Social & Outreach Chair, A Community for Minorities in STEM, 2018-2019

Board Member, LGBT+ in STEM, 2018-2019

Graduate Teaching Fellow, University of Oregon, 2017-2019

GRANTS, AWARDS, AND HONORS:

NSF Graduate Research Fellow, National Science Foundation, 2019-2022

First Year Merit Award, University of Oregon, 2017

PUBLICATIONS:

Kawamura, K.E.; Chang, A.S.; Martin, D.J.; Smith, H.M.; Morris, P.T.; Cook, A.K. Modular Ni(0)/Silane Catalytic System for the Isomerization of Alkenes. *Organometallics* **2022**, *41*, 486-496.

ACKNOWLEDGMENTS

First and foremost, I want to thank Professor Amanda Cook for her perfect timing of coming to the UO in 2018 and letting me be part of building the Cook Lab. I learned so much from you in terms of both science and being a mentor and leader. I also want to thank Dr. Michael Hurst, the other original Cook Lab member, for sticking with me throughout the years, and all of the mentees (and friends) who contributed scientific knowledge, moral support, and friendship throughout the years, in particular Alison Sy-min Chang, Daryl J. Martin and Parker T. Morris. I also want to acknowledge all the wonderful adventure, crafting, wine drinking and baking buddies that I made throughout the years. Grad school was hard, but there were so many fun times that were because of the people and friends.

I want to thank my family (my pottery wielding parents, Jon and Maija, and my fabulous sister and brother-in-law, Malia and Justin), who helped me stay grounded throughout grad school. I also want to thank my partner, Dr. Matt Cerda for the constant support throughout the years and for letting Max live with me the last few years so I could have daily cat snuggles.

To my family.

TABLE OF CONTENTS

LIST OF FIGURES

Figure Page

LIST OF TABLES

Table Page

LIST OF SCHEMES

Scheme Page

CHAPTER I

NICKEL-CATALYZED TRANSFORMATION OF ALKENES: MOTIVATIONS AND MECHANISTIC APPROACHES

This chapter was written by Kiana E. Kawamura and presents an unpublished perspective on work developed and presented in Chapters II-V.

1.1 Introduction

The development of transition metal-catalyzed transformations has enabled access to chemical targets that are difficult to synthesize through traditional pathways. The development of regioselective catalytic processes broadens substrate scope of transformations, minimizing protection/deprotection steps and overall increases the atom economy of transformations. The transformation of alkenes through isomerization[1,2] (**Figure 1.1.a.**) or other reactions such as oxidation,[3–7] polymerization[8,9] or functionalization[10,11] has played a key role in developing synthetic routes to desired target molecules (**Figure 1.1.b.**). Focusing specifically on the functionalization of alkenes through transition metal-catalyzed approaches, catalysts are often designed to be selective for alkenes in specific environments (*i.e.* allyl ethers,[12] terminal alkenes,[13] 1,1-disubstitutes alkenes,[14,15] amongst others). The regioselectivity of these transformations is key to practically applying catalytic systems to synthesis, and often the origin of selectivity is not fully understood.[16]

In the hydrofunctionalization of alkenes, selectivity is determined by many factors including steric accessibility, coordination sphere on the metal center, and substrate structure (electronic bias,[17–20] directing group participation,[21,22] etc.). Due to lower thermodynamic stability, terminal alkenes typically react more readily with metal catalysts. In fact, some hydrofunctionalization reactions (such as hydrosilylation[23,24]), are hindered when catalyst decomposition leads to the formation of species that are active for alkene isomerization to the internal alkene. With catalysts that are selective for

hydrofunctionalization of terminal alkenes, this leads to a decreased efficiency and potential mixture of products.[25]

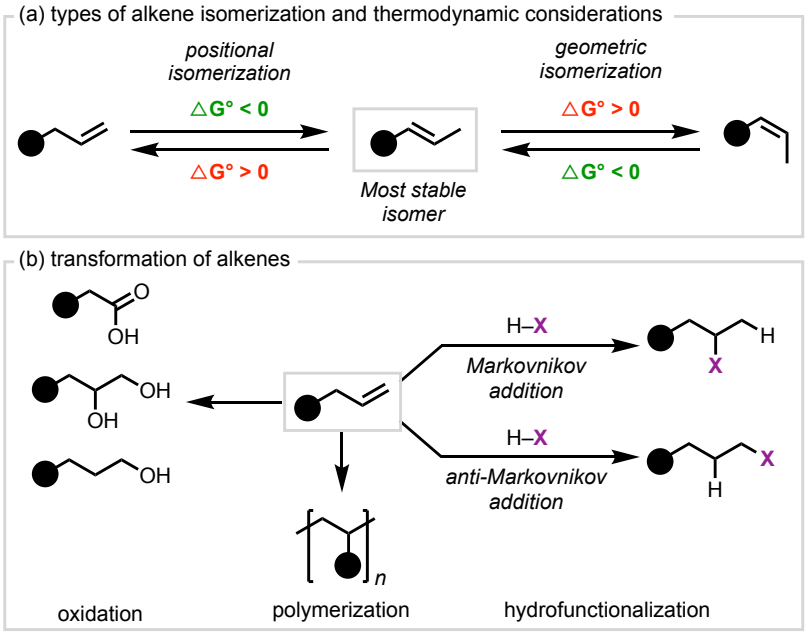

Figure 1.1. (a) Thermodynamic considerations of alkene isomerization and (b) select transformations of alkenes.

Nickel-catalyzed hydrofunctionalization reactions are of particular interest due to the mechanistic versatility of nickel compared to second and third row transition metals, which allows for complementary reactivity to be achieved. Nickel is also abundant and cost-effective compared to the other group 10 metals, particularly palladium and platinum, making it a more economical choice.[26,27] While the presence of a species active for alkene isomerization is often undesirable in (hydro)functionalization reactions, the high activity for isomerization, if harnessed, could provide mechanistic insight into isomerization catalysts that are compatible with functionalization reactions, enabling more efficient processes for the remote functionalization of alkenes (Chapter V). Nickel-catalyzed isomerization reactions have achieved high efficiency and selectivity with many approaches, with the most active systems dominated by the formation of active catalysts in situ, often requiring additives to reduce the metal center or form an active species.[28]

Focusing specifically on the generation of Ni–H species, which are the proposed active catalysts or reactive intermediates in many transformations of alkenes, the primary routes to form Ni–H species have used non-modular hydride sources such as strong acids

or main group metal hydrides (see Chapter II for a more thorough summary). In the early 1970s, Tolman investigated the mechanism of 1-butene isomerization with $Ni[P(OEt)_3]_4$ in acidic conditions (H_2SO_4), showing via mechanistic investigation that the reaction proceeded through a hydride insertion-elimination pathway (**Figure 1.2**., top pathway) and reactivity was very sensitive to the concentration of H_2SO_4.[29] More recently, Schoenebeck elucidated the reactivity of a Ni(I) dimer that efficiently isomerizes alkenes via a radical mechanism (**Figure 1.2**, bottom), supported by a radical clock experiment.[30] This work from Schoenebeck is one of the cleanest catalytic systems with nickel that effects alkene isomerization at mild conditions (no additives, no byproduct formation, room temperature, <3 h). Other nickel-based systems rely on stoichiometric reductants or additives (*e.g.* Zn[13], Mn[31]) or difficult-to-handle reagents such as Ph_2PH.[13] While systems with these approaches have achieved high selectivity and yield, there is still a strong desire to develop mild and tunable isomerization systems that do not require stoichiometric additives or harsh reducing agents.

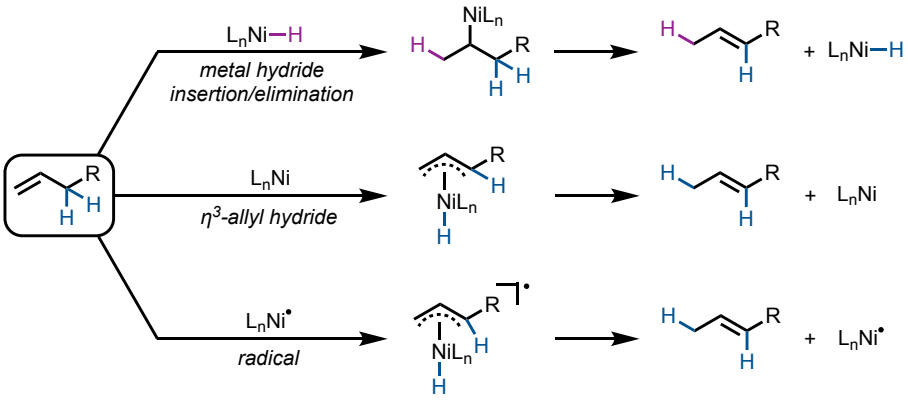

Figure 1.2. Mechanisms of Ni-catalyzed alkene isomerization.

The use of silanes offers immense potential as a modular, mild, and commercially available hydride sources in nickel-catalyzed alkene isomerization. Nickel plays an important role in the catalytic hydrosilylation of alkenes, with mechanistic investigations showing the feasibility of chain walking in certain conditions.[32,33] As mentioned above, many catalytic systems developed for hydrosilylation are designed to inhibit substrate isomerization to prevent undesirable side reactivity and the formation of isomerization or internal hydrosilylation products.[34,35] Recently, the Chirik Group showed through deuterium incorporation studies with $DSi(OEt)_3$ that during the hydrosilylation of 1-octene,

deuterium is incorporated along the entire alkyl chain while functionalizing selectively at the terminal position (**Figure 1.3.a.**), demonstrating that the active species formed in situ is active for rapid chain walking.[32] This work demonstrates the feasibility of utilizing nickel with molecular silanes to effect Ni migration along a carbon chain. The Hu group, in a similar pursuit, studied the hydrosilylation of 3- and 4-octene with H_2SiPh_2 catalyzed by a pincer nickel complex in the presence of NaO*t*-Bu to selectively form the terminal, linear hydrosilylation product, showing the ability of the catalytic system to travel along the alkyl chain prior to selective terminal functionalization (**Figure 1.3.b.**).[33] Both of these systems proceed through a proposed Ni–H species.

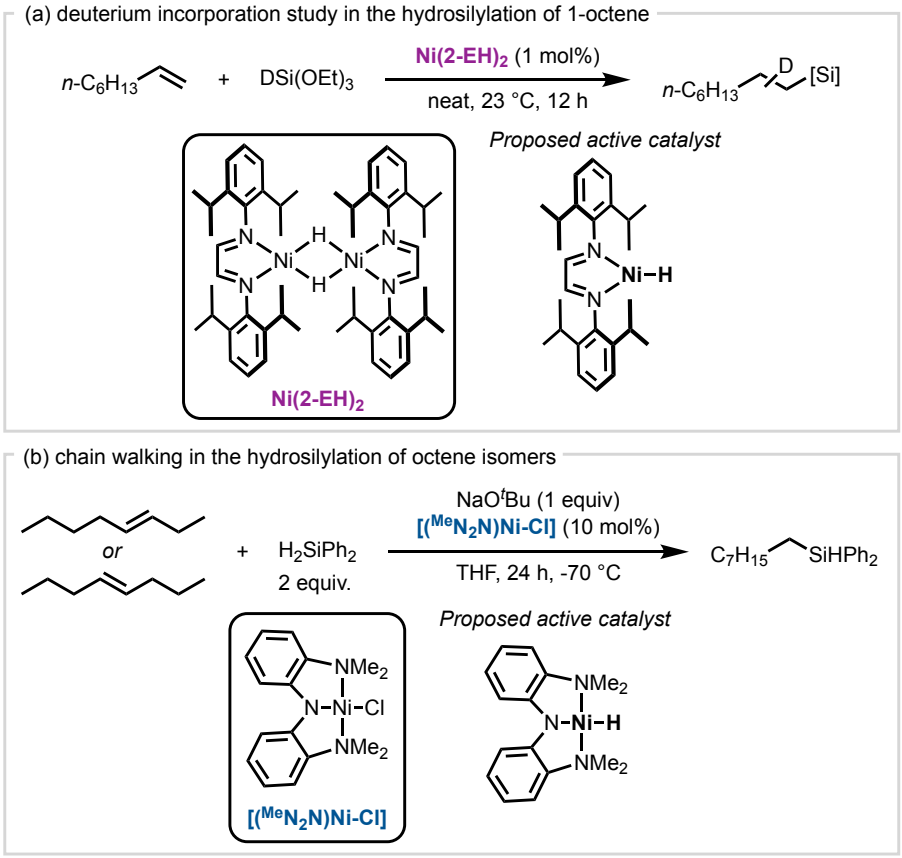

Figure 1.3. Precedent for chain walking in Ni-catalyzed hydrosilylation.

This work on Ni-catalyzed hydrosilylation demonstrates the feasibility of using molecular silanes with Ni to form active species for chain walking. The use of molecular silanes in transition metal-catalyzed alkene isomerization is limited despite the

complementary reactivity of nickel (and other transition metal) complexes with molecular silanes in hydrosilylation systems. Current examples are limited to Co,[15] Pd[36,37] and Ir[12] (**Figure 1.4.**). Our interest focuses on the development of related Ni systems due to the precedent in hydrosilylation as well as direct oxidative addition of silanes to Ni(0) complexes to form (silyl)Ni–H species.

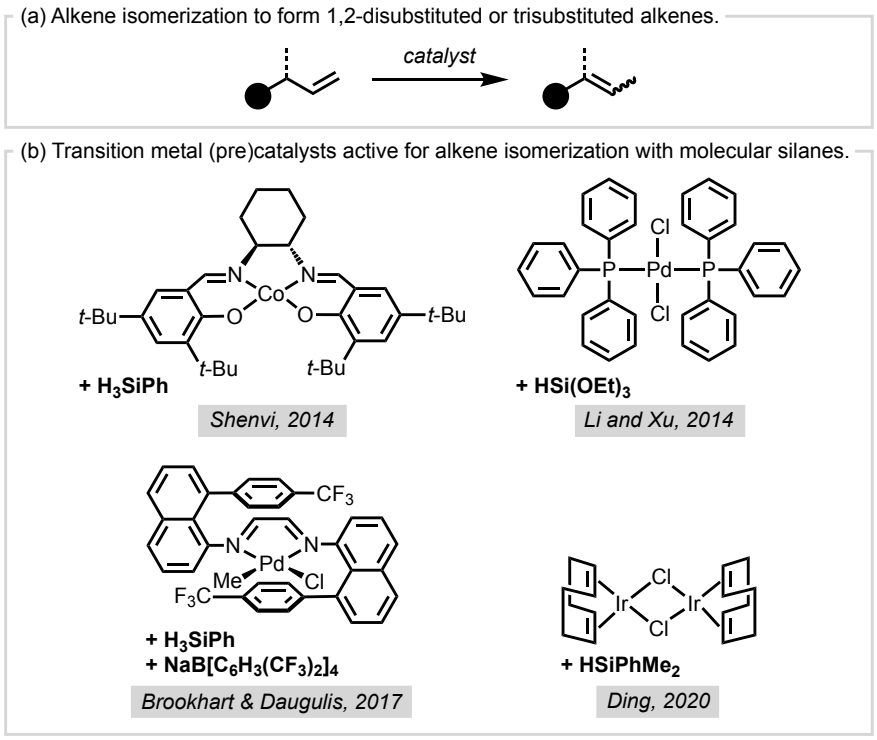

Figure 1.4. Prior work on transition metal catalyzed alkene isomerization with molecular silanes. (a) general scheme of alkene isomerization. (b) (pre)catalysts used in reactivity with silanes to form active isomerization catalysts.

Specific examples of oxidative addition of the Si–H bond of molecular silanes include alkene-stabilized Ni(0) complexes with phosphine or *N*-heterocyclic carbene (NHC) ligands as shown in **Figure 1.5**. In the Hillhouse work,[38] the formed (silyl)Ni–H species (**Figure 1.5.**, top) was shown to be in dynamic exchange with the σ-complex. In the work from Radius,[39,40] the silane identity was critical to controlling the formation of either the isolable (silyl)Ni–H species (observed with 3° silanes) or the formation bis-silyl complexes (with 2° silanes). With these examples in mind, we set out to investigate the oxidative addition of 3° silanes to alkene-stabilized (NHC)Ni(0) complexes as a possible

route to form catalytically active (silyl)Ni–H species, with a desire to gain a better understanding of the role of the silane in its reactivity with a Ni(0) precursor, the effect of both silane and ligand sphere on reactivity, and the catalytic activity of the Ni(0)/silane combination in the transformation of alkenes.

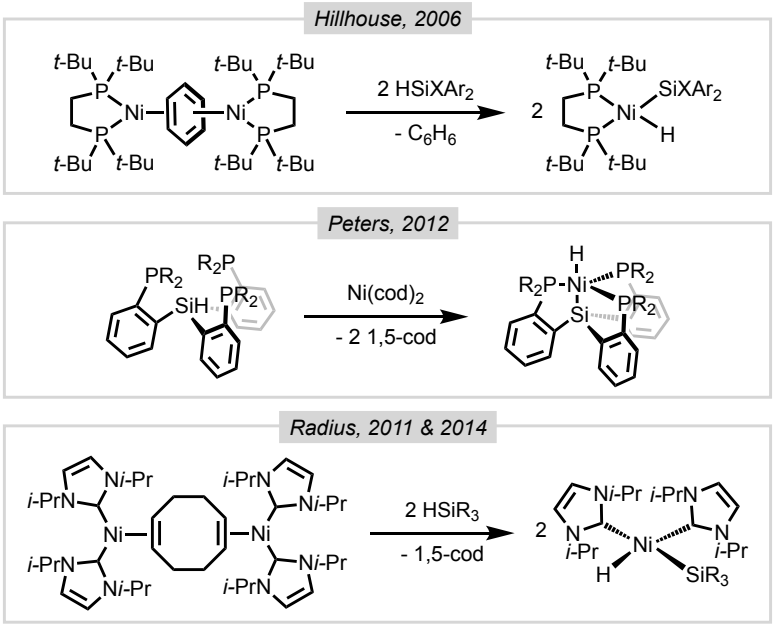

Figure 1.5. Prior work on the oxidative addition of [Si]–H to Ni(0).

1.2 Mechanisms of Nickel-Catalyzed Alkene Isomerization

As mentioned above, the mechanistic versatility of Ni compared to other group 10 metals Pd and Pt is part of our interest in this work which seeks to understand the formation of active Ni species and the mechanism of resulting catalytic transformations. While Pd and Pt typically proceed through two electron processes (*i.e.* oxidative addition/reductive elimination, transmetallation, σ-bond metathesis), Ni is able to proceed through both two electron and one electron processes (*i.e.* hydrogen atom transfer and other radical processes). In fact, Ni has been proposed to proceed through the hydride insertion-elimination,[13,29,41–47] π-allyl[48–51] and radical[30] type mechanisms shown above in **Figure 1.2**. These catalysts, shown in **Figure 1.6.**, have a wide variety of coordination spheres and operate in different reaction conditions, and the experimental elucidation of mechanistic steps is often very difficult.

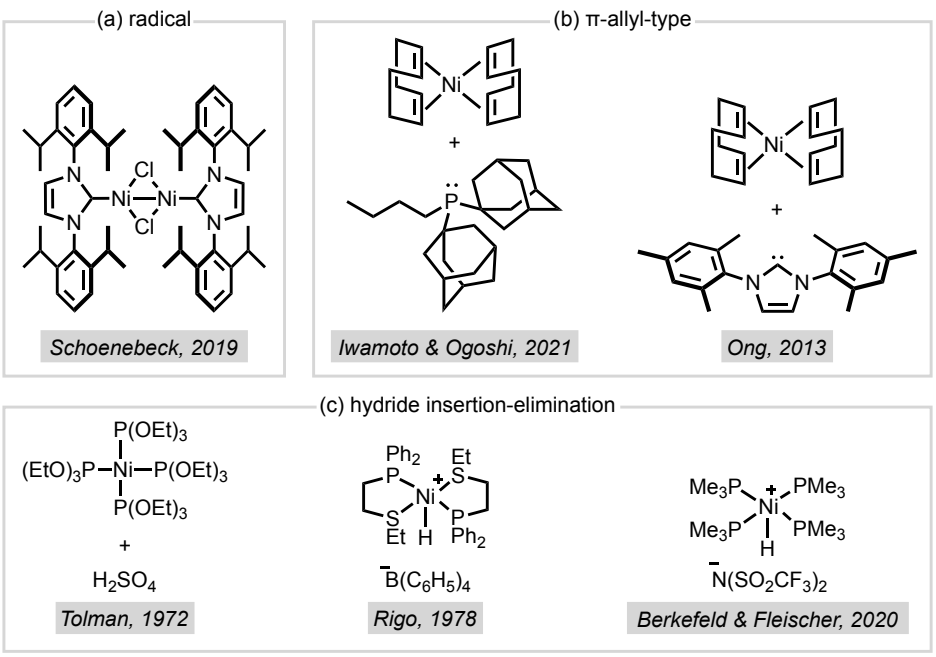

Figure 1.6. Representative examples of Ni isomerization catalysts.

Chapter II of this dissertation describes the initial reaction development for the isomerization of alkenes with low valent (NHC)Ni(0) precatalysts with molecular silanes (**Figure 1.7.**). The scope and modularity of the silane partner is demonstrated to affect reactivity in terms of both conversion and rate. The work in Chapter II was published in *Organometallics* in 2022. The article was written by Kiana E. Kawamura with editorial assistance from Alison Sy-min Chang and Amanda K. Cook. The experimental work was conducted by Kiana E. Kawamura with synthetic contributions from Alison Sy-min Chang, Daryl J. Martin and Parker T. Morris. Haley M. Smith carried out deuterium incorporation studies. While initial mechanistic studies in Chapter II point to a metal hydride insertion-elimination pathway, Chapter III furthers this work with the goal of elucidating specific mechanistic steps in play (*i.e.* identification of rate limiting step(s) and the role of reagents on the reaction kinetic profile). The work in Chapter III was carried out by Kiana E. Kawamura. The chapter is in preparation for publication with editorial assistance from Amanda K. Cook. Of special interest to this dissertation is elucidation of the substrate-divergent kinetic profiles, where allylarene substrates and α-substituted styrene substrates behave distinctly (**Figure 1.8.**). While Chapters II and III focus on the role of the silane and the overall mechanism, Chapter IV delves deeper into the role of the NHC ligand, the stabilizing alkene of the introduced Ni(0) complex, and makes progress toward modifying

the reaction set up to form the active catalyst in situ (**Figure 1.9.**) The work in Chapter IV was developed by Kiana E. Kawamura and the synthetic and mechanistic work presented was carried out primarily by Parker T. Morris and Gaby M. Bailey with guidance from Alison Sy-min Chang and Kiana E. Kawamura. Victor M. Salpino contributed through the synthesis of ligands. The overall goal of the mechanistic investigation outlined in Chapters II-IV is to enable rational and efficient design of catalysts for application in the remote functionalization of alkenes.

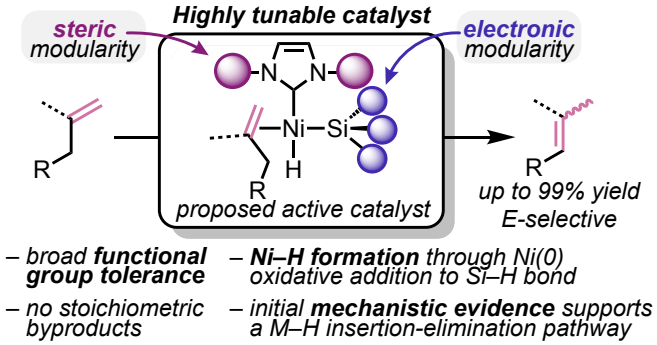

Figure 1.7. The development of a Ni(0)/silane catalytic system for the isomerization of alkenes.

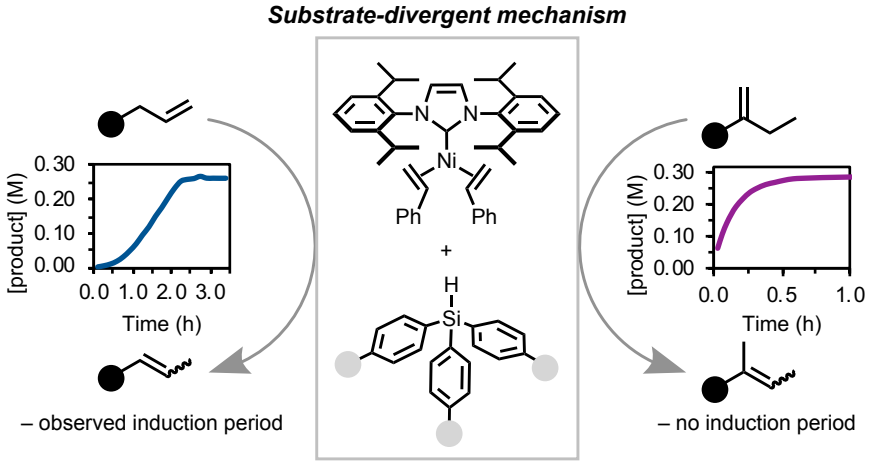

Figure 1.8. Mechanistic investigation of Ni(0)/silane catalyzed alkene isomerization with substrate-divergent mechanisms.

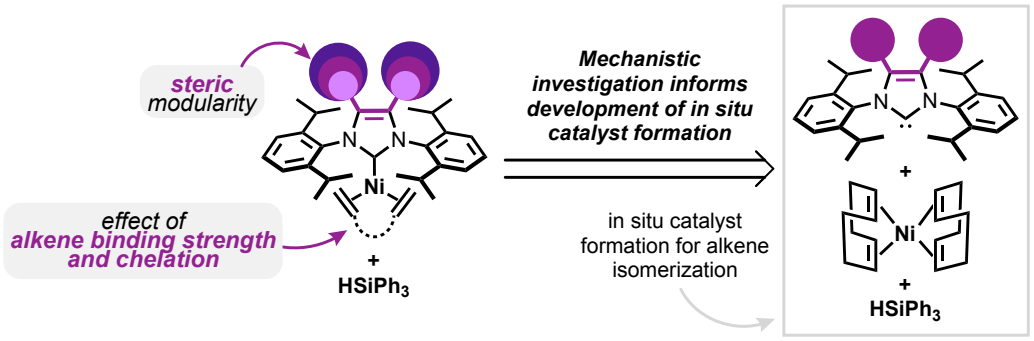

Figure 1.9. Delving into the role of the NHC ligand and developing a practical method for Ni(0)/silane catalyzed isomerization

1.3 Nickel-Catalyzed Remote Functionalization of Alkenes

The application of Ni in remote functionalization reactions has seen recent advances from both alkene and alkyl halide starting materials, summarized in recent reviews.[16,52] While work up to this point has achieved the efficient functionalization at distal sites, many of the Ni-based catalytic systems rely on stoichiometric additives to regenerate the active catalyst. For example, the Martin group developed the temperature-based regiodivergent carboxylation of alkyl halides which required 3.0 equivalents of Mn(0) in order to reduce the NiX_2 species (X = I or Br) introduced as the precatalyst or generated during product formation (**Figure 1.10.**, top).[53]

The Zhu group has also contributed important advances in the remote arylation and alkylation of both alkyl halide and alkene starting materials (see **Figure 1.10.**, bottom for one example).[31,54–58] This work most commonly proceeds through the formation of a Ni–I intermediate, and stoichiometric CsF or KF are added to from Ni–F complexes, which then react with molecular silanes to form the proposed active catalyst, a Ni–H species, and F–SiR_3 as a byproduct. The formed Ni(I)–H species is the proposed active catalyst for the chain walking steps and the Ni(I)-alkyl species that forms is proposed to react with the cross-coupling partner (typically an aryl or alkyl iodide), reforming the Ni–I species to close the catalytic cycle after a reductive elimination step forms the desired functionalized organic product. While these systems have been optimized to be selective for either internal or terminal functionalization, the low-atom economy and difficult mechanistic elucidation leave a gap for the development of more efficient and rational catalyst design.

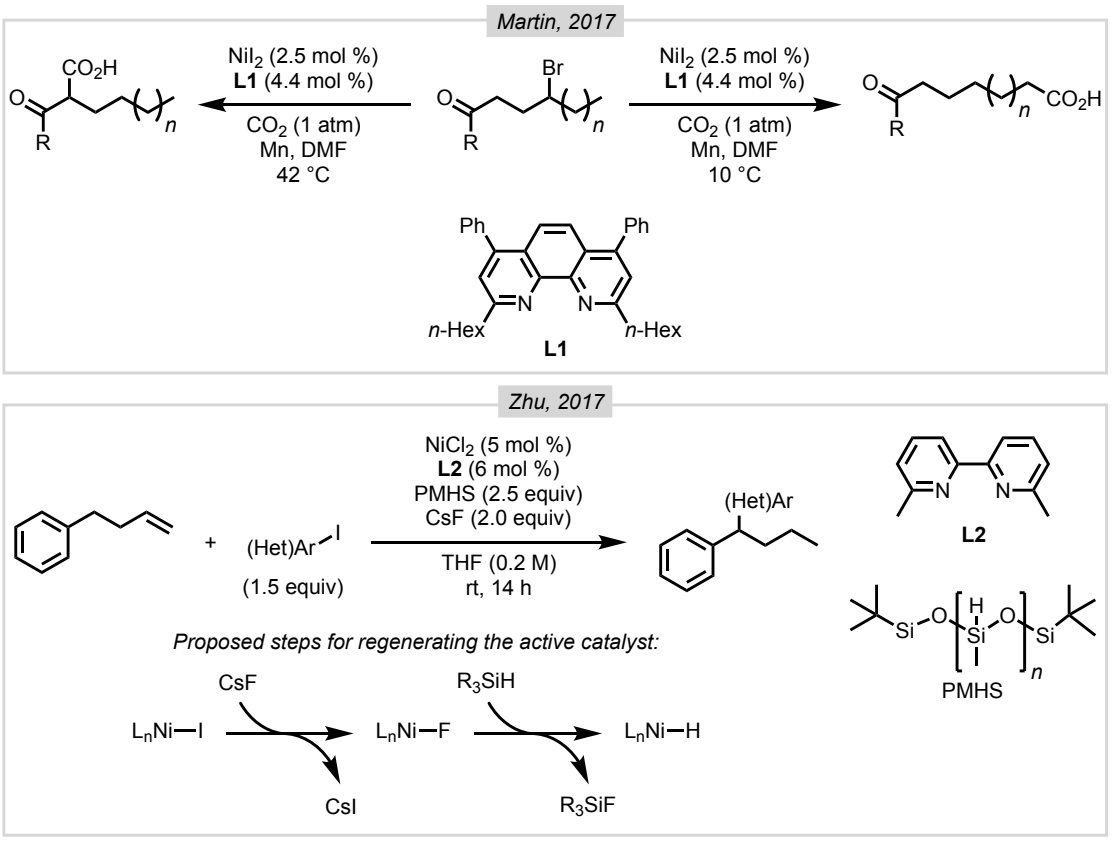

Figure 1.10. Recent examples of Ni-catalyzed remote functionalization.

Our group is interested in applying the catalytic system developed in Chapters II-IV to the remote functionalization of alkenes because the formed Ni–H species has demonstrated the ability to isomerize alkenes over multiple carbon bond lengths and operates in relatively mild reaction conditions (80 °C, toluene or hexanes). In remote functionalization, there are two approaches that we have considered: (i) a single catalyst-system in which the introduced catalyst is capable of both the isomerization and functionalization reactivity and (ii) an orthogonal tandem catalytic approach in which two separate catalysts are introduced to carry out the isomerization and functionalization separately. There are other approaches to tandem catalysis[59–61] (**Figure 1.11.**), but the work presented in Chapter V will focus on the orthogonal tandem catalytic approach for the reasons outlined below.

While the development of catalysts that are active for both chain walking and functionalization (auto-tandem catalysis) is ideal from an atom-economy perspective, in reality, an orthogonal tandem catalytic approach offers the benefit of broader reactivity

potential if systems are designed with a thorough understanding of the mechanistic aspects of both catalytic transformations. The goal of Chapter V is to investigate the compatibility of isomerization and functionalization catalysts in the remote hydroboration of alkenes. One primary challenge in remote functionalization applications is the site of functionalization.[16,62] Often, functionalization is optimized to be selective for either the terminal alkene or a position proximal to an electronically biased functional group.[18,54,63] We are particularly interested in selective functionalization of terminal alkenes and more specifically, the Markovnikov-selective functionalization of aliphatic alkenes. There are very few examples of Markovnikov-selective hydroboration of aliphatic alkenes,[64–68] and we hypothesize that introduction of a catalyst that is able to proceed through chain walking steps with a catalyst that is selective for terminal alkenes would allow for the kinetic trapping of terminal alkenes through rapid functionalization.

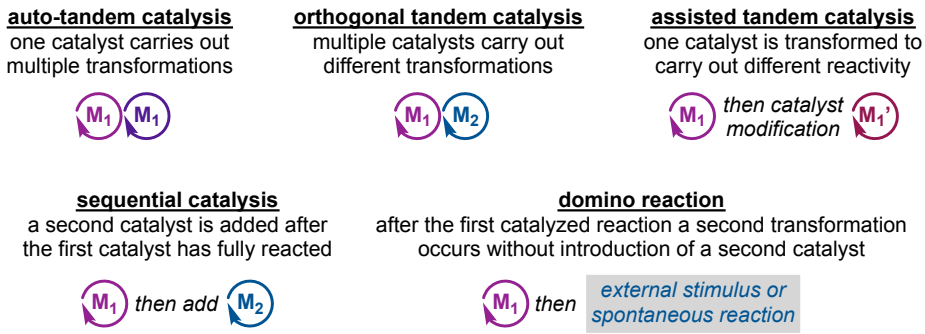

Figure 1.11. Different approaches to tandem catalysis.

Chapter V of this dissertation outlines our preliminary work on the Markovnikov-selective remote hydroboration of aliphatic alkenes (**Figure 1.12.a.**) with a variety of isomerization (**Figure 1.12.b.**) and hydroboration catalysts (**Figure 1.12.c.**). This work builds on the reactivity developed and outlined in Chapters II-IV of this dissertation, as well as preliminary results from the Cook Lab that demonstrates the viability of utilizing sulfated zirconia (SZO)[69] as a hydride source with $Ni[P(OEt)_3]_4$ to isomerize alkenes (building off of the homogeneous analogue developed by Tolman[29] in the 1970s). The work in Chapter V was developed by Kiana E. Kawamura and Amanda K. Cook. Experimental work was carried out by Kiana E. Kawamura. Quinn Valentine contributed sulfated zirconia material for isomerization/hydroboration screening studies.

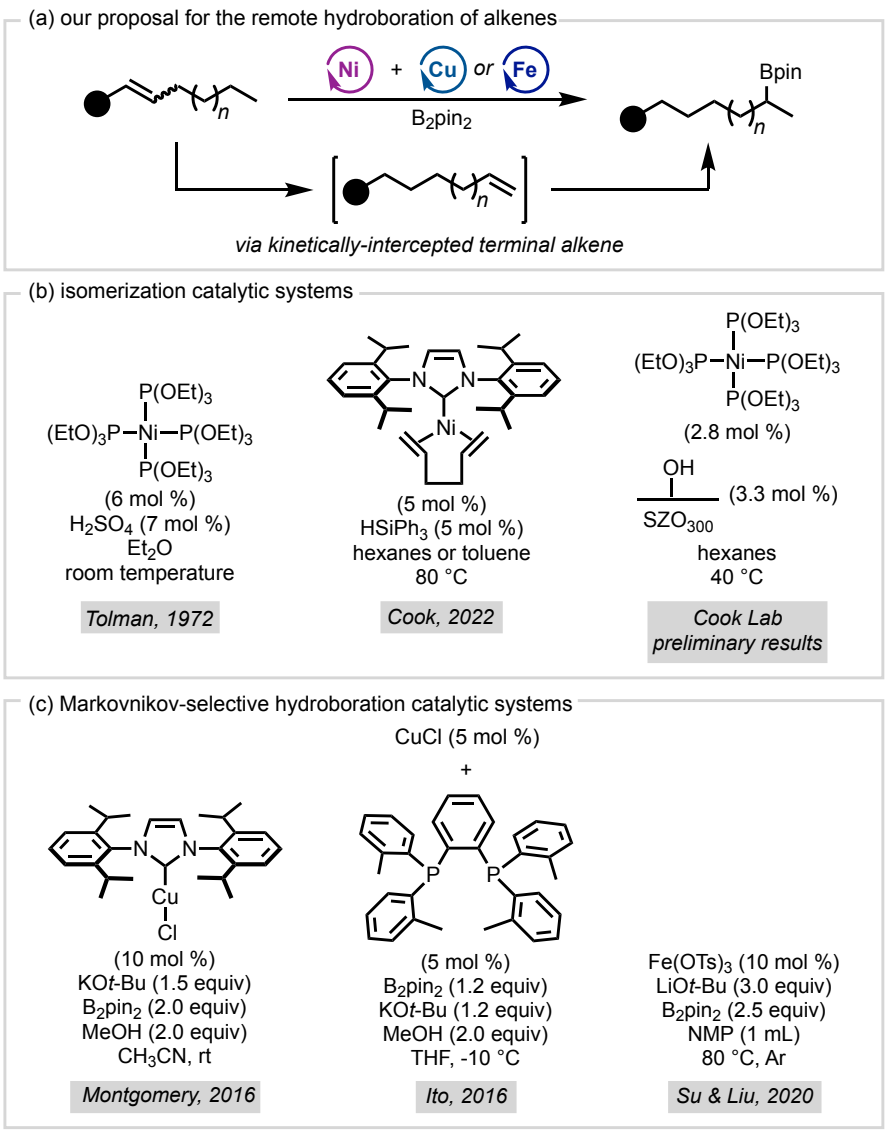

Figure 1.12. Our proposal and initial catalytic targets for the remote Markovnikov-selective hydroboration of aliphatic alkenes.

1.4 Conclusions and Outlook

The development of transition metal-catalyzed processes, particularly utilizing first row transition metals, is an important field of current research due to the remaining gaps in mechanistic understanding. Filling in these gaps by carrying out detailed mechanistic investigations and applying these findings in rational ways to achieve complex reactivity shows the potential to broaden reactivity to new transformations, new classes of substrates, and to optimize current processes.

CHAPTER II

DEVELOPMENT OF A MODULAR NI(0)/SILANE CATALYTIC SYSTEM FOR THE ISOMERIZATION OF ALKENES

This chapter includes previously published and co-authored material from Kawamura, K.E.; Chang, A.S.; Martin, D.J.; Smith, H.M.; Morris, P.T.; Cook, A.K. A Modular Ni(0)/Silane Catalytic System for the Isomerization of Alkenes. *Organometallics* **2022**, 41 (4), 486-496. https://doi.org/10.1021/acs.organomet.2c00010. This article was written by Kiana E. Kawamura with editorial assistance from Alison Sy-min Chang and Professor Amanda K. Cook. Alison Sy-min Chang, Daryl J. Martin, and Parker T. Morris contributed synthetically through the preparation of starting materials. Haley M. Smith carried out deuterium incorporation studies.

2.1 Introduction

The significance of the alkene as a synthetic target and feedstock cannot be overstated; alkenes are found in and are used to synthesize pharmaceuticals,[70,71] natural products,[72] commodity chemicals,[73,74] and materials.[75,76] The functionalization of alkenes is a pillar in organic synthesis from the large scales of industry to the small scales of research labs.[77] As the location and geometry of the alkene dictate the site- and stereoselectivity of subsequent reactions, it is critical to be able to control the location and geometry of alkenes. Numerous strategies exist for the synthesis of alkenes (*e.g.*, specialized P-[78–80] and Si[81]-based reagents for carbonyl olefination, alkene metathesis,[82] semihydrogenation[83,84]), yet few are as atom-economical as alkene isomerization, which is utilized in many industrial processes (*e.g.*, Shell Higher Olefin Process, adiponitrile synthesis).[85]

Transition metal-catalyzed alkene isomerization (**Figure 2.1.a.**) is attractive as a strategy to synthesize internal alkenes because i) accessible terminal alkenes can be used as starting materials, ii) isomerization has inherently high atom economy, and iii) site-, chemo- and stereoselectivity can be controlled by catalyst design.[1,72,85,86] These advantages

are particularly attractive in the context of remote functionalization and convergent syntheses.[16,52,60,62]

State-of-the-art alkene isomerization catalysts have been developed to operate under mild reaction conditions and have a broad substrate scope, yet they either rely on rare and expensive 2nd and 3rd row transition metals,[87–90] require catalyst activators or stoichiometric additives with ill-defined impacts, or utilize non-tunable ancillary ligands, which limits catalyst modularity. Significant contributions to the state-of-the-art have been recently developed and utilize base metals[86] like iron,[91,92] cobalt,[14,15,93–97] and nickel[30,51,98,99] (**Figure 2.1.b.**). Many of these catalysts operate under mild conditions (*e.g.*, low temperatures, short reaction times), give high regio- and stereoselectivities, and exhibit broad substrate scopes including isomerization to trisubstituted alkenes, isomerization of internal alkenes, and large functional group tolerance. Yet, many of these reports lack a demonstration of rational tunability of the catalyst's activity. Additionally, while Fe- and Co-based catalysts for alkene isomerization are operable with low catalyst loadings, Ni-based catalysts still often require high catalyst loadings (≥10 mol %). Devising a structurally modular catalyst system derived from mechanistic understanding has the potential to create a versatile catalyst system that is readily tailored to substrates and thereby can increase compatibility. Catalyst tunability is especially important in the context of tandem catalytic applications, for which the isomerization catalyst must be compatible with a wide range of functionalization reactions.

Transition metal-catalyzed isomerization reactions typically proceed via one of three possible mechanisms: i) radical pathway,[15,30,93,97] ii) π-allyl pathway,[100] or iii) insertion/elimination via a metal-hydride[101] (**Figure 2.2.a.**). Nickel catalysts are particularly attractive not only because Ni is an Earth-abundant, 1st-row transition metal, but also because they are mechanistically versatile (*i.e.*, able to proceed through 1-electron and 2-electron pathways).[30,48,49,101] Ni has been proposed to isomerize alkenes through insertion/elimination,[13,29,41–47] radical,[30] and π-allyl-type mechanisms.[48–51] The insertion/elimination pathway using a Ni–H catalyst is particularly attractive because it is the proposed mechanism for many chain walking applications.[16,31,45,54–57,63,99,102–114]

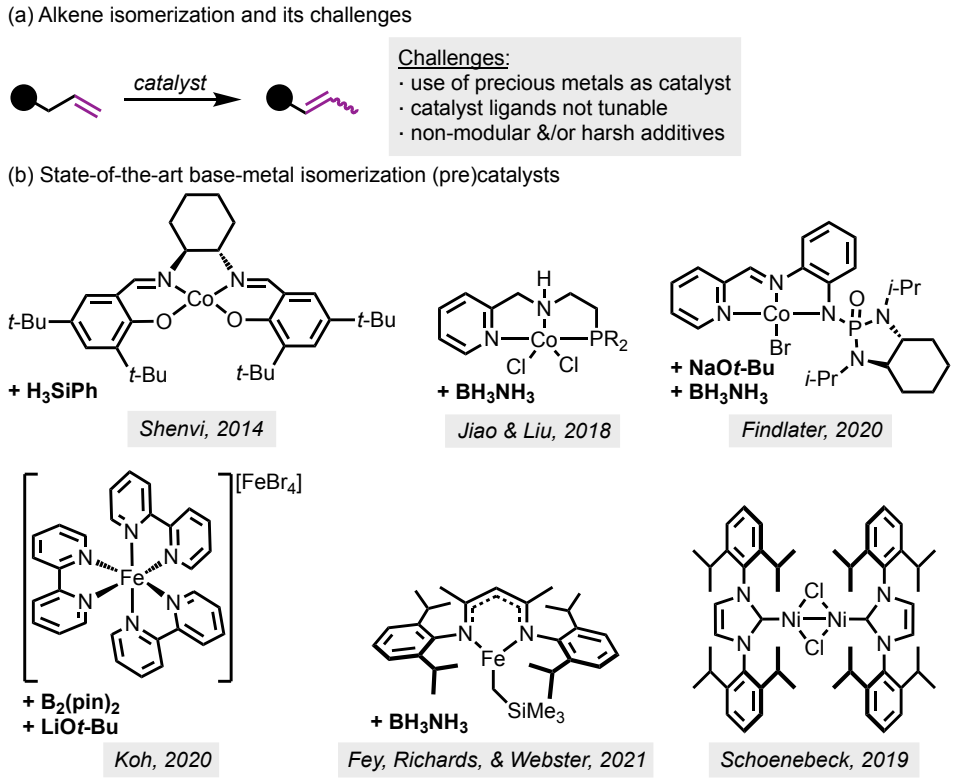

Figure 2.1. Prior work on alkene isomerization. (a) general scheme and challenges of alkene isomerization. (b) state-of-the-art alkene isomerization catalysts using base metals.

Elucidation of the active species structure and the effect of ancillary ligands has been specifically identified as the major challenge in Ni-catalyzed remote functionalization reactions.[16] This task is difficult because multiple steps and processes are occurring in remote functionalization (namely, the chain walking and functionalization processes), which convolutes analysis. The goal of this work is to develop a highly tunable catalyst system for alkene isomerization that will not only be useful for isomerization reactions but will also elucidate mechanistic information about the fundamental reactivity between in situ generated (NHC)Ni catalysts and alkenes.

Previous work has accessed Ni–H species in situ (**Figure 2.2.b.**) for alkene isomerization and remote functionalization[16] by oxidative addition of strong acids (*e.g.*, H_2SO_4,[29,44,46,115] HCl,[116] HBF_4,[41] $HN(SO_2CF_3)_2$[45]) or polar O–H bonds,[107,114] oxidative addition of alkyl halides followed by β-hydride elimination,[31] or by reduction of Ni(II) with additives that can limit functional group tolerance (*e.g.*, Grignard reagents,[117,118] $NaBH_4$,[119–121] $LiAlH_4$,[122] $LiBHEt_3$,[98,123,124] $SnCl_2$,[42] MAO[43]). In remote functionalization

applications, the use of Ni–X (X = halide) complexes in conjunction with a silane as the H-source by the Zhu lab[55,63,110,111] and others[102,105,125] has achieved efficient and selective reactivity for the remote functionalization of alkenes. The silane, which is used in excess, is proposed to react with the Ni–X to form a Ni–H species, generating a silyl halide byproduct each catalytic turnover.

To avoid these byproducts and install an additional handle to control catalyst reactivity, we sought to utilize the direct formation of (silyl)Ni–H species through oxidative addition of Ni(0) to the Si–H bond of silanes for alkene isomerization (**Figure 2.2.c.**). A similar strategy has been used for precious metal-catalyzed alkene isomerization,[12,36,37,126–128] and silanes (primarily $PhSiH_3$) have been used with Co as H-atom sources also for isomerization via 1-electron pathways.[15,97] Promising precedent for Ni(0) oxidative addition to silanes is shown in examples from Hillhouse,[38] Radius[39,40] and Peters,[129] which show the stoichiometric formation of (silyl)Ni–H species through direct oxidative addition of Ni(0) to Si–H bonds of molecular 2° and 3° silanes. Furthermore, Ni-based catalytic systems for hydrosilylation are known,[11,34,130,131] with a key mechanistic step being oxidative addition of the Ni complex to the Si–H bond of the silane reagent prior to reactivity with alkenyl,[132] alkynyl[133] or allenyl[134,135] substrates.

We hypothesized that the (silyl)Ni–H species formed from this oxidative addition could be harnessed for catalytic activity toward the isomerization of alkenes. We identified triaryl silanes as good candidates for mild hydride sources because i) they are less reactive than the reagents currently used to form Ni–H species (namely aluminum- and borohydrides and strong acids), ii) they are typically less active toward hydrosilylation of alkenes with nickel (there are numerous examples of Ni(0)-catalyzed alkene and allene hydrosilylation that require 1° and 2° silanes),[11,34,130,131] and iii) the silane substituents can be rationally tuned to influence the catalytic cycle. With this precedent in mind, we designed and herein disclose a catalytic system with direct generation of (NHC)(silyl)Ni–H species for alkene isomerization with high steric and electronic modularity enabling catalyst tunability based on substrate compatibility.

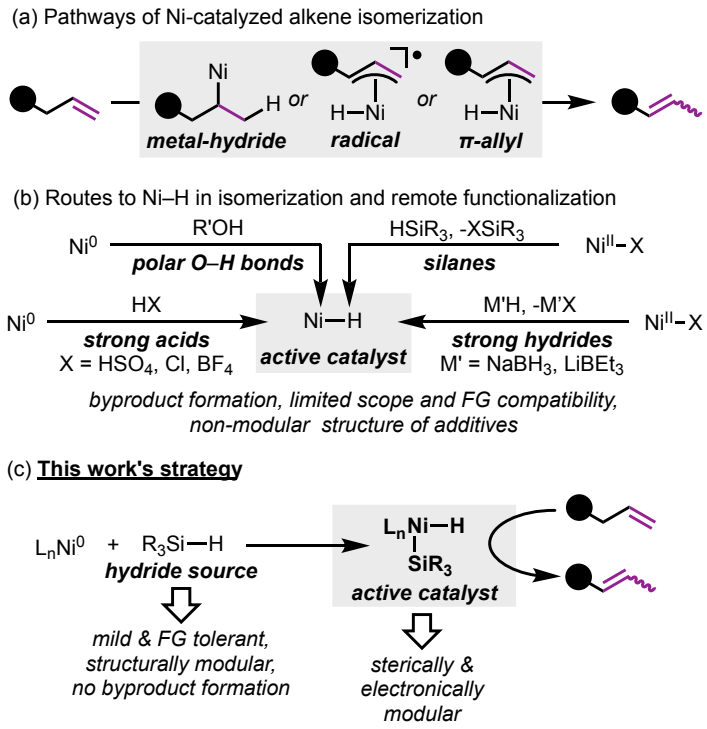

Figure 2.2. Proposed catalyst structures for nickel-catalyzed alkene isomerization. (a) Types of intermediates proposed. (b) Routes to Ni–H proposed in isomerization and/or remote functionalization reactions. (c) The strategy of this work is to generate (silyl)Ni–H as the active catalyst via oxidative addition of Ni(0) complexes to silyl hydrides.

2.2 Results and Discussion

We were particularly attracted to N-heterocyclic carbenes as ancillary ligands because of their demonstrated i) modularity,[136] ii) precedent as ligands for Ni(0) oxidative addition to silanes,[39,40] and iii) use in hydrosilylation[132–135] and remote functionalization[50,99] reactions with Ni. Taking advantage of recent progress in synthesizing thermally stable Ni(0) complexes,[136–139] we began investigating isomerization of our test substrate, allylbenzene[72] (**2a**) to β-methylstyrene (**3a**) with alkene-stabilized (NHC)Ni(0) complexes **1a-e** and with commercially available silanes. The reaction was optimized to give 95% yield with high selectivity for the E-isomer of β-methylstyrene (**3a**) using 5 mol % each of (1,5-hexadiene)Ni(IPr) (**1a**) and $HSiPh_3$ to generate the active catalyst (**Table 2.1.**, entry 1; see Supporting Information for full optimization). Control experiments show the critical role of both Ni and silane for isomerization activity (entries 2 and 3). The catalysts with more strongly coordinating alkenyl ligands[137] (**1b-d**) showed diminished reactivity (entries 4-6), which we hypothesize is based on hindered entry into

the catalytic cycle. The influence of the alkenyl ligand identity on *E/Z* selectivity is possibly due to the ligand remaining coordinated to the Ni center throughout the reaction, but more thorough mechanistic work is needed to elucidate the cause of this effect. Less bulky IMes instead of IPr gave slightly lower, yet still good yield (92%) and similar selectivity for ***E*-3a** (entry 7). Attempts to form the catalyst in situ led to lower yield and selectivity (entry 9), as did using industry-standard[85] basic conditions (entry 8). The identity of the silane partner was investigated next. Use of the secondary silane H_2SiPh_2 led to slightly diminished yield, although high selectivity for the E-alkene was maintained (entry 10). Substitution of smaller, more electron-rich methyl groups in place of phenyl substituents (entries 11-12) led to increasingly lower yields. We hypothesize that this decrease in yield is due to the silane being more electron-rich, and less susceptible to oxidative addition by Ni(0) (vide infra).[140] With the optimal system utilizing **1a**/$HSiPh_3$, the substrate scope of isomerization was investigated (**Scheme 2.1.**).

Scheme 2.1.a. shows results for the formation of 1,2-disubstituted alkenes. The formation of β-methylstyrene derivatives from the corresponding allylbenzene proceeded with high selectivity (≥15:1) for the *E*-alkene (products **3a**-**g**). In cases with particularly volatile products (*e.g.*, **3d**), isolated yields are lower than expected due to evaporation during the isolation process, although conversion and selectivity for the *E*-alkene is excellent (for **3d**: 54% isolated yield, 98% conversion, 23:1). A wide range of electron withdrawing (**3d**, **3g**, **3i**) to electron donating (**3b**, **3c**, **3e**, **3f**, **3h**) substituents were tolerated on phenyl ring of allylbenzene (conversion >95%).

Isomerization to form trisubstituted alkenes, notably challenging substrates because of their increased steric encumbrance and small energetic difference between *E* and *Z* isomers,[14] is shown in **Scheme 2.1.b.**. In the cases of sterically demanding substrates, conversions were low using **1a**/$HSiPh_3$. For example, isomerization of the 1,1-disubstituted alkenes **2w** and **2z** proceeded to only 58% (*E/Z* = 8:1) and 35% conversion, respectively, to form the sterically encumbered trisubstituted alkenes **3w** and **3z**. We reasoned that steric hinderance was potentially slowing down the reaction, and strategized replacing **1a** with **1e**, which has the smaller NHC ligand, IMes, to increase conversion. Accordingly, we found that the conversion of **2w** to **3w** increased to 94% (with a diminished *E/Z* ratio of 4:1) and **2z** to **3z** increased to 86% using **1e**/$HSiPh_3$ (**Scheme 2.1.b.**; increasing the

temperature to 90 °C and catalyst loading to 10 mol % for substrate **2z** did not show improved reactivity; see Appendix A for more details).

Table 2.1. Results of selected reaction optimization parameters

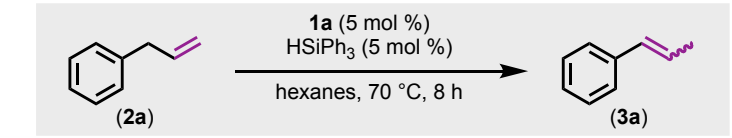

NHC ligands:

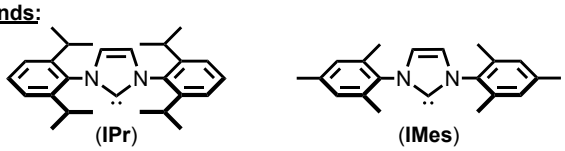

Ni complexes:

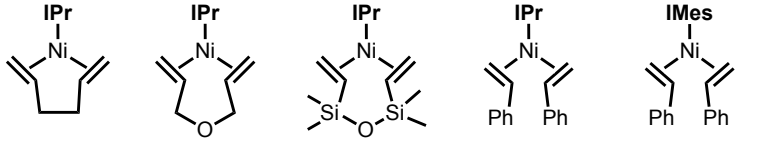

Entry	Deviation from standard conditions[a]	GCMS Yield[b]	*E/Z* ratio
1	No deviation	95%	14:1
2	No **1a**	7%	1:1
3	No silane	9%	2:1
4	**1b** instead of **1a**	10%	2:1
5	**1c** instead of **1a**	9%	2:1
6	**1d** instead of **1a**	67%	11:1
7	**1e** instead of **1a**	92%	13:1
8	5 mol % KOt-Bu instead of **1a** + silane	43%[c]	5:1
9	$Ni(COD)_2$ + IPr•HCl + KOt-Bu instead of **1a**	4%	16:1
10	H_2SiPh_2 instead of $HSiPh_3$	84%	12:1
11	$HSiMePh_2$ instead of $HSiPh_3$	47%	9:1
12	$HSiMe_2Ph$ instead of $HSiPh_3$	19%	3:1

[a]Reaction conditions: **2a** (0.080 mmol), **1a** (0.0040 mmol, 5 mol %), $HSiPh_3$ (0.0040 mmol, 5 mol %), hexanes (0.25 mL), 70 °C, 8 h, under N_2. [b]Yield and selectivity determined by GC-MS analysis of the crude reaction mixture with 1,2,4,5-tetramethylbenzene as an internal standard. [c]Run on 0.50 mmol scale.

While this strategy of enhancing catalyst activity via NHC steric modulation was successful for substrates such as **2w**, it did not lead to significantly improved conversions for all challenging substrates (*e.g.*, **2x**, see Appendix A for a full summary of conditions tested). To further improve the activity of the catalyst, we took advantage of the silane substituents as an additional and complementary reactive handle. We hypothesized that oxidative addition of Ni(0) to electron-poor silanes would proceed more favorably than with electron-rich silanes,[140] and this in turn would lead to enhanced catalytic activity by entering the catalytic cycle more readily.

To test our hypothesis, we systematically altered the electronic character of the silane by synthesizing 4-substituted triaryl silanes $HSi(4\text{-}CF_3\text{-}C_6H_4)_3$, $HSi(4\text{-}OMe\text{-}C_6H_4)_3$, and $HSi(4\text{-}NMe_2\text{-}C_6H_4)_3$ and compared their activity to commercially available $HSiPh_3$ (**Scheme 2.2.a.**).[140,141] Monitoring the conversion of **2a** to **3a** over time shows that the use of the electron-poor $HSi(4\text{-}CF_3\text{-}C_6H_4)_3$ resulted in faster formation of product (triangles), whereas electron-rich silanes $HSi(4\text{-}OMe\text{-}C_6H_4)_3$ (circles) and $HSi(4\text{-}NMe_2\text{-}C_6H_4)_3$ (squares) showed diminished reactivity overall. Therefore, our hypothesis was confirmed: electronic modulation of the silane partner can enhance catalyst activity, affecting the observed induction period and reaching reaction completion faster than $HSiPh_3$.

Utilizing the approach pioneered by Blackmond,[142] we visualized the reaction rate versus time to decouple the maximum reaction rate and the time it takes to reach that maximum rate (**Scheme 2.2.b.**; see Supporting Information for full details). With this approach, we see that while $HSiPh_3$ and $HSi(4\text{-}CF_3\text{-}C_6H_4)_3$ both reach full conversion, the maximum rate is reached more quickly (2 h versus 5 h) with more electron-poor $HSi(4\text{-}CF_3\text{-}C_6H_4)_3$ than $HSiPh_3$, and the maximum rate reached is greater for $HSi(4\text{-}CF_3\text{-}C_6H_4)_3$ (0.13 M/h) than $HSiPh_3$ (0.09 M/h). For $HSi(4\text{-}OMe\text{-}C_6H_4)_3$, the maximum rate is both lower (0.02 M/h) and reached later (6 h) in reaction progress. The low conversion with $HSi(4\text{-}NMe_2\text{-}C_6H_4)_3$ prevented comparable analysis to the other silanes, but the rate never surpasses 0.007 M/h. Comparing selectivity for the other three silanes, we observe no significant impact on *E/Z* ratios at 30% conversion of **2a** to **3a**, with all silanes maintaining high selectivity for the *E*-alkene (>20:1). With this knowledge, we hypothesized that introducing $HSi(4\text{-}CF_3\text{-}C_6H_4)_3$ to the reaction instead of $HSiPh_3$ could enhance rates of reaction with challenging substrates.

Scheme 2.1. Scope of alkene isomerization

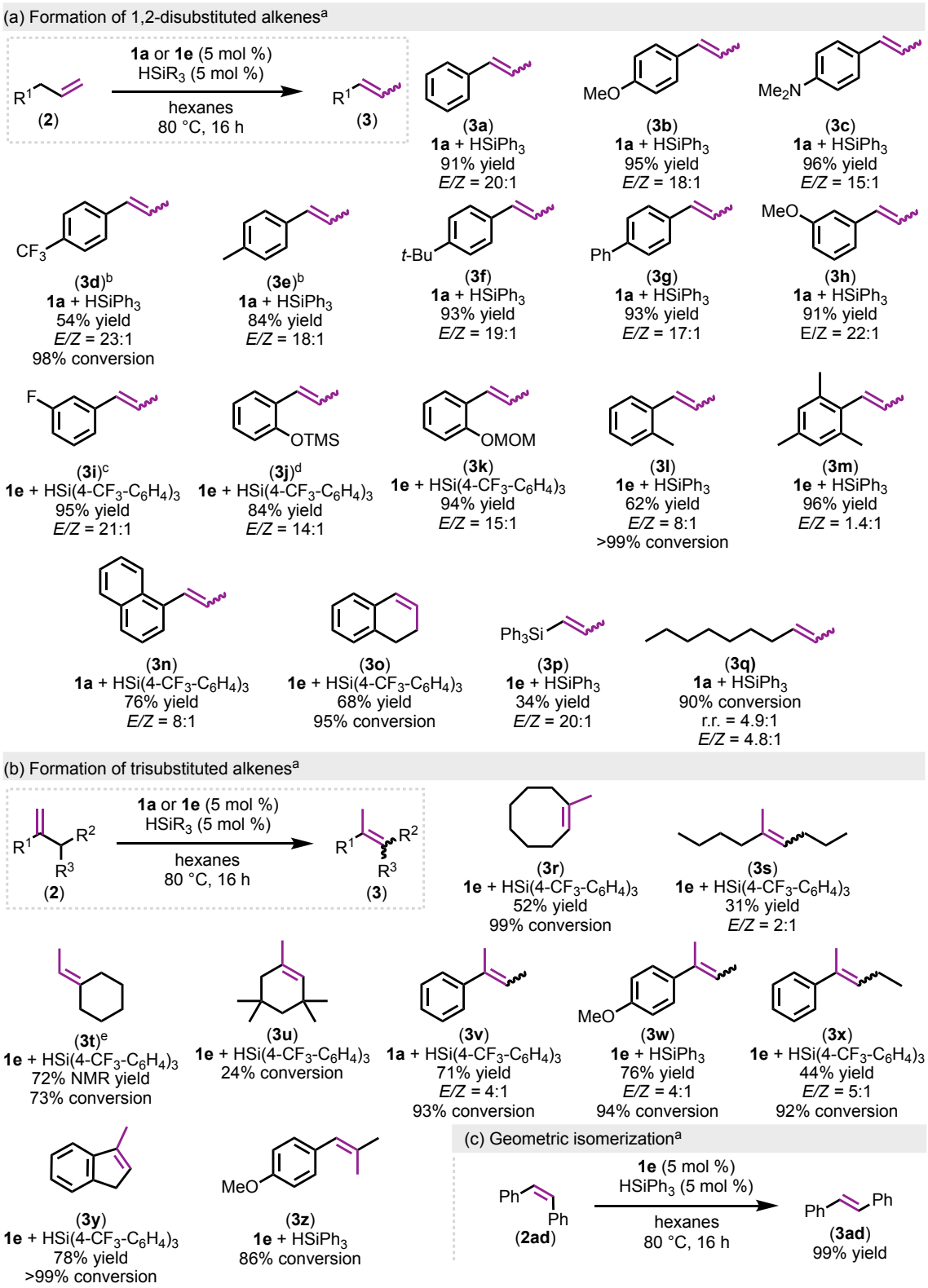

[a]Reaction conditions: **2** (0.5 mmol), **1** (0.025 mmol, 5 mol %), $HSiR_3$ (0.025 mmol, 5 mol %), hexanes (1.6 mL), 80 °C, 16 h, under N_2. Isolated yields are reported. *E/Z* ratios determined by GC analysis of the crude reaction mixture. TMS, trimethylsilyl; MOM, methoxymethyl; r.r. = regiomeric ratio (with the major species corresponding to the drawn isomer). [b]Reaction performed on a 0.3 mmol scale. [c]Reaction performed with 2 mol % **1e**. [d]Isolated as 2-(1-propen-1-yl)phenol. [e]Reaction yield determined by NMR with 1,2,4,5-tetramethylbenzene as an internal standard.

We first targeted the substrate **2j**, which we hypothesized was reacting slowly because of its increased steric bulk near but not exactly at the reactive center (the allyl group). Conversion of **2j** to **3j** with catalyst **1e**/$HSiPh_3$ was 32% (*E/Z* = 10:1). Applying the improved catalyst system **1e**/$HSi(4\text{-}CF_3\text{-}C_6H_4)_3$, we found a dramatic increase in the formation of **3j** (98% conversion) and improved selectivity (*E/Z* = 14:1; **Scheme 2.1.a.**). This strategy of tuning the catalyst activity was successfully applied to additional substrates with monosubstituted alkenes (**2i**, **2k**, and **2n**).

Scheme 2.2. Effect of silane electronics on yield and rate[a]

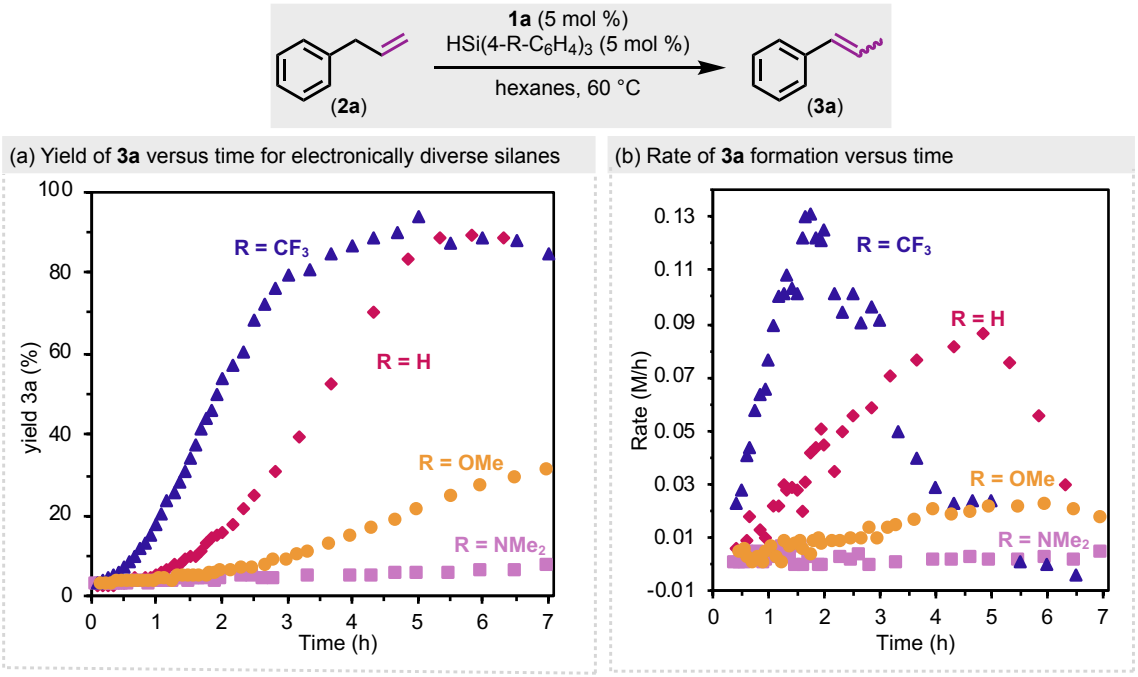

[a]Reaction conditions: **2a** (0.16 mmol), **1a** (0.008 mmol, 5 mol %), $HSi(4\text{-}R\text{-}C_6H_4)_3$ (0.008 mmol, 5 mol %), hexanes (0.5 mL), 60 °C, under N_2. (a) Yield determined by GC-MS analysis of aliquots removed throughout the course of the reaction with 1,2,4,5-tetramethylbenzene as an internal standard. (b) Rate of **3a** formation plotted as a function of time.

Substrates **2j** and **2k** also highlight another advantage to our catalyst system: tolerance of highly sensitive functional groups. Under our isomerization conditions, the acid-labile TMS and MOM groups remain intact, which is not expected using known methods to generate Ni–H active catalysts with acids. Recent advances in isomerization and remote functionalization with Ni that form the active Ni–H through activation with polar O–H bonds[107,114,143] or through high temperature (130 °C) activation of C–H bonds for an allyl-type mechanism[50] could potentially also tolerate acid-labile groups, though few or no substrates with acid-labile groups were tested in these works. Attempted isomerization with unprotected 2-allylphenol (**S3**) was less successful with crude reaction analysis showing 83% remaining **S3**, 14% isomerized alkene, and <3% 2-propylphenol. While the unprotected phenol did diminish isomerization reactivity, no silylation of the unprotected phenol was observed.[144] Non-aromatic substrates such as 1-decene and allyltriphenylsilane were also isomerized to the corresponding 2-alkene (**3q** and **3p**, respectively) with slightly lower efficiency and lower selectivity for the 2-alkene in the case of 1-decene (**2q**), which was isolated as a mixture of isomers (regiomeric ratio (r.r.) = 4.9:1 for 2-decene, *E/Z* 4.8:1).

We next sought to apply our catalyst system to other trisubstituted alkenes.[14] Products **3v**, **3w**, and **3x** are formed in high conversions from substrates **2v**, **2w** and **2x**, but in moderate isolated yield (44-76% yield, >92% conversion) and selectivity (*E/Z* = ~4:1) (**Scheme 2.1.b.**). While this catalytic system does not achieve comparable reactivity to state-of-the-art transition metal-catalyzed formation of trisubstituted alkenes,[14,15,94,123] we hypothesize that further catalyst tuning could improve reactivity for isomerization to trisubstituted alkenes. For example, with substrate **2w**, isomerization with **1a** and $HSiPh_3$ or $HSi(4\text{-}CF_3\text{-}C_6H_4)_3$ led to lower overall yields, but high selectivity for the *E*-alkene (58% conversion, *E/Z* = 8:1 and 85% conversion, *E/Z* = 6:1, respectively). Reactivity with **1e** increased reaction yield while decreasing selectivity (with $HSiPh_3$, 94% conversion, *E/Z* = 4:1; with $HSi(4\text{-}CF_3\text{-}C_6H_4)_3$, 95% conversion, *E/Z* = 3:1). Decreasing the temperature from 80 °C to 70 °C, the reaction conversion decreased to 81%, but the *E/Z* ratio increased to >14:1. Formation of **3r**, **3t**, **3y**, and **3z** all proceeded in high conversions to a single product (99%, 73%, >99%, and 86%, respectively).

Our catalyst system was also applied to substrates where the double bond is migrated across multiple bonds to the most thermodynamically stable products (**Scheme 2.3.**): homoallylbenzene **2aa** was converted in good yield to β-ethylstyrene **3aa** (isolated as a mixture with 18% of 4-phenyl-2-butene (**3aa'**)); 1,5-cod (**2ab**) and allyl indane (**2ac**) were selectively converted in good and excellent yields to 1,3-cod (**3ab**) and 1-propylindene (**3ac**). These examples show that chain walking over long distances can occur, and the driving force is generating a conjugated alkene. Finally, the geometric isomerization of internal alkene *cis*-stilbene (**2ad**) to *trans*-stilbene (**3ad**) was also carried out with full conversion to the *E*-isomer (**Scheme 2.1.c.**). A broad overview of the substrate scope demonstrates applicability to a wide range of electronically (**3a-n**) and sterically (**3j-n**, **3v-z**) diverse allylbenzene derivatives, aliphatic alkenes (**3p**, **3q**, **3r**, **3s**, **3t**, and **3ab**), and internal alkenes (**3o**, **3ab**, **3ad**).

Scheme 2.3. Scope of long chain isomerization

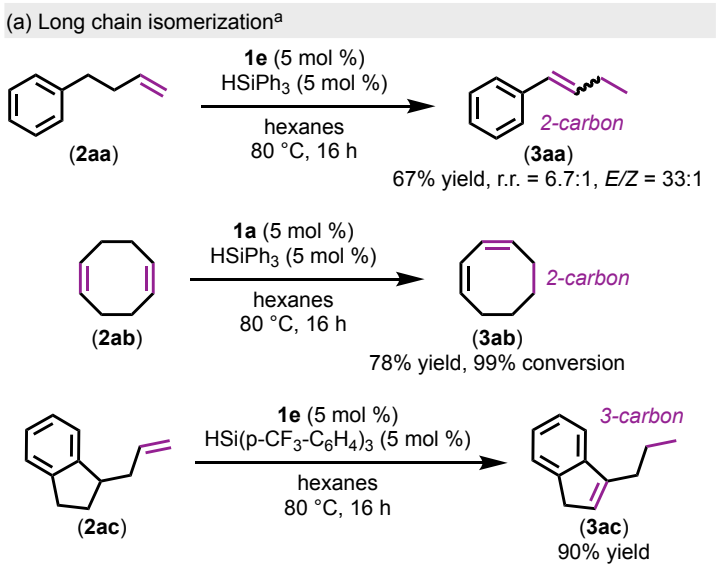

[a]Reaction conditions: **2** (0.5 mmol), **1** (0.025 mmol, 5 mol %), $HSiR_3$ (0.025 mmol, 5 mol %), hexanes (1.6 mL), 80 °C, 16 h, under N_2. Isolated yields are reported. *E/Z* ratios determined by GC analysis of the crude reaction mixture. TMS, trimethylsilyl; MOM, methoxymethyl; r.r. = regiomeric ratio (with the major species corresponding to the drawn isomer). [b]Reaction performed on a 0.3 mmol scale. [c]Reaction performed with 2 mol % **1e**. [d]Isolated as 2-(1-propen-1-yl)phenol. [e]Reaction yield determined by NMR with 1,2,4,5-tetramethylbenzene as an internal standard.

Of particular interest in the scope of remote functionalization applications and chain walking is the feasibility of regioconvergent syntheses, with the formation of a single product from a mixture of starting materials. To test the efficiency of our system for regioconvergent isomerization, we independently synthesized 4-phenyl-2-butene (**3aa'**) a possible intermediate in the isomerization of **2aa**. When introduced to optimized reaction conditions, **3aa'** was isomerized to **3aa** with 66% conversion (**Scheme 2.2.a.**). When a mixture of **3aa'**/**2aa** (75%/25%) was introduced, the mixture was converted to **3aa** in 75% conversion with 21% remaining **3aa'** (**Scheme 2.2.b.**). The higher conversion observed in the regioconvergent reaction suggests our catalytic system is more active with terminal alkenes, but more detailed mechanistic investigation is required to elucidate the mechanism of chain walking.

Scheme 2.2. Application in regioconvergent syntheses.

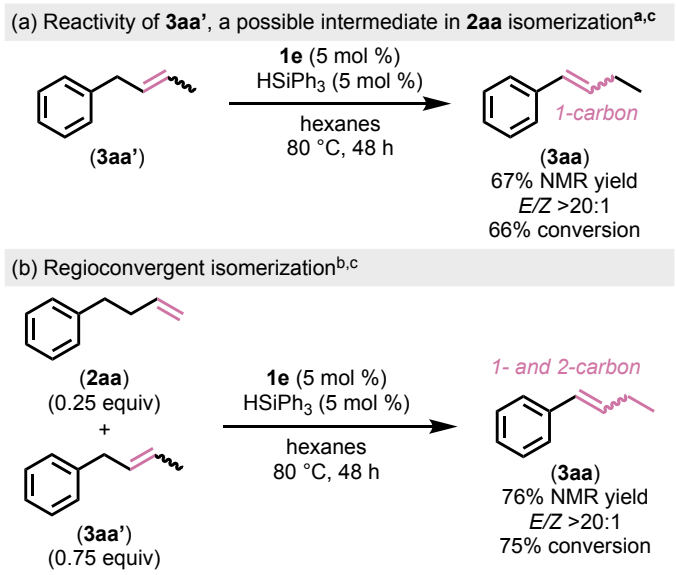

[a]Reaction conditions: **3aa'** (0.50 mmol), **1e** (0.025 mmol, 5 mol %), $HSiPh_3$ (0.025 mmol, 5 mol %), hexanes (1.6 mL), 80 °C, 48 h, under N_2. [b]Reaction conditions: **2aa** (0.13 mmol), **3aa'** (0.37 mmol), **1e** (0.025 mmol, 5 mol %), $HSiPh_3$ (0.025 mmol, 5 mol %), hexanes (1.6 mL), 80 °C, 48 h, under N_2. [c]Reaction yield determined by NMR with 1,2,4,5-tetramethylbenzene as an internal standard.

Having shown the broad applicability of our modular catalyst system, we embarked upon preliminary mechanistic studies. In many Ni-catalyzed chain-walking systems, the mechanism is still elusive, with identification of the active Ni species (Ni(I), Ni(II) or

Ni(III)) difficult.[50,57,145] One of our goals in developing this catalytic system is to extract mechanistic information that will enable more rational and efficient design of Ni-based chain-walking and tandem catalytic systems. We considered the three pathways known for Ni catalysts outlined in **Figure 2.2.a.**: allyl, insertion/elimination, and radical. We devised four experiments to differentiate between these pathways; the results and implications of these experiments are seen in **Scheme 2.3**.

Because we hypothesize that the active catalyst is formed via oxidative addition of the Ni(0) precatalyst to the Si–H bond of the silane, we expected that the silyl group remains ligated to Ni for the entire catalytic cycle and that the H from the silane would be incorporated into at least the first turnover of the product. The impact of silane electronics on the induction period and overall rate of reaction (**Scheme 2..**) is evidence supporting the presence of a (silyl)Ni species throughout the catalytic cycle. To test whether the H from the silane is incorporated into the isomerized product, $DSiPh_3$ was used in place of $HSiPh_3$ (**Scheme 2.3.a.**). For the insertion/elimination and MHAT pathways, D incorporation into the propenyl chain of **3a** is expected, and no D incorporation is expected for the π-allyl pathway. ^2H NMR analysis of **3a** after isomerization with **1a**/$DSiPh_3$ shows incorporation of deuterium at all three positions along the carbon chain. This result is consistent with the result from our control reaction without silane, which shows that silane is required for reactivity (**Table 2.1.**, entry 3), and suggests the silane is acting as the H-source. This data is consistent with the insertion/elimination and MHAT pathways, and inconsistent with the π-allyl pathway.

We next sought to differentiate between an intra- and intermolecular mechanism, since isomerization via the π-allyl pathway is expected to occur intramolecularly, and the insertion/elimination and MHAT pathways can occur intermolecularly, via either ligand exchange or radical cage escape. We designed a crossover experiment between α-ethylstyrene (**2v**) and 4'-OMe-α-ethylstyrene-d_2 (**2w-*d*$_2$**) (**Scheme 2.3.b.**).[14] If a π-allyl or caged MHAT pathway was operative, we expect no deuterium incorporation into **3v**; if the reaction proceeds via insertion/elimination or an uncaged MHAT pathway, we would expect significant deuterium incorporation in **3v** and protium incorporation in **3w**. Analysis of each product with ^2H NMR shows crossover between the two substrates, inconsistent with a concerted, intramolecular pathway. Observation of deuterium crossover suggests an

intermolecular mechanism that is consistent with a hydride insertion/elimination or an uncaged MHAT pathway and inconsistent with a π-allyl pathway.[146] Notably, our data are in contrast with mechanistic experiments performed by Schoenebeck and coworkers using $[(IPr)NiCl]_2$, which show no H/D crossover between substrates, supporting their hypothesized mechanism of an intramolecular 1,3-H shift.[30]

Having excluded the π-allyl pathway with our first two mechanistic experiments, we next sought to differentiate between a hydride insertion/elimination and an MHAT radical pathway. Common radical clock substrates with cyclopropyl groups proximal to the alkene were inconclusive in our system due to the established reactivity of (NHC)Ni(0) complexes with vinylcyclopropanes, which ring-open via oxidative addition to the strained C–C bonds of the cyclopropane.[147] Turning to a radical trap, we introduced 1.0 equivalent of 1,1-diphenylethylene (DPE)[14,93] and monitored the kinetic profile for the isomerization of **2a** (**Scheme 2.3.c.**). The introduction of DPE had no effect on the isomerization of **2a** in terms of overall yield or kinetic profile, and <5% conversion of 1,1-diphenylethene was observed. In particular, we were interested to see if the product of a styrenyl radical undergoing cage escape to react with 1,1-diphenylethylene was formed, but we never observed the products of such reactivity by GC or GCMS. If an MHAT mechanism were in play in which the radicals could diffuse, the rate of $H^{\bullet}$ transfer to 1,1-diphenylethylene should be much faster than to **2a**.[93] These data suggest that either the reaction is not proceeding through an MHAT pathway, or the intermediate radicals react too rapidly to diffuse.[148]

To further probe whether an MHAT mechanism is in play and avoid potential ambiguity regarding caged versus uncaged radical pairs, we introduced the 1,6-diene **2ae**, which should cycloisomerize to the cyclopentane **3ae** if an MHAT mechanism is in play (**Scheme 2.3.d.**).[94] The reaction proceeded in 76% conversion of **2ae**, giving a complex mixture of regioisomeric products. However, the absence of cycloisomerization product **3ae** and presence of 1,6- and 1,5-dienes (determined by ^1H NMR analysis) suggest that free radical intermediates are not forming under our reaction conditions. We also note that our catalyst system performs differently than the known Ni(I) alkene isomerization catalyst[30] in the isomerization of a vinylcyclopropane **S13** and 1,6-diene **2ae** (see Appendix A for details).

Scheme 2.3. Initial mechanistic experiments.

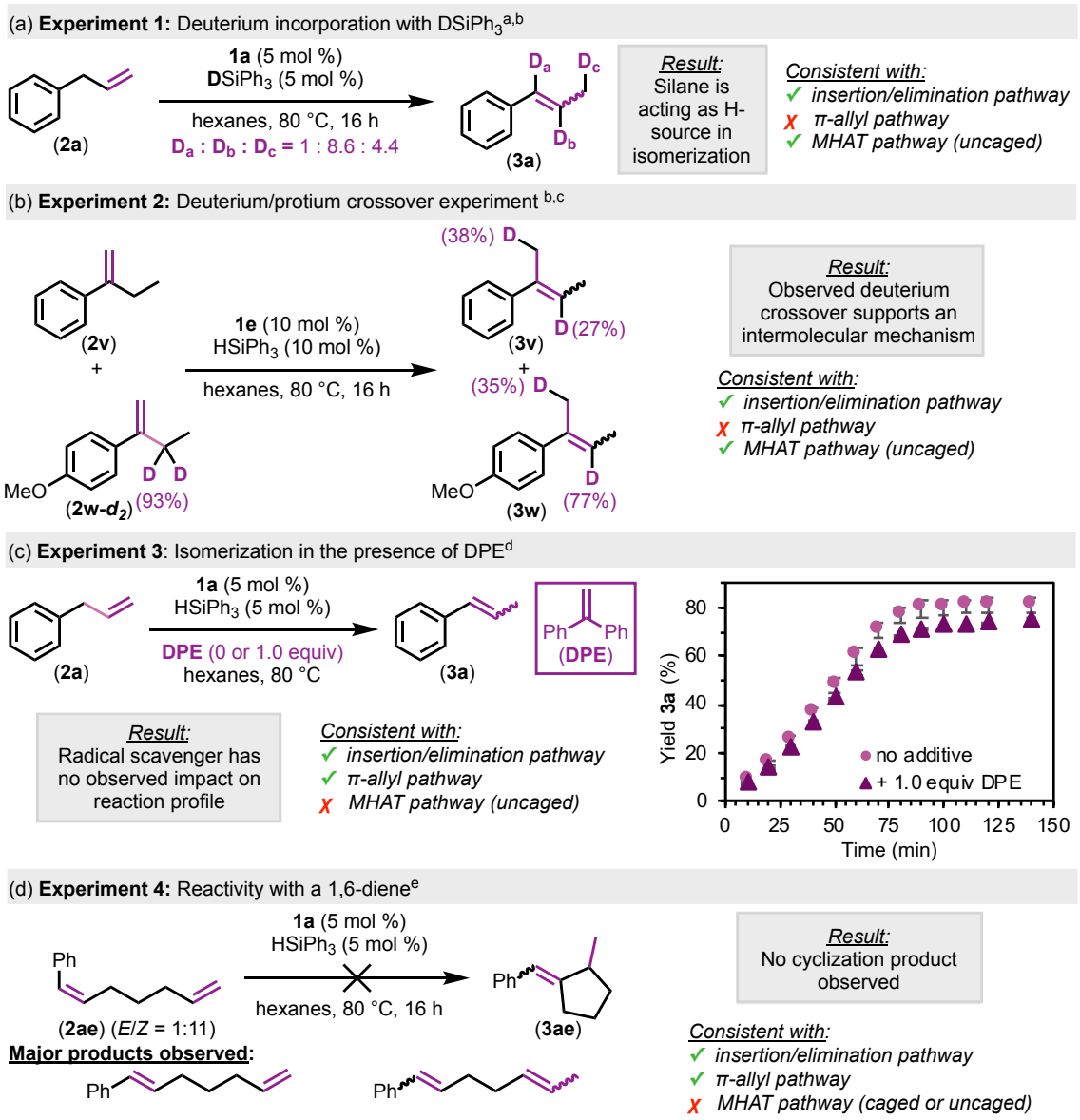

[a]Reaction conditions: **2a** (0.25 mmol), **1a** (0.013 mmol, 5 mol %), $DSiPh_3$ (0.013 mmol, 5 mol %), hexanes (0.8 mL), 80 °C, 16 h, under N_2. [b]Deuterium incorporation was determined using ^2H NMR. [c]Reaction conditions: **2v** (0.13 mmol), **2w-d₂** (0.13 mmol), **1e** (0.013 mmol), $HSiPh_3$ (0.013 mmol), hexanes (0.8 mL), 80 °C, 16 h, under N_2. [d]Reaction conditions: **2a** (0.25 mmol), 1,2-diphenylethylene (**DPE**; 0 or 0.25 mmol), **1a** (0.013 mmol, 5 mol %), $HSiPh_3$ (0.013 mmol, 5 mol %), hexanes (0.8 mL), 80 °C, under N_2. [e]Reaction conditions: **2ae** (0.25 mmol), **1a** (0.013 mmol), $HSiPh_3$ (0.013 mmol), hexanes (0.8 mL), 80 °C, under N_2.

Further support for the 2-electron insertion/elimination pathway comes from monitoring the reaction by ^1H NMR and by analyzing reaction mixtures by EPR.

Monitoring the isomerization of **2a** to **3a** by ^{1}H NMR shows minimal broadening, and no evidence of radicals forming during the reaction are seen by EPR spectroscopy (see Appendix A for details). Collectively, all evidence is consistent with a Ni–H insertion/elimination pathway.

Based on these data, a mechanism for the isomerization of alkenes is proposed (**Scheme 2.4.**). Entry into the catalytic cycle is proposed to occur through reversible oxidative addition of the (NHC)Ni(0) center to the Si–H bond of the silane. Alkene exchange forms intermediate **4**, which then is susceptible to [2,1]-insertion to form the Ni-alkyl complex **5a**, with reversible unproductive [1,2]-insertion occurring to form complex **5b**. β-Hydride elimination of the benzylic hydrogen forms intermediate **6**, which then undergoes ligand exchange with **2a** to release product **3a**. As elucidated in the deuterium incorporation studies with $DSiPh_3$ (**Scheme 2.3.a.**), we hypothesize that the iterative insertion/elimination steps are reversible since D was incorporated at all carbon positions along the alkene chain.

Scheme 2.4. Proposed mechanism of Ni(0)/$HSiR_3$-catalyzed alkene isomerization.

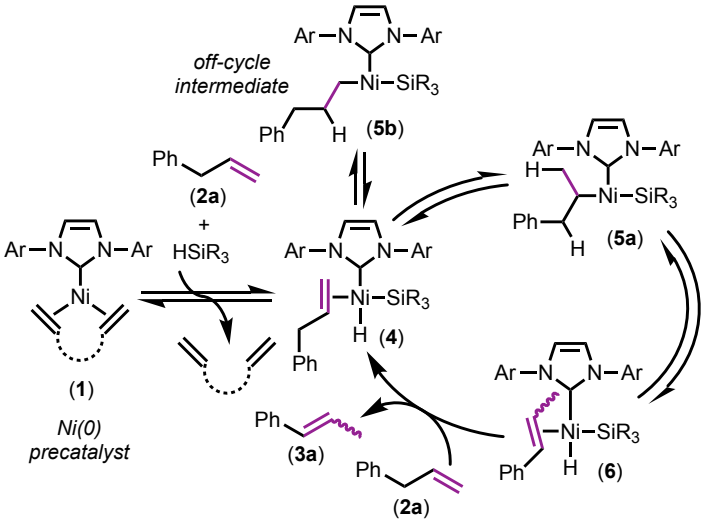

2.3 Conclusions

In summary, a modular and mild Ni(0)/silane catalytic system has been rationally designed for alkene isomerization. The role of the silane as the hydride source in the *in situ* formation of a catalytically active Ni–H represents an important step away from the

functional group intolerant hydride sources required with many Ni-based catalytic systems. The use of readily accessible and thermally stable (NHC)Ni(0) complexes avoids the reliance on expensive and thermally unstable Ni(0) precursors such as $Ni(cod)_2$. This Ni(0)/silane catalytic system offers reliable, efficient and E-selective isomerization of alkenes to form 1,2-disubstituted and trisubstituted alkenes without generation of stoichiometric byproducts. Mechanistic investigation supports a hydride insertion/elimination pathway. Trends and preliminary mechanistic insights are expected to be of significance in the context of remote functionalization reactions, which often use (NHC)Ni complexes and/or silanes under similar reaction conditions.

While the chemistry and reaction development from this chapter contributes to the field of isomerization, we hypothesized that further mechanistic investigation would enable more efficient rational design of remote functionalization or tandem catalysts for isomerization/functionalization applications. Chapters III and IV discuss the physical organic approaches we utilized to better understand what mechanistic steps affect the isomerization reactivity developed in this chapter and also expand our understanding of NHC and alkene ligand effect on catalysis.

CHAPTER III

MECHANISTIC INVESTIGATION OF A NI(0)/SILANE CATALYTIC SYSTEM FOR ALKENE ISOMERIZATION: ORIGINS OF A SUBSTRATE-DIVERGENT MECHANISM

The work in Chapter III was carried out by Kiana E. Kawamura. The chapter is in preparation for publication with editorial assistance from Amanda K. Cook.

3.1 Introduction

The development of base metal catalysts for the alkene isomerization has been established over the last few decades[29,86,115] with contributions as recent as the last few years.[14,15,30,149] Many catalytic systems, however, are still limited to specific classes of substrates such as alkenes with polar functional groups,[116,150,151] terminal alkenes,[13,152,153] or 1,1-disubstituted alkenes to form trisubstituted alkenes.[14,15] Recently, the application of alkene isomerization to more complex synthetic targets through remote functionalization[16,52,62] has received much attention due to the ability to control the site of functionalization through modification of different aspects of the reaction conditions such as temperature[53] or the introduction of additives.[50] Advances specifically with nickel[16] have utilized the ability of nickel to proceed through chain walking prior to functionalization steps including (hydro)arylation, (hydro)alkylation amongst others. The specific mechanistic steps occurring at the Ni center in these systems (*i.e.* mechanism of isomerization,[1,86,146] dissociative vs non-dissociative chain walking[31,107]) and the effect of ligand coordination sphere or additives are not always well understood. The inability to fully elucidate mechanistic information about individual steps in these complex systems has been identified as a current challenge in the further development of Ni-catalyzed remote functionalization.[16]

Our group has focused on the development of mild Ni catalysts[149] for alkene isomerization with the overall goal of applying these catalytic systems in tandem catalytic remote functionalization applications. A key aspect of our approach is our focus on

elucidating mechanistic information about the isomerization process to enable rational design of catalytic systems for remote functionalization. As our goal is to apply the developed catalytic system to remote functionalization processes, we also aimed to develop a catalytic system that was mild and modular for different substrate classes.

The Ni(0)/silane catalytic system developed and outlined in Chapter II demonstrates the feasibility of using triaryl silanes as the H-source in the isomerization of alkenes. While initial mechanistic studies point to a hydride insertion-elimination mechanism, the specific mechanistic steps are not fully understood. Upon kinetic monitoring of the isomerization of different substrates, we observed differences in the kinetic profile: for allylarene substrates, an induction period was observed with overall sigmoidal kinetics while α-substituted styrene derivatives showed linear initial rates. This chapter describes the deeper mechanistic investigation into the reactivity of (NHC)Ni(0) complexes with silanes to form catalytically-active species for the isomerization of alkenes with the goal of determining the divergent mechanism observed with different substrates. A variety of physical organic approaches including rate and order studies, linear free energy relationships, kinetic isotope effect, deuterium incorporation/scrambling, and analysis of catalyst resting states were applied. These data point to differences in Ni speciation, which is dependent on the isomerization substrate and leads to divergent mechanisms.

3.2 Results and Discussion

Mechanistic investigation of Ni(0)/silane-catalyzed isomerization of allylarenes. We first carried out kinetic studies to determine the order in each reagent. In Tolman's isomerization work[29] with $Ni[P(OEt)_3]_4/H_2SO_4$, the reaction was determined to be 1st order in $[HNi[P(OEt)_3]_4]^+$ (the precatalyst), 1st order in substrate, and negative 1st order in $P(OEt)_3$ when applying the steady state approximation. In our proposed catalytic cycle from Chapter II, we hypothesized that once the active Ni–H species was formed, the reaction could be proceeding through a similar mechanism as proposed in Tolman's work, especially since we propose one of the key steps in the activation of the catalyst is dissociation of one or both of the coordinated styrene molecules. To test this hypothesis, the $[(sty)_2Ni(IPr)]$ was varied over a concentration range of 0.011 to 0.060 M (3.5 to 20 mol % Ni loading relative to substrate). Due to variability in reaction rate from day to day,

all data that is directly compared was collected on the same day. The reactions were monitored using GC-FID. As the reaction demonstrates a distinct induction period, leading to sigmoidal kinetic profiles, the maximum rate at the linear portion of the kinetic curve was used to determine the rate at each concentration.[154] Under our reaction conditions, the isomerization of 4-allylanisole showed a half order dependence on Ni (0.50 ± 0.02), which is distinct from the work from Tolman, suggesting our system likely has different rate limiting step(s) or competing side reactivity (**Figure 3.1.**). Specifically, the Tolman work showed that decomposition of the phosphite ligand impacted observed kinetics. We do not observe any transformation or decomposition of styrene ligands in our system and expect the role of styrene to be more important due to its coordination to Ni rather than a possible decomposition path.

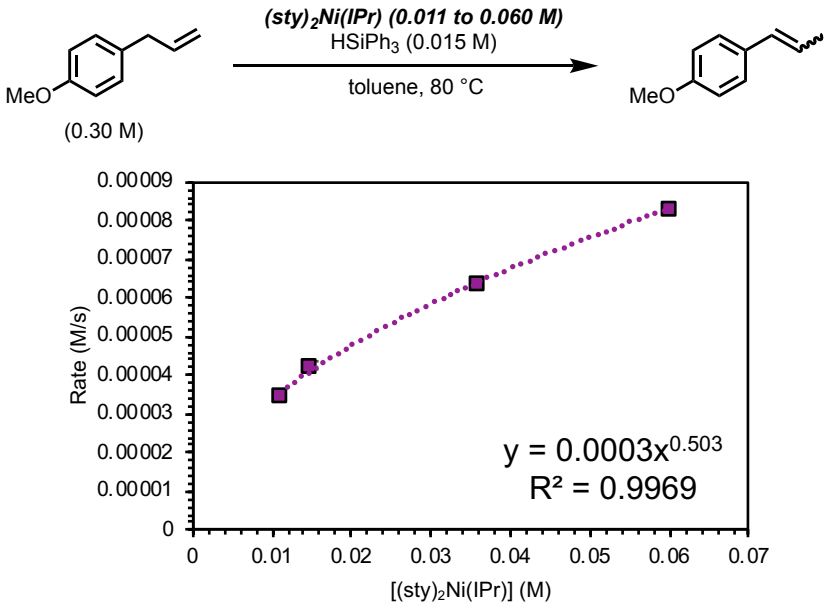

Figure 3.1. Order in $(sty)_2Ni(IPr)$. Trials were run in duplicate with durene as an internal standard. Error in the individual measured rates are present but not visible.

To further probe the roles of other reagents, the kinetic order in $HSiPh_3$ was also measured by varying the $[HSiPh_3]$ over a concentration range of 0.015 to 0.060 M (5 to 20 mol% $HSiPh_3$ loading relative to substrate) while maintaining $[(sty)_2Ni(IPr)]$ constant at 0.015 M. Under our reaction conditions, the reaction also showed a half order dependence on $HSiPh_3$ (0.53 ± 0.01), **Figure 3.2**. We also carried out experiments with different initial

concentrations of 4-allylanisole, ranging from 0.050 to 0.40 M while maintaining [$(sty)_2Ni(IPr)$] and [$HSiPh_3$] constant at 0.015 M. The data show a half order dependence on 4-allylanisole (0.46 ± 0.08), **Figure 3.3**. With these data, we wanted to investigate the role of styrene on reactivity. With no added styrene, the expected concentration of styrene based on 0.015 M of [$(sty)_2Ni(IPr)$] is 0.030 M. We monitored the isomerization of 4-allylanisole with added styrene, achieving a concentration range for [styrene] from 0.030 to 0.50 M. However, attempts to measure the order in styrene were unsuccessful, as any added styrene led to drastically reduced reaction efficiency and did not allow for valid comparison of reaction rates (**Figure 3.4.**).

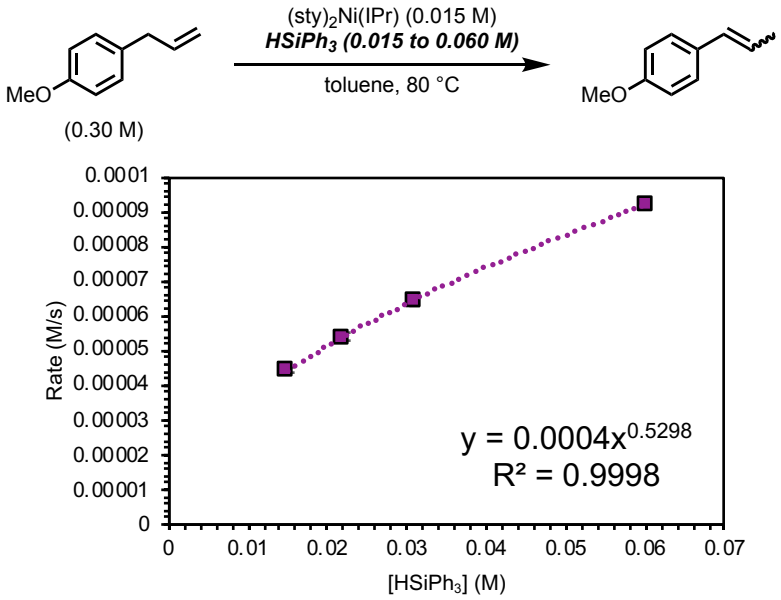

Figure 3.2. Order in $HSiPh_3$. Trials were run in duplicate with durene as an internal standard. Error in the individual measured rates are present but not visible.

Inspired by the work of Blackmond[142] and Burés,[155,156] we also performed kinetic analysis to determine whether the reaction was prone to either catalyst deactivation or product inhibition. Based on monitoring of the [4-allylanisole] (M) over the course of the reaction, we compared standard conditions (0.30 M in 4-allylanisole) to one set of data where the starting [4-allylanisole] was 0.18 M and a second set of data where the reaction was started with 0.18 M 4-allylanisole and 0.12 M 4-OMe-*trans*-β-methylstyrene was added. The three reaction profiles were compared and the complete overlay of all three

kinetic curves with a time shift of 0.42 h suggests that neither catalyst decomposition nor product inhibition are in play at the tested reaction conditions (**Figure 3.5.**).

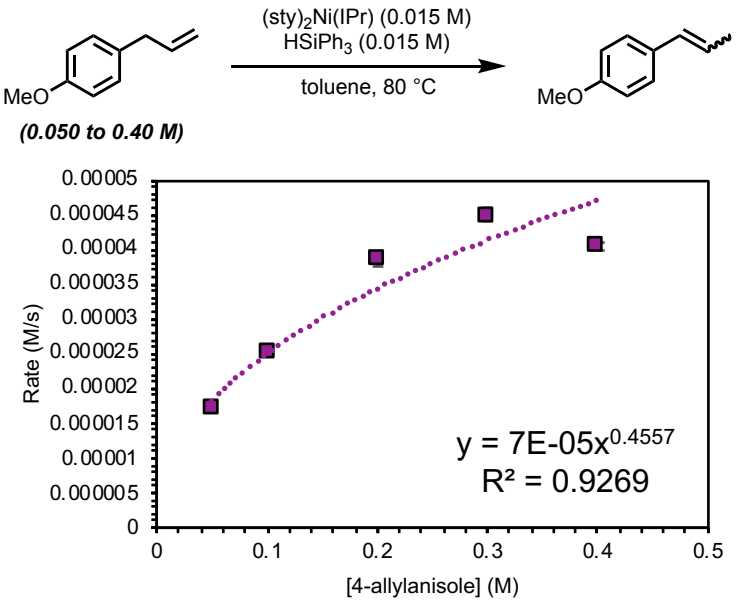

Figure 3.3. Order in 4-allylanisole. Trials were run in duplicate with durene as an internal standard. Error in the individual measured rates are present but not visible.

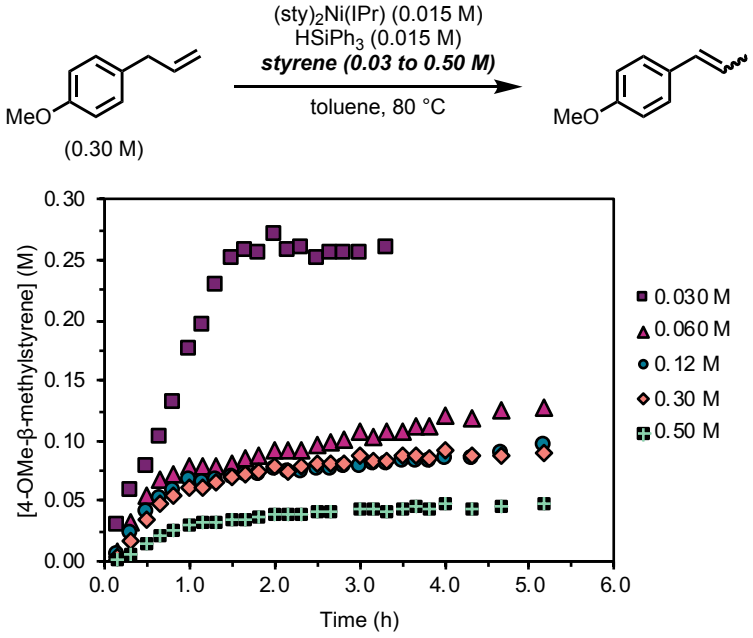

Figure 3.4. Effect of added styrene on the isomerization of 4-allylanisole. Durene was used as an internal standard.

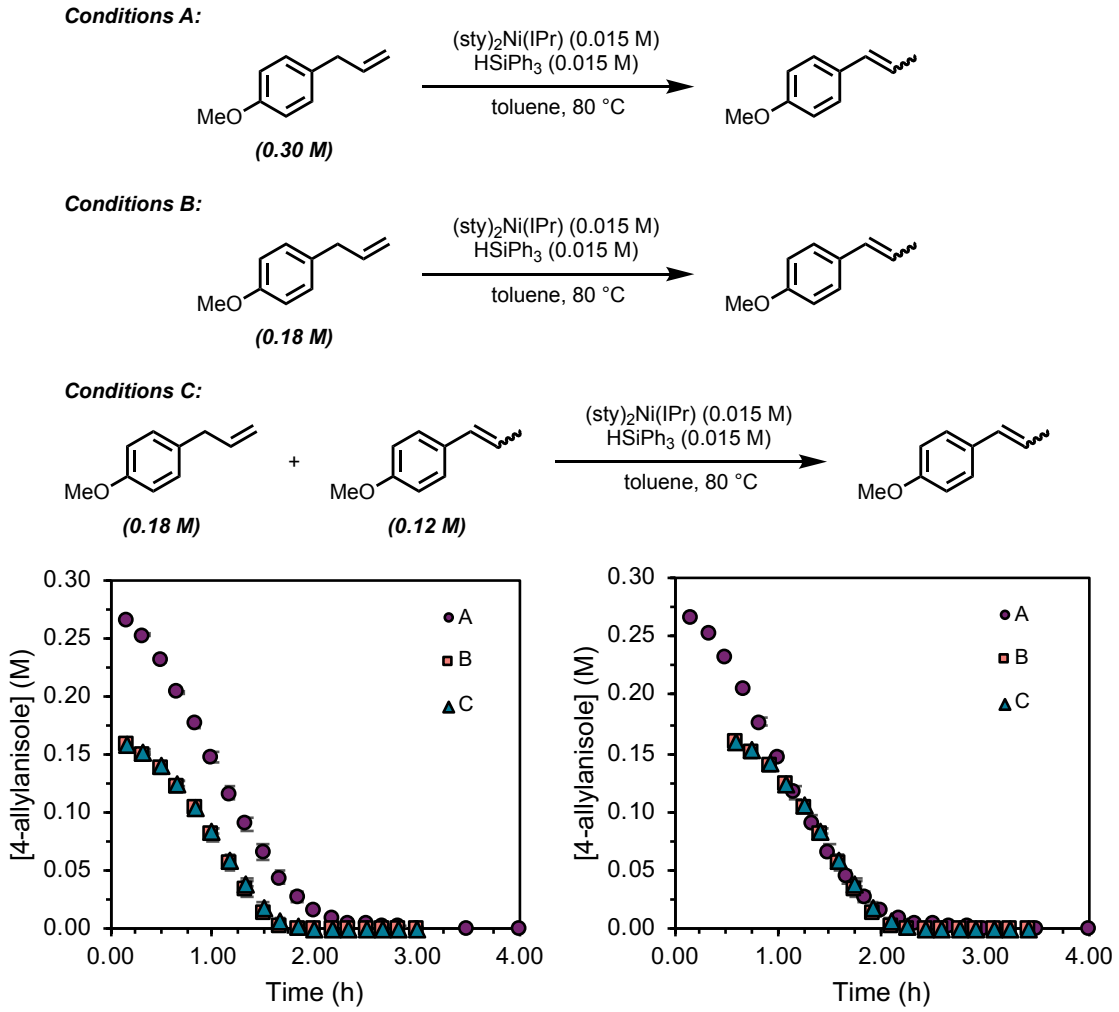

Figure 3.5. Kinetic analysis to investigate possible catalyst decomposition studies or product inhibition. Trials were run in duplicate with durene as an internal standard. Left plot shows unprocessed data. Right plot shows data with a time shift of 0.42 h.

In other kinetic studies, we investigated the kinetic isotope effect (KIE) from introduction of $DSiPh_3$ instead of $HSiPh_3$. Comparing the maximum rate at the linear portion of the kinetic curve, a KIE (k_H/k_D) of 1.09 ± 0.04 was found (**Figure 3.6.**). This small, normal KIE value is inconsistent with cleavage of the Si–H/D bond being the rate determining step. However, due to the many reversible insertion-elimination steps potentially involving the introduced deuterium, the meaning of the KIE value is unclear.

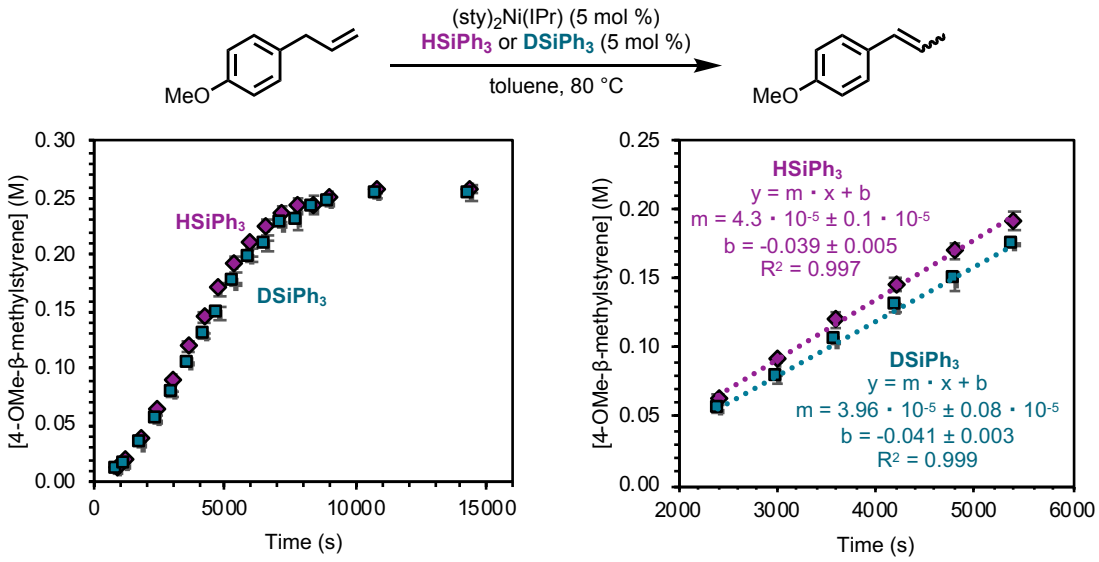

Figure 3.6. H/D kinetic isotope effect for triphenylsilane. Trials were run in duplicate with durene as an internal standard.

To further probe reactivity with $DSiPh_3$, the isomerization of 4-allylanisole was run with 10 mol % each of $(sty)_2Ni(IPr)$ and $DSiPh_3$ and the incorporation of deuterium in 4-OMe-β-methylstyrene was investigated using ^2H NMR and mass spectrometry (**Figure 3.7.**). By GC and GC-MS analysis, the distribution of species in the crude reaction mixture was: 4-allylanisole <1%; 4-propylanisole = 3%; 4-OMe-*cis*-β-methylstyrene = 5%; 4-OMe-*trans*-β-methylstyrene = 92%. Based on analysis of the ^2H NMR spectrum, unexpected incorporation of deuterium into the $–OCH_3$ group is observed along with incorporation along the alkyl chain, consistent with the results observed with allylbenzene with (1,5-hexadiene)Ni(IPr) as the catalyst. First, incorporation of deuterium into the $–OCH_3$ group suggests there is some reactivity in these conditions between either the silane and the $–OCH_3$ directly, or reactivity that is mediated by Ni. The control experiment without Ni (to determine whether reactivity is occurring directly between silane and substrate) must be run to confirm this hypothesis. While the isomerization of 4-allylanisole to 4-OMe-β-methylstyrene still proceeds to completion, the reactivity observed here could be related to the incompatibility of 4-allylansiole with substituted triaryl silanes (*vida infra*).

Aside from ^2H NMR, we also analyzed the mass spectra for the 4-OMe-*trans*-β-methylstyrene and 4-propylanisole (**Figure 3.7.**, bottom). Prediction based on natural

abundance for the distribution of the *m/z* and the *m/z* + 1 peak are shown below each structure. While the *m/z* +1 peak intensity was slightly higher than expected for 4-OMe-*trans*-β-methylstyrene (15% instead of predicted 11%), the *m/z* + 1 peak intensity for 4-propylanisole was a surprising 52% relative intensity to the *m/z* peak compared to a predicted intensity of 11%. Of note, as the formation of 4-propylanisole is hypothesized to be accompanied by the formation of a disilane species, but no such species has been observed to date (via NMR or GC-MS). These data along with observations from integration of the ^{2}H NMR spectrum suggest that formation of the undesired 4-propylanisole likely occurs more rapidly than isomerization of 4-allylanisole. Monitoring the reaction by ^{1}H NMR (Chapter II), we observe $HSiPh_3$ throughout the reaction, suggesting consumption of silane to form the alkane product uses only a fraction of the silane introduced. Further investigation into possible mechanistic routes to the formation of 4-propylanisole are needed to fully elucidate the impact of this path on the isomerization catalytic cycle.

As the use of triphenylsilane as a mild and modular H-source for Ni-catalyzed isomerization is not well studied, we sought to gain more information about the role of the silane in catalysis. To probe the influence of silane electronic character on reactivity, a series of triaryl silanes with different substituents in the 3- or 4-position were synthesized and introduced as the catalytic partner with $(sty)_2Ni(IPr)$. Due to incompatibility of $HSi(4\text{-}CF_3\text{-}C_6H_4)_3$ with 4-allylansiole, the unsubstituted allylbenzene was used in these studies (see Appendix B for the data with 4-allylanisole). The isomerization of allylbenzene to β-methylstyrene proceeded to completion with all silanes introduced, regardless of electronic character (**Figure 3.8.a.**). However, the electron-poor silanes reach completion faster than electronic-deficient silanes. To quantify the observed trend, rates for the first ~40% of the reaction were measured (**Figure 3.8.b.**) and a Hammett plot was constructed (**Figure 3.8.c.**). A ρ value of 0.42 ± 0.04 was found. This small positive slope suggests some dependence on electronic character of the silane.

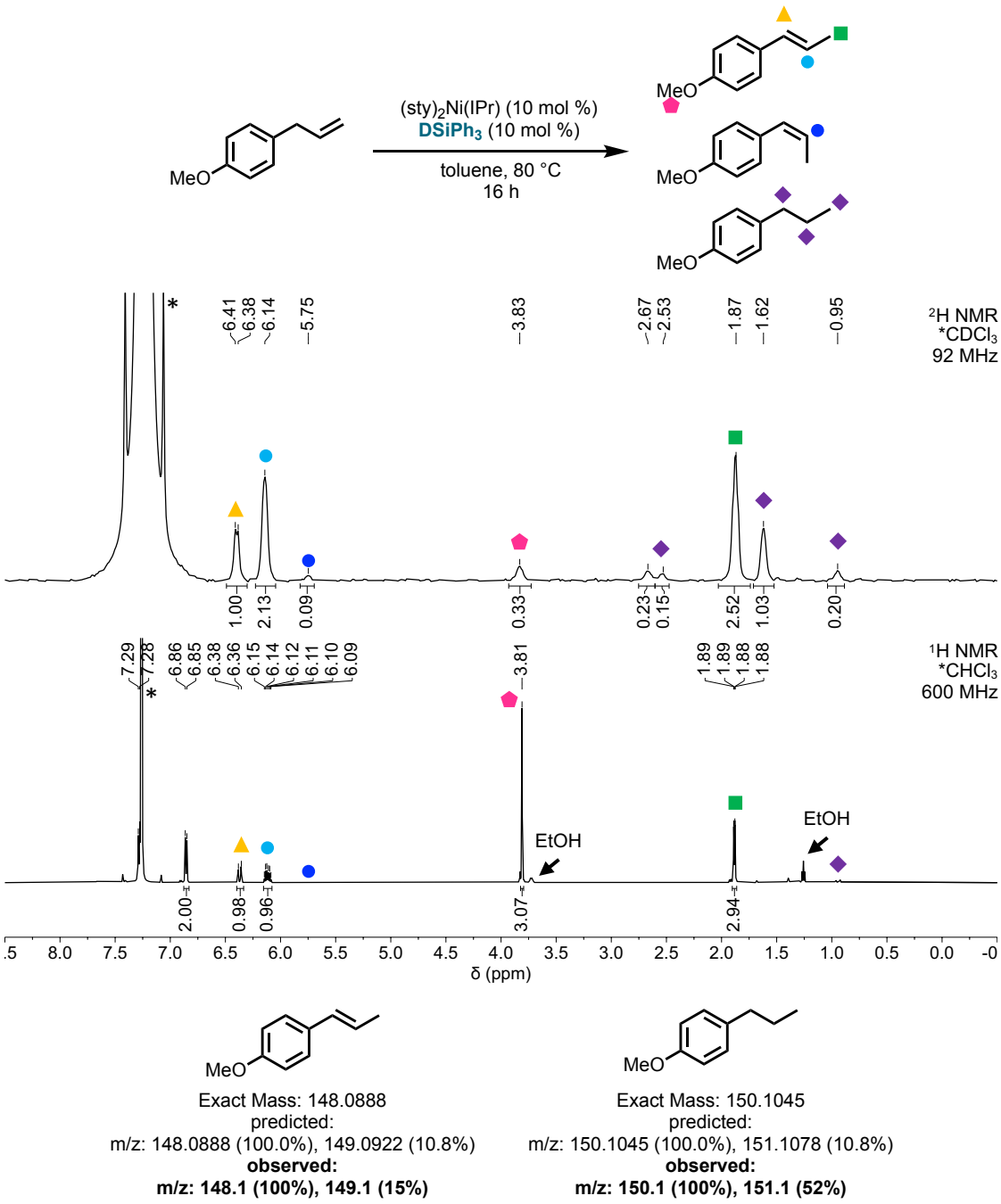

Figure 3.7. Deuterium incorporation with $DSiPh_3$ in the isomerization of 4-allylanisole.

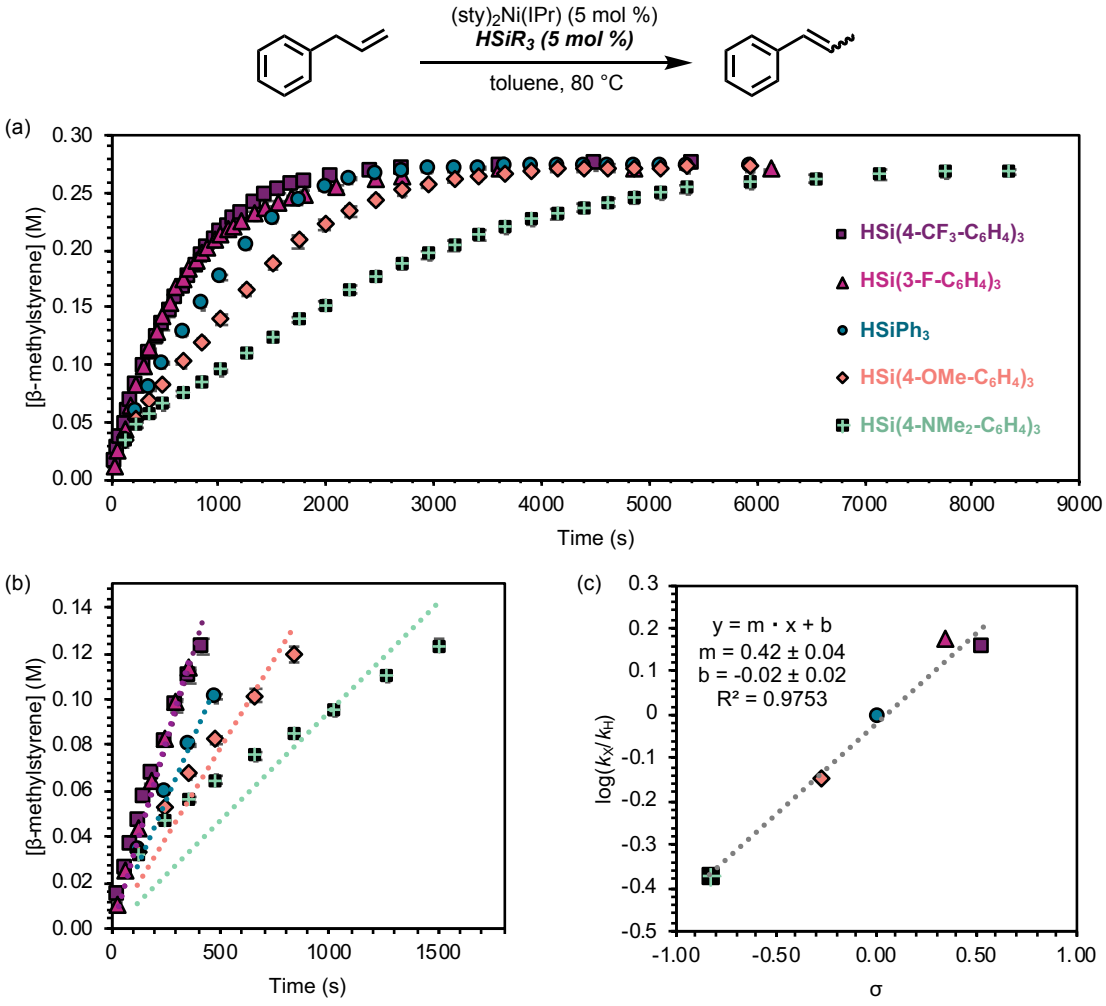

Figure 3.8. Linear free energy relationship with substituted triaryl silanes. Trials were run in duplicate with durene as an internal standard. Linear fits (y = m • x) for each silane are as follows: HSi(4-CF_3-C_6H_4)$_3$: m = 3.2 • 10^{-4} ± 0.1 • 10^{-4}, R^2 = 0.99; HSi(3-F-C_6H_4)$_3$: m = 3.3 • 10^{-4} ± 0.1 • 10^{-4}, R^2 = 0.99; HSiPh$_3$: m = 2.2 • 10^{-4} ± 0.1 • 10^{-4}, R^2 = 0.99; HSi(4-OMe-C_6H_4)$_3$: m = 1.6 • 10^{-4} ± 0.1 • 10^{-4}, R^2 = 0.98; HSi(4-NMe_2-C_6H_4)$_3$: m = 9.4 • 10^{-5} ± 0.1 • 10^{-5}, R^2 = 0.96.

Based on the above mechanistic data, attempts to derive a rate expression for the isomerization of 4-allylanisole were undertaken from a pre-equilibrium approach. From the mechanistic data, we observe an experimental rate law of:

$$rate = k_{obs}[4-allylanisole]^{0.5}[HSiPh_3]^{0.5}[(sty)_2Ni(IPr)]^{0.5}[styrene]^{-n}$$

From deuterium incorporation studies, we see the silane acting as an H-source, but cleavage of the Si–H bond is unlikely to be the rate determining step since only a very

small KIE was observed with $HSiPh_3$ vs $DSiPh_3$. Deuterium incorporation with $DSiPh_3$ suggests that the formation of 4-propylanisole occurs more rapidly than isomerization (but never makes up >3% of the reaction products). Scrambling of deuterium along the alkyl chain of the isomerization product suggests that insertion-elimination steps are all reversible. Based on the current mechanistic data, we propose a mechanism as shown in **Figure 3.9**. From *in situ* NMR studies, the starting complex $(sty)_2Ni(IPr)$ is the catalyst resting state (see Appendix B), but based on the *in situ* monitoring with (hex)Ni(IPr) (see Appendix A), the formation of a bisallylarene-Ni complex is possible. We hypothesize that complicated ligand exchange processes (*i.e.* **1** to **5** to **4** and in between) are convoluting kinetic analysis of the reaction. As the reaction proceeds, the equilibrium between all the ligand exchange reactions is likely to shift. This, along with the observed induction period, makes drawing a conclusive mechanism at this point difficult.

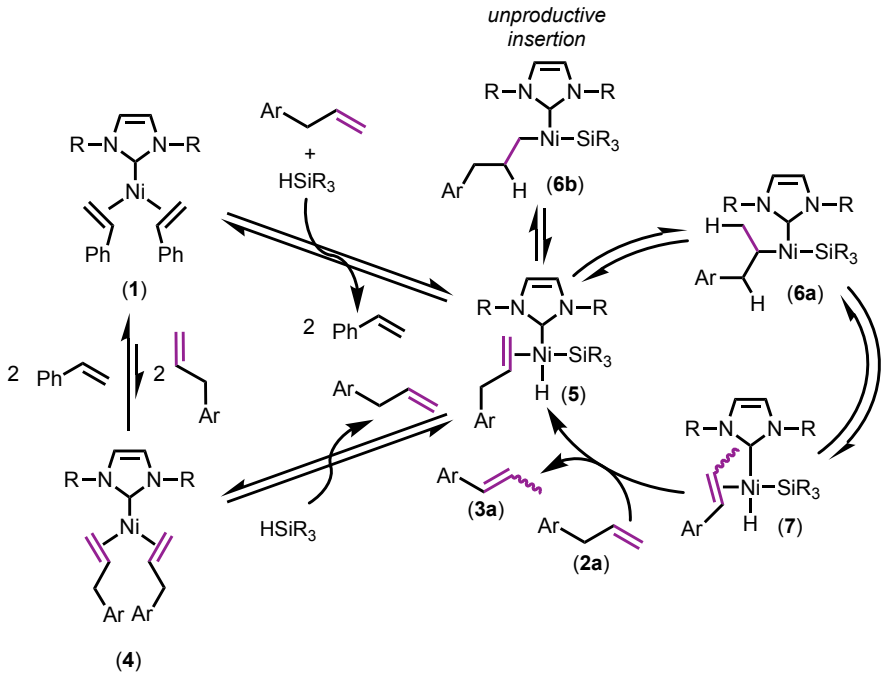

Figure 3.9. Proposed mechanism for the isomerization of allylarenes to β-methylstyrenes.

Mechanistic investigation of Ni(0)/silane-catalyzed isomerization of α-substituted styrenes. As stated in Chapter II, our initial investigation of the Ni(0)/silane catalytic system demonstrated pronounced induction periods. When we moved forward

with further mechanistic investigation to probe the reactivity of α-substituted styrenes, the kinetic profile lacked an induction period at the beginning of the reaction. To discern the origins of the apparent substrate-dependence mechanisms in play, we set out to determine the rate law for the isomerization of 4'-OMe-α-ethylstyrene to 4'-OMe-α,β-dimethylstyrene. Due to variability in reaction rate from day to day, all data that is directly compared was collected on the same day.

We first varied [$HSiPh_3$] from 0.0060 to 0.059 M and monitored the reaction by GC-FID. Attempting to take time points as frequently as every 30 seconds led to minimal formation of product for the first 3 minutes, and so the data was extracted for the time points from 3 minutes forward. The linear portion of product growth was relative rates at each concentration were measured. These data suggest a reaction that is approximately half order in $HSiPh_3$ (0.5 ± 0.1, **Figure 3.10.**), consistent with the results observed in the isomerization of 4-allylansiole.

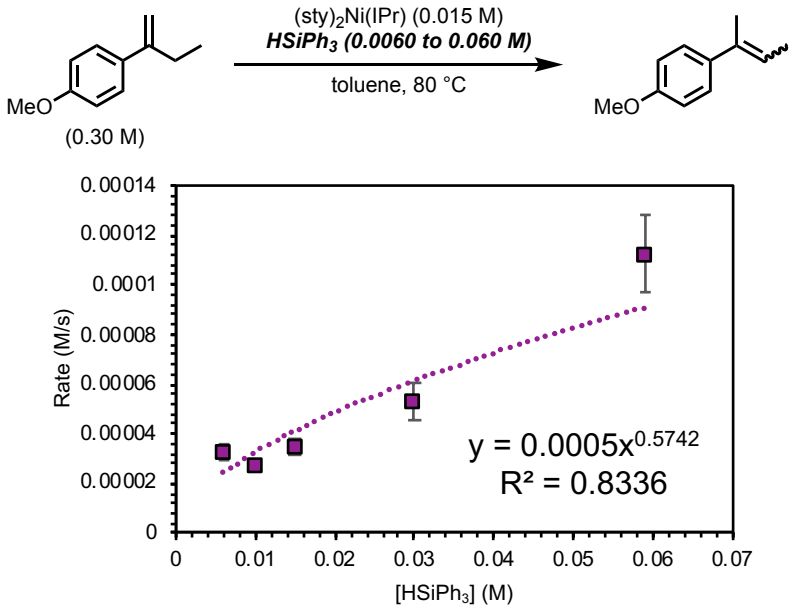

Figure 3.10. Order in $HSiPh_3$. Trials were run in duplicate with durene as an internal standard.

We next varied the concentration of both $(sty)_2Ni(IPr)$ and $HSiPh_3$ together, which will be referred to as "catalyst." Varying [catalyst] from 0.0059 to 0.030 M, we again unexpectedly observed an induction period. Measuring the linear portion of the rate

following the induction period, an order in [catalyst] was found to be approximately half order (0.57 ± 0.08, **Figure 3.11.**). Current efforts are underway to collect comparable data with the 4-allylanisole system, as well as unveil the cause behind the observed induction period.

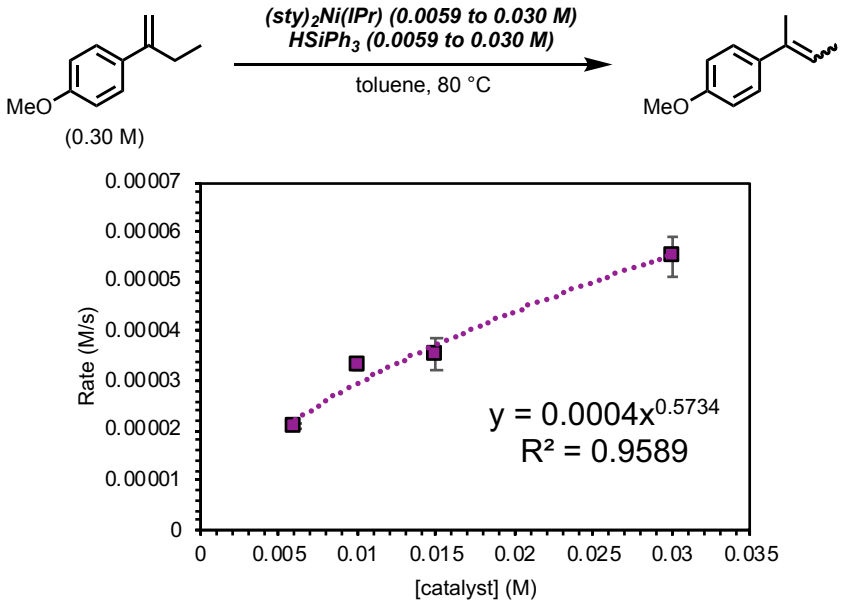

Figure 3.11. Order in catalyst [$(sty)_2Ni(IPr)$ and $HSiPh_3$ varied together]. Trials were run in duplicate with durene as an internal standard.

As with 4-allylanisole, we wanted to also investigate the role of the silane further. For this purpose, isotope labeled $DSiPh_3$ and $HSiPh_3$ were introduced in parallel reactions and the KIE was measured. Comparing the early reaction rates, a KIE (k_H/k_D) of 2.5 ± 0.2 was found (**Figure 3.12.**). The maximum KIE for an Si–H/D bond without invoking tunneling was determined to be 4.0 (see Appendix B for derivation), and so the observed KIE of 2.5 ± 0.2 is not due to tunneling, but rather points to the involvement of the labeled bond in the rate determining step(s) of the reaction since a value of 2.5 is considered a normal, primary KIE.[157] Further work to elucidate the meaning of the large KIE value is underway.

We moved forward with deuterium incorporation with $DSiPh_3$ (**Figure 3.13.**). The isomerization of 4'-OMe-α-ethylstyrene was run with 10 mol % each of $(sty)_2Ni(IPr)$ and $DSiPh_3$ and the incorporation of deuterium in 4'-OMe-α,β-dimethylstyrene was

investigated using ^{2}H NMR and mass spectrometry. By GC and GC-MS analysis, the distribution of species in the crude reaction mixture was: 4'-OMe-α-ethylstyrene (starting material) <1%; 1-methoxy-4-(1-methylpropyl)benzene (hydrogenated product) = 1%; 4'-OMe-α,β-dimethylstyrene (*Z*-product) = 17%; 4'-OMe-α,β-dimethylstyrene (*E*-product) = 78% (**Figure 3.13.**, top). Contrary to the results observed with 4-allylansiole, no deuterium incorporation is observed in the substrate –OCH_3 group. Rather, deuterium is only observed in two positions: primarily in the α-CH_3 group and the C_β–H position of the *E*-product.

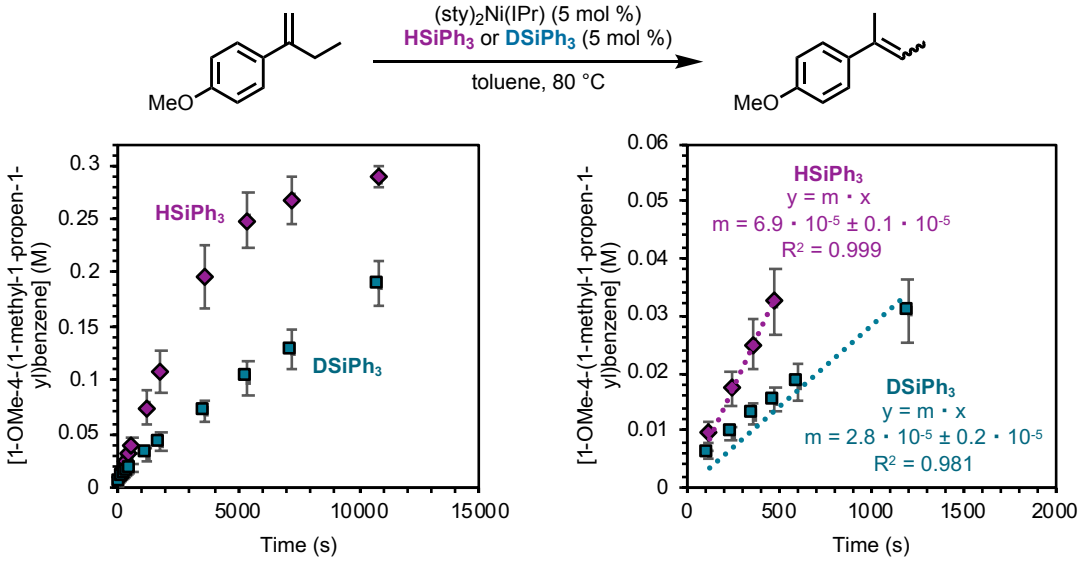

Figure 3.12. H/D kinetic isotope effect for triphenylsilane. Trials were run in duplicate with durene as an internal standard.

Aside from ^{2}H NMR, we also analyzed the mass spectra for the 4'-OMe-α,β-dimethylstyrene and 1-methoxy-4-(1-methylpropyl)benzene (**Figure 3.13.**, bottom). Prediction based on natural abundance for the distribution of the *m/z* and the *m/z* + 1 peak are shown below each structure. While the *m/z* +1 peak intensity was slightly higher than expected for 4'-OMe-α,β-dimethylstyrene (15% instead of predicted 12%), the *m/z* + 1 peak intensity for 1-methoxy-4-(1-methylpropyl)benzene was a surprising 38% relative intensity to the *m/z* peak compared to a predicted intensity of 12%. These data along with observations from integration of the ^{2}H NMR spectrum suggest that, similarly to the isomerization of 4-allylanisole, formation of the undesired 1-methoxy-4-(1-

methylpropyl)benzene likely occurs more rapidly than isomerization of 4'-OMe-α-ethylstyrene, which may be diluting any effect of labeling the Si–H bond in terms of kinetic analysis. Further investigation into the different reactivity in action are needed to fully determine the role of both the silane and the side reaction required to form the reduced 1-methoxy-4-(1-methylpropyl)benzene byproduct.

To further investigate the role of the silane in the catalytic system, we introduced a series of electronically varied triaryl silanes. Based on the incompatibility of 4-allylansiole with $HSi(4\text{-}CF_3\text{-}C_6H_4)_3$, we decided to carry out these experiments with the unsubstituted α-ethylstyrene analogue of 4'-OMe-α-ethylstyrene to avoid any undesirable side reactivity. Monitoring the kinetic profile of the isomerization with the different substituted silanes (**Figure 3.14.a.**) and measuring the early rate of reaction (**Figure 3.14.b.**) provided the data to construct a Hammett plot (**Figure 3.14.c.**). A ρ value (slope) of 0.34 ± 0.06 is within error of that found for the isomerization of 4-allylansiole (ρ = 0.34 ± 0.04), suggesting that the substrates are similarly affected by silane electronics. Based on the KIE with H/D–$SiPh_3$, we were surprised by the similarity in ρ values between the two substrates. To attempt to gain more information, we turned to isotope labeling of the substrate.

Through established methods,[14] 4'-OMe-α-ethylstyrene-d_2 was synthesized and a parallel KIE experiment was carried out (**Figure 3.15.**). A KIE (k_H/k_D) of 1.01 ± 0.03 was found, which is within error of 1, indicating no kinetic isotope effect. These data suggest β-hydride elimination of the labeled C–H/D bond is not involved in the rate determining step(s). From the crossover experiment with 4'-OMe-α-ethylstyrene-d_2 and α-ethylstyrene (Chapter II), we do know that intermolecular H/D-transfer is in play, which suggests that at some point, the labeled atoms are moving from one substrate to the other, which we believe means the reaction must be going through a [Ni]–H/D species at some point. For the α-substituted styrene derivatives, the observation of crossover and the lack of a substrate-based KIE along with a large primary KIE with H/D–$SiPh_3$ strongly suggests the rate determining step(s) are occurring prior to the product-forming elimination step.

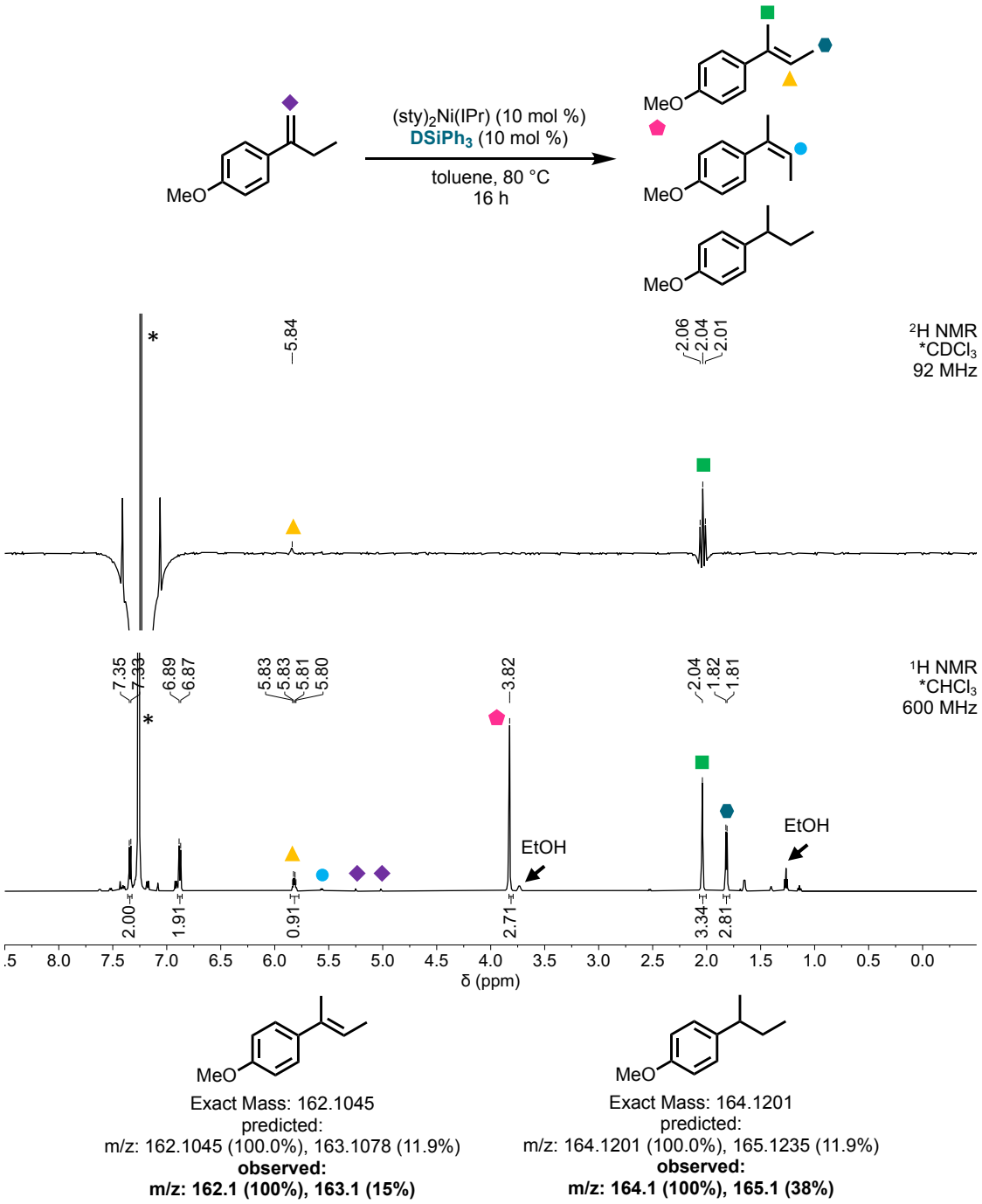

Exact Mass: 162.1045
predicted:
m/z: 162.1045 (100.0%), 163.1078 (11.9%)
observed:
m/z: 162.1 (100%), 163.1 (15%)

Exact Mass: 164.1201
predicted:
m/z: 164.1201 (100.0%), 165.1235 (11.9%)
observed:
m/z: 164.1 (100%), 165.1 (38%)

Figure 3.13. Deuterium incorporation with $DSiPh_3$ in the isomerization of 4'-OMe-α-ethylstyrene.

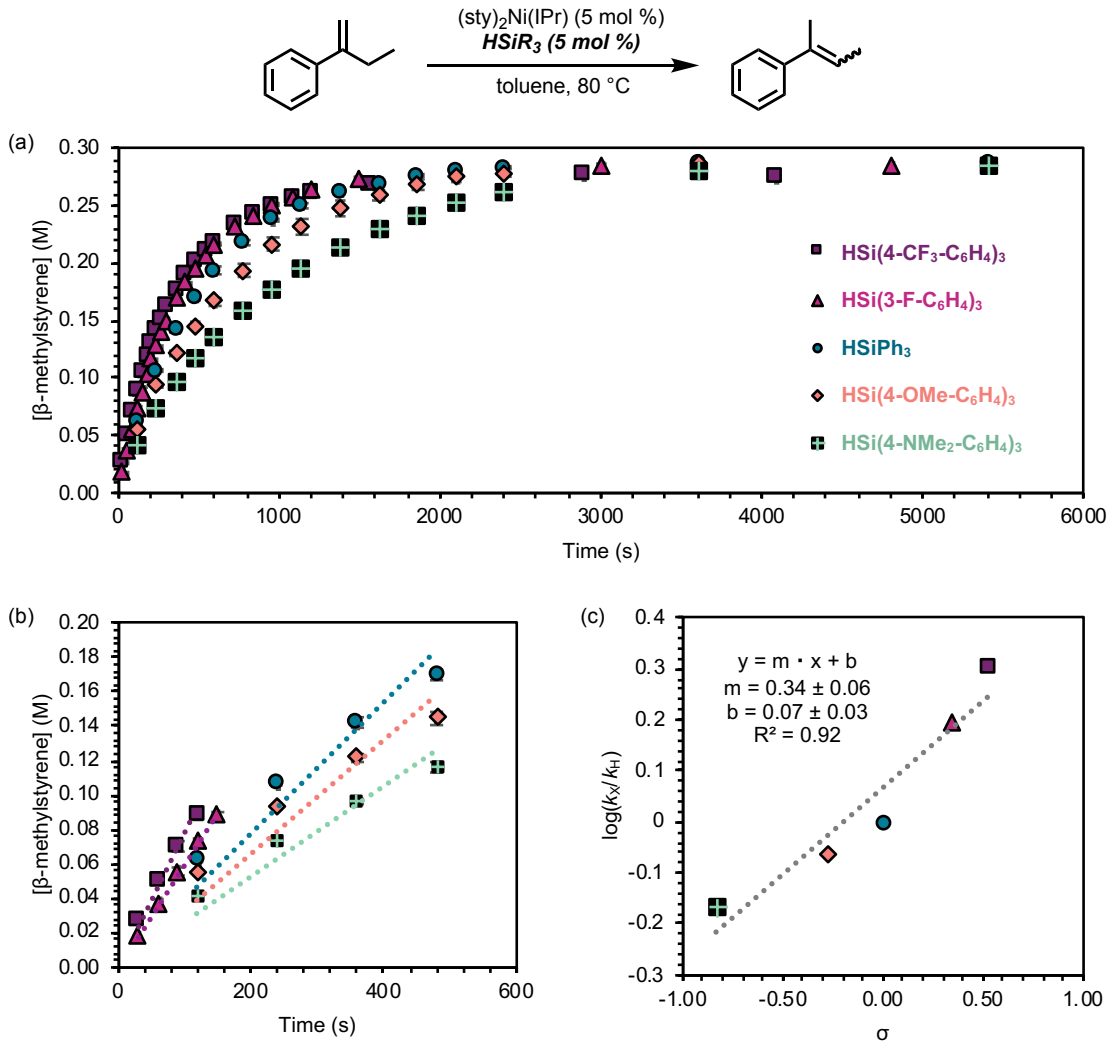

Figure 3.14. Linear free energy relationship with substituted triaryl silanes. Trials were run in duplicate with mesitylene as an internal standard. Linear fits (y = m · x) for each silane are as follows: HSi(4-CF_3-C_6H_4)$_3$: m = 7.7 · 10^{-4} ± 0.3 · 10^{-4}, R^2 = 0.997; HSi(3-F-C_6H_4)$_3$: m = 5.99 · 10^{-4} ± 0.07 · 10^{-4}, R^2 = 0.999; $HSiPh_3$: m = 3.8 · 10^{-4} ± 0.2 · 10^{-4}, R^2 = 0.989; HSi(4-OMe-C_6H_4)$_3$: m = 3.3 · 10^{-4} ± 0.1 · 10^{-4}, R^2 = 0.987; HSi(4-NMe_2-C_6H_4)$_3$: m = 2.6 · 10^{-4} ± 0.1 · 10^{-4}, R^2 = 0.990.

Based on current mechanistic results, we propose the following mechanism for the isomerization of α-substituted styrenes (**Figure 3.16.**). Due to the increased steric bulk of the substrates, we do not propose the formation of a bis-substrate complex (future directions include *in situ* NMR studies to identify catalyst resting state). From deuterium incorporation studies, we propose the insertion step favors the productive insertion. From the substrate-based KIE experiment, we propose that the product-forming β-hydride

elimination step is after the rate determining step. From the silane KIE experiment, we observe a large KIE, suggesting cleavage of the labeled bond or migration of the deuterium atom are possible rate determining steps.

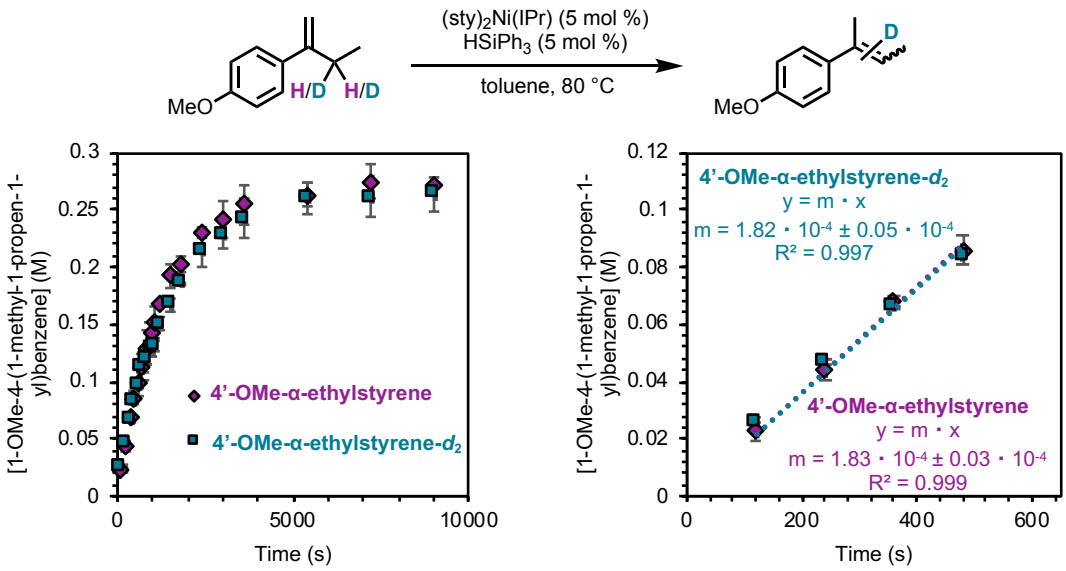

Figure 3.15. H/D kinetic isotope effect for 4'-OMe-α-ethylstyrene. Trials were run in duplicate with durene as an internal standard.

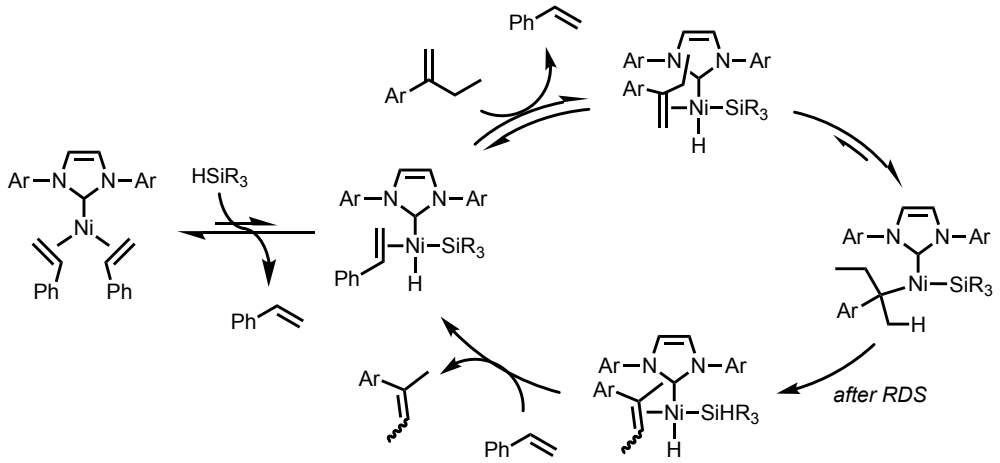

Figure 3.16. Proposed mechanism for the isomerization of α-substituted styrenes.

3.3 Conclusions

In summary, the work in Chapter III applies a broad variety of physical organic approaches toward mechanistic elucidation of alkene isomerization that shows distinct

kinetic profiles based on the substrate substitution pattern. Current efforts focus on synthesis of 4-allylanisole-d_2 in order to compare a possible substrate-based KIE for the two systems (we are particularly interested in pursuing this experiment because of the difference in silane-based KIE for the two systems). Other goals include more detailed *in situ* NMR experiments and identification of catalyst resting state(s). Ni-catalyzed transformations of alkenes are numerous, including, but not limited to hydrofunctionalization, cross coupling and polymerization reactions. Based on our preliminary results, the skeletal structure of the alkene substrates introduced has a profound effect on the rate determining step(s) and overall mechanistic picture of Ni(0)/silane-catalyzed alkene isomerization. Identification of the specific steps within the catalytic cycle (or to enter the catalytic cycle) that are affected by substrate structure could inform not only the current isomerization catalytic system, but other Ni-based catalytic transformations of alkenes.

The work in Chapter III has provided important information to improve our understanding the role of each reagent, including substrate, in the Ni(0)/silane-catalyzed isomerization of alkenes. This work focuses on the structure of substrates and silanes. Chapter IV shifts focus to focus on the impact of the ligand sphere on the Ni complexes introduced as (pre)catalysts. The next chapter investigates the effect of both the NHC ligand and the alkene to enable the rational design of an *in situ* approach to Ni(0)/silane-catalyzed alkene isomerization.

CHAPTER IV

THE ROLE OF LIGAND STERICS ON THE ACTIVITY OF A NI(0)/SILANE CATALYTIC SYSTEM FOR THE ISOMERIZATION OF ALKENES

This chapter includes previously published material from Morris, P.T. The Role of Sterics and Electronics on Nickel Catalyzed Isomerization of Allylbenzene. *Clark Honors College Theses* **2021**, https://scholarsbank.uoregon.edu/xmlui/handle/1794/26547. The work in Chapter IV was developed by Kiana E. Kawamura and the synthetic and mechanistic work presented was carried out primarily by Parker T. Morris and Gaby M. Bailey with guidance from Alison Sy-min Chang and Kiana E. Kawamura. Victor M. Salpino contributed through the synthesis of ligands.

4.1 Introduction

In the introduction of new catalytic systems to the broader chemistry community, practicality is of great importance, with tedious, multi-step reactions being of limited utility in industry.[158] Indeed, on an industrial scale, the isomerization of alkenes most commonly relies on base-mediated processes, which require high loading of base and high temperatures, depending on the substrate. For example, stoichiometric or excess KOH at 200 °C are the industrial conditions for the isomerization of 4-allylanisole or eugenol (**Figure 4.1.a.**), and even these harsh conditions only achive moderate yield (~56%) and low *E*:*Z* selectivity (82:18).[85] As recently as 2015, the development of a polymer-bound Ru catalyst from Grotjahn has enabled conversion of allyl aromatics to the corresponding *E*-propenylbenzene derivatives (>20:1; *E*/*Z*) with low catalyst loading (0.5 mol %), relatively mild conditions (70 °C, 24 h) and recyclability (3-4 cycles) with simple decantation of product from the heterogeneous catalyst (**Figure 4.1.b.**).[159] While the devleopment of heterogenized transition metal catalysts is appealing from a practicality perspective due to the (general) increased ease of product separation from catalyst, we chose to focus on other aspects of practicality, mainly modularity and scalability, with the additional benefit of relying on first row Ni compared to second row Ru. While the work

outlined in Chapters II and III focuses on the application of an isolated Ni(0) complex with a known ligand coordination environment, this Chapter focuses on modifying the approach to make the catalytic system applicable to the average synthetic lab.

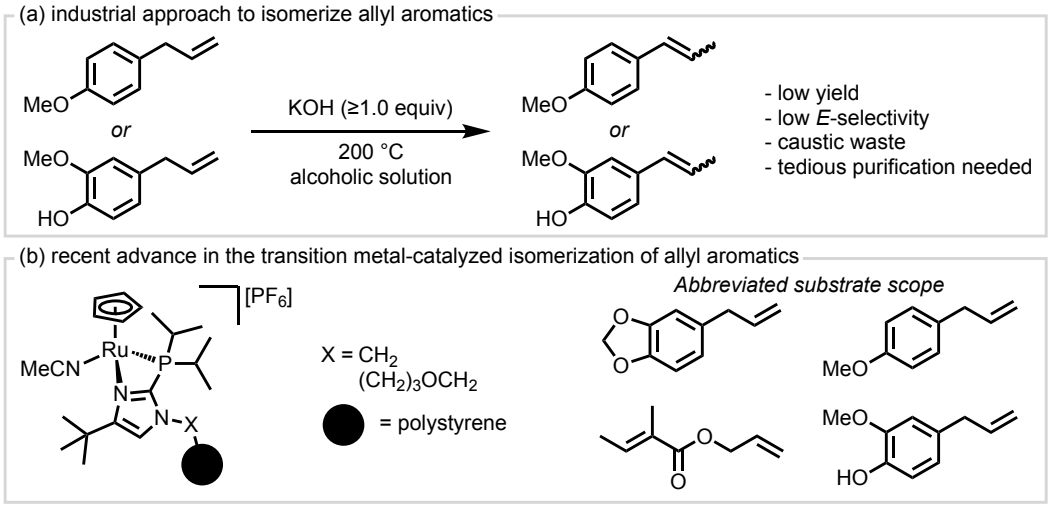

Figure 4.1. (a) Industrial approach to the isomerization of allyl aromatics and (b) recent development in transition metal-catalyzed isomerization.

Our overall goals on this front were to (i) deepen our understanding of the effect of the NHC ligand used and (ii) use this information to develop an *in situ* approach, which only utilizes compounds that are either commercially available or accessible to the general synthetic lab (*i.e.* labs that might not have access to a glovebox). We started by looking at isolated $(sty)_2Ni(NHC)$ complexes before moving on to attempt to form the active catalyst *in situ* to ensure our mechanistic understanding of the catalytic system transferred between the different approaches. We hypothesized that steric and electronic variation of the NHC ligand could affect catalyst activity and/or selectivity, adding a degree of modularity already explored in addition to the silane identity.

4.2 Results and Discussion

Effect of NHC modification on reactivity. To probe the effect of NHC modification, complexes of the form $(sty)_2Ni(NHC)$ were synthesized for the four NHC ligands shown in **Figure 4.2**. All four of these complexes are known[136] with a recent study

on the structure of the NHC providing information on the percent buried volume (%V_{bur}) for each ligand.[136] From Louie & co.'s studies, substitution along the backbone of the NHC ligand disrupts dynamic rotation along of the *N*-aryl substituent. As outlined in **Figure 4.2.**, bottom right, installing larger substituents decreases the C_{Ar}–N–C_1 angle, which results in a more crowded metal center. From the work of Louie, we developed the following hypotheses:

(i) Based on the inhibiting role of styrene to catalytic activity for catalytic activity (see Chapter III), we hypothesized that if styrene dissociation is involved in the rate determining step(s), then *increased %V_{bur} of the ancillary NHC ligand could increase reactivity by encouraging more facile styrene dissociation*.

(ii) Due to crowding at the Ni center, *sterically larger ligands may decrease selectivity for the E-propenylbenzene product*.

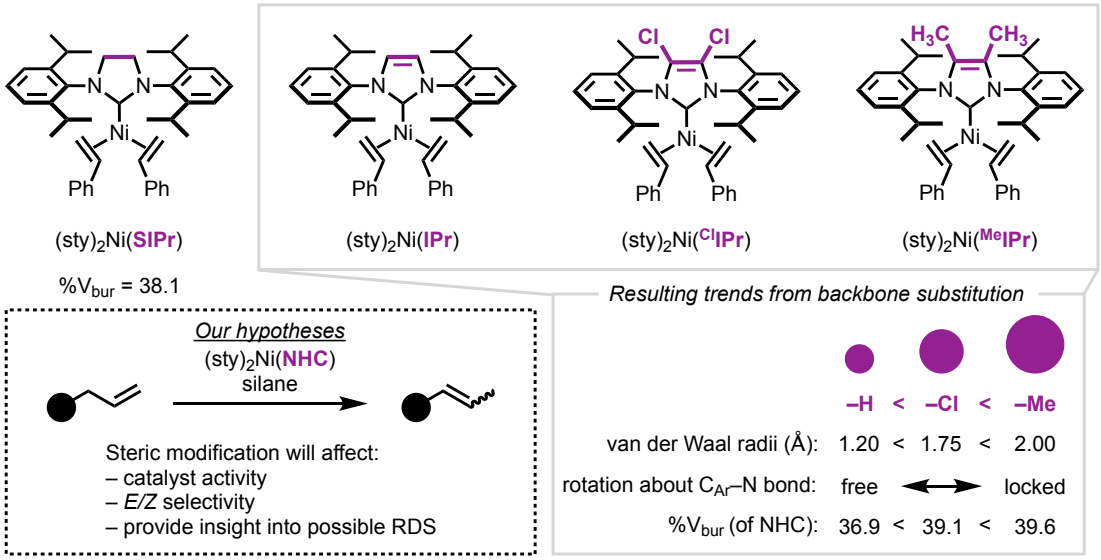

Figure 4.2. Complexes utilized to screen impact of NHC modification on catalytic activity. %V_{bur} values are based on a normalized Ni–C_1 bond length of 2.00 Å. If calculated from the X-ray crystal structures without normalized Ni–C_1 bond lengths, the trend holds, but values change slightly.[136]

To test these hypotheses, the isomerization of allylbenzene to β-methylstyrene was screened with the four complexes shown in **Figure 4.2**. The results of the screening are

shown in **Table 4.1**. To our surprise, at 80 °C, all four complexes reached appreciable conversion to β-methylstyrene. Due to issues with mass balance, the % conversion is reported instead of calibrated yield. Of note is that while the SIPr complex reached high conversion, it was much less selective for the *E*-product. As these results did not provide much insight into the role of the NHC on reactivity (they all performed well), we turned to kinetic monitoring of the reactions to monitor product formation over time.

Table 4.1. Product distribution in the isomerization of allylbenzene screening different $(sty)_2Ni(NHC)$ complexes.

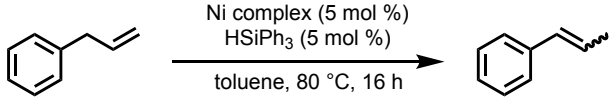

Ni complex	% conversion	*E/Z* ratio
$(sty)_2Ni(SIPr)$	94 ± 2	7 ± 1 : 1
$(sty)_2Ni(IPr)$	99 ± 0	21 ± 1 : 1
$(sty)_2Ni(^{Cl}IPr)$	98 ± 0	21 ± 0 : 1
$(sty)_2Ni(^{Me}IPr)$	98 ± 0	21 ± 1 : 1

Focusing on the three complexes with satisfactory *E/Z* selectivity, the isomerization of allylbenzene was monitored at 80 °C by GC vs durene as an internal standard (**Figure 4.3.**). The formation of β-methylstyrene over time shows that $(sty)_2Ni(^{Me}IPr)$ is much more efficient than the other two complexes, with the unsubstituted backbone, $(sty)_2Ni(IPr)$, being the slowest to reach full conversion. While this data gave us some insight into the overall trends in reactivity, we wanted to observe the initial rates of reactivity for the three complexes, and so we re-ran kinetic trials at reduced a temperature (70 °C) to slow product formation (**Figure 4.4.**). At the reduced temperature, the same trend is seen with $(sty)_2Ni(^{Me}IPr) > (sty)_2Ni(^{Cl}IPr) > (sty)_2Ni(IPr)$. These results support our first hypothesis that increased steric bulk ($\%V_{bur}$) of the ancillary NHC ligand does increase reactivity. While this does not guarantee that the dissociation of styrene (or a different ligand) is one of the rate-determining steps, it does show that modification of the steric bulk can be tuned to increase catalytic activity. We also want to bring attention to the retained high selectivity for the *E*-alkene product, demonstrating that the increased reactivity did not come with a decrease in selectivity as we predicted was a possible undesirable outcome. The modularity

of this catalytic system with respect to the NHC ligand is of particular interest since other Ni catalysts for alkene isomerization are not modular.[30]

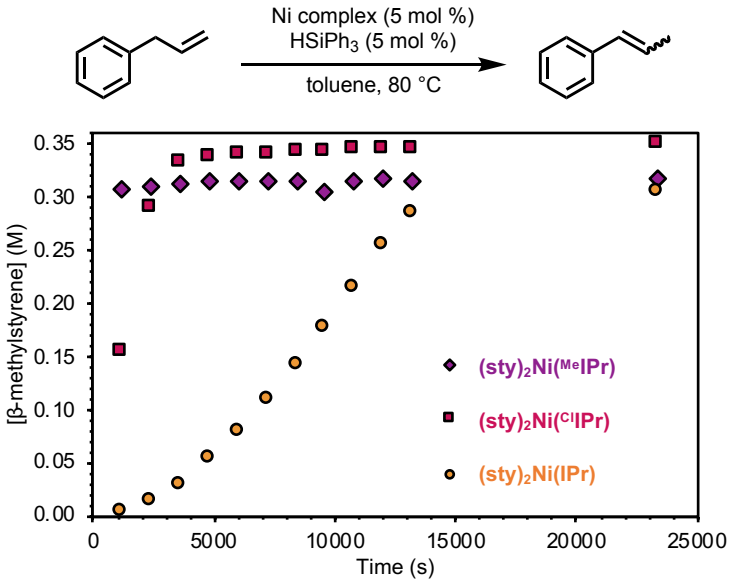

Figure 4.3. Isomerization of allylbenzene to compare the reactivity of different Ni complexes with modified NHC ligands at 80 °C. Product concentration was calculated vs durene as an internal standard.

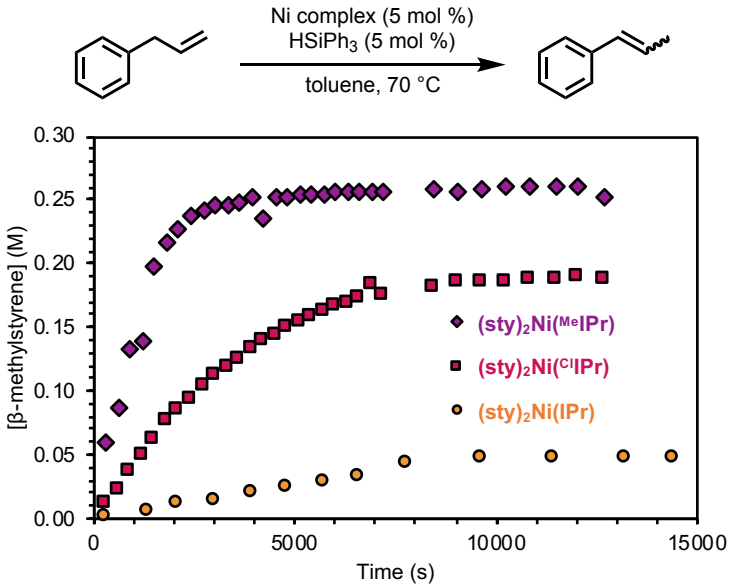

Figure 4.4. Isomerization of allylbenzene to compare the reactivity of different Ni complexes with modified NHC ligands at 70 °C. Product concentration was calculated vs durene as an internal standard.

The final experiment we ran with isolated Ni complexes was directly comparing the reactivity of $(sty)_2Ni(IPr)$ and (hex)Ni(IPr). Based on the ability to readily substitute the 1,5-hexadiene ligand for other bis-alkene ligands (*i.e.* diallylether, divinyltetramethyldisiloxane[160], complexes of which both performed very poorly, reaching <10% conversion in screening studies[149]) and mono-ligated alkene ligands (*i.e.* styrene), we proposed that comparing complexes with the same NHC but different alkene ligands would also support the hypothesis that dissociation of the stabilizing alkene could limit reactivity. While optimization of the original system showed that both $(sty)_2Ni(IPr)$ and (hex)Ni(IPr) reached appreciable yields (67% and 95%, respectively) at 70 °C after 8 h in hexanes,[149] we wanted to compare the reactivity of the two complexes in hexanes (optimized conditions for the 1,5-hexadiene complex). Monitoring the formation of β-methylstyrene over time, we see that the 1,5-hexadiene complex, (hex)Ni(IPr), reaches reaction completion within 5 hours, while $(sty)_2Ni(IPr)$ lags behind, only reaching ~55% conversion at 5 h (**Figure 4.5.**). The reactivity of these two complexes observed in this experiment further supports our hypothesis that the identity (and coordinating ability) of the alkene ligand affects reactivity. These results also help motivate the introduction of a Ni complex such as $Ni(cod)_2$, where the stabilizing alkenes are very labile.

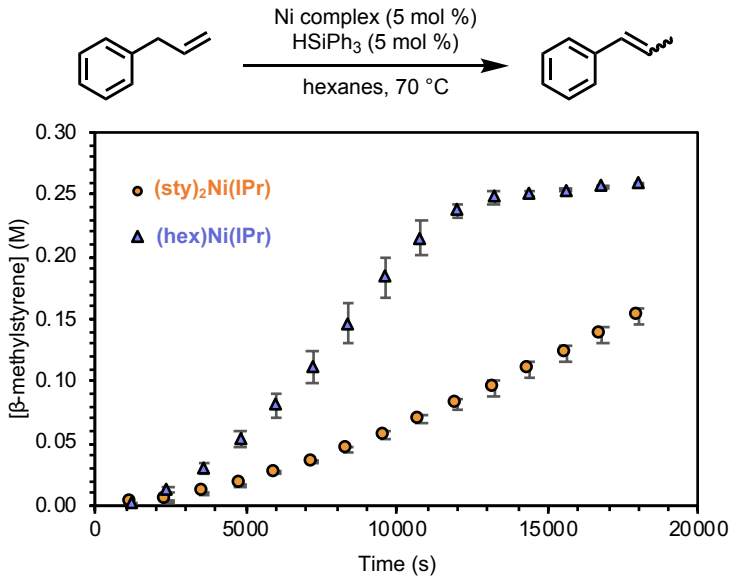

Figure 4.5. Comparing the influence of stabilizing alkene ligands on catalyst activity. Trials were run in duplicate with durene as an internal standard.

We have also shown that 1,5-cyclooctadiene is efficiently isomerized to the conjugated 1,3-cyclooctadiene product when introduced as a substrate. We proposed that if the introduced 1,5-cyclooctadiene reacts readily to form 1,3-cyclooctadiene, the Ni will more readily react with introduced substrate (*i.e.* allylbenzene). This hypothesis, along with the practical aspect of not needing to isolate a variety of Ni complexes in order to screen the effect of ligand identity helped motivate us to develop an *in situ* route to active catalyst formation from $Ni(cod)_2$.

Development of a practical *in situ* approach. Moving forward to address our second goal with this work, which was to develop a practical method in which the catalyst is generated *in situ*, we turned to commercially available $Ni(cod)_2$ and the carbene ligands that were isolable as the free carbene. We decided to focus on the free carbene rather than the corresponding imidazolium salt due to results from reaction optimization for the original catalytic system developed in Chapter II. In optimization of the (hex)Ni(IPr)/$HSiPh_3$ catalytic system, the isomerization of allylbenzene proceeded smoothly with 5 mol % each of $Ni(cod)_2$, IPr and $HSiPh_3$ reaching 98 ± 0 % conversion with high selectivity for the *E*-alkene (*E/Z* ratio = 23:1). However, attempts to introduce 5 mol % each of IPr · HCl and KO*t*-Bu (to deprotonate the imidazolium chloride and generate the free carbene *in situ*) led to severely diminished conversion of allylbenzene to β-methylstyrene (22 ± 7%). As KO*t*-Bu is able to isomerization allylbenzene to β-methylstyrene on its own, it is unclear if the activity observed with IPr · HCl and KO*t*-Bu is due to a catalytically active Ni complex or simply the presence of KO*t*-Bu (isomerization with only KO*t*-Bu led to 43% yield with an *E/Z* selectivity of 5:1). Of note is the critical role of both the NHC ligand and the silane in the reaction. Control studies were conducted with $Ni(cod)_2$ and either IPr or $HSiPh_3$ (but not both), and none of these reactions reached >5 % conversion.

To explore the possibility of an *in situ* approach, three free carbene ligands were screened with $Ni(cod)_2$ and $HSiPh_3$ (**Figure 4.6.**). Of the three ligands screened, IPr performed the best, reaching the highest conversion and reaction completion within three hours. The reaction with IMes eventually reached high conversion, but over a much longer time span. The *N*-alkyl ITMe ligand performed very poorly, with low conversion (~3% yield) over the 19-hour period monitored. This trend agrees with results observed in the

system with isolated $(sty)_2Ni(NHC)$ complexes where NHC ligands with larger $\%V_{bur}$ values reached higher conversion at faster rates (**Figure 4.4.**). The $\%V_{bur}$ value for IMes is smaller than the unsubstituted IPr (35.3 vs 38.5, respectively).[136]

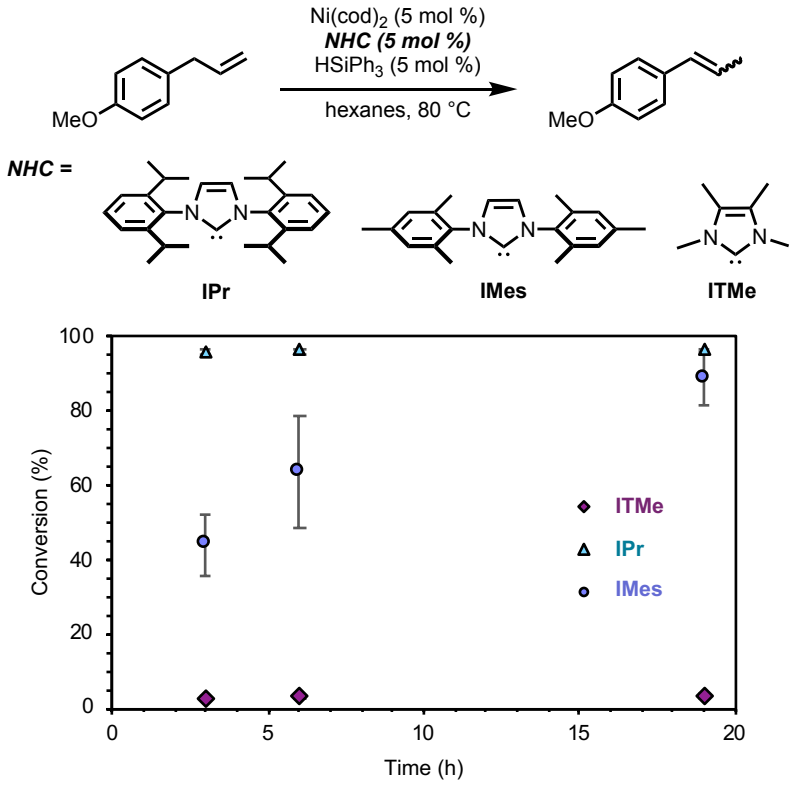

Figure 4.6. Initial screening of different carbene ligands for an *in situ* approach to forming an active catalyst for alkene isomerization. Trials were run in duplicate with durene as an internal standard.

To check whether the *in situ* approach is proceeding through a comparable mechanism as proposed in the system with isolated (NHC)Ni complexes, an abbreviated screening of triaryl silanes was investigated at 80 °C (**Figure 4.7.**). Based on initial rates of reaction, the same trend is observed compared to the reactivity of isolated complexes as precatalysts, with electron-poor silanes leading to faster initial rates. However, in the reactions with $HSi(4\text{-}CF_3\text{-}C_6H_4)_3$, the rate of reaction starts to slow after ~20 minutes, causing the reaction to lag behind the other two silanes. Based on unpublished results, our current hypothesis is that $Ni(cod)_2$ is reacting with $HSi(4\text{-}CF_3\text{-}C_6H_4)_3$, leading to side reactivity that hinders isomerization catalytic activity. Testing different approaches to

setting this reaction up (*i.e.* changing the order of addition of reagents) are underway to try and address the reactivity observed in **Figure 4.7.**

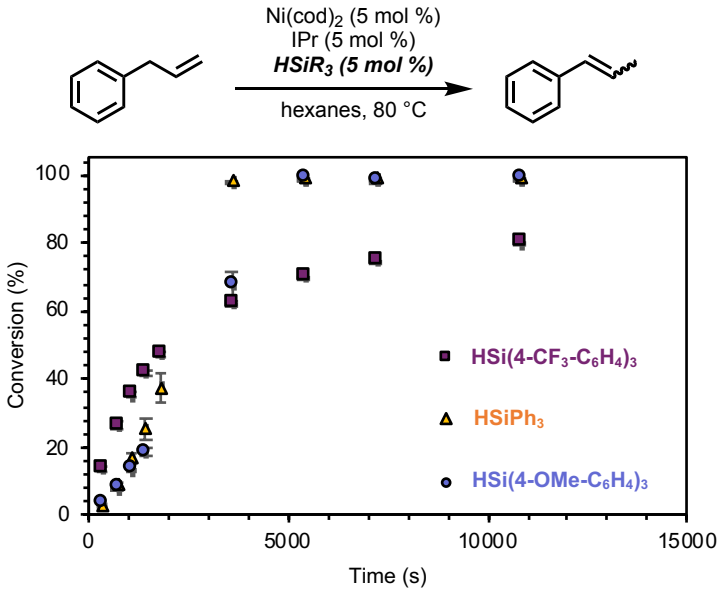

Figure 4.7. Abbreviated silane screening for the isomerization of allylbenzene. Trials were run in duplicate.

From NMR monitoring of the isomerization of 4-allylanisole with $(sty)_2Ni(IPr)/HSiPh_3$, the primary resting state is identified as the starting $(sty)_2Ni(IPr)$ complex (**Figure 4.8.**). The predominance of the starting styrene complex as the resting state throughout the reactions suggests styrene coordinates strongly to the Ni center. From work in Chapter III, we hypothesize that the relative coordination strength of all alkenes in solution plays an important role in the reactivity of the catalytic system. Therefore, next steps for the development of an *in situ* approach will investigate *in situ* reactivity, with the goal of identifying the catalyst resting state (**Scheme 4.1.**).

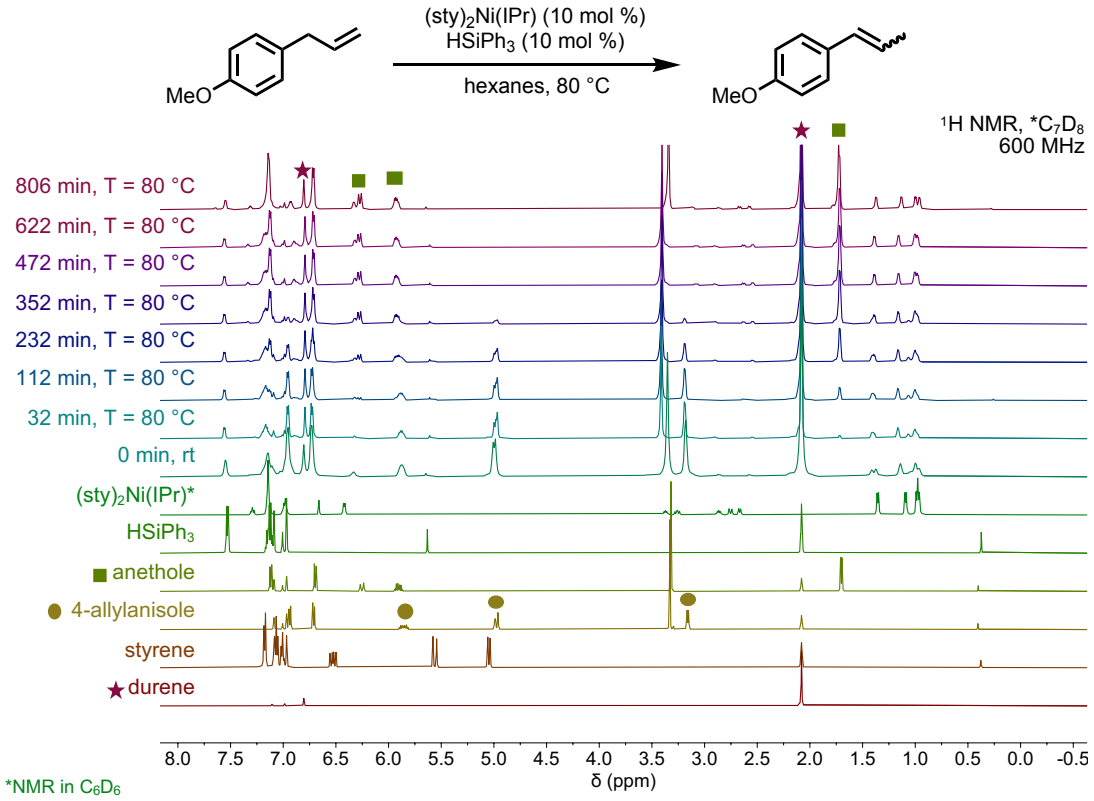

Figure 4.8. ^{1}H NMR monitoring of the isomerization of 4-allylanisole with isolated $(sty)_2Ni(IPr)$.

Scheme 4.1. ^{1}H NMR monitoring of the isomerization of 4-allylanisole with $Ni(cod)_2$/IPr.

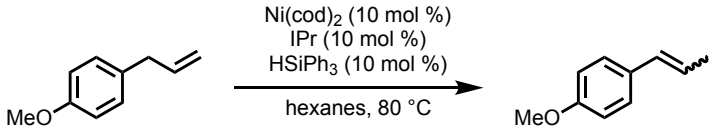

As mentioned above, one goal of developing an *in situ* approach for Ni-catalyzed alkene isomerization was practicality. In our screening studies and kinetic experiments, reactions were run on a <0.5 mmol scale. While running on a small scale was beneficial for reaction development, we want to test the scale up of the method developed in this chapter. Next steps will explore the feasibility of running the isomerization of 4-allylanisole on a 1 g (6.7 mmol) scale, testing whether factors such as catalyst loading can be changed (*i.e.* lowered to 2.5 or 1 mol %).

4.3 Conclusions

In this chapter, we broadened our understanding of the role of the NHC ligand in the Ni(0)/silane-catalyzed isomerization of alkenes, building on work developed in Chapters II and III. The work showed that NHC ligands with larger steric bulk, as measured by $\%V_{bur}$, were able to enhance catalytic activity in terms of both conversion (with milder conditions: 70 °C instead of 80 °C) and rate of reaction. The effect of the stabilizing alkene on isolated Ni(0) complexes was also investigated, showing that the more labile 1,5-hexadiene complex compared to the bis-styrene complex performed better at the lower temperature as well. These results point to the important role of alkene coordination at the Ni center throughout catalysis, suggesting that starting from Ni(0) complexes with strongly stabilizing alkene ligands can hinder entry into the catalytic cycle. Future work on this will focus on the equilibrium and ligand exchange reactions between isolated Ni(0) complexes with substrate molecules to elucidate the impact of relative alkene coordination strength.

The chemistry described in Chapter IV provides insight into the effect of the ligand sphere of the isolated Ni complexes on alkene isomerization. We used this information to inform the development of a system that forms an active species *in situ*. Building off of our interest in developing modular, practical methods for alkene isomerization, the work in Chapter V describes our preliminary work on applying our knowledge of alkene isomerization with known hydroboration catalysts to achieve the remote hydroboration of alkenes, of which a critical consideration is an understanding of how each reagent and ligand affects reactivity at the metal center.

CHAPTER V

DEVELOPMENT OF A TANDEM CATALYTIC SYSTEM FOR THE MARKOVNIKOV-SELECTIVE REMOTE HYDROBORATION OF ALKENES

The work in Chapter V was developed by Kiana E. Kawamura and Amanda K. Cook. Experimental work was carried out by Kiana E. Kawamura. Quinn Valentine contributed sulfated zirconia material for isomerization/hydroboration screening studies.

5.1. Introduction

Remote functionalization has emerged as an appealing route to the transition metal-catalyzed transformation of molecules at sites distal to the site of initial interaction. The overall process proceeds through an initial chain walking step followed by functionalization. Major benefits that arise from remote functionalization systems include elimination of purification steps for intermediates, avoidance of directing group installation, and regioconvergent synthesis. Remote functionalization has been applied in a variety of transformations including hydrofunctionalization,[161–163] hydroalkylation,[56,104] hydroarylation,[31,57,58,107,108,111] and carboxylation,[53,114] amongst many others.[18,54,55,63,103,109,112] The design of remote functionalization catalytic systems can arise from many different approaches including development of a single catalyst capable of both the chain walking and the functionalization, reliance on two different catalysts to carry out the two distinct actions (orthogonal tandem catalysis, OTC), or other tandem catalytic appoaches.[59]

The goals of this work is based on an OTC approach in which a Ni catalyst is introduced to facilitate chain walking along an alkene chain, followed by hydroboration with a Cu or Fe catalyst. Our target with this work is to achieve the terminal-, Markovnikov-selective hydroboration of aliphatic alkenes. Thus far, remote hydroboration has been achived with terminal selectivity using Co-[164–167] and Fe-based[167,168] catalysts, but all of these examples are selective for anti-Markovnikov (linear) functionalization. Indeed, Markovnikov selectivity in the hydroboration of alkenes is most commonly achieved in the

presence of electronically-biased functional groups[17–20] (*i.e.* aryl rings) with very select examples of Markovnikov-selective transition metal catalysts for the hydroboration of aliphatic alkenes.[64–68] The examples shown in **Figure 5.1.** are the only known examples of transition metal catalysts selective for Markovnikov hydroboration of aliphatic alkenes. None of these catalytic systems were active with internal alkenes, and thus there are no examples to date of remote, terminal- and Markovnikov-selective hydroboration of alkenes.

Our specific target is remote hydroboration because organoboron compounds play an important role in organic synthesis. The C–B bond can be further transformed into functional groups such as amides, alkyl fluorides, bromides, alcohols, aldehydes and more.[169] Organoboron compounds also make up one of the coupling partners in Suzuki-Miyaura cross coupling reactions,[170] making them an important precursor for the formation of C–C bonds. While our initial targets are not asymmetric, work from Shi and Hong[66] provides precedent for asymmetric Markovnikov hydroboration, using an (NHC)CuCl catalyst with a chiral and enantiopure NHC. Our reaction development will focus on reactivity with achiral ligands, but hopefully will set the stage for asymmetric work in the future through ligand modification.

Our proposal builds on the work developed in Chapters II-IV and by others in the Cook Lab to develop an OTC system with two catalysts: (i) a Ni catalyst to enable chain walking and kinetic trapping of the terminal alkene which then proceeds through hydroboration with (ii) a Cu or Fe catalyst that is Markovnikov-selective for aliphatic alkenes (**Figure 5.2.**). Two key challenges in the development of OTC systems is the compatibility of the two catalysts in terms of reaction conditions (and additives) and rate of reaction. In order to achieve the desired reactivity, the chain walking catalyst must be able to efficiently "walk" the alkene from a starting position to the terminal position prior to functionalization. The functionalization catalyst must react selectively with terminal alkenes to avoid the formation of a mixture of isomeric products with Bpin installed at multiple positions along the carbon chain.

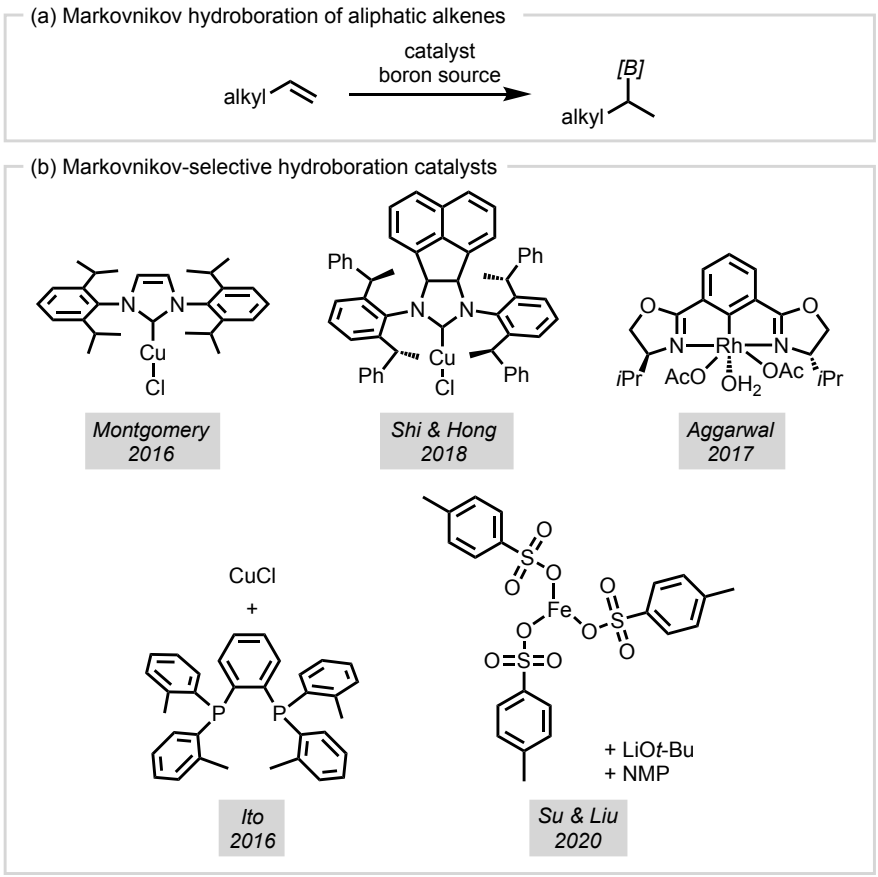

Figure 5.1. Markovnikov hydroboration of aliphatic alkenes. (a) General reaction scheme. (b) Transition metal catalyst selective for Markovnikov hydroboration of aliphatic alkenes.

Beyond relative rates of reactivity, there must be compatibility of reaction conditions and all reagents introduced. For example, hydroboration catalytic systems that use B_2pin_2 as the boron source require an H-source as well. In the Cu work from Montgomery,[64] the H-source is MeOH, while in the Fe work from Su and Liu,[68] the H-source was determined to the the solvent, NMP. If MeOH or NMP react with introduced Ni(0) complex in any way such as oxidative addition of the MeO–H bond or H-atom transfer from NMP to Ni, it's possible Ni will be deactivated and stop being able to carry out its job to move the alkene to a new position. Due to these anticipated challenges, we propose a variety of catalysts and conditions for both transformations for our initial screening based on our hypothesized catalytic cycles, shown specifically with Cu in **Figure 5.3.**

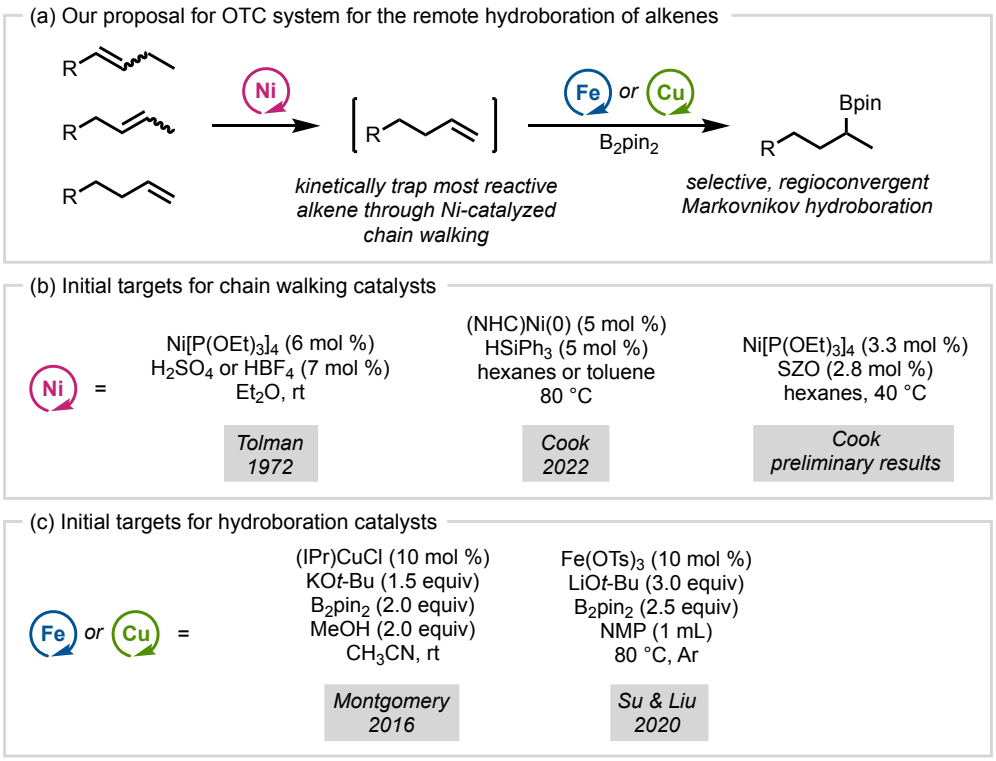

Figure 5.2. Our proposal for the remote, Markovnikov-selective hydroboration of aliphatic alkenes through an OTC approach.

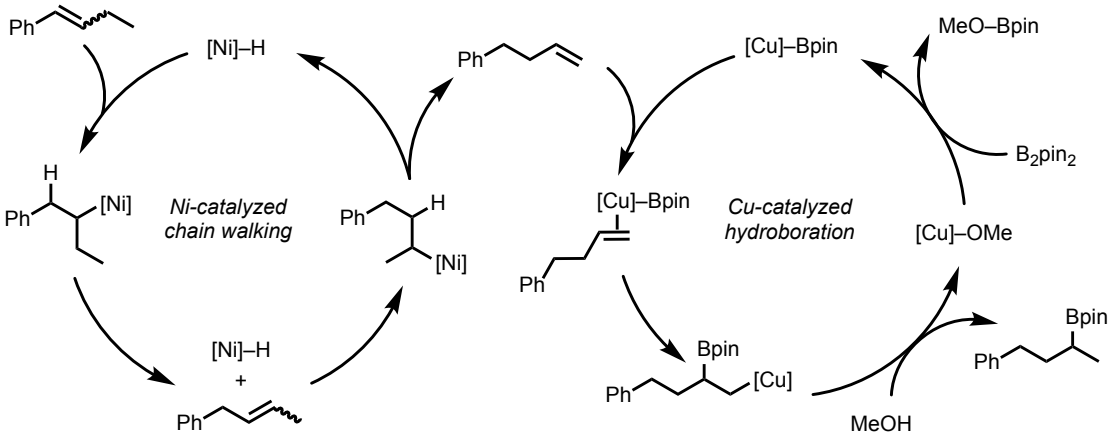

Figure 5.3. Proposed Ni/Cu OTC catalytic cycles for the remote hydroboration of alkenes.

5.2. Results and Discussion

We began our investigation screening and testing catalysts for the individual reacitons (isomerization or hydroboration). Starting with the (NHC)Ni(0)/silane catalytic system developed and studied in Chapters II-IV, we wanted to demonstrate the feasibility

of contra-thermodynamic chain walking, meaning that while the catalytic system developed is selective for the positional isomerization of terminal alkenes to internal positions, the chain walking is dynamic, allowing for Ni to "walk" to all positions along the carbon chain. Our questions included: (i) does the [Ni] complex react with internal alkenes? (ii) is the formation of terminal alkenes favorable enough that the hydroboration catalysts could kinetically trap the terminal alkene? In order to address these questions, we turned to deuterium incorporation studies.

In Chapter II, the isomerization of allylbenzene was carried out with $DSiPh_3$, showing deuterium incorporation at all three carbon positions along the alkenyl chain. To test reactivity with internal alkenes, *trans*-β-methylstyrene was introduced to standard reaction conditions with $DSiPh_3$ (**Figure 5.4.**). Using ^1H NMR spectroscopy, the only species observed is β-methylstyrene. However, using ^2H NMR spectroscopy, we observe deuterium incorporation in all three positions along the carbon chain, indicating that the Ni complex is capable of reacting with internal alkenes, and there must be some dynamic chain walking occurring in solution in order to get deuterium incorporation on the terminal carbon.

Other work in the Cook Lab has focused on the development of heterogenized Ni catlaysts for alkene isomerization, building off work from Tolman in the 1970s.[29] Tolman investigated the formation of an active Ni–H from a $Ni[P(OEt)_3]_4$ complex in acidic conditions. The Cook Lab has been focusing the development of a heterogenized catalytic system by building off of work from Marks[171–174] and Conley[175–177] that makes sulfated zirconia (SZO) surfaces. Early work suggested the surface reacted as a superacidic Brønsted acid, participating in the isomerization of *n*-butane to isobutane.[178,179] However, recent work from the Conley Group studied the reactivity of SZO with phosphines (of the type $(t\text{-Bu})_2ArP$), showing the formation of protonated $[(t\text{-Bu})_2ArPH]^+$ species.[69] Based on electronic variation of the phospine and trends in protonation, Conley concludes that the surface does not actually fall above the "superacidic" threshold. While not considered a superacid, we hypothesized that SZO could function as a solid acid H-source to react with $Ni[P(OEt)_3]_4$ to form an active catalyst for alkene isomerization (**Figure 5.5.**). Tolman's work showed that dissociation of the phosphite ligand, $P(OEt)_3$, played an important role in the catalytic cycle, and any added $P(OEt)_3$ inhibited reactivity.[29] From this, our

hypothesis about the reactivity of the SZO surface expanded to not only involve the possible formation of an active Ni–H, but also possible sequestration of the dissocated $P(OEt)_3$ in solution to further promote catalysis.

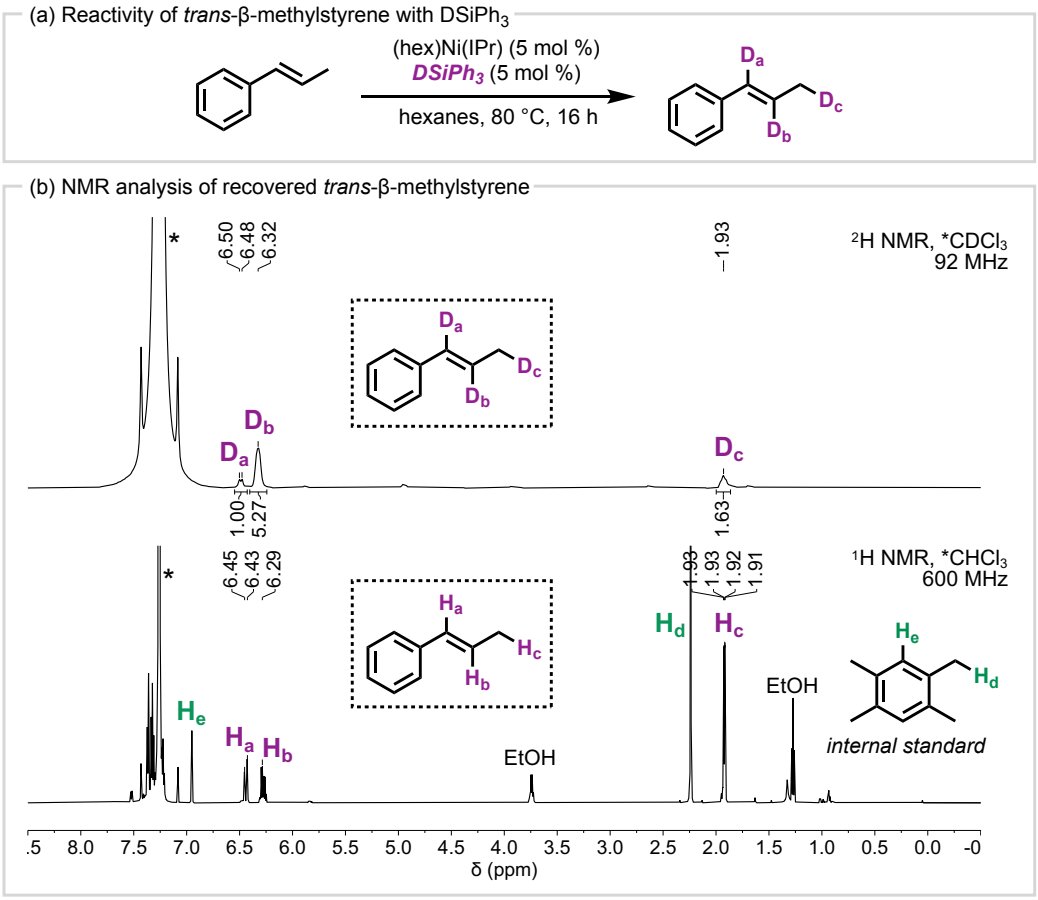

Figure 5.4. Testing the reactivity of (NHC)Ni(0)/silane catalytic system with internal alkene, *trans*-β-methylstyrene. (a) reaction scheme; (b) NMR analysis of isolated *trans*-β-methylstyrene recorded in $CHCl_3/CDCl_3$ (9:1) at 298 K.

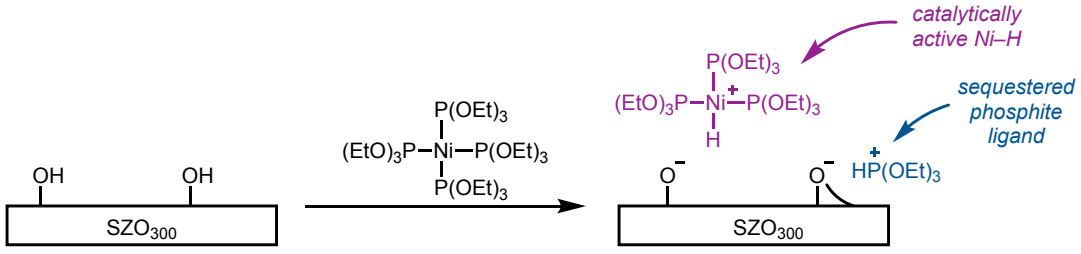

Figure 5.5. Hypothesized reactivity of $Ni[P(OEt)_3]_4$ with SZO.

From these hypotheses, we began testing combinations of possible OTC systems for the remote hydroboration of 1-phenyl-1-butene (**Table 5.1.**). However, as mentioned above, in order for the hydroboration to selectively occur from the terminal alkene, it would be ideal if the hydroboration catalyst were inactive with internal alkenes. Testing the three positional isomers of phenylbutene in the optimized conditions for (IPr)CuCl (**Scheme 5.1.**),[64] only the terminal alkene, 4-phenyl-1-butene, showed appreciable reactivity toward hydroboration (determined by uncalibrated, relative integration in GC-MS) and the product was further identified as the desired γ-functionalized product by ^{1}H NMR (see Appendix D).

With low reactivity of internal alkenes toward hydroboration in the Montgomery conditions, we began screening other conditions and catalyst combinations, starting from the internal 1-phenyl-1-butene (**Table 5.1.**). For initial screenings, we focused efforts on the (IPr)CuCl hydroboration catalytic system developed by Montgomery & co.[64] Thus far, our attempts have resulted in the formation of what we hypothesize is the α- or β-functionalized product based on analysis of the mass spectra (confirmation via ^{1}H NMR is pending), and no formation of the desired γ-functionalized product. Our next steps include testing reactivity with the $Fe(OTs)_3$/LiO*t*-Bu/NMP catalytic system developed by Su and Liu. Synthesis of the $Fe(OTs)_3$ complex is reported in Appendix D.

5.3. Conclusions

We will continue testing different reaction conditions and catalyst combinations, but we are also interested in pivoting to pursue internal aliphatic alkenes (*e.g.* 3-hexene, 4-octene), which may react more readily for chain walking to the terminal alkene without the thermodynamic penalty of breaking conjugation with the proximal phenyl ring with 1-phenyl-1-butene. The formation of what appears to be α- or β-functionalized product could also be due to either the different reaction conditions or reactivity of the introduced Ni species. Therefore, more control studies are also needed to determine which (pre)catalyst is responsible for the observed reactivity.

The work in this chapter explores the feasibility of an OTC approach to the remote hydroboration of alkenes. Preliminary results have demonstrated the reactivity of (NHC)Ni(0) complexes with internal alkenes, including the transient movement of alkenes

from an internal position to a terminal position. Future work will continue to investigate the compatibility of different catalytic systems.

Table 5.1. Catalyst combinations and reaction conditions screened for the remote hydroboration of 1-phenyl-1-butene. Trials were run in duplicate with cyclooctane as an internal standard.

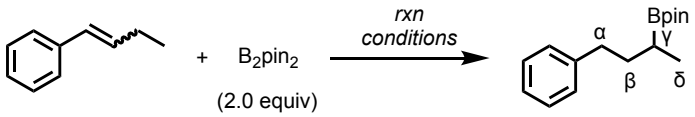

Entry	Reaction conditions
1	$(sty)_2Ni(IPr)$ (5 mol %) $HSiPh_3$ (5 mol %0 (IPr)CuCl (10 mol %) KO*t*-Bu (1.5 equiv) MeOH (2.0 equiv) acetonitrile (0.1 M) 40 °C, 24 h
2	$(sty)_2Ni(IPr)$ (5 mol %) $HSiPh_3$ (5 mol %0 (IPr)CuCl (10 mol %) KO*t*-Bu (1.5 equiv) MeOH (2.0 equiv) toluene (0.1 M) 80 °C, 24 h
3	$Ni[P(OEt)_3]_4$ (5 mol %) SZO (5 mol %) (IPr)CuCl (10 mol %) KO*t*-Bu (1.5 equiv) MeOH (2.0 equiv) acetonitrile (0.1 M) 40 °C, 24 h
4	$Ni[P(OEt)_3]_4$ (5 mol %) HBF_4 (5 mol %) (IPr)CuCl (10 mol %) KO*t*-Bu (1.5 equiv) MeOH (2.0 equiv) acetonitrile (0.1 M) 40 °C, 24 h
5	$Ni(cod)_2$ (5 mol %) $HSiPh_3$ (5 mol %) CuCl (10 mol %) IPr (15 mol %) toluene (0.1 M) 80 °C, 24 h

Scheme 5.1. Reactivity of phenylbutene isomers.

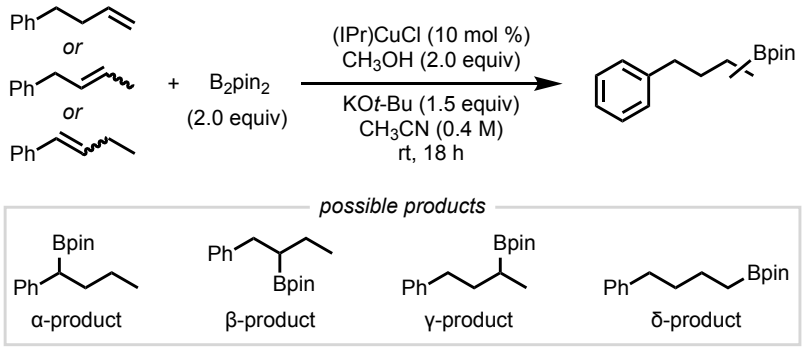

APPENDIX A

SUPPLEMENTARY CONTENT FOR CHAPTER II

Experimental details

A.1.1. Materials and Methods

All syntheses and manipulations were carried out under nitrogen using standard Schlenk (vacuum 10^{-2} mbar) techniques or in a nitrogen-filled glovebox unless otherwise indicated. All reagents and solvents were used after drying and stored under nitrogen, unless otherwise indicated. Tetrahydrofuran (THF; Fisher Chemical; HPLC grade, unstabilized), hexanes (Fisher Chemical; HPLC grade), diethyl ether (Et_2O; B&J Brand; HPLC grade, unstabilized), dichloromethane (DCM; Oakwood Chemical; HPLC grade, unstabilized), dimethylformamide (DMF; Alfa Aesar; HPLC grade, unstabilized) and acetonitrile (MeCN; Fisher Chemical; HPLC grade) were dispensed under nitrogen from an LC Technology SP-1 solvent system. Benzene (ACS grade) and pentane (HPLC grade) were refluxed overnight with CaH_2 and distilled under nitrogen before use. The dried solvents were thereafter stored on activated 4Å molecular sieves under nitrogen. C_6D_6 and $CDCl_3$ were purchased from Cambridge Isotope Laboratories, degassed by freeze-pump-thaw, and thereafter stored on activated 4Å molecular sieves under nitrogen. All stock solutions were prepared by mass and were dispensed into reaction vessel by difference from syringe, as detailed in the procedure for each experiment.

A.1.2. General Experimental

Nuclear magnetic resonance (NMR) spectra were collected at room temperature (298 K) unless otherwise stated on a Bruker AV-III HD 600 NMR (600.13 MHz for ^{1}H; 150.90 MHz for ^{13}C; 564.69 MHz for ^{19}F; 119.23 MHz for ^{29}Si; 232.94 MHz for ^{31}P; 92.12 MHz for ^{2}H), Bruker Avance-III HD 500 NMR (499.90 MHz for ^{1}H; 126 MHz for ^{13}C; 471 MHz for ^{19}F; 99 MHz for ^{29}Si; 202.46 MHz for ^{31}P), or Varian Inova 500 NMR (499.90 MHz for ^{1}H; 126 MHz for ^{13}C; 471 MHz for ^{19}F; 99 MHz for ^{29}Si; 202.46 MHz for ^{31}P). ^{1}H and ^{13}C spectra were referenced to the residual solvent peak ($CDCl_3$: ^{1}H δ = 7.26 ppm, ^{13}C δ = 77.16 ppm; C_6D_6: ^{1}H δ = 7.16 ppm, ^{13}C δ = 128.06 ppm). Chemical shifts are

reported in parts per million (ppm, δ) relative to tetramethylsilane at 0.00 ppm. Peaks are characterized as follows: s (singlet), d (doublet), t (triplet), q (quartet), pent (pentet), hept (heptet), m (multiplet), br (broad), app (apparent), and/or ms (multiple signals). Coupling constants, *J*, are reported in Hz. Electron paramagnetic resonance (EPR) spectra were collected at 77 K on a Bruker Elexsys E500 EPR X-band spectrometer. Infrared spectroscopy was performed on an Agilent Nicolet 6700 FT-IR, and peaks are reported in cm^{-1}. For catalytic reactions, yields were determined using Gas Chromatography-Mass Spectrometry (GCMS) or Gas Chromatography (GC) against an internal standard. GCMS was carried out on a Shimadzu GC-2010 Plus/GCMS-QP2010 SE using a Restek Rtx®-5 (Crossbond 5% diphenyl – 95% dimethyl polysiloxane; 15 m, 0.25 mm ID, 0.25 μm df) column. GC was carried out on a Thermo Fisher Trace 1300 Gas Chromatograph using a Restek Rtx®-5 (Crossbond 5% diphenyl – 95% dimethyl polysiloxane; 15 m, 0.25 mm ID, 0.25 μm df) column. High-resolution mass spectrometry (HRMS) was carried out on a Waters XEVO G2-XS TOF mass spectrometer.

A.1.3. Synthesis of Non-Commercial Reagents

a. Ligand and Catalyst Synthesis

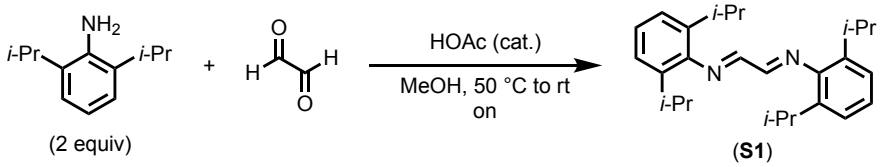

(1*E*,2*E*)-1,2-Bis(2,6-Diisopropylphenylimino)ethane (S1) was synthesized via literature procedure:[180] Under ambient conditions, to a 1000 mL round-bottom flask (RBF) equipped with a magnetic stir bar was added 2,6-diisopropylaniline (19 mL, 0.10 mol, 2.0 equiv), methanol (200 mL), glyoxal (40 wt% aqueous solution, 5.9 mL, 0.050 mol, 1.0 equiv), and glacial acetic acid (0.5 mL). Reaction was stirred and heated to 50 °C for 30 min before the heating was turned off and reaction was left to stir 18 h, slowly cooling to room temperature. After stirring overnight, the solution was placed in the freezer for 2 h before filtering through a glass frit to collect **S1** as a fluffy yellow powder (13 g, 0.034 mol, 69% yield). NMR spectra match values previously reported.[181]

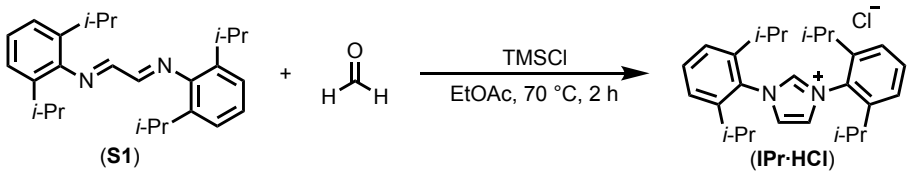

(**S1**) (**IPr·HCl**)

1,3-Bis(2,6-diisopropylphenyl)imidazolium chloride (IPr·HCl) was synthesized via literature procedure:[180] Under ambient conditions, to a 500 mL RBF was added **S1** (12 g, 33 mmol, 1.0 equiv), paraformaldehyde powder (1.0 g, 33 mmol, 1.0 equiv), and ethyl acetate (200 mL). The reaction was heated to 70 °C. To a 25 mL Erlenmeyer flask was added EtOAc (10 mL) and TMSCl (4.1 mL, 33 mmol, 1.0 equiv). To the hot mixture of **S1** and paraformaldehyde was added the TMSCl solution dropwise via glass pipette. After stirring for 2 h at 70 °C, the reaction was removed from heat and placed in the freezer for 2 h before filtering through a glass frit to collect **IPr·HCl** as a pale pink solid (11 g, 26 mmol, 78% yield). NMR spectra match values previously reported.[181]

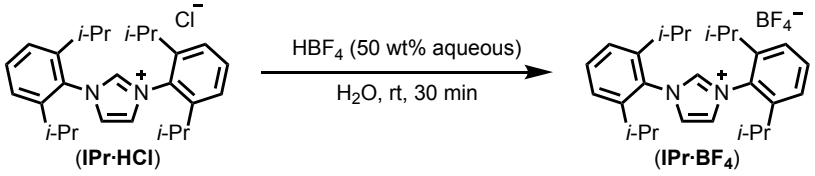

(**IPr·HCl**) (**IPr·BF$_4$**)

1,3-Bis(2,6-diisopropylphenyl)-1*H*-imidazol-3-ium tetrafluoroborate (IPr·HBF$_4$) was synthesized via literature procedure:[182] Under ambient conditions, to a 1000 mL RBF was added **IPr·HCl** (10 g, 24 mmol, 1.0 equiv). Minimal deionized water (500 mL) was added and the reaction was stirred until **IPr·HCl** was dissolved. HBF_4 (50 wt% aqueous solution, 3.6 mL, 29 mmol, 1.1 equiv) was added dropwise and a white precipitate formed. After stirring for 30 min, product was extracted with dichloromethane. The combined organic layers were dried over $MgSO_4$ and filtered, and the filtrate was concentrated under reduced pressure to yield **IPr·HBF$_4$** as an off-white solid (8.6 g, 18 mmol, 72% yield). NMR spectra match values previously reported.[183]

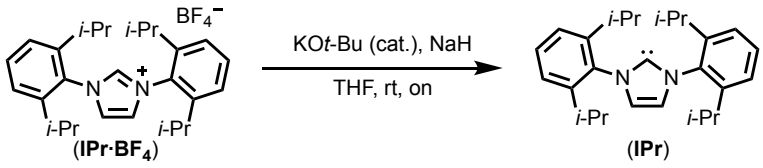

(**IPr·BF$_4$**) (**IPr**)

1,3-Bis(2,6-diisopropylphenyl)-1,3-dihydro-2*H*-imidazol-2-ylidene (IPr) was synthesized via literature procedure:[182] **IPr·HBF$_4$** (1.0 g, 2.1 mmol, 1.0 equiv) was dissolved in THF (8.5 mL) in a flask equipped with a magnetic stir bar. NaH (0.10 g, 4.2 mmol, 2.0 equiv) and a spatula tip of KO*t*-Bu were added to the reaction, which was then stirred overnight at room temperature. The reaction was filtered through a glass frit, and the solid was washed with THF (3 mL). The filtrate and washes were combined and concentrated under reduced pressure to give an off-white solid, which was then washed with hexanes and dried under vacuum to yield **IPr** as a cream-colored solid (0.61 g, 1.6 mmol, 74% yield). NMR spectra match values previously reported.[181]

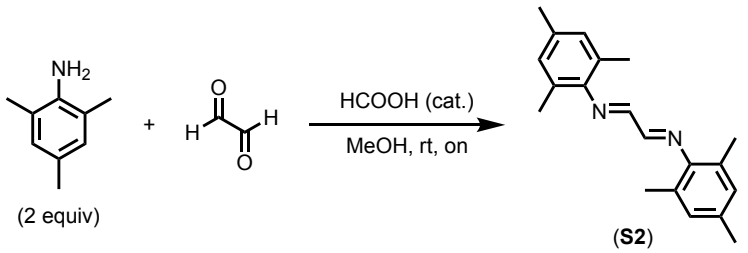

***N*,*N*'-Bis(2,4,6-trimethylphenyl)ethane-1,2-diimine (S2)** was synthesized via literature procedure:[182] Under ambient conditions, 2,4,6-trimethylaniline (16.0 mL, 114 mmol, 2.00 equiv) was dissolved in MeOH (60 mL) in a RBF equipped with a magnetic stir bar. Glyoxal (40 wt% aqueous solution, 6.50 mL, 57.0 mmol, 1.00 equiv) was added and the reaction turned yellow. A few drops of formic acid were added, and a precipitate began forming. The reaction was stirred overnight at room temperature. The reaction was then chilled in the freezer for an hour before it was filtered through a glass frit to yield **S2** as a fluffy yellow powder (12.5 g, 42.7 mmol, 75% yield). No further purification was required. NMR spectra match values previously reported.[182]

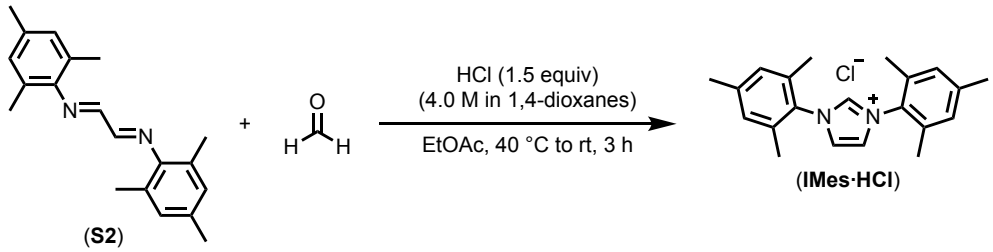

1,3-Bis(2,4,6-trimethylphenyl)imidazolium chloride (IMes·HCl) was synthesized via literature procedure:[182] Under ambient conditions, to a RBF equipped with a magnetic stir bar was added paraformaldehyde (1.35 g, 45.0 mmol, 1.10 equiv) and HCl (4.0 M in 1,4-dioxanes, 15.4 mL, 61.6 mmol, 1.50 equiv). The reaction was then heated at 40 °C for 1 h. In a separate RBF equipped with a magnetic stir bar, **S2** (12.0 g, 41.0 mmol, 1.00 equiv) was dissolved in EtOAc (85 mL). The reaction was heated to 40 °C and the paraformaldehyde/HCl solution was added dropwise to the **S2** solution. The reaction changed color from yellow to brown with the formation of a white precipitate. The reaction was cooled to room temperature and the precipitate was collected by filtration through a glass frit. The solid was then washed with EtOAc (300 mL), yielding the crude product as an off-white solid. This crude product was dissolved in saturated $NaHCO_3$ aqueous solution (30 mL) and this solution was washed with EtOAc (3 x 50 mL). The layers were separated, and the aqueous layer was extracted with DCM (3 x 50 mL). The combined organic layers were dried over $MgSO_4$, filtered, and concentrated under reduced pressure. The product was further purified by crystallization in the freezer after dissolving in minimal DCM and layering with EtOAc. **IMes·HCl** was collected as a white solid (4.20 g, 12.3 mmol, 30% yield) via filtration. NMR spectra match values previously reported.[182]

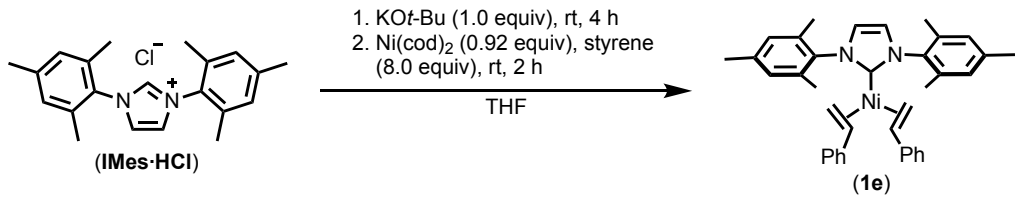

(**IMes·HCl**) (**1e**)

(styrene)$_2$Ni(IMes) (1e) was synthesized via literature procedure:[136] To a vial equipped with a magnetic stir bar was added **IMes·HCl** (0.676 g, 1.98 mmol, 1.00 equiv), KO*t*-Bu (0.223 g, 1.99 mmol, 1.01 equiv) and THF (17 mL). The reaction was stirred at room temperature for 4 h and then filtered through a pad of Celite. A separate solution of $Ni(cod)_2$ (0.500 g, 1.82 mmol, 0.92 equiv) and styrene (1.82 mL, 15.8 mmol, 8.00 equiv) in THF (17 mL) was prepared and stirred for 15 min before the filtrate from the **IMes·HCl** reaction was added dropwise, resulting in an orange solution. The reaction was stirred for 2 h before being concentrated under reduced pressure to yield the crude product. The crude mixture was taken up in minimal THF (~2 mL) and filtered through Celite. Pure product

was collected after recrystallization at -30 °C by dissolving in THF and adding hexanes. The product was collected via vacuum filtration to yield **1e** as an orange powder (0.893 g, 1.56 mmol, 86% yield). NMR spectra match values previously reported.[136]

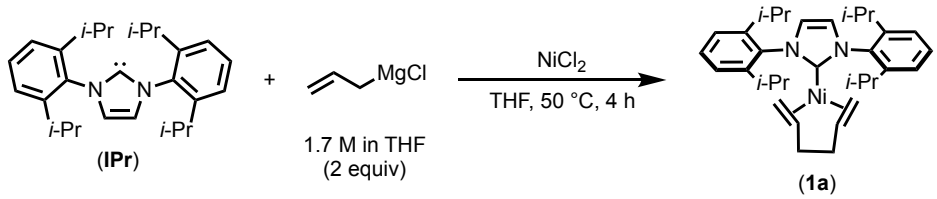

(1,5-hexadiene)Ni(IPr) (1a) was synthesized via literature procedure:[137] To a Schlenk flask equipped with a magnetic stir bar was added $NiCl_2$ (0.653 g, 5.04 mmol, 1.00 equiv), **IPr** (1.97 g, 5.07 mmol, 1.01 equiv) and THF (70 mL) in an N_2-filled glovebox. Allylmagnesium chloride solution (1.7 M in THF, 5.9 mL, 10.1 mmol, 2.0 equiv) was added slowly. The reaction was sealed and removed from the glovebox to be heated at 50 °C on the Schlenk line. After 4 h, the reaction was concentrated under reduced pressure to give an orange/brown solid. In the glovebox, the product was extracted into hexanes (300 mL), and the residual solids were removed by filtration through a glass frit. The filtrate was concentrated under reduced pressure to yield **1a** as an orange powder (2.30 g, 4.34 mmol, 86% yield). NMR spectra match values previously reported.[184]

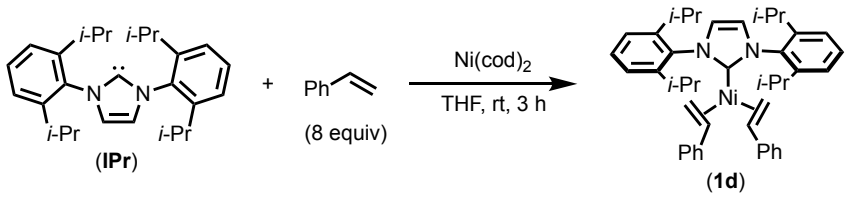

(styrene)$_2$Ni(IPr) (1d) was synthesized via literature procedure:[185] To a vial equipped with a magnetic stir bar was added $Ni(cod)_2$ (0.286 g, 1.04 mmol, 1.05 equiv), styrene (1.00 mL, 8.70 mmol, 8.82 equiv) and THF (9 mL). After stirring for 15 min, a solution of **IPr** (0.383 g, 0.986 mmol, 1.00 equiv) in THF (8.0 mL) was added. After 3 h, the reaction was concentrated under reduced pressure to yield the crude product, which was purified via crystallization out of THF layered beneath hexanes at -30 °C. The precipitate was collected via filtration through a glass frit and dried under reduced pressure

to yield pure **1d** as a yellow-orange powder (0.351 g, 0.535 mmol, 54% yield). NMR spectra match values previously reported.[185]

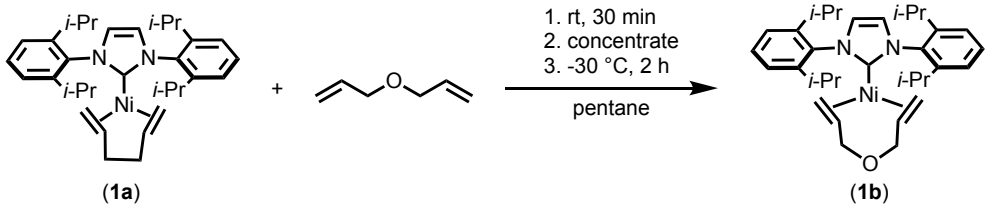

(diallylether)Ni(IPr) (1b) was synthesized via literature procedure:[137] To a vial equipped with a magnetic stir bar was added **1a** (0.101 g, 0.191 mmol, 1.00 equiv), diallylether (25.0 μL, 0.205 mmol, 1.07 equiv) and pentane (6.5 mL). The reaction was stirred at room temperature for 30 min and then concentrated to 2 mL and placed in the freezer to enable crystallization. Purified **1b** was collected as pale-yellow solid after filtration through a glass frit (0.0310 g, 0.0568 mmol, 30% yield). NMR spectra match values previously reported.[137]

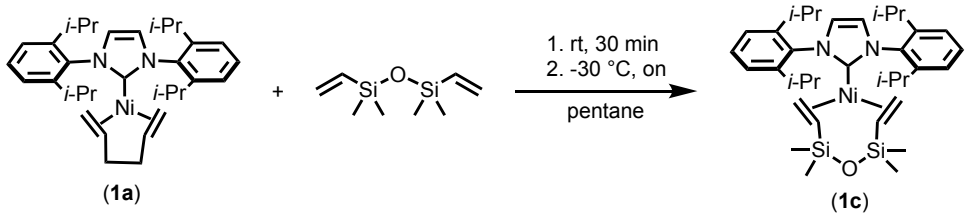

(1,3-divinyltetramethyldisiloxane)Ni(IPr) (1c) was synthesized via literature procedure:[137] To a vial equipped with a magnetic stir bar was added **1a** (0.100 g, 0.189 mmol, 1.00 equiv), 1,3-divinyltetratmethyldisiloxane (44.0 μL, 0.191 mmol, 1.01 equiv), and pentane (1.00 mL). The reaction was stirred at room temperature for 30 min before being placed in the freezer (-25 °C) overnight. Filtration through a glass frit yielded **1c** as a pale brown solid (0.0450 g, 0.0710 mmol, 38% yield). NMR spectra match values previously reported.[137]

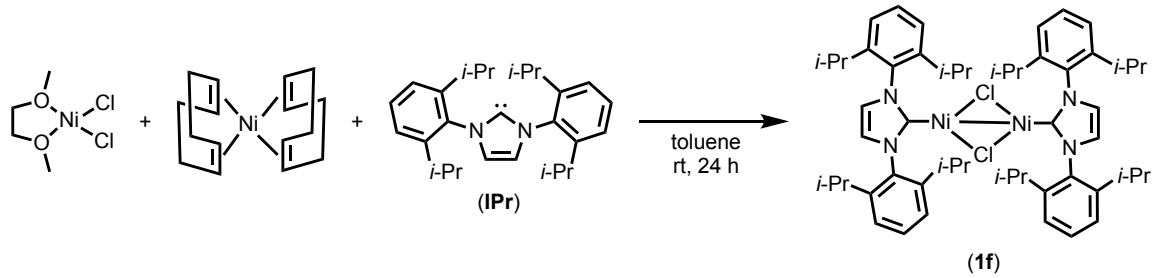

(**IPr**) (**1f**)

[(IPr)Ni(μ-Cl)]$_2$ (1f) was synthesized via literature procedure:[186] In a nitrogen-filled glovebox, Ni(II) chloride ethylene glycol dimethyl ether complex (0.062 g, 0.28 mmol, 1.0 equiv), Ni(cod)$_2$ (0.079 g, 0.29 mmol, 1.0 equiv) and IPr (0.22 g, 0.56 mmol, 2.0 equiv) were added to a 4-dram vial equipped with a magnetic stir bar. Toluene (8.0 mL) was added to the vial and the reaction was stirred at room temperature for 24 h. The reaction was filtered through Celite into a 4-dram vial, concentrated to a third of the volume, and 5 mL hexanes was added. The vial was sealed and placed in the freezer at -30 °C for 12 h. The solution was decanted and the solid was washed with 1 mL cold hexanes to obtain **1f** as bright green crystals (0.14 g, 0.15 mmol, 52% yield). NMR spectra match values previously reported.[186]

b. Allylbenzene Derivatives

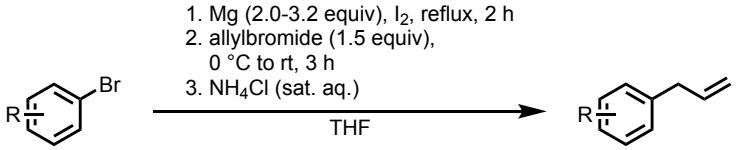

(**2**)

Allylbenzene derivatives were synthesized via modified literature procedure:[187,188] an oven-dried Schlenk flask was charged with Mg (2.0-3.2 equiv) and I$_2$ (cat.) in THF. A portion of aryl bromide (0.33 equiv) was added at room temperature and the reaction was stirred until the yellow color from I$_2$ disappeared. The remaining aryl bromide (0.67 equiv) was added, and the reaction was equipped with a reflux condenser and heated to reflux. Following consumption of the aryl bromide (monitored by TLC), the reaction was cooled to room temperature. The solution was transferred via cannula to a new oven-dried Schlenk flask and cooled to 0 °C with an ice/water bath. Allyl bromide (1.5 equiv) was added dropwise, and the reaction was allowed to slowly warm to room temperature. After stirring 3-18 h at room temperature, the flask was opened to air and quenched with NH$_4$Cl

(saturated aqueous solution). The organic layer was separated, and the aqueous layer extracted three times with Et_2O. The combined organic layers were dried over Na_2SO_4 and filtered, and the filtrate was concentrated under reduced pressure to yield the corresponding crude product. Purification details are included below.

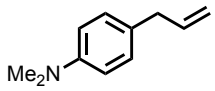

3-[(4-*N*,*N*-Dimethylamino)phenyl]-1-propene (2c)

Synthesis details: 4-bromo-*N,N*-dimethylaniline (2.01 g, 10.0 mmol, 1.0 equiv), magnesium (0.67 g, 28 mmol, 2.8 equiv), iodine (a grain), THF (25 mL), allylbromide (1.30 mL, 15.0 mmol, 1.5 equiv), quenched with NH_4Cl (30 mL), extracted with Et_2O (3 x 50 mL). Clear, yellow oil (0.79 g, 4.9 mmol, 49% yield).

Purification details: A yellow oil was collected after concentration under reduced pressure. The crude oil was purified via column chromatography (silica, gradient eluent 0-5% Et_2O/hexanes) to yield the product as a clear pale-yellow oil.

NMR spectra match values previously reported.[189]

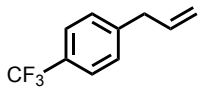

1-Allyl-4-(trifluoromethyl)benzene (2d)

Synthesis details: 4-bromobenzotrifluoride (4.0 mL, 28.6 mmol, 1.0 equiv), magnesium (1.39 g, 57.2 mmol, 2.0 equiv), iodine (a grain), THF (50 mL), allylbromide (3.72 mL, 43.0 mmol, 1.5 equiv), quenched with NH_4Cl (30 mL), extracted with Et_2O (3 x 100 mL). Clear, colorless oil (2.35 g, 12.6 mmol, 44% yield).

Purification details: An orange oil was collected after concentration under reduced pressure. The crude oil was run through a silica plug (90% hexanes, 10% Et_2O) and concentrated to yield a yellow oil. The purified product was obtained via distillation at 50 °C into a collection flask cooled with liquid N_2.

NMR spectra match values previously reported.[190]

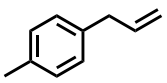

3-(4-Methylphenyl)-1-propene (2e)

Synthesis details: 4-bromotoluene (6.04 g, 35.3 mmol, 1.00 equiv), magnesium (1.81 g, 74.5 mmol, 2.1 equiv), iodine (a grain), THF (70 mL), allylbromide (4.6 mL, 53 mmol, 1.5 equiv), quenched with NH_4Cl (100 mL), extracted with Et_2O (3 x 100 mL). Clear, colorless oil (1.91 g, 14.4 mmol, 41% yield).

Purification details: A yellow oil was collected after concentration under reduced pressure. Purified product was obtained via distillation at 50 °C into a collection flask cooled with liquid N_2.

NMR spectra match values previously reported.[191]

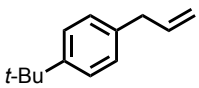

3-(4-*tert*-Butylphenyl)-1-propene (2f)

Synthesis details: 4-*t*-Bu-bromobenzene (4.98 g, 23.4 mmol, 1.00 equiv), magnesium (1.2 g, 49 mmol, 2.1 equiv), iodine (a grain), THF (40 mL), allylbromide (4.25 g, 35.0 mmol, 1.5 equiv), quenched with NH_4Cl (65 mL), extracted with Et_2O (3 x 65 mL). Clear, colorless oil (2.09 g, 12.0 mmol, 51% yield).

Purification details: Column chromatography: silica, hexanes.

NMR spectra match values previously reported.[192]

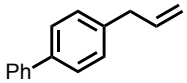

4-(2-Propen-1-yl)-1,1'-biphenyl (2g)

Synthesis details: 4-bromobiphenyl (5.05 g, 21.7 mmol, 1.00 equiv), magnesium (1.16 g, 47.7 mmol, 2.20 equiv), iodine (a grain), THF (36 mL), allylbromide (4.04 g, 33.3 mmol, 1.6 equiv), quenched with NH_4Cl (50 mL), extracted with Et_2O (3 x 50 mL). Clear colorless oil (0.759 g, 3.90 mmol, 18% yield).

Purification details: Column chromatography: silica, pentane.

NMR spectra match values previously reported.[193]

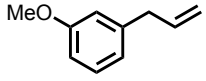

3-(3-Methoxyphenyl)-1-propene (2h)

Synthesis details: 3-bromoanisole (2.0 mL, 15.8 mmol, 1.00 equiv), magnesium (0.846 g, 34.8 mmol, 2.20 equiv), iodine (a grain), THF (30 mL), allylbromide (2.1 mL, 24.3 mmol, 1.54 equiv), quenched with NH_4Cl (30 mL), extracted with Et_2O (3 x 30 mL). Clear, colorless oil (0.692 g, 4.87 mmol, 31% yield).

Purification details: Column chromatography: silica, gradient eluent 3-5% Et_2O/hexanes.

NMR spectra match values previously reported.[194]

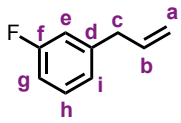

3-(3-Fluorophenyl)-1-propene (2i)

Synthesis details: 1-bromo-3-fluorobenzene (3.0 mL, 26.9 mmol, 1.00 equiv), magnesium (1.34 g, 55.1 mmol, 2.05 equiv), iodine (a grain), THF (60 mL), allylbromide (3.6 mL, 42 mmol, 1.5 equiv), quenched with NH_4Cl (50 mL), extracted with Et_2O (3 x 60 mL). Clear, colorless soil (1.05 g, 7.7 mmol, 29% yield).

Purification details: Column chromatography: silica, hexanes.

NMR spectra match values previously reported.[195]

^1H NMR (500 MHz, $CDCl_3$, 298 K): δ 7.25 (m, 1H, H_h), 6.96 (d, J = 7.6 Hz, H_i), 6.91-6.85 (ms, 2H, $H_{e,g}$), 5.94 (ddt, J = 17.6, 9.4, 6.8 Hz, H_b), 5.14-5.06 (ms, 2H, H_a), 3.38 (d, J = 6.8 Hz, H_c)

$^{13}C\{^1H\}$ NMR (126 MHz, $CDCl_3$, 298 K): δ 163.1 (d, J = 245.2 Hz, C_f), 142.7 (d, J = 7.2 Hz, C_d), 136.7 (C_b), 129.9 (d, J = 8.4 Hz, C_h), 124.3 (d, J = 2.9 Hz, C_i), 116.6 (C_a), 115.6 (d, J = 20.9 Hz, $C_{e\ or\ g}$), 113.1 (d, J = 21.1 Hz, $C_{e\ or\ g}$), 40.0 (C_c)

^{19}F NMR (471 MHz, $CDCl_3$, 298 K): δ -113.72 (m)

ASAP/HRMS (m/z): M^+ calculated for C_9H_9F 136.0688, found 136.0728

IR (ATR, neat) ν: 1590 (m), 1490 (m), 1150 (s), 994 (s), 752 (s) cm^{-1}

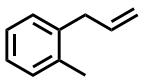

1-Allyl-2-methylbenzene (2l)

Synthesis details: 2-bromotoluene (2.0 mL, 16.6 mmol, 1.0 equiv), magnesium (1.28 g, 52.7 mmol, 3.2 equiv), iodine (a grain), THF (30 mL), allylbromide (2.2 mL, 25 mmol, 1.5 equiv), quenched with NH_4Cl (100 mL), extracted with Et_2O (3 x 60 mL). Clear, yellow oil (1.36 g, 10.3 mmol, 62% yield).

Purification details: A cloudy yellow oil was collected after concentration under reduced pressure. Clean product was obtained after filtration through a silica plug eluting with Et_2O.

NMR spectra match values previously reported.[193]

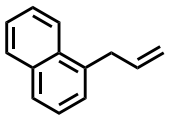

1-Allylnapthalene (2n)

Synthesis details: 1-bromonapthalene (4.0 mL, 29 mmol, 1.0 equiv), magnesium (1.74 g, 71.6 mmol, 2.50 equiv), iodine (a grain), THF (100 mL), allylbromide (3.7 mL, 42.8 mmol, 1.5 equiv), quenched with NH_4Cl (60 mL), extracted with Et_2O (3 x 100 mL). Clear, pale yellow oil (1.49 g, 8.9 mmol, 31% yield).

Purification details: Column chromatography: silica, pentane.

NMR spectra match values previously reported.[193]

c. Other Substrate Syntheses

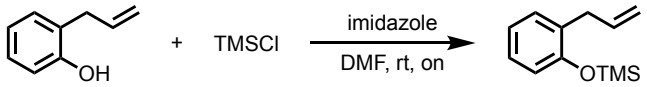

(**S3**) (**2j**)

(2-Allylphenoxy)trimethylsilane (2j) was synthesized via literature procedure:[196] To an oven-dried Schlenk flask equipped with a magnetic stir bar was added 2-allylphenol (0.650 mL, 4.98 mmol, 1.00 equiv), DMF (15 mL) and imidazole (1.09 g, 16.0 mmol, 3.21 equiv). After stirring for 15 min, trimethylsilylchloride (1.30 mL, 10.2 mmol, 2.06 equiv) was added. After stirring 18 h, reaction was quenched with water (10 mL) and extracted with DCM (3 x 20 mL). The combined organic layers were dried over Na_2SO_4, filtered, and the filtrate was concentrated under reduced pressure. Pure product was obtained by

column chromatography (silica, 3% Et_2O/hexanes) to give the product as a colorless oil (0.740 g, 3.59 mmol, 72% yield). NMR spectra match values previously reported.[196]

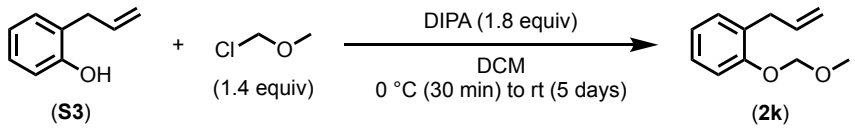

1-(Methoxymethoxy)-2-(2-propen-1-yl)benzene (2k) was synthesized via literature procedure:[197] To an oven-dried Schlenk flask equipped with a magnetic stir bar was added 2-allylphenol (1.00 mL, 7.68 mmol, 1.0 equiv) and DCM (15 mL). The flask was cooled in an ice/water bath for 5 minutes before adding diisopropylamine (DIPA; 1.95 mL, 13.9 mmol, 1.8 equiv). The reaction was stirred for 5 minutes before adding chloromethyl methyl ether (0.82 mL, 10.8 mmol, 1.4 equiv) dropwise. The reaction was stirred at 0 °C for 30 minutes before the ice/water bath was removed and the reaction was warmed to room temperature. After 5 days of stirring at room temperature, the reaction was transferred to a RBF and concentrated under reduced pressure. Et_2O (25 mL) was added to the crude product and the solution was transferred to a separatory funnel. The organic layer was washed with H_2O (2 x 25 mL), NaOH (10 wt%, 2 x 25 mL) and brine (2 x 25 mL). The organic layer was dried with Na_2SO_4, filtered, and concentrated under reduced pressure to an orange oil. Product was purified by column chromatography (silica, hexanes). A Celite plug (acetonitrile) was run to remove grease, yielding the product as a clear oil (0.121 g, 0.679 mmol, 8.8% yield). NMR spectra match values previously reported.[197]

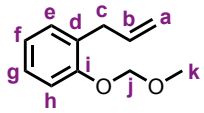

^{1}H NMR (500 MHz, $CDCl_3$, 298 K): δ 7.19-7.13 (ms, 2H, $H_{e,g}$), 7.07 (d, J = 8.0 Hz, 1H, H_h), 6.95 (t, J = 7.4 Hz, 1H, H_f), 6.00 (ddt, J = 16.9, 10.2, 6.5 Hz, 1H, H_b), 5.20 (s, 2H, H_j), 5.08-5.01 (ms, 2H, H_a), 3.48 (s, 3H, H_k), 3.42 (d, J = 6.5 Hz, 2H, H_c)

^{13}C{^{1}H} NMR (126 MHz, $CDCl_3$, 298 K): δ 155.1 (C_i or C_d), 137.1 (C_b), 130.2 (C_e or C_g), 129.4 (C_i or C_d), 127.5 (C_e or C_g), 121.9 (C_f), 115.5 (C_a), 114.2 (C_h), 94.6 (C_j), 56.2 (C_k), 34.5 (C_c)

ASAP/HRMS (m/z): $[M+H]^+$ calculated for $C_{11}H_{15}O_2$ 179.1067, found 179.1069

IR (ATR, neat) ν: 1490 (m), 1232 (m), 1151 (s), 1076 (m), 994 (s), 751 (s) cm^{-1}

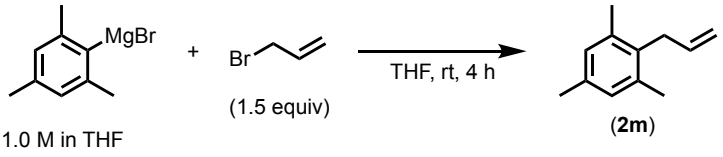

1,3,5-Trimethyl-2-prop-2-enylbenzene (2m) was synthesized via modified literature procedure:[188] To an oven-dried Schlenk flask equipped with a magnetic stir bar was added THF (9 mL) and allylbromide (1.30 mL, 15.0 mmol, 1.50 equiv). Mesityl magnesium bromide solution (1.0 M in THF, 10.0 mL, 10.0 mmol, 1.00 equiv) was added dropwise to the stirring solution. After stirring for 4 h at room temperature, the reaction was quenched with NH_4Cl (20 mL) and extracted with Et_2O (3 x 30 mL). The combined organic layers were dried over Na_2SO_4, filtered, and the filtrate was concentrated under reduced pressure. The crude product was filtered through a silica plug, eluting with hexanes. Mesitylene (the major byproduct) was removed by distillation under reduced pressure (>0.1 torr, Schlenk line) while heating to 60 °C. The pure product was obtained as a clear, colorless oil (0.31 g, 1.9 mmol, 19% yield). NMR spectra match values previously reported.[193]

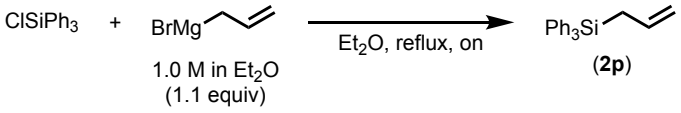

Allyltriphenylsilane (2p) was synthesized via modified literature procedure:[198] To an oven-dried Schlenk flask equipped with a magnetic stir bar was added triphenylchlorosilane (2.01 g, 6.82 mmol, 1.00 equiv) and Et_2O (18 mL). To the stirring solution, allylmagnesium bromide (1.00 M in Et_2O, 7.50 mL, 7.50 mmol, 1.10 equiv) was added dropwise. The reaction was equipped with a reflux condenser and heated to 50 °C in a pre-heated oil bath for 18 h. The reaction was quenched with NH_4Cl (20 mL) and extracted with Et_2O (3 x 60 mL). The combined organic layers were dried over Na_2SO_4, filtered, and concentrated under reduced pressure to give a white solid. This solid was filtered through a silica plug (5% Et_2O/pentane) and the filtrate was concentrated under reduced pressure. The collected solid was dissolved in a minimal amount of ethanol and the product crystallized in the freezer overnight. White crystals formed and were collected

and washed with cold ethanol. The product was dissolved in acetonitrile and filtered through Celite to remove grease. After concentrating under reduced pressure, pure product was obtained as a white solid (0.602 g, 2.00 mmol, 29% yield). NMR spectra match values previously reported.[199]

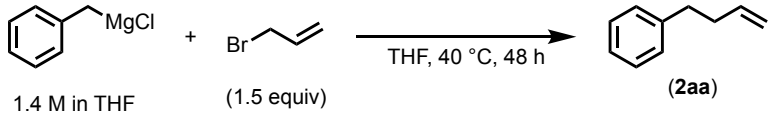

4-Phenyl-1-butene (2aa): To an oven-dried Schlenk flask equipped with a magnetic stir bar was added THF (25 mL) and allylbromide (2.10 mL, 24.3 mmol, 1.08 equiv). To the stirring reaction, benzylmagnesium chloride (1.4 M in THF, 16.0 mL, 22.4 mmol, 1.00 equiv) was added dropwise. Upon full addition of benzylmagnesium chloride, the reaction was heated to 40 °C and allowed to react for 48 h. The reaction was quenched with NH_4Cl (20 mL) and extracted with Et_2O (3 x 50 mL). The combined organic layers were dried over Na_2SO_4, filtered, and the filtrate was concentrated under reduced pressure. Clean product was obtained via distillation at 50 °C into a collection flask cooled with liquid N_2. Clear, colorless liquid (0.871 g, 6.59 mmol, 29% yield). NMR spectra match values previously reported.[30]

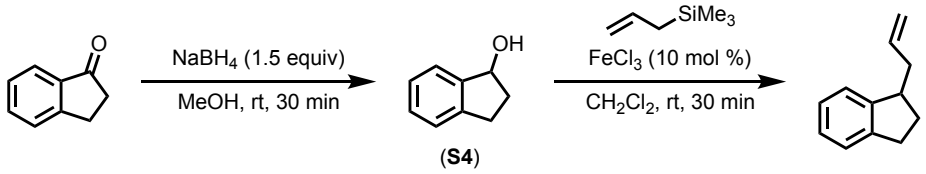

2,3-Dihydro-1-(2-propen-1-yl)-1*H*-indene (2ac) was synthesized via literature procedure:[96] To an oven-dried Schlenk flask equipped with a magnetic stir bar was added 1-indanone (1.00 g, 7.57 mmol, 1.00 equiv) and MeOH (15 mL). The mixture was stirred until indanone was completely dissolved. The reaction was then cooled slightly with a water bath, $NaBH_4$ was added in one portion (0.430 g, 11.4 mmol, 1.50 equiv), and the reaction was stirred for 30 min. The reaction was then opened to air and extracted with Et_2O (3 x 80 mL). The combined organic layers were washed with brine (3 x 30 mL) and dried over Na_2SO_4, filtered, and the filtrate was concentrated under reduced pressure. 1-indanol (**S4**) was collected as a viscous yellow oil (0.945 g, 7.04 mmol, 93% yield) and

carried forward without further purification. NMR spectra match values previously reported.[200]

To an oven-dried Schlenk flask equipped with a magnetic stir bar was added **S4** (0.390 g, 2.91 mmol, 1.0 equiv) and DCM (25 mL). Allyltrimethylsilane (0.88 mL, 5.54 mmol, 1.90 equiv) and $FeCl_3$ (0.061 g, 0.38 mmol, 0.13 equiv) were added, and the reaction was stirred for 90 min before being opened to air and quenched with water (10 mL). The organic layer was separated, and the aqueous layer was extracted with Et_2O (3 x 30 mL). The combined organic layers were dried over $MgSO_4$, filtered, and the filtrate was concentrated under reduced pressure to a red oil. Crude product was filtered through a silica plug with pentane to yield the product as a clear oil (0.428 g, 2.70 mmol, 93% yield). NMR match values previously reported.[201]

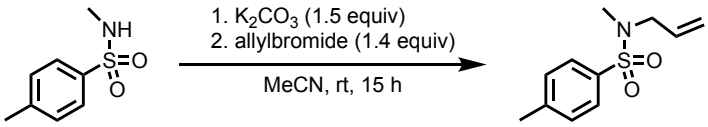

(**S5**)

***N*,4-dimethyl-*N*-2-propen-1-ylbenzenesulfondamide (S5)** was synthesized via literature procedure:[30] To an oven-dried Schlenk flask equipped with a magnetic stir bar was added *N*-methyl-*para*-toluenesulfonamide (0.51 g, 2.8 mmol, 1.0 equiv), acetonitrile (40 mL), and K_2CO_3 (0.57 g, 4.1 mmol, 1.5 equiv). After stirring for 30 minutes, allylbromide (0.35 mL, 4.0 mmol, 1.4 equiv) was added. The reaction was stirred for 15 h at room temperature before it was quenched with H_2O (20 mL). The aqueous layer was extracted with EtOAc (3 x 30 mL) and the combined organic layers were dried over $MgSO_4$, filtered, and concentrated under reduced pressure to a yellow oil. The product was purified by column chromatography (silica, gradient eluent 0-20% EtOAc/hexanes) to give the product as a clear oil (0.26 g, 1.2 mmol, 41% yield). NMR spectra match values previously reported.[202]

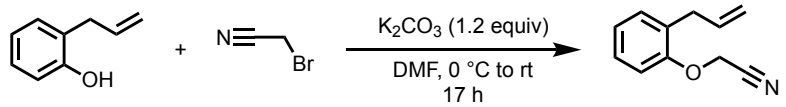

(**S3**) (**S6**)

2-[2-(2-propen-1-yl)phenoxy]acetonitrile (S6) To an oven-dried Schlenk flask equipped with a magnetic stir bar was added 2-allylphenol (0.96 mL, 7.4 mmol, 1.0 equiv), DMF (12 mL) and K_2CO_3 (1.22 g, 8.8 mmol, 1.2 equiv). The heterogeneous mixture was cooled to 0 °C with an ice/water bath for 5 minutes before 2-bromoacectonitrile (0.51 mL, 7.4 mmol, 1.0 equiv) was added dropwise. After full addition of 2-bromoacetonitrile, the reaction was removed from the ice/water bath and warmed to room temperature. After 45 minutes, the reaction color had changed from white to yellow. The reaction was stirred for 17 h before being quenched with H_2O (10 mL). The aqueous layer was extracted with EtOAc (3 x 30 mL), dried with Na_2SO_4, filtered and concentrated under reduced pressure. The crude product was taken up in 30 mL EtOAc, transferred to a separatory funnel, and washed with LiCl (3 x 30 mL, saturated aqueous solution). The organic layers were dried over Na_2SO_4, filtered and concentrated under reduced pressure to a dark green/brown oil. The product was purified by column chromatography (silica, gradient eluent 0-20% EtOAc/hexanes) to give the product as a clear oil (0.87 g, 5.0 mmol, 68% yield). NMR spectra match values previously reported.[196]

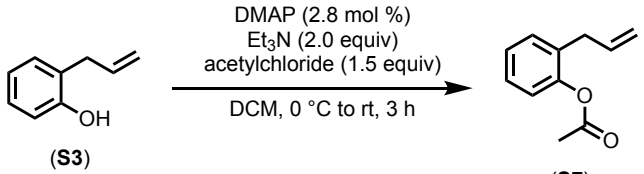

(**S3**) (**S7**)

1-acetate-2-(2-propen-1-yl)phenol (S7) was synthesized via literature procedure:[203] To an oven-dried Schlenk flask equipped with a magnetic stir bar was added 2-allylphenol (0.96 mL, 7.4 mmol, 1.0 equiv) and DCM (20 mL). The reaction was cooled to 0 °C with an ice/water bath for 5 minutes before Et_3N (2.1 mL, 15 mmol, 2.0 equiv) and 4-dimethylaminopyridine (25 mg, 0.20 mmol, 0.028 equiv) were added. After 5 minutes, acetyl chloride (0.79 mL, 11 mmol, 1.5 equiv) was added slowly. During addition of acetyl chloride, a precipitate formed and the reaction became a dark yellow slurry. After stirring for 30 minutes at 0 °C, the ice/water bath was removed and the reaction was warmed to room temperature. After 3 h, the reaction was quenched with $NaHCO_3$ (30 mL, saturated aqueous solution). The DCM layer was separated and the aqueous layer was extracted with Et_2O (2 x 50 mL). Et_2O and DCM layers were combined and washed with H_2O (2 x 50

mL) and brine (2 x 50 mL). The organic layer was dried over Na_2SO_4, filtered, and concentrated under reduced pressure to give an orange/yellow oil. The product was purified by column chromatography (silica, hexanes) to give the product as a light yellow oil (1.1 g, 6.1 mmol, 83% yield). NMR spectra match values previously reported.[203]

d. Wittig Reactions

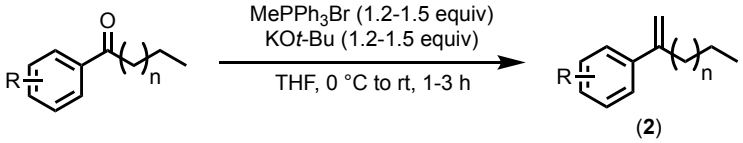

(**2**)

Wittig reactions were carried out via modified literature procedure:[14] an oven-dried Schlenk flask equipped with a magnetic stir bar was charged with $MePPh_3Br$ (1.2-1.5 equiv) and THF and cooled to 0 °C with an ice/water bath for 10 min before KO*t*-Bu (1.2-1.5 equiv) was added in one portion. *Note:* KO*t*-Bu needs to be rigorously dried before use – in our syntheses, KO*t*-Bu was removed from the glovebox within 1 h of running the reaction. Once the distinctive bright yellow color appeared, the reaction was stirred for 30 min at 0 °C before adding the ketone (1.0 equiv) dropwise. If the yellow color failed to appear, the deprotonation of $MePPh_3Br$ was not successful. The reaction was stirred at 0 °C for 30 min to 1 h before stirring at room temperature or being heated to 40 °C. Upon consumption of ketone (determined by TLC) flask was opened to air and reaction was quenched with water. The organic layer was separated, and the aqueous layer was extracted three times with Et_2O. The combined organic layers were dried over Na_2SO_4 and filtered, and the filtrate was concentrated under reduced pressure to yield the corresponding crude product. Purification details are included below.

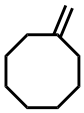

Methylenecyclooctane (2r)

Synthesis details: $MePPh_3Br$ (6.43 g, 18.0 mmol, 1.2 equiv), KO*t*-Bu (2.02 g, 18.0 mmol, 1.2 equiv), THF (100 mL), cyclooctanone (1.90 g, 15.0 mmol, 1.0 equiv). Clear liquid (0.48 g, 3.9 mmol, 26% yield).

Purification details: Silica plug with hexanes.

NMR spectra match values previously reported.[204]

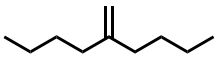

2-Butylpentene (2s)

Synthesis details: $MePPh_3Br$ (8.04 g, 22.5 mmol, 1.5 equiv), KO*t*-Bu (2.52 g, 22.5 mmol, 1.5 equiv), THF (100 mL), 5-nonanone (2.57 mL, 15.0 mmol, 1.0 equiv). Clear liquid (1.12 g, 7.98 mmol, 53% yield).

Purification details: Silica plug with hexanes.

NMR spectra match values previously reported.[205]

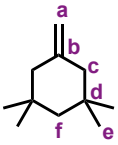

3,3,5,5-tetramethylmethylenecyclohexane (2u)

Synthesis details: $MePPh_3Br$ (5.36 g, 15.0 mmol, 1.5 equiv), KO*t*-Bu (1.68 g, 15.0 mmol, 1.5 equiv), THF (70 mL), 3,3,5,5-tetramethylcyclohexanone (1.70 mL, 10.0 mmol, 1.0 equiv). Clear liquid (0.52 g, 3.4 mmol, 34% yield).

Purification details: Silica plug with hexanes.

^{1}H NMR (500 MHz, $CDCl_3$, 298 K): δ 4.69 (br s, 2H, **H_a**), 1.87 (br s, 4 H, **H_c**), 1.25 (br s, 2H, **H_f**), 0.92 (br s, 12H, **H_e**)

^{13}C NMR (126 MHz, $CDCl_3$, 298 K): δ 146.6 (**C_b**), 109.8 (**C_a**), 52.6 (**C_f**), 48.7 (**C_c**), 33.3 (**C_d**), 31.0 (**C_e**)

ASAP/HRMS (m/z): $[M+H]^+$ calculated for $C_{11}H_{20}$ 153.1638, found 153.1623

IR (ATR, neat) ν: 2951 (m), 1651 (m), 1365 (m), 879 (s)

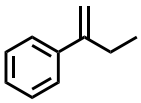

2-Phenyl-1-butene (2v)

Synthesis details: $MePPh_3Br$ (10.01 g, 28.0 mmol, 1.24 equiv), KO*t*-Bu (3.18 g, 28.3 mmol, 1.25 equiv), THF (125 mL), propiophenone (3.00 mL, 22.6 mmol, 1.00 equiv). Clear oil (1.90 g, 14.3 mmol, 63% yield).

Purification details: Silica plug with pentane.

NMR spectra match values previously reported.[206]

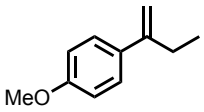

2-(4-Methoxyphenyl)-1-butene (2w)

Synthesis details: $MePPh_3Br$ (10.1 g, 28.2 mmol, 1.24 equiv), KO*t*-Bu (3.17 g, 28.3 mmol, 1.24 equiv), THF (150 mL), 4'-methoxypropiophenone (4.00 mL, 22.8 mmol, 1.00 equiv). Yellow oil (3.17 g, 19.5 mmol, 86% yield).

Purification details: Column chromatography: silica, gradient eluent (0-10% Et_2O/pentane).

NMR spectra match values previously reported.[207]

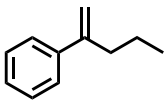

2-Phenyl-1-pentene (2x)

Synthesis details: $MePPh_3Br$ (8.04 g, 22.5 mmol, 1.48 equiv), KO*t*-But (2.53 g, 22.5 mmol, 1.48 equiv), THF (60 mL), butyrophenone (2.20 mL, 15.2 mmol, 1.00 equiv). Clear oil (1.31 g, 8.96 mmol, 59% yield).

Purification details: Silica plug with hexanes.

NMR spectra match values previously reported.[206]

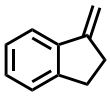

2,3-dihydro-1-methylene-1*H*-indene (2y)

Synthesis details: $MePPh_3Br$ (5.36 g, 15.0 mmol, 1.5 equiv), KO*t*-Bu (1.68 g, 15.0 mmol, 1.5 equiv), THF (70 mL), 1-indanone (1.32 g, 10.0 mmol, 1.0 equiv). Clear oil (1.01 g, 7.8 mmol, 78% yield).

Purification details: Column chromatography: silica, hexanes

NMR spectra match values previously reported.[208]

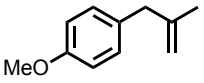

1-Methoxy-4-(2-methyl-2-propenyl)benzene (2z)

Synthesis details: $MePPh_3Br$ (4.98 g, 13.9 mmol, 1.07 equiv), KO*t*-Bu (1.54 g, 13.7 mmol, 1.05 equiv), THF (80 mL), 4-methoxyphenylacetone (2.00 mL, 13.0 mmol, 1.00 equiv). Clear oil (1.47 g, 9.06 mmol, 70% yield).

Purification details: Column chromatography: silica, gradient eluent (0-10% Et_2O/pentane).

NMR spectra match values previously reported.[209]

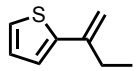

2-(But-1-en-2-yl)thiophene (S8)

Synthesis details: $MePPh_3Br$ (8.04 g, 22.5 mmol, 1.5 equiv), KO*t*-Bu (2.52 g, 22.5 mmol, 1.5 equiv), THF (100 mL), 1-(2-thienyl)-1-propanone (1.86 mL, 15.0 mmol, 1.0 equiv). Yellow oil (1.00 g, 7.23 mmol, 48% yield).

Purification details: Column chromatography: silica, gradient eluent (0-10% Et2O/hexanes).

NMR spectra match values previously reported.[210]

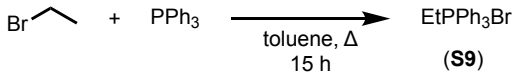

Ethyltriphenylphosphonium bromide (S9) was synthesized via literature procedure:[211] To a 500 mL 3-neck RBF was added triphenylphosphine (30 g, 110 mmol, 1.1 equiv), toluene (100 mL) and bromoethane (7.8 mL, 100 mmol, 1.0 equiv). The reaction was heated to reflux for 15 h before being cooled to room temperature. The product was collected via filtration with a glass frit before being dried under reduced pressure to yield a white powder (24 g, 65 mmol, 65% yield). NMR spectra match values previously reported.[212]

ASAP/HRMS (m/z): M^+ calculated for $C_{20}H_{20}P$ 291.1297, found 291.1225

IR (ATR, neat) ν: 2908 (w), 1431 (m), 1113 (m), 688 (s)

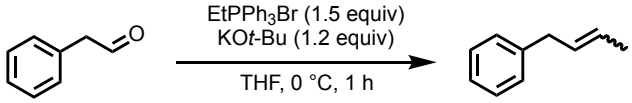

4-Phenyl-2-butene (3aa') To an oven-dried 200 mL Schlenk flask was added **S9** (12 g, 32 mmol, 1.5 equiv) and THF (110 mL). The reaction was cooled to 0 °C with an ice/water bath for 5 min before KO*t*-Bu (3.0 g, 27 mmol, 1.3 equiv) was added in one portion. A bright orange color appeared within a minute. This mixture was stirred for 30 min before phenylacetaldehyde (2.5 mL, 22 mmol, 1.0 equiv) was added dropwise. The

reaction was stirred at 0 °C for one hour before water (80 mL) was added and the reaction was exposed to atmosphere. The aqueous layer was extracted with Et_2O (3 x 100 mL) and the combined organic layers were dried over Na_2SO_4, filtered, and concentrated under reduced pressure. The crude material was purified by column chromatography (silica, hexanes) to yield the product as a clear liquid (1.4 g, 11 mmol, 50% yield). NMR spectra match values previously reported.[95]

IR (ATR, neat) ν: 3020 (w), 1495 (m), 1452 (m), 694 (s)

e. Triaryl Silanes

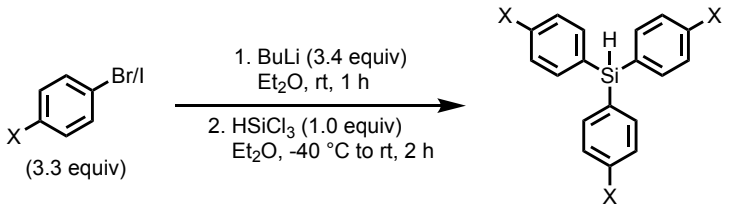

(**S4-6**)

Triaryl silanes were synthesized via modified literature procedure:[141] To an oven-dried Schlenk flask was added aryl iodide or aryl bromide (3.3 equiv) and Et_2O. BuLi (2.5 M in hexanes, 3.4 equiv) was added dropwise and the reaction was stirred at room temperature for 1 h before being cooled to -40 °C with a dry ice/MeCN bath. $HSiCl_3$ (1.0 equiv) was slowly added, and the reaction stirred for 1 h at -40 °C before the bath was removed and the reaction was slowly warmed to room temperature before stirring for an additional 1 h. The flask was cooled to 0 °C with an ice/water bath before being opened to air and quenched with NH_4Cl (saturated aqueous solution). The organic layer was separated, and the aqueous layer was extracted twice with Et_2O. The combined organic layers were dried over $MgSO_4$ and filtered, and the filtrate was concentrated under reduced pressure to yield the corresponding crude product. Purification details are included below.

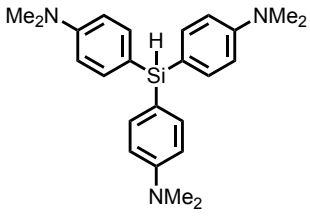

Tris[4-(*N,N*-dimethylamino)phenyl]silane (HSi(4-NMe_2-C_6H_4)$_3$)

Synthesis details: 4-Bromo-*N,N*-dimethylaniline (2.00 g, 10.0 mmol, 3.33 equiv), Et_2O (20 mL), BuLi (4.12 mL, 10.3 mmol, 3.41 equiv), $HSiCl_3$ (0.30 mL, 3.0 mmol, 1.0 equiv),

quenched with NH_4Cl (10 mL), extracted with Et_2O (2 x 25 mL). White solid (1.08 g, 2.77 mmol, 92% yield).

Purification details: A white solid was collected after concentration under reduced pressure. To the solid was added cold hexane, and the insoluble solid was separated by filtration. The filtrate was concentrated under reduced pressure to yield the product as a white solid.

^{1}H NMR (500 MHz, C_6D_6, 298 K): δ 7.80 (d, J = 8.6 Hz, 6H), 6.65 (d, J = 8.6 Hz, 6H), 6.06 (s, 1H), 2.50 (s, 18H)

$^{13}C\{^1H\}$ NMR (126 MHz, C_6D_6, 298 K) δ 151.7, 137.4, 121.0, 112.6, 39.8

$^{29}Si\{^1H\}$ NMR (99 MHz, C_6D_6, 298 K): δ -19.10

IR (ATR, neat) ν: 2070 (Si–H, m), 1592 (m), 1108 (m), 789 (s) cm^{-1}

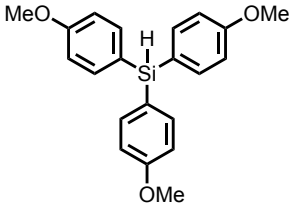

Tris(4-methoxyphenyl)silane (HSi(4-OMe-C_6H_4)$_3$)

Synthesis details: 4-iodoanisole (2.34 g, 10.0 mmol, 3.33 equiv), Et_2O (20 mL), BuLi (4.12 mL, 10.3 mmol, 3.41 equiv), $HSiCl_3$ (0.30 mL, 3.0 mmol, 1.0 equiv), quenched with NH_4Cl (10 mL), extracted with Et_2O (2 x 25 mL). White solid (1.05 g, 3.00 mmol, 100% yield)

Purification details: A white, waxy solid was collected after concentration under reduced pressure. To the solid was added cold hexane, and the insoluble solid was separated by filtration. The filtrate was concentrated under reduced pressure to saturation and the product crystallized after cooling in the freezer to give a white solid.

^{1}H NMR (500 MHz, C_6D_6, 298 K): δ 7.63 (d, *J* = 7.7 Hz, 6H), 6.85 (d, *J* = 7.7 Hz, 6H), 5.85 (s, 1H), 3.28 (s, 9H)

^{13}C{^{1}H} NMR (126 MHz, C_6D_6, 298 K) δ 161.6, 137.7, 125.3, 114.3, 54.5

^{29}Si{^{1}H} NMR (99 MHz, C_6D_6, 298 K): δ -18.99

IR (ATR, neat) ν: 2136 (Si–H, m), 1500 (m), 1106 (s), 777 (s) cm^{-1}

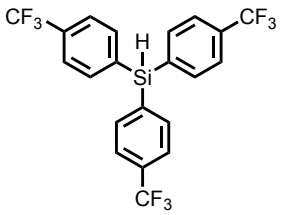

Tris[4-(trifluoromethyl)phenyl]silane (HSi(4-CF_3-C_6H_4)$_3$)

Synthesis details: 4-iodobenzotrifluoride (1.47 mL, 10.0 mmol, 3.33 equiv), Et_2O (20 mL), BuLi (4.12 mL, 10.3 mmol, 3.41 equiv), $HSiCl_3$ (0.30 mL, 3.0 mmol, 1.0 equiv), quenched with NH_4Cl (10 mL), extracted with Et_2O (2 x 25 mL). Pale yellow solid (0.40 g, 0.86 mmol, 29% yield).

Purification details: A yellow, waxy solid was collected after concentration under reduced pressure. To the solid was added cold hexanes, and the insoluble material was separated by filtration. The filtrated was concentrated under reduced pressure to saturation and the product crystallized after cooling in the freezer to give a pale yellow solid.

^{1}H NMR (600 MHz, C_6D_6, 298 K): δ 7.36 (d, *J* = 7.7 Hz, 6H), 7.20 (d, *J* = 7.7 Hz, 6H), 5.32 (s, 1H)

^{13}C{^{1}H} NMR (151 MHz, C_6D_6, 298 K) δ 136.4, 136.2, 132.6 (q, *J* = 32.4 Hz), 125.2 (q, *J* = 3.8 Hz), 124.7 (q, *J* = 277.5 Hz)

^{19}F NMR (565 MHz, C_6D_6, 298 K): δ -62.90

^{29}Si{^{1}H} NMR (99 MHz, C_6D_6, 298 K): δ -18.92

IR (ATR, neat) ν: 2159 (Si–H, w), 1323 (m), 1115 (s), 696 (s) cm^{-1}

f. Deuterated Substrates

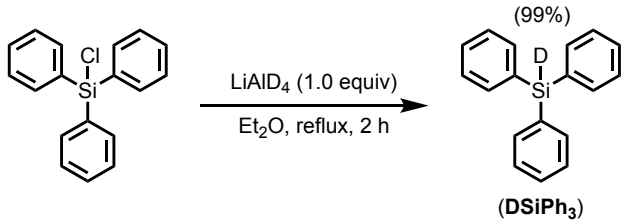

Triphenylsilane-*d*$_1$ (DSiPh$_3$) was synthesized via modified literature procedure:[213] To an oven-dried Schlenk flask equipped with a magnetic stir bar was added $ClSiPh_3$ (300 mg, 1.0 mmol, 1.0 equiv) and Et_2O (15 mL). $LiAlD_4$ (42 mg, 1.0 mmol, 1.0 equiv) was added to the stirring reaction, and the flask was equipped with a reflux condenser and heated to reflux and stirred 23 h. The reaction was cooled to room temperature and quenched with H_2O (10 mL). The mixture was extracted twice with Et_2O (10 mL) and the organic layer was filtered through Celite. The filtrate was concentrated under reduced pressure to yield **S7-*d*$_1$** as a viscous, clear, colorless oil (250 mg, 0.96 mmol, 96% yield). NMR spectra match values previously reported.[213]

ASAP/HRMS (m/z): M^+ calculated for $C_{18}H_{15}DSi$ 261.1084, found 261.0945

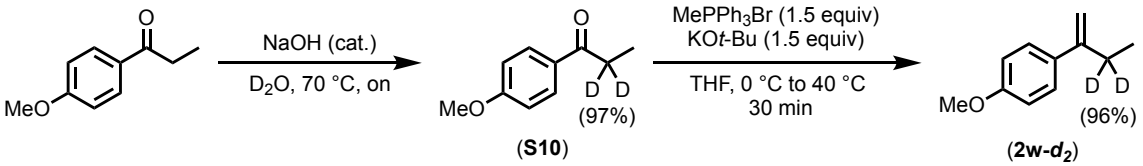

2-(4-Methoxyphenyl)-1-butene-*d*$_2$ (2w-*d*$_2$) was synthesized via literature procedure:[14] To a RBF equipped with a magnetic stir bar was added D_2O (12 mL), which was sparged with N_2 gas for 30 min. The NaOH (60 mg, 1.5 mmol, 0.13 equiv) was added in one portion and reaction was stirred until NaOH was fully dissolved. 4'-methoxypropiophenone (2.0 mL, 11 mmol, 1.0 equiv) was added and reaction was placed in an oil bath to heat at 70 °C for 18 h. After the reaction cooled to room temperature, the reaction was extracted with Et_2O (3 x 30 mL). The combined organic layers were dried over Na_2SO_4, filtered, and the filtrate was concentrated under reduced pressure to give **S10**

as a yellow oil (1.88 g, 11.3 mmol, 99% yield). NMR spectra match values previously reported.[214]

ASAP/HRMS (m/z): M^+ calculated for $C_{10}H_{10}D_2O_2$ 166.0963, found 166.0968

To an oven-dried Schlenk flask equipped with a magnetic stir bar was added $MePPh_3Br$ (4.9 g, 14 mmol, 1.5 equiv) and THF (75 mL). The reaction was cooled with an ice/water bath for 10 minutes before KO*t*-Bu (1.6 g, 14 mmol, 1.5 equiv) was added in one portion. The reaction was stirred for 30 minutes before **S10** (1.6 mL, 9.0 mmol, 1.0 equiv) was added with a disposable syringe. After full addition of **S10**, the reaction was moved to an oil bath at 40 °C and stirred for 30 minutes. The reaction was opened to air and quenched with water (50 mL). The organic layer was separated, and the aqueous layer was extracted with Et_2O (3 x 30 mL). The combined organic layers were dried over Na_2SO_4, filtered, and the filtrate was concentrated under reduced pressure to a gooey white solid. Triphenylphosphine oxide (the main byproduct) was separated by running a silica plug with 5% Et_2O/hexanes. **2w-*d*$_2$** was isolated as a clear oil (1.09 g, 6.64 mmol, 74% yield). NMR spectra match values previously reported.[207]

ASAP/HRMS (m/z): M^+ calculated for $C_{11}H_{12}D_2O$ 164.1170, found 164.1168

A.1.4. Alkene Isomerization

a. Reaction Optimization

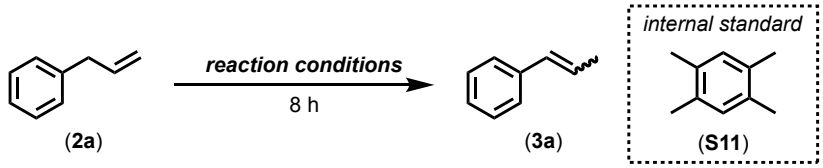

In a nitrogen-filled glovebox, stock solutions of silanes were prepared by weighing out the silane, dissolving it in the appropriate volume of hexanes using volumetric glassware, and distributing the stock solutions by microliter syringe. Ni complexes were added via stock solutions prepared by weighing out the complex, dissolving it in the appropriate volume of hexanes using volumetric glassware, and distributing the stock solutions by microliter syringe. KO*t*-Bu, **IPr** and **IPr·HCl** were weighed out directly into the appropriate vial(s). Additional hexanes was added using a disposable plastic syringe to bring the total reaction volume to the appropriate volume. Vials were sealed with septum caps, removed from the glovebox and placed on a pre-heated vial block at the appropriate

temperature. After 30 minutes, allylbenzene (1.0 equiv) was distributed using a 250-µL or a 25-µL microliter syringe, depending on the scale of the reaction. After 8 h, the vial was quenched by cooling in a liquid N_2 bath, opening to air, and **S11** was added to the reaction as a stock solution (0.25-0.30 equiv). An aliquot was removed and filtered with hexanes through a Celite plug. The filtrate from the Celite plug was analyzed by GCMS to assess the progress and selectivity of the reaction.

Results from optimization screening reactions are summarized below in **Table A.1.** with any deviations from standard procedures explained therein.

Table A.1. Reaction screening and optimization.

Entry	*Ni complex (loading)*	*Silane (loading)*	*Additive*	*Solvent*	*Temp.*	*Time*	*Yield **3a***	*E/Z ratio*
1	**1a** (5 mol %)	$HSiPh_3$ (5 mol %)	None	Hexanes	70 °C	8 h	95%	14:1
2[a]	**1b** (5 mol %)	$HSiPh_3$ (5 mol %)	None	Hexanes	70 °C	8 h	10%	2:1
3[a]	**1c** (5 mol %)	$HSiPh_3$ (5 mol %)	None	Hexanes	70 °C	8 h	9%	2:1
4[a]	**1d** (5 mol %)	$HSiPh_3$ (5 mol %)	None	hexanes	70 °C	8 h	67%	11:1
5[b]	**1e** (5 mol %)	$HSiPh_3$ (5 mol %)	None	Hexanes	70 °C	8 h	92%	13:1
6	**1f** (5 mol %)	None	None	Hexanes	70 °C	8 h	44%	8:1
7[c]	**1f** (5 mol %)	None	None	ClPh	r.t.	3 h	81%	18:1
8	$Ni(cod)_2$ (5 mol %)	$HSiPh_3$ (5 mol %)	None	Hexanes	70 °C	8 h	5%	2:1
9	**1a** (2.5 mol %)	$HSiPh_3$ (2.5 mol %)	None	Hexanes	70 °C	8 h	64%	12:1
10	**1a** (10 mol %)	$HSiPh_3$ (10 mol %)	None	Hexanes	70 °C	8 h	91%	13:1
11	**1a** (5 mol %)	$HSiPh_3$ (20 mol %)	None	Hexanes	70 °C	8 h	94%	14:1
12	None	$HSiPh_3$ (5 mol %)	None	Hexanes	70 °C	8 h	7%	1:1
13	**1a** (5 mol %)	None	None	Hexanes	70 °C	8 h	9%	2:1
14	**1a** (5 mol %)	$HSiPh_3$ (5 mol %)	None	Hexanes	r.t.	8 h	7%	1:1
15	**1a** (5 mol %)	$HSiPh_3$ (5 mol %)	None	Hexanes	50 °C	8 h	37%	8:1

16	**1a** (5 mol %)	$HSiPh_3$ (5 mol %)	None	Hexanes	80 °C	8 h	93%	11:1
17	**1a** (5 mol %)	$HSiPh_3$ (5 mol %)	None	Toluene	70 °C	8 h	94%	13:1
18	**1a** (5 mol %)	$HSiPh_3$ (5 mol %)	None	1,4-dioxane	70 °C	8 h	19%	4:1
19	**1a** (5 mol %)	H_2SiPh_2 (5 mol %)	None	Hexanes	70 °C	8 h	84%	12:1
20	**1a** (5 mol %)	$HSiMePh_2$ (5 mol %)	None	Hexanes	70 °C	8 h	47%	9:1
21	**1a** (5 mol %)	$HSiMe_2Ph$ (5 mol %)	None	Hexanes	70 °C	8 h	19%	3:1
22	**1a** (5 mol %)	$HSi(OEt)_3$ (5 mol %)	None	Hexanes	70 °C	8 h	34%	4:1
23[d]	None	None	KO*t*-Bu (5 mol %)	Hexanes	70 °C	8 h	43%	5:1
24	$Ni(cod)_2$ (5 mol %)	None	IPrHCl (5 mol %) + KO*t*-Bu (5 mol %)	Hexanes	70 °C	8 h	4%	16:1
25	$Ni(cod)_2$ (5 mol %)	$HSiPh_3$ (5 mol %)	IPrHCl (5 mol %) + KO*t*-Bu (5 mol %)	Hexanes	70 °C	8 h	18%	42:1

[a] catalyst stock solution prepared in THF, evaporated before reaction.
[b] **1e** weighed out directly into vial.
[c] run at 0.4 M.
[d] run on a 0.5 mmol scale, KO*t*-Bu weighed out directly into vial

b. General Procedures for Isomerization and Isolation of Products

i. General procedure A (GP-A): In a nitrogen-filled glovebox, stock solutions of **1a** (0.028 M) and silane (0.036 M) were prepared by weighing out the reagent and dissolving in the appropriate volume of hexanes. The stock solutions of **1a** (0.90 mL, 0.025 mmol, 0.05 equiv) and silane (0.70 mL, 0.025 mmol, 0.05 equiv) were added to a 1-dram vial equipped with a stir bar using disposable 1-mL syringes. The vial was sealed with a septum cap, removed from the glovebox, and placed on an aluminum vial block pre-heated to 80 °C. The reaction was heated for 30 minutes before the substrate (0.50 mmol, 1.0 equiv) was added using a 250-µL microliter

syringe. After 16 h, the reaction was quenched by cooling in a liquid N_2 bath, opening to air, and diluting with hexanes (0.10-0.20 mL). An aliquot was removed and filtered with hexanes through a Celite plug. The filtrate from the Celite plug was analyzed by GC to assess the progress and selectivity of the reaction. The product was purified as detailed below for each substrate.

ii. **General procedure B (GP-B):** In a nitrogen-filled glovebox, the nickel complex (**1a** or **1e**, 0.025 mmol, 0.05 equiv) was weighed out directly into a 1-dram vial equipped with a magnetic stir bar. A stock solution of silane (0.05 M) was prepared by weighing out the reagent and dissolving in the appropriate volume of hexanes. The stock solution of silane (0.50 mL, 0.025 mmol, 0.05 equiv) was added to the vial using a disposable 1-mL syringe. Hexanes (1.1 mL) was added to the vial. The vial was sealed with a septum cap, removed from the glovebox, and placed on an aluminum vial block pre-heated to 80 °C. The reaction was heated for 30 minutes before substrate (0.50 mmol, 1.0 equiv) was added using a 250-µL microliter syringe. After 16 h, the reaction was quenched by cooling in a liquid N_2 bath, opening to air, and diluting with hexanes (0.10-0.20 mL). An aliquot was removed and filtered with hexanes through a Celite plug. The filtrate from the Celite plug was analyzed by GC to assess the progress and selectivity of the reaction. The product was purified as detailed below for each substrate.

iii. **General procedure C (GP-C):** In a nitrogen-filled glovebox, the nickel complex (**1a** or **1e**, 0.015 mmol, 0.05 equiv) was weighed out directly into a 1-dram vial equipped with a magnetic stir bar. A stock solution of silane (0.015 M) was prepared by weighing out the reagent and dissolving in the appropriate volume of hexanes. The stock solution of silane (1.0 mL, 0.015 mmol, 0.05 equiv) was added to the vial using a disposable 1-mL syringe. The vial was sealed with a septum cap, removed from the glovebox, and placed on an

aluminum vial block pre-heated to 80 °C. The reaction was heated for 30 min before the substrate (0.30 mmol, 1.0 equiv) was added using a 250 μL microliter syringe. After 16 h, the reaction was quenched by cooling in a liquid N_2 bath, opening to air, and diluting with hexanes (0.10-0.20 mL). An aliquot was removed and filtered with hexanes through a Celite plug. The filtrate from the Celite plug was analyzed by GC to assess the progress and selectivity of the reaction. The product was purified as detailed below for each substrate.

iv. **General procedure D (GP-D):** In a nitrogen-filled glovebox, **1e** (5.7 mg, 0.010 mmol, 0.02 equiv) was weighed out directly into a 1-dram vial equipped with a magnetic stir bar. A stock solution of silane (0.015 M) was prepared by weighing out the reagent and dissolving in the appropriate volume of hexanes. The stock solution of silane (1.6 mL, 0.024 mmol, 0.05 equiv) was added to the vial using a disposable 1-mL syringe. The vial was sealed with a septum cap, removed from the glovebox, and placed on an aluminum vial block pre-heated to 80 °C. The reaction was heated for 30 min before the substrate (0.50 mmol, 1.0 equiv) was added using a 250 μL microliter syringe. After 16 h, the reaction was quenched by cooling in a liquid N_2 bath, opening to air, and diluting with hexanes (0.10-0.20 mL). An aliquot was removed and filtered with hexanes through a Celite plug. The filtrate from the Celite plug was analyzed by GC to assess the progress and selectivity of the reaction. The product was purified as detailed below for each substrate.

v. **General procedure E (GP-E):** In a nitrogen-filled glovebox, the nickel complex (**1a** or **1e**) was weighed directly into a 1-dram vial equipped with a magnetic stir bar. The substrate (0.50 mmol, 1.0 equiv) was weighed directly into the 1-dram vial. A stock solution of silane (0.015 M) was prepared by weighing out the reagent and dissolving in the appropriate volume of hexanes. The stock solution

of silane (1.6 mL, 0.024 mmol, 0.05 equiv) was added to the vial using a disposable 1-mL syringe. The vial was sealed with a septum cap, removed from the glovebox, and placed on an aluminum vial block pre-heated to 80 °C. After 16 h, the reaction was quenched by cooling in a liquid N_2 bath, opening to air, and diluting with hexanes (0.10-0.20 mL). An aliquot was removed and filtered with hexanes through a Celite plug. The filtrate from the Celite plug was analyzed by GC to assess the progress and selectivity of the reaction. The product was purified as detailed below for each substrate.

c. Isomerization of (2-allylphenoxy)trimethylsilane (XX)

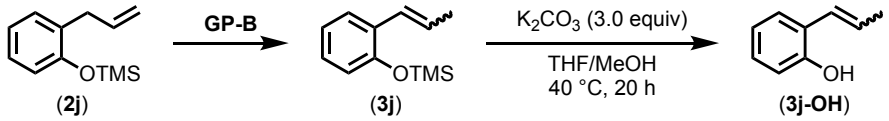

GP-B (catalyst **1e**, $HSi(p\text{-}CF_3\text{-}C_6H_4)_3$, substrate **2j**) was followed to generate **3j**. The *E*/*Z* ratio was determined to be 14:1 by GC analysis of the crude reaction mixture after the reaction was quenched by cooling in a liquid N_2 bath, opened to air and diluted with hexanes. The crude reaction mixture was concentrated under reduced pressure and a ^1H NMR sample was prepared by filtering a portion of the reaction through Celite with $CDCl_3$. The crude ^1H NMR spectrum shows survival of the trimethylsilyl-protecting group at 0.27 ppm, corresponding to the 9H of the TMS group in **3j** (Figure S76) and 100% conversion of **2j**. Attempts to isolate **3j** by column chromatography led to partial deprotection of the phenol. NMR spectra match values previously reported.[215]

^1H NMR (500 MHz, $CDCl_3$, 298 K): δ 7.40 (d, J = 7.7 Hz, 1H), 7.07 (t, J = 7.7 Hz, 1H), 6.91 (t, J = 7.5 Hz, 1H), 6.77 (d, J = 8.0 Hz, 1H), 6.62 (d, J = 15.9 Hz, 1H), 6.19 (dq, J = 15.9, 6.6 Hz, 1H), 1.89 (d, J = 6.6 Hz, 3H), 0.27 (s, 9H).

The NMR sample was recombined with the reaction and re-concentrated under reduced pressure. To the crude **3j** was added THF/MeOH (3.0 mL, 1:1 THF/MeOH) and K_2CO_3 (0.21 g, 1.5 mmol, 3.0 equiv). The vial was sealed and stirred for 20 h in an oil bath at 40 °C before being quenched with water (5.0 mL), which formed two layers. The organic layer was separated, and the aqueous layer extracted with EtOAc (3 x 10 mL). The combined organic layers were dried over Na_2SO_4 and filtered, and the filtrate was

concentrated under reduced pressure to yield the crude deprotected product as a red oil. The crude product was purified via column chromatography (silica, gradient eluent 0-7% EtOAc/hexanes) to give the deprotected product (2-(1-propen-1-yl)phenol, **3j-OH**) as a clear yellow oil (58 mg, 0.43 mmol, 86% yield). NMR spectra match values previously reported.[90,216]

The major product isolated is the *E*-isomer, and the *Z*-isomer is seen in the NMR spectra as well. The ratio of these isomers determined by integration of H in the β-position was found to be 14:1 (*E/Z*). The *E*-product is fully characterized below, and the peaks visible and clearly assignable to the *Z*-isomer are given directly following the NMR characterization of the *E*-product.

<u>*E*-product:</u>

^{1}H NMR (500 MHz, $CDCl_3$, 298 K): δ 7.29 (d, *J* = 7.6 Hz, 1H), 7.08 (t, *J* = 7.6 Hz, 1H), 6.87 (t, *J* = 7.5 Hz, 1H), 6.77 (d, *J* = 8.0 Hz, 1H), 6.57 (d, *J* = 15.8 Hz, 1H), 6.20 (dq, *J* = 15.8, 6.6 Hz, 1H), 5.05 (br s, 1H), 1.90 (dd, *J* = 6.6, 1.3 Hz, 3H).

^{13}C{^{1}H} NMR (126 MHz, $CDCl_3$, 298 K): δ 152.4, 128.5, 128.1, 127.5, 125.4, 125.2, 121.0, 115.8, 19.0

<u>*Z*-product:</u>

^{1}H NMR (500 MHz, $CDCl_3$, 298 K): δ 6.38 (d, *J* = 11.5 Hz), 6.01 (dq, *J* = 11.2, 6.9 Hz), 1.71 (dd, *J* = 6.9, 1.5 Hz)

^{13}C{^{1}H} NMR (126 MHz, $CDCl_3$, 298 K): δ 152.7, 131.3, 129.8, 128.7, 126.4, 124.2, 120.4, 115.2

d. Characterization Data for Isomerized Alkenes

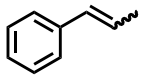

β-Methylstyrene (3a)

<u>Synthesis details:</u> **GP-A**, catalyst **1a**, $HSiPh_3$, substrate **2a**, crude *E*/*Z* ratio determined by GC = 20:1

<u>Purification details:</u> Column chromatography: silica, pentane to give the product as a clear oil (53 mg, 0.45 mmol, 90% yield). NMR spectra match values from commercial material.

The major product isolated is the *E*-isomer, and the *Z*-isomer is seen in the NMR spectra as well. The ratio of these isomers determined by integration of H in the β-position was found to be 25:1 (*E/Z*). The *E*-product is fully characterized below, and the peaks visible and clearly assignable to the *Z*-isomer are given directly following the NMR characterization of the *E*-product.

<u>*E*-product:</u>

^{1}H NMR (500 MHz, $CDCl_3$, 298 K): δ 7.33-7.25 (ms, 4H), 7.17 (t, *J* = 7.2 Hz, 1H), 6.39 (d, *J* = 15.8 Hz, 1H), 6.23 (dq, *J* = 15.7, 6.7 Hz, 1H), 1.87 (dd, *J* = 6.5, 1.0 Hz, 3H).

^{13}C{^{1}H} NMR (126 MHz, $CDCl_3$, 298 K): δ 138.1, 131.2, 128.6, 126.9, 126.0, 125.8, 18.6.

<u>*Z*-product:</u>

^{1}H NMR (500 MHz, $CDCl_3$, 298 K): δ 7.47 (d, *J* = 7.2 Hz), 5.79 (dq, *J* = 11.6, 7.2 Hz)

^{13}C{^{1}H} NMR (126 MHz, $CDCl_3$, 298 K): δ 135.3, 129.9, 129.0, 128.2, 127.8, 29.9

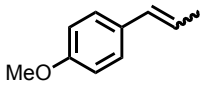

Anethole (3b)

<u>Synthesis details:</u> **GP-A**, **1a**, $HSiPh_3$, substrate **2b**, crude *E*/*Z* ratio determined by GC = 18:1

<u>Purification details:</u> Column chromatography: silica, hexane to give the product as a clear oil (69 mg, 0.47 mmol, 93% yield).

NMR spectra match values previously reported[30] and values from commercial material.

The major product isolated is the *E*-isomer, and the *Z*-isomer is seen in the NMR spectra as well. The ratio of these isomers determined by integration of H in the β-position was found to be 20:1 (*E/Z*). The *E*-product is fully characterized below, and the peaks visible

and clearly assignable to the *Z*-isomer are given directly following the NMR characterization of the *E*-product.

<u>*E*-product:</u>

^{1}H NMR (500 MHz, $CDCl_3$, 298 K): δ 7.25 (d, *J* = 8.6 Hz, 2H), 6.83 (d, *J* = 8.6 Hz, 2H), 6.34 (d, *J* = 15.8 Hz, 1H), 6.09 (dq, *J* = 15.7, 6.6 Hz, 1H), 3.79 (s, 3H), 1.85 (d, *J* = 6.6 Hz, 3H)

^{13}C{^{1}H} NMR (126 MHz, $CDCl_3$, 298 K): δ 158.7, 131.0, 130.5, 127.0, 123.6, 114.0, 55.4, 18.5

<u>*Z*-product:</u>

^{1}H NMR (500 MHz, $CDCl_3$, 298 K): δ 7.09 (d, *J* = 8.2 Hz), 6.87 (d, *J* = 8.6 Hz), 5.69 (dq, *J* = 11.6, 7.2 Hz), 3.81 (s), 1.89 (d, *J* = 7.2 Hz)

^{13}C{^{1}H} NMR (126 MHz, $CDCl_3$, 298 K): δ 130.1, 129.44, 129.41, 125.2, 113.7

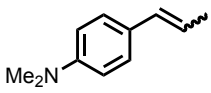

_N_,_N_-Dimethyl-4-(1-propen-1-yl)benzenamine (3c)

<u>Synthesis details:</u> **GP-A**, **1a**, $HSiPh_3$, substrate **2c**, crude *E*/*Z* ratio determined by GC = 15:1

<u>Purification details:</u> Column chromatography: silica, gradient eluent 0-3% Et_2O/pentane to give the product as a cream colored solid (77 mg, 0.48 mmol, 96% yield).

NMR spectra match values previously reported.[217]

The major product isolated is the *E*-isomer, and the *Z*-isomer is seen in the NMR spectra as well. The ratio of these isomers determined by integration of H in the β-position was found to be 20:1 (*E*/*Z*). The *E*-product is fully characterized below, and the peaks visible and clearly assignable to the *Z*-isomer are given directly following the NMR characterization of the *E*-product.

<u>*E*-product:</u>

^{1}H NMR (500 MHz, $CDCl_3$, 298 K): δ 7.22 (d, *J* = 8.8 Hz, 2H), 6.67 (d, *J* = 8.8 Hz, 2H), 6.32 (d, *J* = 15.7 Hz, 1H), 6.02 (dq, *J* = 15.7, 6.6 Hz, 1H), 2.93 (s, 6H), 1.84 (dd, *J* = 6.6, 1.2 Hz, 3H)
^{13}C{^{1}H} NMR (126 MHz, $CDCl_3$, 298 K): δ 149.8, 130.9, 126.9, 126.8, 121.6, 112.8, 40.8, 18.6

Z-product:

^{1}H NMR (500 MHz, $CDCl_3$, 298 K): δ 6.71 (d, *J* = 8.7 Hz), 5.61 (dq, *J* = 11.5, 7.2 Hz), 2.95 (s), 1.91 (dd, *J* = 7.2, 1.5 Hz)
^{13}C{^{1}H} NMR (126 MHz, $CDCl_3$, 298 K): δ 135.3, 129.9, 127.8, 123.5, 112.3, 40.7, 14.9

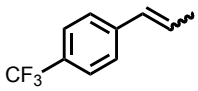

1-(4-Trifluoromethylphenyl)-1-propene (3d)

Synthesis details: **GP-C**, **1a**, $HSiPh_3$, substrate **2d**, crude *E*/*Z* ratio determined by GC = 23:1

Purification details: Column chromatography: silica, hexanes to give the product as a clear oil (30 mg, 0.16 mmol, 54% yield).

NMR spectra match values previously reported.[30]

The major product isolated is the *E*-isomer, and the *Z*-isomer is seen in the NMR spectra as well. The ratio of these isomers determined by integration of H in the β-position was found to be 50:1 (*E*/*Z*). The *E*-product is fully characterized below, and the peaks visible and clearly assignable to the *Z*-isomer are given directly following the NMR characterization of the *E*-product.

Note: the volatility of this product is likely the cause of the low isolated yield. Analysis of the crude reaction mixture shows no side-products and full consumption of starting alkene **3d**.

E-product:

^{1}H NMR (500 MHz, $CDCl_3$, 298 K): δ 7.52 (d, *J* = 8.0 Hz, 2H), 7.39 (d, *J* = 8.0 Hz, 2H), 6.42 (d, *J* = 15.9 Hz), 6.33 (dq, *J* = 15.9, 6.4 Hz, 1H), 1.90 (d, *J* = 6.4 Hz, 3H)

^{13}C{^{1}H} NMR (126 MHz, $CDCl_3$, 298 K): δ 141.5, 130.1, 128.8, 128.7 (q, *J* = 32 Hz), 126.1, 125.6 (q, J = 3.9 Hz), 124.5 (q, J = 272 Hz), 18.7

^{19}F NMR (471 MHz, $CDCl_3$, 298 K): δ -62.40

Z-product:

^{1}H NMR (500 MHz, $CDCl_3$, 298 K): δ 7.57 (d, *J* = 8.1 Hz), 5.89 (dq, *J* = 11.6, 7.2 Hz)

^{19}F NMR (471 MHz, $CDCl_3$, 298 K): δ -62.44

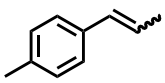

1-(4-Methylphenyl)-1-propene (3e)

Synthesis details: **GP-C**, **1a**, $HSiPh_3$, substrate **2e**, crude *E*/*Z* ratio determined by GC = 18:1

Purification details: Column chromatography: silica, pentane to give the product as a clear oil (38 mg, 0.29 mmol, 96% yield).

NMR spectra match values previously reported.[217]

The major product isolated is the *E*-isomer, and the *Z*-isomer is seen in the NMR spectra as well. The ratio of these isomers determined by integration of H in the β-position was found to be 20:1 (*E*/*Z*). The *E*-product is fully characterized below, and the peaks visible and clearly assignable to the *Z*-isomer are given directly following the NMR characterization of the *E*-product.

E-product:

^{1}H NMR (500 MHz, $CDCl_3$, 298 K): δ 7.21 (d, *J* = 7.9 Hz, 2H), 7.08 (d, *J* = 7.9 Hz, 2H), 6.36 (d, *J* = 15.7 Hz, 1H), 6.16 (dq, *J* = 15.7, 6.7 Hz, 1H), 2.31 (s, 3H), 1.85 (d, *J* = 6.7 Hz, 3H)

$^{13}C\{^{1}H\}$ NMR (126 MHz, $CDCl_3$, 298 K): δ 136.5, 135.3, 131.0, 129.3, 125.9, 124.7, 21.2, 18.6

Z-product:

^{1}H NMR (500 MHz, $CDCl_3$, 298 K): δ 7.13 (d, J = 7.8 Hz), 5.73 (dq, J = 11.6, 7.2 Hz), 2.33 (s), 1.88 (dd, J = 7.2, 1.5 Hz)

$^{13}C\{^{1}H\}$ NMR (126 MHz, $CDCl_3$, 298 K): δ 128.95, 128.88, 29.9, 22.5

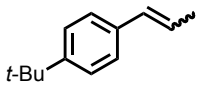

1-(1,1-Dimethylethyl)-4-(1-propen-1-yl)benzene (3f)

Synthesis details: **GP-B**, **1a**, $HSiPh_3$, substrate **2f**, crude *E*/*Z* ratio determined by GC = 19:1

Purification details: Column chromatography: silica, hexanes to give the product as a clear oil (81 mg, 0.46 mmol, 93% yield).

NMR spectra match values previously reported.[218]

The major product isolated is the *E*-isomer, and the *Z*-isomer and the starting material **2f** are seen in the NMR spectra as well. The ratio of these isomers determined by integration of H in the β-position was found to be 25:1 (*E*/*Z*) and <5% **2f**. The *E*-product is fully characterized below, and the peaks visible and clearly assignable to the *Z*-isomer are given directly following the NMR characterization of the *E*-product.

E-product:

^{1}H NMR (500 MHz, $CDCl_3$, 298 K): δ 7.31 (d, J = 8.3 Hz, 2H), 7.26 (d, J = 8.1 Hz, 2H), 6.38 (d, J = 15.8 Hz, 1H), 6.18 (dq, J = 15.8, 6.7 Hz, 1H), 1.86 (dd, J = 6.7, 1.1 Hz, 3H), 1.30 (s, 3H)

$^{13}C\{^{1}H\}$ NMR (126 MHz, $CDCl_3$, 298 K): δ 149.8, 135.3, 130.9, 125.7, 125.5, 125.0, 34.6, 31.5, 18.6

Z-product:

^{1}H NMR (500 MHz, $CDCl_3$, 298 K): δ 7.35 (d, J = 8.3 Hz), 5.74 (dq, J = 11.5, 7.2 Hz), 1.90 (dd, J = 7.2, 1.5 Hz), 1.32 (s)

$^{13}C\{^{1}H\}$ NMR (126 MHz, $CDCl_3$, 298 K): δ 128.7, 126.3, 125.2, 31.6

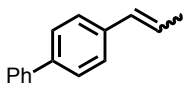

4-(1-Propen-1-yl)-1,1'-biphenyl (3g)

Synthesis details: **GP-A**, **1a**, $HSiPh_3$, substrate **2g**, crude *E*/*Z* ratio determined by GC = 17:1

Purification details: Column chromatography: silica, pentane to give the product as a clear oil (90 mg, 46 mmol, 93% yield).

NMR spectra match values previously reported.[219]

The major product isolated is the *E*-isomer, and the *Z*-isomer and the starting material **2g** are seen in the NMR spectra as well. The ratio of these isomers determined by integration of H in the β-position was found to be 25:1 (*E*/*Z*) and <2% **2g**. The *E*-product is fully characterized below, and the peaks visible and clearly assignable to the *Z*-isomer are given directly following the NMR characterization of the *E*-product.

E-product:

^{1}H NMR (500 MHz, $CDCl_3$, 298 K): δ 7.58 (d, *J* = 7.7 Hz, 2H), 7.52 (d, *J* = 8.1 Hz, 2H), 7.44-7.37 (ms, 4H), 7.31 (t, *J* = 7.4 Hz, 4H), 6.43 (d, *J* = 15.9 Hz, 1H), 6.27 (dq, *J* = 15.7, 6.7 Hz, 1H), 1.90 (dd, *J* = 6.6, 0.9 Hz, 3H)

$^{13}C\{^{1}H\}$ NMR (126 MHz, $CDCl_3$, 298 K): δ 141.0, 139.6, 137.1, 130.7, 128.9, 127.31, 127.26, 127.0, 126.4, 126.0, 18.7

Z-product:

^{1}H NMR (500 MHz, $CDCl_3$, 298 K): δ 7.47 (d, *J* = 7.2 Hz), 5.82 (dq, 11.6, 7.2 Hz), 1.94 (dd, *J* = 7.2, 1.4 Hz)

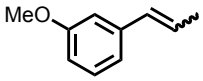

1-Methoxy-3-(1-propen-1-yl)benzene (3h)

Synthesis details: **GP-A**, **1a**, $HSiPh_3$, substrate **2h**, crude *E*/*Z* ratio determined by GC = 22:1

Purification details: Column chromatography: silica, gradient eluent 0-5% Et_2O/pentane to give the product as a clear oil (68 mg, 0.46 mmol, 92% yield).

NMR spectra match values previously reported.[217]

The major product isolated is the *E*-isomer, and the *Z*-isomer is seen in the NMR spectra as well. The ratio of these isomers determined by integration of H in the β-position was found to be 50:1 (*E*/*Z*). The *E*-product is fully characterized below, and the peaks visible and clearly assignable to the *Z*-isomer are given directly following the NMR characterization of the *E*-product.

E-product:

^1H NMR (500 MHz, $CDCl_3$, 298 K): δ 7.18 (t, *J* = 7.9 Hz, 1H), 6.91 (d, *J* = 7.7 Hz, 1H), 6.86 (m, 1H), 6.74 (dd, *J* = 8.1, 2.4 Hz, 1H), 6.35 (dd, *J* = 15.7, 1.4 Hz, 1H), 6.22 (dq, *J* = 15.7, 6.6 Hz, 1H), 3.78 (s, 3H), 1.87 (dd, *J* = 6.6, 1.5 Hz, 3H)

$^{13}C\{^1H\}$ NMR (151 MHz, $CDCl_3$, 298 K): δ 159.9, 139.6, 131.1, 129.9, 126.2, 118.6, 112.5, 111.3, 55.3, 18.6

Z-product:

^1H NMR (500 MHz, $CDCl_3$, 298 K): δ 5.78 (dq, *J* = 11.6, 7.2 Hz), 1.89 (dd, *J* = 7.2, 1.8 Hz)

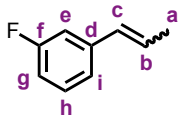

1-Fluoro-3-(1-propen-1-yl)benzene (3i)

Synthesis details: **GP-D**, **1e**, $HSi(p\text{-}CF_3\text{-}C_6H_4)_3$, substrate **2i**, crude *E*/*Z* ratio determined by GC = 21:1

Purification details: Column chromatography: silica, hexanes to give the product as a clear oil (51 mg, 0.37 mmol, 75% yield).

The major product isolated is the *E*-isomer, and the *Z*-isomer is seen in the NMR spectra as well. The ratio of these isomers determined by integration of H in the β-position was found to be 25:1 (*E/Z*). The *E*-product is fully characterized below, and the peaks visible and clearly assignable to the *Z*-isomer are given directly following the characterization of the *E*-product.

<u>*E*-product:</u>

^{1}H NMR (500 MHz, $CDCl_3$, 298 K): δ 7.22 (m, 1H, H_h), 7.07 (d, *J* = 7.8 Hz, 1H, H_i), 7.01 (dt, *J* = 10.4, 1.5 Hz, 1H, H_e), 6.87 (td, *J* = 8.5, 2.1 Hz, 1H, H_g), 6.36 (d, *J* = 15.8 Hz, 1H, H_c), 6.23 (dq, *J* = 15.8, 6.5 Hz, 1H, H_b), 1.88 (dd, *J* = 6.5, 0.8 Hz, 3H, H_a)

^{13}C{^{1}H} NMR (126 MHz, $CDCl_3$, 298 K): δ 163.3 (d, *J* = 244.6 Hz, C_f), 140.5 (d, *J* = 7.7 Hz, C_d), 130.2 (d, *J* = 2.7 Hz, C_c), 130.0 (d, *J* = 8.4 Hz, C_h), 127.4 (C_b), 121.8 (d, *J* = 2.7 Hz, C_i), 113.6 (d, *J* = 21.6 Hz, C_g), 112.4 (d, *J* = 21.7 Hz, C_e), 18.6 (C_a)

^{19}F NMR (471 MHz, $CDCl_3$, 298 K): δ -113.93 (m)

<u>*Z*-product:</u>

^{1}H NMR (500 MHz, $CDCl_3$, 298 K): δ 5.82 (dq, *J* = 11.6, 7.2 Hz)

^{13}C{^{1}H} NMR (126 MHz, $CDCl_3$, 298 K): δ 129.6 (d, *J* = 8.5 Hz), 129.0 (d, *J* = 2.3 Hz), 128.2, 124.7 (d, *J* = 2.8 Hz), 115.6 (d, *J* = 21.3 Hz), 113.4 (d, *J* = 21.4 Hz)

^{19}F NMR (471 MHz, $CDCl_3$, 298 K): δ -113.84 (m)

ASAP/HRMS (m/z): M^+ calculated for C_9H_9F 136.0688, found 136.0752

IR (ATR, neat) ν: 1608 (m), 1581 (m), 1141 (m), 958 (s), 767 (s), 680 (s) cm^{-1}

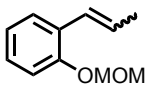

1-(Methoxymethoxy)-2-(1E)-1-propen-1-ylbenzene (3k)

<u>Synthesis details:</u> **GP-C**, **1e**, $HSi(4\text{-}CF_3\text{-}C_6H_4)_3$, substrate **2k**, crude *E*/*Z* ratio determined by GC = 15:1

Purification details: Column chromatography: silica, gradient eluent 0-4% Et2O/hexanes to give the product as a clear, yellow oil (51 mg, 0.29 mmol, 95% yield).
NMR spectra match values previously reported.[220]

The major product isolated is the *E*-isomer, and the *Z*-isomer is seen in the NMR spectra as well. The ratio of these isomers determined by integration of H in the β-position was found to be 33:1 (*E*/*Z*). The *E*-product is fully characterized below, and the peaks visible and clearly assignable to the *Z*-isomer are given directly following the NMR characterization of the *E*-product.

E-product:

^{1}H NMR (500 MHz, $CDCl_3$, 298 K): δ 7.41 (d, *J* = 7.6 Hz, 1H), 7.14 (t, *J* = 7.7 Hz, 1H), 7.06 (d, *J* = 8.2 Hz, 1H), 6.95 (t, *J* = 7.4 Hz, 1H), 6.73 (d, *J* = 15.8 Hz, 1H), 6.22 (dq, *J* = 15.8, 6.6 Hz, 1H), 5.19 (s, 2H), 3.48 (s, 3H), 1.90 (d, *J* = 6.6 Hz, 3H)

^{13}C{^{1}H} NMR (126 MHz, $CDCl_3$, 298 K): δ 154.0, 128.0, 127.9, 126.6, 126.5, 125.6, 122.1, 115.0, 94.93, 56.2, 19.0

Z-product:

^{1}H NMR (500 MHz, $CDCl_3$, 298 K): δ 7.27 (d, *J* = 7.5 Hz), 7.19 (t, *J* = 7.9 Hz), 6.55 (d, *J* = 11.4 Hz), 5.83 (dq, *J* = 11.5, 7.0 Hz), 3.47 (s), 1.83 (d, *J* = 7.0 Hz)

^{13}C{^{1}H} NMR (126 MHz, $CDCl_3$, 298 K): δ 154.9, 130.4, 128.1, 127.1, 125.4, 121.5, 114.8, 94.86, 14.7

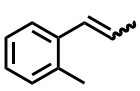

1-(2-Methylphenyl)-1-propene (3l)

Synthesis details: **GP-B**, **1a**, $HSiPh_3$, substrate **2l**, crude *E*/*Z* ratio determined by GC = 8:1

Purification details: Column chromatography: silica, hexanes to give the product as a clear oil (42 mg, 0.32 mmol, 64% yield).

NMR spectra match values previously reported.[217]

The major product isolated is the *E*-isomer, and the *Z*-isomer is seen in the NMR spectra as well. The ratio of these isomers determined by integration of H in the β-position was found to be 33:1 (*E/Z*). The *E*-product is fully characterized below, and the peaks visible and clearly assignable to the *Z*-isomer are given directly following the NMR characterization of the *E*-product.

<u>*E*-product:</u>

^{1}H NMR (500 MHz, $CDCl_3$, 298 K): δ 7.38 (d, *J* = 7.2 Hz, 1H), 7.16-7.04 (ms, 3H), 6.58 (d, *J* = 15.6 Hz, 1H), 6.09 (dq, *J* = 15.6, 6.7 Hz, 1H), 2.32 (s, 3H), 1.89 (d, *J* = 6.5, 1.1 Hz, 3H)

^{13}C{^{1}H} NMR (126 MHz, $CDCl_3$, 298 K): δ 137.2, 134.9, 130.3, 129.0, 127.1, 126.8, 126.1, 125.6, 19.9, 18.9

<u>*Z*-product:</u>

^{1}H NMR (500 MHz, $CDCl_3$, 298 K): δ 6.45 (d, *J* = 11.5 Hz), 5.81 (dq, *J* = 11.5, 7.0 Hz), 2.24 (s), 1.73 (d, *J* = 7.0 Hz)

^{13}C{^{1}H} NMR (126 MHz, $CDCl_3$, 298 K): δ 129.9, 129.2, 125.4, 22.8, 14.5

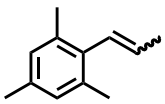

1,3,5-Trimethyl-2-(1-propen-1-yl)benzene (3m)

<u>Synthesis details:</u> **GP-B**, **1e**, $HSiPh_3$, substrate **2m**, crude *E*/*Z* ratio determined by GC = 1.4:1

<u>Purification details:</u> Silica plug with hexanes to give the product as a clear oil (77 mg, 0.48 mmol, 96% yield).

NMR spectra match values previously reported.[217]

The ratio of the *E*- and *Z*-isomers, determined by integration of H in the β-position, was found to be 1.4:1 (*E/Z*). The *E*-product is fully characterized below, and the peaks visible and clearly assignable to

the *Z*-isomer are given directly following the NMR characterization of the *E*-product.

E-product:

^{1}H NMR (600 MHz, $CDCl_3$, 298 K): δ 6.84 (s, 2H), 6.34-6.23 (ms, 1.7H, both isomers), 5.65 (dq, *J* = 16.1, 6.5 Hz, 1H), 2.25 (s, 9H), 1.89 (d, *J* = 6.3 Hz, 3H)

^{13}C{^{1}H} NMR (151 MHz, $CDCl_3$, 298 K): δ 136.1, 136.0, 135.7, 134.9, 130.2, 128.52, 21.02, 21.00, 19.0

Z-product:

^{1}H NMR (600 MHz, $CDCl_3$, 298 K): δ 6.85 (s), 5.81 (dq, *J* = 11.2, 6.7 Hz), 2.27 (s), 2.16 (s), 1.45 (d, *J* = 6.7 Hz)

^{13}C{^{1}H} NMR (151 MHz, $CDCl_3$, 298 K): δ 135.9, 133.7, 128.50, 127.9, 127.4, 21.1, 20.3

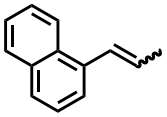

1-(1-Propen-1-yl)naphthalene (3n)

Synthesis details: **GP-B**, **1a**, $HSi(p\text{-}CF_3\text{-}C_6H_4)_3$, substrate **2n**, crude *E*/*Z* ratio determined by GC = 8:1

Purification details: Column chromatography: silica, hexanes to give the product as a clear oil (65 mg, 0.39 mmol, 77% yield).

NMR spectra match values previously reported.[221]

The major product isolated is the *E*-isomer, and the *Z*-isomer and the starting material **2n** are seen in the NMR spectra as well. The ratio of these isomers determined by integration of H in the β-position was found to be 8:1 (*E*/*Z*) and <3% **2n**. The *E*-product is fully characterized below, and the peaks visible and clearly assignable to the *Z*-isomer are given directly following the NMR characterization of the *E*-product.

E-product:

^{1}H NMR (500 MHz, $CDCl_3$, 298 K): δ 8.11 (d, *J* = 8.1 Hz, 1H), 7.81 (d, *J* = 7.8 Hz, 1H), 7.71 (d, *J* = 8.1 Hz, 1H), 7.52 (d, *J* = 7.1 Hz, 1H), 7.46 (pd, *J* = 7.2, 1.8 Hz, 2H), 7.40 (t, *J* = 7.7 Hz, 1H), 7.12 (d, *J* = 15.5 Hz, 1H), 6.22 (dq, *J* = 15.5, 6.7 Hz, 1H), 1.98 (dd, *J* = 6.6, 1.4 Hz, 3H)

^{13}C{^{1}H} NMR (126 MHz, $CDCl_3$, 298 K): δ 135.9, 133.8, 131.2, 129.1, 128.6, 128.4, 127.3, 125.9, 125.8, 125.7, 124.1, 123.6, 19.1

Z-product:

^{1}H NMR (500 MHz, $CDCl_3$, 298 K): δ 7.34 (d, *J* = 7.0 Hz), 6.89 (d, *J* = 11.4 Hz), 6.03 (dq, *J* = 11.4, 7.0 Hz), 1.73 (dd, *J* = 7.0, 1.5 Hz)

^{13}C{^{1}H} NMR (126 MHz, $CDCl_3$, 298 K): δ 134.7, 132.0, 128.7, 128.5, 128.0, 127.2, 126.6, 125.4, 125.2, 14.8

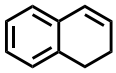

1,2-dihydronaphthalene (3o)

Synthesis details: **GP-B**, catalyst **1e**, $HSi(4\text{-}CF_3\text{-}C_6H_4)_3$, substrate 1,4-dihydronaphthalene **2o** (commercial)

Purification details: Column chromatography: silica, hexanes to give the product as a clear oil (44 mg, 0.34 mmol, 68% yield).

NMR spectra match values previously reported.[222]

The major product isolated is 1,2-dihydronaphthalene. The starting material contained 10% naphthalene, and the isolated product contains 8% naphthalene along with remaining <2% **2o**. The peaks listed below correspond to the desired product, 1,2-dihydronaphthalene.

^{1}H NMR (500 MHz, $CDCl_3$, 289 K): δ 7.18-7.05 (ms, 3H), 7.01 (d, *J* = 6.8 Hz, 1H), 6.45 (d, *J* = 9.4 Hz, 1H), 6.02 (m, 1H), 2.79 (t, *J* = 8.2 Hz, 2H), 2.30 (m, 2H).

^{13}C NMR (126 MHz, $CDCl_3$, 298 K): δ 135.6, 134.3, 128.8, 127.9, 127.6, 127.0, 126.6, 126.0, 27.6, 23.3

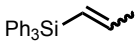

(1-Propen-1-yl)triphenylsilane (3p)

Synthesis details: **GP-E**, **1e**, $HSi(p\text{-}CF_3\text{-}C_6H_4)_3$, substrate **2p**

Purification details: Column chromatography: silica, hexanes to separate product from remaining starting material. Product was recrystallized out of EtOH in the freezer to yield white crystals (51 mg, 0.17 mmol, 34% yield).

NMR spectra match values previously reported.[30]

The major product isolated is the *E*-isomer, and the *Z*-isomer is seen in the NMR spectra as well. The ratio of these isomers determined by integration of methyl group was found to be 30:1 (*E/Z*). The *E*-product is fully characterized below, and the peaks visible and clearly assignable to the *Z*-isomer are given directly following the NMR characterization of the *E*-product.

E-product:

^{1}H NMR (500 MHz, $CDCl_3$, 298 K): δ 7.59 (d, J = 7.1 Hz, 6H), 7.50-7.39 (ms, 9H), 6.32-6.20 (ms, 2H), 1.99 (d, J = 4.3 Hz, 3H)

$^{13}C\{^1H\}$ NMR (151 MHz, $CDCl_3$, 298 K): δ 148.5, 136.1, 135.1, 129.5, 127.9, 125.3, 23.1

Z-product:

^{1}H NMR (500 MHz, $CDCl_3$, 298 K): δ 7.64 (d, J = 7.0 Hz), 1.68 (d, J = 6.8 Hz)

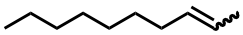

2-Decene (3q)

Synthesis details: **GP-B**, **1a**, $HSiPh_3$, substrate **2q**

Purification details: Column chromatography: silica, pentane to give the product as a clear liquid (57 mg, 0.41 mmol, 81% yield).

NMR spectra match values previously reported.[223–226]

The major product isolated is (*E*)-2-decene, and the *Z*-isomer, other internal isomers, and starting material **2q** are seen in the NMR spectra as well. The ratio of 2-decene isomers, determined by integration of H in the terminal methyl group was found to be 12:1 (*E/Z*) and ~9% **2q**. The *E*-product is fully characterized below, and the peaks visible and clearly assignable to the *Z*-isomer are given directly following the NMR characterization of the *E*-product.

<u>*E*-product:</u>

^{1}H NMR (500 MHz, $CDCl_3$, 298 K): δ 5.46-5.33 (ms, 2H), 1.64 (d, *J* = 3.9 Hz), 1.41-1.20 (ms, 12H), 0.88 (t, *J* = 6.7 Hz)

$^{13}C\{^{1}H\}$ NMR (151 MHz, $CDCl_3$, 298 K): δ 131.9, 124.7, 32.8, 32.1, 29.8, 29.39, 29.35, 22.9, 18.1, 14.3

<u>*Z*-product:</u>

^{1}H NMR (500 MHz, $CDCl_3$, 298 K): δ 1.60 (d, *J* = 6.2 Hz), 0.96 (t, *J* = 7.4 Hz)

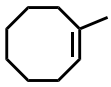

***Cis*-1-methylcyclooctene (3r)**

<u>Synthesis details:</u> **GP-B**, catalyst **1e**, $HSi(4\text{-}CF_3\text{-}C_6H_4)_3$, substrate **2r**

<u>Purification details:</u> Column chromatography: silica, hexanes to give the product as a clear liquid (32 mg, 0.26 mmol, 52% yield). NMR spectra match values previously reported.[227]

^{1}H NMR (500 MHz, $CDCl_3$, 289 K): δ 5.34 (t, *J* = 8.0 Hz, 1H), 2.13 (m, 2H), 2.06 (br s, 2H), 1.68 (s, 3H), 1.55-1.42 (ms, 8H)

^{13}C NMR (126 MHz, CDCl3, 298 K): δ 137.1, 124.3, 30.5, 30.4, 28.2, 26.8, 26.7, 26.4, 23.6

ASAP/HRMS (m/z): M^+ calculated for C_9H_{16} 124.1252, found 124.1229

IR (ATR, neat) ν: 2920 (s), 2848 (m), 1444 (m), 818 (m) cm^{-1}

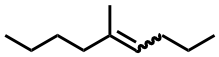

5-Methyl-4-nonene (3s)

Synthesis details: **GP-B**, catalyst **1e**, $HSi(4\text{-}CF_3\text{-}C_6H_4)_3$, substrate **2s**

Purification details: Column chromatography: silica, hexanes to give the product as a clear liquid (22 mg, 0.16 mmol, 31% yield). NMR spectra match values previously reported.[228]

The major product isolated is the *E*-isomer, and the *Z*-isomer is seen in the NMR spectra as well. The ratio of these isomers determined by integration of the branched CH_3 methyl group was found to be 2:1 (*E*/*Z*). The peaks visible and clearly assignable to each isomer are given below. We also observed ~4% formation of 5-methyl-3-nonene, characterized by the peaks at 5.40 ppm and 5.25 ppm in the ^1H NMR spectrum, according to values previously reported.[229]

E-product:

^1H NMR (500 MHz, $CDCl_3$, 289 K): δ 5.12 (t, J = 6.8 Hz, 1H), 1.58 (s, 3H)

^{13}C NMR (126 MHz, $CDCl_3$, 298 K): δ 135.5, 124.5, 39.6, 31.7, 30.4, 30.2, 23.2, 22.5, 14.17, 13.96

Z-product:

^1H NMR (500 MHz, $CDCl_3$, 289 K): δ 1.67 (s, 1.5 H)

^{13}C NMR (126 MHz, $CDCl_3$, 298 K): δ 135.7, 125.2, 30.5, 30.1, 23.6, 23.4, 22.9, 14.23, 14.05

ASAP/HRMS (m/z): $[M+H]^+$ calculated for $C_{10}H_{21}$ 141.1638, found 141.1595

IR (ATR, neat) ν: 2956 (s), 2926 (s), 2860 (m), 1456 (m) cm^{-1}

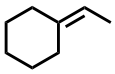

Ethylidenecyclohexane (3t)

Synthesis details: **GP-B**, **1e**, $HSi(p\text{-}CF_3\text{-}C_6H_4)_3$, substrate **2t**. After dilution of the quenched reaction mixture with hexanes, a stock solution of **S9** (0.19 M in hexanes) using volumetric glassware was prepared. A portion of this stock solution (0.40 mL, 0.076 mmol) was added to the reaction mixture using a 250-μL microliter syringe. The crude reaction mixture was then filtered through a short silica plug with hexanes. A portion (0.5 mL) of this filtered reaction mixture and $CDCl_3$ (0.2 mL) was added to an NMR tube, and a ^1H NMR spectrum was recorded.

NMR spectra match values previously reported.[230]

^1H NMR (500 MHz, $CDCl_3$, 298 K): δ 5.11 (q, J = 6.7 Hz, 1H), other peaks obscured by hexanes

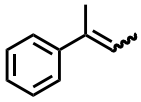

α,β-dimethylstyrene (3v)

Synthesis details: **GP-B**, **1a**, $HSi(p\text{-}CF_3\text{-}C_6H_4)_3$, substrate **2v**, crude *E*/*Z* ratio determined by GC = 4:1

Purification details: Column chromatography: silica, pentane to give the product as a clear oil (48 mg, 0.36 mmol, 73% yield).

NMR spectra match values previously reported.[231]

The major product isolated is the *E*-isomer, and the *Z*-isomer and the starting material **3v** are seen in the NMR spectra as well. The ratio of these isomers determined by integration of H in the β-position was found to be 7.7:1 (*E*/*Z*) and <4% **3v**. The *E*-product is fully characterized below, and the peaks visible and clearly assignable to the *Z*-isomer are given directly following the NMR characterization of the *E*-product.

E-product:

^{1}H NMR (600 MHz, $CDCl_3$, 298 K): δ 7.36 (d, *J* = 7.7 Hz, 2H), 7.29 (t, *J* = 7.6 Hz, 2H), 7.20 (t, *J* = 7.2 Hz, 1H), 5.86 (q, *J* = 6.7 Hz, 1H), 2.02 (br s, 3H), 1.79 (d, *J* = 6.7 Hz, 3H)

^{13}C{^{1}H} NMR (151 MHz, $CDCl_3$, 298 K): δ 144.2, 135.6, 128.3, 126.5, 125.7, 122.6, 15.6, 14.5

Z-product:

^{1}H NMR (600 MHz, $CDCl_3$, 298 K): δ 5.56 (q, *J* = 6.9 Hz), 1.59 (dd, *J* = 6.9, 1.1 Hz).

^{13}C{^{1}H} NMR (151 MHz, $CDCl_3$, 298 K): δ 142.0, 136.9, 128.21, 128.15, 121.7, 25.5, 15.0

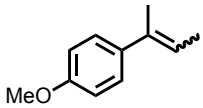

1-Methoxy-4-(1-methyl-1-propen-1-yl)benzene (3w)

Synthesis details: **GP-B**, **1e**, $HSiPh_3$, substrate **2w**, crude *E*/*Z* ratio determined by GC = 4:1

Purification details: Column chromatography: silica, gradient eluent 0-5% DCM/hexanes to give the product as a clear oil (62 mg, 0.38 mmol, 76% yield).

NMR spectra match values previously reported.[232] Only the *E*-isomer is observed by NMR after purification.

^{1}H NMR (500 MHz, $CDCl_3$, 298 K): δ 7.30 (d, *J* = 8.7 Hz, 2H), 6.84 (d, *J* = 8.7 Hz, 2H), 5.78 (q, *J* = 6.7 Hz, 1H), 3.79 (s, 3H), 2.00 (s, 3H), 1.78 (d, *J* = 6.7 Hz, 3H)

^{13}C{^{1}H} NMR (151 MHz, $CDCl_3$, 298 K): δ 158.4, 136.8, 134.9, 126.6, 121.0, 113.6, 55.4, 15.6, 14.4

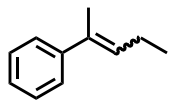

2-Phenyl-2-pentene (3x)

Synthesis details: **GP-B**, **1e**, $HSi(p\text{-}CF_3\text{-}C_6H_4)_3$, substrate **2x**, crude *E*/*Z* ratio determined by GC = 5:1

Purification details: Column chromatography: silica, cyclohexanes to give the product as a clear oil (33 mg, 0.23 mmol, 45% yield). NMR spectra match values previously reported.[233]

The major product isolated is the *E*-isomer, and the *Z*-isomer and the starting alkene **2x** are seen in the NMR spectra as well. The ratio of these isomers determined by integration of H in the β-position was found to be 25:1 (*E/Z*) and <4% **2x**. The *E*-product is fully characterized below, and the peaks visible and clearly assignable to the *Z*-isomer are given directly following the NMR characterization of the *E*-product.

E-product:

^{1}H NMR (500 MHz, $CDCl_3$, 298 K): δ 7.38 (d, *J* = 7.7 Hz, 2H), 7.29 (t, *J* = 7.6 Hz, 2H), 7.20 (t, *J* = 7.2 Hz, 1H), 5.77 (t, *J* = 7.1 Hz, 1H), 2.20 (pent, *J* = 7.5 Hz, 2H), 2.02 (s, 3H), 1.05 (t, *J* = 7.5 Hz, 3H)

^{13}C{^{1}H} NMR (126 MHz, $CDCl_3$, 298 K): δ 144.1, 134.2, 130.4, 128.3, 126.6, 125.7, 22.2, 15.7, 14.2

Z-product:

^{1}H NMR (500 MHz, $CDCl_3$, 298 K): δ 5.45 (t, *J* = 7.2 Hz)

^{13}C{^{1}H} NMR (126 MHz, $CDCl_3$, 298 K): δ 129.7, 128.14, 128.09, 25.6, 22.6, 14.8

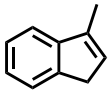

1-Methylindene (3y)

Synthesis details: **GP-B**, **1e**, $HSi(p\text{-}CF_3\text{-}C_6H_4)_3$, substrate **2y**.

Purification details: Column chromatography: silica, hexanes to give the product as a clear oil (51 mg, 0.39 mmol, 78% yield)

NMR spectra match values previously reported.[234]

^{1}H NMR (500 MHz, $CDCl_3$, 298 K): δ 7.43 (d, *J* = 7.4 Hz, 1H), 7.35-7.26 (ms, 2H), 7.19 (t, *J* = 7.3 Hz, 1H), 6.18 (s, 1H), 3.29 (br s, 2H), 2.16 (d, *J* = 1.4 Hz, 3H)

^{13}C{^{1}H} NMR (126 MHz, $CDCl_3$, 298 K): 146.2, 144.5, 140.1, 128.9, 126.2, 124.6, 123.7, 119.0, 37.8, 13.2

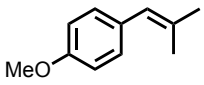

1-(4-Methoxyphenyl)-2-methyl-1-propene (3z)

Synthesis details: **GP-B**, **1e**, $HSiPh_3$, substrate **2z**

Purification details: Column chromatography: silica, gradient eluent 0-2% DCM/hexanes to give the product as a clear oil that is 87% product, 13% starting alkene (69 mg, 0.43 mmol, 85% yield of mixture, 74% yield of **3z**).

NMR spectra match values previously reported.[235]

^{1}H NMR (500 MHz, $CDCl_3$, 298 K): δ 7.15 (d, *J* = 8.6 Hz, 2H), 6.85 (d, *J* = 8.6 Hz, 2H), 6.20 (s, 1H), 3.78 (s, 3H), 1.88 (s, 3H), 1.84 (s, 3H)

^{13}C{^{1}H} NMR (126 MHz, $CDCl_3$, 298 K): δ 157.8, 134.0, 131.5, 129.9, 124.7, 113.6, 55.3, 26.9, 19.4

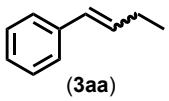
(**3aa**)

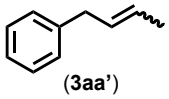
(**3aa'**)

1-buten-1-ylbenzene (3aa)

Synthesis details: **GP-B**, **1e**, $HSiPh_3$, substrate **2aa**, crude ratio of products determined by GC = 38:1:9:2 (***E*-3aa**/***Z*-3aa**/***E*-3aa'**/***Z*-3aa'**)

Purification details: Silica plug with pentane to give the product as a clear oil that is a mixture of 87:13 **3aa**/2-buten-1-ylbenzene (**3aa'**) (44 mg, 0.33 mmol, 67% yield of mixture, 58% yield **3aa**, 8.7% yield **3aa'**).

NMR spectra match values previously reported.[45,236]

The major product isolated is ***E*-3aa**, which is fully characterized below. ***Z*-3aa** was not clearly identifiable in the NMR spectra. The

peaks visible and clearly assignable to **3aa'** are given directly following the NMR characterization of **3aa**.

^{1}H NMR (500 MHz, $CDCl_3$, 298 K): δ 7.39 (d, *J* = 7.6 Hz, 2H), 7.33 (t, *J* = 7.6 Hz, 2H), 7.23 (m, 2H), 6.43 (d, *J* = 15.9 Hz, 1H), 6.32 (dt, *J* = 15.9, 6.4 Hz, 1H), 2.28 (pent, *J* = 7.1 Hz, 2H), 1.14 (t, *J* = 7.4 Hz, 3H)

^{13}C{^{1}H} NMR (151 MHz, $CDCl_3$, 298 K): δ 138.1, 132.8, 128.9, 128.6, 126.9, 126.0, 26.2, 13.8

E-2-buten-1-ylbenzene

^{1}H NMR (500 MHz, $CDCl_3$, 298 K): δ 3.37 (d, *J* = 6.3 Hz), 1.74 (d, *J* = 5.9 Hz)

^{13}C{^{1}H} NMR (151 MHz, $CDCl_3$, 298 K): δ 141.2, 136.6, 136.0, 128.5, 128.2, 126.5, 39.2, 18.0

Z-2-buten-1-ylbenzene

^{1}H NMR (500 MHz, $CDCl_3$, 298 K): δ 3.46 (d, *J* = 4.7 Hz), 1.77 (d, *J* = 4.5 Hz)

^{13}C{^{1}H} NMR (151 MHz, $CDCl_3$, 298 K): δ 135.3, 134.9, 130.2, 130.0, 127.8, 126.0

1,3-Cyclooctadiene (3ab)

Synthesis details: **GP-B**, **1a**, $HSiPh_3$, substrate **2ab**

Purification details: Column chromatography: silica, pentane to give the product as a clear liquid (42 mg, 0.39 mmol, 78% yield). NMR spectra match values from commercial material.

^{1}H NMR (500 MHz, $CDCl_3$, 298 K): δ 5.81 (d, *J* = 10.5 Hz, 2H), 5.62 (m, 2H), 2.18 (br s, 4H), 1.51 (m, 4H)

^{13}C{^{1}H} NMR (151 MHz, $CDCl_3$, 298 K): δ 131.4, 126.1, 28.2, 23.3

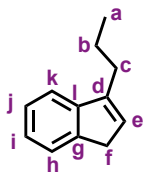

3-Propyl-1*H*-indene (3ac)

Synthesis details: **GP-B**, **1e**, HSi(p-CF_3-C_6H_4)$_3$, substrate **2ac**

Purification details: Column chromatography: silica, hexanes to give the product as a pale yellow oil (73 mg, 0.46 mmol, 92% yield).

^{1}H NMR (500 MHz, $CDCl_3$, 298 K): δ 7.43 (d, J = 7.4 Hz, 1H, H_k), 7.35 (d, J = 7.5 Hz, 1H, H_h), 7.27 (t, J = 7.4 Hz, 1H H_i), 7.17 (t, J = 7.3 Hz, 1H, H_j), 6.17 (br s, 1H, H_e), 3.29 (br s, 2H, H_f), 2.51 (t, J = 7.1 Hz, 2H, H_c), 1.70 (app sext, J = 7.3 Hz, 2H, H_b), 1.00 (t, J = 7.3 Hz, 3H, H_a)

^{13}C{^{1}H} NMR (151 MHz, $CDCl_3$, 298 K): δ 145.8 (C_l), 144.7 ($C_{d\ or\ g}$), 144.6 ($C_{d\ or\ g}$), 127.8 (C_e), 126.1 (C_i), 124.5 (C_j), 123.8 (C_k), 119.1 (C_h), 37.8 (C_f), 30.0 (C_c), 21.4 (C_b), 14.3 (C_a)

ASAP/HRMS (m/z): $[M+H]^+$ calculated for $C_{12}H_{15}$ 159.1168, found 159.1167

IR (ATR, neat) ν: 1680 (w), 1460 (m), 963 (m), 769 (s), 718 (s) cm^{-1}

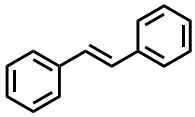

***trans*-Stilbene (3ad)**

Synthesis details: **GP-B**, **1e**, HSi(p-CF_3-C_6H_4)$_3$, substrate **2ad**

Purification details: Column chromatography: silica, hexanes to give the product as a white solid (91 mg, 0.50 mmol, >99% yield). NMR spectra match values from commercial material and values previously reported.[237]

^{1}H NMR (500 MHz, $CDCl_3$, 298 K): δ 7.52 (d, J = 7.6 Hz, 4H), 7.36 (t, J = 7.6 Hz, 4H), 7.26 (m, overlapping with $CHCl_3$, 2H), 7.11 (s, 2H)

^{13}C{^{1}H} NMR (151 MHz, $CDCl_3$, 298 K): δ 137.4, 128.8, 127.8, 126.6

e. Isomerization of 4-phenyl-2-butene (XX) and Regioconvergent Isomerization

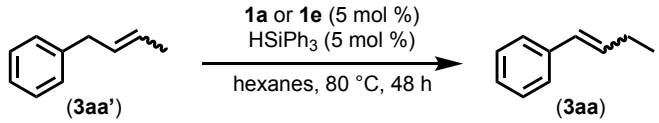

GP-B (catalyst **1a** or **1e**, $HSiPh_3$, substrate **3aa'**) was followed to generate **3aa**. Reaction progress was monitored by removal of aliquots (5 µL), which were filtered through Celite and analyzed by GC. After 48 h, the reaction composition was steady, so the reactions were quenched by cooling in a liquid N_2 bath, opened to air, and diluted with hexanes. A stock solution of **S11** (0.6 M) was prepared and distributed (0.2 mL, 0.13 mmol) to each vial. The reaction mixtures were filtered through short silica plugs with hexanes and concentrated under reduced pressure. The reaction yield of **3aa** was determined via integration against **S11**. NMR spectra match values previously reported.[45,236]

Results are summarized in **Table A.**, entry 29.

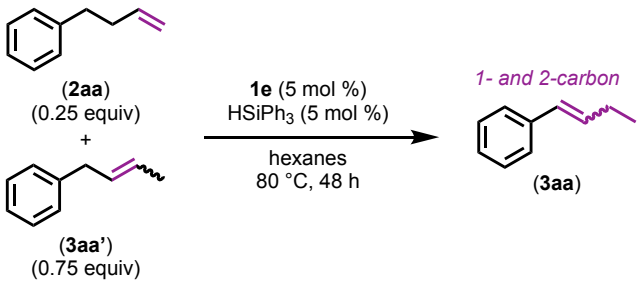

GB-B (catalyst **1e**, $HSiPh_3$, substrates **2aa**, **3aa'**) was followed to generate **3aa**. Reaction progress was monitored by removal of aliquots (5 µL), which were filtered through Celite and analyzed by GC. After 48 h, the reaction composition was steady, so the reaction was quenched by cooling in a liquid N_2 bath, opening to air, and diluting with hexanes. A stock solution of **S11** (0.6 M) was prepared and distributed (0.2 mL, 0.13 mmol) to the vial. The reaction mixture was filtered through short silica plugs with hexanes and concentrated under reduced pressure. The final reaction yield of **3aa** was determined via integration against **S11** in the ^1H NMR spectrum. NMR spectra match values previously reported.[45,236]

Results of GC monitoring are summarized in **Table A.2.** The conversion of **2aa** is 96%.

Table A.2. Results of regioconvergent isomerization. Percentages are calculated based on total mmol of alkene present in the reaction.

Entry	*Time (h)*	*% **2aa***	*% **3aa'***	*% **3aa***
1	14.5	2	46	52
2	23	1	33	65
3	47	1	23	75

f. Catalyst/Silane Combination Screening

Table A.3. Screening of different conditions for isomerization.

Entry	*Substrate*	*Ni complex (mol %)*	*Silane (mol %)*	*Rxn time (h)*	*Rxn T (°C)*	*Rxn scale (mmol)*	*GC conv. to **3** (%)*	*GC E/Z ratio*
1	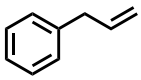 **2a**	**1a** (5 mol %)	$HSiPh_3$ (5 mol %)	16	80	0.5	98	20:1
2	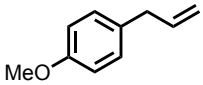 **2b**	**1a** (5 mol %)	$HSiPh_3$ (5 mol %)	16	80	0.5	98	18:1
3	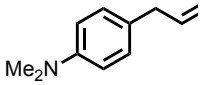 **2c**	**1a** (5 mol %)	$HSiPh_3$ (5 mol %)	16	80	0.5	>98	15:1
4	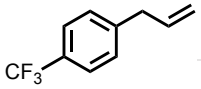 **2d**	**1a** (5 mol %)	$HSiPh_3$ (5 mol %)	16	80	0.5	84	27:1
		1a (5 mol %)	$HSiPh_3$ (5 mol %)	16	80	0.3	98	23:1
5	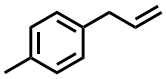 **2e**	**1a** (5 mol %)	$HSiPh_3$ (5 mol %)	16	80	0.5	92	21:1
		1a (5 mol %)	$HSiPh_3$ (5 mol %)	16	80	0.3	98	18:1
6	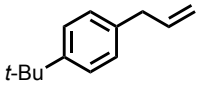 **2f**	**1a** (5 mol %)	$HSiPh_3$ (5 mol %)	16	80	0.5	97	19:1
7	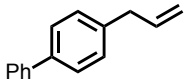 **2g**	**1a** (5 mol %)	$HSiPh_3$ (5 mol %)	16	80	0.5	95	17:1
8	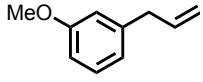 **2h**	**1a** (5 mol %)	$HSiPh_3$ (5 mol %)	16	80	0.5	97	22:1
9		**1a** (5 mol %)	$HSiPh_3$ (5 mol %)	16	80	0.5	81	23:1

		1a (5 mol %)	$HSiPh_3$ (5 mol %)	16	80	0.3	80	22:1
		1e (5 mol %)	HSi(4-CF_3-C_6H_4)$_3$ (5 mol %)	16	80	0.5	96	21:1
	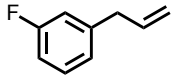 **2i**	**1e** (2 mol %)	HSi(4-CF_3-C_6H_4)$_3$ (2 mol %)	16	80	0.5	77	13:1
		1e (2 mol %)	HSi(4-CF_3-C_6H_4)$_3$ (5 mol %)	16	80	0.5	98	21:1
10	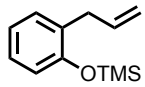 **2j**	**1e** (5 mol %)	$HSiPh_3$ (5 mol %)	16	80	0.5	32	10:1
		1e (5 mol %)	HSi(4-CF_3-C_6H_4)$_3$ (5 mol %)	16	80	0.5	98	14:1
11	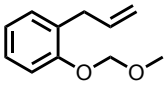 **2k**	**1e** (5 mol %)	HSi(4-CF_3-C_6H_4)$_3$ (5 mol %)	16	80	0.5	99	15:1
12	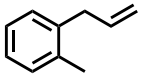 **2l**	**1a** (5 mol %)	$HSiPh_3$ (5 mol %)	16	80	0.5	75	9:1
		1e (2 mol %)	HSi(4-CF_3-C_6H_4)$_3$ (5 mol %)	16	80	0.5	76	4:1
		1e (5 mol %)	$HSiPh_3$ (5 mol %)	16	80	0.5	99	8:1
13	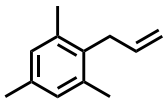 **2m**	**1a** (5 mol %)	$HSiPh_3$ (5 mol %)	16	80	0.5	39	1.7:1
		1e (5 mol %)	$HSiPh_3$ (5 mol %)	16	80	0.5	99	1.4:1
14	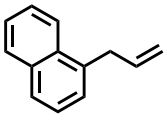 **2n**	**1e** (5 mol %)	$HSiPh_3$ (5 mol %)	16	80	0.5	72[a]	See note
		1a (5 mol %)	HSi(4-CF_3-C_6H_4)$_3$ (5 mol %)	16	80	0.5	83[a]	See note
15	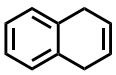 **2o**	**1e** (5 mol %)	HSi(4-CF_3-C_6H_4)$_3$ (5 mol %)	16	80	0.5	95	n/a

16	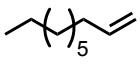 **2q**	**1a** (5 mol %)	$HSiPh_3$ (5 mol %)	16	80	0.5	90[b]	
		1a (10 mol %)	$HSiPh_3$ (10 mol %)	16	90	0.5	~98 [c]	
17	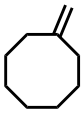 **2r**	**1e** (5 mol %)	HSi(4-CF_3-C_6H_4)$_3$ (5 mol %)	16	80	0.5	>99	n/a
18	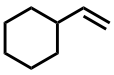 **2t**	**1e** (5 mol %)	HSi(4-CF_3-C_6H_4)$_3$ (5 mol %)	16	80	0.5	73	n/a
19	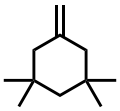 **2u**	**1a** (5 mol %)	$HSiPh_3$ (5 mol %)	16	80	0.5	15	n/a
		1a (5 mol %)	$HSiPh_3$ (5 mol %)	48	80	0.5	41	n/a
		1e (5 mol %)	$HSiPh_3$ (5 mol %)	16	80	0.5	8	n/a
		1e (5 mol %)	HSi(4-CF_3-C_6H_4)$_3$ (5 mol %)	16	80	0.5	24	n/a
20	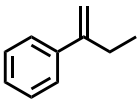 **2v**	**1a** (5 mol %)	$HSiPh_3$ (5 mol %)	16	80	0.5	78	8:1
		1e (5 mol %)	$HSiPh_3$ (5 mol %)	16	80	0.5	94	4:1
		1a (5 mol %)	HSi(4-CF_3-C_6H_4)$_3$ (5 mol %)	16	80	0.5	93	4:1
		1a (10 mol %)	HSi(4-CF_3-C_6H_4)$_3$ (10 mol %)	16	90	0.5	92	4:1
21	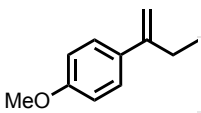 **2w**	**1a** (5 mol %)	$HSiPh_3$ (5 mol %)	16	80	0.5	58	8:1
		1e (5 mol %)	$HSiPh_3$ (5 mol %)	16	80	0.5	94	4:1
		1e (5 mol %)	$HSiPh_3$ (5 mol %)	16	70	0.5	81	14:1

		1a (5 mol %)	HSi(4-CF_3-C_6H_4)$_3$ (5 mol %)	16	80	0.5	85	6:1
		1e (5 mol %)	HSi(4-CF_3-C_6H_4)$_3$ (5 mol %)	16	80	0.5	95	3:1
		1e (10 mol %)	$HSiPh_3$ (10 mol %)	16	90	0.5	94	3:1
22	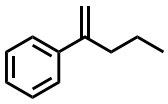 **2x**	**1a** (5 mol %)	$HSiPh_3$ (5 mol %)	16	80	0.5	69	5:1
		1e (5 mol %)	$HSiPh_3$ (5 mol %)	16	80	0.5	77	10:1
		1a (5 mol %)	HSi(4-CF_3-C_6H_4)$_3$ (5 mol %)	16	80	0.5	77	7:1
		1e (5 mol %)	HSi(4-CF_3-C_6H_4)$_3$ (5 mol %)	16	80	0.5	92	5:1
		1e (10 mol %)	HSi(4-CF_3-C_6H_4)$_3$ (10 mol %)	16	90	0.5	92	3:1
23	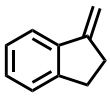 **2y**	**1e** (5 mol %)	HSi(4-CF_3-C_6H_4)$_3$ (5 mol %)	16	80	0.5	>99	n/a
24	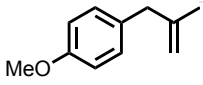 **2z**	**1a** (5 mol %)	$HSiPh_3$ (5 mol %)	16	80	0.5	35	n/a
		1e (5 mol %)	$HSiPh_3$ (5 mol %)	16	80	0.5	86	n/a
		1e (5 mol %)	HSi(4-CF_3-C_6H_4)$_3$ (5 mol %)	16	80	0.5	70	n/a
		1e (10 mol %)	$HSiPh_3$ (10 mol %)	16	90	0.5	85	n/a
25	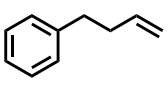	**1a** (5 mol %)	HSi(4-CF_3-C_6H_4)$_3$	16	80	0.5	77[d]	39:1

	2aa		(5 mol %)					
		1e (5 mol %)	$HSiPh_3$ (5 mol %)	16	80	0.5	98[e]	33:1
		1e (5 mol %)	HSi(4-CF_3-C_6H_4)$_3$ (5 mol %)	16	80	0.5	93[f]	35:1
26	 **2ab**	**1a** (5 mol %)	$HSiPh_3$ (5 mol %)	16	80	0.5	99	n/a
27	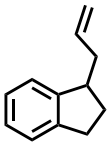 **2ac**	**1a** (5 mol %)	$HSiPh_3$ (5 mol %)	16	80	0.5	47	n/a
		1e (5 mol %)	HSi(4-CF_3-C_6H_4)$_3$ (5 mol %)	16	80	0.5	98	n/a
28	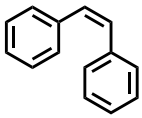 **2ad**	**1a** (5 mol %)	$HSiPh_3$ (5 mol %)	16	80	0.5	95	18:1
		1e (5 mol %)	$HSiPh_3$ (5 mol %)	16	80	0.5	98	59:1
29	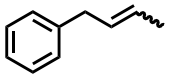 **3aa'**	**1a** (5 mol %)	$HSiPh_3$ (5 mol %)	48	80	0.5	84[g]	1:2
		1e (5 mol %)	$HSiPh_3$ (5 mol %)	48	80	0.5	68[g]	1:2

The GC conversions for the following substrates are not reported above due to overlap between starting material and product:

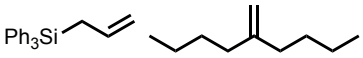

[a] Conversion reported for ***E*-3n** because ***Z*-3n** overlaps with remaining **2n**
[b] Conversion of **2q** reported, r.r. = 4.9:1 for 2-decene:other internal isomers
[c] Conversion of **2q** reported, r.r. = 1:2.3 for 2-decene: other internal isomers
[d] Conversion of **2aa** reported, r.r = 3:1 for **3aa':3aa,** *E/Z* ratio reported for **3aa**
[e] Conversion of **2aa** reported, r.r. = 1:1 for **3aa':3aa**, *E/Z* ratio reported for **3aa**
[f] Conversion of **2aa** reported, r.r. = 1:3 for **3aa':3aa**, *E/Z* ratio reported for **3aa**
[g] Conversion of **3aa'** to **3aa** reported

g. Substrates that did not undergo efficient isomerization

Table A.4. Summary of substrates that did not undergo isomerization in high conversion.

Entry	Substrate	Ni complex (mol %)	Silane (mol %)	Rxn time (h)	Rxn T (°C)	Rxn scale (mmol)	GC conv. (%)

1	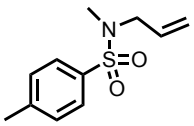 **S5**	**1a** (5 mol %)	$HSiPh_3$ (5 mol %)	16	80	0.5	6
2	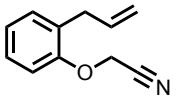 **S6**	**1a** (5 mol %)	$HSiPh_3$ (5 mol %)	16	80	0.5	12
		1e (5 mol %)	$HSiPh_3$ (5 mol %)	16	80	0.5	1
3	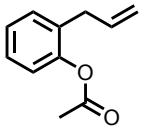 **S7**	**1a** (5 mol %)	HSi(4-CF_3-C_6H_4)$_3$ (5 mol %)	16	80	0.5	7
4	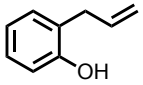 **S3**	**1e** (5 mol %)	HSi(4-CF_3-C_6H_4)$_3$ (5 mol %)	16	80	0.5	17
5	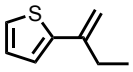 **S8**	**1a** (5 mol %)	$HSiPh_3$ (5 mol %)	16	80	0.5	3
		1a (5 mol %)	HSi(4-CF_3-C_6H_4)$_3$ (5 mol %)	16	80	0.5	2

A.1.5. Kinetic Studies

a. Effect of Silane Electronics on Reaction Kinetics

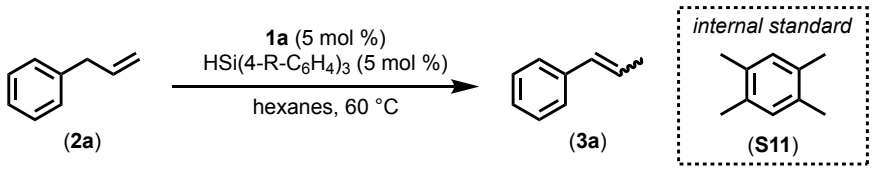

In a nitrogen-filled glovebox, silane ($HSiPh_3$, HSi(4-CF_3-C_6H_4)$_3$, HSi(4-NMe_2-C_6H_4)$_2$ or HSi(4-OMe-C_6H_4)$_3$) was weighed out directly into 1-dram vials. Stock solutions of **1a** (0.023 M) and **S11** (0.30 M) were prepared and distributed (**1a**: 0.35 mL, 0.008 mmol, 0.05 equiv; **S11**: 0.15 mL, 0.045 mmol, 0.28 equiv) to each vial. The vial was sealed with a septum cap, removed from the glovebox, and placed on an aluminum vial block pre-heated to 60 °C. After 30 minutes, allylbenzene (22 μL, 0.16 mmol, 1.0 equiv) was added with a 25-μL microliter syringe. Throughout the course of the reaction, 5 μL aliquots were removed and filtered through Celite with DCM. The filtrate was analyzed by GC-MS to assess the progress and selectivity of the reaction. The product concentration was

determined by relative integration (by GC-MS) of the product peaks against **S11**, in accordance with calibration curves prepared independently using the commercial compounds.

Table A.5. Formation of **3a** over time.

Silane	*Time (min)*	*% yield **3a***
$HSiPh_3$	5	*3*
	10	3
	15	3
	20	3
	25	4
	30	3
	35	4
	40	5
	45	4
	50	5
	55	5
	60	5
	65	6
	70	7
	75	8
	80	8
	85	9
	90	10
	95	10
	100	11
	105	14
	110	14
	115	15
	120	16
	130	18
	140	22
	150	25
	170	31
	190	39
	220	53
	260	70
	290	83
	320	89
	350	89
	380	89
Silane	*Time (s)*	*% yield **3a***
$HSi(4\text{-}CF_3\text{-}C_6H_4)_3$	5	4

	10	4
	15	5
	20	6
	25	6
	30	7
	35	9
	40	10
	45	12
	50	13
	55	14
	60	18
	65	21
	70	24
	75	26
	80	28
	85	31
	90	34
	95	38
	100	41
	105	44
	110	46
	115	50
	120	54
	130	57
	140	61
	150	68
	160	72
	170	76
	180	79
	200	81
	220	84
	240	87
	260	88
	280	90
	300	94
	330	87
	360	88
	390	88
	420	85

Silane	*Time (s)*	*% yield **3a***
$HSi(4\text{-}OMe\text{-}C_6H_4)_3$	10	3
	15	3
	20	3
	25	3

	30	4
	35	4
	40	3
	45	3
	50	4
	55	4
	60	4
	65	4
	70	4
	75	4
	80	5
	85	5
	90	5
	95	5
	100	5
	107	5
	110	6
	115	5
	120	6
	130	6
	140	7
	150	7
	161	8
	170	9
	180	9
	190	10
	200	10
	220	13
	240	15
	260	16
	280	18
	300	21
	332	25
	360	27
	390	29
	420	31
Silane	*Time (s)*	*% yield **3a***
$HSi(4\text{-}NMe_2\text{-}C_6H_4)_3$	5	3
	10	3
	15	3
	20	3
	25	3
	30	3
	35	3

	40	4
	45	3
	50	4
	55	3
	60	4
	65	4
	70	4
	75	4
	80	4
	85	4
	90	4
	95	4
	100	4
	105	4
	115	4
	120	4
	140	5
	150	5
	160	4
	170	4
	200	5
	240	5
	260	5
	280	5
	300	5
	330	6
	360	6
	390	6
	420	8
	660	11

To visualize the reaction rate versus time, the rate (M/h) over 5 points was calculated and plotted versus time:

$$Rate \approx \frac{\Delta[\mathbf{3a}]}{\Delta(time)} = \frac{[\mathbf{3a}]_{t_n} - [\mathbf{3a}]_{t_{n-5}}}{t_n - t_{n-5}}$$

Example calculation using the rate at time = 0.67 h:

$$Rate \approx \frac{\Delta[\mathbf{3a}]}{\Delta(time)} = \frac{[\mathbf{3a}]_{0.67\ h} - [\mathbf{3a}]_{0.33\ h}}{t_{0.67\ h} - t_{0.33\ h}} = \frac{0.017\ M - 0.011\ M}{0.67\ h - 0.33\ h} = 0.18$$

The data is summarized in **Table A.6.** Bolded entries are the maximum rates observed.

Table A.6. Formation of **3a** over time.

Silane	*Time (h)*	*[**3a**] (M)*	*Δ[**3a**]/Δ(time) (M/h)*
$HSiPh_3$	0.08	0.011	---
	0.17	0.011	---
	0.25	0.011	---
	0.33	0.011	---
	0.42	0.013	0.0058
	0.50	0.012	0.0035
	0.58	0.014	0.0094
	0.67	0.017	0.018
	0.75	0.014	0.0040
	0.83	0.016	0.014
	0.92	0.017	0.010
	1.00	0.018	0.0052
	1.08	0.021	0.022
	1.17	0.023	0.022
	1.25	0.027	0.030
	1.33	0.028	0.028
	1.42	0.031	0.029
	1.50	0.033	0.028
	1.58	0.034	0.020
	1.67	0.038	0.031
	1.75	0.045	0.042
	1.83	0.048	0.044
	1.92	0.051	0.051
	2.00	0.053	0.045
	2.17	0.059	0.035
	2.33	0.073	0.050
	2.50	0.083	0.055
	2.83	0.10	0.059
	3.17	0.13	0.071
	3.67	0.18	0.077
	4.33	0.23	0.082
	4.83	**0.28**	**0.087**
	5.33	0.29	0.076
	5.83	0.30	0.055
	6.33	0.30	0.031

Silane	*Time (h)*	*[**3a**] (M)*	*Δ[**3a**]/Δ(time) (M/h)*
$HSi(4\text{-}CF_3\text{-}C_6H_4)_3$	0.08	0.012	---
	0.17	0.015	---
	0.25	0.016	---
	0.33	0.019	---
	0.42	0.020	0.023

	0.50	0.024	0.028
	0.58	0.029	0.041
	0.67	0.033	0.044
	0.75	0.039	0.058
	0.83	0.045	0.064
	0.92	0.051	0.066
	1.00	0.059	0.077
	1.08	0.069	0.089
	1.17	0.079	0.10
	1.25	0.085	0.10
	1.33	0.095	0.11
	1.42	0.10	0.10
	1.50	0.11	0.10
	1.58	0.13	0.12
	1.67	0.14	0.13
	1.75	0.15	0.13
	1.83	0.15	0.12
	1.92	0.17	0.12
	2.00	**0.18**	**0.13**
	2.17	0.19	0.10
	2.33	0.20	0.095
	2.50	0.23	0.10
	2.67	0.24	0.090
	2.83	0.25	0.096
	3.00	0.26	0.092
	3.33	0.27	0.051
	3.67	0.28	0.040
	4.00	0.29	0.029
	4.33	0.29	0.023
	4.67	0.30	0.024
	5.00	0.31	0.024
	5.50	0.29	0.00087
	6.00	0.29	0
	6.50	0.29	-0.0042
	7.00	0.28	-0.015

Silane	*Time (h)*	*[**3a**] (M)*	*Δ[**3a**]/Δ(time) (M/h)*
$HSi(4\text{-}OMe\text{-}C_6H_4)_3$	0.17	0.011	---
	0.25	0.011	---
	0.33	0.011	---
	0.42	0.012	---
	0.50	0.012	0.0041
	0.58	0.013	0.0054
	0.67	0.011	0.0020
	0.75	0.012	0.00037

	0.83	0.013	0.0021
	0.92	0.013	-0.00013
	1.00	0.013	0.0041
	1.08	0.014	0.0059
	1.17	0.013	0.0020
	1.25	0.013	0
	1.33	0.016	0.0086
	1.42	0.016	0.0064
	1.50	0.016	0.0075
	1.58	0.015	0.0084
	1.67	0.017	0.0050
	1.75	0.017	0.0034
	1.83	0.019	0.0086
	1.92	0.019	0.0097
	2.00	0.20	0.0069
	2.17	0.020	0.0077
	2.33	0.023	0.0078
	2.50	0.024	0.0092
	2.67	0.026	0.0091
	2.83	0.029	0.013
	3.00	0.029	0.0090
	3.17	0.033	0.013
	3.33	0.035	0.014
	3.67	0.042	0.016
	4.00	0.049	0.020
	4.33	0.054	0.018
	4.67	0.061	0.020
	5.00	0.070	0.021
	5.33	0.082	0.021
	6.00	**0.091**	**0.022**
	6.50	0.097	0.020
	7.00	0.10	0.017

Silane	*Time (h)*	*[**3a**] (M)*	*Δ[**3a**]/Δ(time) (M/h)*
$HSi(4\text{-}NMe_2\text{-}C_6H_4)_3$	0.08	0.011	---
	0.17	0.011	---
	0.25	0.011	---
	0.33	0.011	---
	0.42	0.011	0
	0.50	0.011	0
	0.58	0.011	0
	0.67	0.012	0.0044
	0.75	0.012	0.0033
	0.83	0.012	0.0046
	0.92	0.011	0

	1.00	0.013	0.0016
	1.08	0.013	0.0033
	1.17	0.013	0.0027
	1.25	0.013	0.0062
	1.33	0.014	0.0041
	1.42	0.013	0.0018
	1.50	0.013	-0.0011
	1.58	0.015	0.0058
	1.67	0.014	-0.0010
	1.75	0.014	0.0022
	1.83	0.012	-0.00022
	1.92	0.014	-0.00047
	2.00	0.015	0.0026
	2.33	0.015	0.0018
	2.50	0.015	0.0029
	2.67	0.015	-0.00038
	2.83	0.014	0
	3.33	0.014	0.00089
	4.00	0.015	0.0014
	4.67	0.017	0.0024
	5.00	0.018	0.0014
	5.50	0.018	0.0013
	6.0	0.021	0.0023
	6.50	0.021	0.0016
	7.00	0.026	0.0041
	11.00	0.36	0.0031

A.1.6. Deuterium Incorporation and Crossover Studies

a. General Procedure H: Deuterium Incorporation

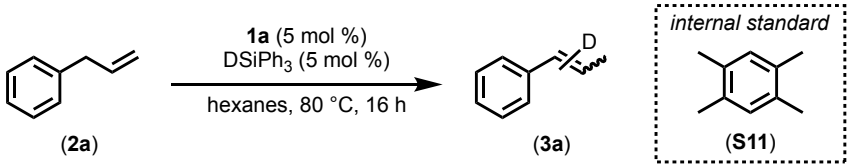

In a nitrogen-filled glovebox, a stock solution of **$DSiPh_3$** (0.048 M) was prepared by weighing out **$DSiPh_3$** and dissolving in the appropriate volume of hexanes. **1a** (6.6 mg, 0.013 mmol, 0.05 equiv) and **S11** (6.3 mg, 0.047 mmol, 0.19 equiv), were weighed out directly into a 1-dram vial equipped with a magnetic stir bar. **$DSiPh_3$** stock solution was distributed (0.27 mL of stock solution; 3.4 mg, 0.013 mmol, 0.05 equiv) with a disposable 1-mL syringe. Hexanes (0.53 mL) was added to the vial. Vial was sealed with a septum cap, removed from the glovebox, and placed on an aluminum vial block pre-heated to 80

°C. After 30 minutes, allylbenzene (33 uL, 0.25 mmol, 1.0 equiv) was distributed via two portions from a 25-µL microliter syringe. After 16 h, the reaction was quenched by cooling in a liquid N_2 bath, opening to air, and diluting with hexanes (0.10-0.20 mL). An aliquot was removed and filtered with hexanes through a Celite plug. The filtrate from the Celite plug was analyzed by GC to assess the progress and selectivity of the reaction (<1% **2a** remaining, *E*/*Z* 21:1 for **3a**). The crude reaction mixture was filtered through silica with hexanes and the filtrate was concentrated under reduced pressure. NMR samples were prepared for ^{1}H NMR and ^{2}H NMR (in $CHCl_3$/$CDCl_3$, 9:1, note that $CHCl_3$ from Fisher Chemical is stabilized with 0.75% EtOH, which appears in the NMR spectra below) analysis. ^{2}H NMR shows deuterium incorporation into all three positions of the propenyl chain (D_a/D_b/D_c = 1:8.6:4.4).

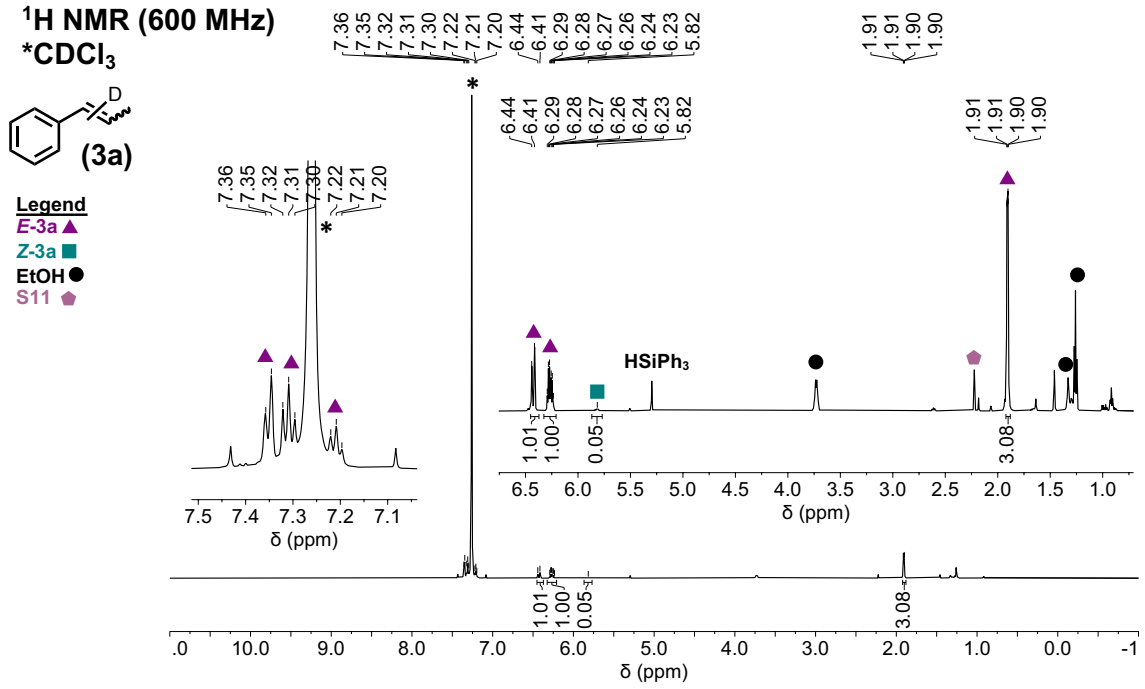

Figure A.1. ^{1}H NMR spectrum of **3a** after isomerization of **2a** with **DSiPh$_3$** recorded in $CHCl_3$/$CDCl_3$ (9:1) at 298 K.

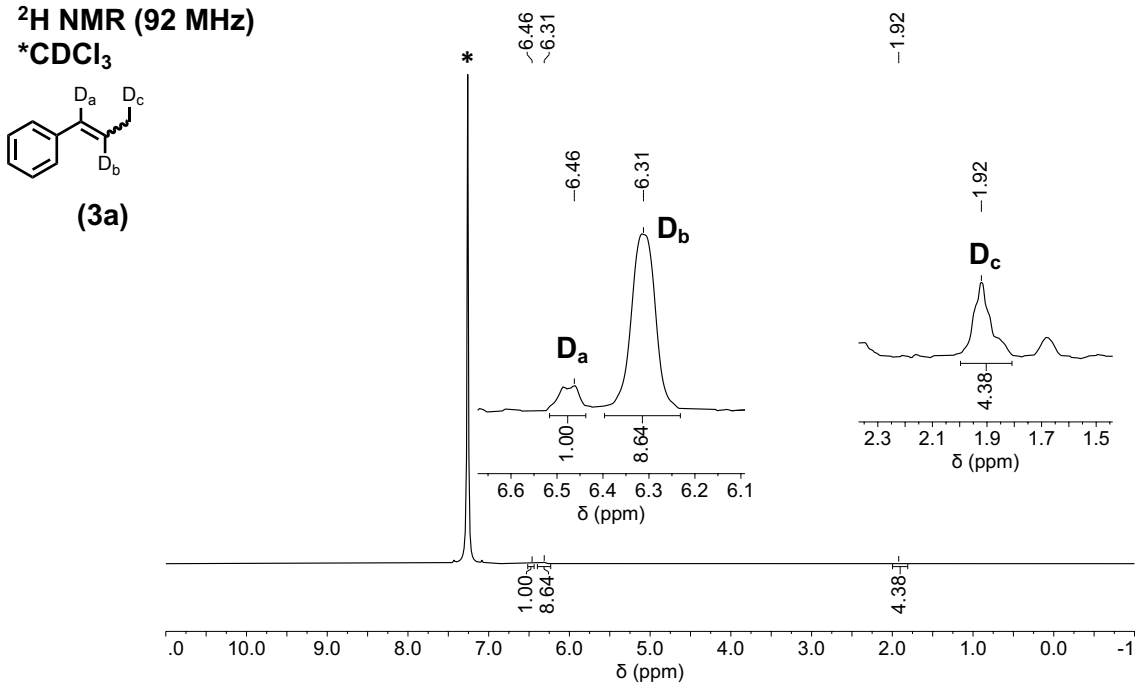

Figure A.2. ^{2}H NMR spectrum of **3a** after isomerization of **2a** with **DSiPh$_3$** recorded in $CHCl_3/CDCl_3$ (9:1) at 298 K.

b. Crossover Procedure

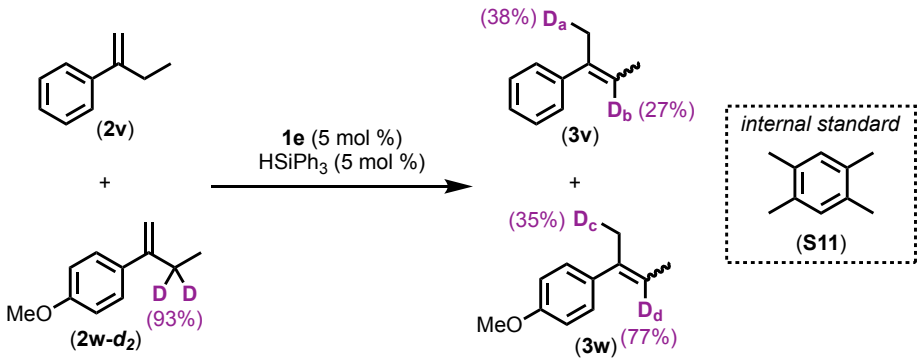

In a nitrogen-filled glovebox, **1e** (7.2 mg, 0.013 mmol, 0.05 equiv) and **S11** (8.3 mg, 0.062 mmol, 0.25 equiv) were weighed out directly into a 1-dram vial equipped with a magnetic stir bar. A stock solution of **HSiPh$_3$** (0.13 M) was prepared by weighing out **HSiPh$_3$** and dissolving in the appropriate volume of hexanes. The **HSiPh$_3$** stock solution was added to the vial (0.10 mL of the stock solution; 3.4 mg, 0.013 mmol, 0.05 equiv) with a 250-μL microliter syringe. Addition hexanes (0.70 mL) was added to the vial with a disposable 1-mL syringe. The vial was sealed with a septum cap, removed from the glovebox and placed on an aluminum vial block pre-heated to 80 °C. After 30 minutes, **2v**

(19 μL, 0.13 mmol, 0.50 equiv) and **2w-*d*$_2$** (23 μL, 0.13 mmol, 0.50 equiv) were added to the reaction with a 25-μL microliter syringe. After 16 h, the reaction was quenched by cooling in a liquid N_2 bath, opening to air, and diluting with hexanes (0.10-0.20 mL). An aliquot was removed and filtered with hexanes through a Celite plug. The filtrate from the Celite plug was analyzed by GCMS to assess the progress and selectivity of the reaction (~6% **2v** and 8% **2w-*d*$_2$** remaining, *E*/*Z* 4:1 for **3v** and *E*/*Z* 9:1 for **3w**). **2v**/**3v** and **2w**/**3w** were separated via column chromatography (silica, gradient eluent 0-2% Et_2O/pentane). NMR samples of each product were prepared for ^{1}H NMR (in $CDCl_3$) and ^{2}H NMR (in $CHCl_3$/$CDCl_3$, 9:1) analysis. ^{2}H NMR shows deuterium incorporation into the D_a and D_b positions of the butenyl chain (for **3v**, 38% D incorporation at D_a, 27% D incorporation at D_b; for **3w**, 35% D incorporation at D_a, 77% D incorporation at D_b).

Example calculation for %D incorporation:

For substrate **3v**, the peak at 2.04 ppm corresponds to the methyl group in the α position (marked with D_a in scheme above), and in the per-proteo isotopolog, integrates for 3H. In the ^{1}H NMR of the isotopolog isolated from the crossover experiment, this methyl group in the α position integrates for 1.85 H. Therefore:

$$\%H\ incorporation = \frac{1.85\ H}{3\ H} * 100\% = 62\%\ H$$

$$\%D\ incorporation = 100\% - \%H\ incorporation = 100\% - 62\% = 38\%\ D$$

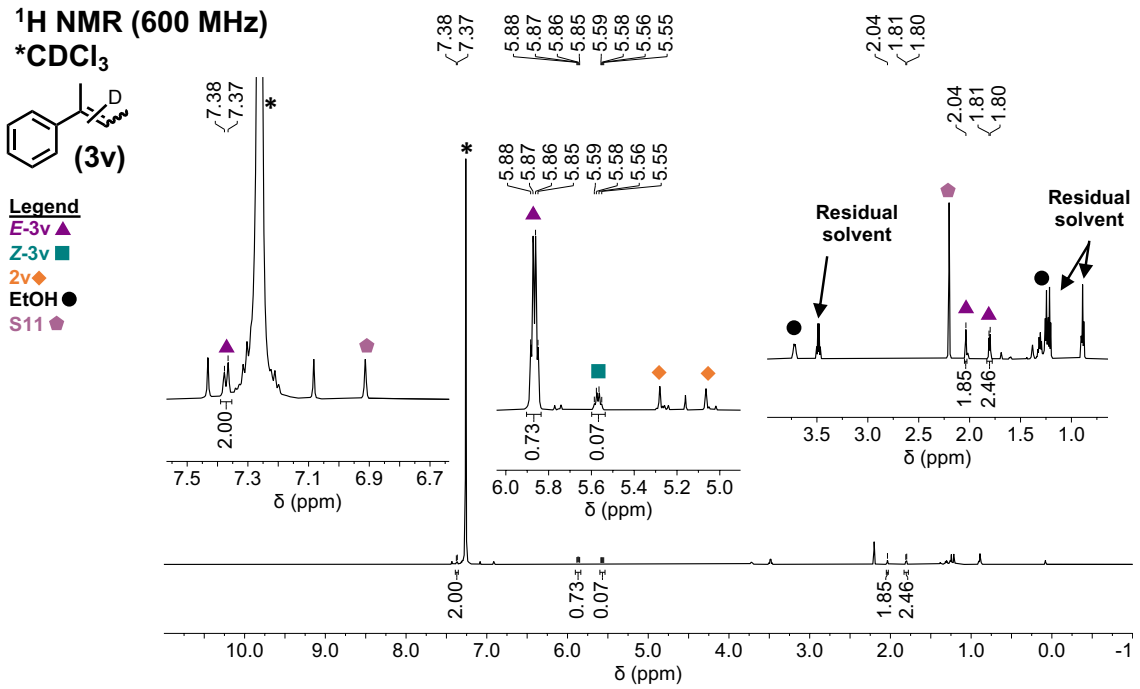

Figure A.3. ^{1}H NMR spectrum of **3v** after isomerization of **2v** in the presence of **2w-*d*$_2$** recorded in $CHCl_3/CDCl_3$ (9:1) at 298 K.

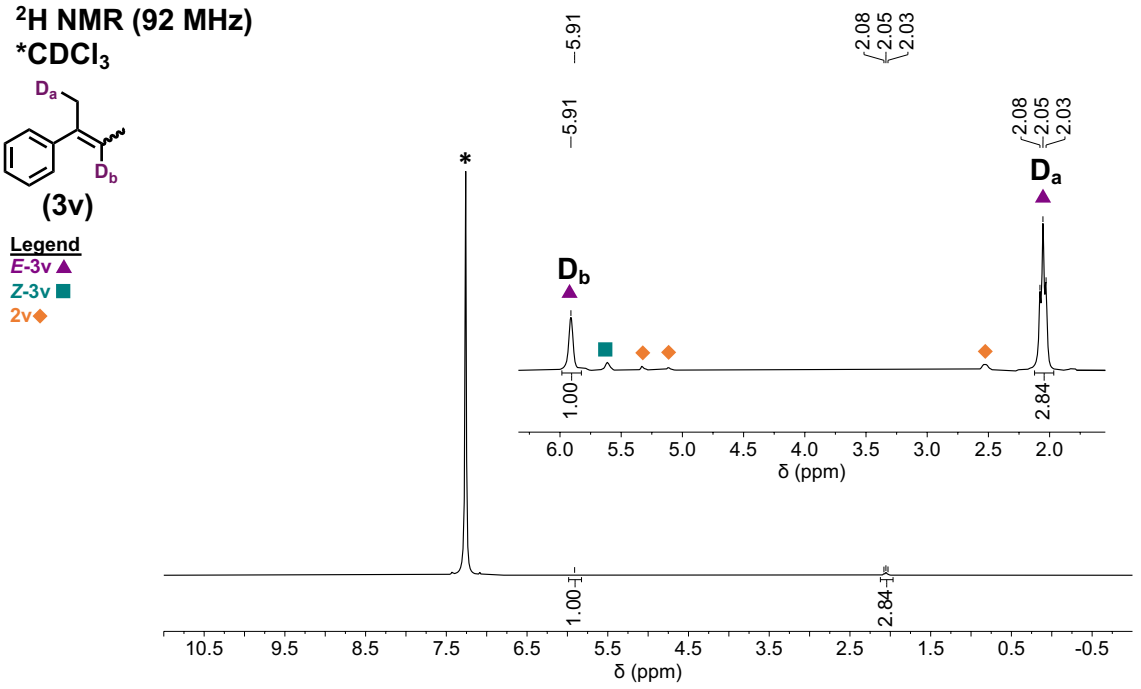

Figure A.4. 2H NMR spectrum of **3v** after isomerization of **2v** in the presence of **2w-*d*$_2$** recorded in $CHCl_3/CDCl_3$ (9:1) at 298 K.

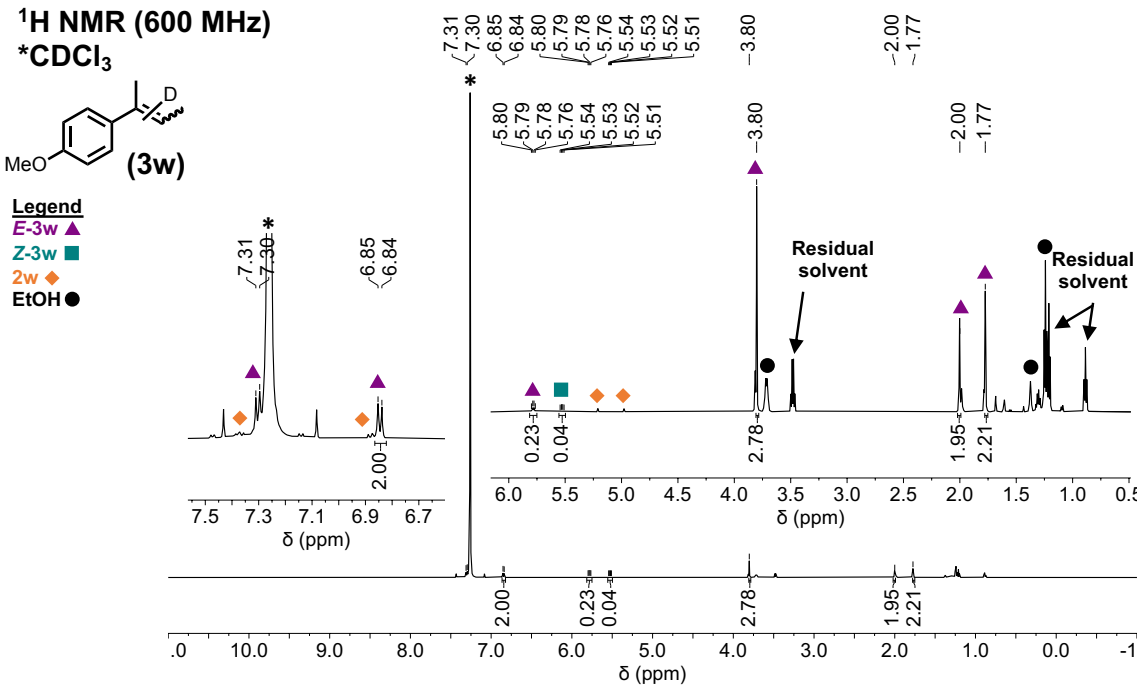

Figure A.5. ^{1}H NMR spectrum of **3w** after isomerization of **2w-*d*$_2$** in the presence of **2v** recorded in $CHCl_3/CDCl_3$ (9:1) at 298 K.

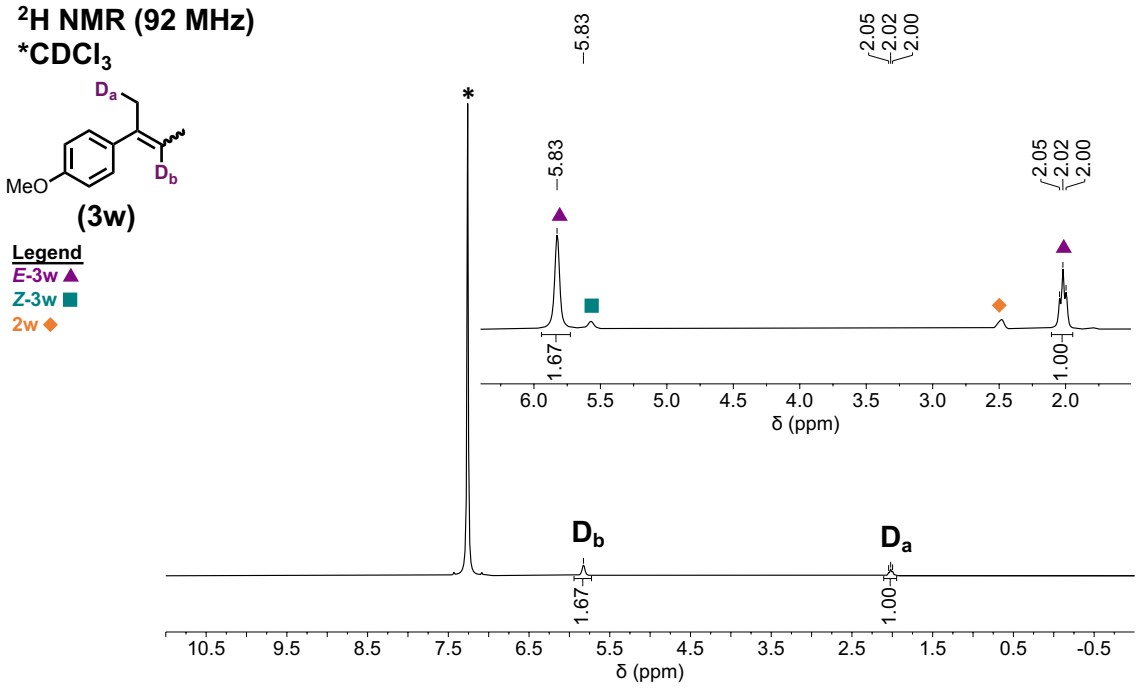

Figure A.6. ^{2}H NMR spectrum of **3w** after isomerization of **2w-*d*$_2$** in the presence of **2v** recorded in $CHCl_3/CDCl_3$ (9:1) at 298 K.

A.1.7. Mechanistic Investigation to Differentiate Between MHAT and Insertion-Elimination Pathways

a. Reactivity in the Presence of a Radical Scavenger

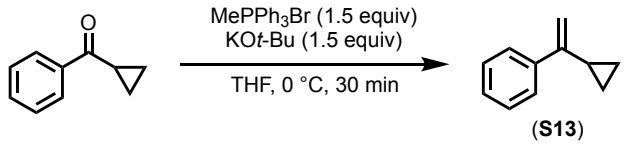

(**S13**)

1,1-Diphenylethylene (DPE) was synthesized via literature procedure:[14] To an oven-dried Schlenk flask equipped with a magnetic stir bar was added $MePPh_3Br$ (8.37 g, 23.4 mmol, 1.48 equiv) and THF (60 mL). The reaction was cooled to 0 °C with an ice/water bath for 5 minutes before adding KO*t*-Bu (2.54 g, 22.6 mmol, 1.43 equiv) in one portion. The reaction was stirred for 30 minutes following the appearance of the distinctive bright yellow color before benzophenone (2.88 g, 15.8 mmol, 1.00 equiv) was added slowly. After full addition of benzophenone, the reaction was warmed to room temperature and then placed in a pre-heated oil bath at 40 °C to stir 16 hours. The reaction was cooled to room temperature before being quenched with H_2O (30 mL). The organic layer was separated, and the aqueous layer was extracted with Et_2O (3 x 100 mL). The combined organic layers were rotovapped down to a gooey white solid. The crude reaction was purified by column chromatography (silica, hexanes) to yield the product as a clear oil (1.6 g, 8.9 mmol, 56% yield). NMR spectra match values previously reported.[238,239]

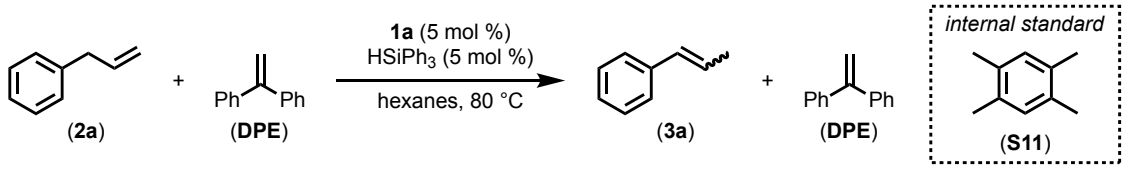

(**2a**) (**DPE**) (**3a**) (**DPE**) (**S11**)

In a nitrogen-filled glovebox, **1a** (6.6 mg, 0.013 mmol, 0.05 equiv) was weighed out directly into a 1-dram vial equipped with a magnetic stir bar. A stock solution of $HSiPh_3$ and **S11** was prepared by weighing out the reagent and dissolving in the appropriate amount of hexanes using a 5-mL volumetric flask. The $HSiPh_3$/**S11** stock solution was added to the vial (0.8 mL, $HSiPh_3$: 0.013 mmol, 0.05 equiv; **S11**: 0.086 mmol, 0.34 equiv) with a 1-mL disposable syringe. The vial was sealed with a septum cap, removed from the glovebox and placed on an aluminum vial block pre-heated to 80 °C. After 30 minutes, **DPE** (45 µL, 0.25 mmol, 1.0 equiv) and **2a** (33 µL, 0.25 mmol, 1.0 equiv) were added to the reaction with a 25-µL microliter syringe. Throughout the course of the reaction, 5 µL aliquots were

removed and filtered through Celite with hexanes. The filtrate from the Celite plug was analyzed by GC to assess the progress and selectivity of the reaction. The product concentration was determined by relative integration (by GC) against **S11**, in accordance with calibration curves prepared independently using the commercial compounds.

As the isomerization of **2a** to **3a** proceeds to completion in the presence of **DPE** without observation of any significant byproducts (aside from <2% each of propylbenzene and 1,1'-ethylidenebisbenzene), we suggest the reaction is not proceeding through an uncaged radical mechanism. If a radical mechanism were in effect, we would expect either low conversion of **2a** to **3a** and/or the formation of oligomers arising from stabilized di-benzylic radicals.

Table A.7. Formation of **3a** over time.

Time (min)	*% yield **3a** at standard conditions*	*% yield **3a** in the presence of 1.0 equiv of **DPE***
10	8±0	7±0
20	16±1	14±0
30	25±2	22±1
40	36±3	33±0
50	48±3	43±0
60	60±3	53±1
70	71±3	62±1
80	77±3	68±1
90	80±3	71±1
100	80±3	73±0
110	81±3	73±0
120	81±3	74±1
140	81±3	75±1
310	83±1	81±1

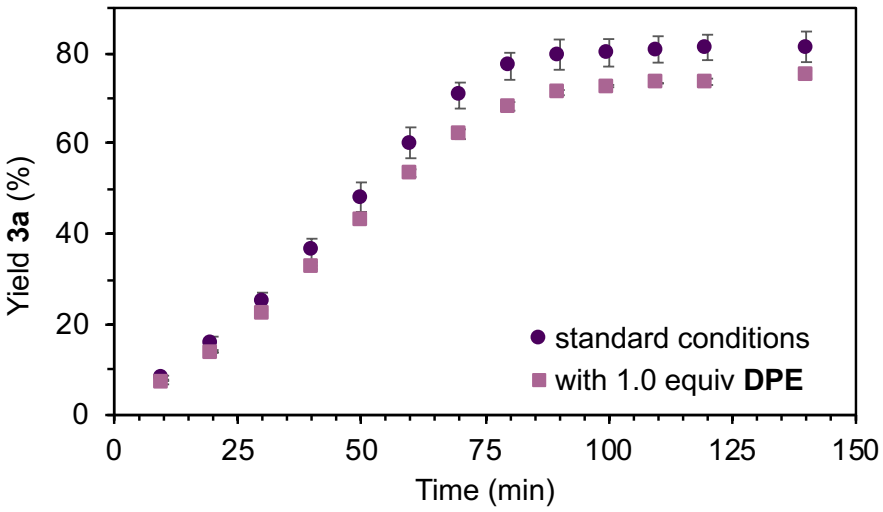

Figure A.7. Formation of **3a** in standard conditions (circles) and in the presence of 1.0 equiv of **DPE** (squares) over time.

b. Reactivity with a 1,6-diene

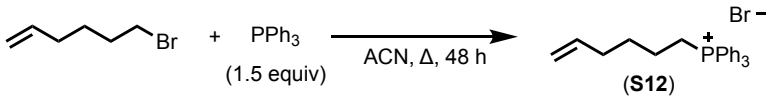

Hex-5-en-1-yltriphenylphosphonium bromide (S12) was synthesized via literature procedure:[240] PPh_3 (10.9 g, 41.5 mmol, 1.50 equiv), acetonitrile (25 mL) and 6-bromohex-1-ene (3.7 mL, 28 mmol, 1.0 equiv) were added to a 100 mL Schlenk flaks equipped with a magnetic stir bar. The reaction was equipped with a nitrogen-flushed condenser and placed in a pre-heated oil bath set to 95 °C. The reaction was heated for 48 h before being cooled to room temperature. Once the reaction was cool, the mixture was transferred to a round bottom flask and concentrated under reduced pressure to approximately 15 mL. Et_2O (70 mL) was layered until a white precipitate began forming at the acetonitrile/Et_2O interface. The reaction was placed in the freezer for 18 hours before the white precipitate was collected by filtration on a glass frit. The solid was washed with Et_2O (50 mL) and dried under reduced pressure in the presence of P_2O_5 overnight before use. The product was collected as a white powder (11.1 g, 26.1 mmol, 93% yield).

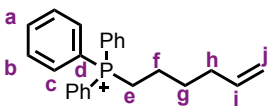

^{1}H NMR (500 MHz, $CDCl_3$, 298 K): δ 7.91-7.84 (m, 6H, **H_b**), 7.79 (t, *J* = 7.4 Hz, 3H, **H_a**), 7.73-7.67 (m, 6H, **H_c**), 5.68 (ddt, *J* = 17.0, 10.2, 6.7 Hz, 1H, **H_i**), 4.92 (d, *J* = 17.0 Hz, 1H, ***trans*-H_j**), 4.88 (d, *J* = 10.2 Hz, 1H, ***cis*-H_j**), 3.90 (m, 2H, **H_e**), 2.08 (q, *J* = 6.9 Hz, 2H, **H_h**), 1.79 (p, *J* = 7.3 Hz, 2H, **H_f**), 1.63 (m, 2H, overlapping with H_2O, **H_g**)

^{13}C{^{1}H} (126 MHz, $CDCl_3$, 298 K): δ 137.7 (**C_i**), 135.1 (d, *J* = 3.0 Hz, **C_a**), 133.7 (d, *J* = 10.0 Hz, **C_b**), 130.6 (d, *J* = 12.5 Hz, **C_c**), 118.3 (d, *J* = 85.9 Hz, **C_d**), 115.4 (**C_j**), 33.0 (d, *J* = 0.9 Hz, **C_h**), 29.2 (d, *J* = 16.0 Hz, **C_f**), 22.7 (d, *J* = 50.0 Hz, **C_e**), 21.9 (d, *J* = 4.4 Hz, **C_g**)

^{31}P{^{1}H} (202 MHz, $CDCl_3$, 298 K): δ 24.62

ASAP/HRMS (m/z): M^+ calculated for $C_{24}H_{26}P$ 345.1767, found 345.1791

IR (ATR, neat) ν: 2856 (w), 1485 (w), 1437 (m), 1109 (s)

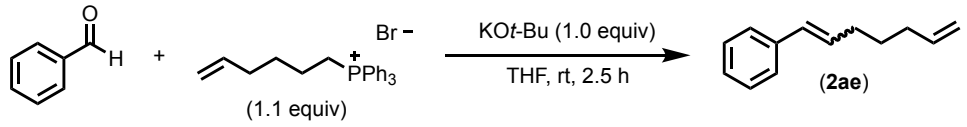

(1*E*)-1,6-heptadien-1-ylbenzene (2ae) was synthesized via literature procedure:[106] **S12** (5.50 g, 12.9 mmol, 1.10 equiv) and THF (80 mL) were added to a 200 mL Schlenk flask and stirred for 5 minutes before KO*t*-Bu (1.32 g, 11.8 mmol, 1.0 equiv) was added in one portion. The reaction turned a bright pumpkin orange and was stirred for 1 h before benzaldehyde (1.20 mL, 11.8 mmol, 1.0 equiv) was added dropwise. Over the course of benzaldehyde addition, the color faded to a pale yellow. The reaction was monitored by TLC and quenched with NH_4Cl (saturated aqueous, 50 mL) when benzaldehyde was fully consumed. The aqueous layer was extracted with EtOAc (3 x 80 mL). The combined organic layers were dried over Na_2SO_4, filtered, and concentrated under reduced pressure. The product was purified by running a silica plug with hexanes. The product was collected as a clear liquid (1.28 g, 7.4 mmol, 63% yield). NMR spectra match values previously reported.[241]

ASAP/HRMS (m/z): M^+ calculated for $C_{13}H_{16}$ 172.1252, found 172.1220

IR (ATR, neat) ν: 2924 (w), 1639 (w), 1493 (w), 910 (m), 696 (s)

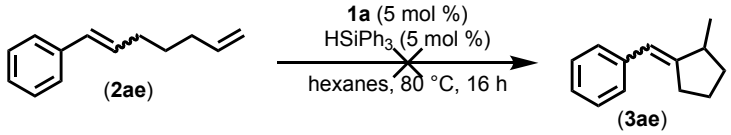

In a nitrogen-filled glovebox, the Ni complex was massed out into 1-dram vials (**1a**: 6.6 mg, 0.013 mmol, 0.05 equiv; **1f**: 12.2 mg, 0.013 mmol, 0.05 equiv). A stock solution of $HSiPh_3$ (0.16 M) was prepared by weighing out the reagent and dissolving in the appropriate amount of hexanes. For entries 1 and 4 in Table S8, 0.8 mL of the silane stock solution was added to the vials. For entries 2 and 3, 0.8 mL of hexanes was added to the vials. For entries 5 and 6, 0.8 mL of chlorobenzene was added to the vials. To all the vials, **2ae** (45 µL, 0.25 mmol, 1.0 equiv) was added in two portions using a 250-µL microliter syringe. All vials were sealed and removed from the glovebox. Vials for entries 1-4 were placed on a pre-heated aluminum vial block at 80 °C. Aliquots from each vial were removed overtime and filtered through Celite for GC analysis. After 24 h, the vials were quenched by submerging in liquid N_2, opening to air and diluting with ~0.1-0.2 mL hexanes. Reaction mixtures were run through short SiO_2 plugs with hexanes, concentrated under reduced pressure and analyzed by NMR. All trials were run in duplicate. NMR spectra match values previously reported.[94]

Table A.8. Screening reactivity of **2ae** in various conditions.

Entry	*Reaction conditions*	*Conversion of **2ae** (%)*
1	**1a** (5 mol %), $HSiPh_3$ (5 mol %), hexanes, 80 °C	77 ± 2
2	**1a** (5 mol %), hexanes, 80 °C	<1 ± 0
3	**1f** (5 mol %), hexanes, 80 °C	7 ± 2
4	**1f** (5 mol %), $HSiPh_3$ (5 mol %), hexanes, 80 °C	21 ± 1
5	**1f** (5 mol %), chlorobenzene, room temp	3 ± 0
6	**1a** (5 mol %), chlorobenzene, room temp	2 ± 0

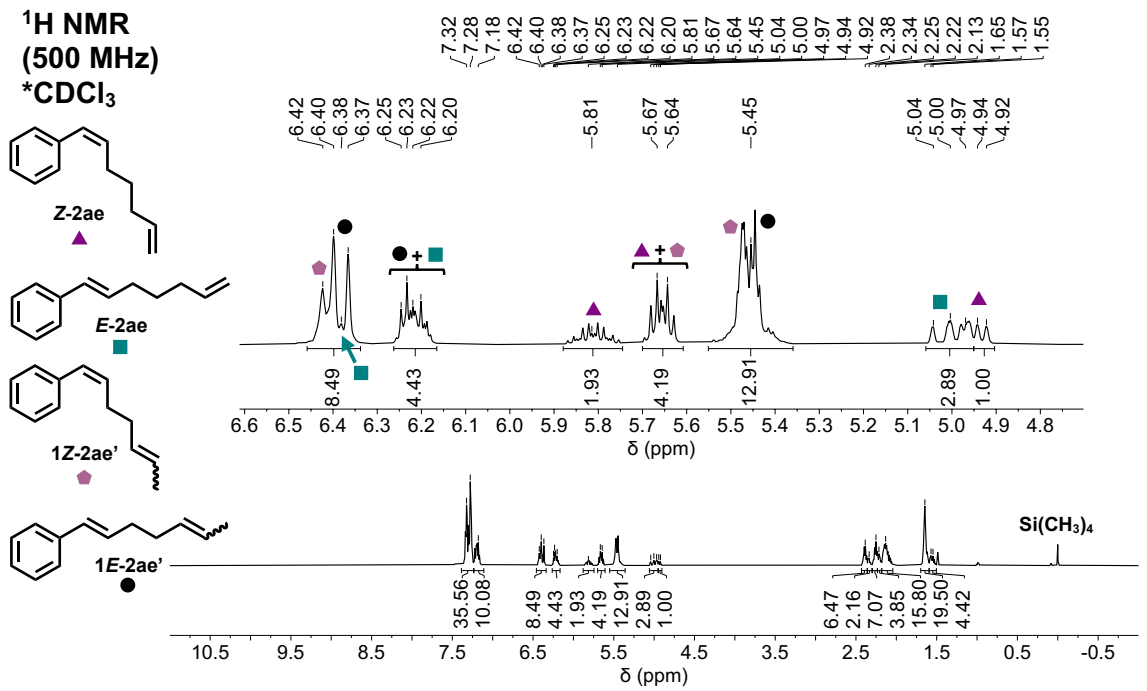

Figure A.8. [1]H NMR spectrum for the crude reaction mixture from **Table A.8.**, entry 1.

While the major product of the isomerization of **2ae** with **1a**/$HSiPh_3$ was identified as the 1,5-diene, forming from the 1-carbon isomerization of the terminal alkene, to further confirm the absence of the cycloisomerized product **3ae**, we independently synthesized **3ae** through a Wittig pathway.

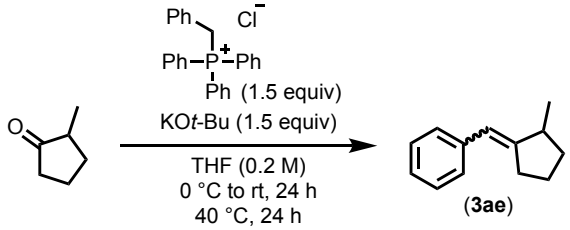

(2-Methylcyclopentylidene)methylbenzene (3ae) To an oven dried 100 mL Schlenk flask was added benzyltriphenylphosphonium chloride (5.83 g, 15.0 mmol, 1.5 equiv) and THF (50 mL). The reaction was cooled to 0 °C with an ice/water bath for 5 min before KO*t*-Bu (1.7 g, 15 mmol, 1.5 equiv) was added in one portion. Following the appearance of the distinctive red/orange color, the reaction was stirred for 30 min before 2-methylcyclopentanone (1.1 mL, 10 mmol, 1.0 equiv) was added dropwise. The ice/water bath was removed and the reaction was warmed to room temperature for 24 h. After 24 h, the reaction was placed in an oil bath at 40 °C for 24 h. The reaction was opened to air and

80 mL H_2O was added. The aqueous layer was extracted with 3 x 100 mL Et_2O and the combined organic layers were dried over Na_2SO_4, filtered, and concentrated under reduced pressure. Crude product was obtained by running a silica plug with hexanes to remove triphenylphosphine oxide. The formation of **3ae** was confirmed by ^{1}H NMR compared to previously reported values.[242,243]

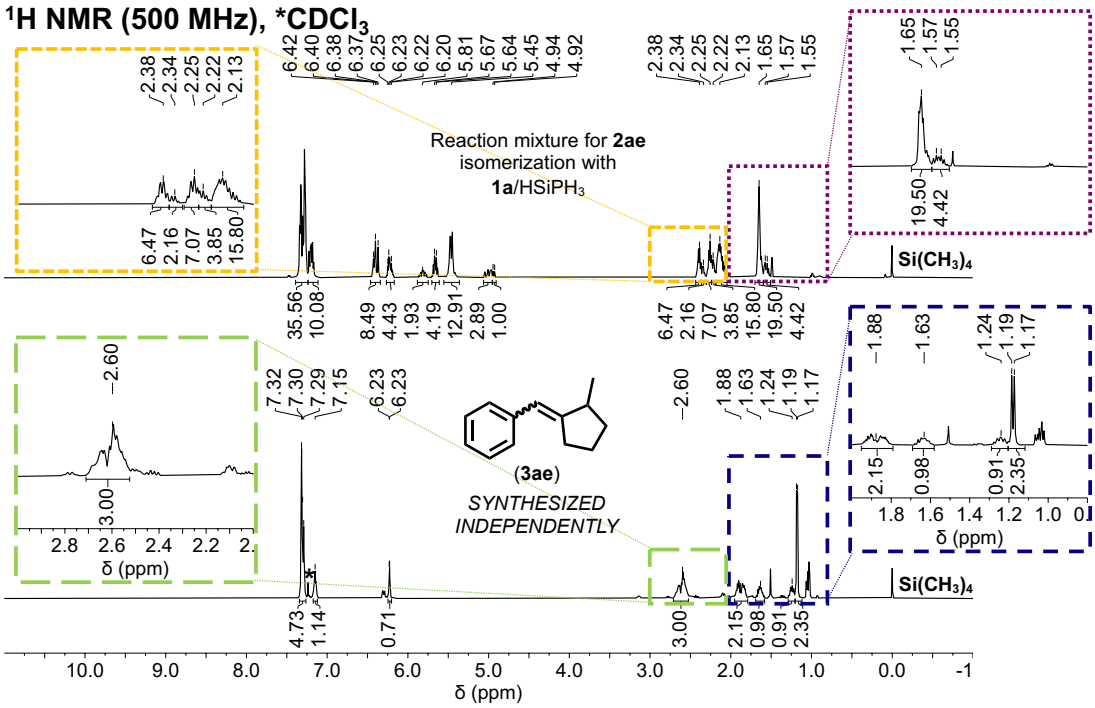

Figure A.9. ^{1}H NMR spectra for the reaction mixture from the isomerization of **2ae** with **1a**/$HSiPh_3$ (top) and *independently synthesized* **3ae** (bottom).

c. Reactivity with a Vinylcyclopropane

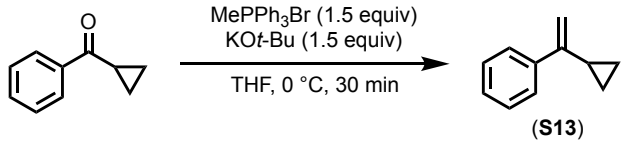

(1-cyclopropylethenyl)benzene (S13) was synthesized via literature procedure:[14] $MePPh_3Br$ (8.05 g, 22.5 mmol, 1.5 equiv) and THF (60 mL) were added to an oven-dried 200 mL Schlenk flask equipped with a magnetic stir bar. The reaction was cooled with an ice/water bath for 20 minutes before KO*t*-Bu (2.53 g, 22.5 mmol, 1.5 equiv) was added in one portion. A vibrant yellow color appeared within 10 seconds. The mixture was stirred for 20 minutes before cyclopropyl phenyl ketone (2.1 mL, 15.2 mmol, 1.0 equiv) was added dropwise. The vibrant yellow color faded, but reaction remained yellow, upon full addition

of the ketone. Reaction progress was monitored by TLC. Upon consumption of starting ketone, the reaction was quenched with H_2O (30 mL). The aqueous layer was extracted with Et_2O (3 x 100 mL) and the combined organic layers were dried over Na_2SO_4 before being filtered and concentrated under reduced pressure to give **S13** as a clear liquid (1.97 g, 13.7 mmol, 90% yield). NMR spectra match values previously reported.[244]

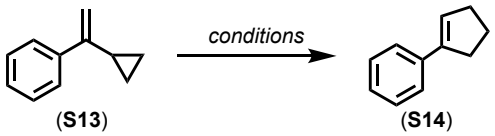

In a nitrogen-filled glovebox, the Ni complex was massed out into 1-dram vials (**1a**: 6.6 mg, 0.013 mmol, 0.05 equiv; **1f**: 12.2 mg, 0.013 mmol, 0.05 equiv). A stock solution of $HSiPh_3$ (0.16 M) was prepared by weighing out the reagent and dissolving in the appropriate amount of hexanes. For entries 1 and 4 in Table S9, 0.8 mL of the silane stock solution was added to the vials. For entries 2 and 3, 0.8 mL of hexanes was added to the vials. For entries 5 and 6, 0.8 mL of chlorobenzene was added to the vials. To all the vials, **S13** (38 µL, 0.25 mmol, 1.0 equiv) was added in two portions using a 25-µL microliter syringe. All vials were sealed and removed from the glovebox. Vials for entries 1-4 were placed on a pre-heated aluminum vial block at 80 °C. After 3 h, the reactions were quenched by freezing in liquid N_2 and opening to air. A stock solution of **S11** (0.38 M) was prepared by weighing out **S11** into a 10-mL volumetric flask and dissolving in 10 mL hexanes. A disposable 1-mL syringe was used to distribute 0.2 mL of the **S11** stock solution to each vial. Aliquots from each vial were removed and filtered through Celite for GC analysis. All trials were run in duplicate.

Table A.9. Screening reactivity of **S13** in various conditions.

Entry	*Reaction conditions*	*Conversion (%) to **S14***
1	**1a** (5 mol %), $HSiPh_3$ (5 mol %), hexanes, 80 °C, 3 h	100±0
2	**1a** (5 mol %), hexanes, 80 °C, 3 h	100±0
3	**1f** (5 mol %), hexanes, 80 °C, 3 h	62±1
4	**1f** (5 mol %), $HSiPh_3$ (5 mol %), hexanes, 80 °C, 3 h	65±1
5	**1f** (5 mol %), chlorobenzene, room temp, 3 h	1±0
6	**1a** (5 mol %), chlorobenzene, room temp, 3 h	1±0

d. EPR Spectroscopy

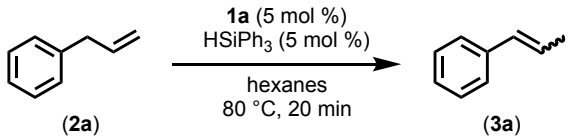

In a nitrogen filled glovebox, **1a** (6.6 mg, 0.013 mmol, 0.05 equiv) was weighed into a 1-dram vial. A stock solution of $HSiPh_3$ (0.016 M) was prepared by weighing out $HSiPh_3$ and dissolving in the appropriate volume of hexanes. 0.8 mL of the $HSiPh_3$ stock solution was added to the vial with **1a** via a 1-mL disposable syringe. The vial was shaken until **1a** was fully solvated before being transferred to a 3 mm EPR tube with a disposable pipet. The EPR tube was sealed with a septum and removed from the glovebox. The tube was heated for 30 minutes in a pre-heated water bath at 80 °C before **2a** (33 µL, 0.25 mmol, 1.0 equiv) was added to the solution via a 25-µL microliter syringe. The reaction was heated for 20 minutes before being removed from the water bath and submerged in liquid N_2. The sample was kept in the liquid N_2 bath for the duration of the experiment.

Prior to sample collection, a sample of TEMPO was prepared as a stock solution (0.016 M; same concentration as **1a** under catalytic conditions) by weighing TEMPO directly into a 20-mL vial and adding the appropriate amount of hexanes. The stock solution (0.8 mL) was added via a 1-mL disposable syringe to a nitrogen-flushed 3 mm EPR tube. The sample was submerged in liquid N_2. The EPR instrument was tuned and a spectrum for TEMPO was recorded prior to analysis of the quenched reaction mixture.

EPR

Experiment parameters
Center field: 3000 G
Field range: 2000 G
Number of points: 4096
Sweep time: 409.60 s
Receiver gain: 60 dB
Attenuation: 25 dB
Sample phase: solid
Solvent: hexanes
Temperature: 77 K
Modulation amplitude: 5.000 G
Modulation frequency: 100 KHz
Time constant: 327.68 ms
Microwave power: 0.6852 mW
Scans: 10

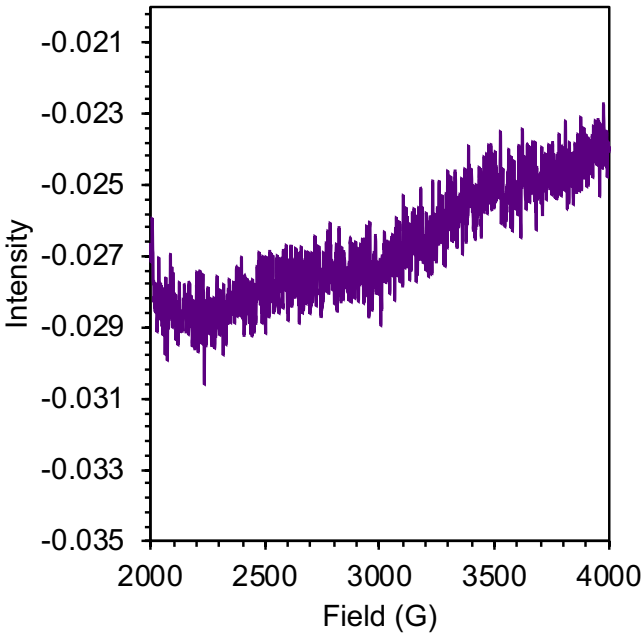

Figure A.10. EPR spectrum of the reaction mixture after 20 minutes of heating.

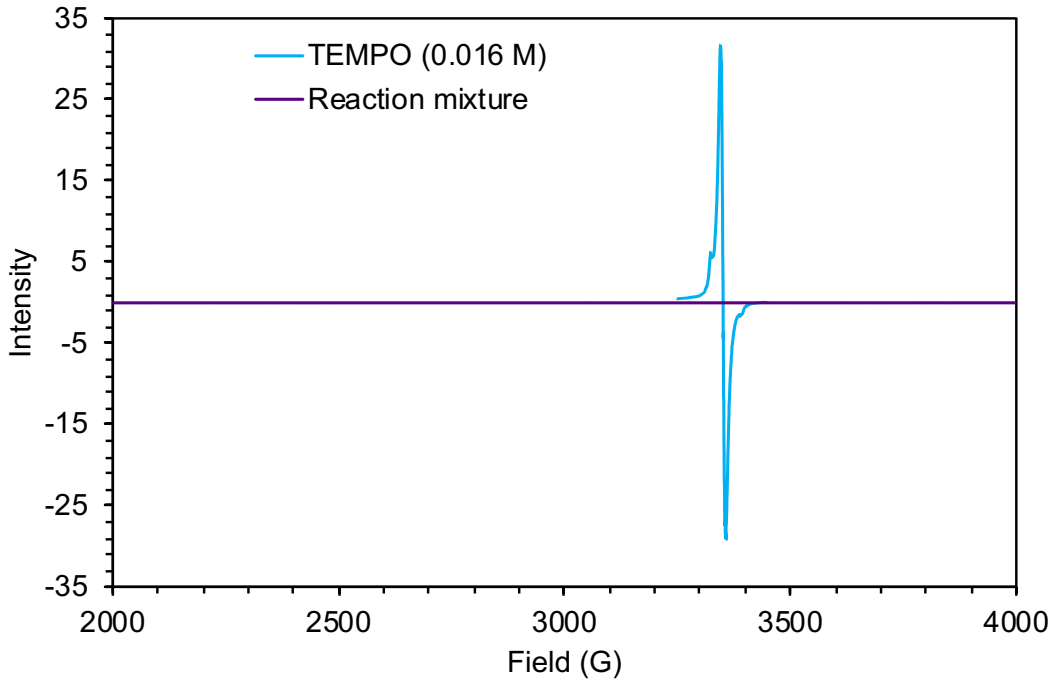

Figure A.11. EPR spectra for the reaction mixture after 20 minutes of heating (purple line) compared to the spectrum of TEMPO (blue line) at the same concentration of **1a**/$HSiPh_3$.

e. In Situ NMR Reaction Monitoring

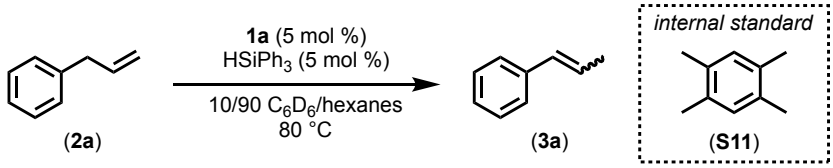

In a nitrogen filled glovebox, **1a** (6.6 mg, 0.013 mmol, 0.05 equiv), $HSiPh_3$ (3.3 mg, 0.013 mmol, 0.05 equiv) and **S11** (5.8 mg, 0.043 mmol, 0.17 equiv) were massed into a 1-dram vial. A solution of 10/90 (v/v) C_6D_6/hexanes was prepared and 0.8 mL was added to the 1-dram vial. **2a** (33 µL, 0.25 mmol, 1.0 equiv) was added to the solution via a 25-µL microliter syringe. The reaction mixture was transferred to a J-Young NMR tube with a glass pipet. The NMR tube was sealed and removed from the glovebox. The reaction was placed in the NMR instrument (pre-heated to 80 °C) and allowed to equilibrate to 80 °C for 5 minutes before the first ^{1}H NMR spectrum was recorded. The instrument was held at 80 °C over the course of the reaction and ^{1}H NMR spectra were recorded periodically. Minimal broadening of peaks is observed over the course of the reaction, indicating the observable resting state of the catalyst does not have an unpaired electron.

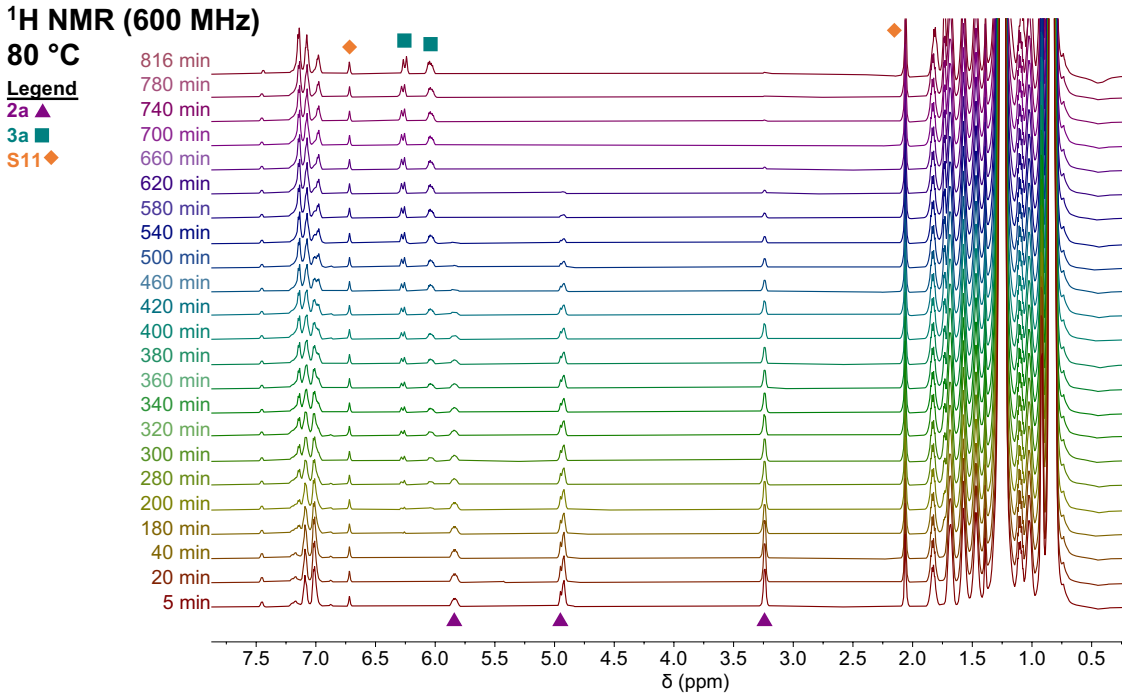

Figure A.12. ^{1}H NMR spectra of the reaction mixture over time (5 minutes to 816 minutes) monitoring the disappearance of **2a** (triangles) and the appearance of **3a** (squares).

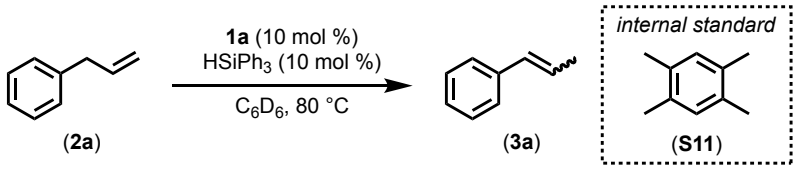

In a nitrogen filled glovebox, **1a** (13.2 mg, 0.025 mmol, 0.10 equiv), $HSiPh_3$ (6.6 mg, 0.025 mmol, 0.10 equiv) and **S11** (16.0 mg, 0.12 mmol, 0.48 equiv) were massed into a 1-dram vial. C_6D_6 (0.8 mL) was added to the 1-dram vial. **2a** (33 µL, 0.25 mmol, 1.0 equiv) was added to the solution via a 25-µL microliter syringe. The reaction mixture was transferred to a J-Young NMR tube with a glass pipet. The NMR tube was sealed and removed from the glovebox. The reaction was placed in the NMR instrument (pre-heated to 70 °C) and allowed to equilibrate to 70 °C before the first ^{1}H spectrum was recorded. The instrument was held at 70 °C over the course of the reaction and spectra were recorded periodically. Minimal broadening of peaks is observed over the course of the reaction, indicating the observable resting state of the catalyst does not have an unpaired electron.

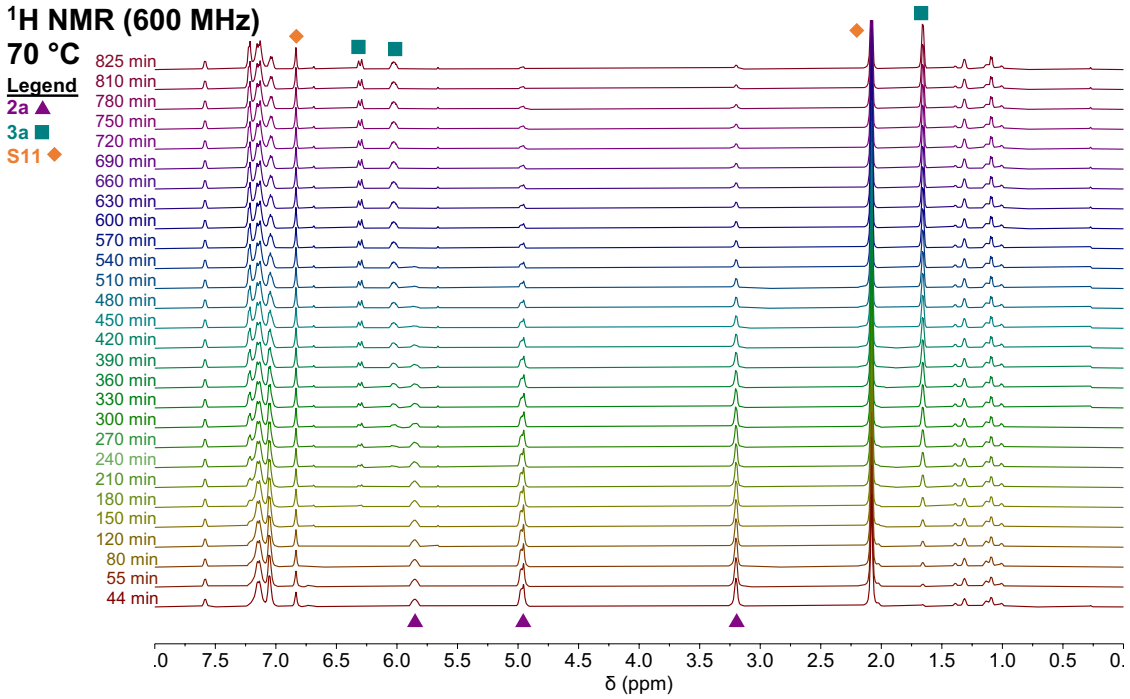

Figure A.13. ^{1}H NMR spectra of the reaction mixture over time (40 minutes to 825 minutes) monitoring the disappearance of **2a** (triangles) and the appearance of **3a** (squares).

A.1.8. NMR and IR Spectra

a. Starting Alkenes

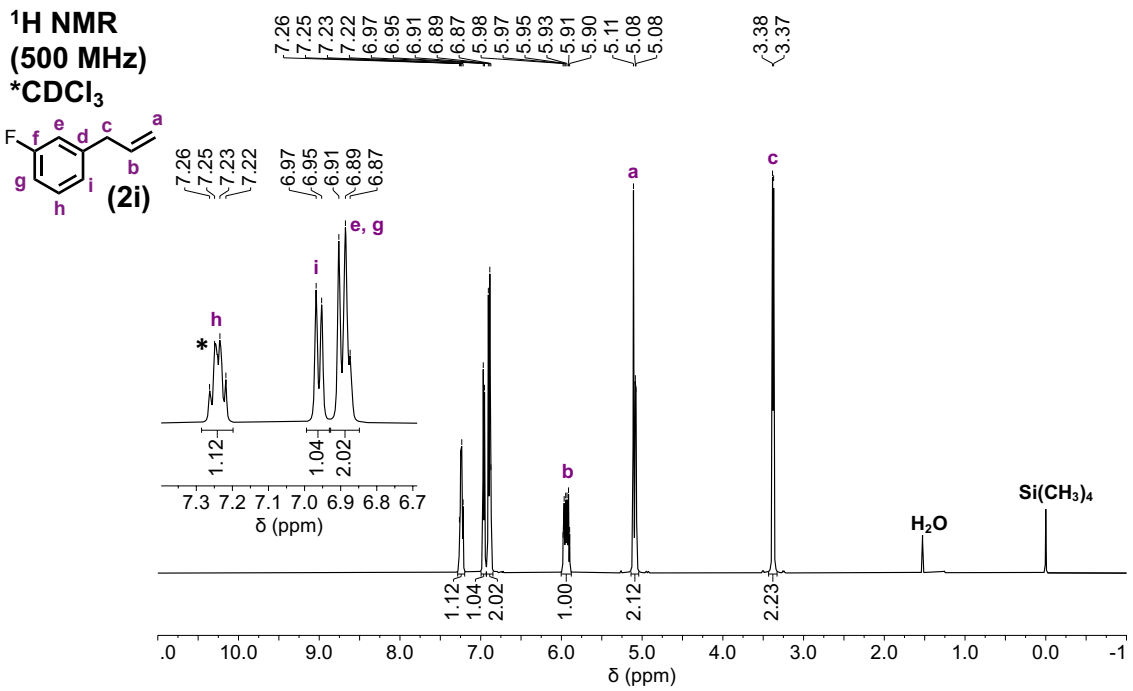

Figure A.14. [1]H NMR spectrum of 3-(3-fluorophenyl)-1-propene (**2i**) recorded in CDCl3 at 298 K.

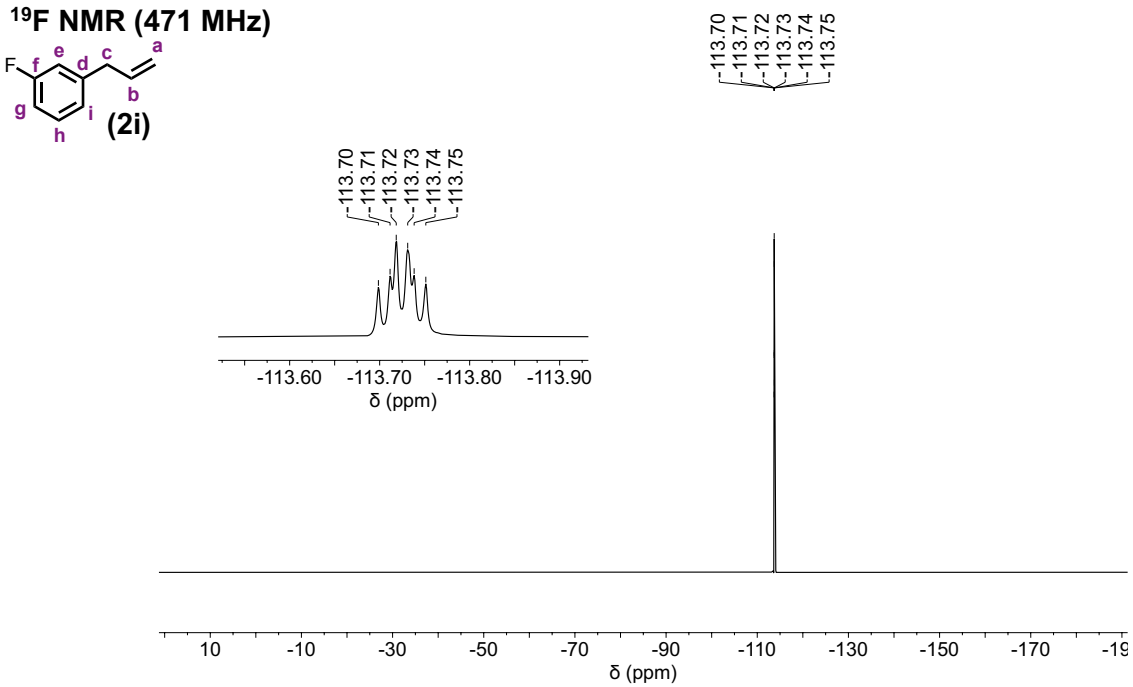

Figure A.15. [19]F NMR spectrum of 3-(3-fluorophenyl)-1-propene (**2i**) recorded in CDCl3 at 298 K.

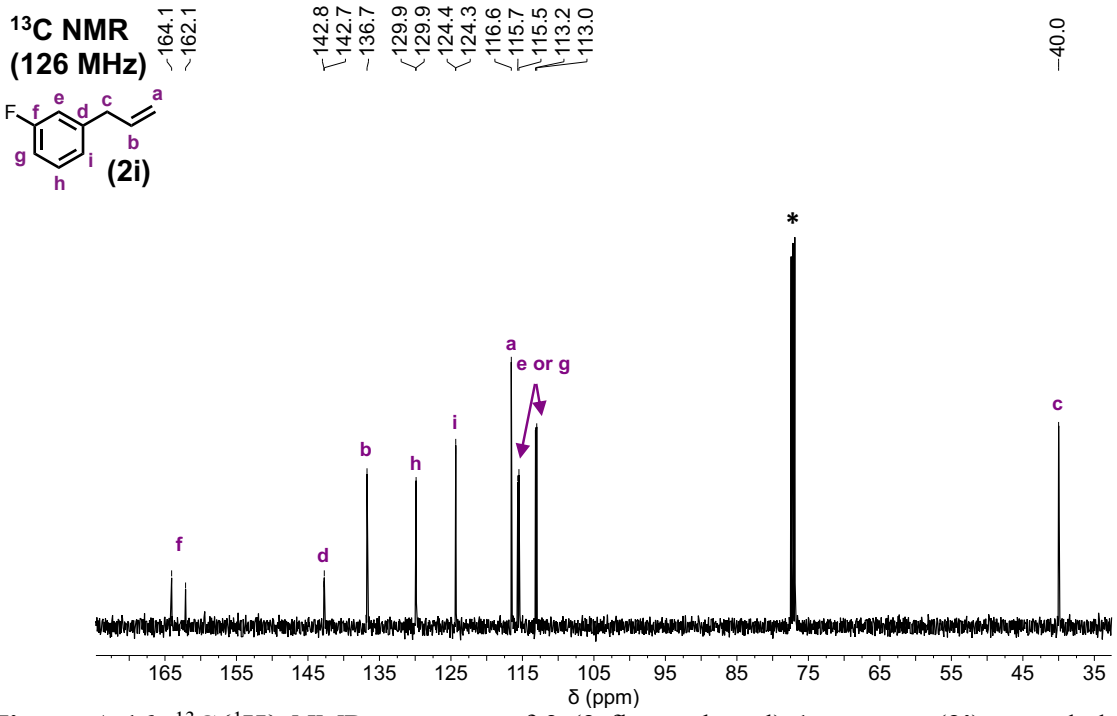

Figure A.16. $^{13}C\{^{1}H\}$ NMR spectrum of 3-(3-fluorophenyl)-1-propene (**2i**) recorded in CDCl3 at 298 K.

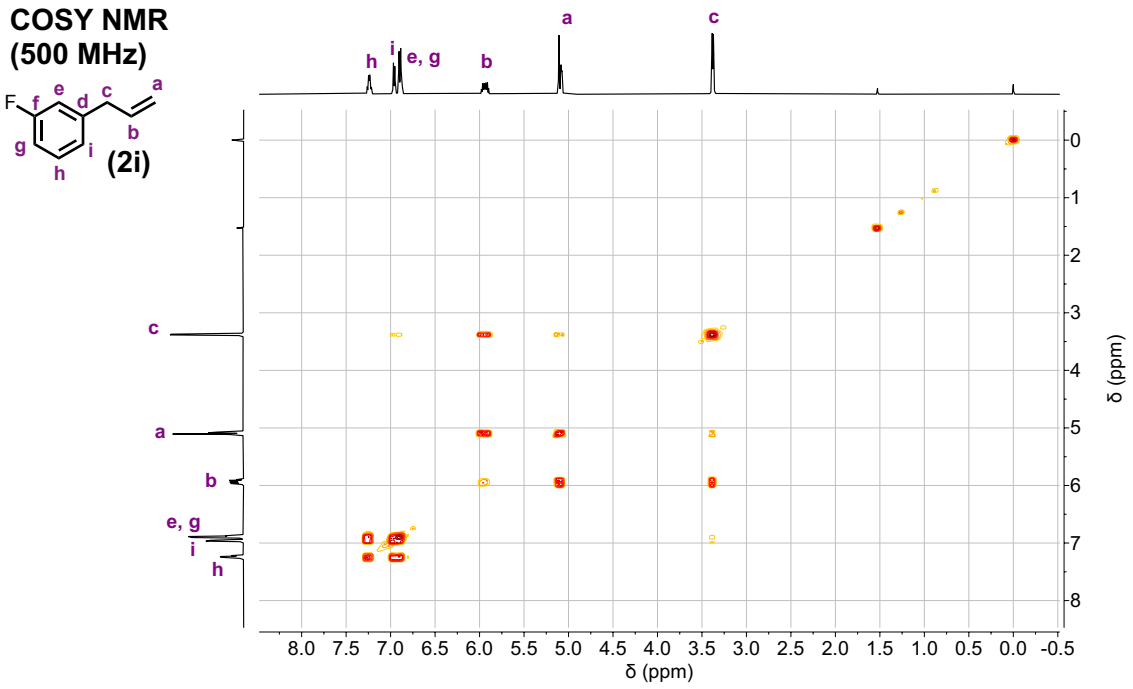

Figure A.17. COSY NMR spectrum of 3-(3-fluorophenyl)-1-propene (**2i**) recorded in CDCl3 at 298 K.

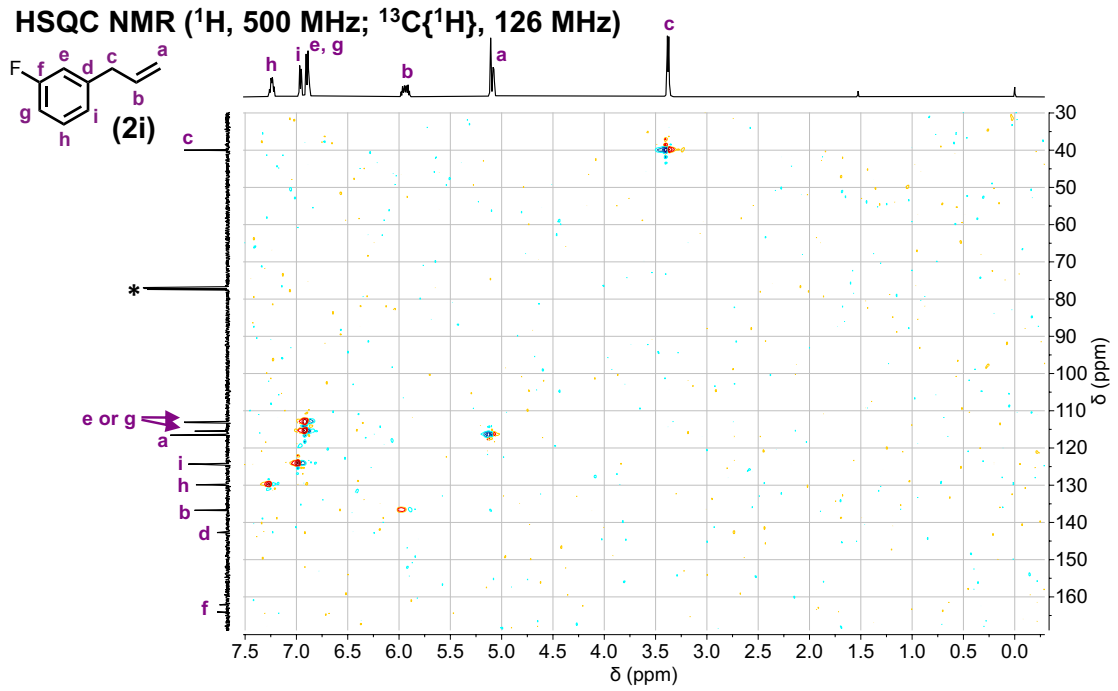

Figure A.18. HSQC NMR spectrum of 3-(3-fluorophenyl)-1-propene (**2i**) recorded in CDCl3 at 298 K.

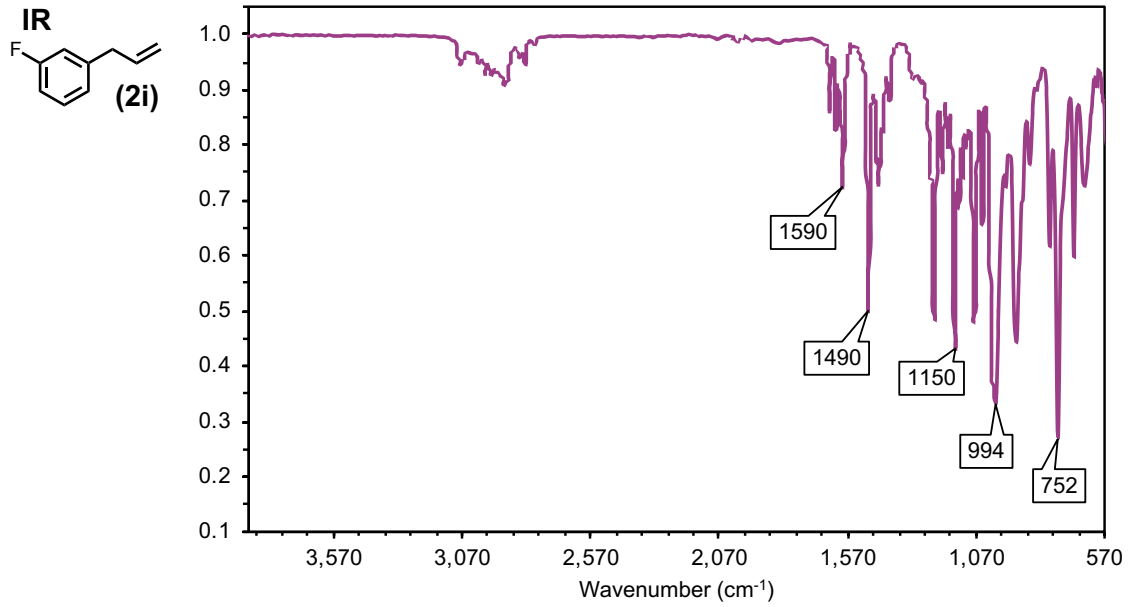

Figure A.19. IR spectrum of 3-(3-fluorophenyl)-1-propene (**2i**) recorded neat at room temperature.

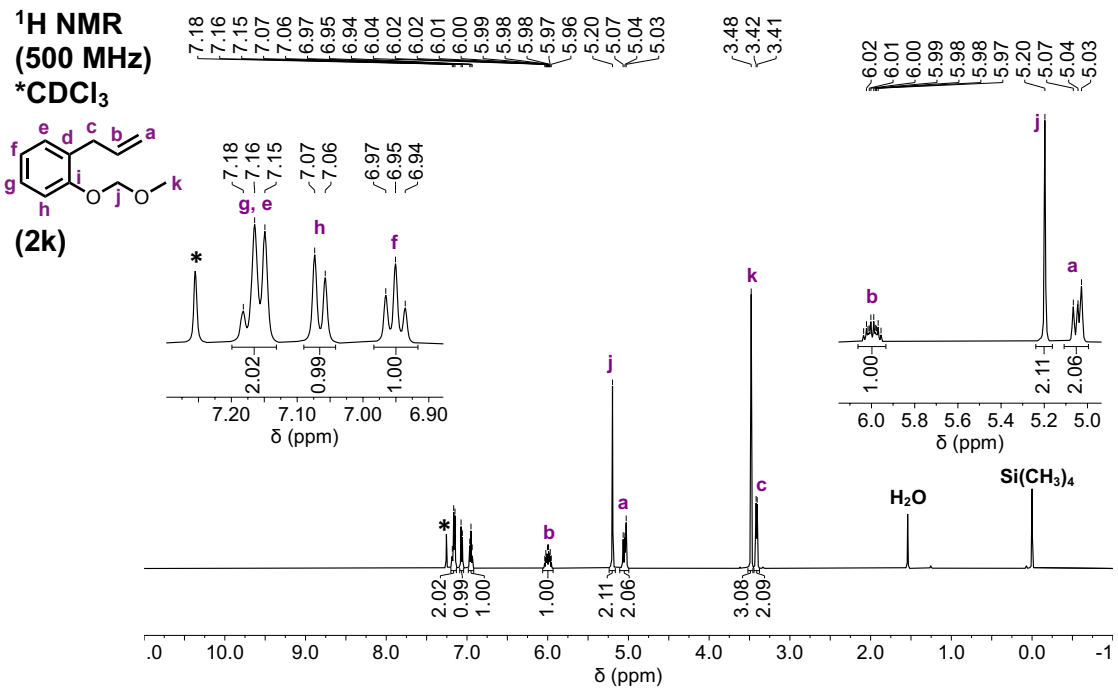

Figure A.20. ^{1}H NMR spectrum of 1-(methoxymethoxy)-2-(2-propen-1-yl)benzene (**2k**) recorded in $CDCl_3$ at 298 K.

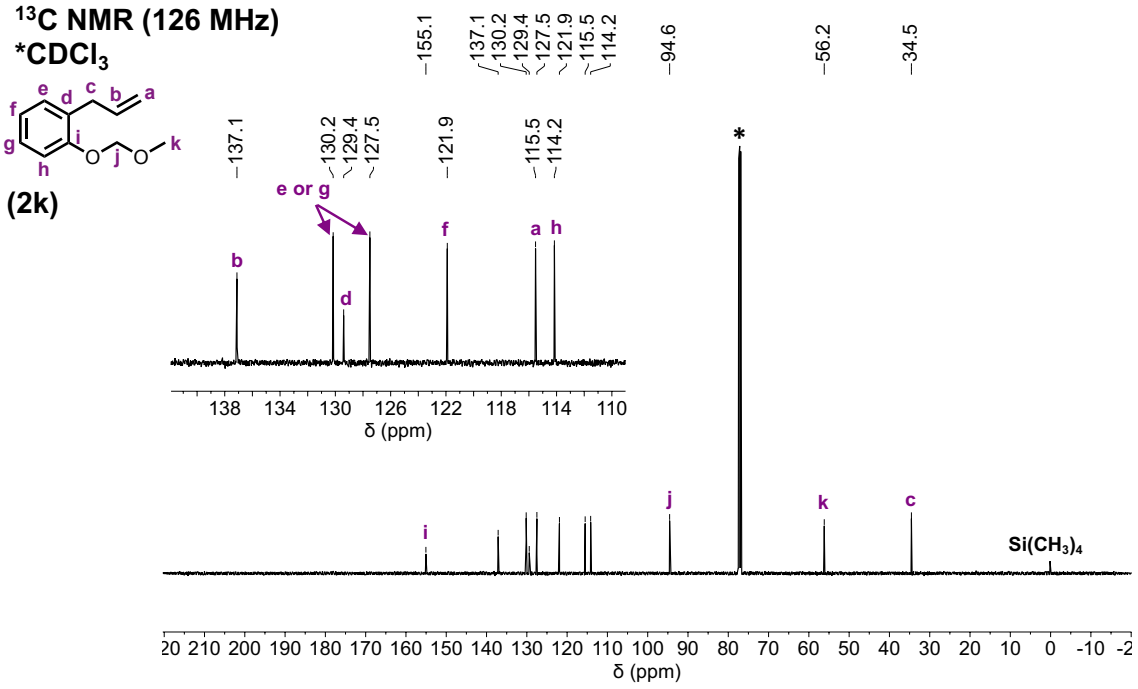

Figure A.21. ^{13}C{^{1}H} NMR spectrum of 1-(methoxymethoxy)-2-(2-propen-1-yl)benzene (**2k**) recorded in $CDCl_3$ at 298 K.

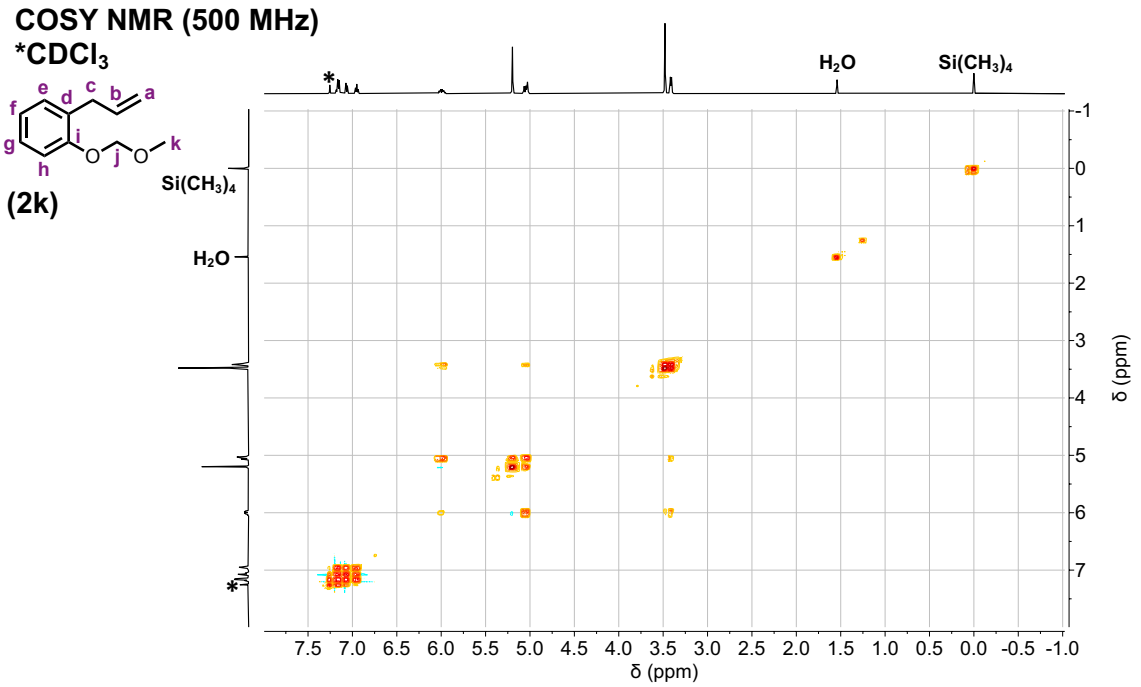

Figure A.22. COSY NMR spectrum of 1-(methoxymethoxy)-2-(2-propen-1-yl)benzene (**2k**) recorded in $CDCl_3$ at 298 K.

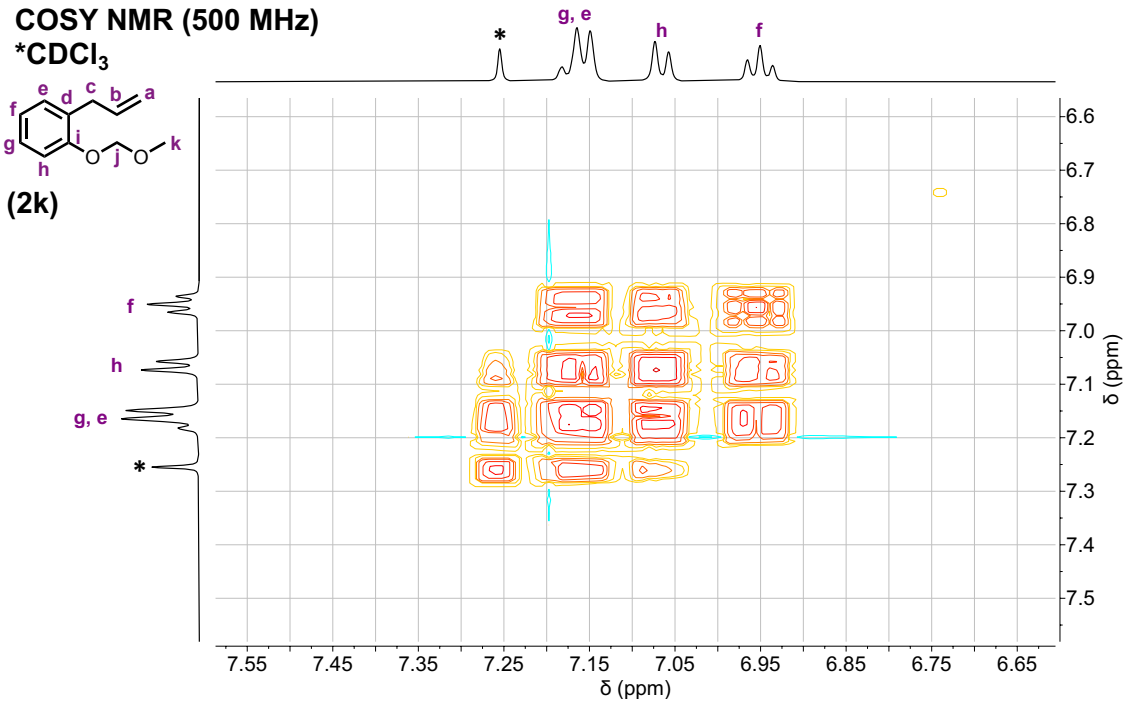

Figure A.23. Aryl region of COSY NMR spectrum of 1-(methoxymethoxy)-2-(2-propen-1-yl)benzene (**2k**) recorded in $CDCl_3$ at 298 K.

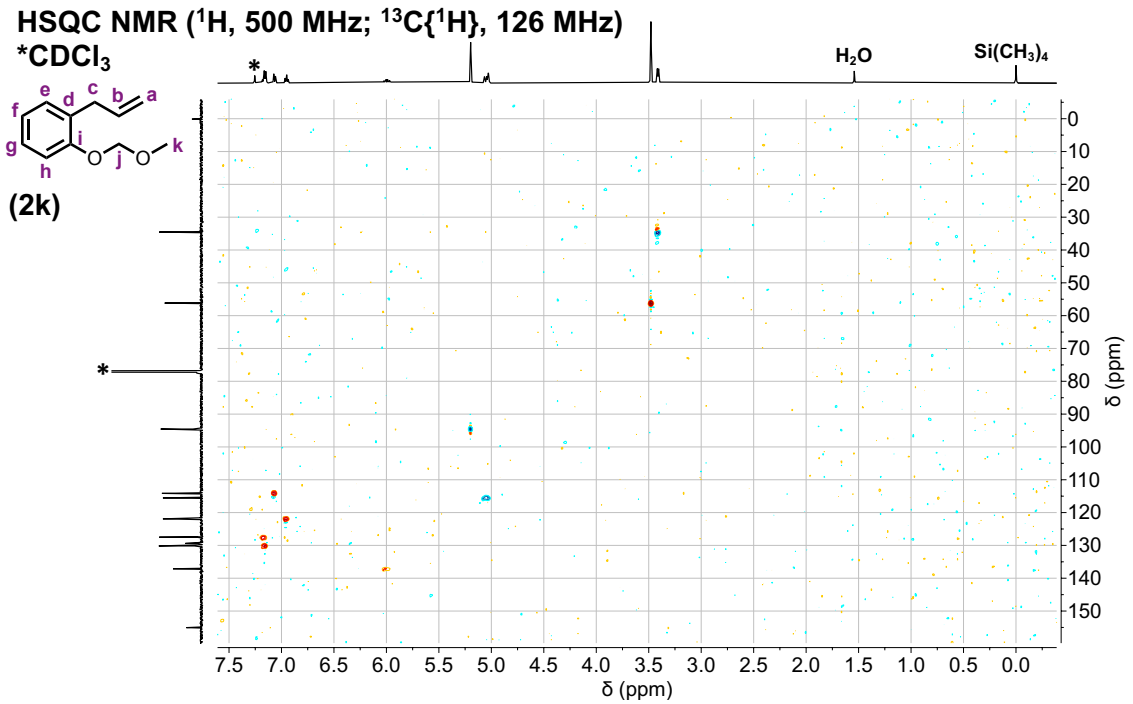

Figure A.24. HSQC NMR spectrum of 1-(methoxymethoxy)-2-(2-propen-1-yl)benzene (**2k**) recorded in $CDCl_3$ at 298 K.

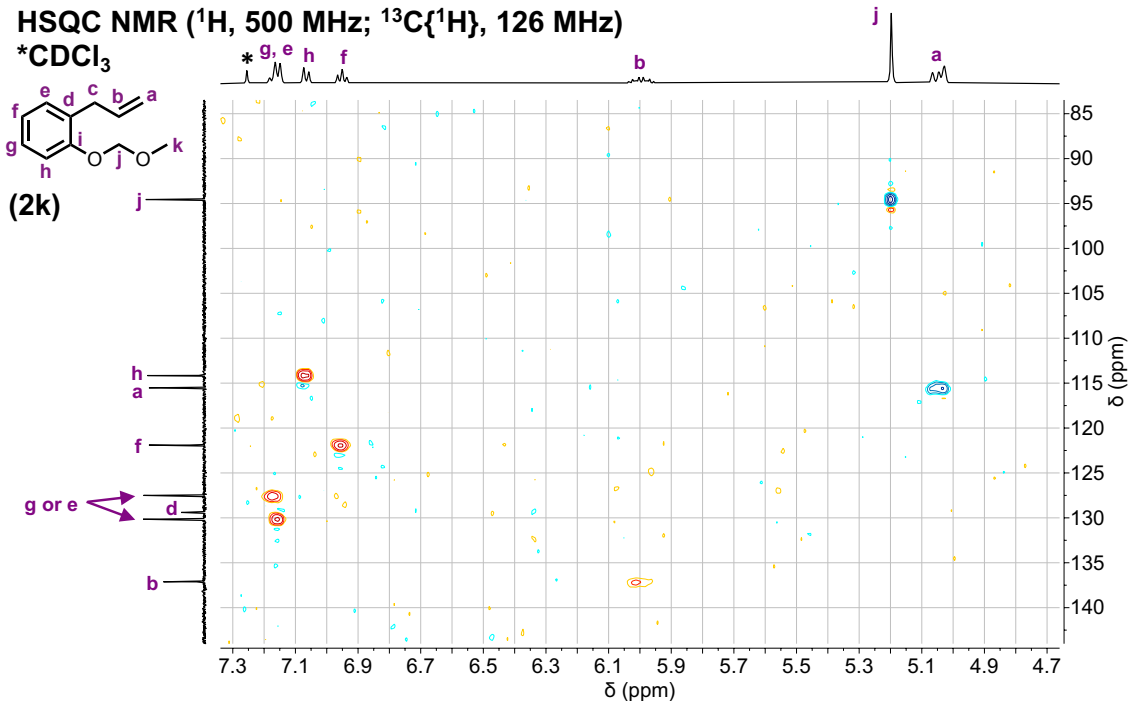

Figure A.25. Aryl and alkenyl region of HSQC NMR spectrum of 1-(methoxymethoxy)-2-(2-propen-1-yl)benzene (**2k**) recorded in $CDCl_3$ at 298 K.

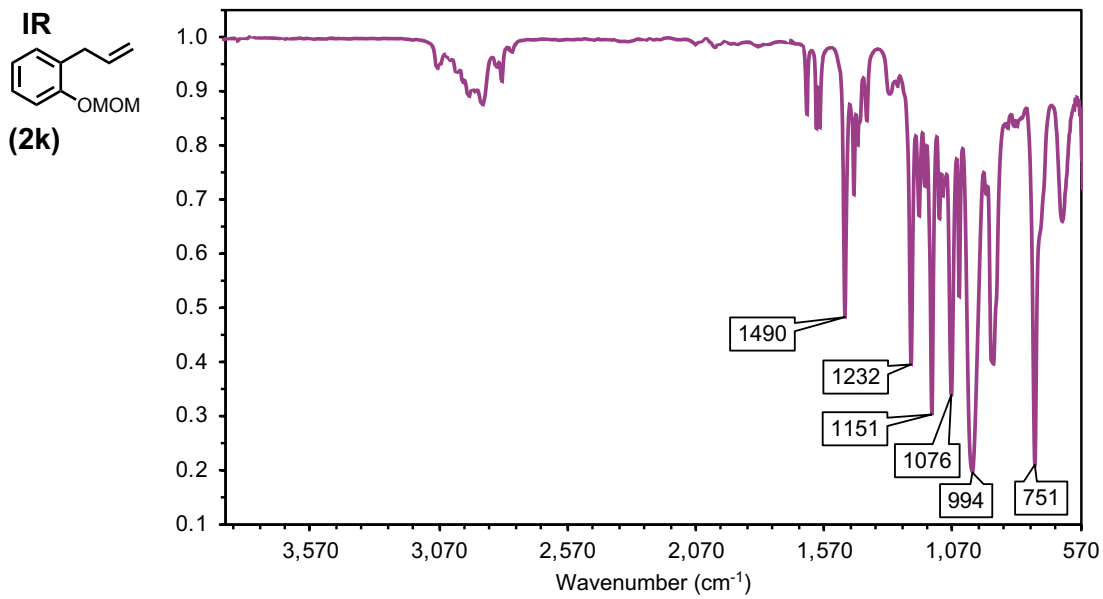

Figure A.26. IR spectrum of 1-(methoxymethoxy)-2-(2-propen-1-yl)benzene (**2k**) recorded neat at room temperature.

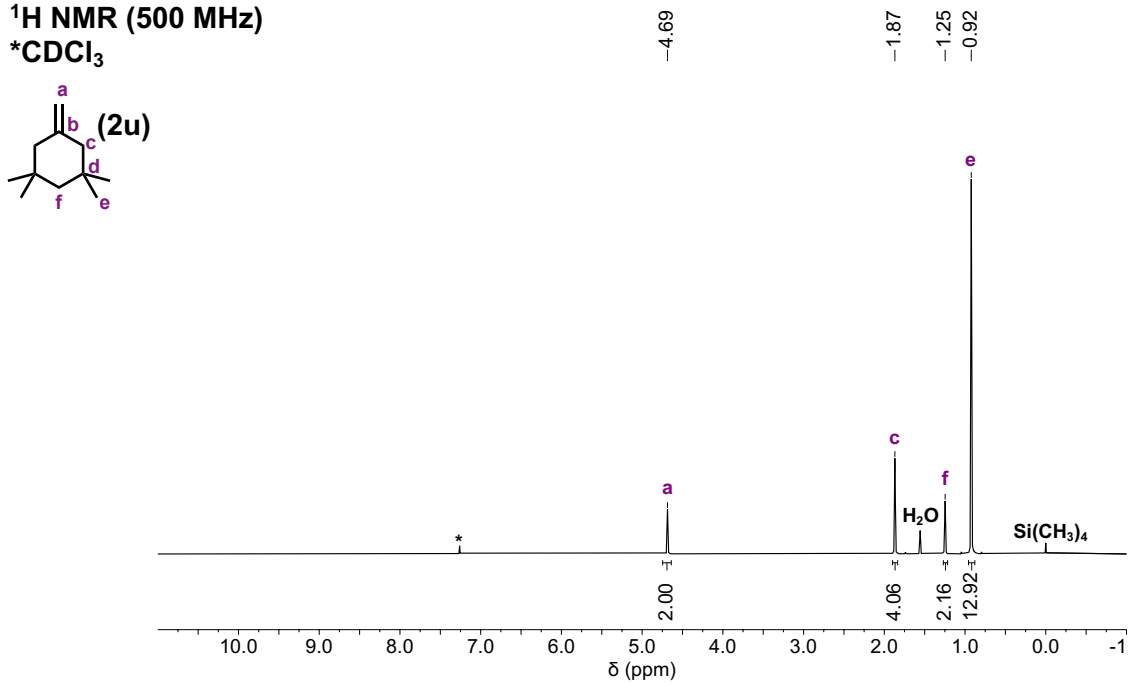

Figure A.27. ^{1}H NMR spectrum of 3,3,5,5-tetramethylmethylenecyclohexane (**2u**) recorded in $CDCl_3$ at 298 K.

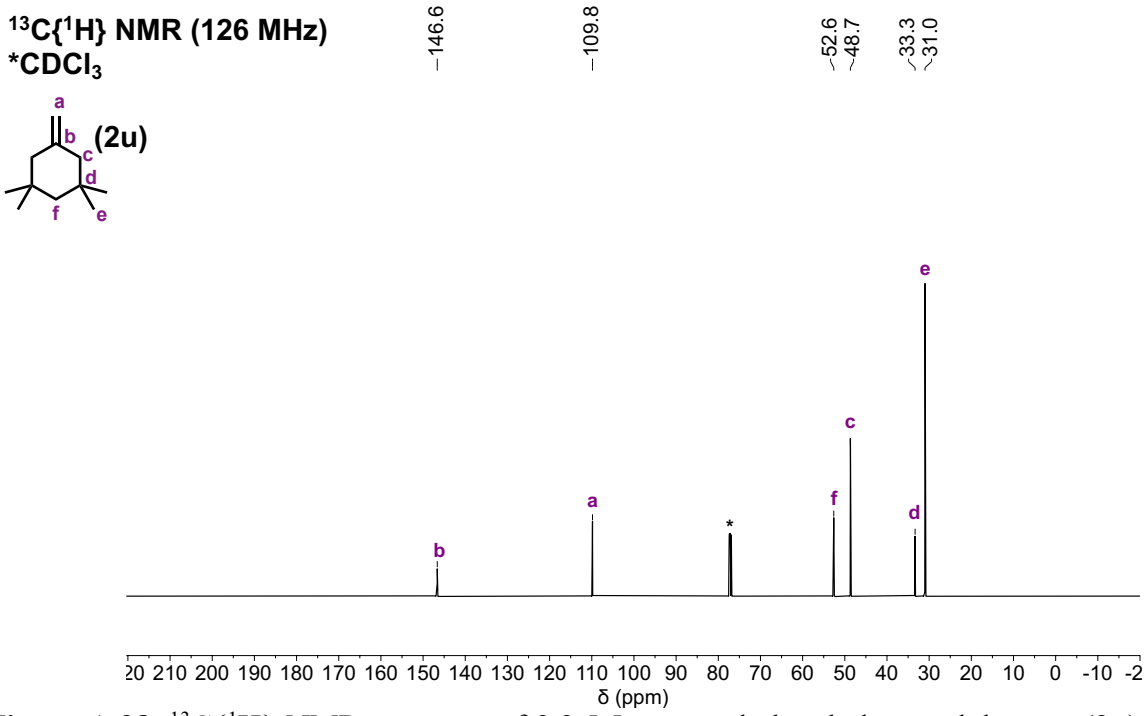

Figure A.28. $^{13}C\{^{1}H\}$ NMR spectrum of 3,3,5,5-tetramethylmethylenecyclohexane (**2u**) recorded in $CDCl_3$ at 298 K.

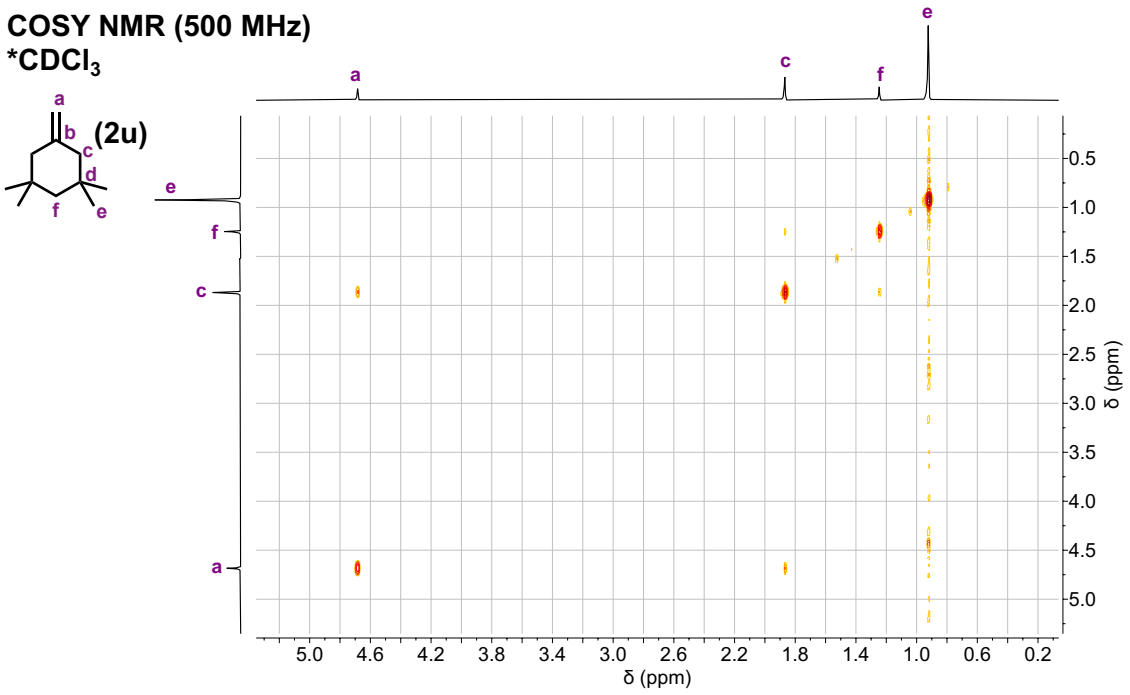

Figure A.29. COSY NMR spectrum of 3,3,5,5-tetramethylmethylenecyclohexane (**2u**) recorded in $CDCl_3$ at 298 K.

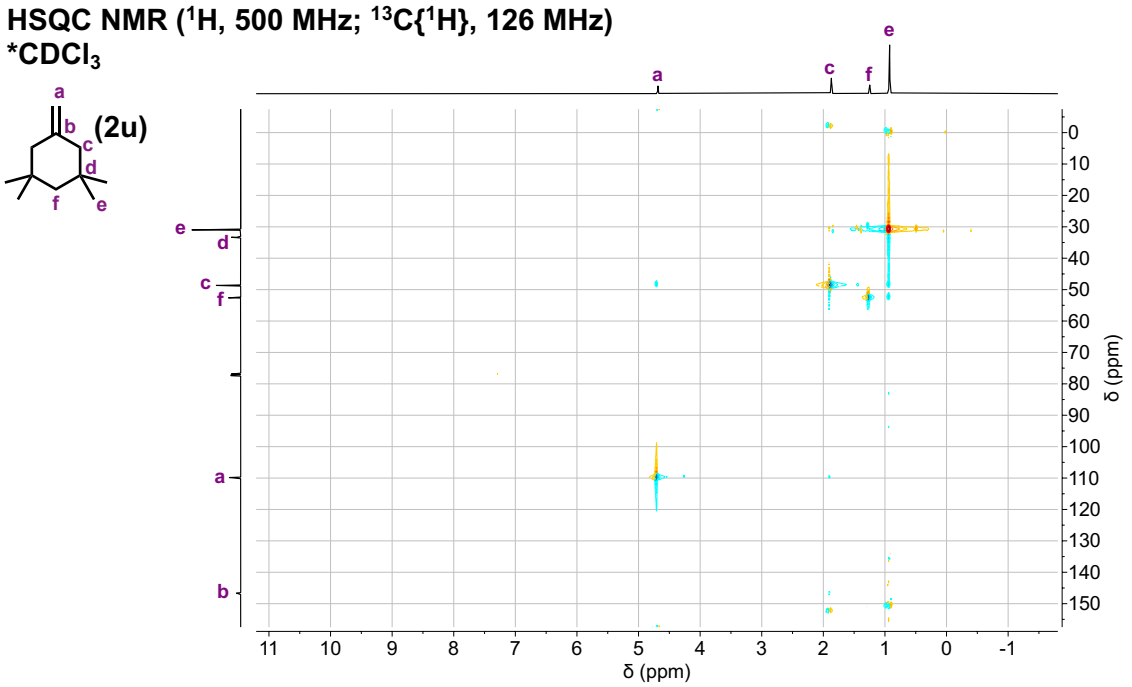

Figure A.30. HSQC NMR spectrum of 3,3,5,5-tetramethylmethylenecyclohexane (**2u**) recorded in $CDCl_3$ at 298 K.

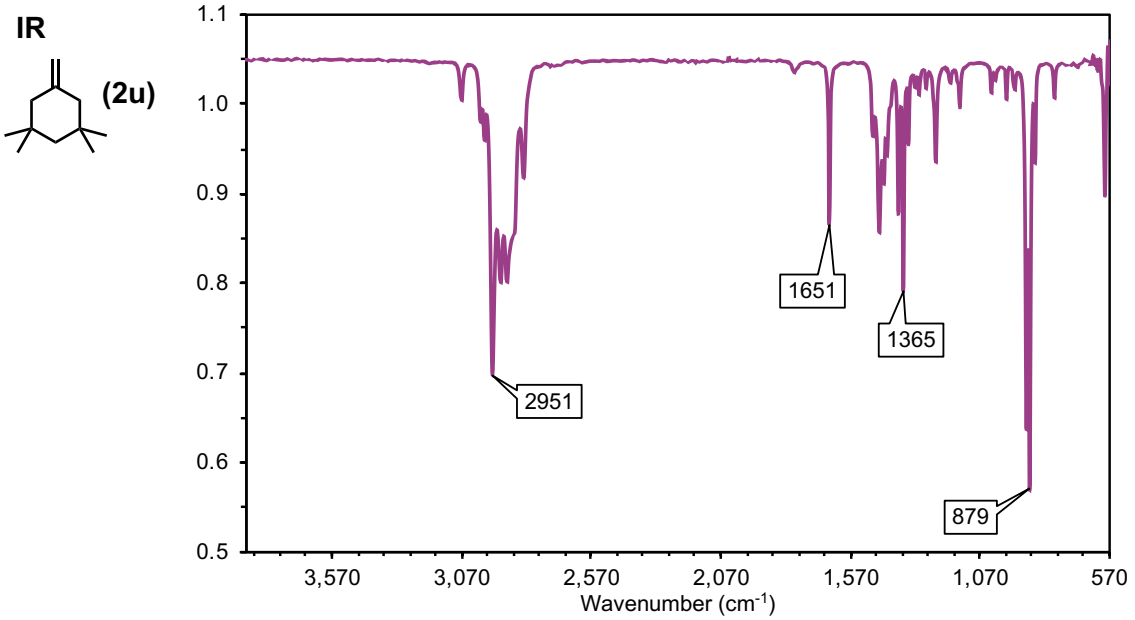

Figure A.31. IR spectrum of 3,3,5,5-tetramethylmethylenecyclohexane (**2u**) recorded neat at room temperature.

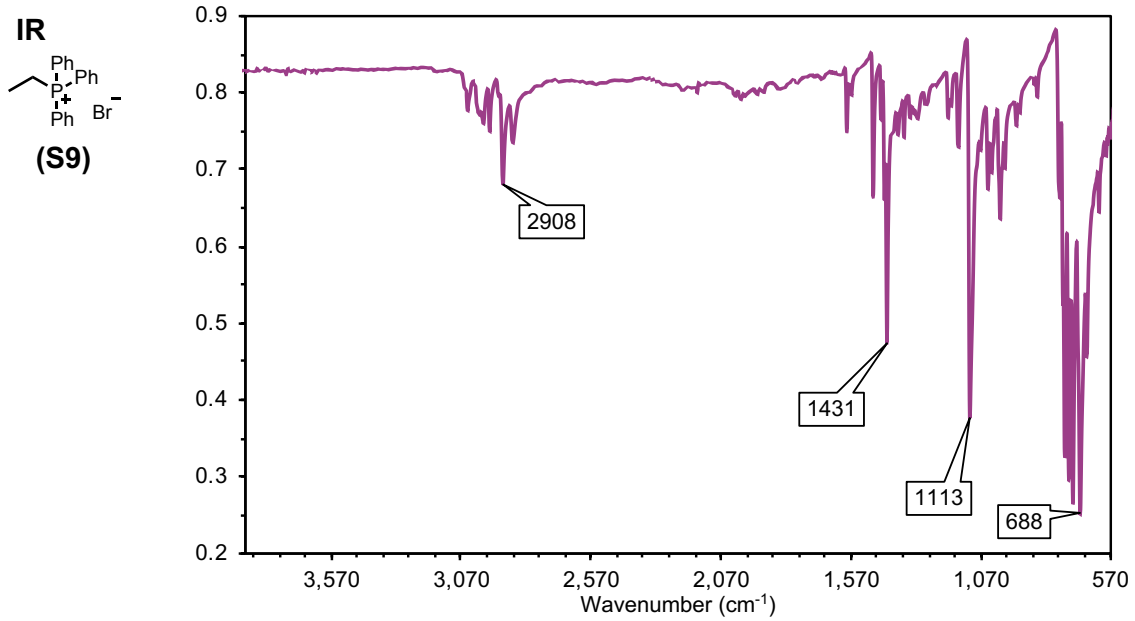

Figure A.32. IR spectrum of ethyltriphenylphosphonium bromide (**S9**) recorded neat at room temperature.

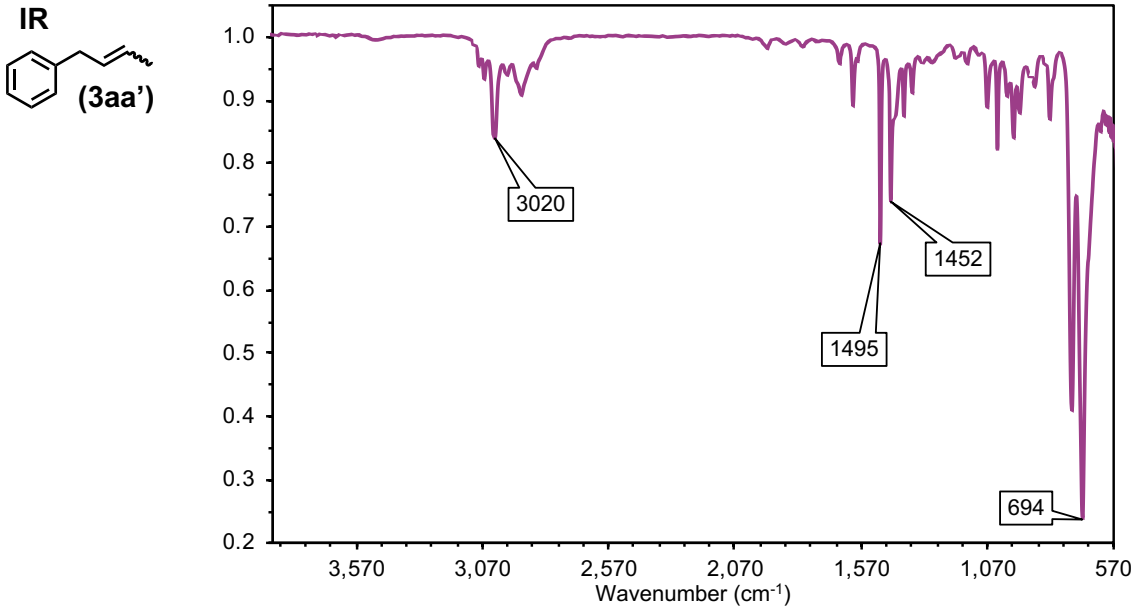

Figure A.33. IR spectrum of 4-phenyl-2-butene (**3aa'**) recorded neat at room temperature.

b. Silanes

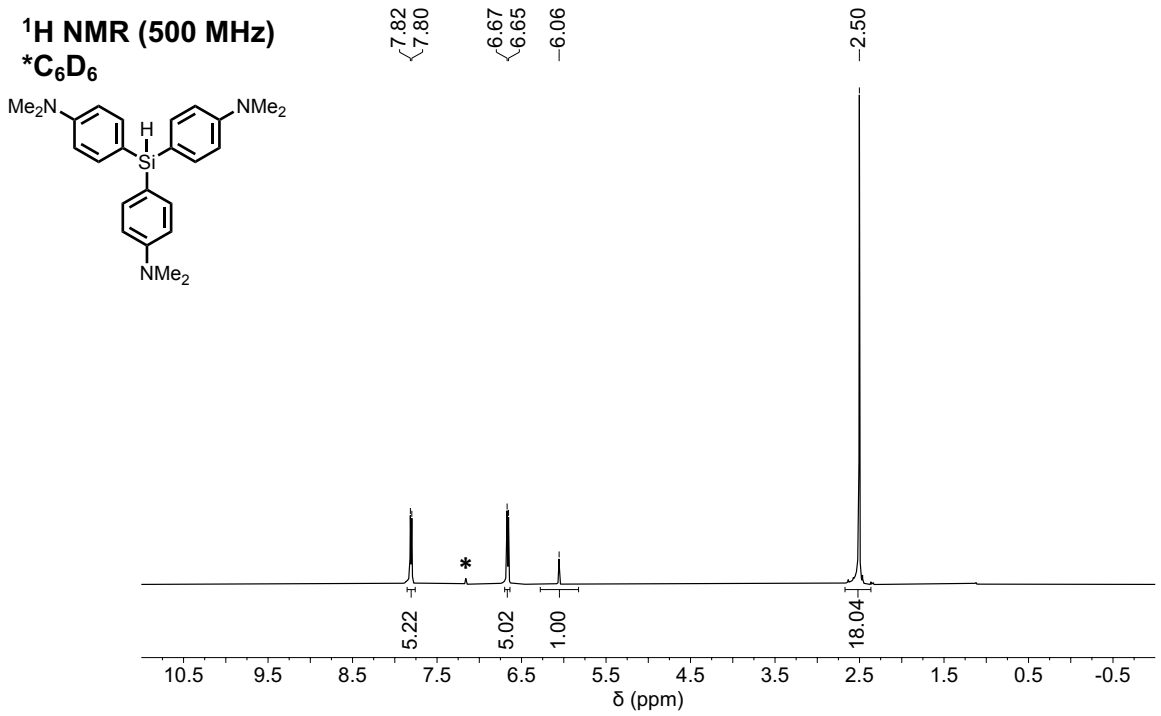

Figure A.34. ^{1}H NMR spectrum of tris[4-(*N,N*-dimethylamino)phenyl]silane (HSi(4-NMe_2-C_6H_4)$_3$) recorded in C_6D_6 at 298 K.

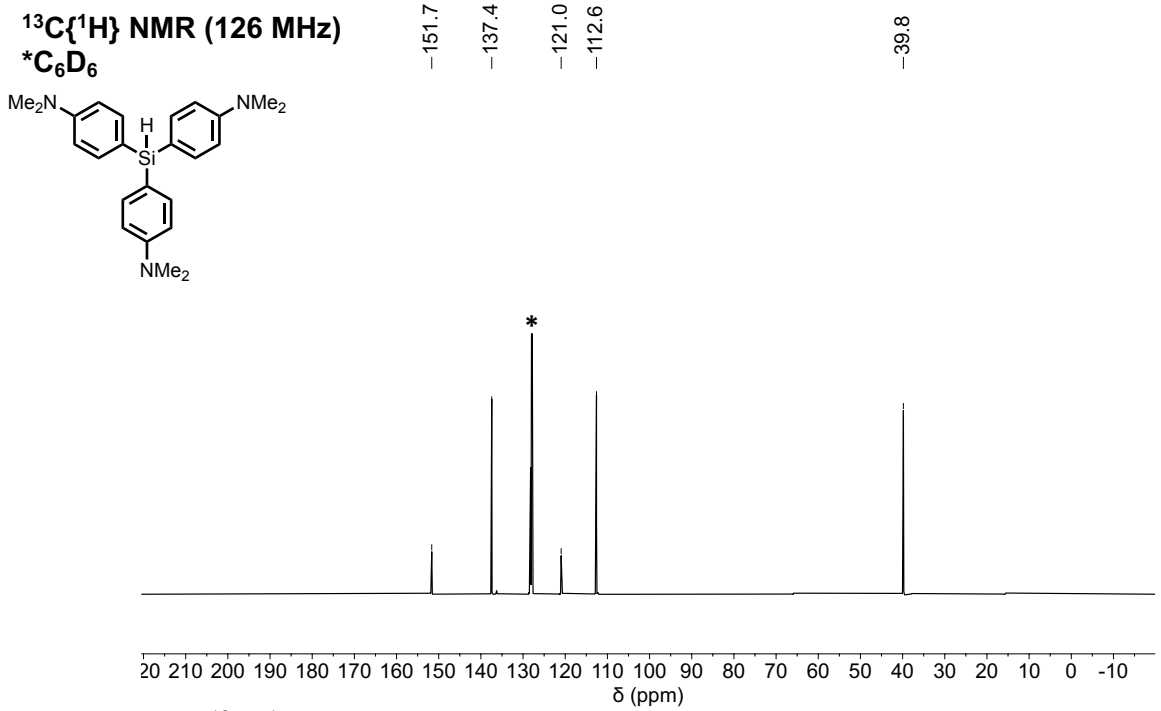

Figure A.35. ^{13}C{^{1}H} NMR spectrum of tris[4-(*N,N*-dimethylamino)phenyl]silane (HSi(4-NMe_2-C_6H_4)$_3$) recorded in C_6D_6 at 298 K.

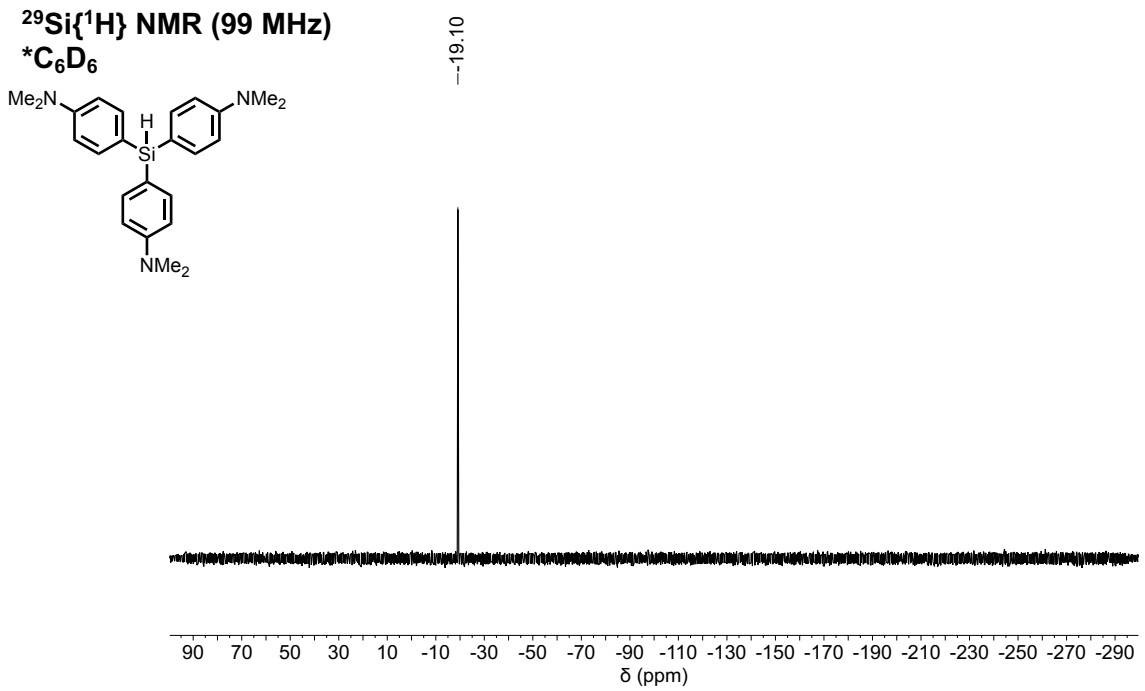

Figure A.36. $^{29}Si\{^{1}H\}$ NMR spectrum of tris[4-(*N,N*-dimethylamino)phenyl]silane ($HSi(4\text{-}NMe_2\text{-}C_6H_4)_3$) recorded in C_6D_6 at 298 K.

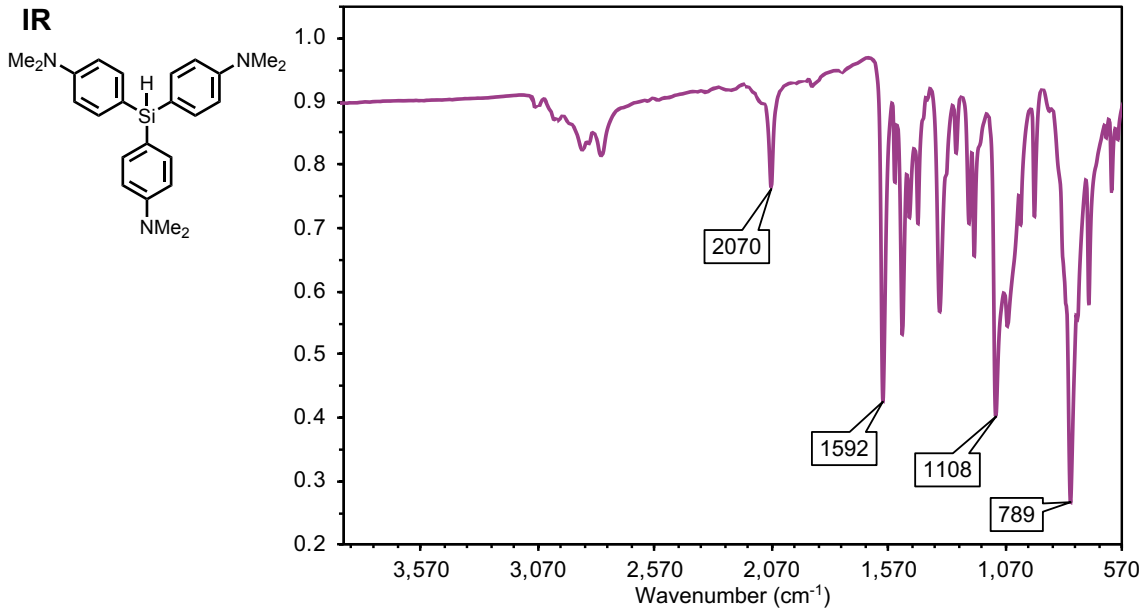

Figure A.37. IR spectrum of tris[4-(*N,N*-dimethylamino)phenyl]silane ($HSi(4\text{-}NMe_2\text{-}C_6H_4)_3$) recorded neat at room temperature.

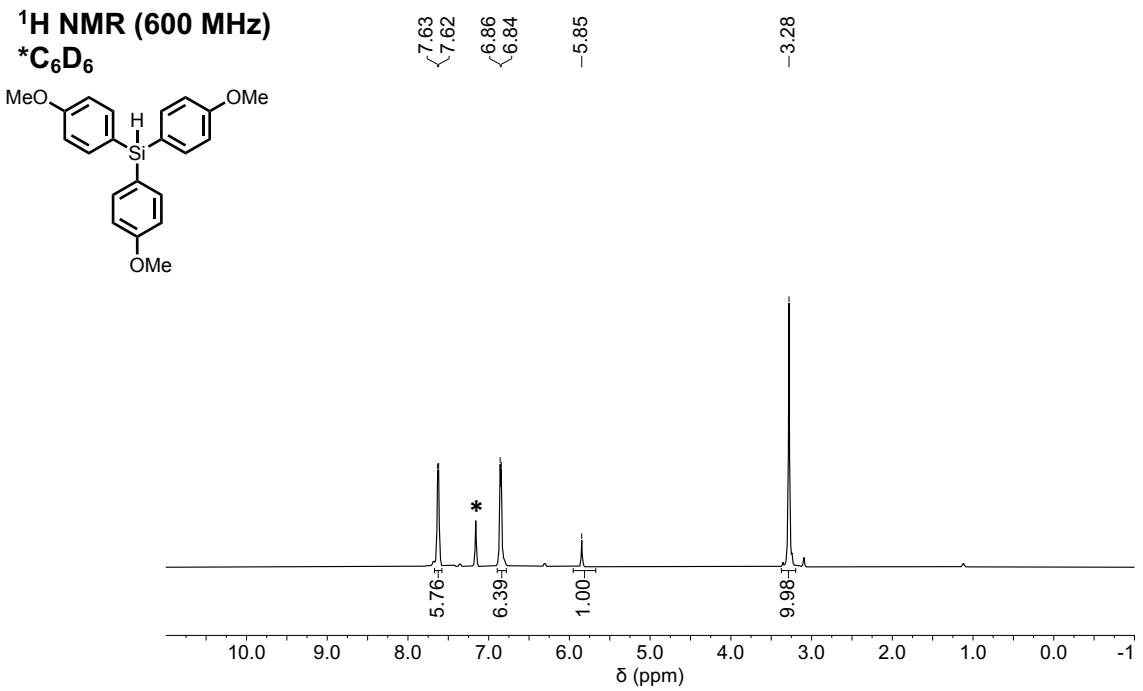

Figure A.38. ^{1}H NMR spectrum of tris(4-methoxyphenyl)silane ($HSi(4\text{-}OMe\text{-}C_6H_4)_3$) recorded in C_6D_6 at 298 K.

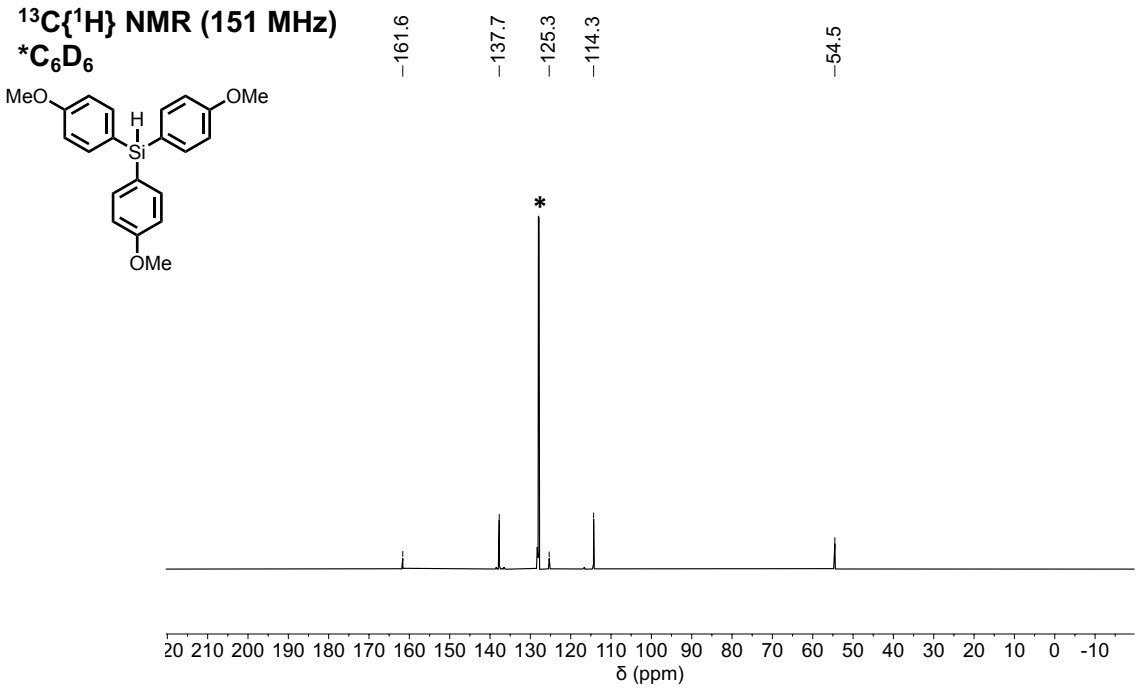

Figure A.39. $^{13}C\{^{1}H\}$ NMR spectrum of tris(4-methoxyphenyl)silane ($HSi(4\text{-}OMe\text{-}C_6H_4)_3$) recorded in C_6D_6 at 298 K.

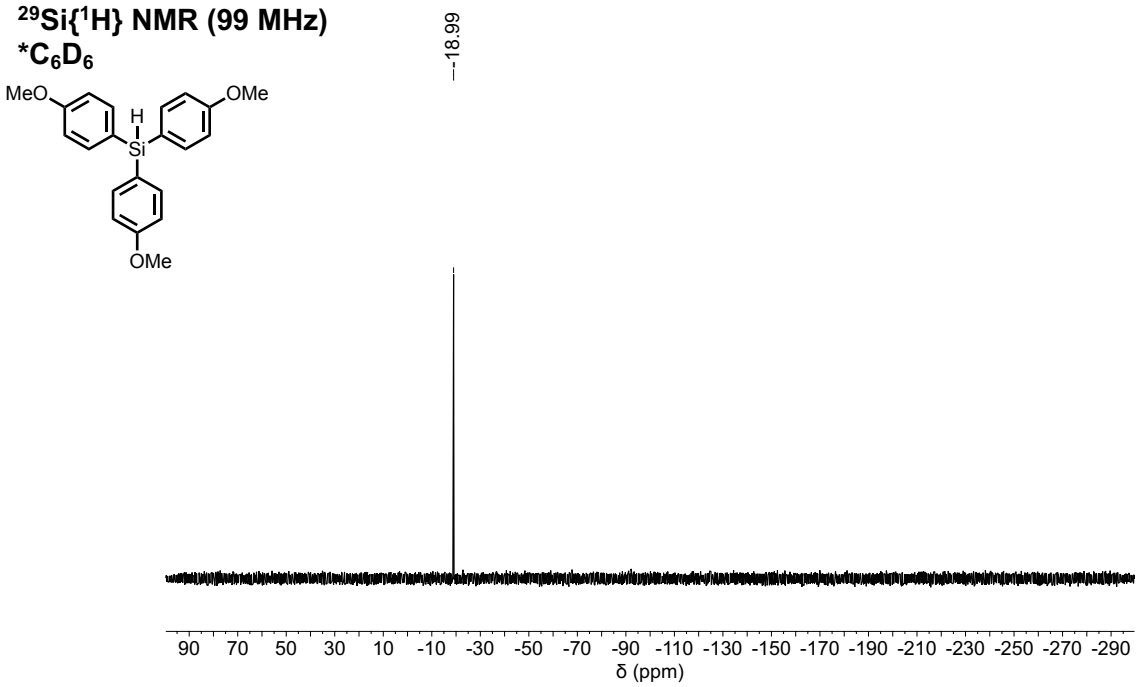

Figure A.40. $^{29}Si\{^{1}H\}$ NMR spectrum of tris(4-methoxyphenyl)silane (HSi(4-OMe-$C_6H_4)_3$) recorded in C_6D_6 at 298 K.

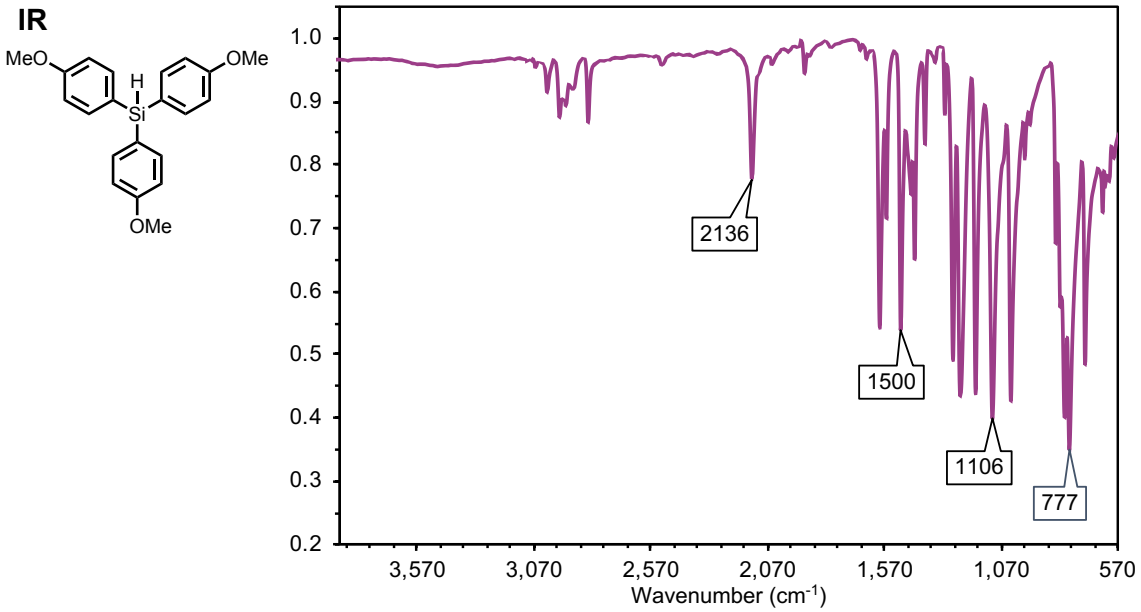

Figure A.41. IR spectrum of tris(4-methoxyphenyl)silane (HSi(4-OMe-$C_6H_4)_3$) recorded neat at room temperature.

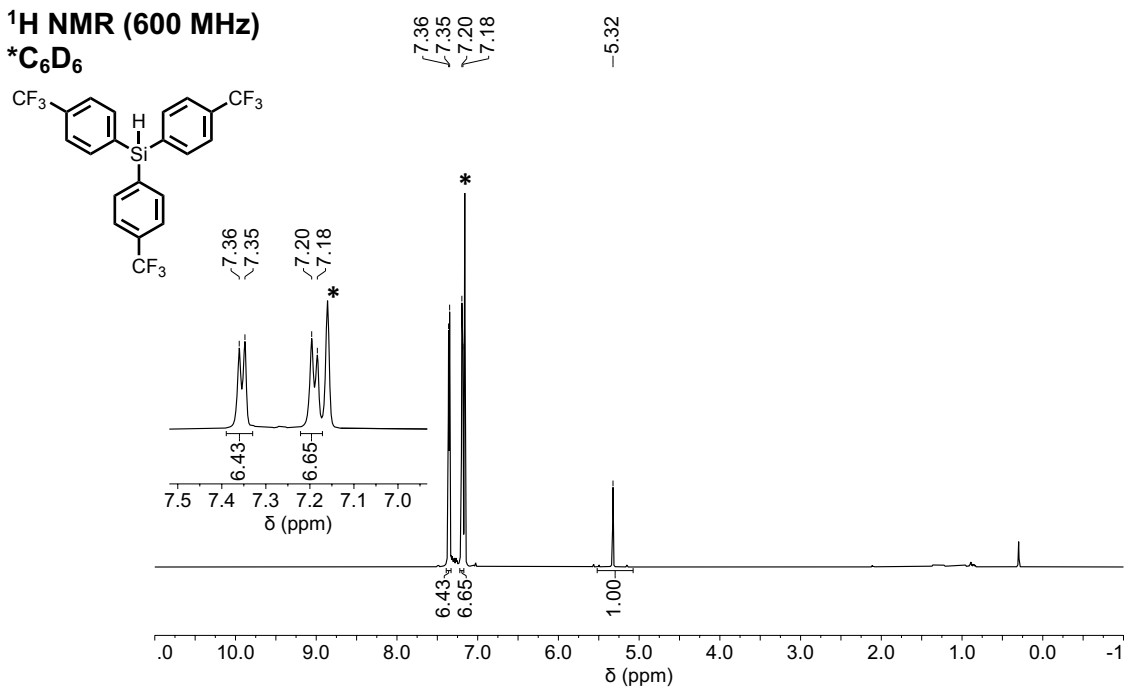

Figure A.42. ^{1}H NMR spectrum of tris[4-(trifluoromethyl)phenyl]silane ($HSi(4\text{-}CF_3\text{-}C_6H_4)_3$) recorded in C_6D_6 at 298 K.

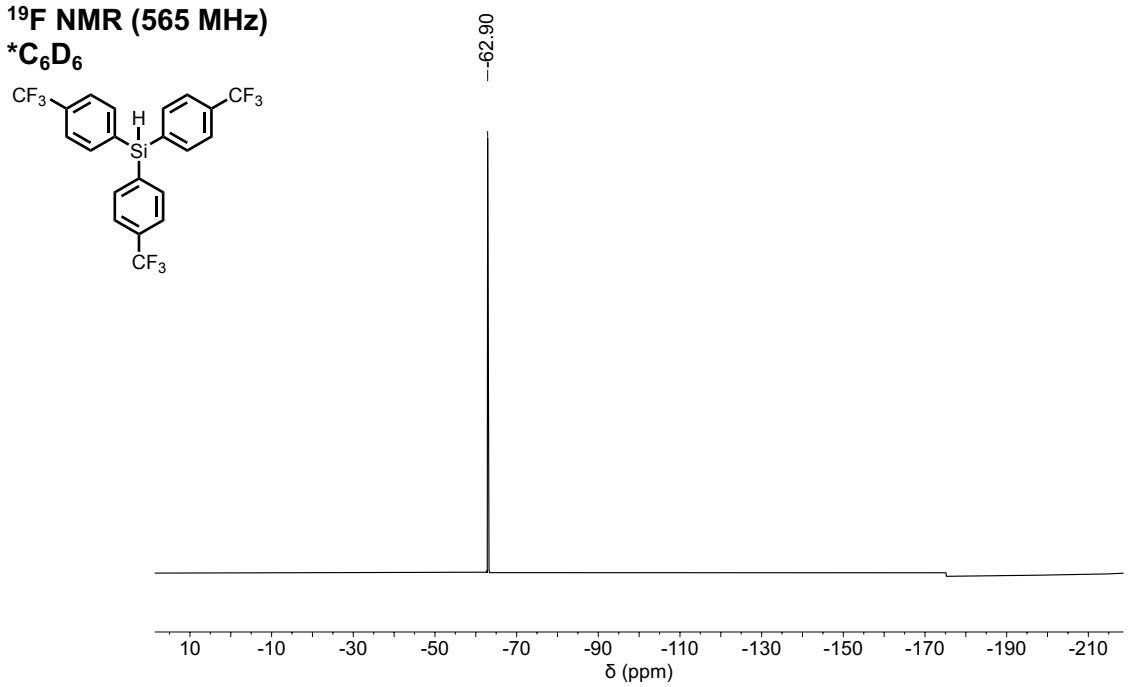

Figure A.43. ^{19}F NMR spectrum of tris[4-(trifluoromethyl)phenyl]silane ($HSi(4\text{-}CF_3\text{-}C_6H_4)_3$) recorded in C_6D_6 at 298 K.

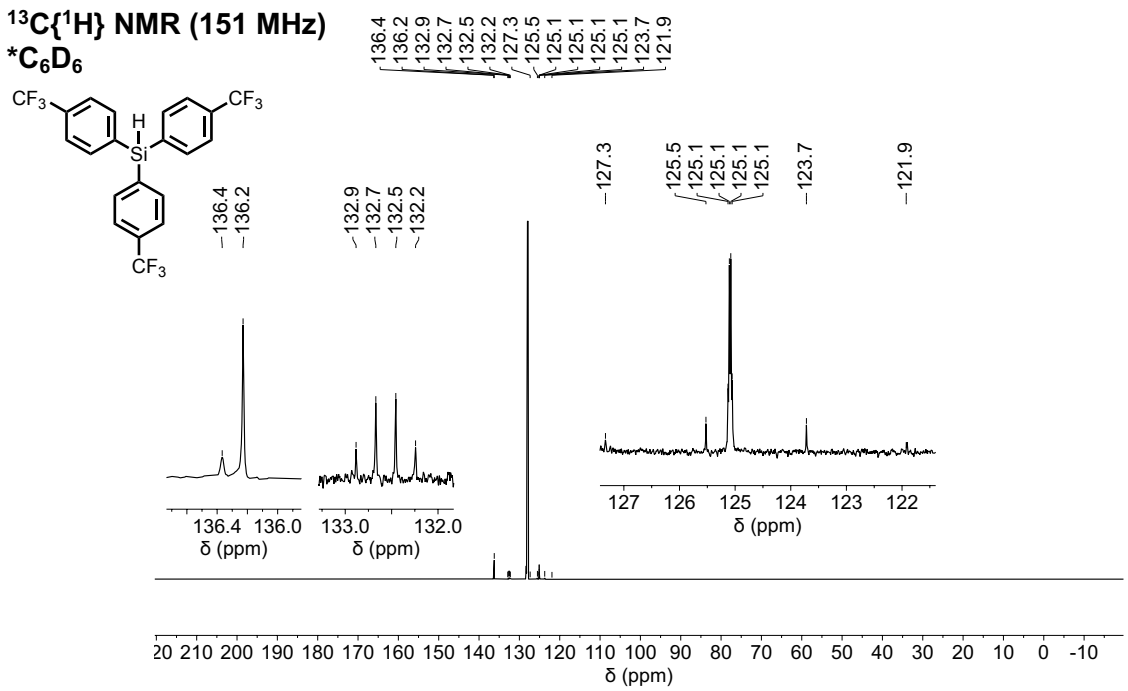

Figure A.44. $^{13}C\{^{1}H\}$ NMR spectrum of tris[4-(trifluoromethyl)phenyl]silane (HSi(4-CF_3-$C_6H_4)_3$) recorded in C_6D_6 at 298 K.

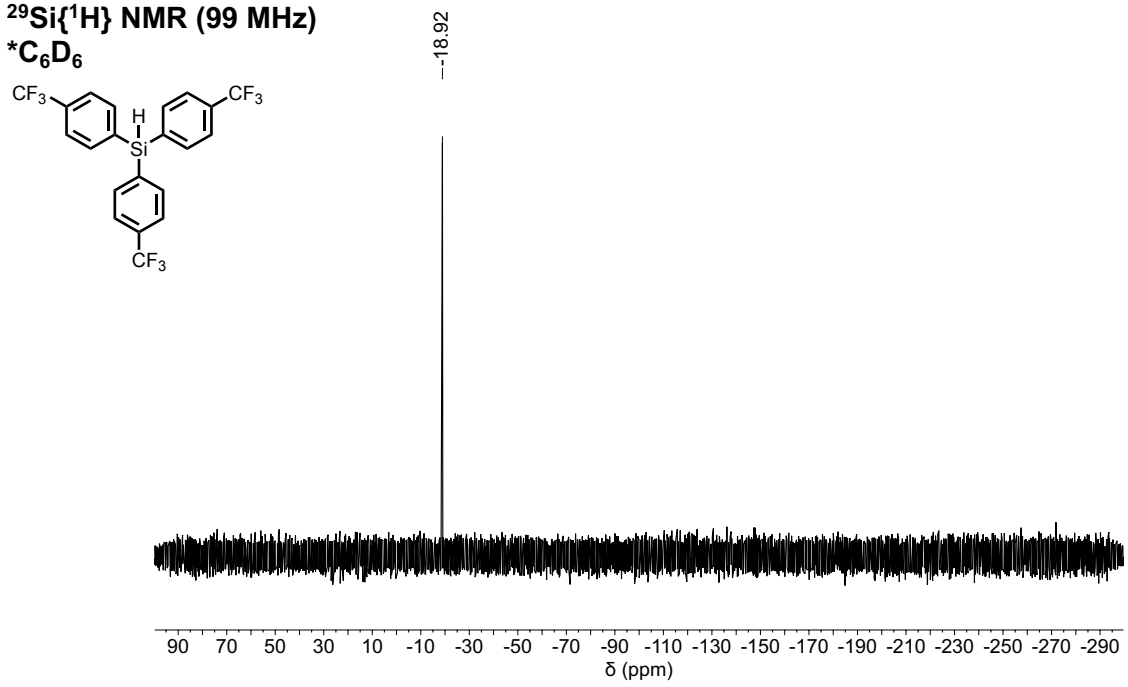

Figure A.45. $^{29}Si\{^{1}H\}$ NMR spectrum of tris[4-(trifluoromethyl)phenyl]silane (HSi(4-CF_3-$C_6H_4)_3$) recorded in C_6D_6 at 298 K.

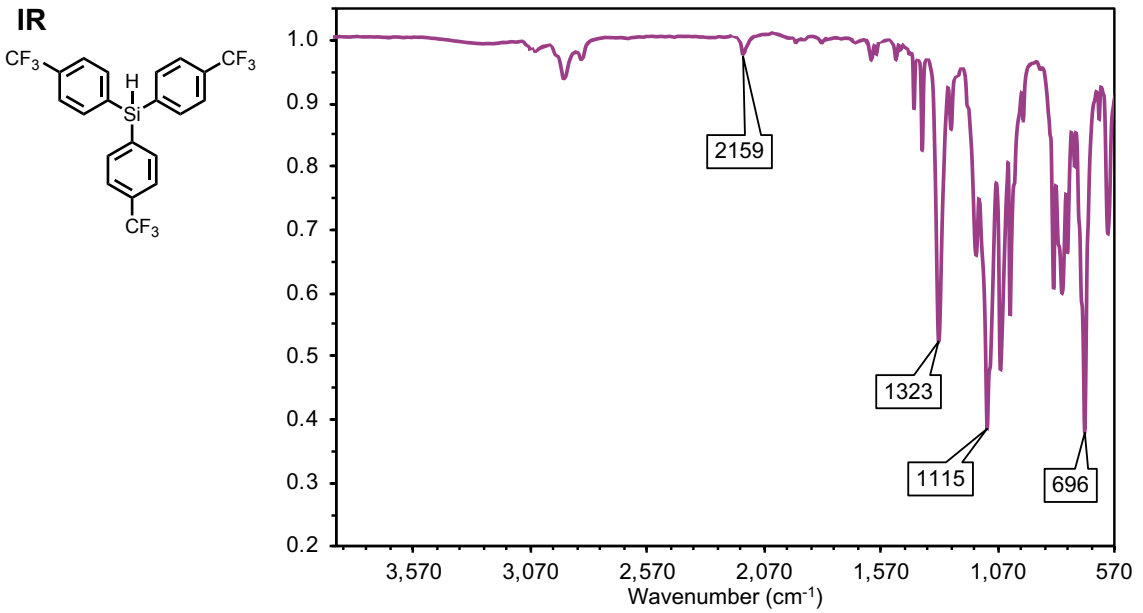

Figure A.46. IR spectrum of tris[4-(trifluoromethyl)phenyl]silane ($HSi(4\text{-}CF_3\text{-}C_6H_4)_3$) recorded neat at room temperature.

c. Deuterated Substrates

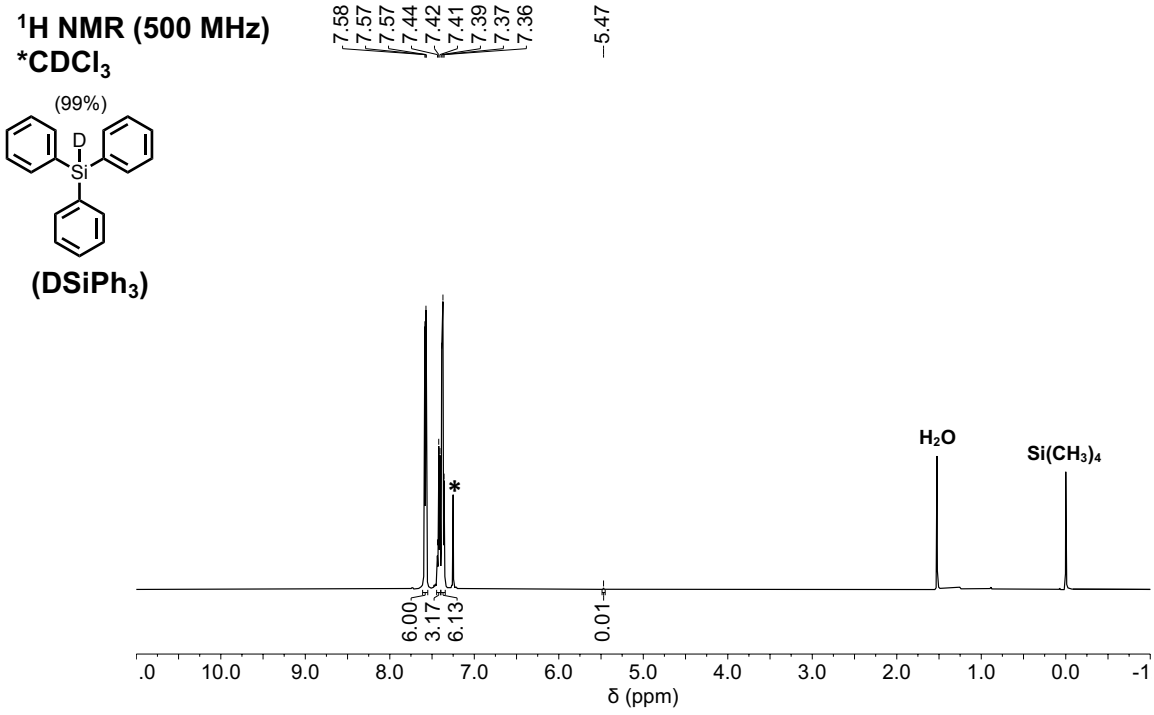

Figure A.47. ^1H NMR spectrum of triphenylsilane-d_1 ($DSiPh_3$) recorded in $CDCl_3$ at 298 K.

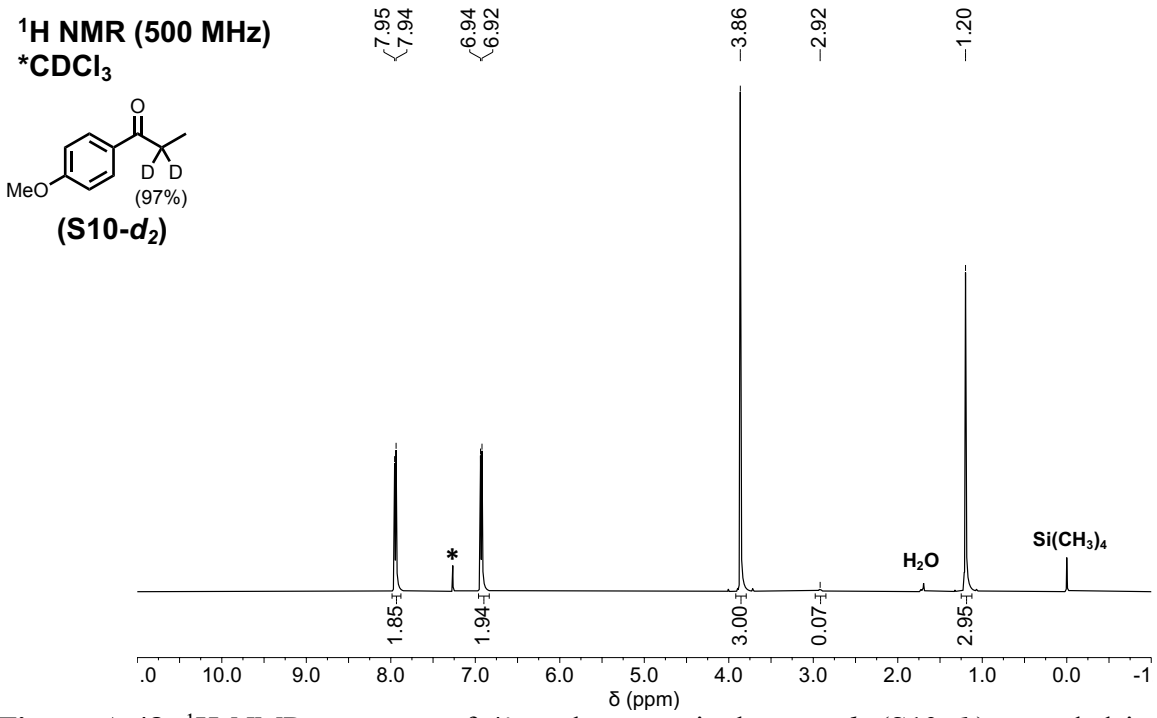

Figure A.48. ^{1}H NMR spectrum of 4'-methoxypropiophenone-d_2 (**S10-*d*$_2$**) recorded in $CDCl_3$ at 298 K.

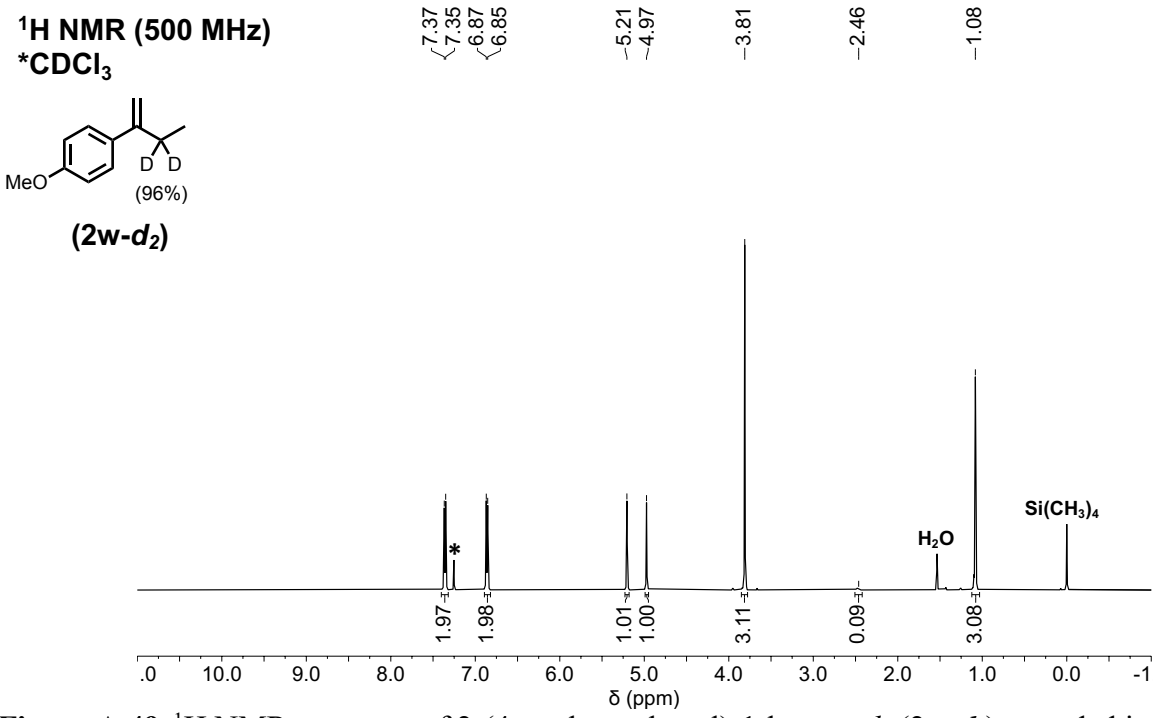

Figure A.49. ^{1}H NMR spectrum of 2-(4-methoxyphenyl)-1-butene-d_2 (**2w-*d*$_2$**) recorded in $CDCl_3$ at 298 K.

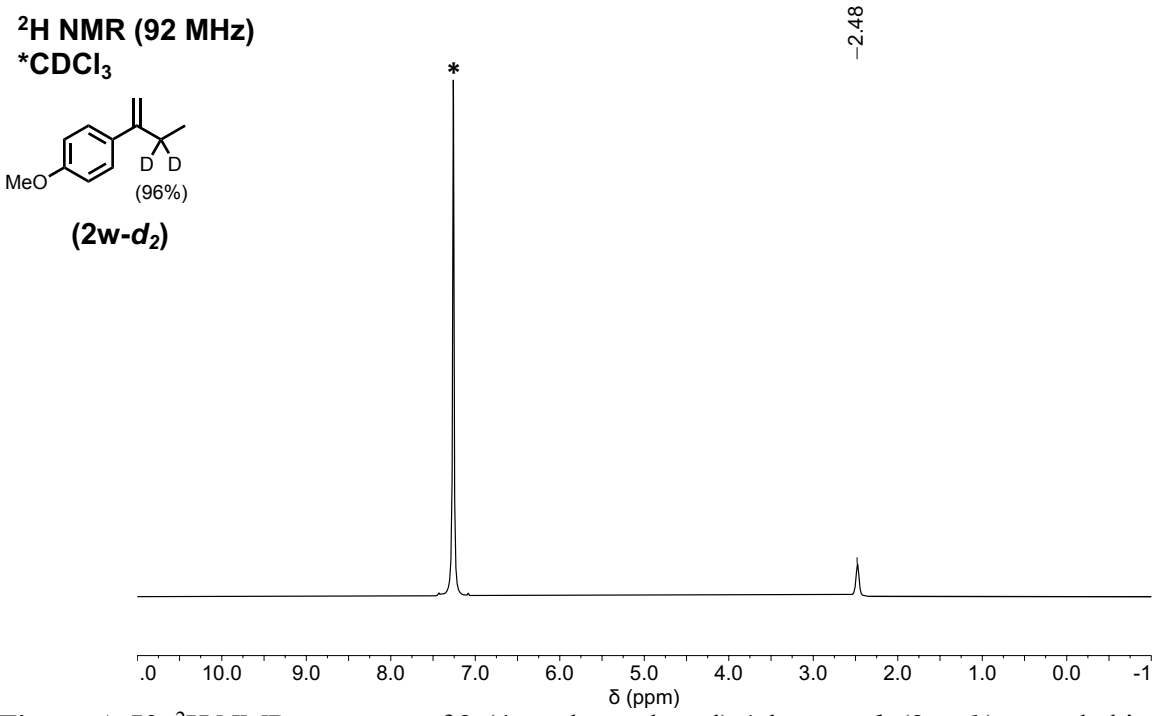

Figure A.50. ^{2}H NMR spectrum of 2-(4-methoxyphenyl)-1-butene-d_2 (**2w-*d*$_2$**) recorded in $CDCl_3$ at 298 K.

d. Isomerization Products

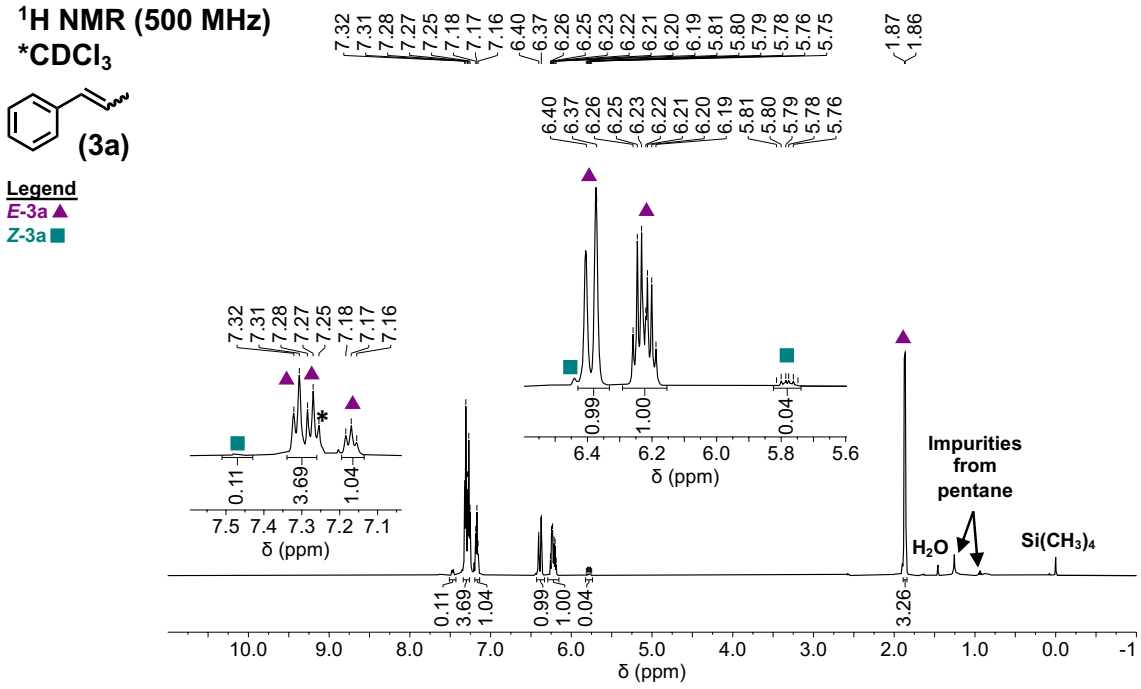

Figure A.51. ^{1}H NMR spectrum of β-methylstyrene (**3a**) recorded in $CDCl_3$ at 298 K.

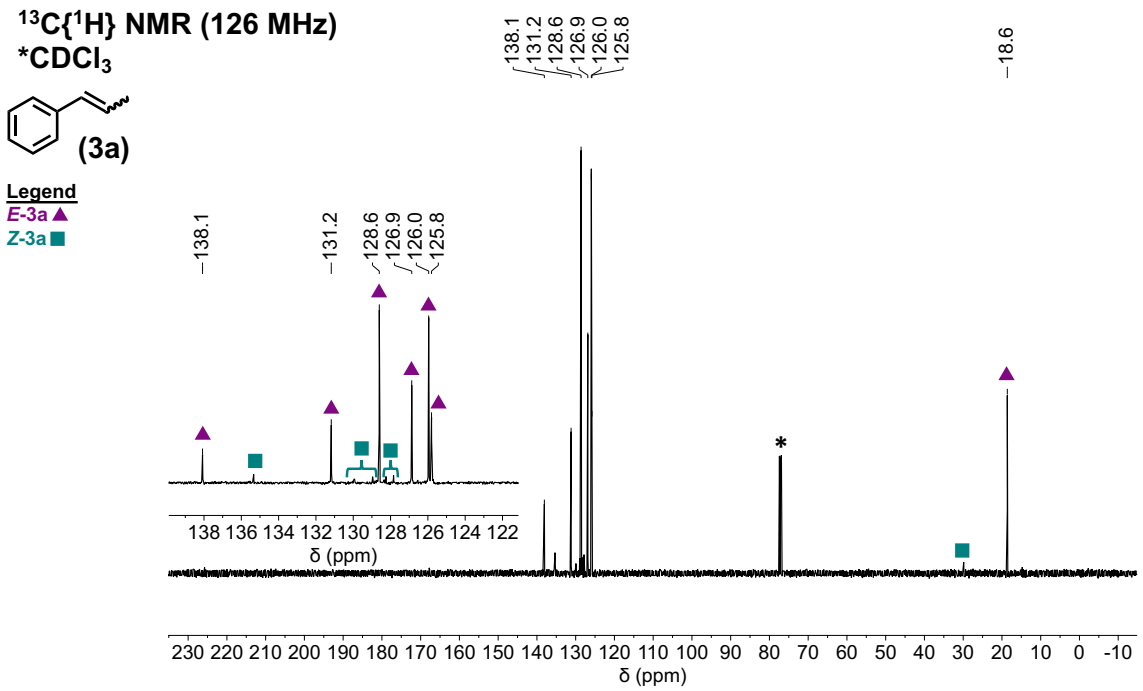

Figure A.52. $^{13}C\{^{1}H\}$ NMR spectrum of β-methylstyrene (**3a**) recorded in $CDCl_3$ at 298 K.

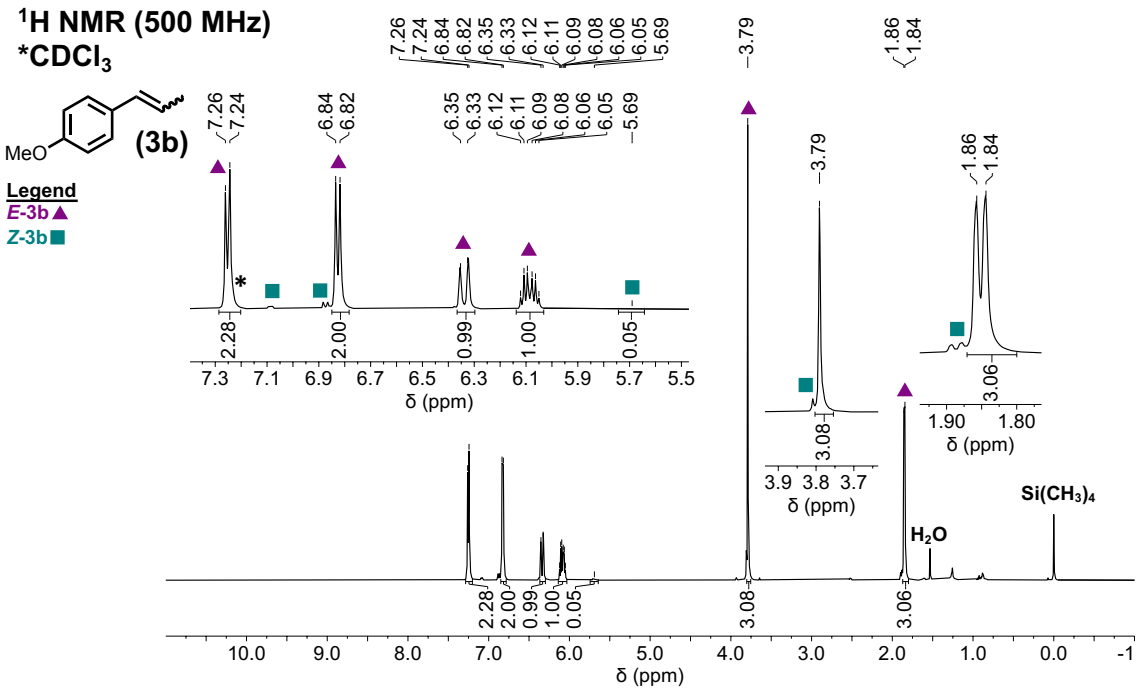

Figure A.53. ^{1}H NMR spectrum of anethole (**3b**) recorded in $CDCl_3$ at 298 K.

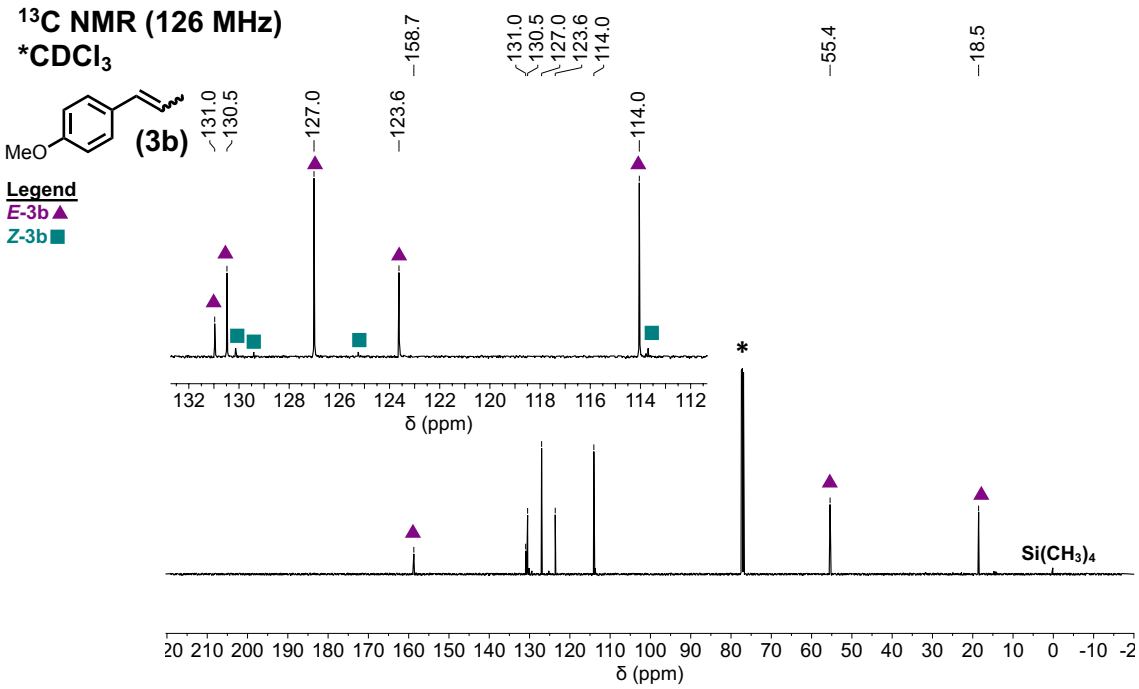

Figure A.54. $^{13}C\{^{1}H\}$ NMR spectrum of anethole (**3b**) recorded in $CDCl_3$ at 298 K.

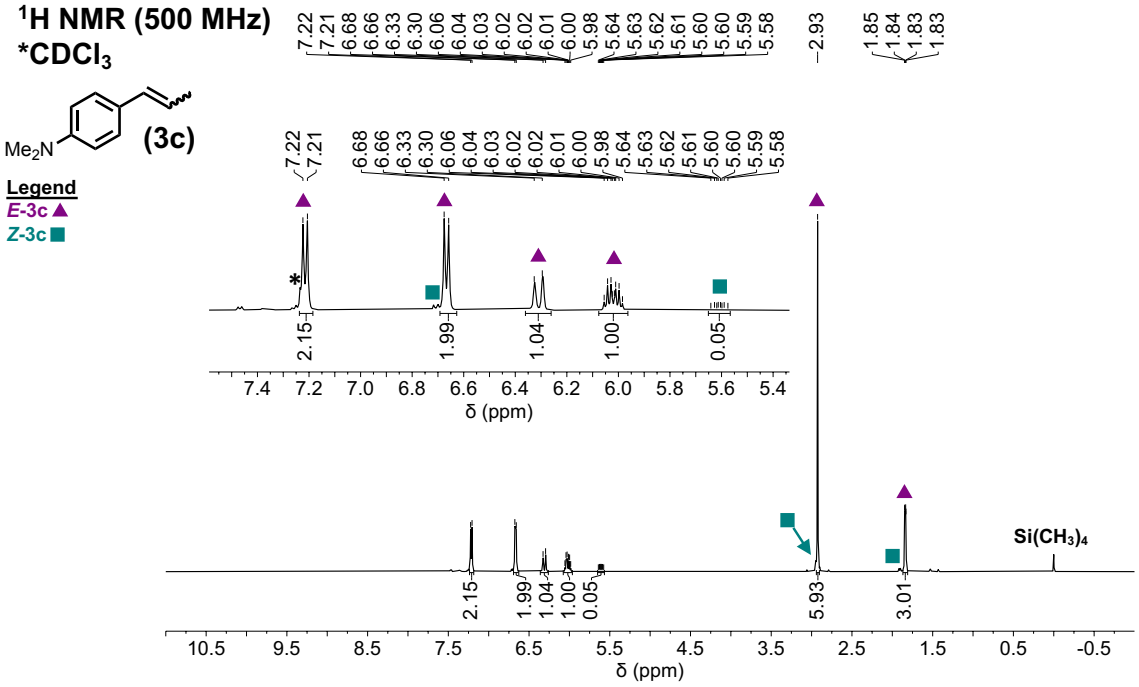

Figure A.55. ^{1}H NMR spectrum of *N,N*-dimethyl-4-(1-propen-1-yl)benzeneamine (**3c**) recorded in $CDCl_3$ at 298 K.

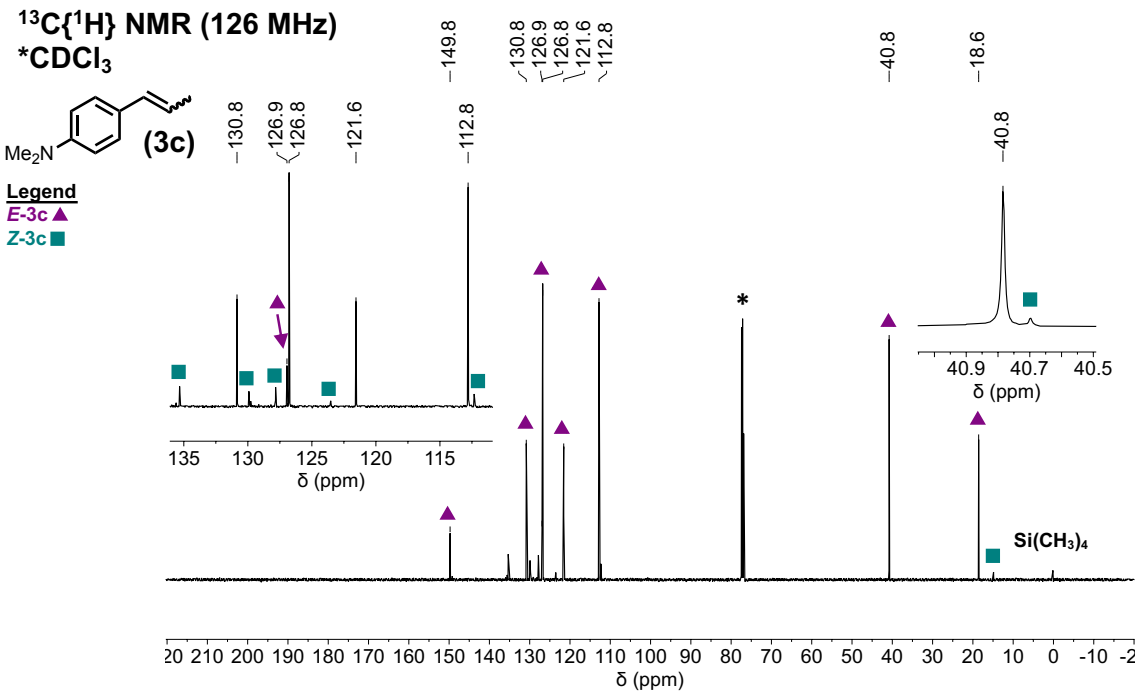

Figure A.56. $^{13}C\{^{1}H\}$ NMR spectrum of *N,N*-dimethyl-4-(1-propen-1-yl)benzeneamine (**3c**) recorded in $CDCl_3$ at 298 K.

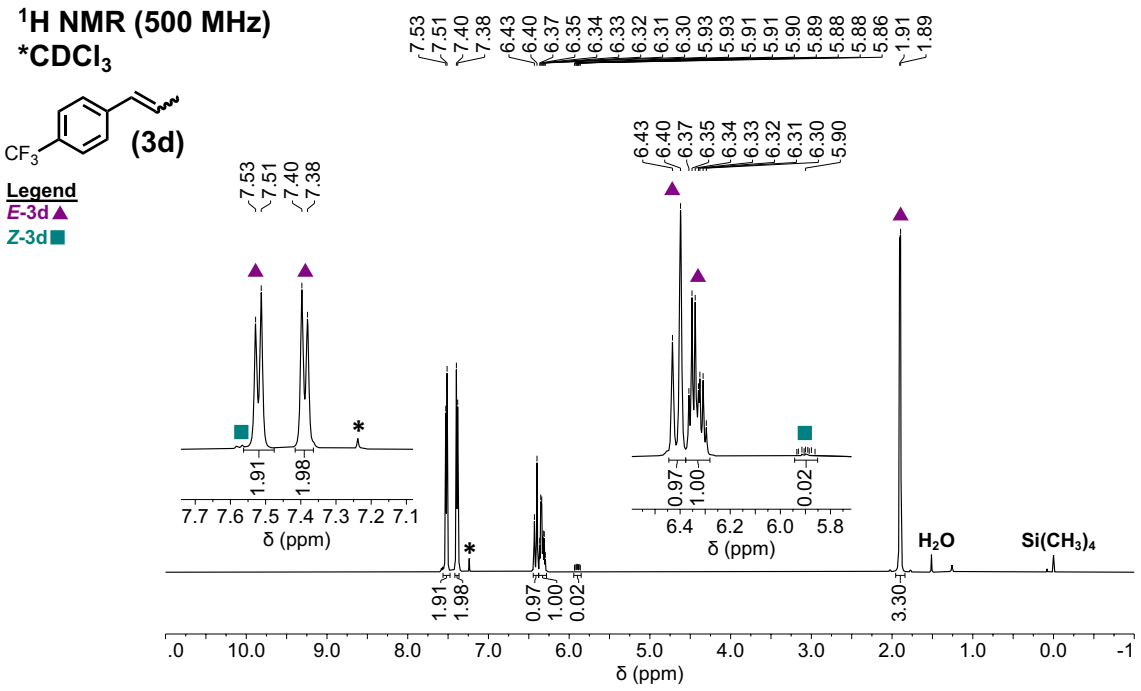

Figure A.57. ^{1}H NMR spectrum of 1-(4-trifluoromethylphenyl)1-propene (**3d**) recorded in $CDCl_3$ at 298 K.

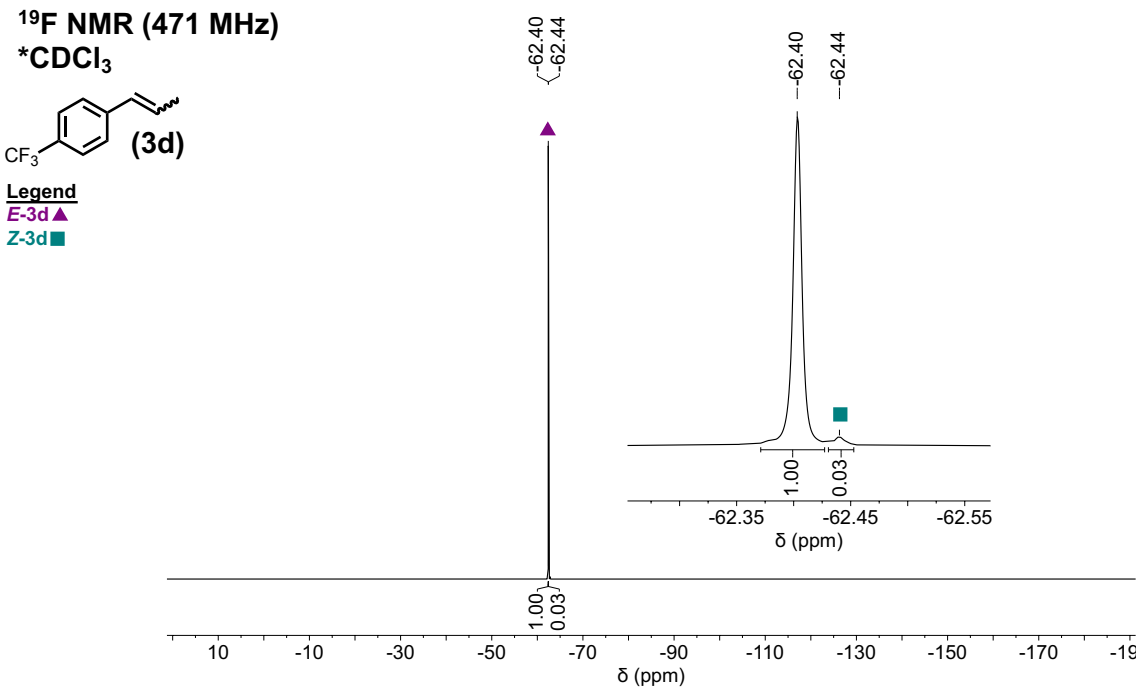

Figure A.58. ^{19}F NMR spectrum of 1-(4-trifluoromethylphenyl)1-propene (**3d**) recorded in $CDCl_3$ at 298 K.

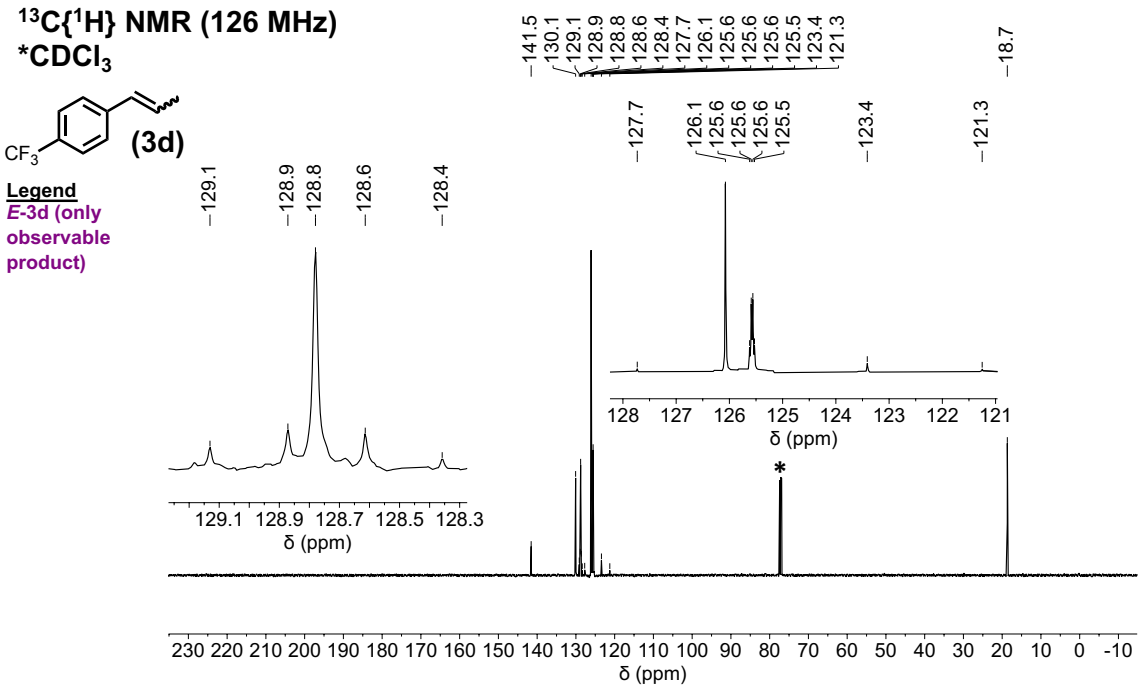

Figure A.59. $^{13}C\{^{1}H\}$ NMR spectrum of 1-(4-trifluoromethylphenyl)1-propene (**3d**) recorded in $CDCl_3$ at 298 K.

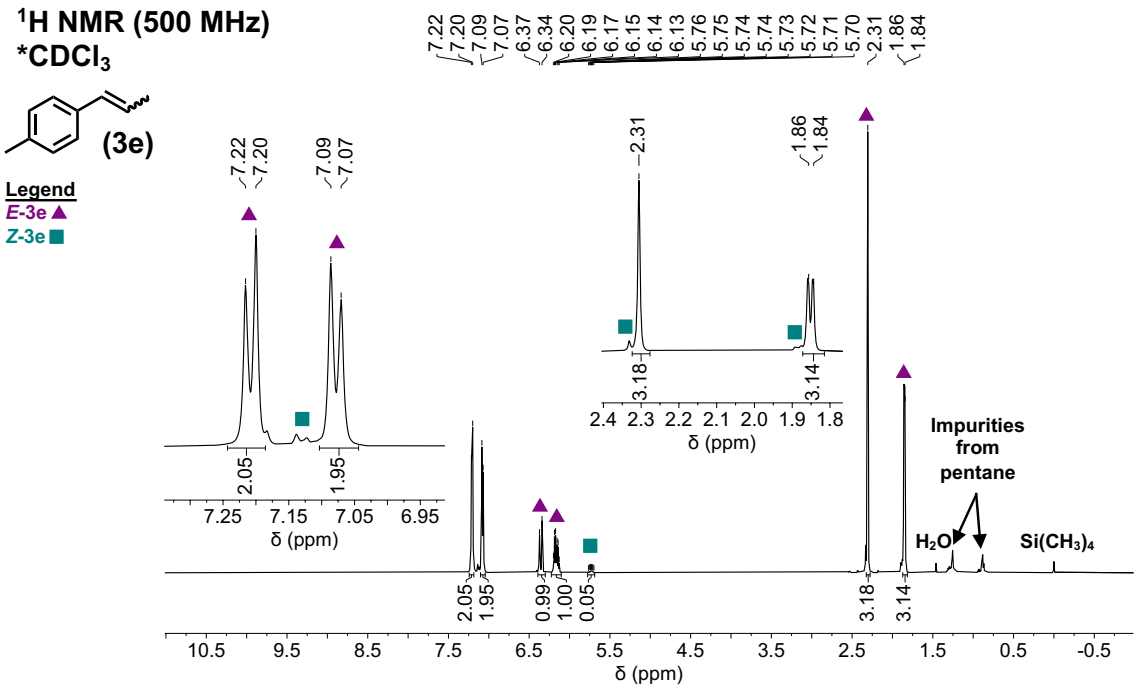

Figure A.60. ^{1}H NMR spectrum of 1-(4-methylphenyl)1-propene (**3e**) recorded in $CDCl_3$ at 298 K.

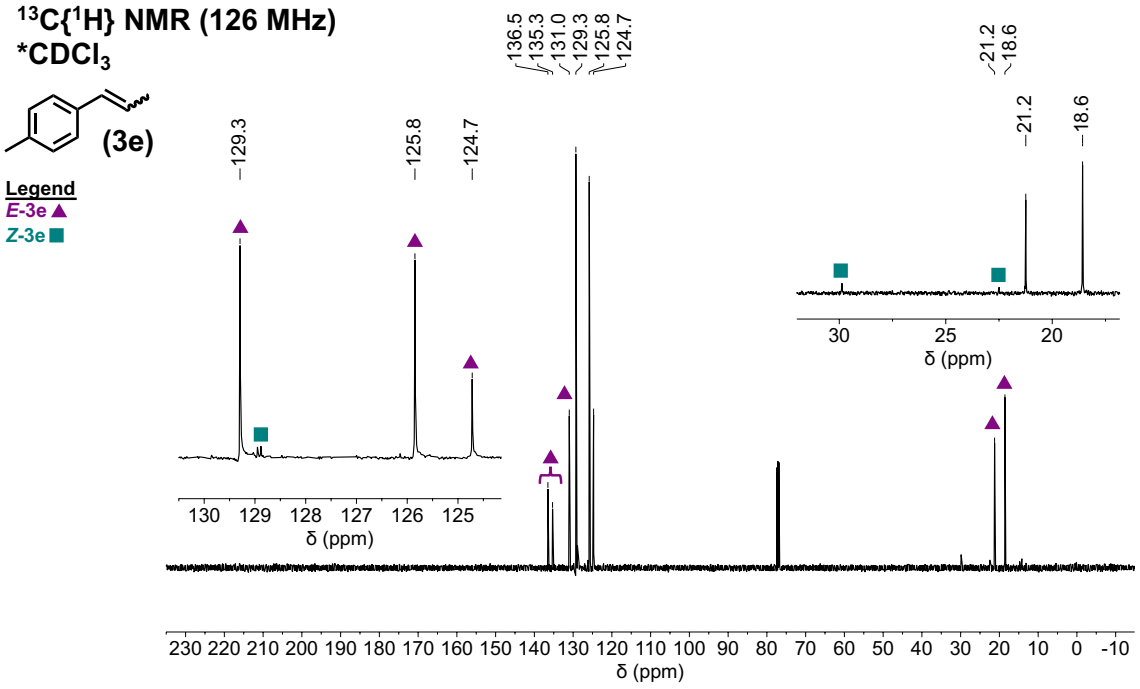

Figure A.61. $^{13}C\{^{1}H\}$ NMR spectrum of 1-(4-methylphenyl)1-propene (**3e**) recorded in $CDCl_3$ at 298 K.

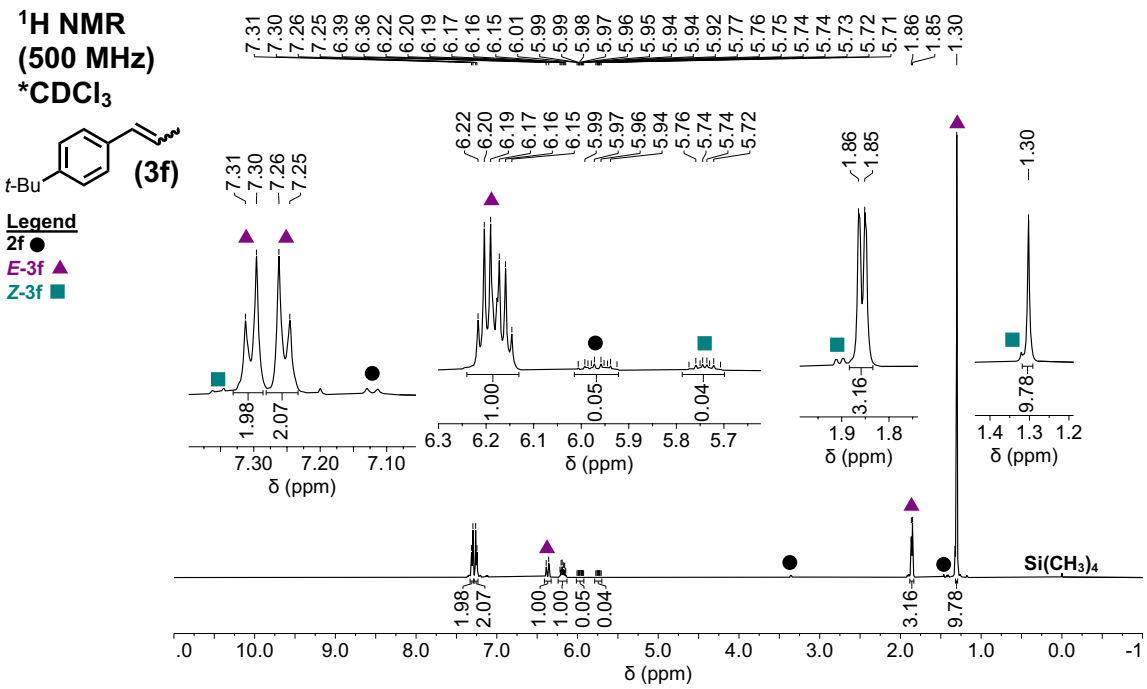

Figure A.62. ^{1}H NMR spectrum of 1-(1,1-dimethylethyl)-4-(1-propen-1-yl)benzene (**3f**) recorded in $CDCl_3$ at 298 K.

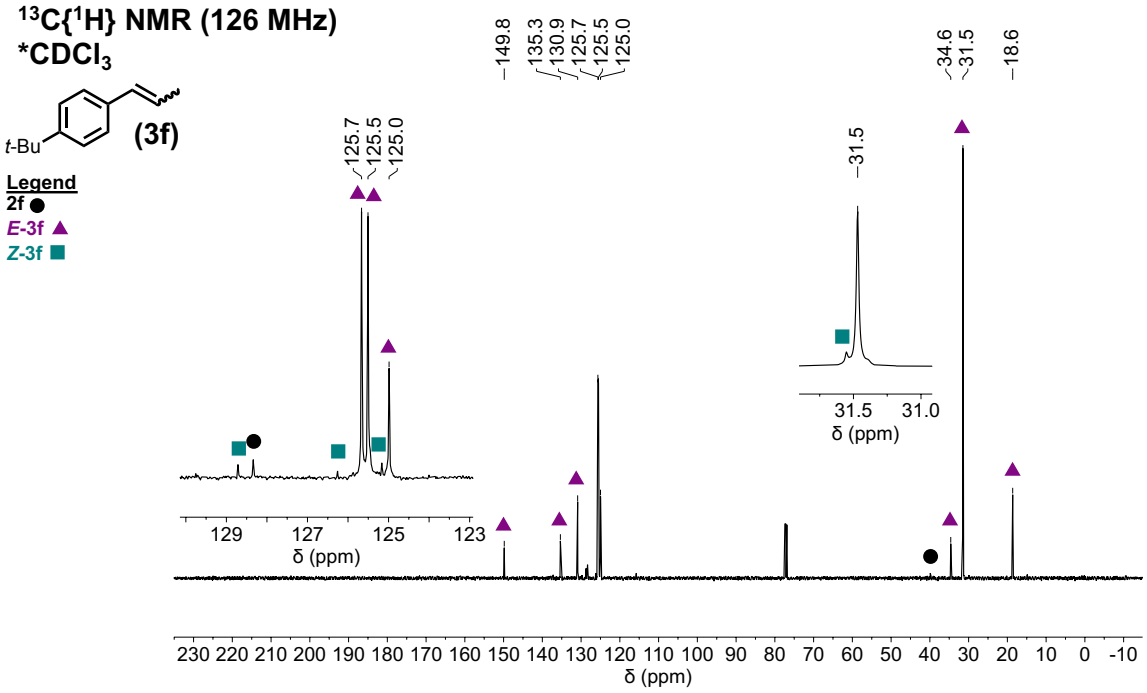

Figure A.63. ^{13}C{^{1}H} NMR spectrum of 1-(1,1-dimethylethyl)-4-(1-propen-1-yl)benzene (**3f**) recorded in $CDCl_3$ at 298 K.

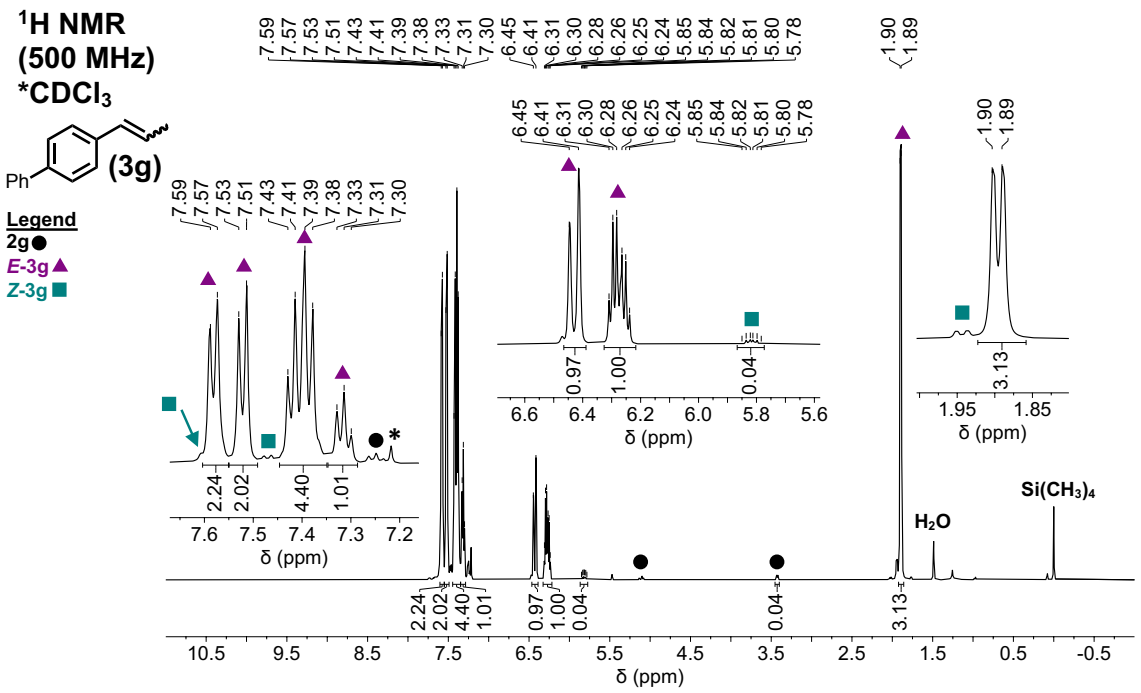

Figure A.64. ^{1}H NMR spectrum of 4-(1-propen-1-yl)-1,1'-biphenyl (**3g**) recorded in $CDCl_3$ at 298 K.

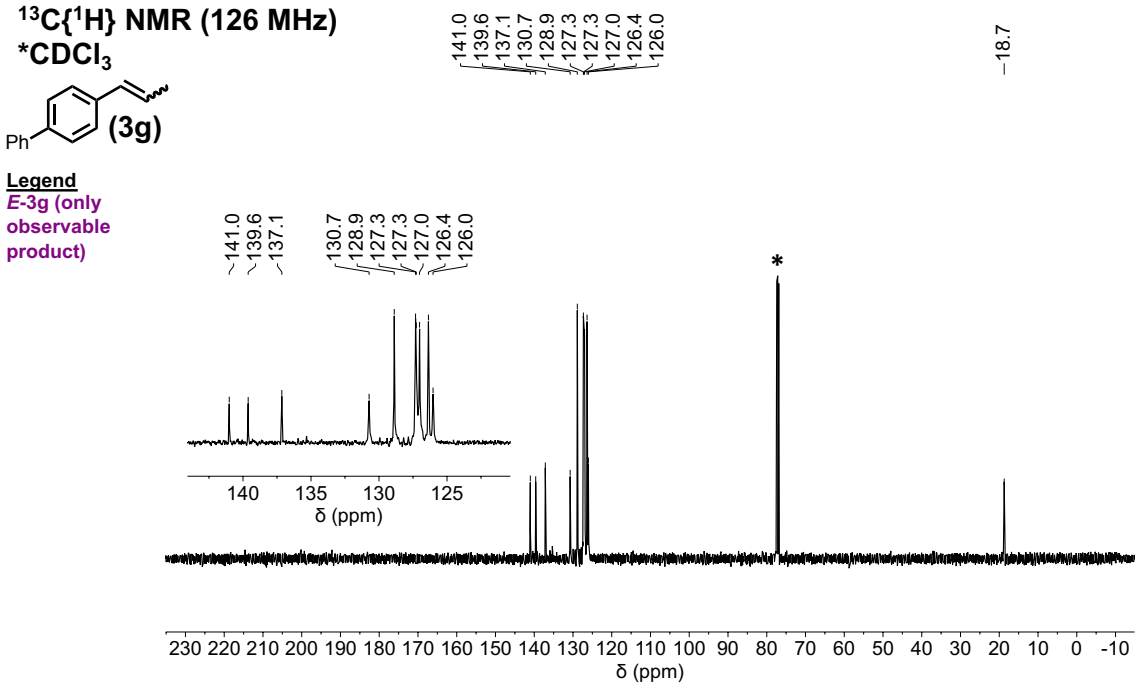

Figure A.65. ^{13}C{^{1}H} NMR spectrum of 4-(1-propen-1-yl)-1,1'-biphenyl (**3g**) recorded in $CDCl_3$ at 298 K.

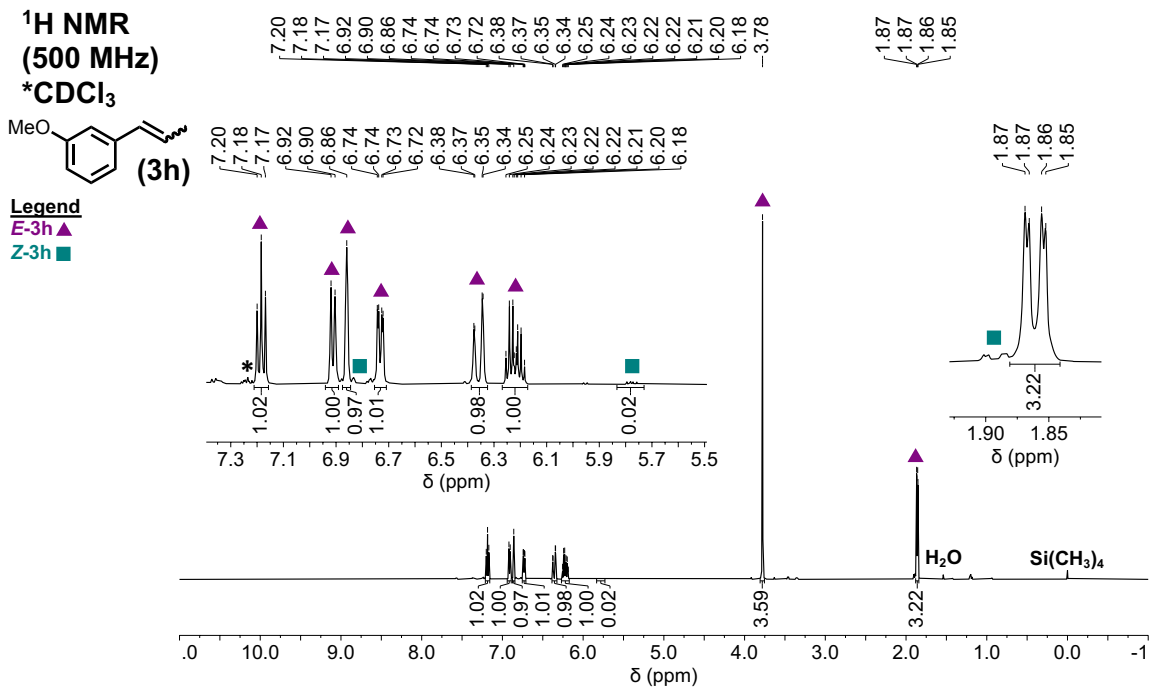

Figure A.66. ^{1}H NMR spectrum of 1-methoxy-3-(1-propen-1-yl)benzene (**3h**) recorded in $CDCl_3$ at 298 K.

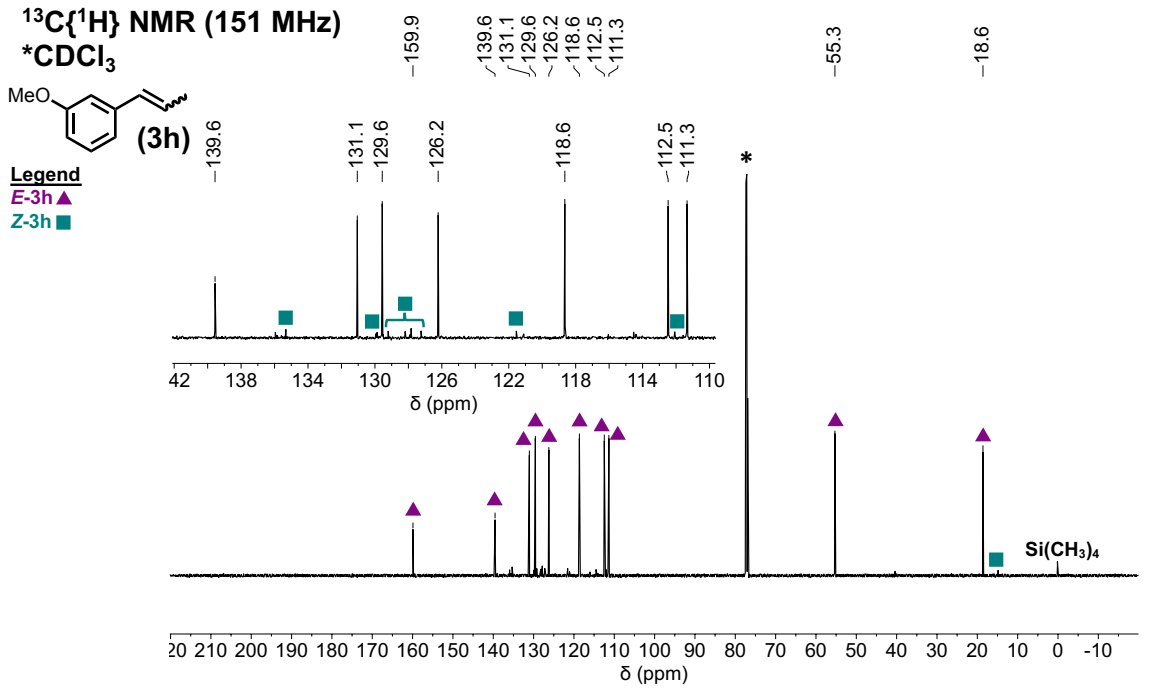

Figure A.67. ^{13}C{^{1}H} NMR spectrum of 1-methoxy-3-(1-propen-1-yl)benzene (**3h**) recorded in $CDCl_3$ at 298 K.

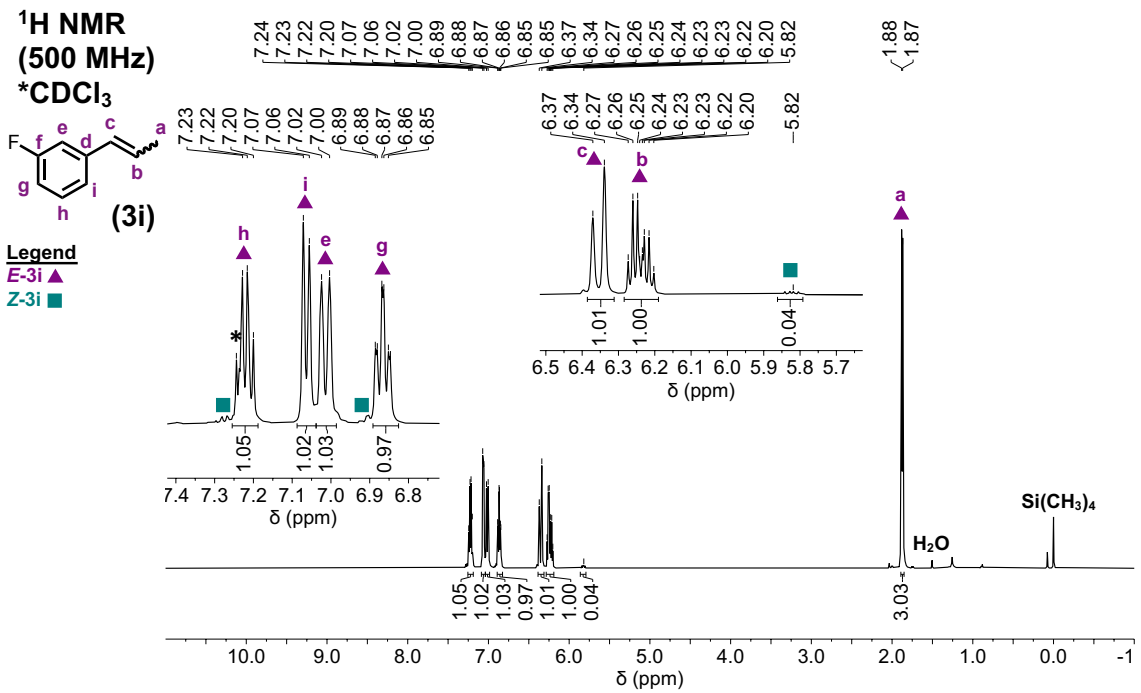

Figure A.68. ^{1}H NMR spectrum of 1-fluoro-3-(1-propen-1-yl)benzene (**3i**) recorded in $CDCl_3$ at 298 K.

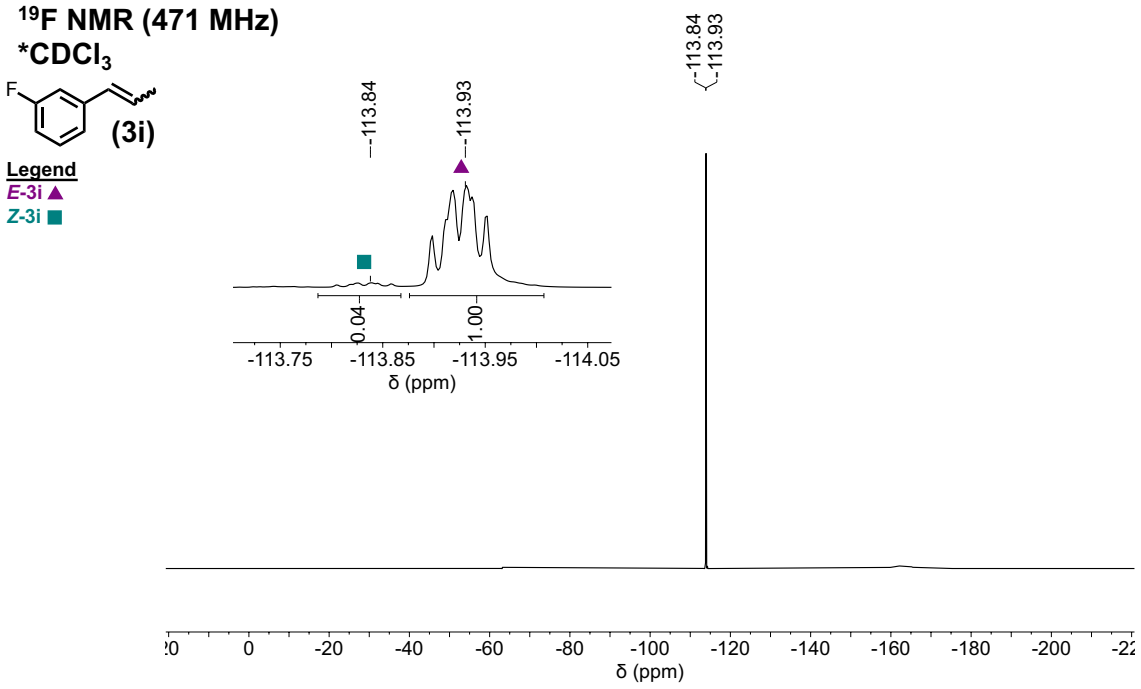

Figure A.69. ^{19}F NMR spectrum of 1-fluoro-3-(1-propen-1-yl)benzene (**3i**) recorded in $CDCl_3$ at 298 K.

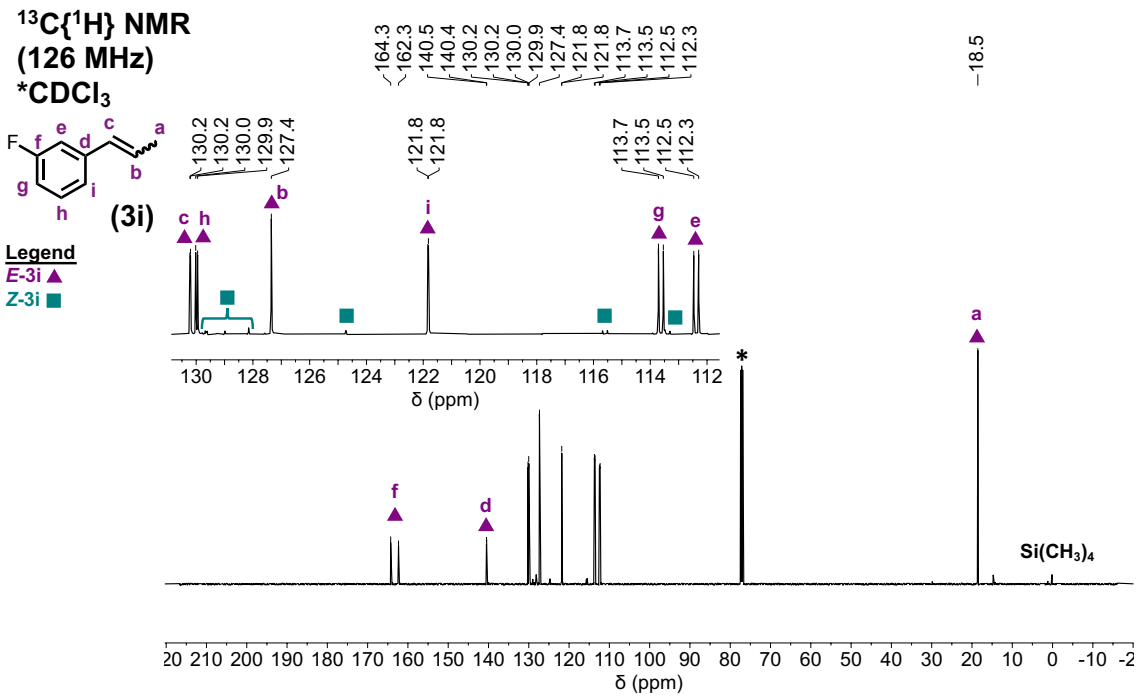

Figure A.70. $^{13}C\{^{1}H\}$ NMR spectrum of 1-fluoro-3-(1-propen-1-yl)benzene (**3i**) recorded in $CDCl_3$ at 298 K.

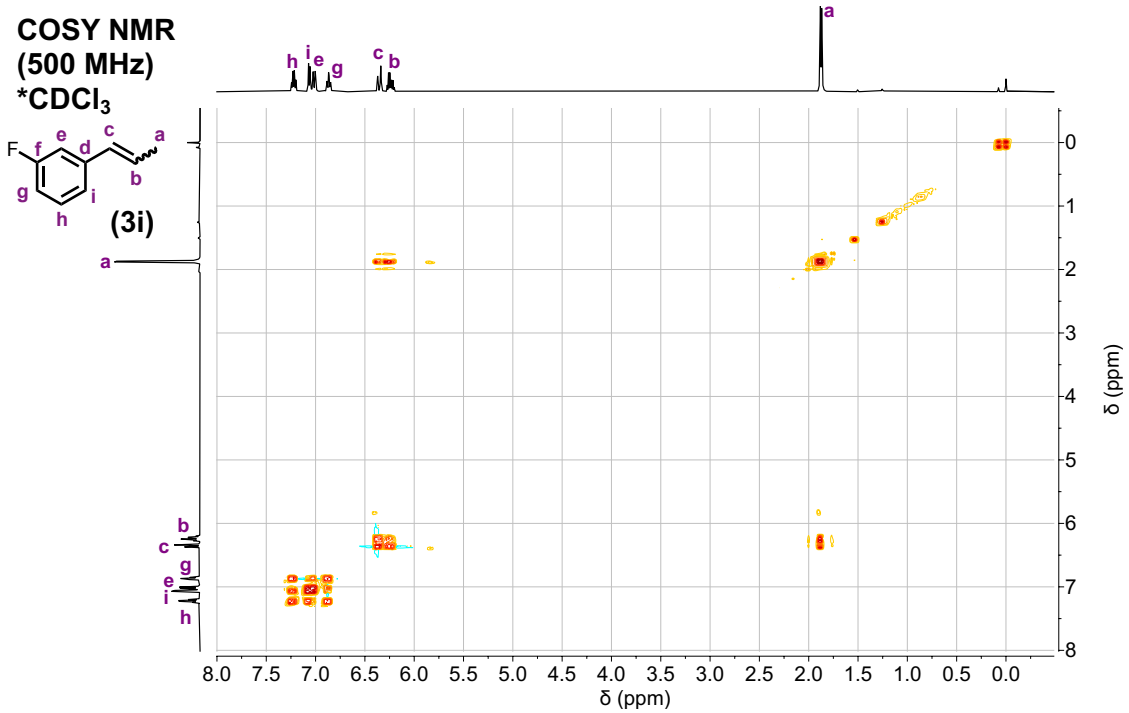

Figure A.71. COSY NMR spectrum of 1-fluoro-3-(1-propen-1-yl)benzene (**3i**) recorded in $CDCl_3$ at 298 K.

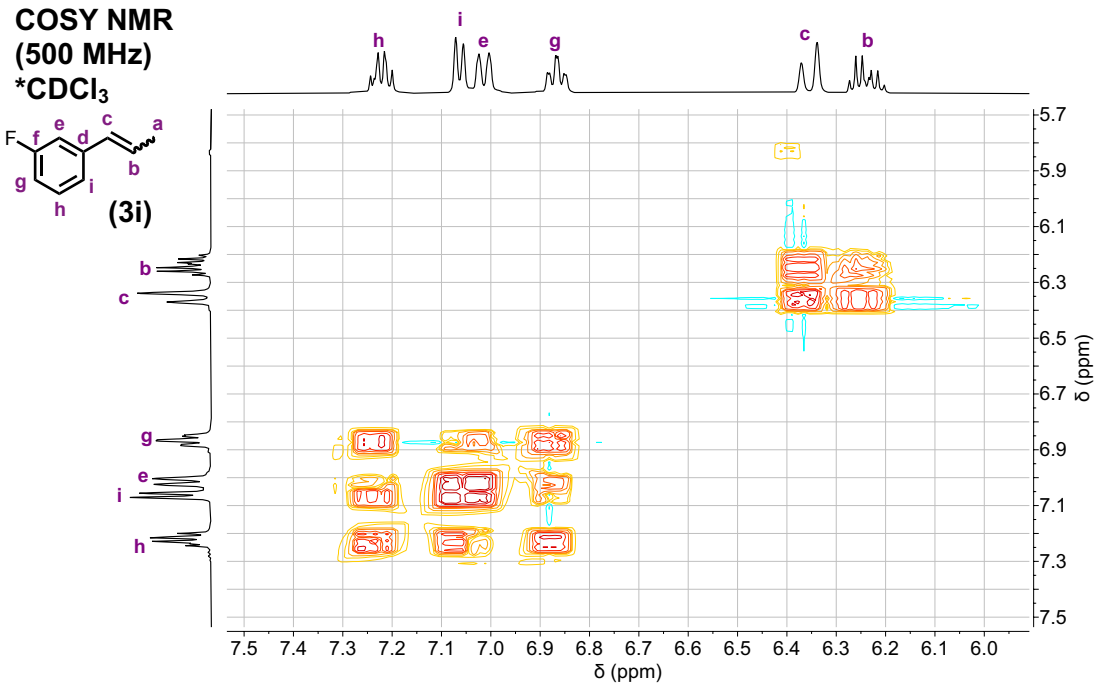

Figure A.72. Aryl region of COSY NMR spectrum of 1-fluoro-3-(1-propen-1-yl)benzene (**3i**) recorded in $CDCl_3$ at 298 K.

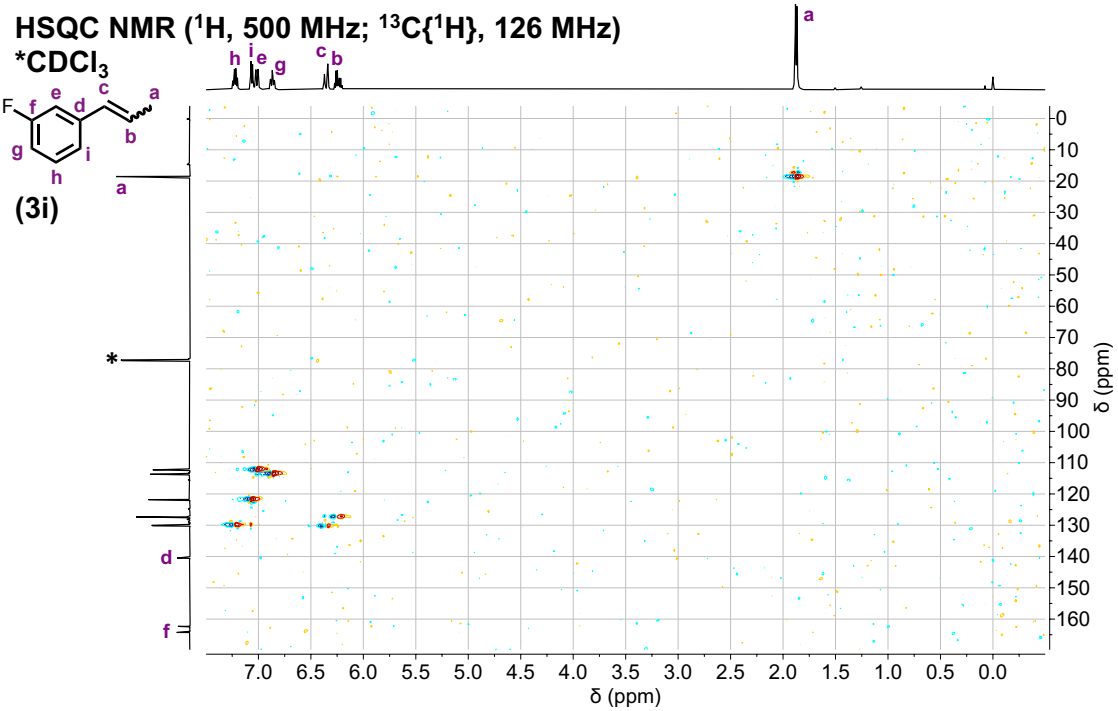

Figure A.73. HSQC NMR spectrum of 1-fluoro-3-(1-propen-1-yl)benzene (**3i**) recorded in $CDCl_3$ at 298 K.

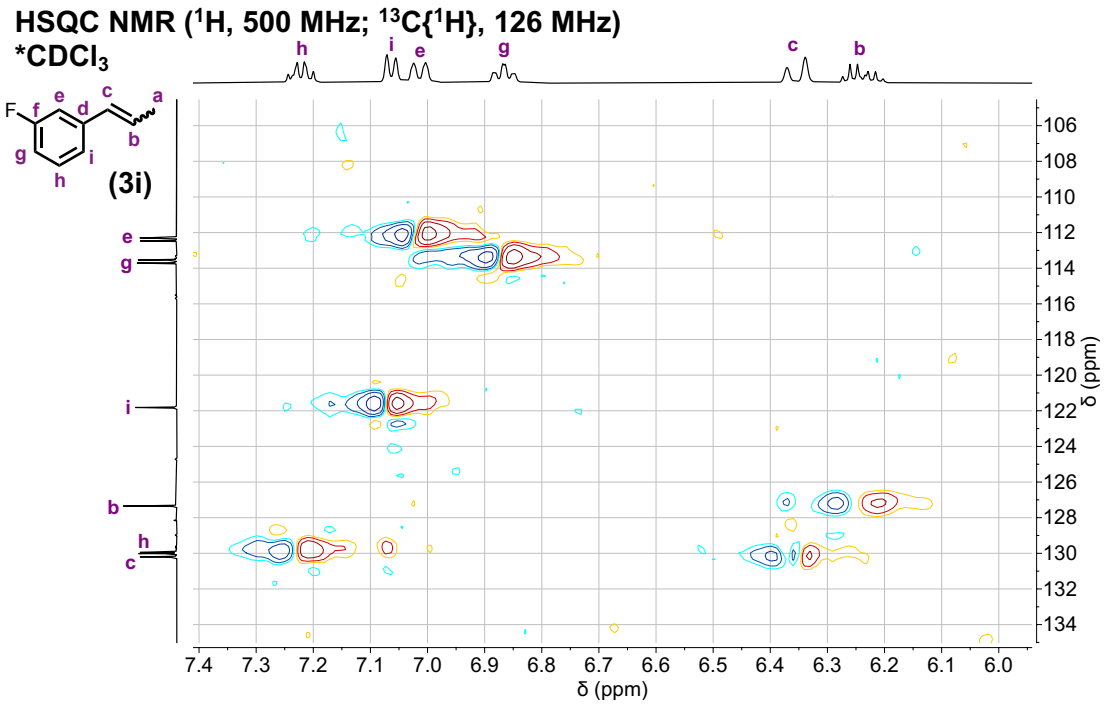

Figure A.74. Aryl and alkenyl region of HSQC NMR spectrum of 1-fluoro-3-(1-propen-1-yl)benzene (**3i**) recorded in $CDCl_3$ at 298 K.

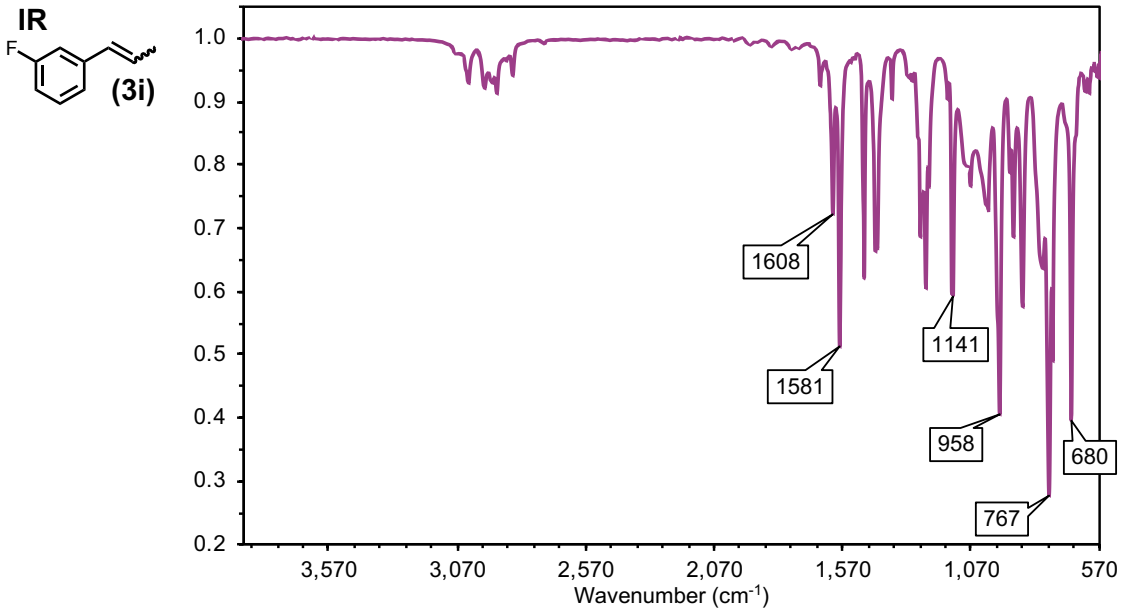

Figure A.75. IR spectrum of 1-fluoro-3-(1-propen-1-yl)benzene (**3i**) recorded neat at room temperature.

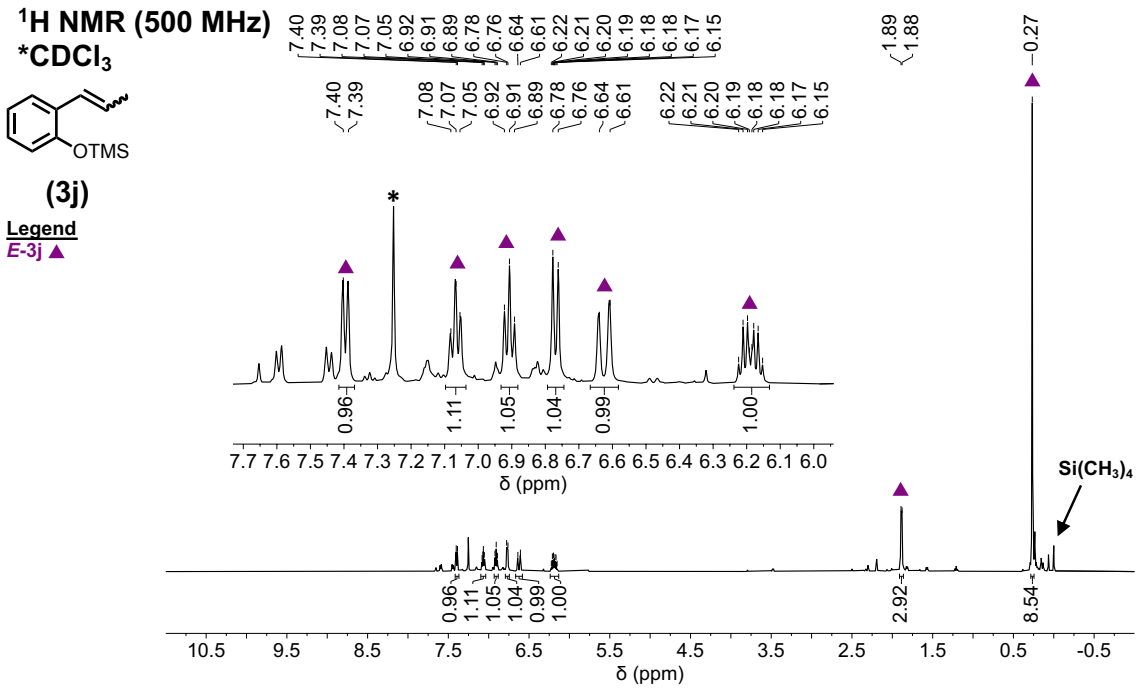

Figure A.76. ^{1}H NMR spectrum of 1-(1-propen-1-yl)-2-[(trimethylsilyl)oxy]benzene (**3j**) recorded in $CDCl_3$ at 298 K.

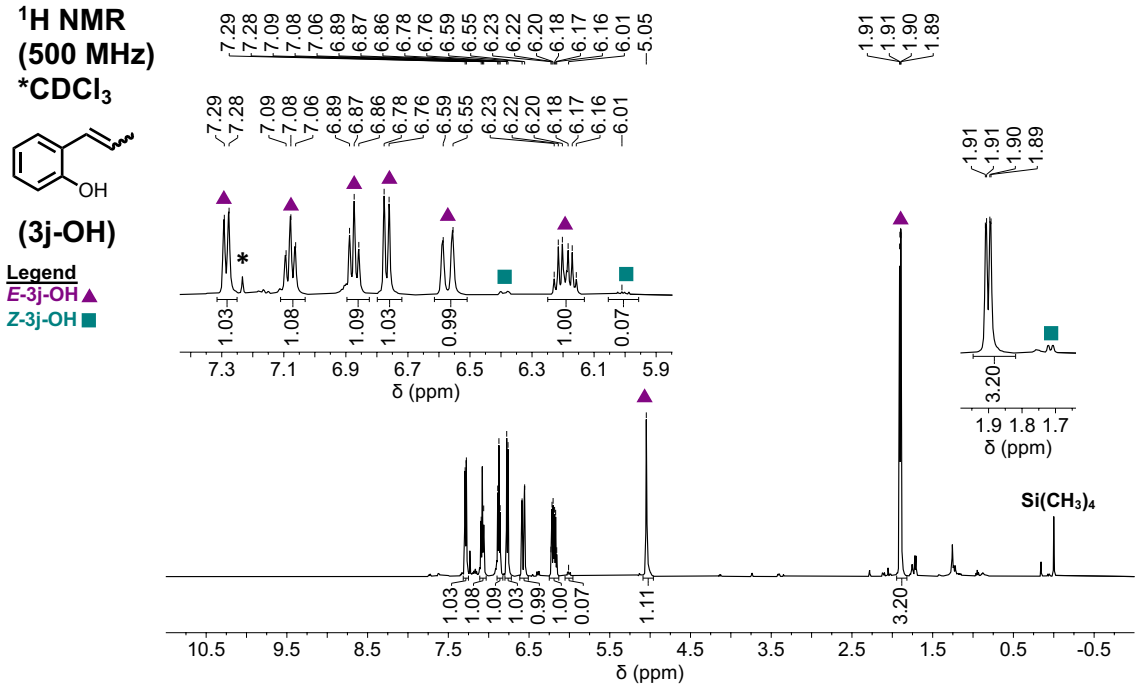

Figure A.77. ^{1}H NMR spectrum of 2-(1-propen-1-yl)phenol (**3j-OH**) recorded in $CDCl_3$ at 298 K.

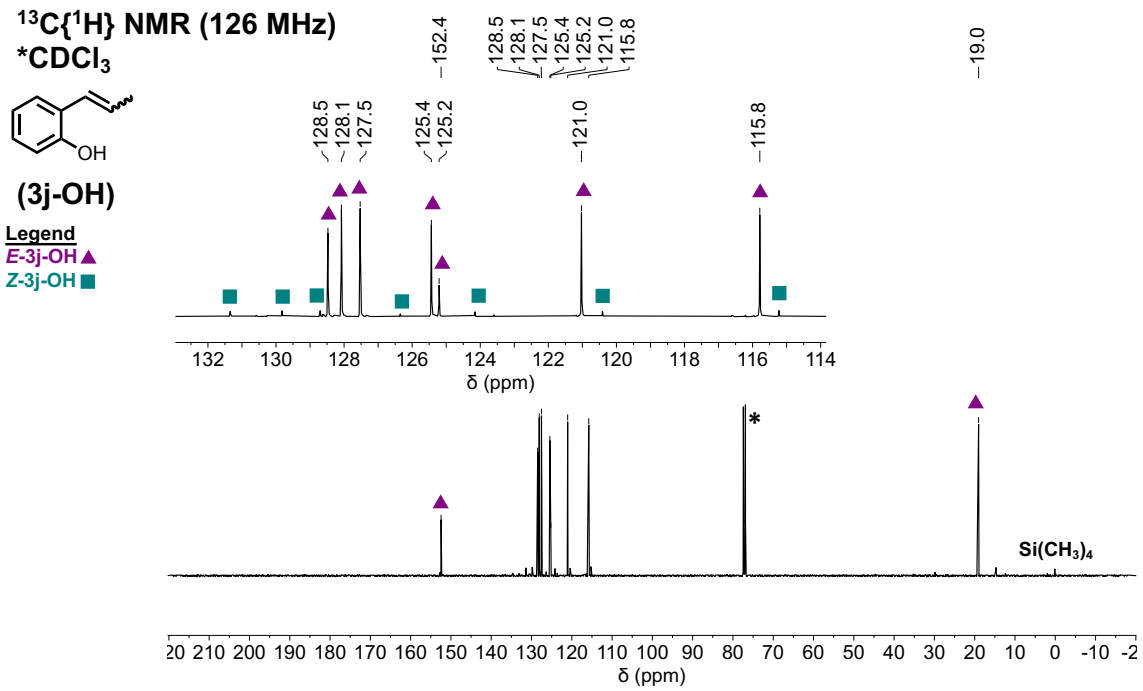

Figure A.78. $^{13}C\{^{1}H\}$ NMR spectrum of 2-(1-propen-1-yl)phenol (**3j-OH**) recorded in $CDCl_3$ at 298 K.

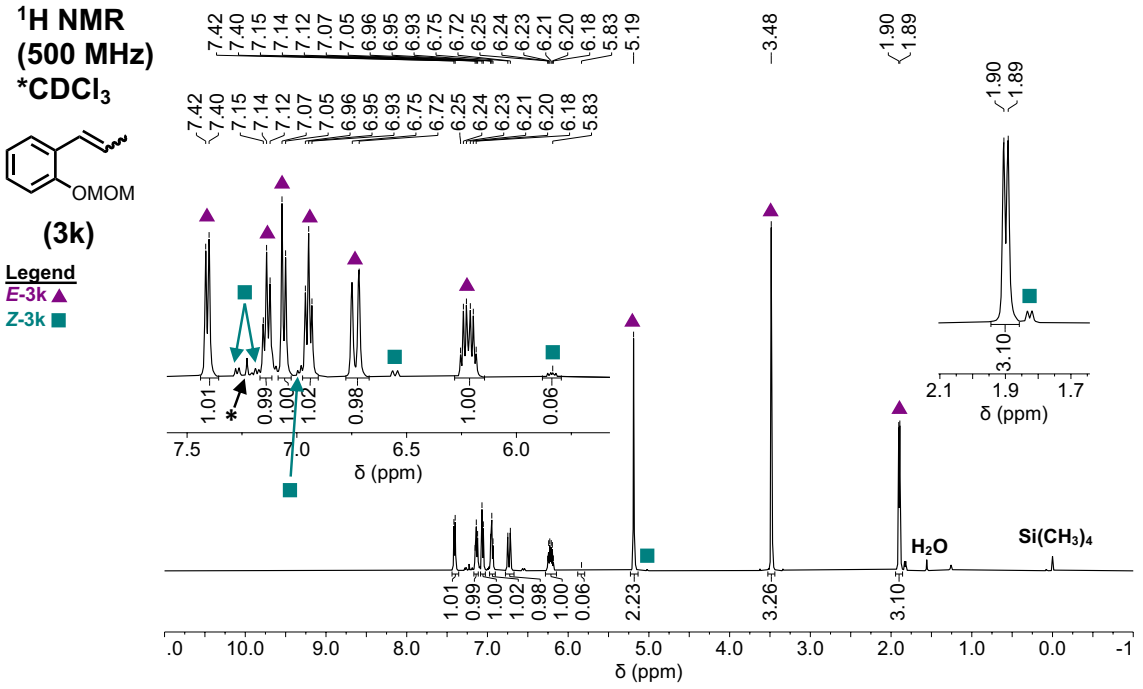

Figure A.79. ^{1}H NMR spectrum of 1-(methoxymethoxy)-2-propen-1-ylbenzene (**3k**) recorded in $CDCl_3$ at 298 K.

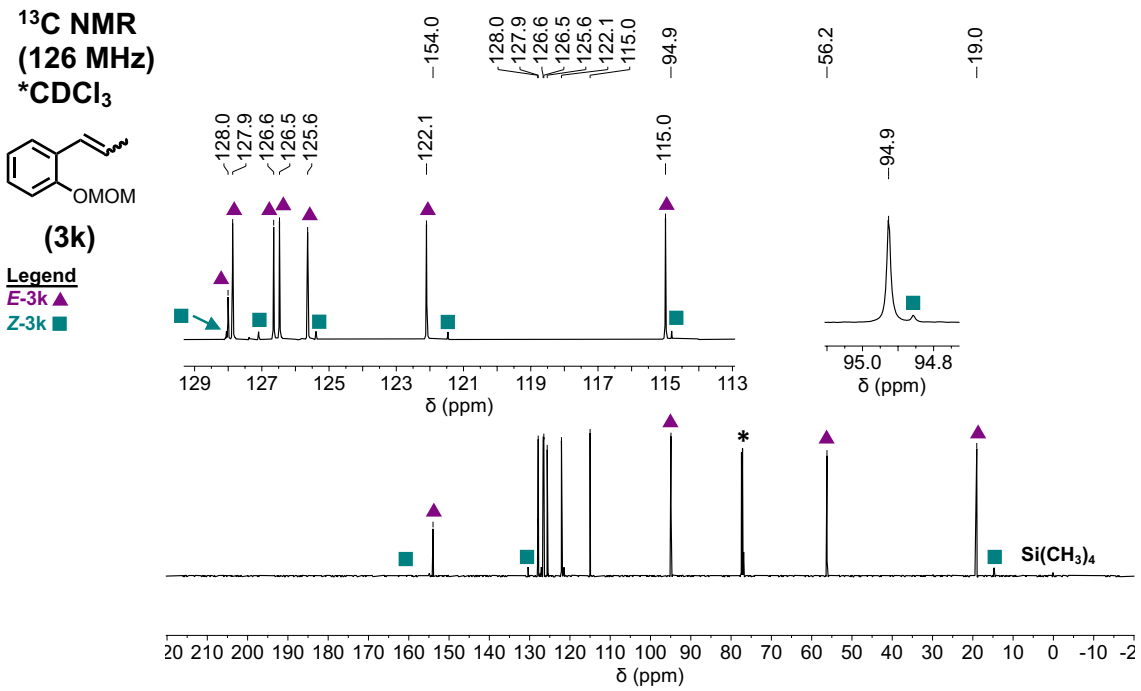

Figure A.80. $^{13}C\{^{1}H\}$ NMR spectrum of 1-(methoxymethoxy)-2-propen-1-ylbenzene (**3k**) recorded in $CDCl_3$ at 298 K.

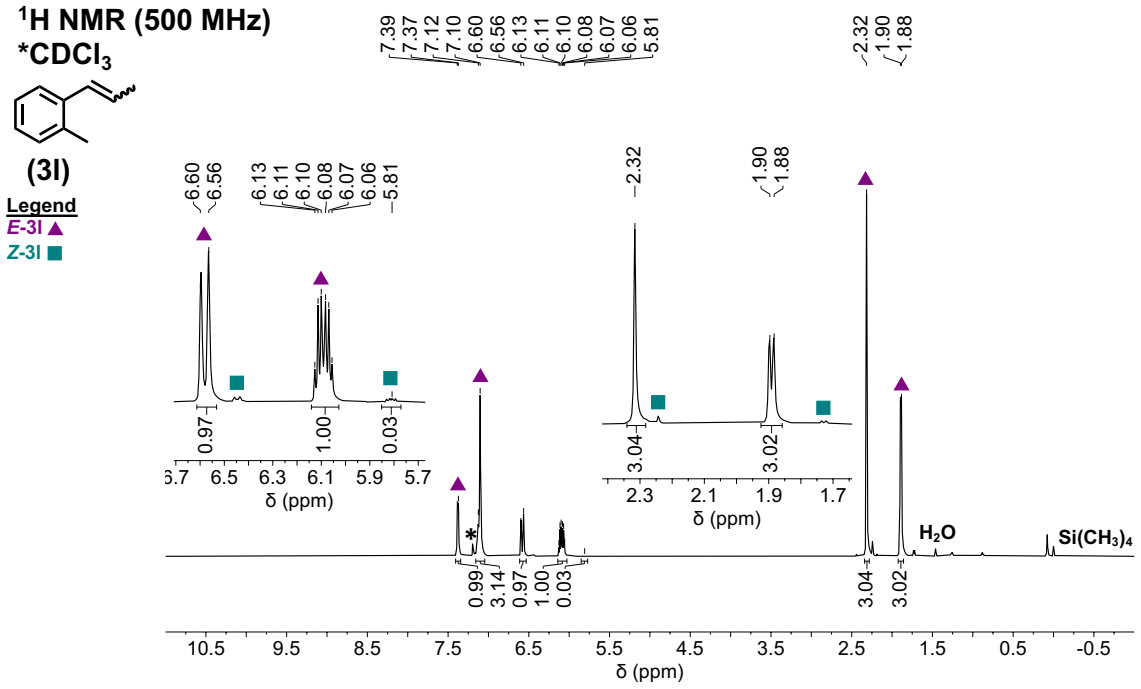

Figure A.81. ^{1}H NMR spectrum of 1-(2-methylphenyl)-1-propene (**3l**) recorded in $CDCl_3$ at 298 K.

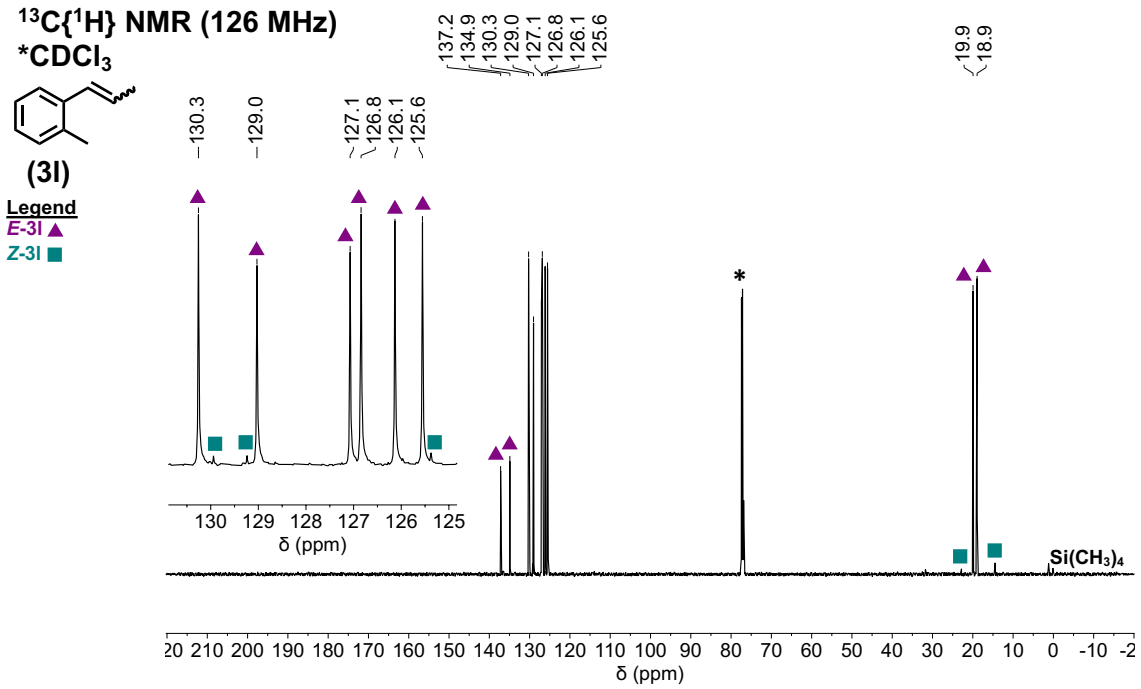

Figure A.82. $^{13}C\{^{1}H\}$ NMR spectrum of 1-(2-methylphenyl)-1-propene (**3l**) recorded in $CDCl_3$ at 298 K.

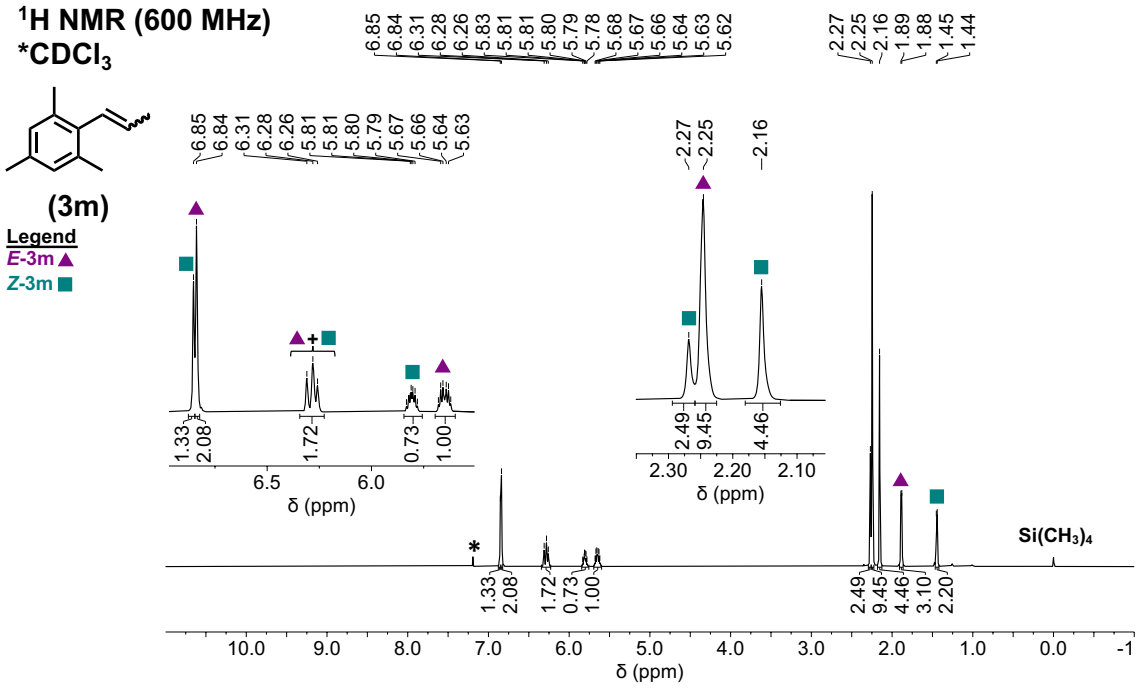

Figure A.83. ^{1}H NMR spectrum of 1,3,5-trimethyl-2-(1-propen-1-yl)benzene (**3m**) recorded in $CDCl_3$ at 298 K.

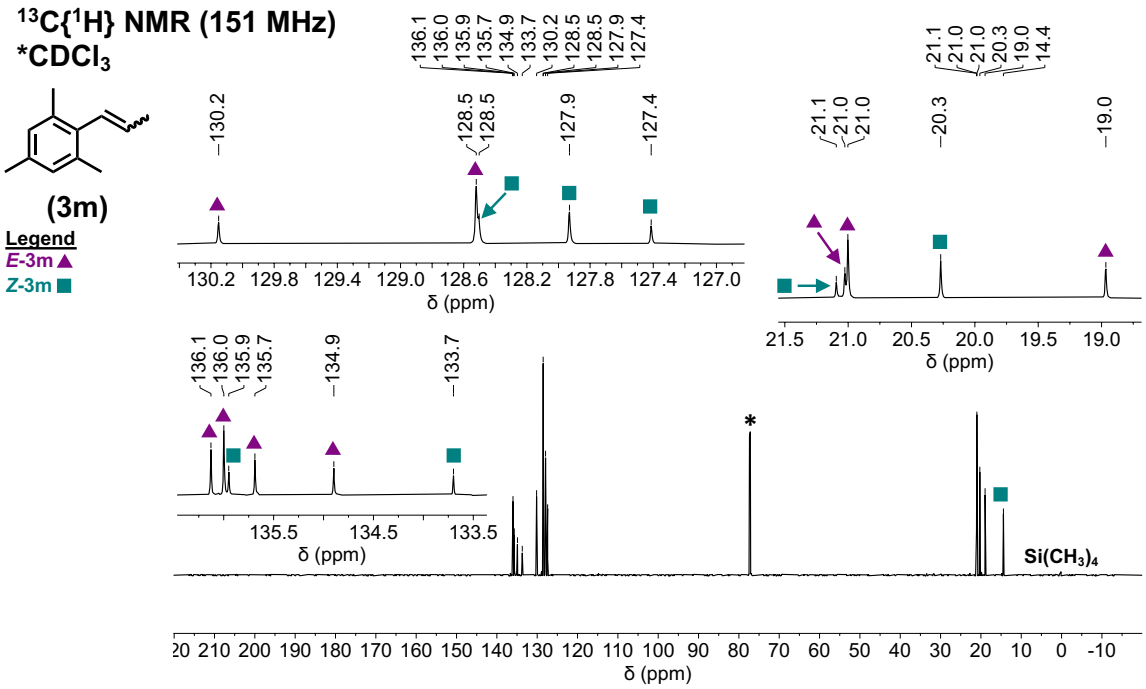

Figure A.84. $^{13}C\{^{1}H\}$ NMR spectrum of 1,3,5-trimethyl-2-(1-propen-1-yl)benzene (**3m**) recorded in $CDCl_3$ at 298 K.

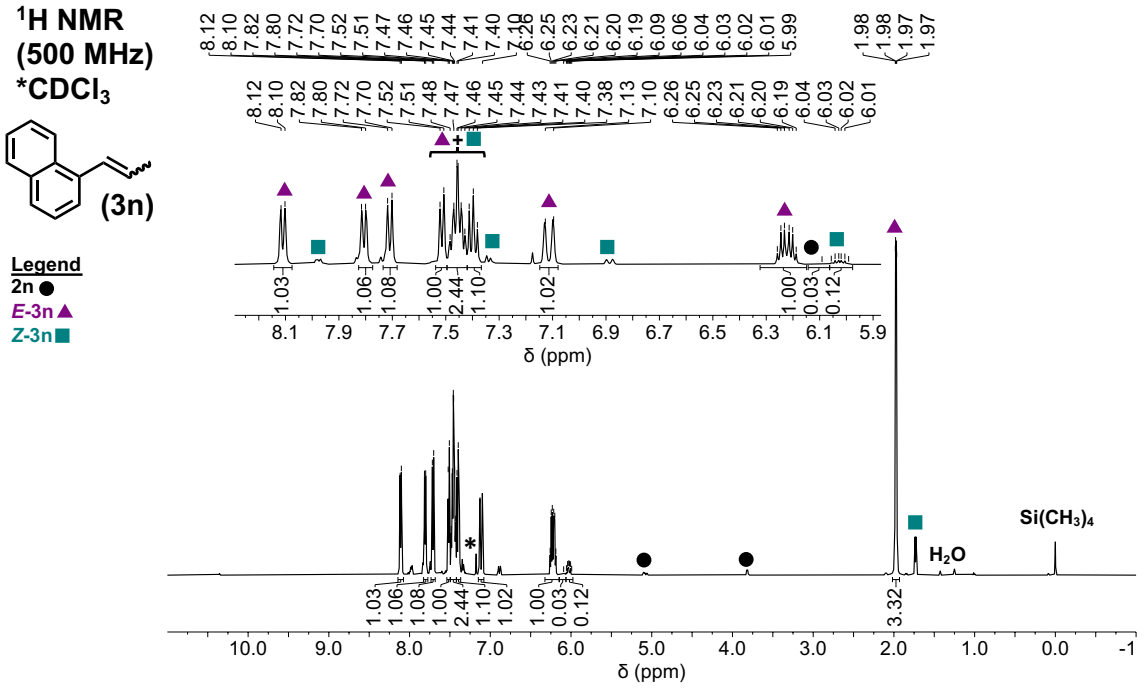

Figure A.85. ^{1}H NMR spectrum of 1-(1-propen-1-yl)naphthalene (**3n**) recorded in $CDCl_3$ at 298 K.

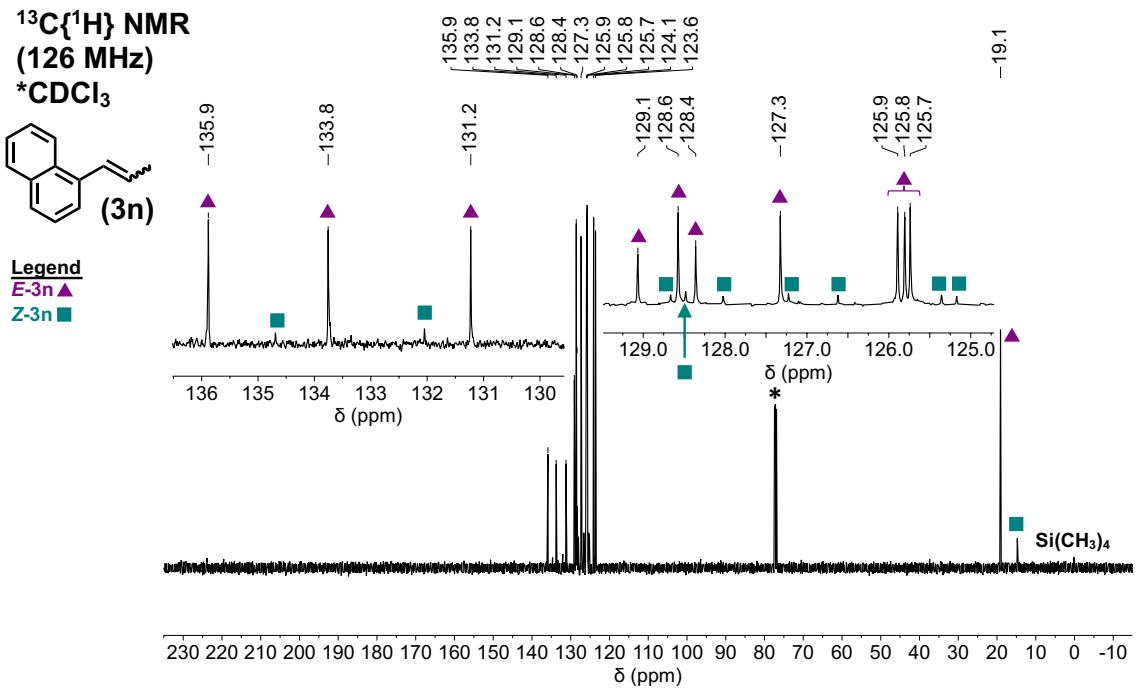

Figure A.86. $^{13}C\{^{1}H\}$ NMR spectrum of 1-(1-propen-1-yl)naphthalene (**3n**) recorded in $CDCl_3$ at 298 K.

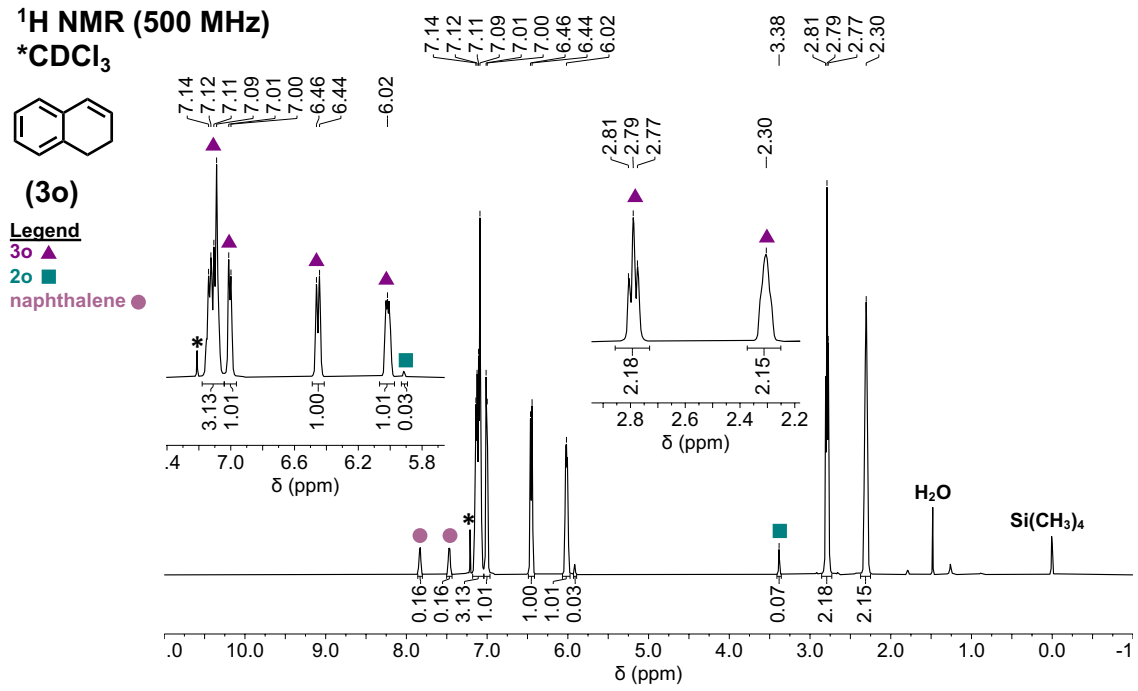

Figure A.87. ^{1}H NMR spectrum of 1,2-dihydronaphthalene (**3o**) recorded in $CDCl_3$ at 298 K.

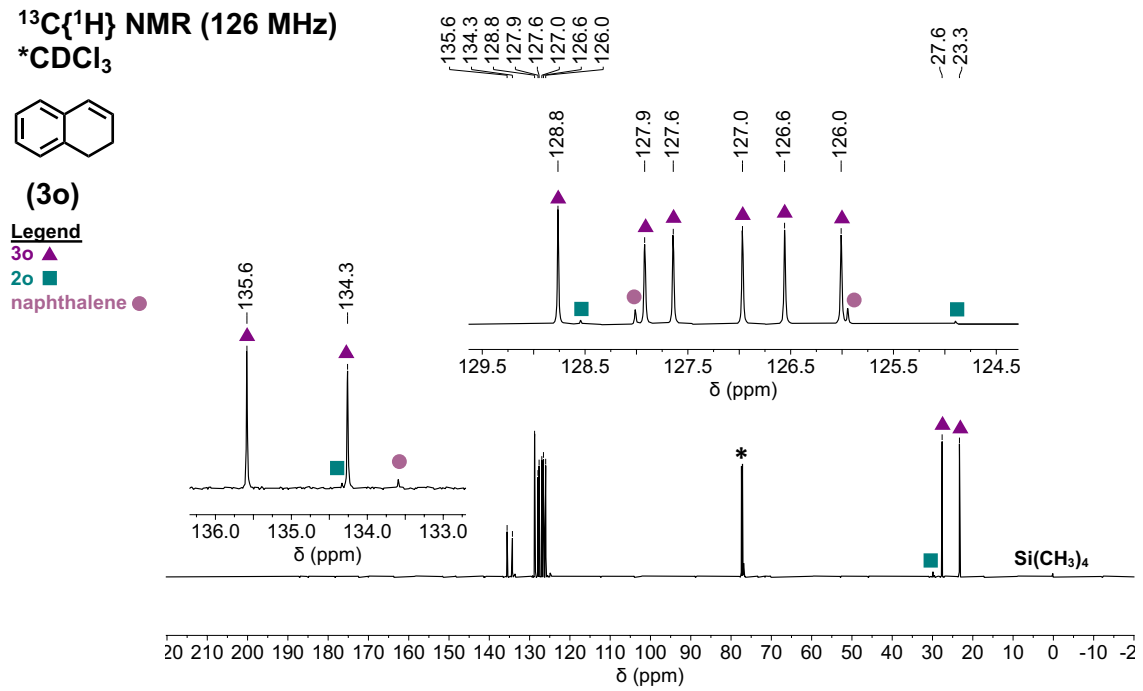

Figure A.88. $^{13}C\{^{1}H\}$ NMR spectrum of 1,2-dihydronaphthalene (**3o**) recorded in $CDCl_3$ at 298 K.

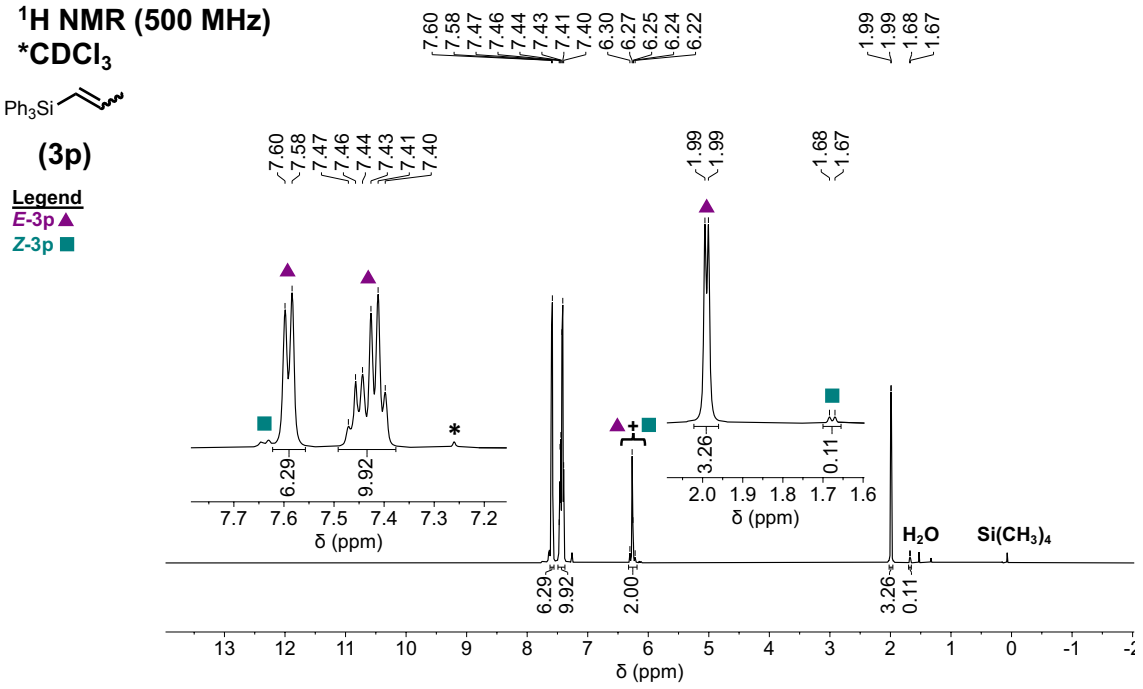

Figure A.89. ^{1}H NMR spectrum of (1-propen-1-yl)triphenylsilane (**3p**) recorded in $CDCl_3$ at 298 K.

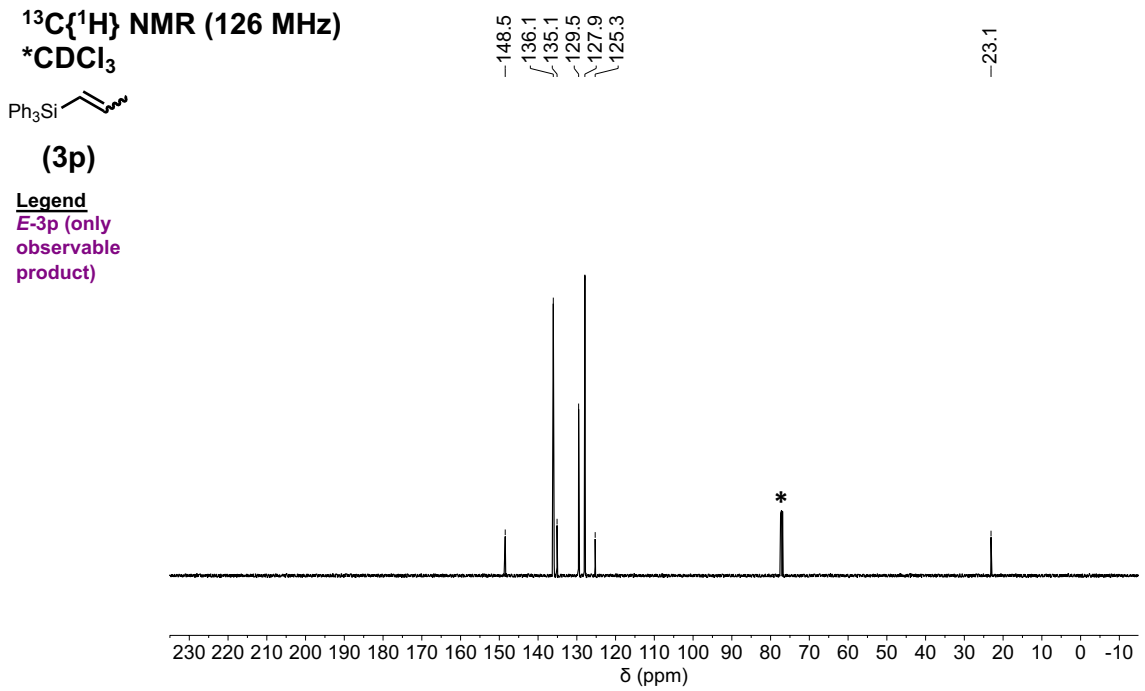

Figure A.90. $^{13}C\{^{1}H\}$ NMR spectrum of (1-propen-1-yl)triphenylsilane (**3p**) recorded in $CDCl_3$ at 298 K.

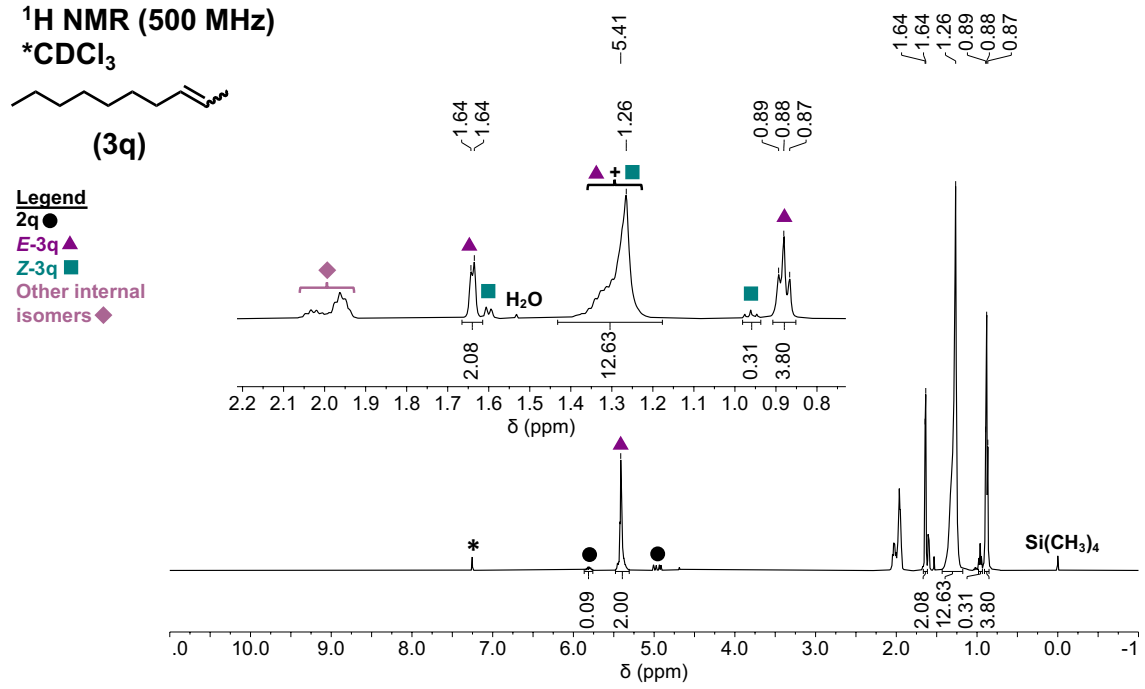

Figure A.91. ^{1}H NMR spectrum of 2-decene (**3q**) recorded in $CDCl_3$ at 298 K.

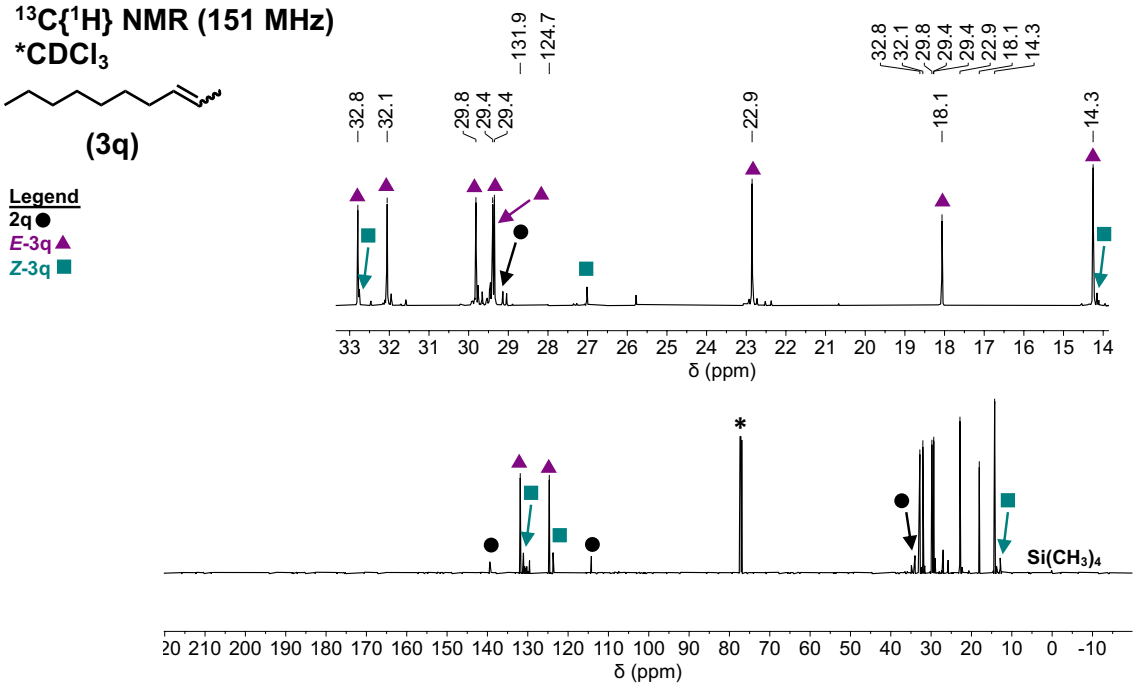

Figure A.92. $^{13}C\{^{1}H\}$ NMR spectrum of 2-decene (**3q**) recorded in $CDCl_3$ at 298 K.

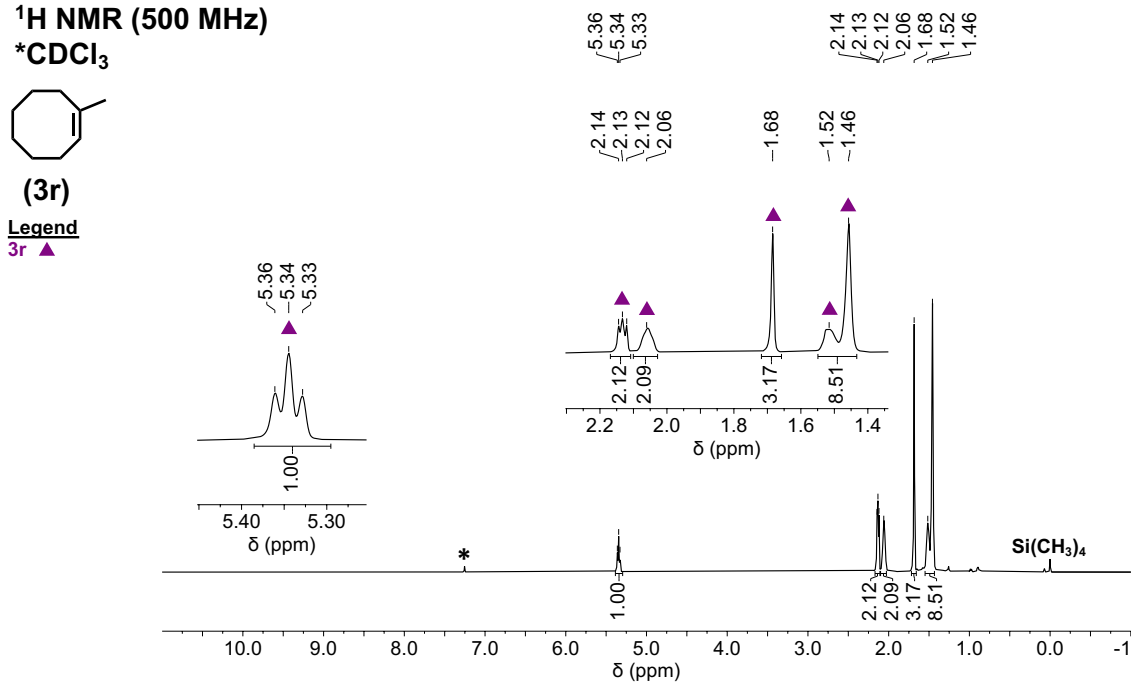

Figure A.93. ^{1}H NMR spectrum of *cis*-1-methylcyclooctene (**3r**) recorded in $CDCl_3$ at 298 K.

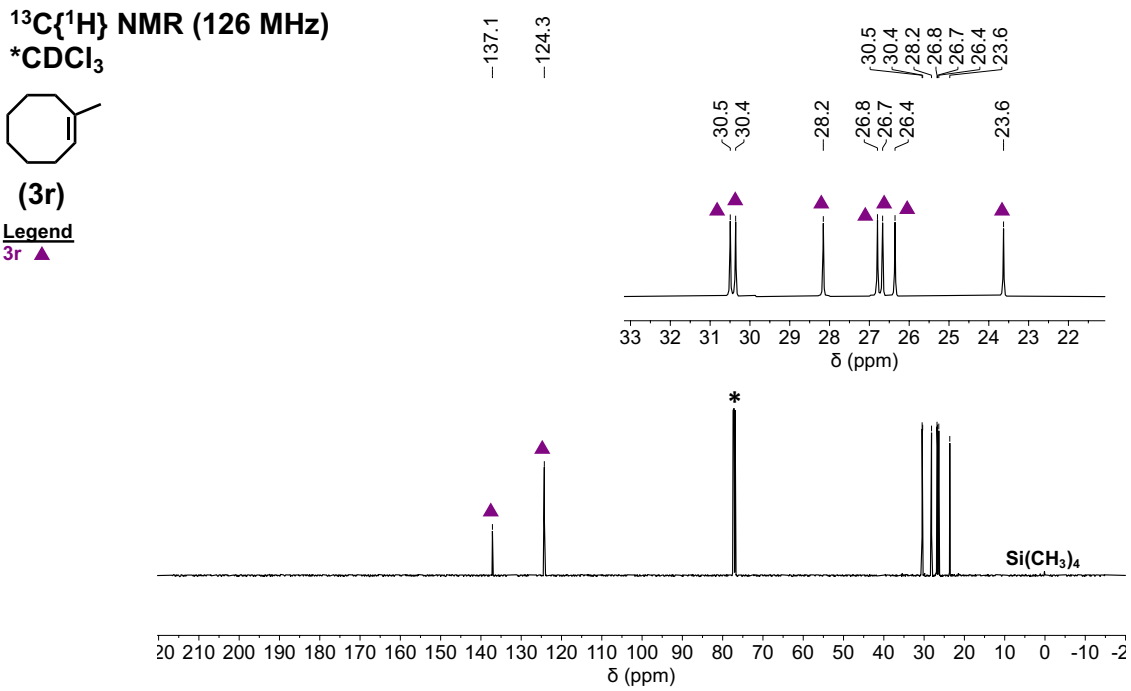

Figure A.94. $^{13}C\{^{1}H\}$ NMR spectrum of *cis*-1-methylcyclooctene (**3r**) recorded in $CDCl_3$ at 298 K.

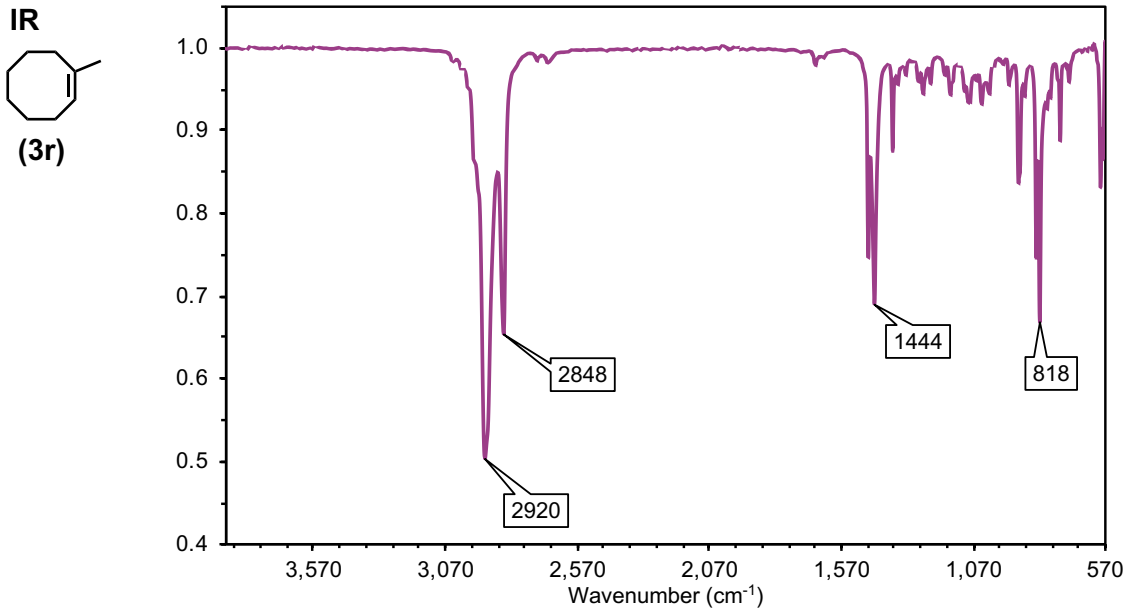

Figure A.95. IR spectrum of *cis*-1-methylcyclooctene (**3r**) recorded neat at room temperature.

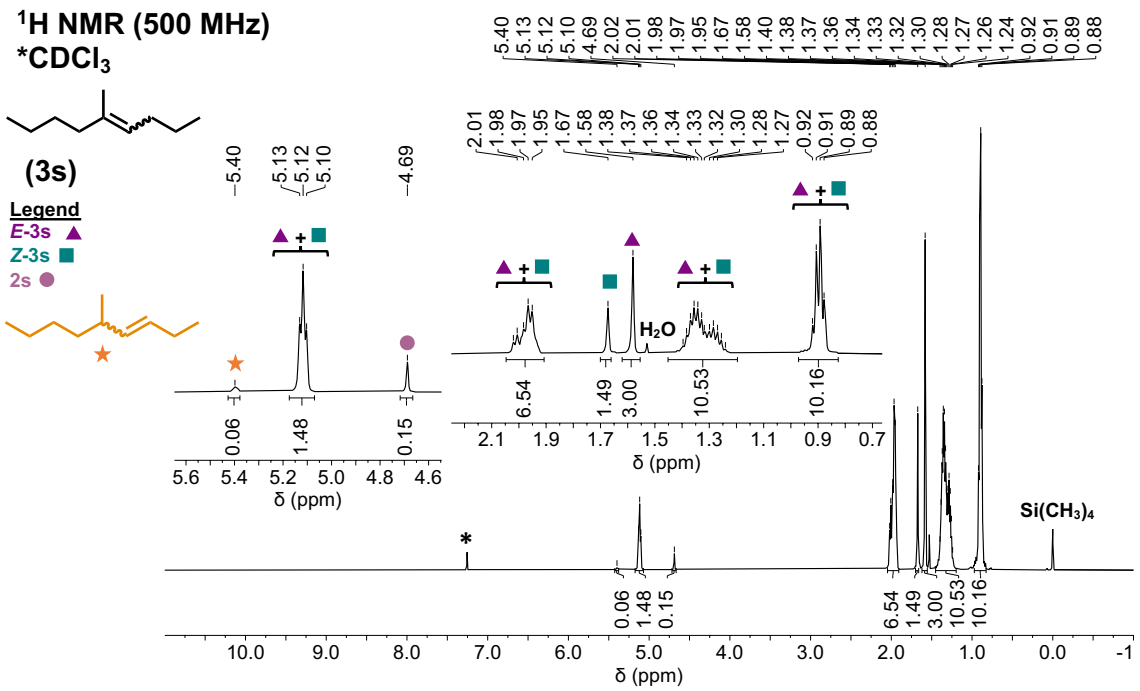

Figure A.96. ^{1}H NMR spectrum of 5-methyl-4-nonene (**3s**) recorded in $CDCl_3$ at 298 K.

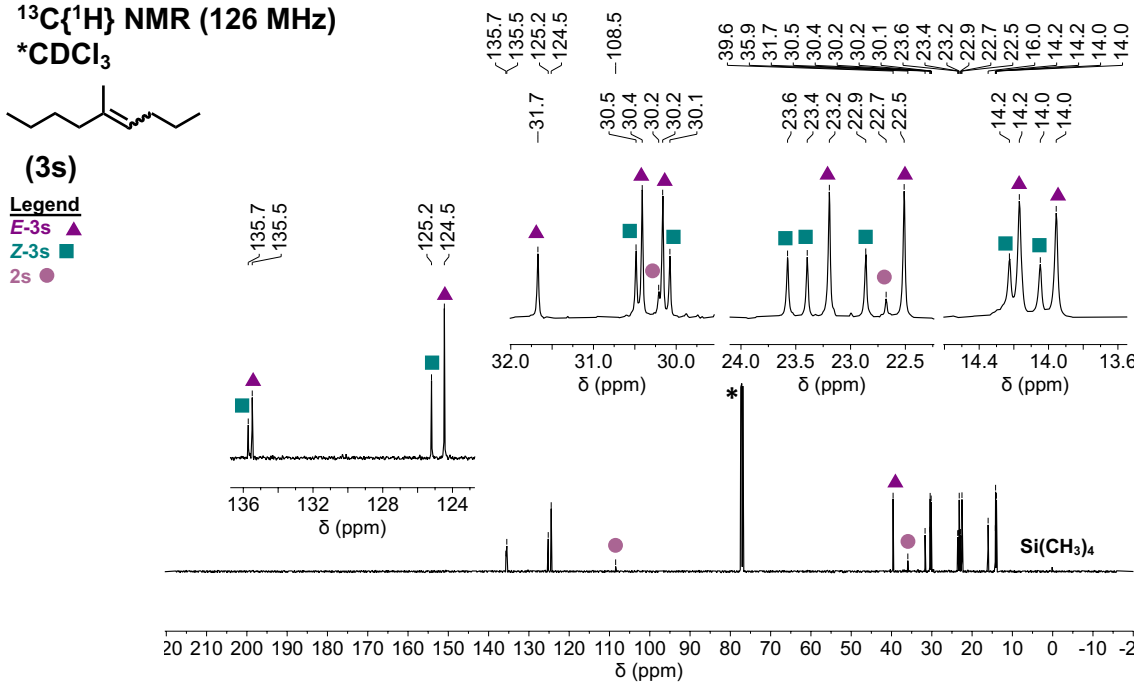

Figure A.97. ^{13}C{^{1}H} NMR spectrum of 5-methyl-4-nonene (**3s**) recorded in $CDCl_3$ at 298 K.

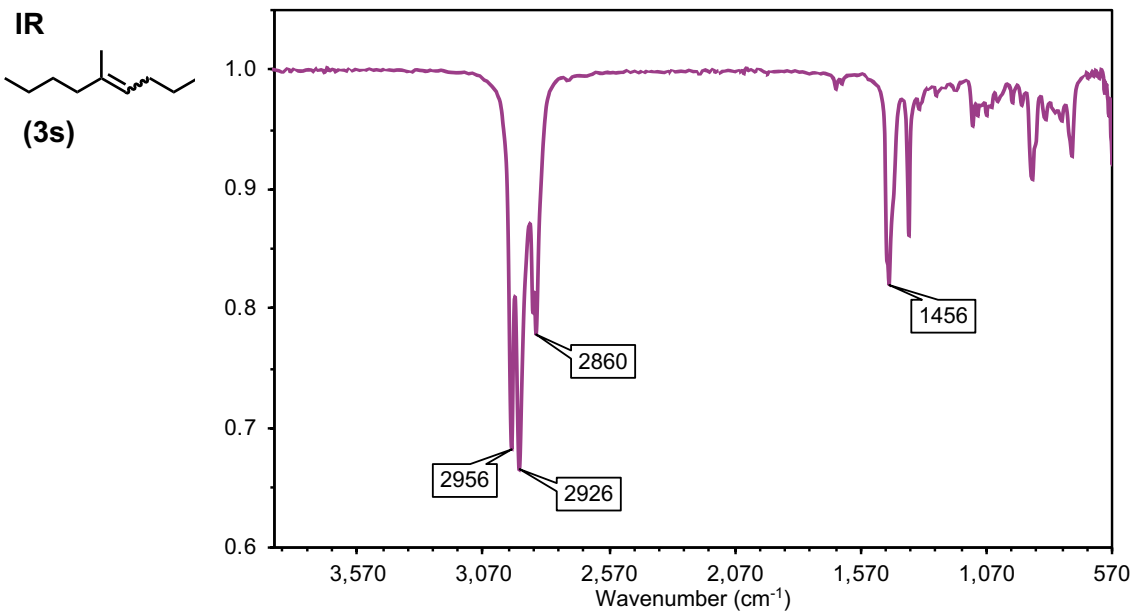

Figure A.98. IR spectrum of 5-methyl-4-nonene (**3s**) recorded neat at room temperature.

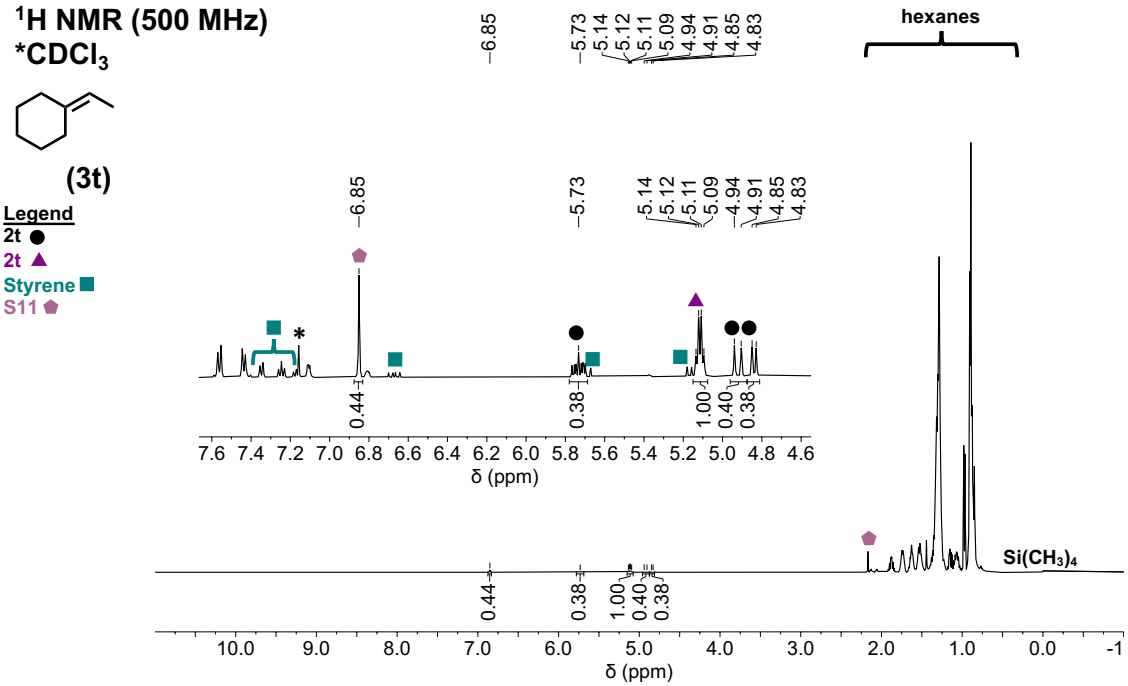

Figure A.99. ^{1}H NMR spectrum of ethylidenecyclohexane (**3t**) recorded in $CDCl_3$ at 298 K.

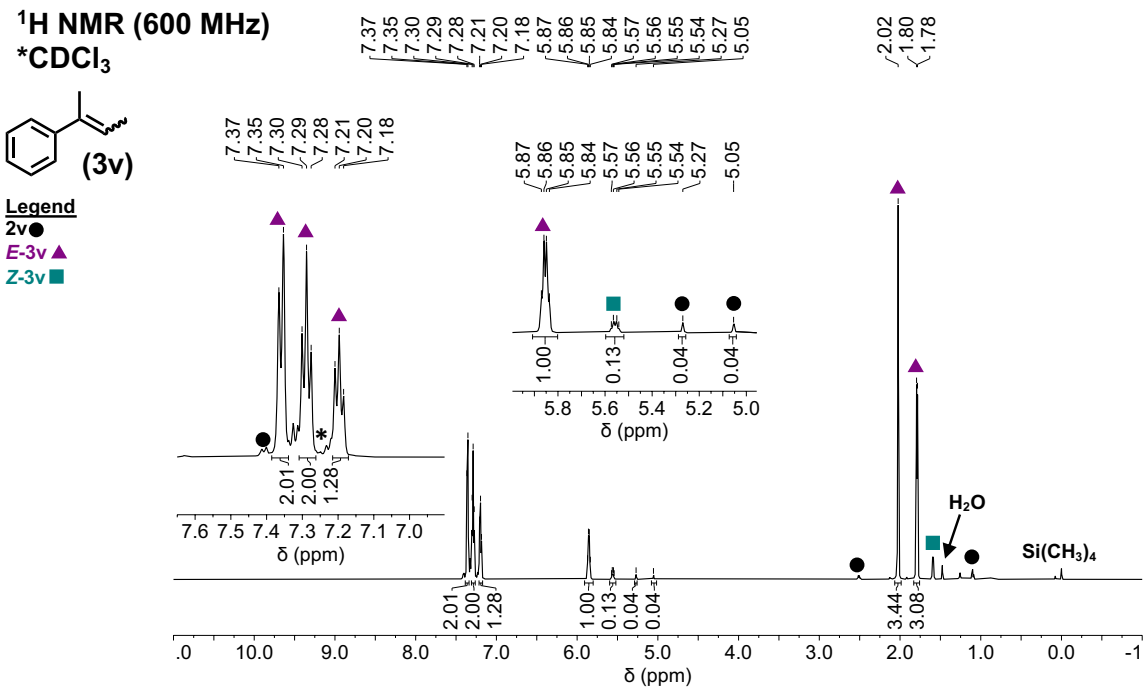

Figure A.100. ^{1}H NMR spectrum of α,β-dimethylstyrene (**3v**) recorded in $CDCl_3$ at 298 K.

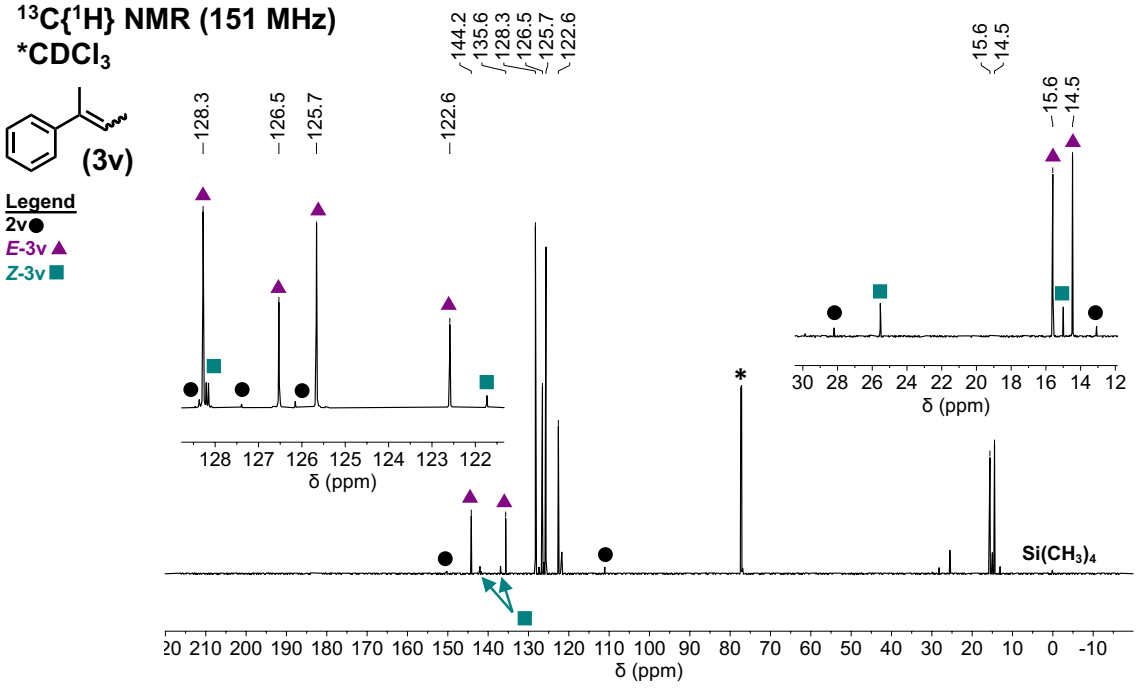

Figure A.101. $^{13}C\{^1H\}$ NMR spectrum of α,β-dimethylstyrene (**3v**) recorded in $CDCl_3$ at 298 K.

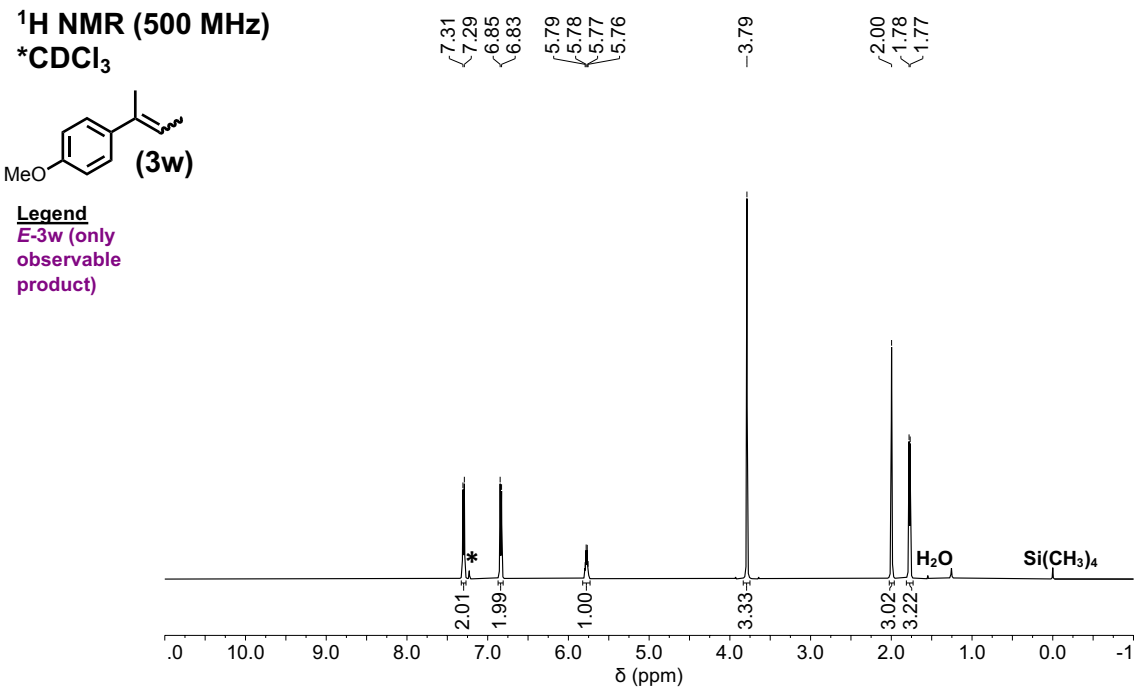

Figure A.102. ^{1}H NMR spectrum of 1-methoxy-4-(1-methyl-1-propen-1-yl)benzene (**3w**) recorded in $CDCl_3$ at 298 K.

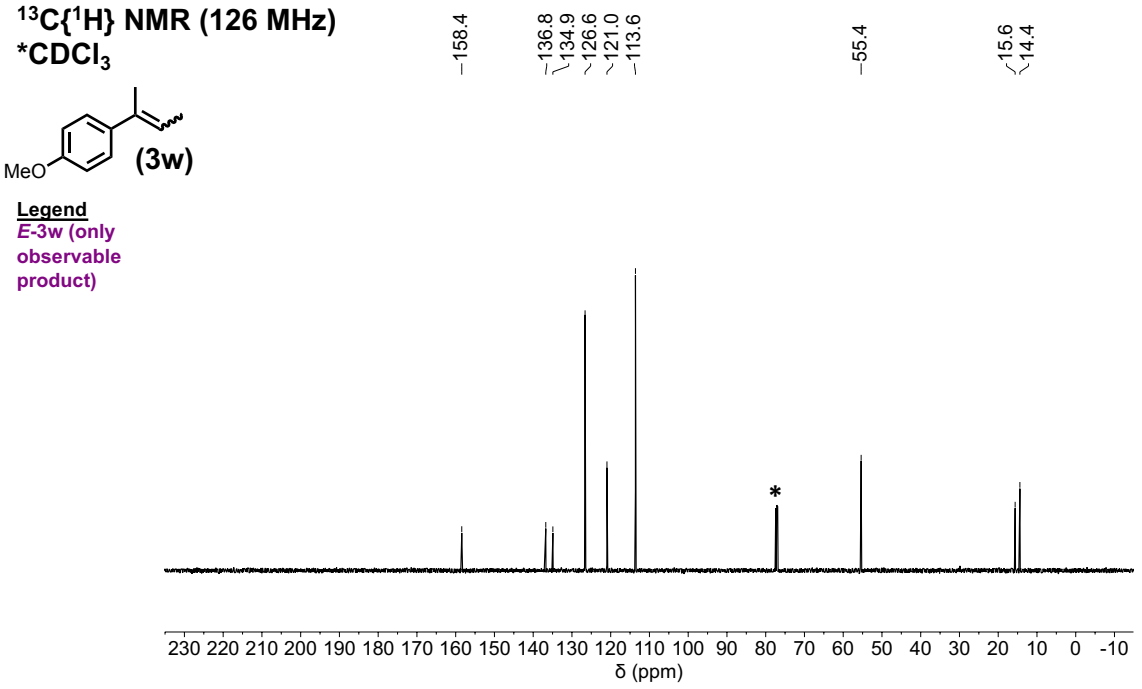

Figure A.103. ^{13}C{^{1}H} NMR spectrum of 1-methoxy-4-(1-methyl-1-propen-1-yl)benzene (**3w**) recorded in $CDCl_3$ at 298 K.

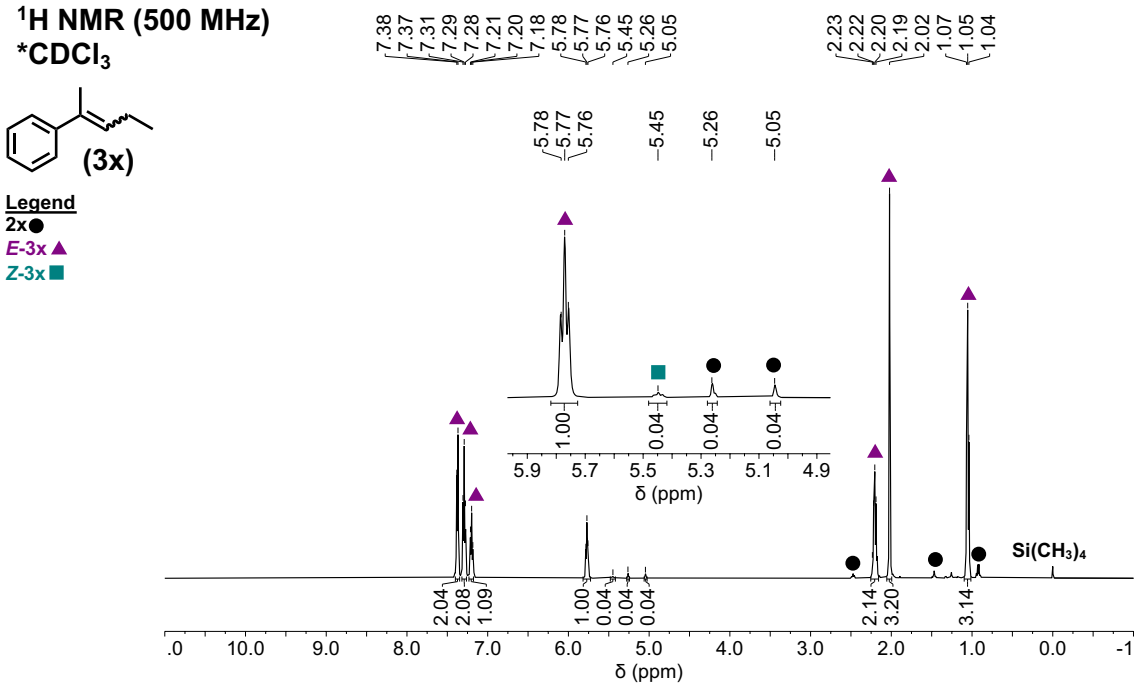

Figure A.104. ^{1}H NMR spectrum of 2-phenyl-2-pentene (**3x**) recorded in $CDCl_3$ at 298 K.

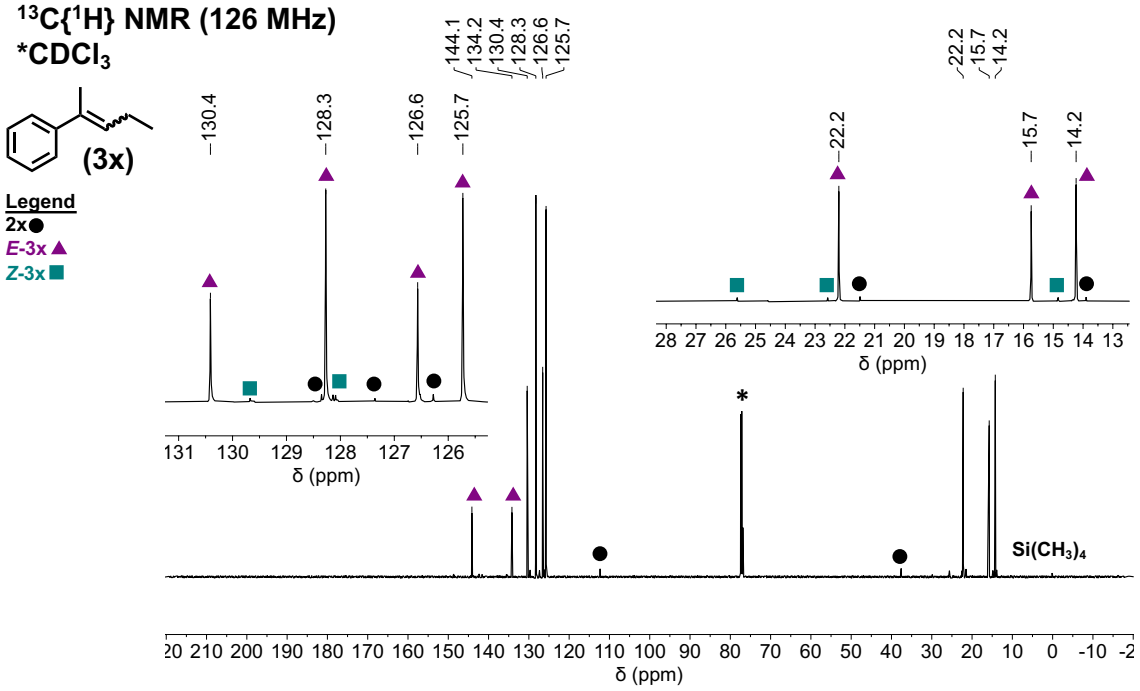

Figure A.105. $^{13}C\{^1H\}$ NMR spectrum of 2-phenyl-2-pentene (**3x**) recorded in $CDCl_3$ at 298 K.

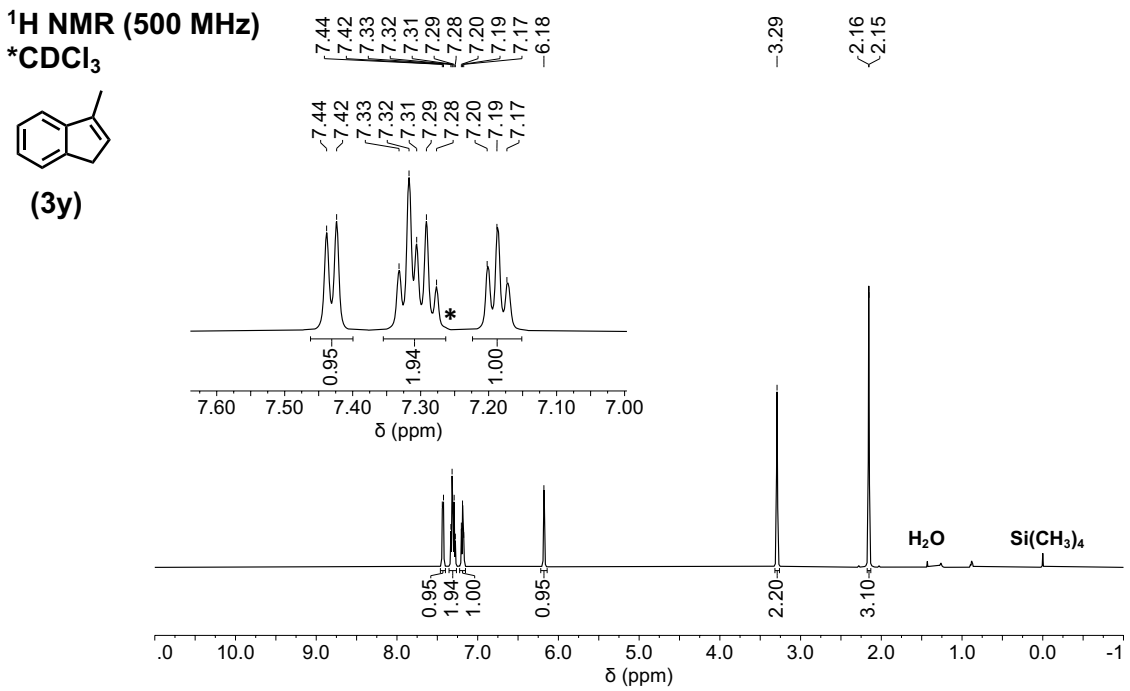

Figure A.106. ^{1}H NMR spectrum of 1-methylindene (**3y**) recorded in $CDCl_3$ at 298 K.

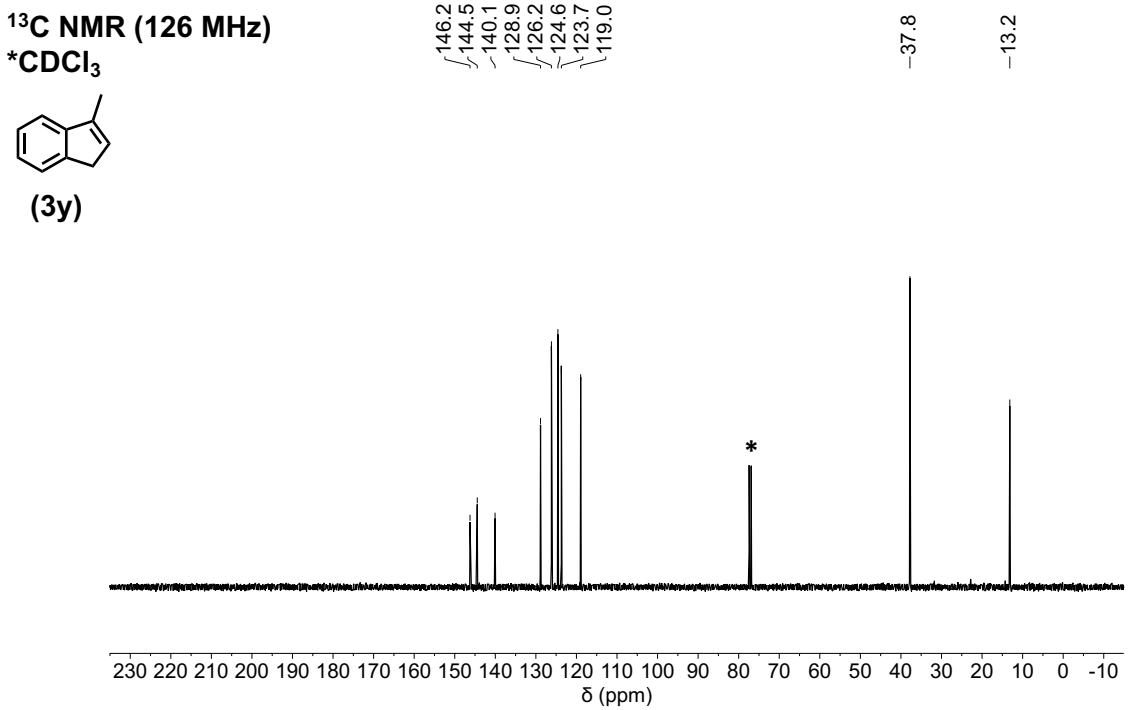

Figure A.107. $^{13}C\{^1H\}$ NMR spectrum of 1-methylindene (**3y**) recorded in $CDCl_3$ at 298 K.

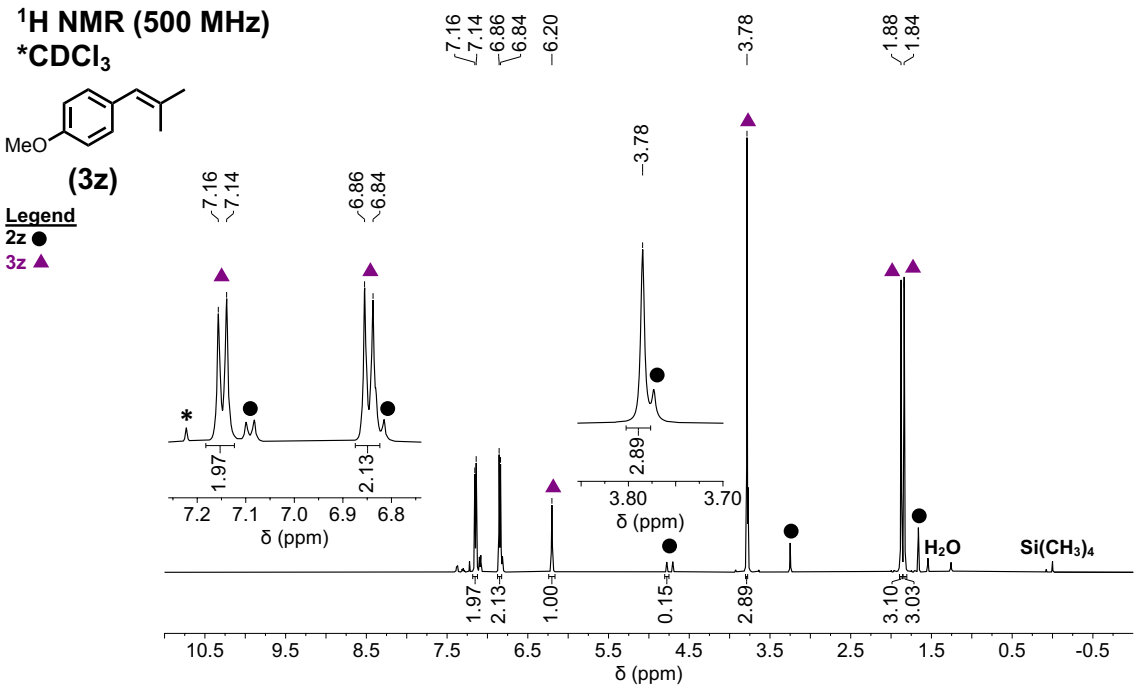

Figure A.108. ^{1}H NMR spectrum of 1-(4-methoxyphenyl)-2-methyl-1-propene (**3z**) recorded in $CDCl_3$ at 298 K.

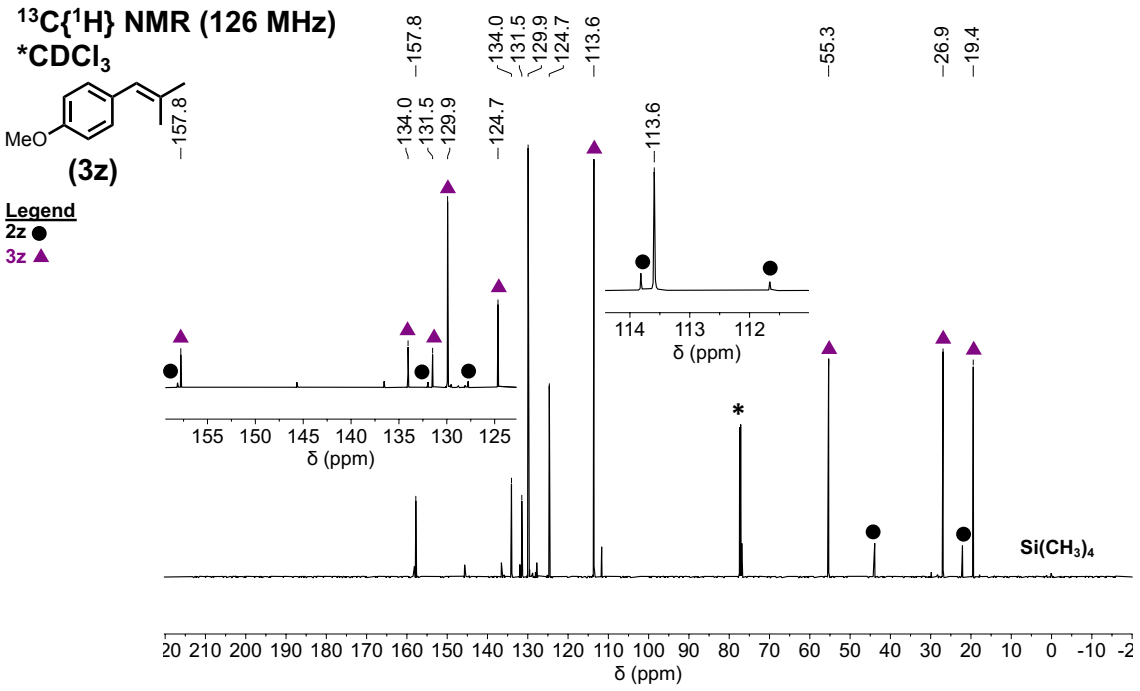

Figure A.109. ^{13}C{^{1}H} NMR spectrum of 1-(4-methoxyphenyl)-2-methyl-1-propene (**3z**) recorded in $CDCl_3$ at 298 K.

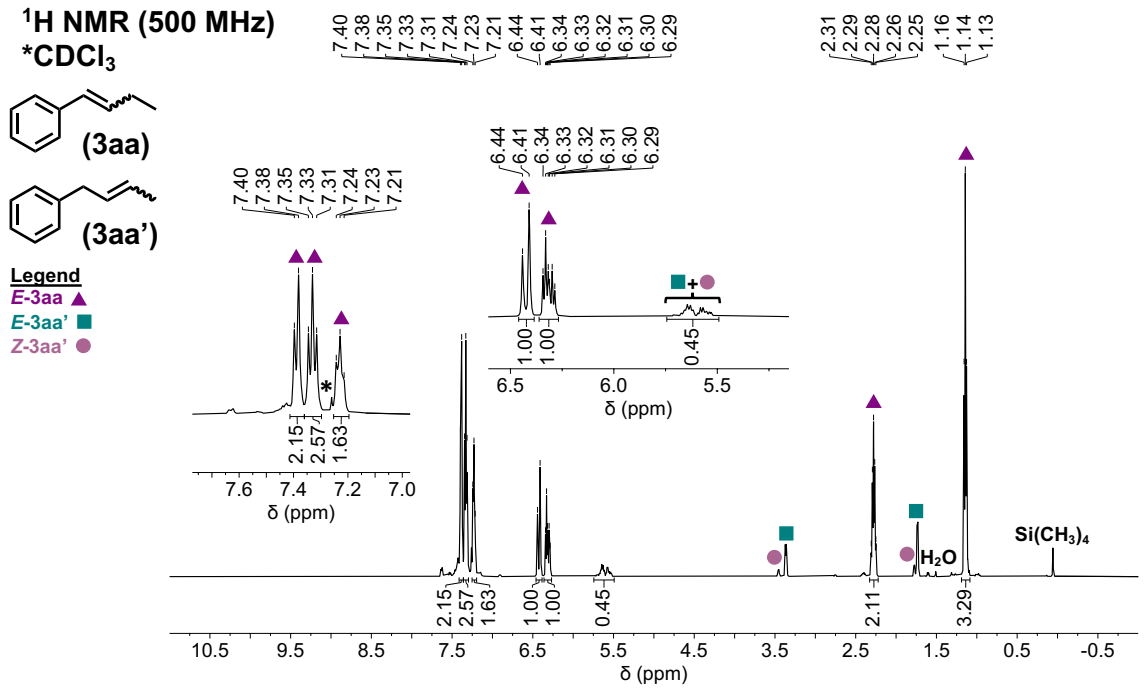

Figure A.110. ^{1}H NMR spectrum of 1-buten-1-ylbenzene (**3aa**) recorded in $CDCl_3$ at 298 K.

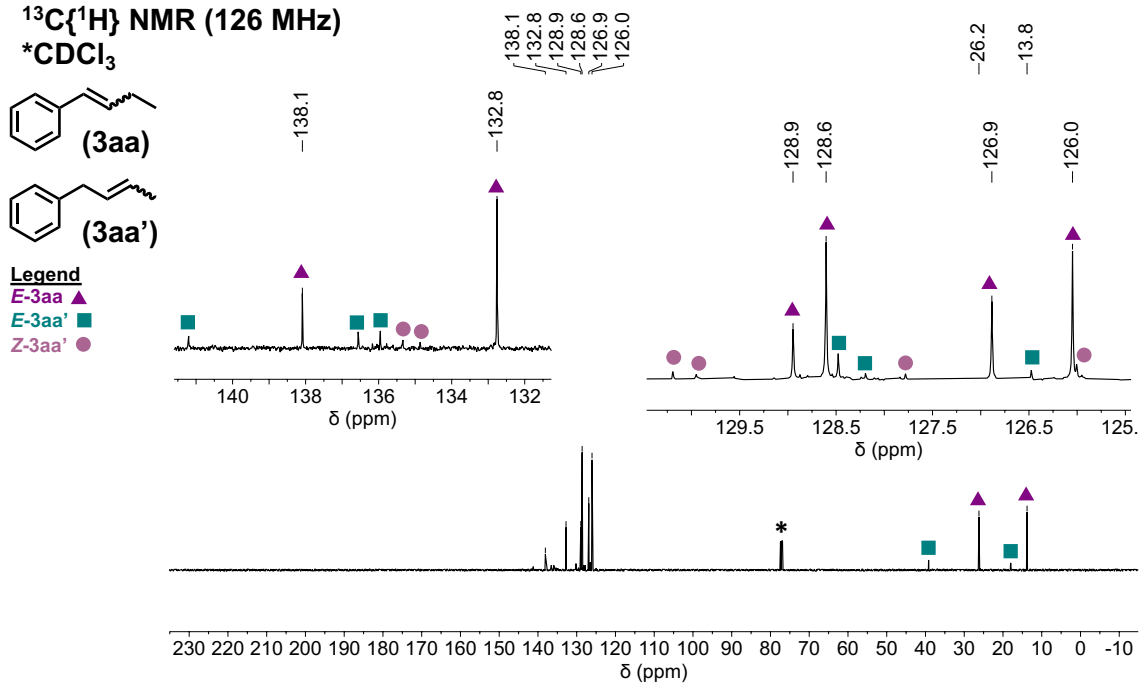

Figure A.111. ^{13}C{^{1}H} NMR spectrum of 1-buten-1-ylbenzene (**3aa**) recorded in $CDCl_3$ at 298 K.

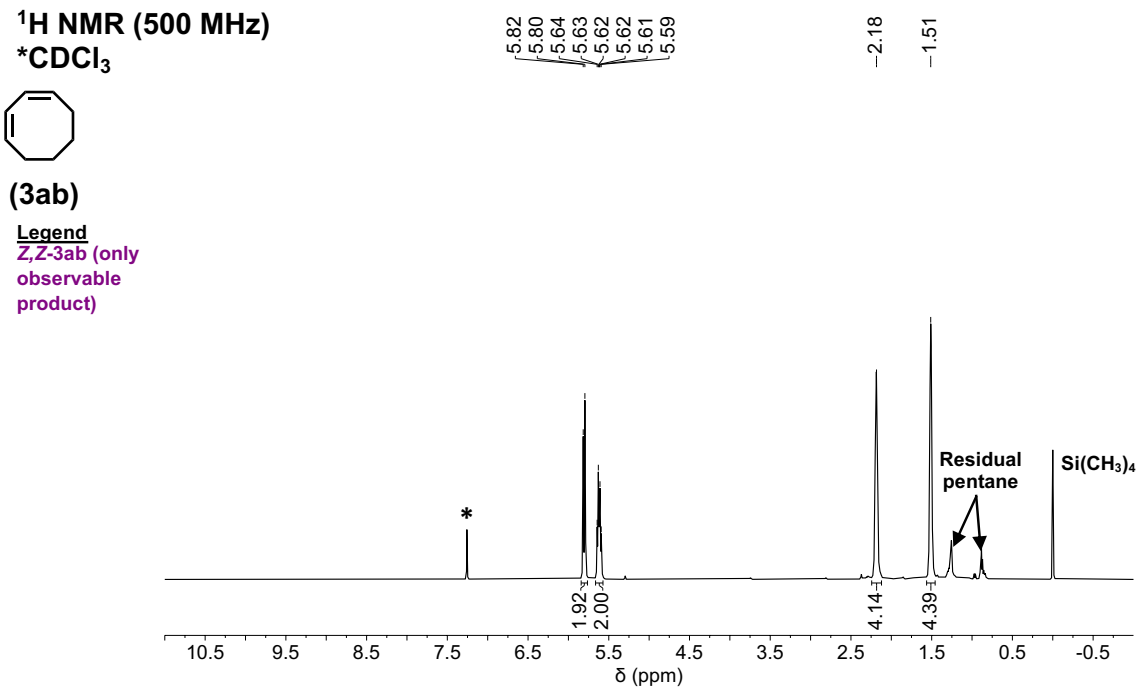

Figure A.112. ^{1}H NMR spectrum of 1,3-cyclooctadiene (**3ab**) recorded in $CDCl_3$ at 298 K.

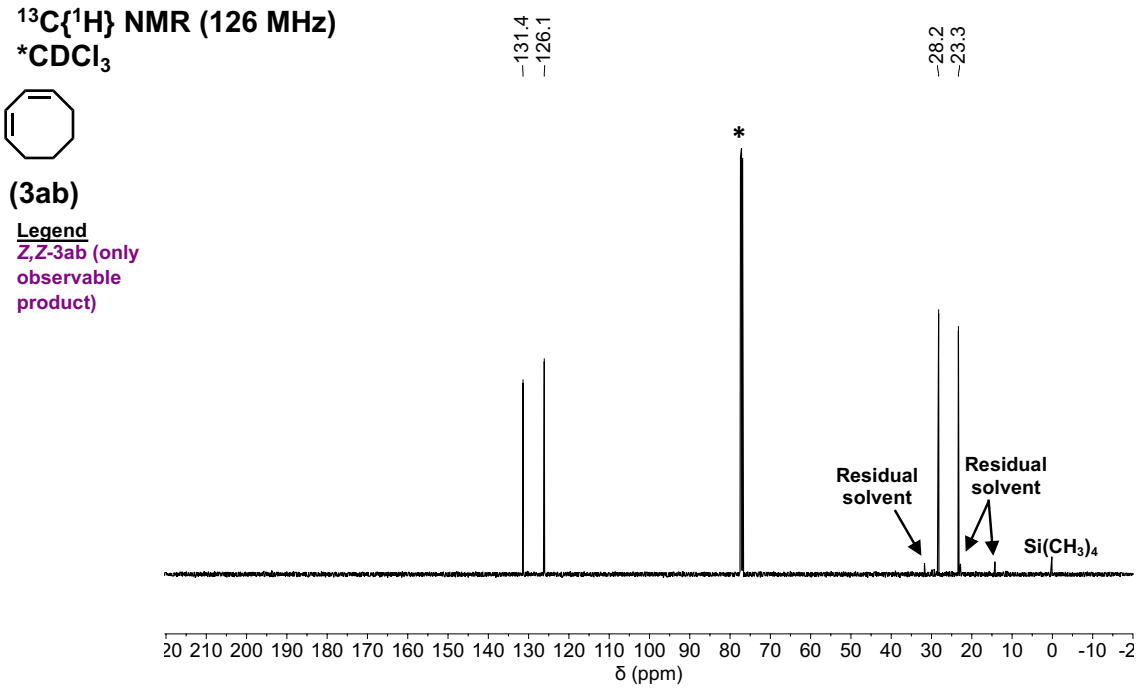

Figure A.113. ^{13}C{^{1}H} NMR spectrum of 1,3-cyclooctadiene (**3ab**) recorded in $CDCl_3$ at 298 K.

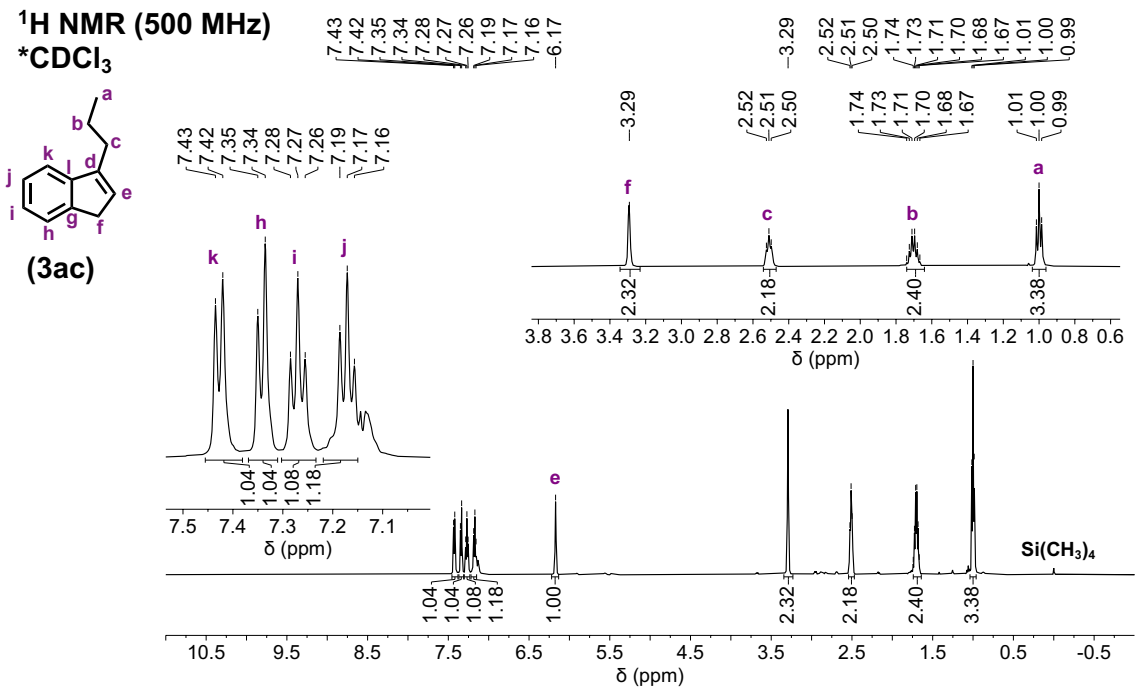

Figure A.114. ^{1}H NMR spectrum of 3-propyl-1*H*-indene (**3ac**) recorded in $CDCl_3$ at 298 K.

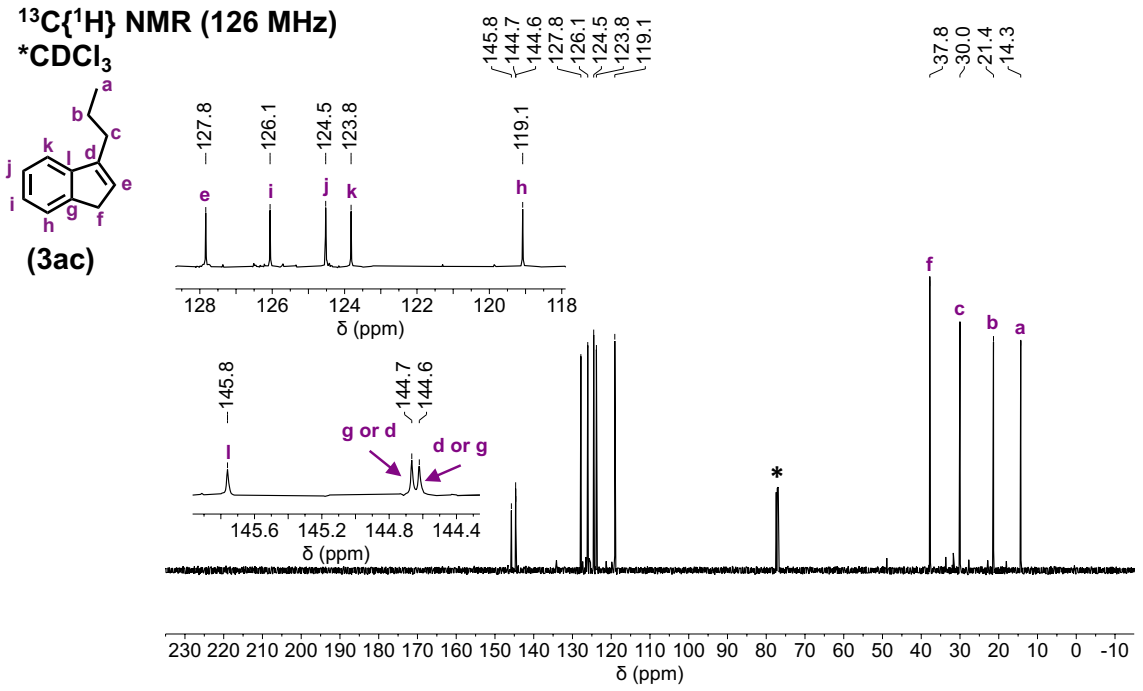

Figure A.115. ^{13}C{^{1}H} NMR spectrum of 3-propyl-1*H*-indene (**3ac**) recorded in $CDCl_3$ at 298 K.

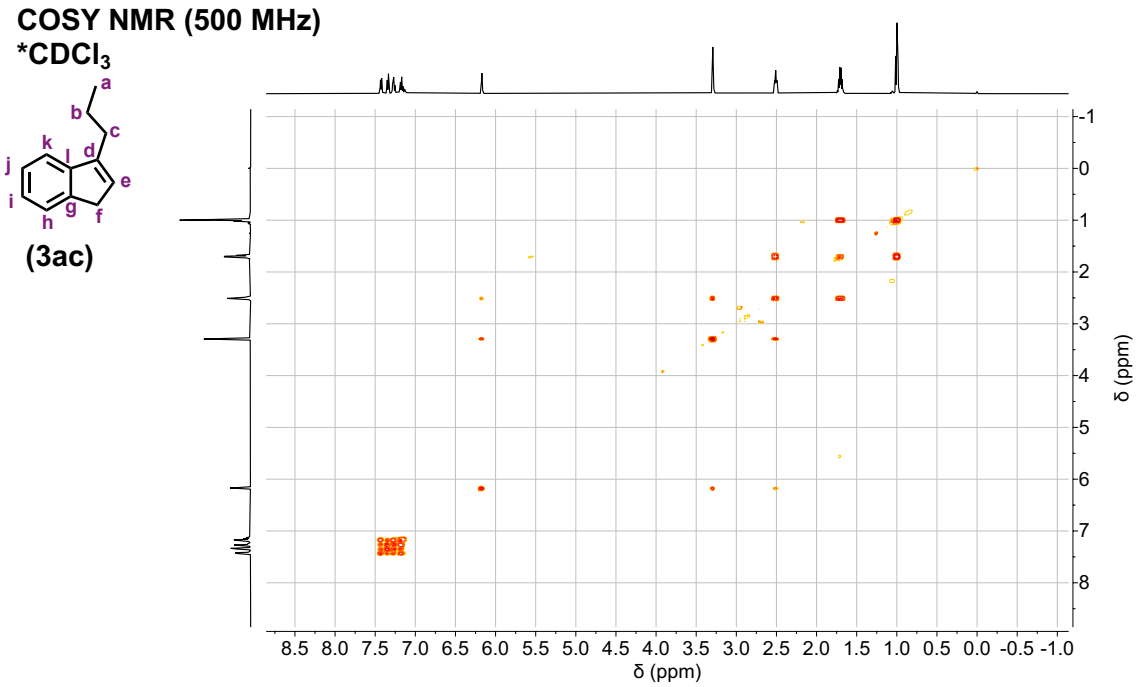

Figure A.116. COSY NMR spectrum of 3-propyl-1*H*-indene (**3ac**) recorded in $CDCl_3$ at 298 K.

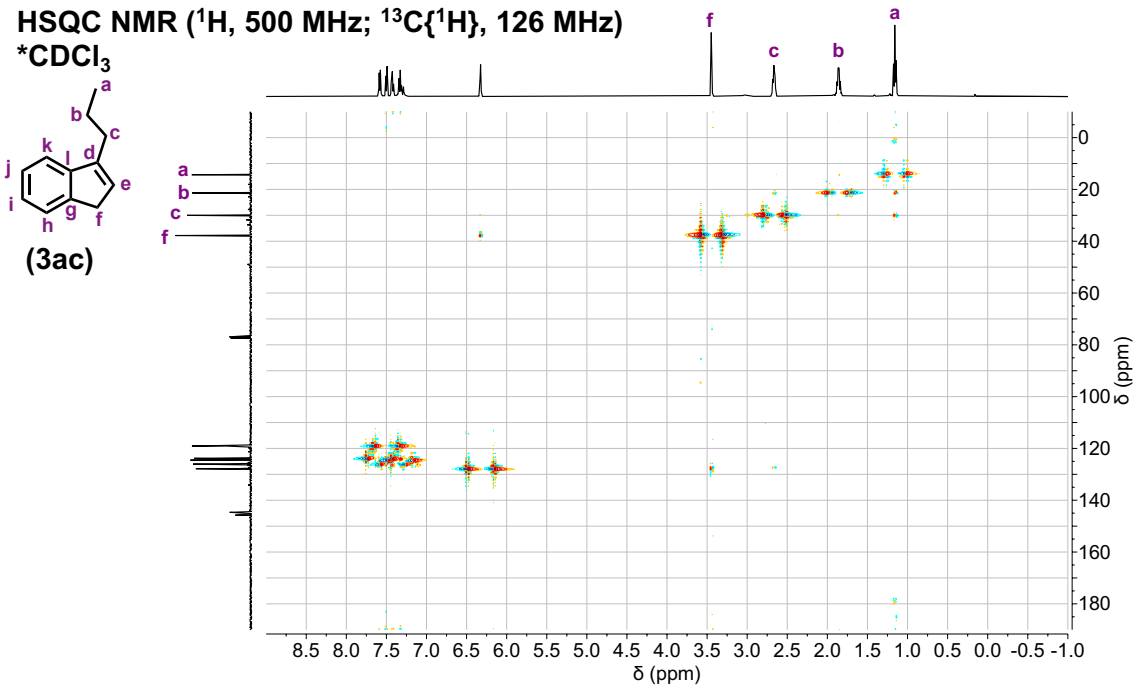

Figure A.117. HSQC NMR spectrum of 3-propyl-1*H*-indene (**3ac**) recorded in $CDCl_3$ at 298 K.

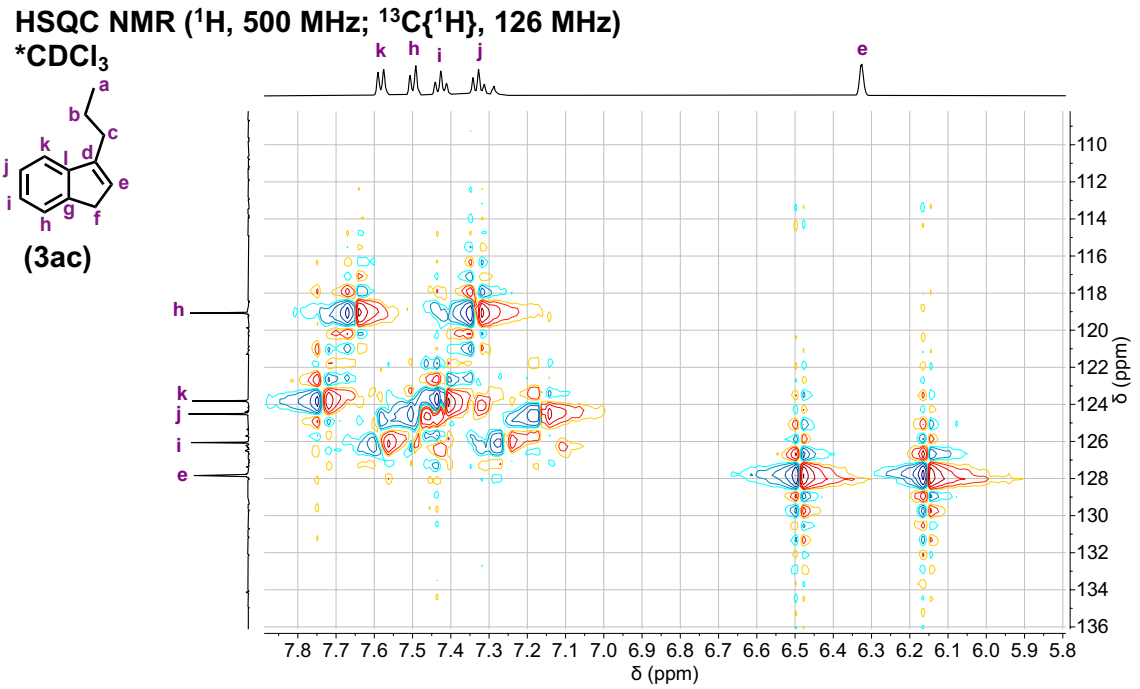

Figure A.118. Aryl region of the HSQC NMR spectrum of 3-propyl-1*H*-indene (**3ac**) recorded in $CDCl_3$ at 298 K.

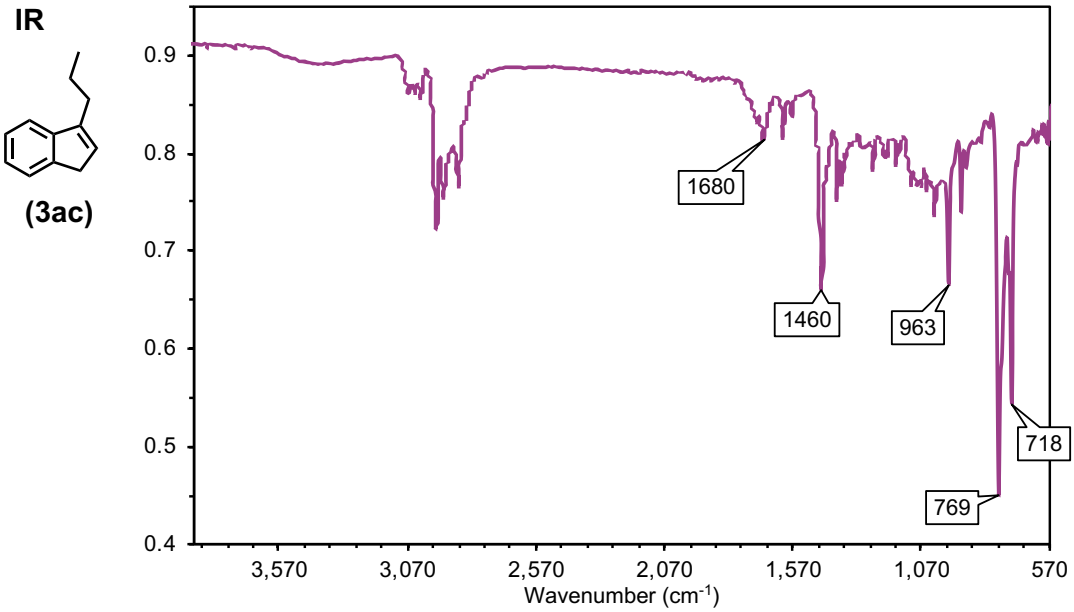

Figure A.119. IR spectrum of 3-propyl-1*H*-indene (**3ac**) recorded neat at room temperature.

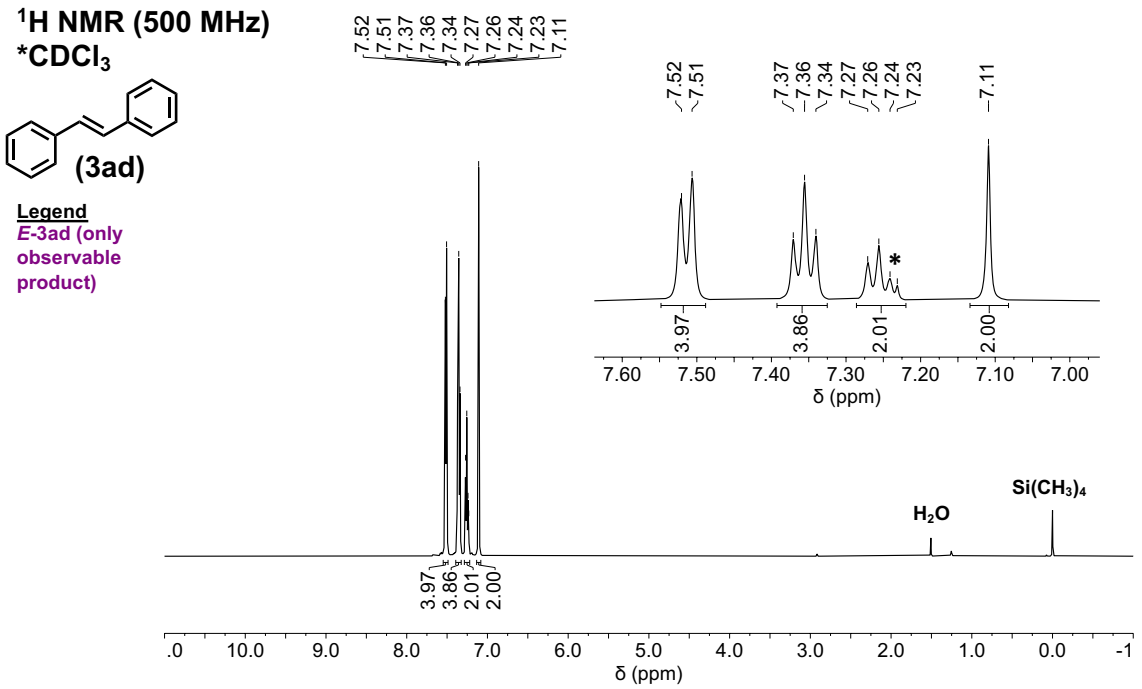

Figure A.120. ^{1}H NMR spectrum of *trans*-stilbene (**3ad**) recorded in $CDCl_3$ at 298 K.

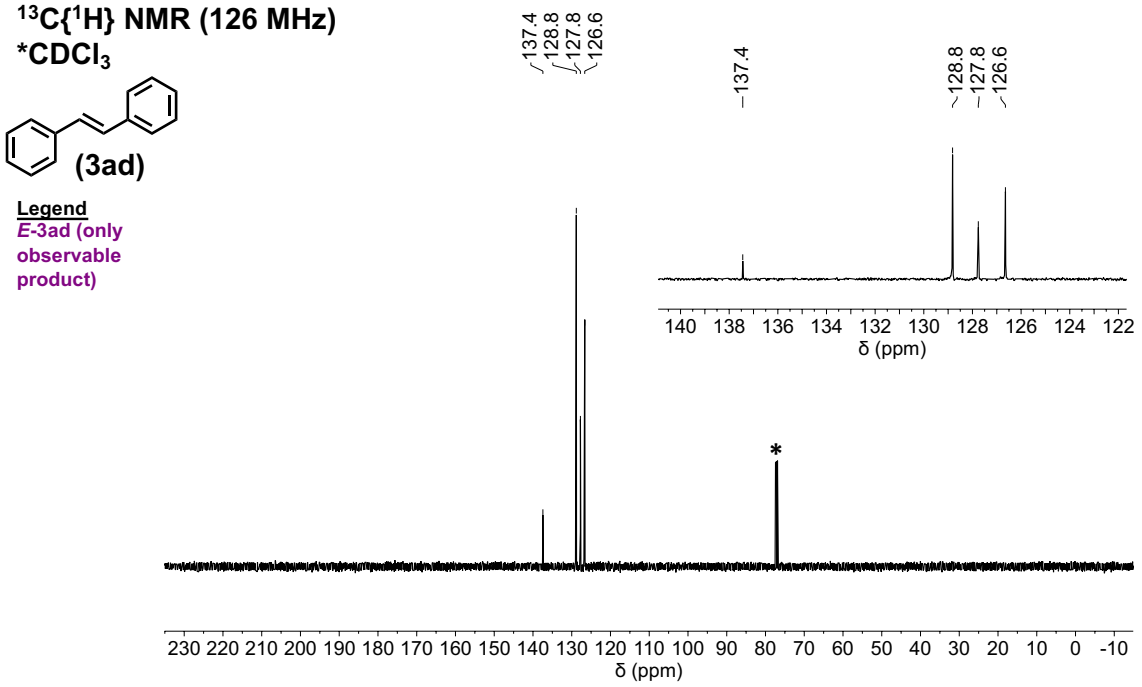

Figure A.121. $^{13}C\{^{1}H\}$ NMR spectrum of *trans*-stilbene (**3ad**) recorded in $CDCl_3$ at 298 K.

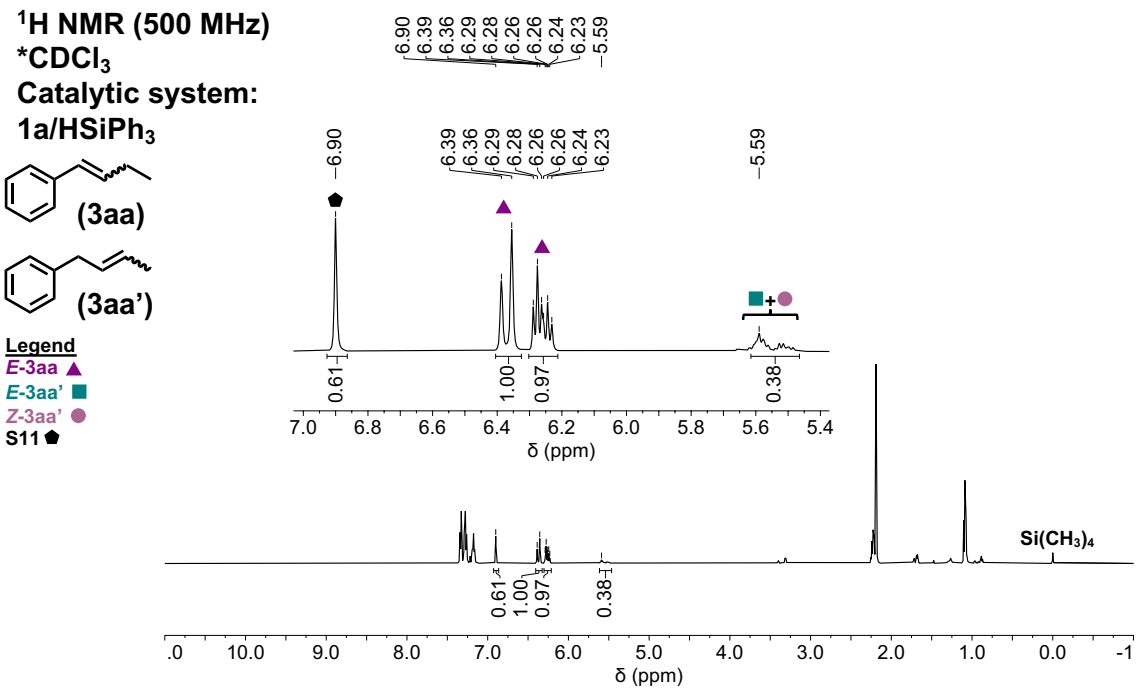

Figure A.122. ^{1}H NMR spectrum of 4-phenyl-2-butene (**3aa'**) isomerization with **1a**/HSiPh$_3$ recorded in CDCl$_3$ at 298 K.

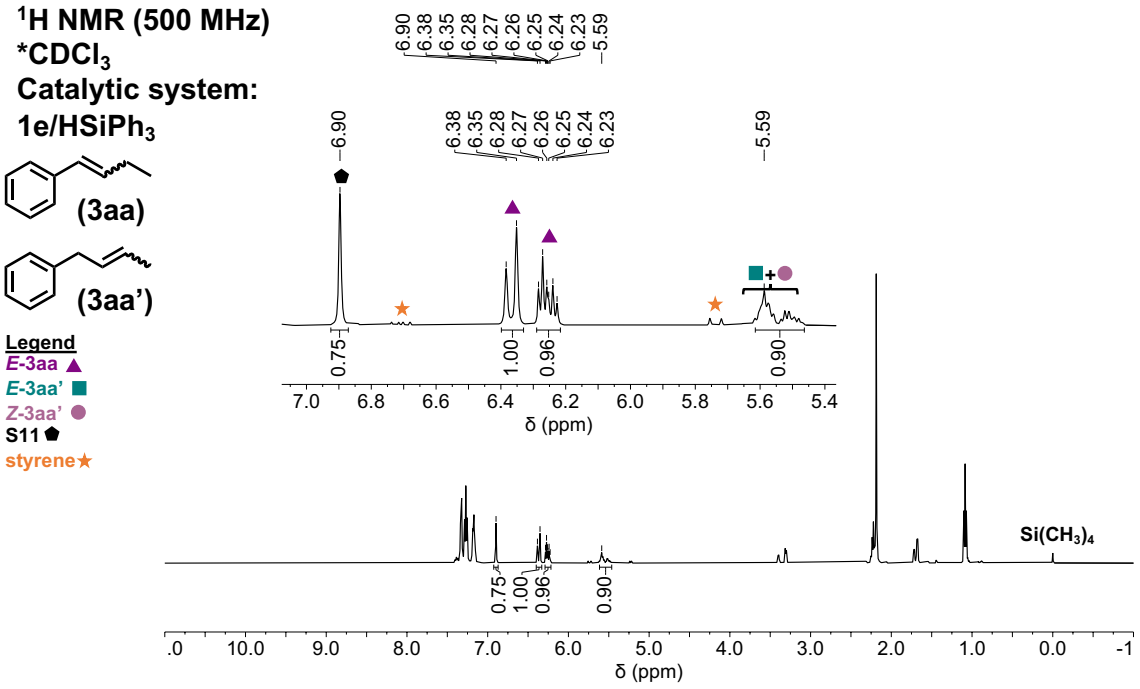

Figure A.123. ^{1}H NMR spectrum of 4-phenyl-2-butene (**3aa'**) isomerization with **1e**/HSiPh$_3$ recorded in CDCl$_3$ at 298 K.

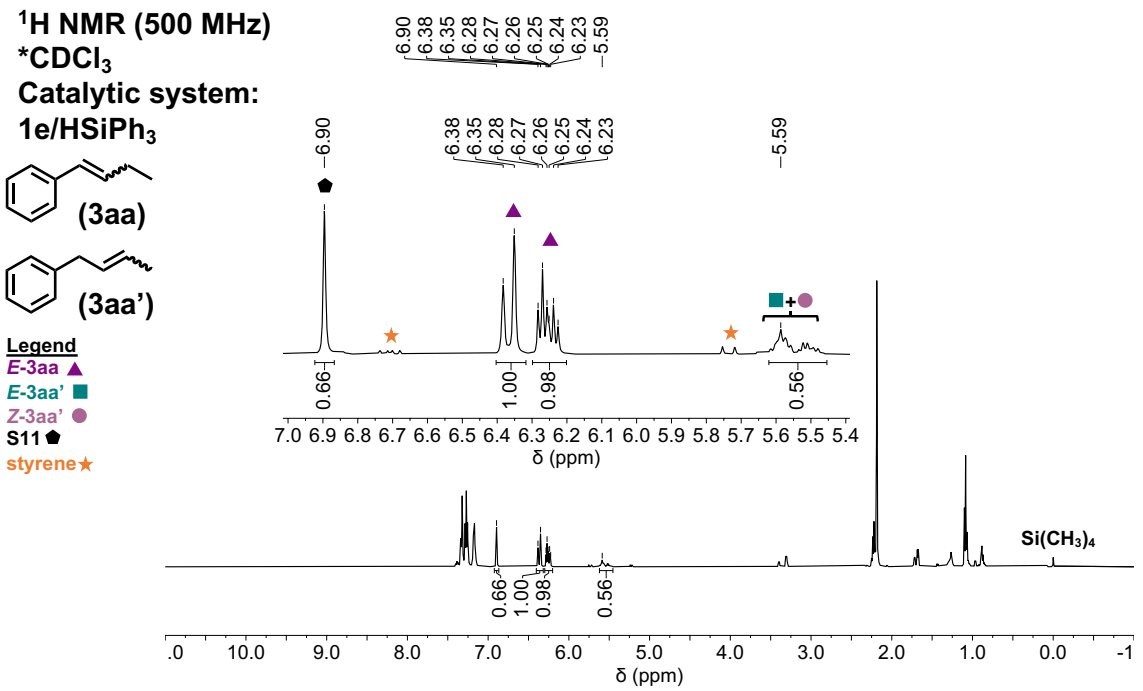

Figure A.124. ^{1}H NMR spectrum of 4-phenyl-1-butene (**2aa**) and 4-phenyl-2-butene (**3aa'**) isomerization with **1e**/$HSiPh_3$ recorded in $CDCl_3$ at 298 K. **Table A.**

e. Compounds for Mechanistic Investigation

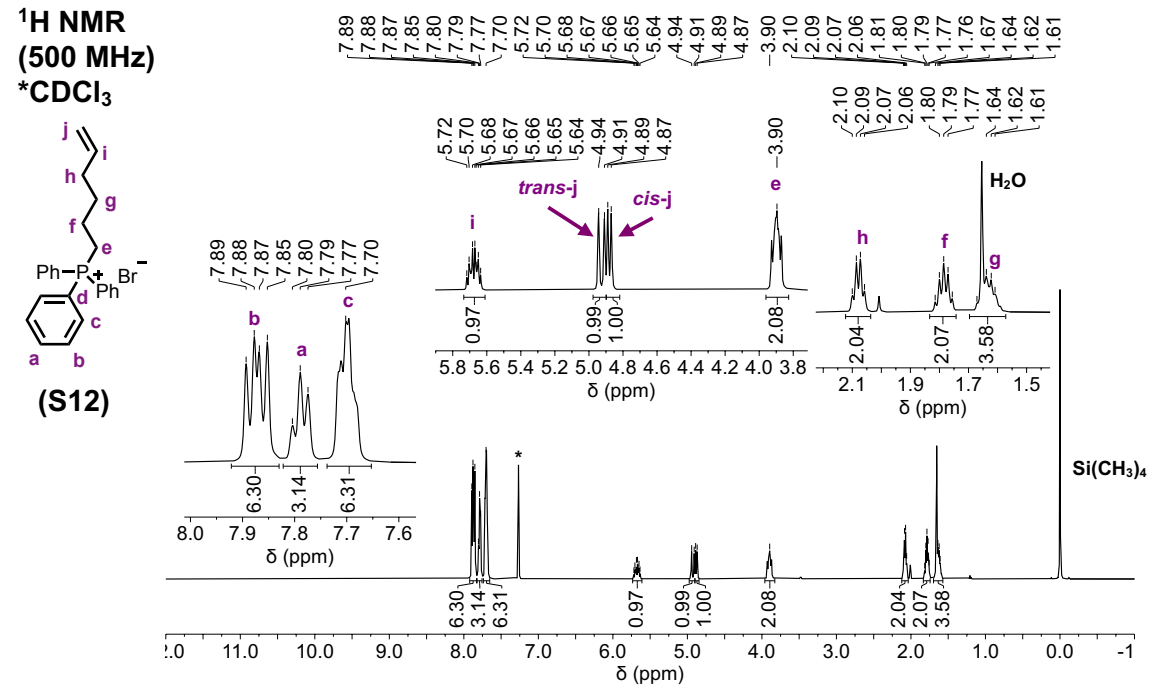

Figure A.125. ^{1}H NMR spectrum of hex-5-en-1-yltriphenylphosphonium bromide (**S12**) recorded in $CDCl_3$ at 298 K.

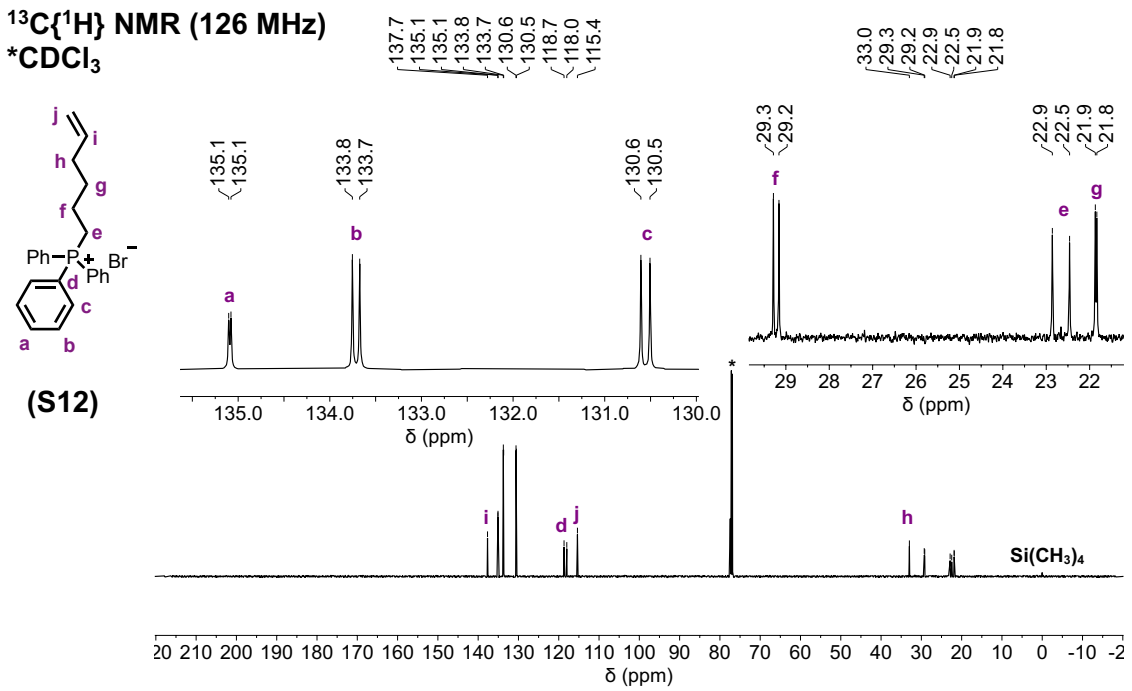

Figure A.126. $^{13}C\{^{1}H\}$ NMR spectrum of hex-5-en-1-yltriphenylphosphonium bromide (**S12**) recorded in $CDCl_3$ at 298 K.

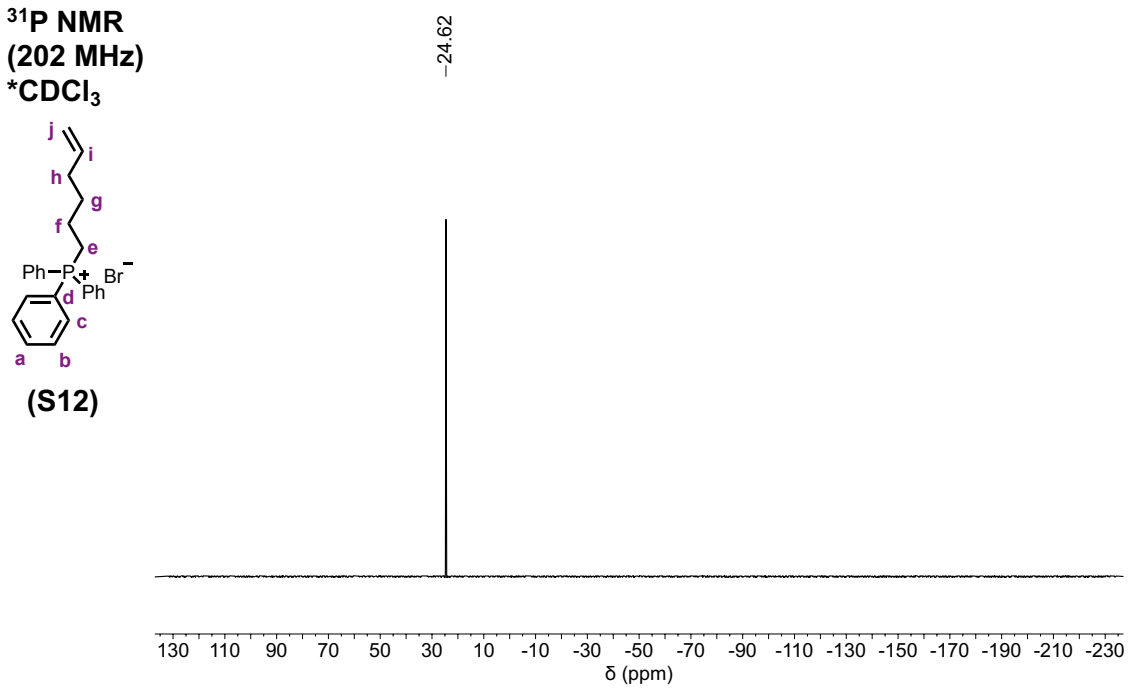

Figure A.127. ^{31}P NMR spectrum of hex-5-en-1-yltriphenylphosphonium bromide (**S12**) recorded in $CDCl_3$ at 298 K.

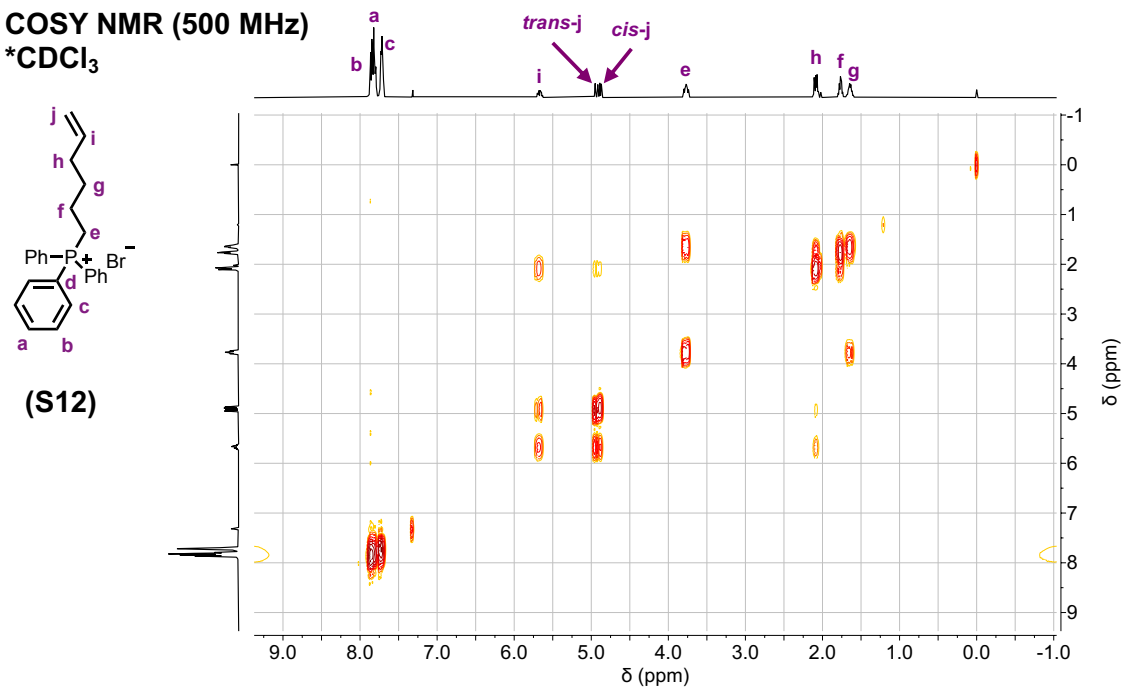

Figure A.128. COSY NMR spectrum of hex-5-en-1-yltriphenylphosphonium bromide (**S12**) recorded in $CDCl_3$ at 298 K.

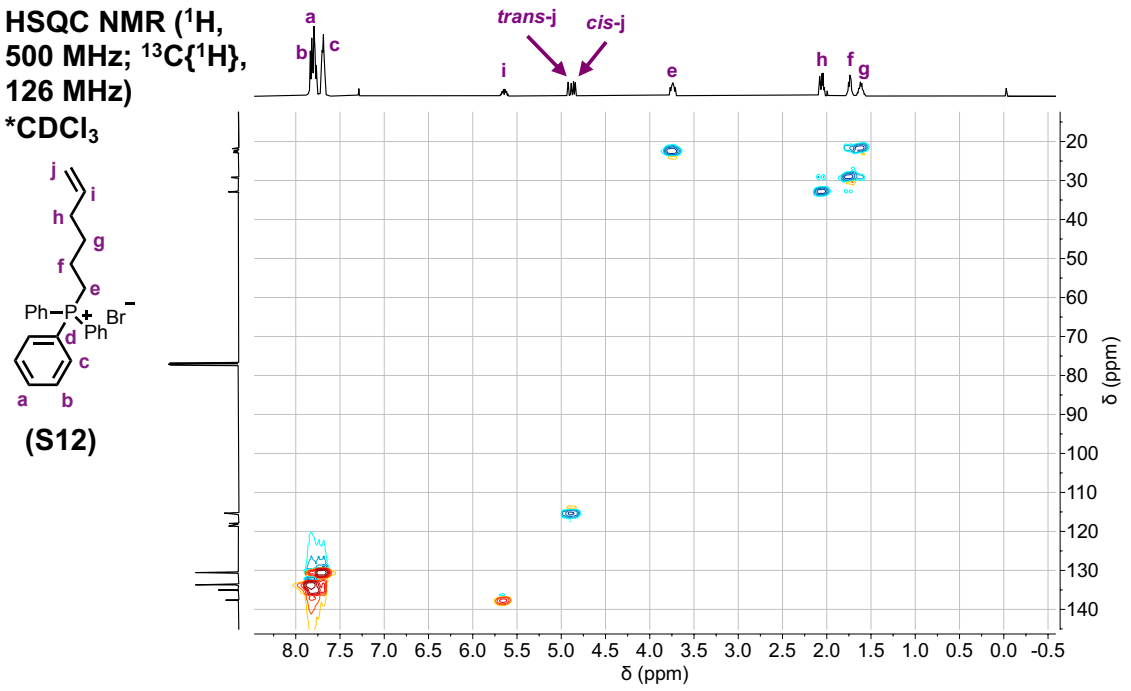

Figure A.129. HSQC NMR spectrum of hex-5-en-1-yltriphenylphosphonium bromide (**S12**) recorded in $CDCl_3$ at 298 K.

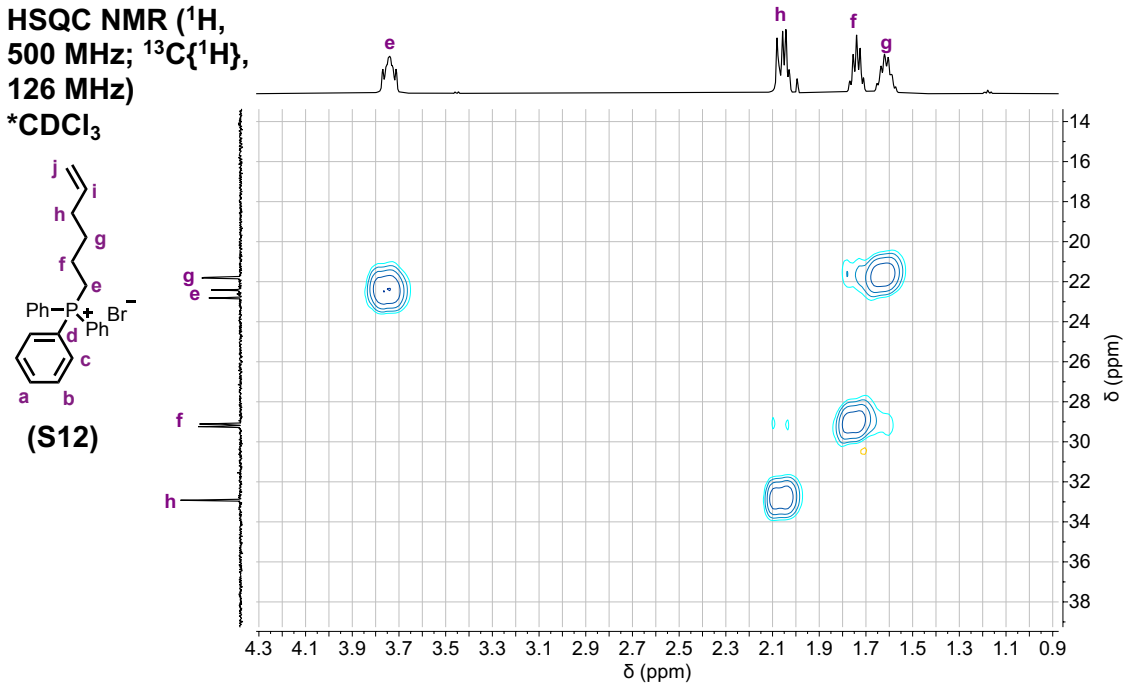

Figure A.130. Alkyl region of HSQC NMR spectrum of hex-5-en-1-yltriphenylphosphonium bromide (**S12**) recorded in $CDCl_3$ at 298 K.

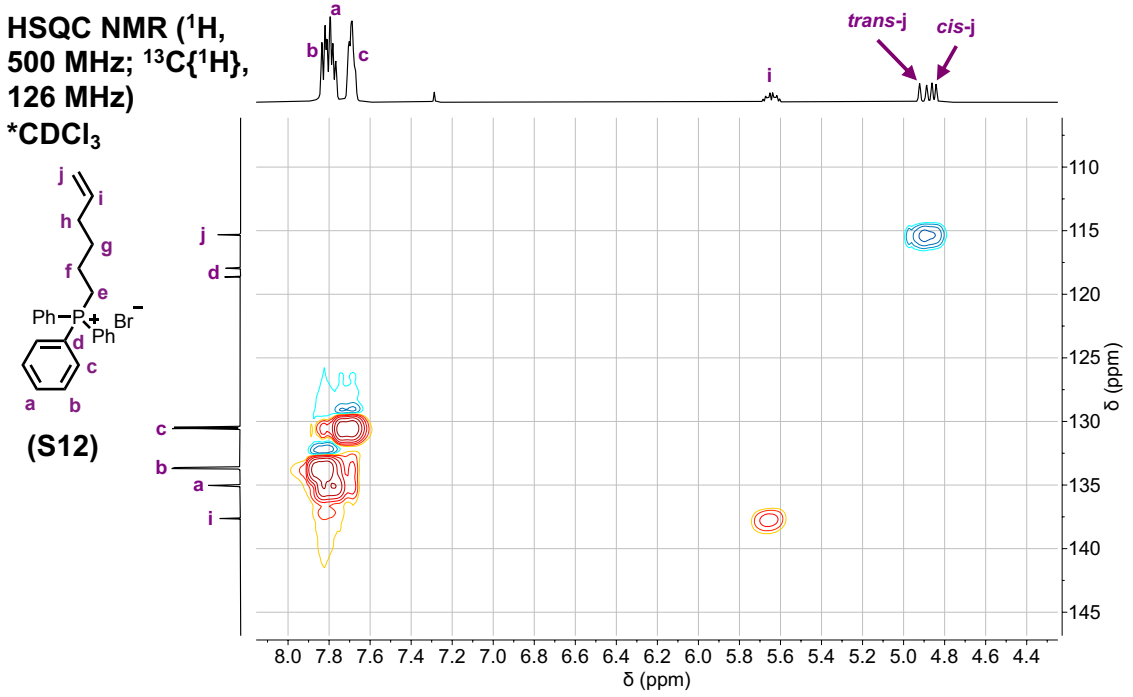

Figure A.131. Aryl region of HSQC NMR spectrum of hex-5-en-1-yltriphenylphosphonium bromide (**S12**) recorded in $CDCl_3$ at 298 K.

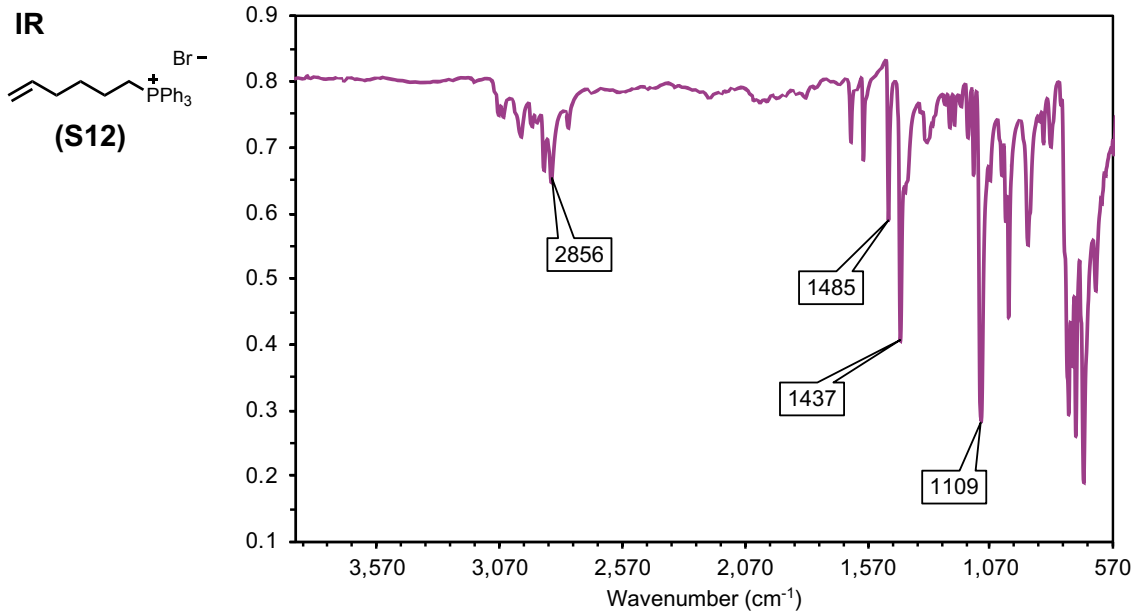

Figure A.132. IR spectrum of hex-5-en-1-yltriphenylphosphonium bromide (**S12**) recorded neat at room temperature.

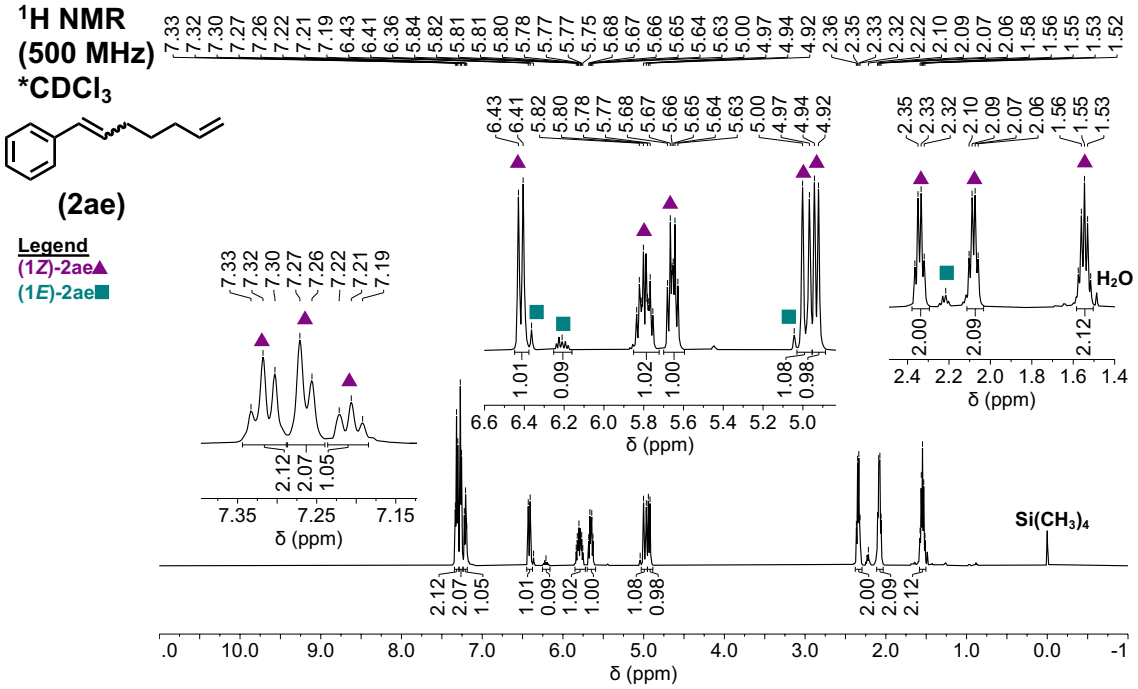

Figure A.133. ^{1}H NMR spectrum of 1,6-heptadien-1-ylbenzene (**2ae**) recorded in $CDCl_3$ at 298 K.

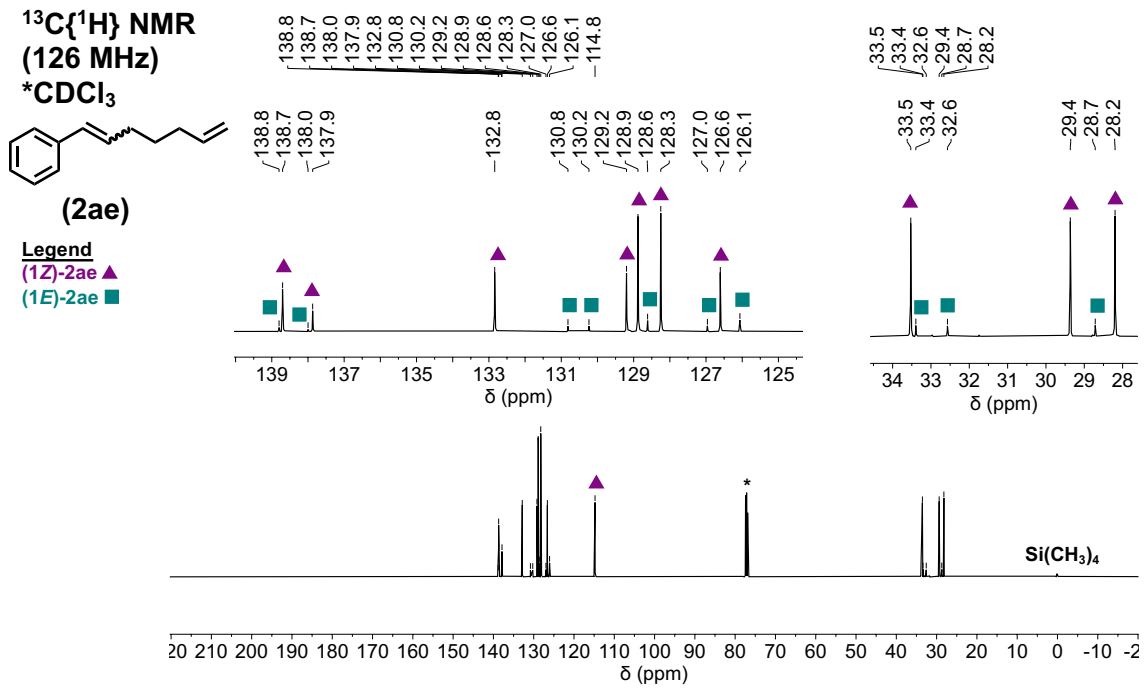

Figure A.134. $^{13}C\{^{1}H\}$ NMR spectrum of 1,6-heptadien-1-ylbenzene (**2ae**) recorded in $CDCl_3$ at 298 K.

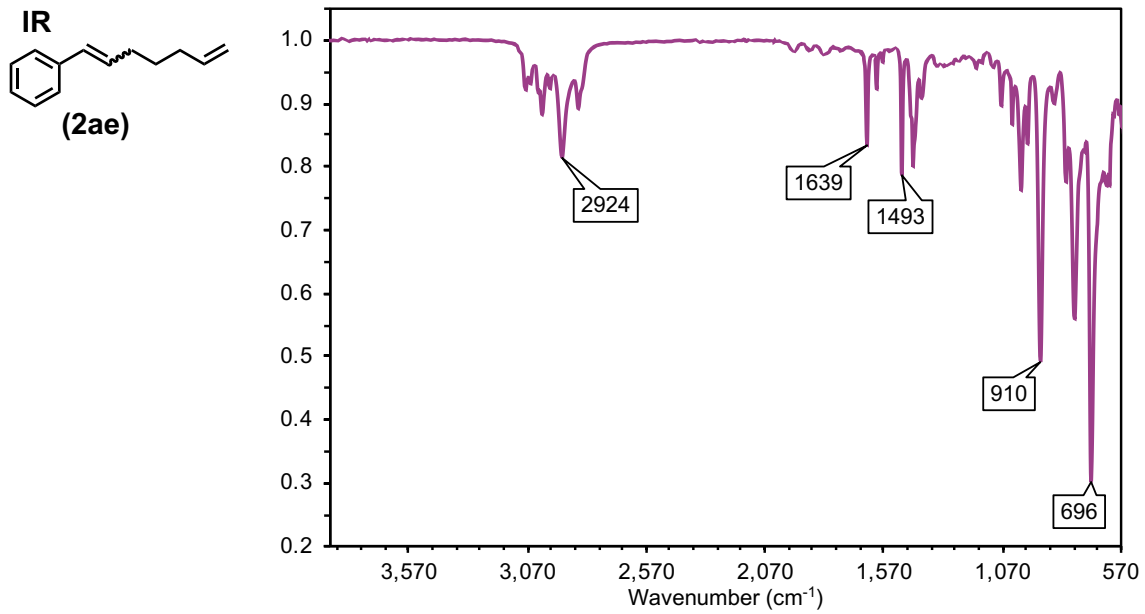

Figure A.135. IR spectrum of 1,6-heptadien-1-ylbenzene (**2ae**) recorded neat at room temperature.

APPENDIX B

SUPPLEMENTARY CONTENT FOR CHAPTER III

Experimental details

B.1.1. Materials and Methods

All syntheses and manipulations were carried out under nitrogen using standard Schlenk (vacuum 10^{-2} mbar) techniques or in a nitrogen-filled glovebox unless otherwise indicated. All reagents and solvents were used after drying and stored under nitrogen, unless otherwise indicated. Tetrahydrofuran (THF; Fisher Chemical; HPLC grade, unstabilized), hexanes (Fisher Chemical; HPLC grade), diethyl ether (Et_2O; B&J Brand; HPLC grade, unstabilized), dichloromethane (DCM; Oakwood Chemical; HPLC grade, unstabilized), dimethylformamide (DMF; Alfa Aesar; HPLC grade, unstabilized) and acetonitrile (MeCN; Fisher Chemical; HPLC grade) were dispensed under nitrogen from an LC Technology SP-1 solvent system. Benzene (ACS grade) and pentane (HPLC grade) were refluxed overnight with CaH_2 and distilled under nitrogen before use. The dried solvents were thereafter stored on activated 4Å molecular sieves under nitrogen. C_6D_6 and $CDCl_3$ were purchased from Cambridge Isotope Laboratories, degassed by freeze-pump-thaw, and thereafter stored on activated 4Å molecular sieves under nitrogen. All stock solutions were prepared by mass and were dispensed into reaction vessel by difference from syringe, as detailed in the procedure for each experiment.

B.1.2. General Experimental

Nuclear magnetic resonance (NMR) spectra were collected at room temperature (298 K) unless otherwise stated on a Bruker AV-III HD 600 NMR (600.13 MHz for ^{1}H; 150.90 MHz for ^{13}C; 564.69 MHz for ^{19}F; 119.23 MHz for ^{29}Si; 232.94 MHz for ^{31}P; 92.12 MHz for ^{2}H), Bruker Avance-III HD 500 NMR (499.90 MHz for ^{1}H; 126 MHz for ^{13}C; 471 MHz for ^{19}F; 99 MHz for ^{29}Si; 202.46 MHz for ^{31}P), or Varian Inova 500 NMR (499.90 MHz for ^{1}H; 126 MHz for ^{13}C; 471 MHz for ^{19}F; 99 MHz for ^{29}Si; 202.46 MHz for ^{31}P). ^{1}H and ^{13}C spectra were referenced to the residual solvent peak ($CDCl_3$: ^{1}H δ = 7.26 ppm,

^{13}C δ = 77.16 ppm; C_6D_6: ^{1}H δ = 7.16 ppm, ^{13}C δ = 128.06 ppm). Chemical shifts are reported in parts per million (ppm, δ) relative to tetramethylsilane at 0.00 ppm. Peaks are characterized as follows: s (singlet), d (doublet), t (triplet), q (quartet), pent (pentet), hept (heptet), m (multiplet), br (broad), app (apparent), and/or ms (multiple signals). Coupling constants, *J*, are reported in Hz. Electron paramagnetic resonance (EPR) spectra were collected at 77 K on a Bruker Elexsys E500 EPR X-band spectrometer. Infrared spectroscopy was performed on an Agilent Nicolet 6700 FT-IR, and peaks are reported in cm^{-1}. For catalytic reactions, yields were determined using Gas Chromatography-Mass Spectrometry (GCMS) or Gas Chromatography (GC) against an internal standard. GCMS was carried out on a Shimadzu GC-2010 Plus/GCMS-QP2010 SE using a Restek Rtx®-5 (Crossbond 5% diphenyl – 95% dimethyl polysiloxane; 15 m, 0.25 mm ID, 0.25 μm df) column. GC was carried out on a Thermo Fisher Trace 1300 Gas Chromatograph using a Restek Rtx®-5 (Crossbond 5% diphenyl – 95% dimethyl polysiloxane; 15 m, 0.25 mm ID, 0.25 μm df) column. High-resolution mass spectrometry (HRMS) was carried out on a Waters XEVO G2-XS TOF mass spectrometer.

B.1.3. Synthesis of Non-Commercial Reagents

a. Tris(3-fluorophenyl)silane, $HSi(3\text{-}F\text{-}C_6H_4)_3$

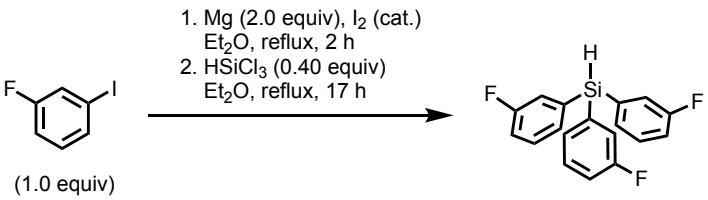

(1.0 equiv)

Tris(3-fluorophenyl)silane was prepared via a literature procedure:[245] To an oven-dried 100-mL Schlenk flask equipped with a magnetic stir bar was added Mg (1.22 g, 40 mmol, 2.0 equiv), Et_2O (30 mL), and I_2 (a grain). 3-Fluoroiodobenzene (2.4 mL, 20 mmol, 1.0 equiv) was added slowly and the reaction was equipped with a condenser before being placed in a preheated oil bath at 60 °C. The reaction was refluxed for 2 hours before being cooled to room temperature. Once cool, the reaction solution was transferred via cannula to a 200-mL oven dried Schlenk flask. The reaction was cooled to 0 °C with an ice/water for 10 minutes. In the meantime, in an oven dried 40 mL Schlenk flask, a solution of $HSiCl_3$ (0.81 mL, 8.0 mmol, 0.40 equiv) in Et_2O (20 mL) was prepared. After 10 minutes, the

solution of $HSiCl_3$ was added slowly to the Grignard solution. The reaction was equipped with a condenser again and placed back in the oil bath at 60 °C to reflux. After 17 h, the reaction was deemed complete by analysis of an aliquot by GC-MS and cooled to room temperature. The reaction was opened to air and quenched with ~10 mL HCl (3 M). The reaction was transferred to a separatory funnel and ~30 mL H_2O was added. The aqueous layer was isolated and extracted with Et_2O (3 x 80 mL). The combined organic layers were dried over Na_2SO_4, filtered and concentrated under reduced pressure. The crude material was purified via column chromatography (silica, hexanes) to yield the product as a white solid (1.50 g, 3.2 mmol, 40% yield).

B.1.4. Isomerization of allylarenes

a. Reaction order determination

i. Kinetics to measure order in $(sty)_2Ni(IPr)$

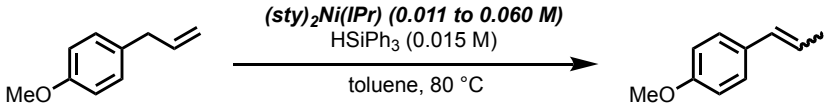

In a nitrogen-filled glovebox, $(sty)_2Ni(IPr)$ was weighed into 1-dram vials (5.8 to 32.8 mg, 0.009 to 0.050 mmol, 0.035 to 0.20 equiv). Magnetic stir bars were added to each vial. A stock solution of $HSiPh_3$ (0.016 M) and durene (0.081 M) was prepared by weighing out each reagent directly into a 10-mL volumetric flask and adding the appropriate volume of toluene. The stock solution was distributed (0.80 mL) using a 1-mL disposable syringe. Vials were sealed with septum caps, removed from the glovebox, and placed on a preheated aluminum vial block at 80 °C. After 30 minutes, 4-allylanisole (38 μL, 0.25 mmol, 1.0 equiv) was distributed in two portions using a 25-μL microliter syringe. Over the course of the reaction, ~5 μL aliquots were removed from the reaction and filtered through Celite with hexanes directly into a GC vial for analysis by GC-FID. The concentration of 4-OMe-β-methylstyrene was found versus durene as an internal standard based on an independent calibration curve prepared with commercial reagents.

Table B.1. Concentration of 4-OMe-β-methylstyrene formed over time at differing initial concentrations of $(sty)_2Ni(IPr)$. Linear portion of kinetic curve values used to find the order are **bolded**. Concentrations of 4-OMe-β-methylstyrene were determined using GC-FID against durene as an internal standard.

$[(sty)_2Ni(IPr)]$ = 0.060 M				$[(sty)_2Ni(IPr)]$ = 0.036 M			
Time (s)	**[4-OMe-β-methylstyrene] (M)**			**Time (s)**	**[4-OMe-β-methylstyrene] (M)**		
300	0.015	±	0.003	300	0.0095	±	0.001
600	0.027	±	0.006	600	0.018	±	0.001
900	0.037	±	0.008	900	0.024	±	0.000
1200	0.048	±	0.008	1200	0.031	±	0.00
1500	0.062	±	0.008	1500	0.040	±	0.00
1800	0.080	±	0.007	1800	0.051	±	0.00
2160	**0.10**	**±**	**0.01**	2160	0.069	±	0.01
2400	**0.12**	**±**	**0.01**	**2400**	**0.081**	**±**	**0.01**
2760	**0.15**	**±**	**0.00**	**2760**	**0.10**	**±**	**0.01**
3000	**0.17**	**±**	**0.01**	**3000**	**0.12**	**±**	**0.01**
3360	**0.20**	**±**	**0.00**	**3360**	**0.14**	**±**	**0.01**
3600	**0.22**	**±**	**0.00**	**3600**	**0.16**	**±**	**0.01**
4200	0.26	±	0.01	**4200**	**0.19**	**±**	**0.01**
4800	0.26	±	0.01	4800	0.23	±	0.01
5400	0.27	±	0.01	5400	0.26	±	0.01
6000	0.27	±	0.00	6000	0.27	±	0.01
6600	0.26	±	0.00	6600	0.27	±	0.01
7200	0.26	±	0.00	7200	0.26	±	0.01
8400	0.27	±	0.00	8400	0.27	±	0.01
9600	0.26	±	0.01	9600	0.27	±	0.01
10800	0.27	±	0.01	10800	0.27	±	0.01
12600	0.27	±	0.01	12600	0.27	±	0.01

$[(sty)_2Ni(IPr)]$ = 0.015 M				$[(sty)_2Ni(IPr)]$ = 0.011 M			
Time (s)	**[4-OMe-β-methylstyrene] (M)**			**Time (s)**	**[4-OMe-β-methylstyrene] (M)**		
300	0.011	±	0.002	300	0.014	±	0.007
600	0.028	±	0.004	600	0.04	±	0.01
1200	0.052	±	0.008	1200	0.08	±	0.03
1800	0.067	±	0.008	1800	0.09	±	0.03
2400	**0.09**	**±**	**0.01**	**2400**	**0.12**	**±**	**0.04**
3000	**0.11**	**±**	**0.01**	**3000**	**0.13**	**±**	**0.04**
3600	**0.13**	**±**	**0.01**	**3600**	**0.15**	**±**	**0.03**
4200	**0.16**	**±**	**0.02**	**4800**	**0.20**	**±**	**0.04**
4800	**0.19**	**±**	**0.02**	**5400**	**0.22**	**±**	**0.03**
5400	**0.21**	**±**	**0.02**	**6000**	**0.24**	**±**	**0.03**
6000	0.24	±	0.01	6600	0.25	±	0.02
6600	0.26	±	0.01	7200	0.26	±	0.01

7200	0.27	±	0.00	7800	0.27	±	0.00
8400	0.27	±	0.00	8400	0.27	±	0.00
9600	0.26	±	0.00	9600	0.27	±	0.00
10800	0.26	±	0.00	10800	0.25	±	0.02
12600	0.26	±	0.00	12600	0.27	±	0.00
				14400	0.27	±	0.00

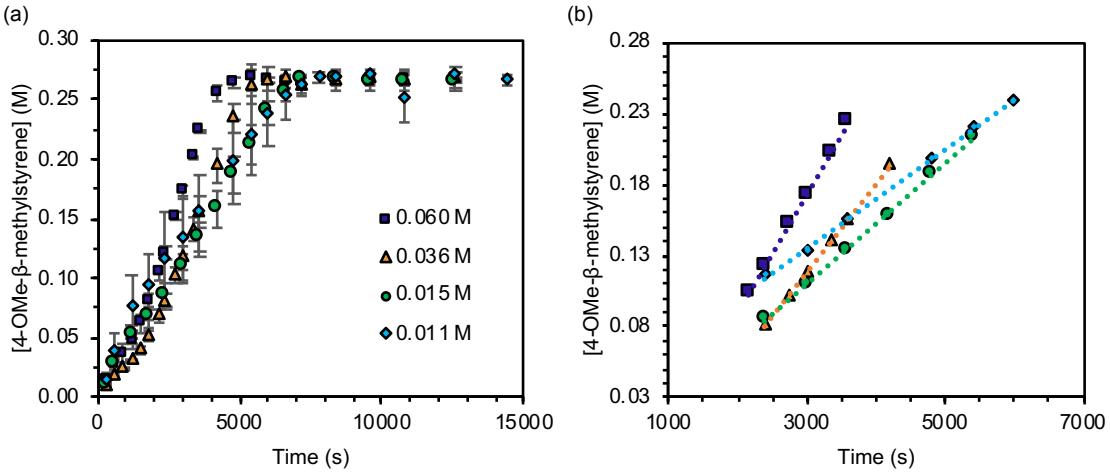

Figure B.1. Formation of 4-OMe-β-methylstyrene formed over time at differing initial concentrations of $(sty)_2Ni(IPr)$. (a) Full reaction profiles and (b) linear portion of kinetic curve.

Table B.2. Rates of formation of 4-OMe-β-methylstyrene at varying initial concentrations of $(sty)_2Ni(IPr)$.

$[(sty)_2Ni(IPr)]$ (M)	**Rate (M/s)**	**$\log([(sty)_2Ni(IPr)]$ / M)**	**log(Rate / M/s)**
0.060	$8.32 \cdot 10^{-5} \pm 0.08 \cdot 10^{-5}$	-1.22	-4.08
0.036	$6.35 \cdot 10^{-5} \pm 0.06 \cdot 10^{-5}$	-1.44	-4.20
0.015	$4.26 \cdot 10^{-5} \pm 0.08 \cdot 10^{-5}$	-1.82	-4.37
0.011	$3.46 \cdot 10^{-5} \pm 0.05 \cdot 10^{-5}$	-1.96	-4.46

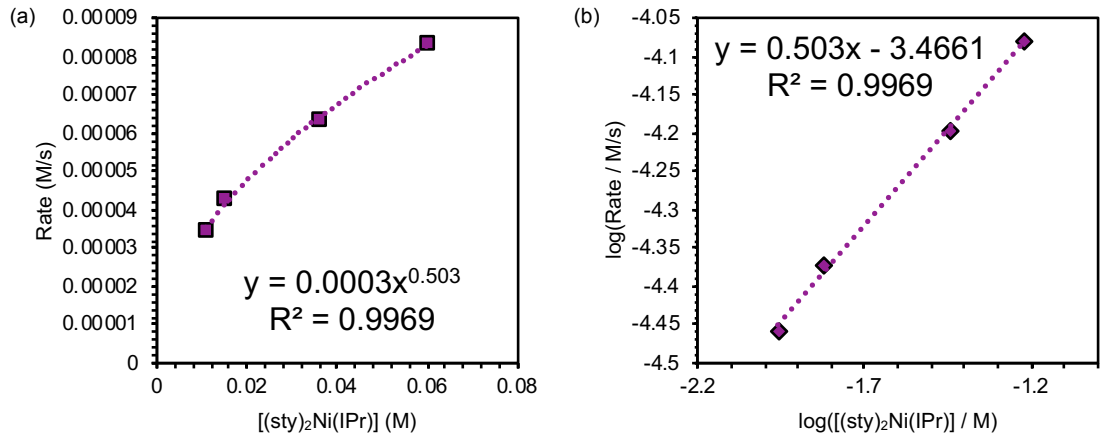

Figure B.2. Order plot for $(sty)_2Ni(IPr)$. (a) Power function fit of form $y = a \cdot x^b$; a = 0.0003, b = 0.50, $R^2 = 0.997$ and (b) linearized log-log plot of form $y = m \cdot x + b$; m = 0.50 ± 0.02, b = 3.47 ± 0.03, $R^2 = 0.997$.

ii. Kinetics to measure order in $HSiPh_3$

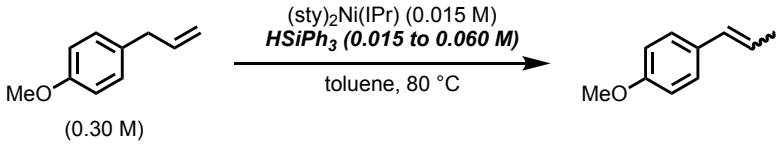

In a nitrogen-filled glovebox, $(sty)_2Ni(IPr)$ (8.2 mg, 0.013 mmol, 0.05 equiv) was weighed directly into 1-dram vials. Magnetic stir bars were added to each vial. Stock solution of durene (0.15 M) and HSiPh3 (0.13 M) were prepared in 5.0- and 10.0-mL volumetric flasks, respectively, by weighing out the reagent and adding the appropriate volume of toluene. The durene stock solution (0.40 mL, 0.061 mmol, 0.24 equiv) was distributed to each vial using a 1-mL disposable syringe. Silane stock solution and toluene (to keep the total volume in each vial consistent) were distributed each vial using a 250-µL microliter syringe (see **Table B.3.** for specific details). Vials were sealed with septum caps, removed from the glovebox and placed on a preheated aluminum vial block at 80 °C. After 30 minutes, 4-allylanisole (38 µL, 0.25 mmol, 1.0 equiv) was distributed in two portions using a 25-µL microliter syringe. Throughout the course of the reaction, ~5 µL aliquots were removed from the reaction, filtered through Celite with hexanes directly in to a GC and analyzed by GC-FID. The concentration of 4-OMe-β-methylstyrene was found versus durene as an internal standard based on an independent calibration curve prepared with commercial reagents.

Table B.3. Amounts and concentrations of $HSiPh_3$ used to collect rate data.

Final [$HSiPh_3$] (M)	Volume of $HSiPh_3$ stock solution added	mmol $HSiPh_3$ added	Volume of extra toluene added
0.015	400 µL	0.050	0
0.022	205 µL	0.025	195 µL
0.031	145 µL	0.018	255 µL
0.060	100 µL	0.013	300 µL

Table B.4. Concentration of 4-OMe-β-methylstyrene formed over time at differing initial concentrations of $HSiPh_3$. Linear portion of kinetic curve values used to find the order are **bolded**. Concentrations of 4-OMe-β-methylstyrene were determined using GC-FID against durene as an internal standard.

[$HSiPh_3$] = 0.060 M	
Time (s)	[4-OMe-β-methylstyrene] (M)
300	0.0033 ± 0.0001
600	0.0059 ± 0.0002
900	0.0091 ± 0.0004
1200	0.014 ± 0.001
1500	0.022 ± 0.001
1800	0.034 ± 0.002
2100	0.048 ± 0.003
2400	0.064 ± 0.003
2700	0.085 ± 0.005
3000	**0.11 ± 0.01**
3300	**0.13 ± 0.01**
3600	**0.16 ± 0.01**
3900	**0.19 ± 0.01**
4500	0.25 ± 0.01
5100	0.27 ± 0.00
5700	0.27 ± 0.00
6300	0.27 ± 0.00
6900	0.27 ± 0.00
8100	0.27 ± 0.00
9300	0.27 ± 0.00
10500	0.27 ± 0.00
12300	0.27 ± 0.00

[$HSiPh_3$] = 0.031 M	
Time (s)	[4-OMe-β-methylstyrene] (M)
300	0.0032 ± 0.0002
600	0.0054 ± 0.0007
900	0.008 ± 0.001
1200	0.011 ± 0.002
1500	0.016 ± 0.003
1800	0.023 ± 0.004
2100	0.031 ± 0.006
2400	0.041 ± 0.008
2700	0.053 ± 0.009
3000	0.07 ± 0.01
3300	**0.08 ± 0.01**
3600	**0.10 ± 0.01**
3900	**0.12 ± 0.02**
4500	**0.16 ± 0.02**
5100	**0.20 ± 0.02**
5700	0.24 ± 0.02
6300	0.26 ± 0.01
6900	0.26 ± 0.01
8100	0.26 ± 0.01
9300	0.26 ± 0.01
10500	0.26 ± 0.01
12300	0.26 ± 0.01

[$HSiPh_3$] = 0.022 M	
Time (s)	[4-OMe-β-methylstyrene] (M)
300	0.0031 ± 0.0002
900	0.0070 ± 0.0003

[$HSiPh_3$] = 0.015 M	
Time (s)	[4-OMe-β-methylstyrene] (M)
300	0.0024 ± 0.0001
900	0.0057 ± 0.0002

1500	0.013	±	0.000	1500	0.011	±	0.000
2100	0.023	±	0.001	2100	0.019	±	0.000
2700	0.039	±	0.001	2700	0.031	±	0.000
3300	0.061	±	0.001	3300	0.049	±	0.001
3900	**0.085**	**±**	**0.00**	**3900**	**0.069**	**±**	**0.001**
4500	**0.12**	**±**	**0.00**	**4500**	**0.093**	**±**	**0.002**
5100	**0.15**	**±**	**0.00**	**5100**	**0.12**	**±**	**0.00**
5700	**0.18**	**±**	**0.00**	**5700**	**0.15**	**±**	**0.00**
6300	**0.21**	**±**	**0.01**	**6300**	**0.17**	**±**	**0.00**
6900	0.24	±	0.01	**6900**	**0.20**	**±**	**0.00**
7500	0.26	±	0.01	7500	0.23	±	0.00
8100	0.26	±	0.01	8100	0.25	±	0.00
8700	0.26	±	0.01	8700	0.26	±	0.00
9300	0.26	±	0.01	9300	0.26	±	0.00
9900	0.26	±	0.01	9900	0.26	±	0.00
10500	0.26	±	0.01	10500	0.26	±	0.00
11100	0.26	±	0.01	11100	0.26	±	0.00
12300	0.26	±	0.00	11700	0.26	±	0.00
				12300	0.26	±	0.00

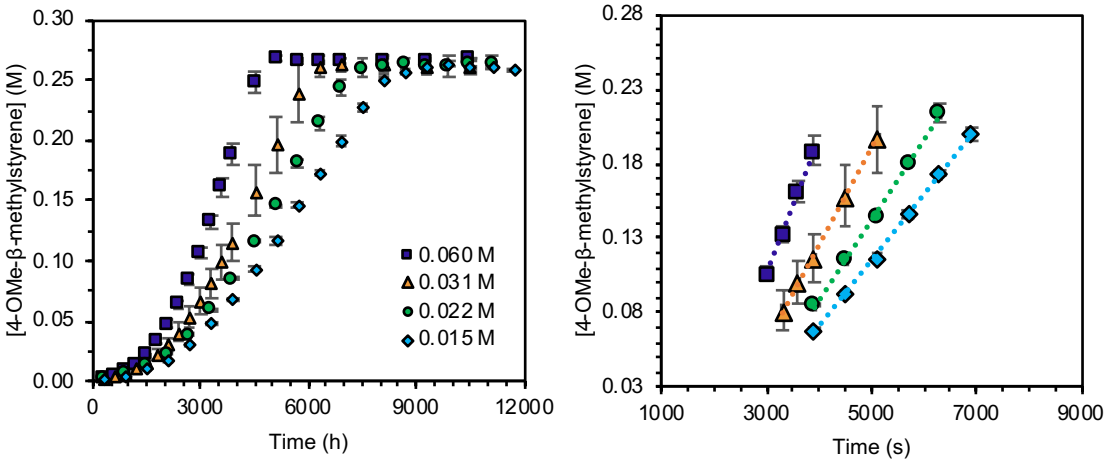

Figure B.3. Formation of 4-OMe-β-methylstyrene formed over time at differing initial concentrations of $HSiPh_3$. (a) Full reaction profiles and (b) linear portion of kinetic curve.

Table B.5. Rates of formation of 4-OMe-β-methylstyrene at varying initial concentrations of $HSiPh_3$.

[$HSiPh_3$] (M)	**Rate (M/s)**	**log([$HSiPh_3$] / M)**	**log(Rate / M/s)**
0.060	$9.2 \cdot 10^{-5} \pm 0.1 \cdot 10^{-5}$	-1.22	-4.04
0.033	$6.4 \cdot 10^{-5} \pm 0.1 \cdot 10^{-5}$	-1.51	-4.19
0.022	$5.4 \cdot 10^{-5} \pm 0.1 \cdot 10^{-5}$	-1.66	-4.27
0.015	$4.42 \cdot 10^{-5} \pm 0.07 \cdot 10^{-5}$	-1.82	-4.35

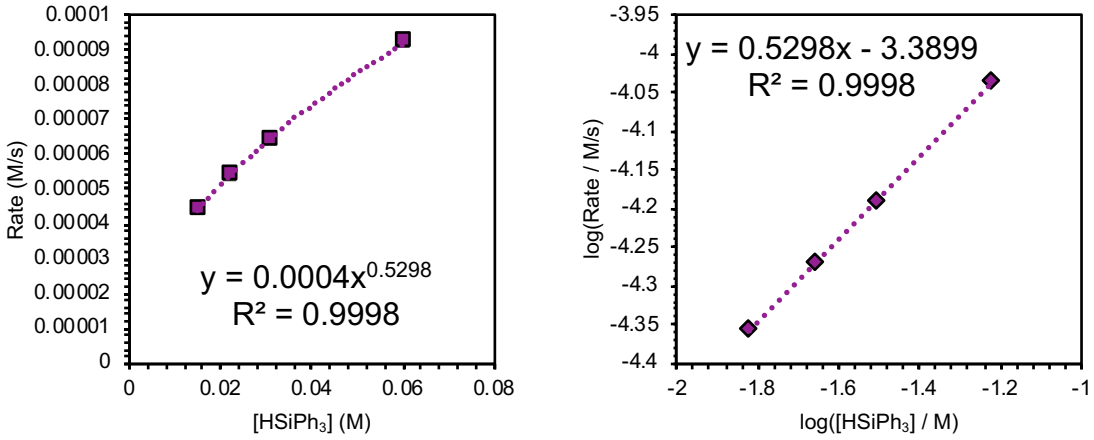

Figure B.4. Order plot for $HSiPh_3$. (a) Power function fit of form $y = a \cdot x^b$; a = 0.0004, b = 0.53, R^2 = 0.999 and (b) linearized log-log plot of form $y = m \cdot x + b$; m = 0.53 ± 0.01, b = -3.4 ± 0.01, R^2 = 0.999.

iii. Kinetics to measure order in 4-allylanisole

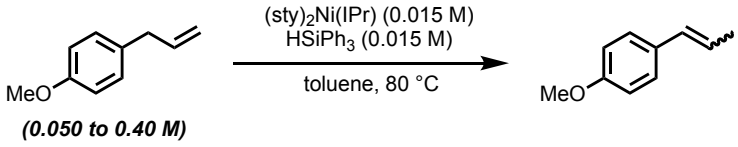

In a nitrogen-filled glovebox, $(sty)_2Ni(IPr)$ was weighed into 1-dram vials (8.2 mg, 0.013 mmol). Magnetic stir bars were added to each vial. A stock solution of $HSiPh_3$ (0.021 M) and durene (0.11 M) was prepared by weighing out each reagent directly into a 10-mL volumetric flask and adding the appropriate volume of toluene. The stock solution was distributed (0.60 mL) using a 1-mL disposable syringe. Toluene was distributed using a 250-µL microliter syringe to bring the total volume (including 4-allylanisole) to 0.84 mL (**Table B.6.**). Vials were sealed with septum caps, removed from the glovebox, and placed on a preheated aluminum vial block at 80 °C. After 30 minutes, 4-allylanisole (6 to 52 µL, 0.042 to 0.34 mmol) was distributed using a 25-µL or 100-µL microliter syringe. Over the course of the reaction, ~5 µL aliquots were removed from the reaction and filtered through Celite with hexanes directly into a GC vial for analysis by GC-FID. The concentration of 4-OMe-β-methylstyrene was found versus durene as an internal standard based on an independent calibration curve prepared with commercial reagents.

Table B.6. Amounts and concentrations of 4-allylanisole used to collect rate data.

Final [4-allylanisole] (M)	Volume of 4-allylanisole added	mmol 4-allylanisole added	Volume of extra toluene added
0.050	6.0 μL	0.042	194 μL
0.10	13 μL	0.084	187 μL
0.20	26 μL	0.17	174 μL
0.30	38 μL	0.25	162 μL
0.40	52 μL	0.34	148 μL

Table B.7. Concentration of 4-OMe-β-methylstyrene formed over time at differing initial concentrations of 4-allylanisole. Linear portion of kinetic curve values used to find the order are **bolded**. Concentrations of 4-OMe-β-methylstyrene were determined using GC-FID against durene as an internal standard.

$[4\text{-allylanisole}]_0 = 0.050$ M	
Time (s)	[4-OMe-β-methylstyrene] (M)
300	0.0048 ± 0.001
600	0.0062 ± 0.0001
900	0.0092 ± 0.0004
1200	**0.014 ± 0.000**
1500	**0.019 ± 0.001**
1800	**0.024 ± 0.001**
2100	**0.029 ± 0.002**
2400	0.034 ± 0.002
2700	0.038 ± 0.000
3000	0.039 ± 0.000
3300	0.039 ± 0.000
3600	0.039 ± 0.001
4200	0.039 ± 0.001
4800	0.039 ± 0.000
5400	0.039 ± 0.001
6000	0.039 ± 0.001
6600	0.039 ± 0.001
7200	0.038 ± 0.000

$[4\text{-allylanisole}]_0 = 0.10$ M	
Time (s)	[4-OMe-β-methylstyrene] (M)
300	0.0041 ± 0.0002
600	0.0067 ± 0.0003
900	0.0099 ± 0.0001
1200	0.014 ± 0.000
1500	0.019 ± 0.000
1800	0.024 ± 0.001
2100	**0.030 ± 0.001**
2400	**0.037 ± 0.002**
2700	**0.045 ± 0.003**
3000	**0.052 ± 0.004**
3300	**0.060 ± 0.005**
3600	0.068 ± 0.006
4200	0.082 ± 0.004
4800	0.085 ± 0.002
5400	0.083 ± 0.000
6000	0.085 ± 0.002
6600	0.084 ± 0.000
7200	0.085 ± 0.002

$[4\text{-allylanisole}]_0 = 0.20$ M	
Time (s)	[4-OMe-β-methylstyrene] (M)
300	0.0044 ± 0.0000
600	0.0094 ± 0.0004
900	0.016 ± 0.001
1200	0.022 ± 0.002
1500	0.027 ± 0.002
1800	0.034 ± 0.002

$[4\text{-allylanisole}]_0 = 0.30$ M	
Time (s)	[4-OMe-β-methylstyrene] (M)
600	0.018 ± 0.006
1200	0.043 ± 0.01
1800	0.058 ± 0.01
2400	0.078 ± 0.01
3000	**0.099 ± 0.02**
3600	**0.12 ± 0.01**

2100	0.040	±	0.002
2400	0.048	±	0.002
2700	0.056	±	0.002
3000	0.063	±	0.002
3300	0.074	±	0.002
3600	**0.082**	**±**	**0.003**
3900	**0.093**	**±**	**0.003**
4200	**0.11**	**±**	**0.00**
4500	**0.12**	**±**	**0.00**
4800	**0.13**	**±**	**0.00**
5100	**0.14**	**±**	**0.00**
5400	**0.15**	**±**	**0.00**
5700	0.16	±	0.00
6000	0.17	±	0.00
6300	0.17	±	0.00
6600	0.18	±	0.00
6900	0.18	±	0.00
7200	0.18	±	0.00
7800	0.18	±	0.00
8400	0.18	±	0.00
9000	0.18	±	0.00
9600	0.18	±	0.00
10200	0.18	±	0.00
10800	0.18	±	0.00

[4-allylanisole]$_0$ = 0.40 M			
Time (s)	**[4-OMe-β-methylstyrene] (M)**		
600	0.044	±	0.006
1200	**0.083**	**±**	**0.01**
1800	**0.10**	**±**	**0.01**
2400	**0.13**	**±**	**0.01**
3000	**0.15**	**±**	**0.01**
3600	**0.18**	**±**	**0.01**
4200	**0.20**	**±**	**0.01**
4800	**0.23**	**±**	**0.01**
5400	0.25	±	0.02
6000	0.27	±	0.01
6600	0.28	±	0.01
7200	0.30	±	0.01
7800	0.31	±	0.00
8400	0.32	±	0.01
9000	0.33	±	0.01
9600	0.34	±	0.01
10200	0.35	±	0.00
10800	0.35	±	0.00
4200	**0.15**	**±**	**0.01**
4800	**0.18**	**±**	**0.01**
5400	**0.21**	**±**	**0.01**
6000	0.23	±	0.01
6600	0.26	±	0.02
7200	0.26	±	0.00
7800	0.27	±	0.00
8400	0.27	±	0.00
9000	0.27	±	0.00
9600	0.26	±	0.00
10800	0.26	±	0.00
12000	0.26	±	0.00
13200	0.26	±	0.00
14400	0.26	±	0.00

11400	0.35	±	0.00
12000	0.35	±	0.00
12600	0.36	±	0.00
13200	0.35	±	0.00
13800	0.36	±	0.00
14400	0.36	±	0.00
15600	0.36	±	0.00
16800	0.36	±	0.00
18000	0.36	±	0.00
19200	0.37	±	0.00

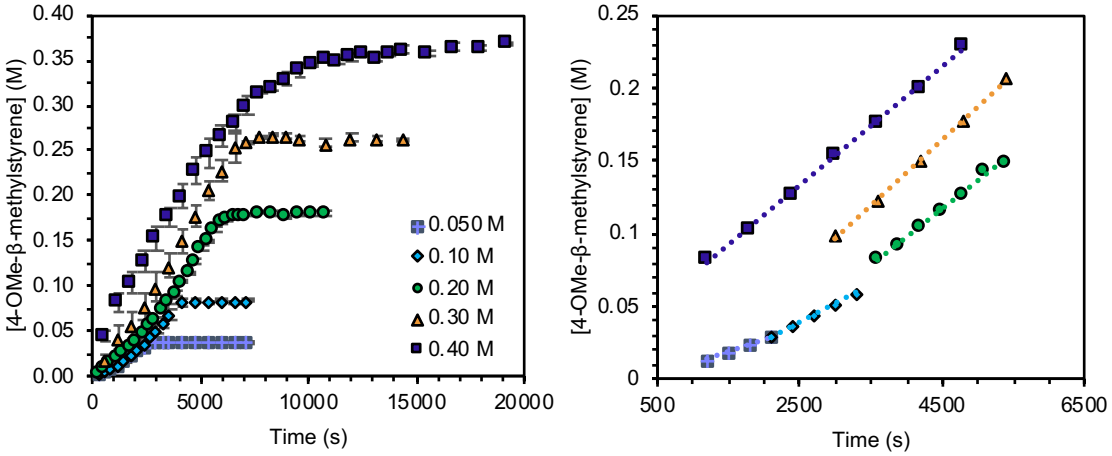

Figure B.5. Formation of 4-OMe-β-methylstyrene formed over time at differing initial concentrations of 4-allylanisole. (a) Full reaction profiles and (b) linear portion of kinetic curve.

Table B.8. Rates of formation of 4-OMe-β-methylstyrene at varying initial concentrations of 4-allylanisole.

$[4\text{-allylanisole}]_0$ (M)	**Rate (M/s)**	**$\log([4\text{-allylanisole}]_0$ / M)**	**log(Rate / M/s)**
0.050	$1.73 \cdot 10^{-5} \pm 0.01 \cdot 10^{-5}$	-1.30	-4.76
0.10	$2.52 \cdot 10^{-5} \pm 0.05 \cdot 10^{-5}$	-1.00	-4.60
0.20	$3.9 \cdot 10^{-5} \pm 0.1 \cdot 10^{-5}$	-0.699	-4.41
0.30	$4.50 \cdot 10^{-5} \pm 0.09 \cdot 10^{-5}$	-0.523	-4.35
0.40	$4.05 \cdot 10^{-5} \pm 0.07 \cdot 10^{-5}$	-0.398	-4.39

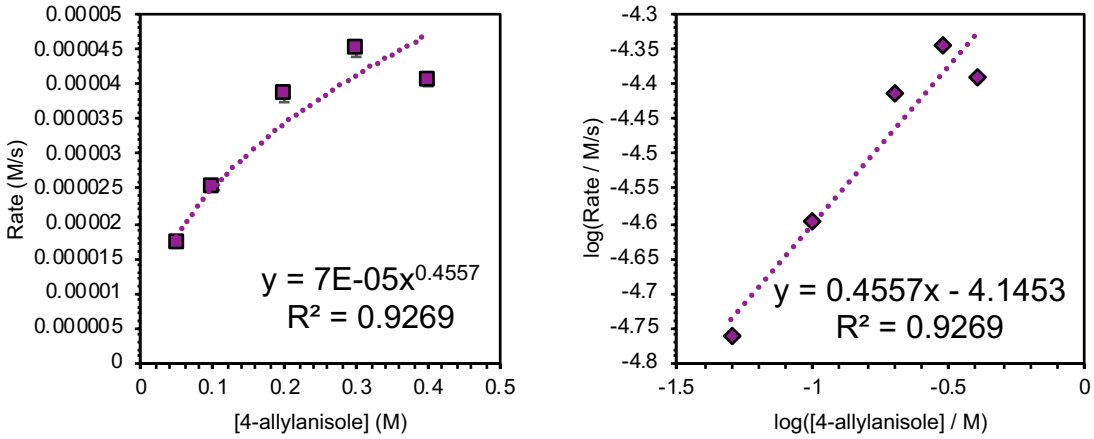

Figure B.6. Order plot for 4-allylanisole. (a) Power function fit of form $y = a \cdot x^b$; $a = 7.0 \cdot 10^{-5}$, $b = 0.46$, $R^2 = 0.927$ and (b) linearized log-log plot of form $y = m \cdot x + b$; $m = 0.46 \pm 0.7$, $b = -4.15 \pm 0.06$, $R^2 = 0.927$.

iv. Kinetics to measure order in styrene

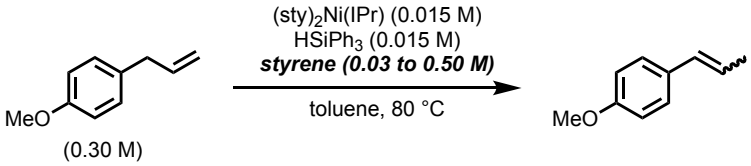

In a nitrogen-filled glovebox, $(sty)_2Ni(IPr)$ was weighed into 1-dram vials (8.2 mg, 0.013 mmol). Magnetic stir bars were added to each vial. A stock solution of $HSiPh_3$ (0.021 M) and durene (0.11 M) was prepared by weighing out each reagent directly into a 10-mL volumetric flask and adding the appropriate volume of toluene. The stock solution was distributed (0.60 mL) using a 1-mL disposable syringe. Styrene was distributed using a 25-µL microliter syringe and toluene was distributed using a 250-µL microliter syringe to bring the total volume (including 4-allylanisole and styrene) to 0.84 mL (**Table B.9.**). For the trial with 0.030 M styrene, [styrene] was calculated based on 2 molar equiv of styrene per molar equiv of $(sty)_2Ni(IPr)$ and no additional styrene was added. Vials were sealed with septum caps, removed from the glovebox, and placed on a preheated aluminum vial block at 80 °C. After 30 minutes, 4-allylanisole (38 µL, 0.25 mmol, 1.0 equiv) was distributed using a 100-µL microliter syringe. Over the course of the reaction, ~5 µL aliquots were removed from the reaction and filtered through Celite with hexanes directly into a GC vial for analysis by GC-FID. The concentration of 4-OMe-β-methylstyrene was

found versus durene as an internal standard based on an independent calibration curve prepared with commercial reagents.

Table B.9. Amounts and concentrations of 4-allylanisole used to collect rate data.

Final [styrene] (M)	Volume of styrene added	mmol styrene added	Volume of extra toluene added
0.030	0	0.025	200 μL
0.060	6.0 μL	0.050	194 μL
0.12	11 μL	0.10	189 μL
0.30	29 μL	0.25	171 μL
0.50	48 μL	0.42	152 μL

Table B.10. Concentration of 4-OMe-β-methylstyrene formed over time at differing initial concentrations of styrene. Concentrations of 4-OMe-β-methylstyrene were determined using GC-FID against durene as an internal standard. One trial per [styrene] was run.

[styrene] = 0.030 M	
Time (s)	[4-OMe-β-methylstyrene] (M)
600	0.031
1200	0.060
1800	0.081
2400	0.103
3000	0.133
3600	0.178
4200	0.197
4800	0.229
5400	0.253
6000	0.260
6600	0.256
7200	0.271
7800	0.259
8400	0.260
9000	0.253
9600	0.256
10200	0.258
10800	0.256
12000	0.261

[styrene] = 0.060 M	
Time (s)	[4-OMe-β-methylstyrene] (M)
600	0.009
1200	0.033
1800	0.055
2400	0.068
3000	0.073
3600	0.080
4200	0.079
4800	0.080
5400	0.083
6000	0.086
6600	0.088
7200	0.094
7800	0.092
8400	0.094
9000	0.097
9600	0.099
10200	0.101
10800	0.109
11400	0.104
12000	0.107
12600	0.108
13200	0.112
13800	0.113
14400	0.123
15600	0.120

16800	0.126
18600	0.128

[styrene] = 0.12 M	
Time (s)	[4-OMe-β-methylstyrene] (M)
600	0.006
1200	0.024
1800	0.043
2400	0.054
3000	0.060
3600	0.068
4200	0.066
4800	0.069
5400	0.072
6000	0.073
6600	0.072
7200	0.077
7800	0.076
8400	0.076
9000	0.078
9600	0.078
10200	0.080
10800	0.080
11400	0.082
12000	0.083
12600	0.083
13200	0.084
13800	0.084
14400	0.087
15600	0.087
16800	0.090
18600	0.098

[styrene] = 0.30 M	
Time (s)	[4-OMe-β-methylstyrene] (M)
600	0.004
1200	0.018
1800	0.035
2400	0.048
3000	0.056
3600	0.062
4200	0.063
4800	0.068
5400	0.071
6000	0.074
6600	0.075
7200	0.079
7800	0.076
8400	0.080
9000	0.083
9600	0.082
10200	0.083
10800	0.089
11400	0.085
12000	0.085
12600	0.089
13200	0.088
13800	0.086
14400	0.093
15600	0.089
16800	0.088
18600	0.091

[styrene] = 0.40 M	
Time (s)	[4-OMe-β-methylstyrene] (M)
600	0.002
1200	0.007
1800	0.015
2400	0.023
3000	0.027
3600	0.030
4200	0.033
4800	0.034
5400	0.035

6000	0.036
6600	0.037
7200	0.040
7800	0.040
8400	0.040
9000	0.042
9600	0.041
10800	0.044
11400	0.046
12000	0.043
12600	0.045
13200	0.046
13800	0.044
14400	0.048
15600	0.044
16800	0.047
18600	0.050

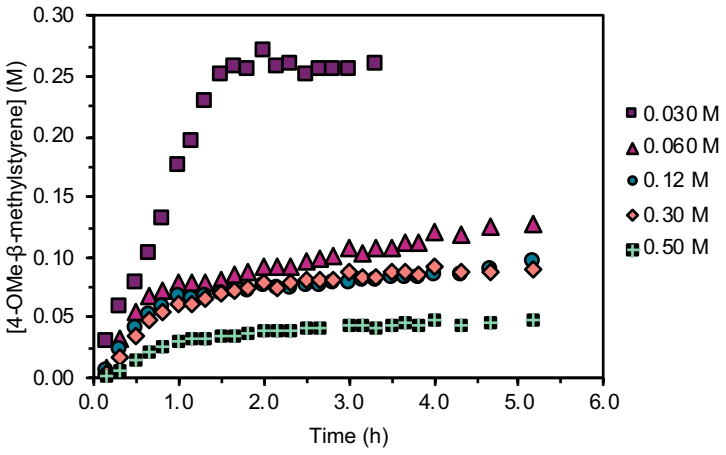

Figure B.7. Formation of 4-OMe-β-methylstyrene formed over time at differing initial concentrations of 4-allylanisole.

v. Kinetics to test for product inhibition or catalyst decomposition

Conditions A:

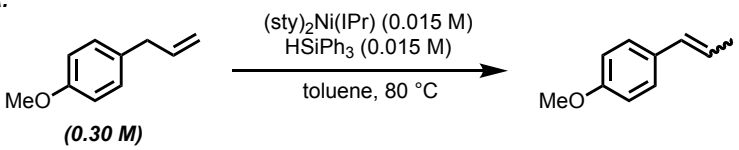

(0.30 M)

Conditions B:

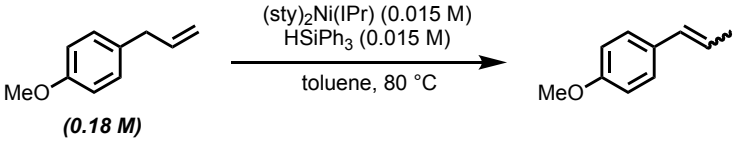

(0.18 M)

Conditions C:

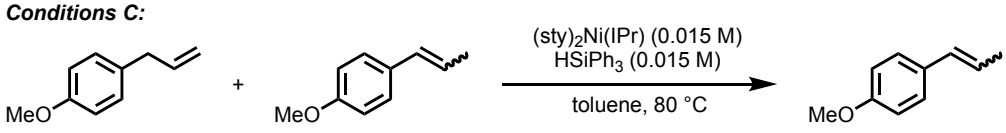

(0.18 M) ***(0.12 M)***

In a nitrogen-filled glovebox, $(sty)_2Ni(IPr)$ was weighed into 1-dram vials (8.2 mg, 0.013 mmol). Magnetic stir bars were added to each vial. A stock solution of $HSiPh_3$ (0.021 M) and durene (0.11 M) was prepared by weighing out each reagent directly into a 10-mL volumetric flask and adding the appropriate volume of toluene. The stock solution was distributed (0.60 mL) using a 1-mL disposable syringe. To the vials, 1 250-μL microliter syringe was used to add toluene to bring the total volume to 0.84 mL. Vials were sealed with septum caps, removed from the glovebox, and placed on a preheated aluminum vial block at 80 °C. After 30 minutes, 4-allylanisole and 4-OMe-*trans*-β-methylstyrene were distributed using a 100-μL microliter syringe. See **Table B.11.** for amounts and concentrations of each reagent. Over the course of the reaction, ~5 μL aliquots were removed from the reaction and filtered through Celite with hexanes directly into a GC vial for analysis by GC-FID. The concentration of 4-OMe-β-methylstyrene was found versus durene as an internal standard based on an independent calibration curve prepared with commercial reagents.

Table B.11. Amounts and concentrations for catalyst decomposition and product inhibition studies. 4-aa = 4-allylanisole; 4-OMe-bs = 4-OMe-*trans*-β-methylstyrene.

Conditions	$[4\text{-aa}]_0$ (M)	Volume of 4-aa added	mmol 4-aa added	$[4\text{-OMe-bs}]_0$ (M)	Volume 4-OMe-bs added	mmol 4-OMe-bs added	Volume of extra toluene added
A	0.30	38 µL	0.25	0	0	0	200 µL
B	0.18	23 µL	0.15	0	0	0	215 µL
C	0.18	23 µL	0.15	0.12	15 µL	0.10	200 µL

Table B.12. Concentration of 4-allylanisole over time at differing initial conditions. Concentrations of 4-allylanisole were determined using GC-FID against durene as an internal standard.

Conditions A	
Time (s)	[4-allylanisole] (M)
600	0.267 ± 0.002
1200	0.253 ± 0.001
1800	0.2323 ± 0.0004
2400	0.205 ± 0.001
3000	0.177 ± 0.003
3600	0.148 ± 0.004
4200	0.117 ± 0.006
4800	0.091 ± 0.006
5400	0.067 ± 0.006
6000	0.046 ± 0.006
6600	0.028 ± 0.005
7200	0.017 ± 0.002
7800	0.010 ± 0.001
8400	0.0066 ± 0.0004
9000	0.0045 ± 0.0002
9600	0.0031 ± 0.0000
10200	0.0023 ± 0.0001
10800	0.0018 ± 0.0002
12600	0.0011 ± 0.0001
14400	0.0009 ± 0.0000

Conditions B	
Time (s)	[4-allylanisole] (M)
600	0.160 ± 0.001
1200	0.151 ± 0.002
1800	0.140 ± 0.003
2400	0.124 ± 0.003
3000	0.105 ± 0.004
3600	0.082 ± 0.005
4200	0.057 ± 0.006
4800	0.035 ± 0.006
5400	0.015 ± 0.005
6000	0.004 ± 0.002
6600	0.0008 ± 0.0003
7200	0.0004 ± 0.0000
7800	0.0004 ± 0.0000
8400	0.0004 ± 0.0000
9000	0.0003 ± 0.0000
9600	0.0004 ± 0.0000
10200	0.0004 ± 0.0000
10800	0.0004 ± 0.0000

Conditions C	
Time (s)	[4-allylanisole] (M)
600	0.160 ± 0.003
1200	0.153 ± 0.002
1800	0.142 ± 0.001
2400	0.125 ± 0.002
3000	0.106 ± 0.002
3600	0.084 ± 0.003

4200	0.061	±	0.003
4800	0.040	±	0.003
5400	0.020	±	0.003
6000	0.007	±	0.002
6600	0.0021	±	0.0008
7200	0.0008	±	0.0001
7800	0.0006	±	0.0000
8400	0.0005	±	0.0000
9000	0.0005	±	0.0000
9600	0.0006	±	0.0000
10200	0.0006	±	0.0000
10800	0.0006	±	0.0000

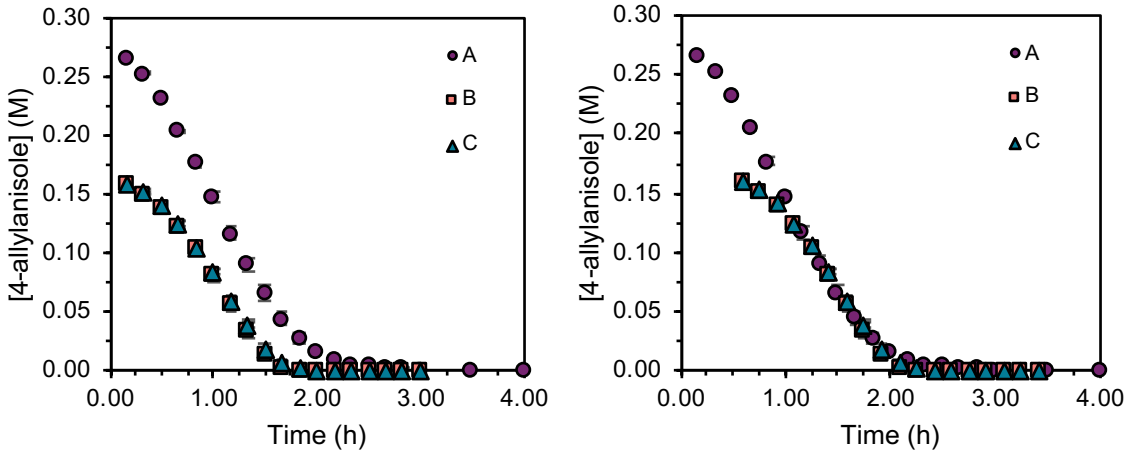

Figure B.8. Kinetic analysis to investigate possible catalyst decomposition studies or product inhibition. Trials were run in duplicate with durene as an internal standard. Left plot shows unprocessed data. Right plot shows data with a time shift of 0.42 h.

b. Silane kinetic isotope experiment

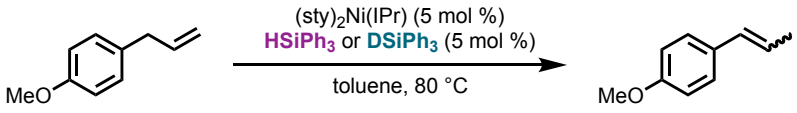

In a nitrogen-filled glovebox, $(sty)_2Ni(IPr)$ (8.2 mg, 0.013 mmol, 0.05 equiv) was weighed directly into 1-dram vials. Magnetic stir bars were added to each vial. Stock solution of durene (0.18 M), $HSiPh_3$ (0.62 M) and $DSiPh_3$ (0.62 M) were prepared in 5.0-, 2.0- and 1.0-mL volumetric flasks, respectively, by weighing out the reagent and adding the appropriate volume of toluene. The durene stock solution (0.60 mL, 0.11 mmol, 0.43 equiv) was distributed to each vial using a 1-mL disposable syringe. Silane stock solution (200 µL, 0.012 mmol, 0.05 equiv) was distributed to each vial using a 250-µL microliter

syringe. Vials were sealed with septum caps, removed from the glovebox and placed on a preheated aluminum vial block at 80 °C. After 30 minutes, 4-allylanisole (38 μL, 0.25 mmol, 1.0 equiv) was distributed in two portions using a 25-μL microliter syringe. Throughout the course of the reaction, ~5 μL aliquots were removed from the reaction, filtered through Celite with hexanes directly into a GC and analyzed by GC-FID. The concentration of 4-OMe-β-methylstyrene was found versus durene as an internal standard based on an independent calibration curve prepared with commercial reagents.

Table B.13. Concentration of 4-OMe-β-methylstyrene formed over time. Concentrations of 4-OMe-β-methylstyrene were determined using GC-FID against durene as an internal standard. Linear portion of kinetic curve values used to find the order are **bolded**.

Silane = $HSiPh_3$	
Time (s)	**[4-OMe-β-methylstyrene] (M)**
900	0.013 ± 0.001
1200	0.016 ± 0.003
1800	0.03 ± 0.01
2400	**0.05 ± 0.02**
3000	**0.08 ± 0.02**
3600	**0.11 ± 0.02**
4200	**0.13 ± 0.02**
4800	**0.16 ± 0.02**
5400	**0.18 ± 0.02**
6000	0.20 ± 0.02
6600	0.22 ± 0.02
7200	0.23 ± 0.02
7800	0.24 ± 0.01
8400	0.24 ± 0.01
9000	0.24 ± 0.01
10800	0.25 ± 0.01
14400	0.26 ± 0.00

Silane = $DSiPh_3$	
Time (s)	**[4-OMe-β-methylstyrene] (M)**
900	0.0104 ± 0.0003
1200	0.013 ± 0.004
1800	0.02 ± 0.01
2400	**0.04 ± 0.02**
3000	**0.07 ± 0.02**
3600	**0.09 ± 0.02**
4200	**0.12 ± 0.02**
4800	**0.14 ± 0.01**
5400	**0.16 ± 0.02**
6000	0.19 ± 0.02
6600	0.20 ± 0.01
7200	0.22 ± 0.02
7800	0.23 ± 0.01
8400	0.23 ± 0.01
9000	0.24 ± 0.00
10800	0.25 ± 0.01
14400	0.25 ± 0.00

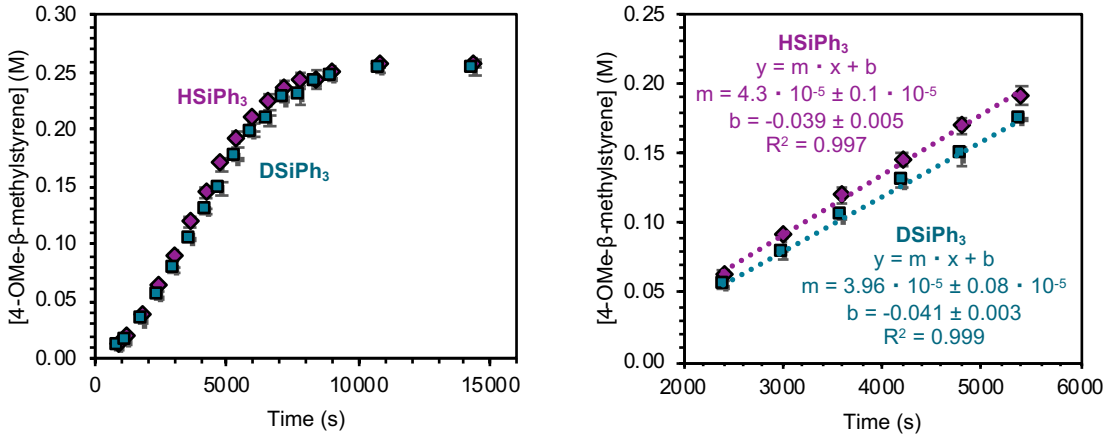

Figure B.9. H/D kinetic isotope effect for triphenylsilane. Trials were run in duplicate with durene as an internal standard.

The assumption used above that k_H/k_D = rate$_H$/rate$_D$ is true if the reactions with $HSiPh_3$ and $DSiPh_3$ undergo the same mechanism, which we assume to be true. The maximum KIE for Si–H/D without tunneling was determined using the following equation:

$$KIE_{max} = e^{\frac{h \cdot c \cdot \Delta\bar{\nu}}{k_B \cdot T}}$$

Where…

h = 6.63×10^{-34} J•s (Planck's constant)

c = 2.998×10^{10} cm•s^{-1} (Speed of light)

$\Delta\bar{\nu}$ = $\nu_H - \nu_D$

$\bar{\nu}_H$ = Stretching frequency of the Si–H bond (cm^{-1})

$\bar{\nu}_D$ = Stretching frequency of the Si–D bond (cm^{-1})

k_B = 1.38×10^{-23} J•K^{-1} (Boltzmann constant)

T = Temperature (K)

For $HSiPh_3$, ν_H = 2118 cm^{-1} and for $DSiPh_3$, ν_D = 1539 cm^{-1}. Calculated at 298 K (the temperature at which the IR spectra were measured):

$$KIE_{max} = e^{\frac{(6.63 \cdot 10^{-34}\ J \cdot K^{-1})(3.0 \cdot 10^{10}\ cm \cdot s^{-1})(2118\ cm^{-1} - 1539\ cm^{-1})}{(1.38 \cdot 10^{-23}\ J \cdot K^{-1})(298\ K)}} = 4.0$$

c. Deuterium incorporation with $DSiPh_3$

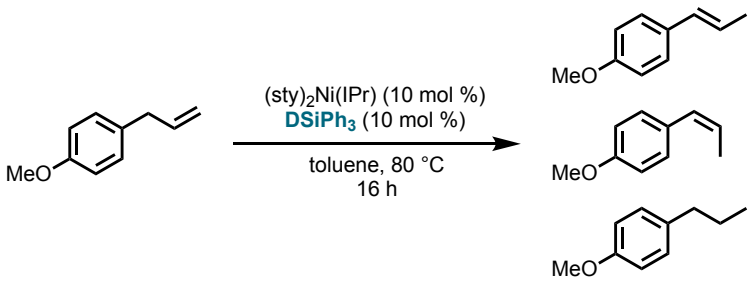

In a nitrogen-filled glovebox, (sty)2Ni(IPr) (32.8 mg, 0.050 mmol, 0.10 equiv) was weighed into 1-dram vials. Magnetic stir bars were added to each vial. A stock solution of silane (0.031 M) was prepared by weighing out DSiPh3 and adding the appropriate volume of toluene. DSiPh3 stock solution was distributed (1.6 mL, 0.050 mmol, 0.10 equiv) using two portions of a 1-mL disposable syringe. Vials were sealed with septum caps, removed from the glovebox, and placed on a preheated aluminum vial block at 80 °C. After 30 minutes, 4-allylanisole (76 µL, 0.50 mmol, 1.0 equiv) was added using a 100-µL microliter syringe. After 16 h, the reactions were quenched by cooling with liquid N2 and opening to air. Small aliquots were removed and filtered through Celite with hexanes directly into GC-MS vials for analysis by GC-MS and GC-FID. A summary of relative composition for the crude reaction is shown in **Table B.14.** Approximately half of the crude reaction mixture was then filtered through a short silica plug using hexanes, solvent was removed under reduced pressure, and samples for NMR were prepared in solutions of $CHCl_3/CDCl_3$ (9:1). ^1H and ^2H NMR spectra were recorded, shown in **Figure B.10.**

Table B.14. Summary of crude reaction composition and analysis of mass spectra from GC-MS.

Component	Relative % composition	Predicted and observed mass fragmentation
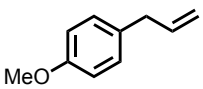	<1%	Exact Mass: 148.0888 predicted: m/z: 148.0888 (100.0%), 149.0922 (10.8%) **observed:** **m/z: 148.1 (100%), 149.1 (10%)**
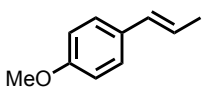	92%	Exact Mass: 148.0888 predicted: m/z: 148.0888 (100.0%), 149.0922 (10.8%) **observed:** **m/z: 148.1 (100%), 149.1 (15%)**

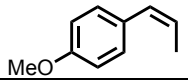	5%	
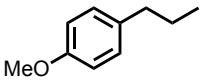	3%	Exact Mass: 150.1045 predicted: m/z: 150.1045 (100.0%), 151.1078 (10.8%) **observed:** **m/z: 150.1 (100%), 151.1 (52%)**

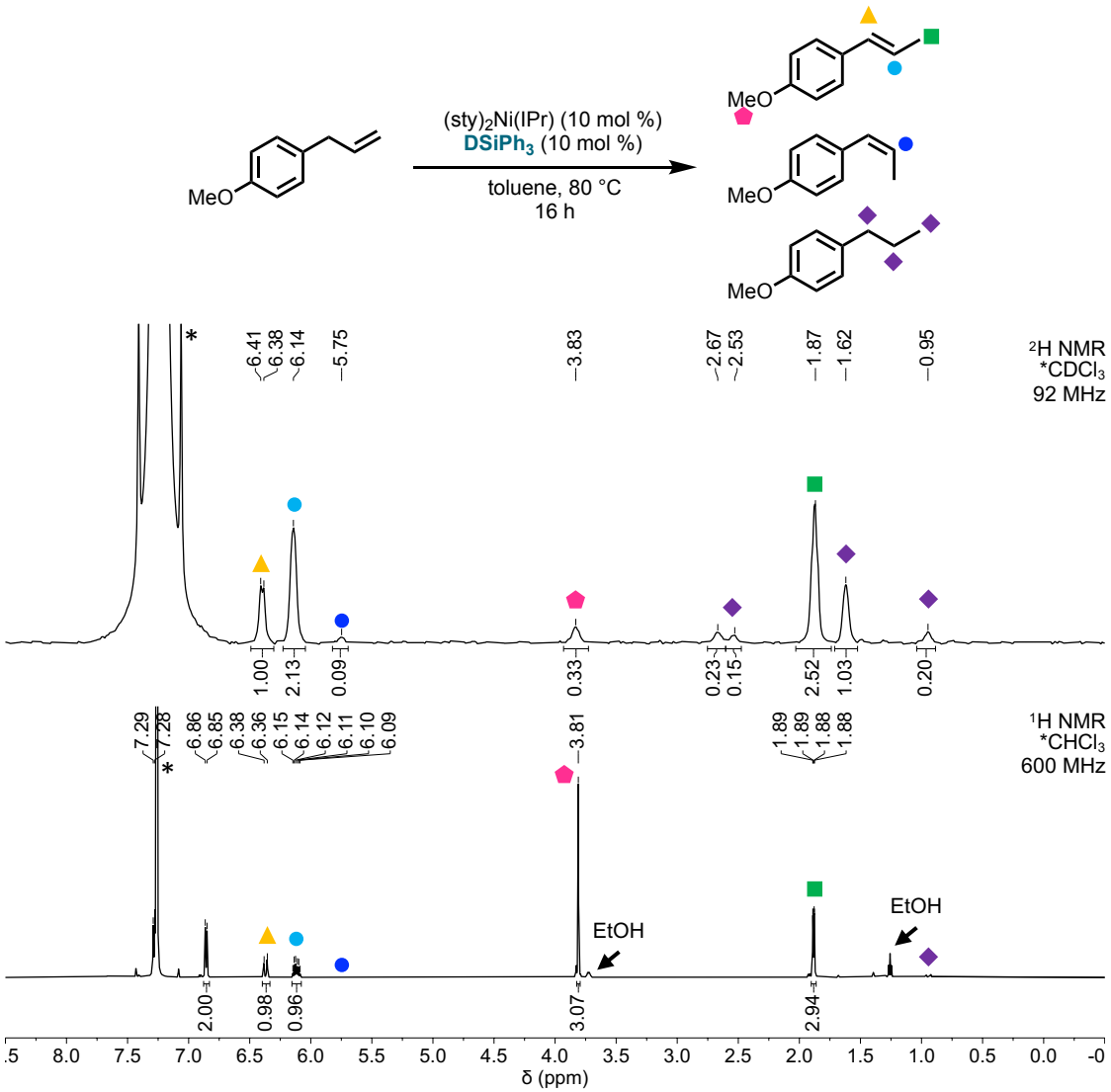

Figure B.10. NMR analysis of deuterium incorporation study with $DSiPh_3$. NMR spectra were recorded at 298 K. $CHCl_3$ was stabilized with EtOH (visible in the ^1H NMR spectrum).

d. Silane linear free energy relationship with 4-allylanisole

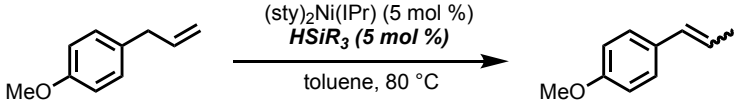

In a nitrogen-filled glovebox, $(sty)_2Ni(IPr)$ (8.2 mg, 0.013 mmol, 0.05 equiv) was weighed directly into 1-dram vials. Magnetic stir bars were added to each vial. Stock solutions of $HSiPh_3$ (0.031 M), $HSi(3\text{-}F\text{-}C_6H_4)_3$ (0.031 M), $HSi(4\text{-}OMe\text{-}C_6H_4)_3$ (0.031 M) and durene (0.28 M) were prepared by weighing out the reagent into volumetric flasks and adding the appropriate volume of toluene. $HSi(4\text{-}NMe_2\text{-}C_6H_4)_3$ (4.9 mg, 0.013 mmol, 0.05 equiv) and $HSi(4\text{-}CF_3\text{-}C_6H_4)_3$ (5.8 mg, 0.013 mmol, 0.05 equiv) were weighed directly into vials with $(sty)_2Ni(IPr)$. Durene stock solution (0.40 mL, 0.11 mmol, 0.44 equiv) was distributed to each vial using a 1-mL disposable syringe. Silane stock solution (0.40 mL, 0.12 mmol, 0.05 equiv) or toluene (0.40 mL) were distributed to vials using a 1-mL disposable syringe. Vials were sealed with septum caps, removed from the glovebox and placed on a preheated aluminum vial block at 80 °C. After 30 minutes, 4-allylanisole (38 μL, 0.25 mmol, 1.0 equiv) was distributed using a 100-μL microliter syringe. Throughout the course of the reaction, ~5 μL aliquots were removed from the reaction, filtered through Celite with hexanes directly into a GC and analyzed by GC-FID. The concentration of 4-OMe-β-methylstyrene was found versus durene as an internal standard based on an independent calibration curve prepared with commercial reagents.

Table B.15. Concentration of 4-OMe-β-methylstyrene formed over time. Concentrations of 4-OMe-β-methylstyrene were determined using GC-FID against durene as an internal standard.

Silane = $HSi(4\text{-}CF_3\text{-}C_6H_4)_3$	
Time (s)	**[4-OMe-β-methylstyrene] (M)**
600	0.0390 ± 0.0009
1200	0.0448 ± 0.0005
1800	0.0474 ± 0.0006
2400	0.0496 ± 0.0006
3000	0.0509 ± 0.0006
3600	0.0525 ± 0.0008
4200	0.0536 ± 0.0008
4800	0.0548 ± 0.0006
5400	0.0560 ± 0.0008
6000	0.0573 ± 0.0006
6600	0.058 ± 0.001
7200	0.060 ± 0.001
9000	0.063 ± 0.001

Silane = $HSi(3\text{-}F\text{-}C_6H_4)_3$	
Time (s)	**[4-OMe-β-methylstyrene] (M)**
300	0.0521 ± 0.0006
600	0.0994 ± 0.0008
900	0.1206 ± 0.0006
1200	0.135 ± 0.002
1500	0.149 ± 0.002
1800	0.160 ± 0.002
2100	0.168 ± 0.002
2400	0.175 ± 0.002
2700	0.181 ± 0.003
3000	0.187 ± 0.002
3300	0.192 ± 0.002
3600	0.198 ± 0.003
4200	0.205 ± 0.002
4800	0.211 ± 0.002

5400	0.218 ± 0.003
6000	0.223 ± 0.002
6600	0.228 ± 0.002
7200	0.233 ± 0.002
9000	0.245 ± 0.002

Silane = $HSiPh_3$	
Time (s)	[4-OMe-β-methylstyrene] (M)
600	0.0112 ± 0.0007
1200	0.0241 ± 0.0004
1800	0.0487 ± 0.0008
2400	0.079 ± 0.003
3000	0.113 ± 0.004
3600	0.147 ± 0.006
4200	0.175 ± 0.006
4800	0.200 ± 0.006
5400	0.219 ± 0.005
6000	0.231 ± 0.005
6600	0.240 ± 0.003
7200	0.247 ± 0.003
7800	0.251 ± 0.004
9000	0.257 ± 0.003

Silane = $HSi(4\text{-}OMe\text{-}C_6H_4)_3$	
Time (s)	[4-OMe-β-methylstyrene] (M)
600	0.0044
1200	0.0081
1800	0.0129
3000	0.0307
4200	0.0530
5400	0.0761
6600	0.0991
7800	0.1228
9000	0.1464
10200	0.1665
11400	0.1878
12600	0.2020
13800	0.2157
15000	0.2236
16200	0.2363
18000	0.2396
19200	0.2454
20400	0.2482
21600	0.2519
25200	0.2557

Silane = $HSi(4\text{-}NMe_2\text{-}C_6H_4)_3$	
Time (s)	[4-OMe-β-methylstyrene] (M)
600	0.018 ± 0.003
1200	0.031 ± 0.005
1800	0.043 ± 0.006
3000	0.067 ± 0.008
4200	0.08 ± 0.01
5400	0.10 ± 0.01
6600	0.11 ± 0.01
7800	0.12 ± 0.01
9000	0.12 ± 0.01
10200	0.13 ± 0.02
11400	0.14 ± 0.02
12600	0.14 ± 0.02
13800	0.15 ± 0.02

15000	0.15	±	0.02
16200	0.15	±	0.02
18000	0.17	±	0.02
19200	0.16	±	0.02
20400	0.16	±	0.02
21600	0.17	±	0.02
25200	0.17	±	0.02

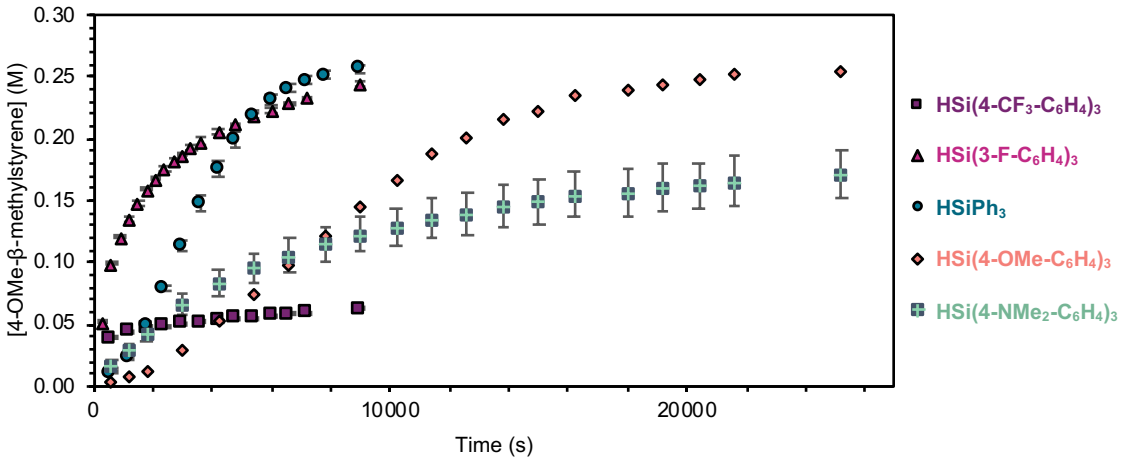

Figure B.11. Linear free energy relationship with substituted triaryl silanes. Trials were run in duplicate, except for HSi(4-OMe-C_6H_4)$_3$, with durene as an internal standard.

e. Silane linear free energy relationship with allylbenzene

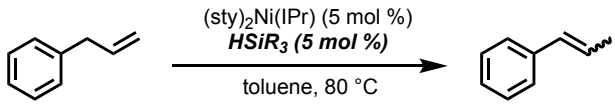

In a nitrogen-filled glovebox, (sty)$_2$Ni(IPr) (8.2 mg, 0.013 mmol, 0.05 equiv) was weighed into 1-dram vials. Magnetic stir bars were added to each vial. HSi(4-CF_3-C_6H_4)$_3$ (5.8 mg, 0.013 mmol, 0.05 equiv) and HSi(4-NMe_2-C_6H_4)$_3$ (4.9 mg, 0.013 mmol, 0.05 equiv) were weighed into respective vials. Stock solutions of $HSiPh_3$ (0.031 M), HSi(3-F-C_6H_4)$_3$ (0.031 M) and HSi(4-OMe-C_6H_4)$_3$ (0.031 M) were prepared in volumetric flasks by weighing out the reagent and adding the appropriate volume of toluene. A stock solution of durene (0.16 M) was prepared by weighing out durene into a 10-mL volumetric flask and adding the appropriate volume of toluene. Silane stock solutions were distributed (400 µL, 0.013 mmol, 0.05 equiv) in two portions using a 250-µL microliter syringe to the respective vials. Durene stock solution (400 µL, 0.065 mmol, 0.26 equiv) was distributed in two portions using a 250-µL microliter syringe to each vial. Vials were sealed with

septum caps, removed from the glovebox and placed on a pre-heated aluminum vial block at 80 °C. After 30 minutes of heating, allylbenzene (33 μL, 0.25 mmol, 1.0 equiv) was added using a 100-μL microliter syringe. Throughout the course of the reaction, ~5 μL aliquots were removed from the reaction, filtered through Celite with hexanes directly into a GC and analyzed by GC-FID. The concentration of β-methylstyrene was found versus durene as an internal standard based on an independent calibration curve prepared with commercial reagents.

Table B.16. Amounts and concentrations of silanes used to collect rate data.

Silane	Volume of volumetric flask	Amount silane added
$HSi(3\text{-}F\text{-}C_6H_4)_3$	1.0 mL	9.7 mg
$HSiPh_3$	5.0 mL	40.3 mg
$HSi(4\text{-}OMe\text{-}C_6H_4)_3$	2.0 mL	21.6 mg

Table B.17. Concentration of β-methylstyrene formed over time. Concentrations of β-methylstyrene were determined using GC-FID against durene as an internal standard. Linear portion of kinetic curve values used to construct the Hammett plot are **bolded**.

Silane = $HSi(4\text{-}CF_3\text{-}C_6H_4)_3$	
Time (s)	**[β-methylstyrene] (M)**
30	**0.015 ± 0.001**
60	**0.026 ± 0.001**
90	**0.0362 ± 0.0009**
120	**0.0472 ± 0.0007**
150	**0.058 ± 0.001**
180	**0.067 ± 0.002**
240	**0.081 ± 0.002**
300	**0.097 ± 0.003**
360	**0.110 ± 0.003**
420	**0.123 ± 0.003**
480	0.135 ± 0.004
540	0.146 ± 0.003
600	0.158 ± 0.003
660	0.167 ± 0.004
720	0.177 ± 0.004
780	0.186 ± 0.003
840	0.194 ± 0.003
900	0.201 ± 0.004

Silane = $HSi(3\text{-}F\text{-}C_6H_4)_3$	
Time (s)	**[β-methylstyrene] (M)**
30	**0.011 ± 0.001**
60	**0.025 ± 0.001**
120	**0.043 ± 0.002**
180	**0.065 ± 0.001**
240	**0.0828 ± 0.0008**
300	**0.0989 ± 0.0005**
360	**0.1134 ± 0.0008**
420	0.1275 ± 0.0008
480	0.1412 ± 0.0006
540	0.1533 ± 0.0001
600	0.1662 ± 0.0003
660	0.1745 ± 0.0001
720	0.1825 ± 0.0005
780	0.1909 ± 0.0007
840	0.1966 ± 0.0008
900	0.202 ± 0.001
960	0.208 ± 0.001
1020	0.213 ± 0.001

960	0.208	±	0.004
1020	0.215	±	0.003
1080	0.221	±	0.004
1140	0.226	±	0.003
1200	0.231	±	0.003
1320	0.240	±	0.002
1440	0.247	±	0.003
1560	0.252	±	0.003
1680	0.256	±	0.002
1800	0.260	±	0.003
2040	0.264	±	0.002
2400	0.268	±	0.002
2700	0.270	±	0.002
3600	0.273	±	0.001
4500	0.274	±	0.002
5400	0.275	±	0.002

1080	0.217	±	0.001
1140	0.220	±	0.001
1200	0.224	±	0.001
1320	0.231	±	0.003
1440	0.236	±	0.003
1560	0.241	±	0.003
1680	0.244	±	0.003
1800	0.248	±	0.003
2100	0.254	±	0.003
2460	0.260	±	0.003
2700	0.263	±	0.003
3600	0.270	±	0.002
4860	0.2707	±	0.0006
6120	0.2700	±	0.0007

Silane = $HSiPh_3$			
Time (s)	**[β-methylstyrene] (M)**		
120	**0.0347**	**±**	**0.0005**
240	**0.0599**	**±**	**0.0003**
360	**0.0805**	**±**	**0.0000**
480	**0.101**	**±**	**0.001**
660	0.1280	±	0.0007
840	0.152	±	0.002
1020	0.176	±	0.002
1260	0.204	±	0.002
1500	0.226	±	0.002
1740	0.243	±	0.001
1980	0.2540	±	0.0004
2220	0.2620	±	0.0003
2460	0.2663	±	0.0009
2700	0.2692	±	0.0001
2940	0.2701	±	0.0005
3180	0.2710	±	0.0002
3420	0.2715	±	0.0009
3660	0.273	±	0.002
3900	0.272	±	0.001
4140	0.272	±	0.002
4380	0.2725	±	0.0009
4620	0.272	±	0.002
4860	0.272	±	0.002
5100	0.272	±	0.002
5340	0.272	±	0.002
5940	0.272	±	0.003

Silane = $HSi(4\text{-}OMe\text{-}C_6H_4)_3$			
Time (s)	**[β-methylstyrene] (M)**		
120	**0.0337**	**±**	**0.0002**
240	**0.0531**	**±**	**0.0003**
360	**0.0673**	**±**	**0.0008**
480	**0.082**	**±**	**0.001**
660	**0.102**	**±**	**0.002**
840	**0.120**	**±**	**0.004**
1020	0.139	±	0.004
1260	0.165	±	0.005
1500	0.188	±	0.005
1740	0.207	±	0.005
1980	0.221	±	0.005
2220	0.234	±	0.004
2460	0.244	±	0.003
2700	0.251	±	0.003
2940	0.256	±	0.002
3180	0.2614	±	0.0007
3420	0.265	±	0.001
3660	0.2669	±	0.0006
3900	0.2686	±	0.0003
4140	0.2699	±	0.0002
4380	0.2708	±	0.0004
4620	0.2709	±	0.0003
4860	0.2713	±	0.0002
5100	0.271	±	0.001
5340	0.2723	±	0.0004
5940	0.272	±	0.001

Silane = $HSi(4\text{-}NMe_2\text{-}C_6H_4)_3$			
Time (s)	**[β-methylstyrene] (M)**		
120	**0.0327**	**±**	**0.0008**
240	**0.048**	**±**	**0.001**
360	**0.056**	**±**	**0.001**
480	**0.065**	**±**	**0.002**
660	**0.075**	**±**	**0.002**
840	**0.085**	**±**	**0.002**
1020	**0.095**	**±**	**0.002**
1260	**0.110**	**±**	**0.002**
1500	**0.123**	**±**	**0.003**
1740	0.139	±	0.003
1980	0.152	±	0.003
2220	0.165	±	0.003
2460	0.177	±	0.003
2700	0.187	±	0.004
2940	0.196	±	0.004
3180	0.204	±	0.004
3420	0.213	±	0.005
3660	0.219	±	0.004
3900	0.226	±	0.004
4140	0.232	±	0.005
4380	0.237	±	0.004
4620	0.241	±	0.004
4860	0.246	±	0.005
5100	0.249	±	0.004
5340	0.253	±	0.004
5940	0.258	±	0.005
6540	0.262	±	0.004
7140	0.265	±	0.004
7740	0.267	±	0.003
8340	0.269	±	0.003

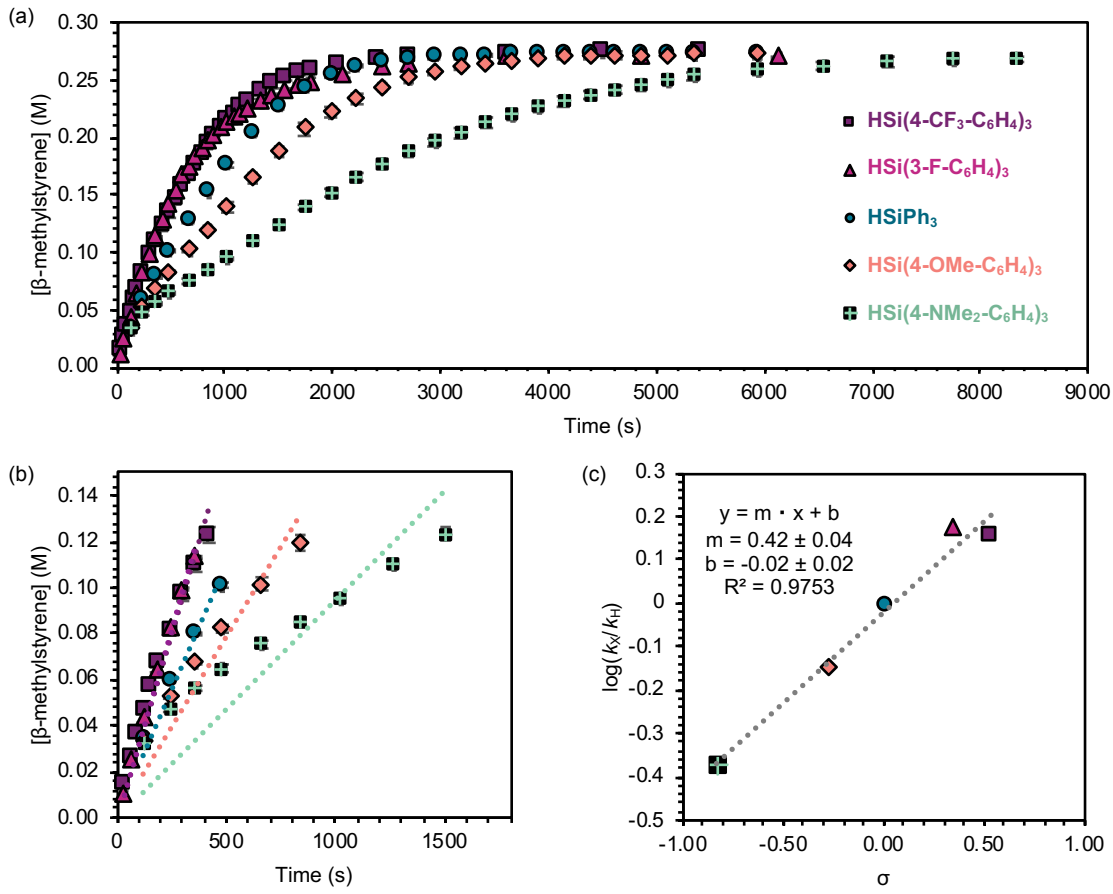

Figure B.12. Linear free energy relationship with substituted triaryl silanes. Trials were run in duplicate with durene as an internal standard. (a) Full reaction profiles; (b) early reaction rates; linear fits (y = m • x) for each silane are as follows: HSi(4-CF_3-C_6H_4)$_3$: m = 3.2 • 10^{-4} ± 0.1 • 10^{-4}, R^2 = 0.99; HSi(3-F-C_6H_4)$_3$: m = 3.3 • 10^{-4} ± 0.1 • 10^{-4}, R^2 = 0.99; $HSiPh_3$: m = 2.2 • 10^{-4} ± 0.1 • 10^{-4}, R^2 = 0.99; HSi(4-OMe-C_6H_4)$_3$: m = 1.6 • 10^{-4} ± 0.1 • 10^{-4}, R^2 = 0.98; HSi(4-NMe_2-C_6H_4)$_3$: m = 9.4 • 10^{-5} ± 0.1 • 10^{-5}, R^2 = 0.96; (c) Hammett plot.

f. In situ NMR monitoring

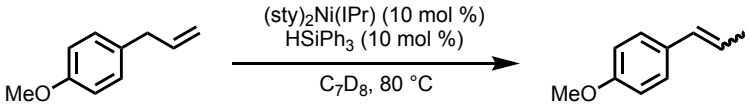

In a nitrogen-filled glovebox, (sty)$_2$Ni(IPr) (16.2 mg, 0.025 mmol, 0.10 equiv) was weighed into a 1-dram vial. A stock solution of $HSiPh_3$ (0.03 M), durene (0.15 M) and 4-allylanisole (0.30 M) was prepared in a 1-mL volumetric flask by weighing the reagents directly into the flask and adding the appropriate volume of C_7D_8. To the weighed out (sty)$_2$Ni(IPr) was added 0.83 mL of the stock solution using a 1-mL disposable syringe and

the reaction was shaken until everything was in solution. The solution was transferred to a J-Young NMR tube, sealed and removed from the glovebox. A ^{1}H NMR spectrum was recorded at room temperature before the instrument was warmed to 80 °C. ^{1}H NMR spectra were recorded periodically up to 806 minutes. Select spectra are shown below.

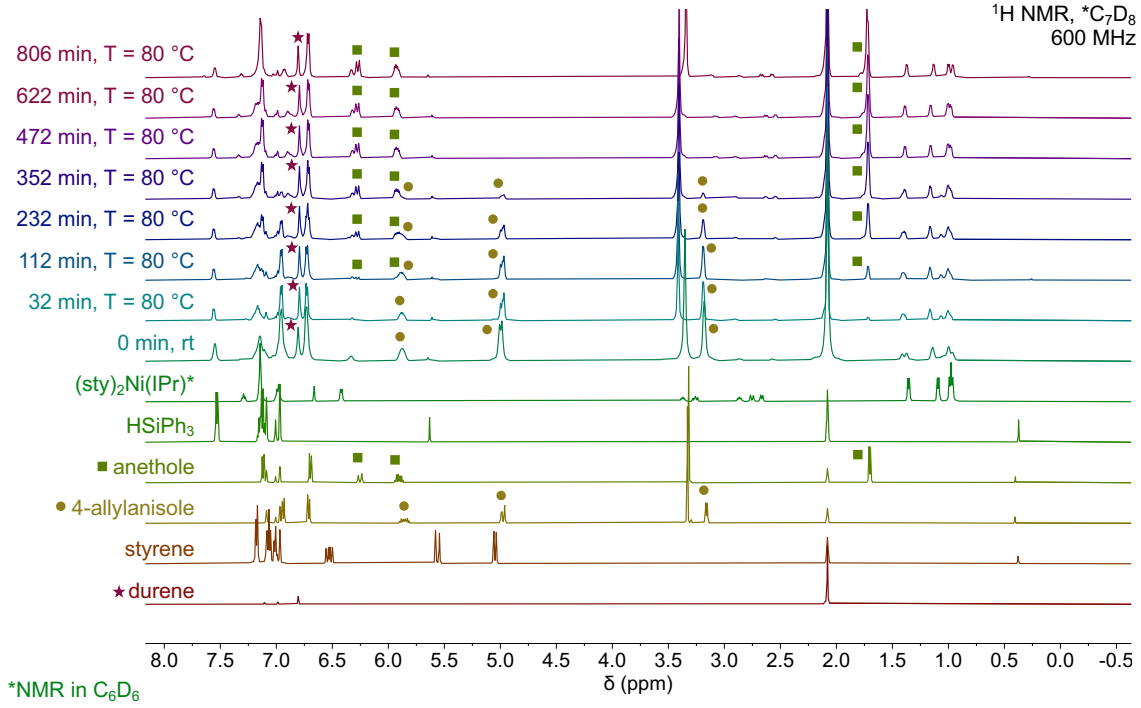

Figure B.13. In situ ^{1}H NMR monitoring of the isomerization of 4-allylanisole. Spectra were recorded at 298 K unless otherwise noted.

B.1.5. Isomerization of α-substituted styrenes

a. Reaction order determination

i. Kinetics to measure order in HSiPh$_3$

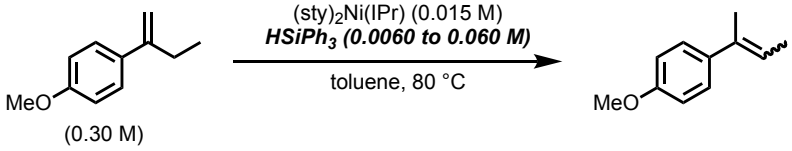

In a nitrogen-filled glovebox, (sty)$_2$Ni(IPr) (8.2 mg, 0.013 mmol, 0.05 equiv) was weighed into 1-dram vials. Magnetic stir bars were added to each vial. Stock solutions of HSiPh$_3$ (0.13 M) and durene (0.15 M) were prepared by weighing each reagent directly into a volumetric flask and adding the appropriate volume of toluene. Durene stock solution (0.40 mL, 0.061 mmol, 0.25 equiv) was distributed to each vial using a 1-mL disposable syringe. Silane stock solution and toluene were distributed to each vial to range [HSiPh$_3$]

from 0.0060 to 0.060 M and maintain a total volume of 0.84 mL (**Table B.18.**). Vials were sealed with septum caps, removed from the glovebox, and placed on an aluminum vial block preheated to 80 °C. After 30 minutes, 4'-OMe-α-ethylstyrene (45 μL, 0.25 mmol, 1.0 equiv) was added using a 100-μL microliter syringe. Throughout the course of the reaction, ~5 μL aliquots were removed from the reaction, filtered through Celite with hexanes directly in to a GC and analyzed by GC-FID. The concentration of 4'-OMe-α,β-dimethylstyrene was found versus durene as an internal standard based on an independent calibration curve of 4'-OMe-α-ethylstyrene and durene.

Table B.18. Summary of reagent distribution for rate data collection.

Final [$HSiPh_3$] (M)	Volume $HSiPh_3$ stock solution added	mmol $HSiPh_3$ added	Volume toluene added
0.060	400 μL	0.050	0 μL
0.030	205 μL	0.026	195 μL
0.015	100 μL	0.013	300 μL
0.010	70 μL	0.0088	330 μL
0.0060	40 μL	0.0050	360 μL

Table B.19. Concentration of 4'-OMe-α,β-dimethylstyrene formed over time. Concentrations of 4'-OMe-α,β-dimethylstyrene were determined using GC-FID against durene as an internal standard (based on starting material, 4'-OMe-α-ethylstyrene). Linear portion of kinetic curve values used to find the order are **bolded**.

[$HSiPh_3$] = 0.060 M		[$HSiPh_3$] 0.030 M	
Time (s)	[4'-OMe-α,β-dimethylstyrene] (M)	Time (s)	[4'-OMe-α,β-dimethylstyrene] (M)
30	0.0038 ± 0.0006	30	0.0040 ± 0.0002
60	0.0048 ± 0.0007	60	0.0045 ± 0.0005
90	0.0052 ± 0.0006	90	0.0054 ± 0.0005
120	0.0056 ± 0.0009	120	0.0054 ± 0.0002
150	0.0059 ± 0.0006	150	0.0053 ± 0.0002
180	**0.006 ± 0.001**	**180**	**0.0055 ± 0.0002**
480	**0.022 ± 0.004**	**480**	**0.0135 ± 0.0001**
780	**0.06 ± 0.01**	**780**	**0.031 ± 0.002**
1080	**0.11 ± 0.02**	**1080**	**0.053 ± 0.005**
1380	0.14 ± 0.02	1380	0.076 ± 0.007
1680	0.18 ± 0.02	1710	0.10 ± 0.01
3480	0.274 ± 0.009	3450	0.19 ± 0.02
5220	0.27 ± 0.03	5190	0.23 ± 0.02

6960	0.298	±	0.002
10800	0.298	±	0.002

7110	0.26	±	0.02
10800	0.282	±	0.009

[$HSiPh_3$] = 0.015 M			
Time (s)	**[4'-OMe-α,β-dimethylstyrene] (M)**		
30	0.0033	±	0.0001
60	0.0038	±	0.0003
90	0.0042	±	0.0004
120	0.0042	±	0.0004
150	0.0044	±	0.0002
180	**0.0044**	**±**	**0.0001**
480	**0.0105**	**±**	**0.0005**
780	**0.0227**	**±**	**0.0005**
1080	**0.035**	**±**	**0.001**
1380	0.048	±	0.002
1680	0.059	±	0.003
3420	0.104	±	0.009
5340	0.14	±	0.01
7230	0.169	±	0.008
10800	0.213	±	0.005

[$HSiPh_3$] = 0.010 M			
Time (s)	**[4'-OMe-α,β-dimethylstyrene] (M)**		
30	0.0031	±	0.0008
60	0.0039	±	0.0009
90	0.0039	±	0.0006
120	0.0045	±	0.0002
150	0.0047	±	0.0006
180	**0.0048**	**±**	**0.0005**
480	**0.010**	**±**	**0.001**
780	**0.019**	**±**	**0.002**
1080	**0.0278**	**±**	**0.002**
1380	**0.037**	**±**	**0.002**
1650	0.046	±	0.002
3570	0.083	±	0.002
5460	0.114	±	0.001
7230	0.1393	±	0.0009
10800	0.184	±	0.003

[$HSiPh_3$] = 0.0060 M			
Time (s)	**[4'-OMe-α,β-dimethylstyrene] (M)**		
30	0.0043	±	0.0009
60	0.0052	±	0.0004
90	0.0047	±	0.0004
120	0.006	±	0.001
150	0.0055	±	0.0008
180	**0.006**	**±**	**0.002**
480	**0.012**	**±**	**0.003**
780	**0.022**	**±**	**0.007**
1080	**0.04**	**±**	**0.01**
1380	0.05	±	0.02
1800	0.06	±	0.02
3690	0.11	±	0.04
5460	0.14	±	0.04
7230	0.16	±	0.04
10800	0.20	±	0.04

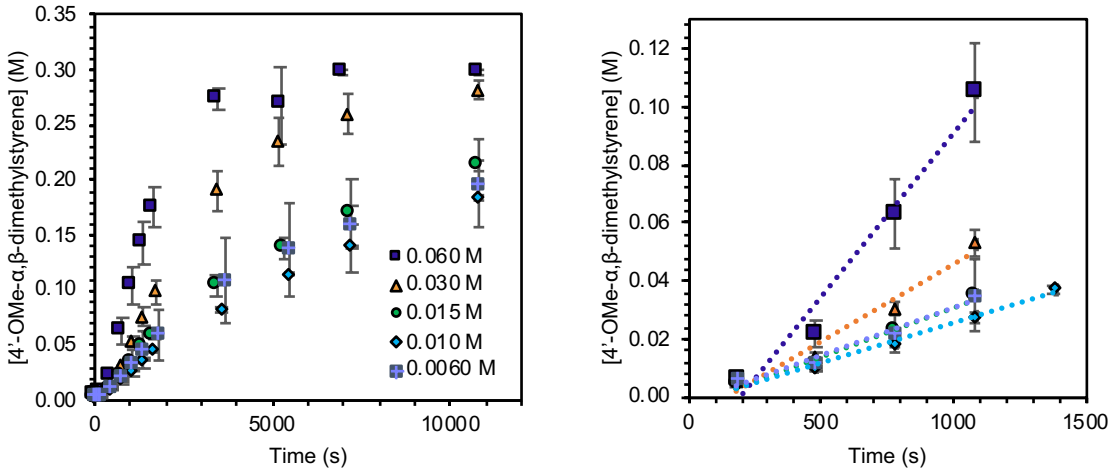

Figure B.14. Formation of 4'-OMe-α,β-dimethylstyrene formed over time at differing initial concentrations of $HSiPh_3$. (a) Full reaction profiles and (b) linear portion of kinetic curve.

Table B.20. Rates of formation of 4'-OMe-α,β-dimethylstyrene at varying initial concentrations of $HSiPh_3$.

[$HSiPh_3$] (M)	Rate (M/s)	log([$HSiPh_3$] / M)	log(Rate / M/s)
0.060	$11 \cdot 10^{-5} \pm 2 \cdot 10^{-5}$	-1.23	-3.95
0.030	$5.29 \cdot 10^{-5} \pm 0.08 \cdot 10^{-5}$	-1.52	-4.28
0.015	$3.46 \cdot 10^{-5} \pm 0.04 \cdot 10^{-5}$	-1.82	-4.46
0.010	$2.74 \cdot 10^{-5} \pm 0.02 \cdot 10^{-5}$	-2.00	-4.56
0.0060	$3.25 \cdot 10^{-5} \pm 0.03 \cdot 10^{-5}$	-2.22	-4.49

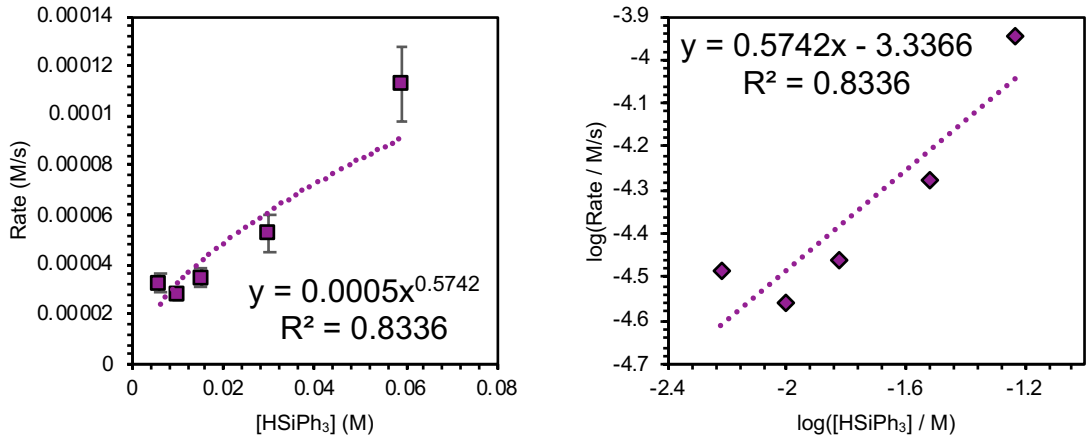

Figure B.15. Order plot for $HSiPh_3$. (a) Power function fit of form $y = a \cdot x^b$; a = 0.0005, b = 0.57, R^2 = 0.834 and (b) linearized log-log plot of form $y = m \cdot x + b$; m = 0.6 ± 0.1, b = -3.3 ± 0.3, R^2 = 0.834.

i. Kinetics to measure order in catalyst

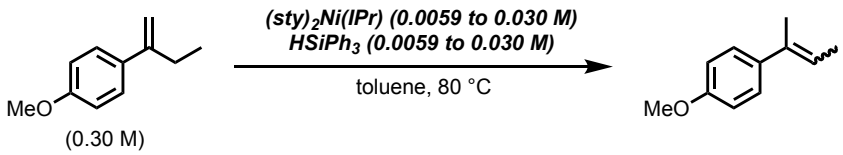

In a nitrogen-filled glovebox, (sty)2Ni(IPr) (see **Table B.21.**) was weighed into 1-dram vials. Magnetic stir bars were added to each vial. Stock solutions of HSiPh3 (0.13 M) and durene (0.15 M) were prepared by weighing the reagent directly into a volumetric flask and adding the appropriate volume of toluene. Durene stock solution (0.40 mL, 0.061 mmol, 0.25 equiv) was distributed to each vial using a 1-mL disposable syringe. Silane stock solution and toluene were distributed to each vial to range [$HSiPh_3$] from 0.0059 to 0.030 M and maintain a total volume of 0.84 mL (see **Table B.21.**). Vials were sealed with septum caps, removed from the glovebox, and placed on an aluminum vial block preheated to 80 °C. After 30 minutes, 4'-OMe-α-ethylstyrene (45 μL, 0.25 mmol, 1.0 equiv) was added using a 100-μL microliter syringe. Throughout the course of the reaction, ~5 μL aliquots were removed from the reaction, filtered through Celite with hexanes directly into a GC and analyzed by GC-FID. The concentration of 4'-OMe-α,β-dimethylstyrene was found versus durene as an internal standard based on an independent calibration curve of 4'-OMe-α-ethylstyrene and durene.

Table B.21. Summary of reagent distribution for rate data collection.

Final [catalyst] (M)	Mass $(sty)_2Ni(IPr)$ (mg)	Volume $HSiPh_3$ stock solution added	mmol $HSiPh_3$ added	Volume toluene added
0.030	16.4	205 μL	0.026	195 μL
0.015	8.2	100 μL	0.013	300 μL
0.011	5.8	70 μL	0.0088	330 μL
0.0059	3.3	40 μL	0.0050	360 μL

Table B.22. Concentration of 4'-OMe-α,β-dimethylstyrene formed over time. Concentrations of 4'-OMe-α,β-dimethylstyrene were determined using GC-FID against durene as an internal standard (based on starting material, 4'-OMe-α-ethylstyrene). Linear portion of kinetic curve values used to find the order are **bolded**.

[catalyst] = 0.030 M	**[catalyst] 0.015 M**

Time (s)	[4'-OMe-α,β-dimethylstyrene] (M)
30	0.006 ± 0.001
60	0.007 ± 0.002
90	0.008 ± 0.002
120	0.008 ± 0.002
150	0.009 ± 0.002
180	0.009 ± 0.002
240	**0.011 ± 0.002**
300	**0.013 ± 0.002**
360	**0.015 ± 0.001**
480	**0.022 ± 0.002**
600	**0.030 ± 0.002**
900	0.054 ± 0.003
1740	0.115 ± 0.004
2760	0.174 ± 0.004
3480	0.203 ± 0.005
5220	0.243 ± 0.006
10740	0.276 ± 0.005
16140	0.287 ± 0.005
25200	0.289 ± 0.004
32400	0.289 ± 0.004

Time (s)	[4'-OMe-α,β-dimethylstyrene] (M)
30	0.0038 ± 0.0002
60	0.0038 ± 0.0005
90	0.0045 ± 0.0004
120	0.0043 ± 0.0005
150	0.0049 ± 0.0002
180	0.0050 ± 0.0007
240	0.0057 ± 0.0002
300	**0.0067 ± 0.0000**
360	**0.0079 ± 00000**
480	**0.0104 ± 0.0001**
600	**0.0143 ± 0.0005**
900	**0.028 ± 0.002**
1740	0.065 ± 0.007
2760	0.10 ± 0.01
3480	0.12 ± 0.02
5220	0.15 ± 0.02
10740	0.23 ± 0.02
16140	0.261 ± 0.006
30600	0.288 ± 0.001

[catalyst] = 0.011 M	
Time (s)	[4'-OMe-α,β-dimethylstyrene] (M)
30	0.0035 ± 0.0006
60	0.005 ± 0.001
120	0.004 ± 0.001
180	0.005 ± 0.001
240	0.0055 ± 0.0008
300	0.006 ± 0.001
360	0.007 ± 0.001
480	**0.009 ± 0.000**
600	**0.013 ± 0.002**
720	**0.015 ± 0.002**
900	**0.022 ± 0.003**
1200	**0.032 ± 0.004**
1800	0.052 ± 0.006
2640	0.077 ± 0.009
3540	0.10 ± 0.01
5340	0.13 ± 0.01
10800	0.21 ± 0.01
14940	0.24 ± 0.01
21600	0.271 ± 0.003
28800	0.281 ± 0.001

[catalyst] = 0.0059 M	
Time (s)	[4'-OMe-α,β-dimethylstyrene] (M)
60	0.004 ± 0.001
120	0.0042 ± 0.0005
180	0.0050 ± 0.0002
240	0.0051 ± 0.0001
300	0.0059 ± 0.0000
360	0.0065 ± 0.0005
480	0.0078 ± 0.0002
600	0.0091 ± 0.0004
720	**0.0107 ± 0.0005**
900	**0.0143 ± 0.0002**
1200	**0.0213 ± 0.0003**
1500	**0.0269 ± 0.0008**
1800	**0.0332 ± 0.0001**
2700	0.050 ± 0.002
3600	0.065 ± 0.002
5400	0.094 ± 0.004
10800	0.165 ± 0.008
13200	0.188 ± 0.007
19800	0.22 ± 0.01
27000	0.23 ± 0.01

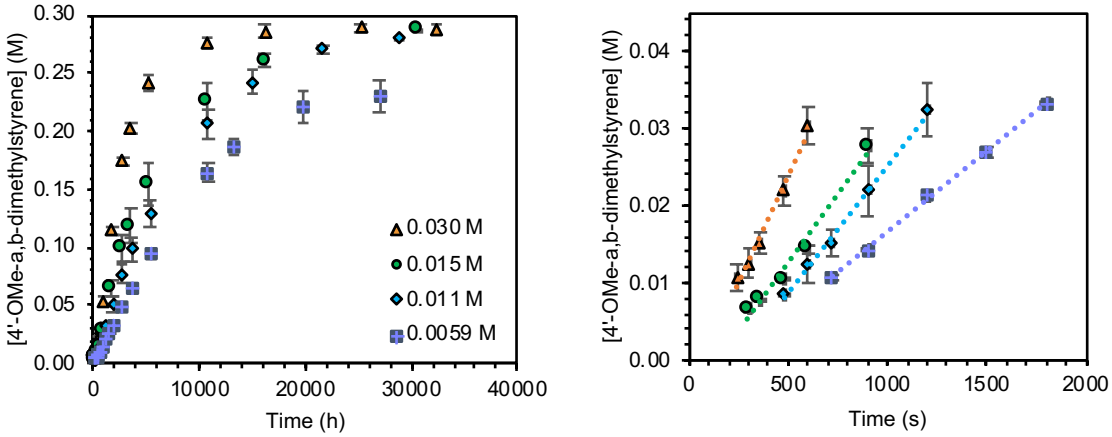

Figure B.16. Formation of 4'-OMe-α,β-dimethylstyrene formed over time at differing initial concentrations of catalyst. (a) Full reaction profiles and (b) linear portion of kinetic curve.

Table B.23. Rates of formation of 4-OMe-β-methylstyrene at varying initial concentrations of catalyst.

[catalyst] (M)	Rate (M/s)	log([catalyst] / M)	log(Rate / M/s)
0.030	$5.5 \cdot 10^{-5} \pm 0.4 \cdot 10^{-5}$	-1.52	-4.26
0.015	$3.5 \cdot 10^{-5} \pm 0.3 \cdot 10^{-5}$	-1.82	-4.45
0.011	$3.3 \cdot 10^{-5} \pm 0.1 \cdot 10^{-5}$	-2.00	-4.48
0.0059	$2.08 \cdot 10^{-5} \pm 0.04 \cdot 10^{-5}$	-2.22	-4.68

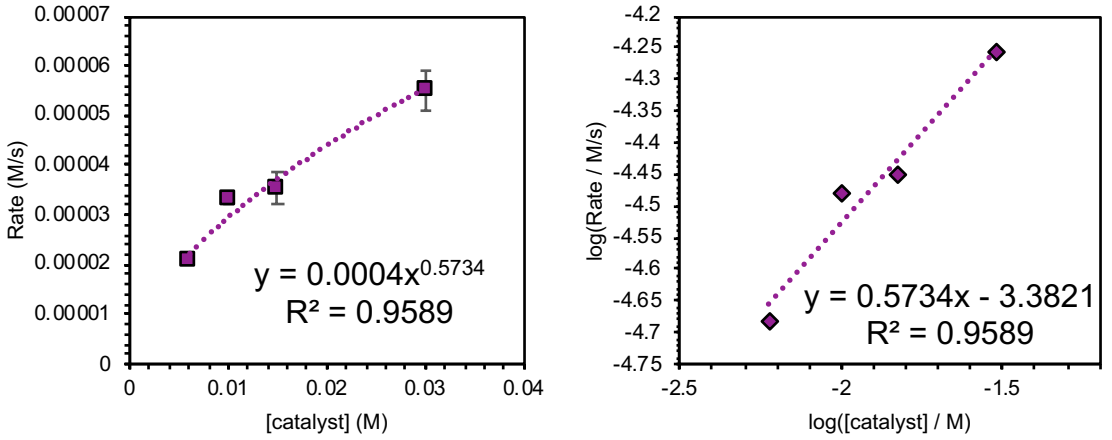

Figure B.17. Order plot for catalyst. (a) Power function fit of form $y = a \cdot x^b$; a = 0.0004, b = 0.57, $R^2 = 0.959$ and (b) linearized log-log plot of form $y = m \cdot x + b$; m = 0.57 ± 0.8, b = -3.4 ± 0.2, $R^2 = 0.959$.

b. Silane kinetic isotope experiment

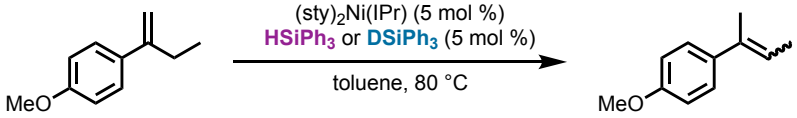

In a nitrogen-filled glovebox, $(sty)_2Ni(IPr)$ (8.2 mg, 0.013 mmol, 0.05 equiv) was weighed directly into 1-dram vials. Magnetic stir bars were added to each vial. Stock solution of durene (0.18 M), $HSiPh_3$ (0.62 M) and $DSiPh_3$ (0.62 M) were prepared in 5.0-, 2.0- and 1.0-mL volumetric flasks, respectively, by weighing out the reagent and adding the appropriate volume of toluene. The durene stock solution (0.60 mL, 0.11 mmol, 0.43 equiv) was distributed to each vial using a 1-mL disposable syringe. Silane stock solution (200 µL, 0.012 mmol, 0.05 equiv) was distributed to each vial using a 250-µL microliter syringe. Vials were sealed with septum caps, removed from the glovebox and placed on a preheated aluminum vial block at 80 °C. After 30 minutes, 4'-OMe-α-ethylstyrene (45 µL, 0.25 mmol, 1.0 equiv) was distributed using a 100-µL microliter syringe. Throughout the course of the reaction, ~5 µL aliquots were removed from the reaction, filtered through Celite with hexanes directly in to a GC and analyzed by GC-FID. The concentration of 4'-OMe-α,β-dimethylstyrene was found versus durene as an internal standard based on an independent calibration curve of 4'-OMe-α-ethylstyrene and durene.

Table B.24. Concentration of 4'-OMe-α,β-dimethylstyrene formed over time. Concentrations of 4'-OMe-α,β-dimethylstyrene were determined using GC-FID against durene as an internal standard (based on starting material, 4'-OMe-α-ethylstyrene).

Silane = $HSiPh_3$	
Time (s)	[4'-OMe-α,β-dimethylstyrene] (M)
120	0.010 ± 0.002
240	0.017 ± 0.003
360	0.025 ± 0.004
480	0.033 ± 0.006
600	0.040 ± 0.007
1200	0.08 ± 0.02
1800	0.11 ± 0.02
3600	0.20 ± 0.03
5400	0.25 ± 0.03
7200	0.27 ± 0.02
10800	0.29 ± 0.01

Silane = $DSiPh_3$	
Time (s)	[4'-OMe-α,β-dimethylstyrene] (M)
120	0.0059 ± 0.0007
240	0.010 ± 0.001
360	0.013 ± 0.002
480	0.015 ± 0.002
600	0.018 ± 0.003
1200	0.031 ± 0.005
1800	0.043 ± 0.008
3600	0.07 ± 0.01
5400	0.10 ± 0.02
7200	0.13 ± 0.02
10800	0.19 ± 0.02

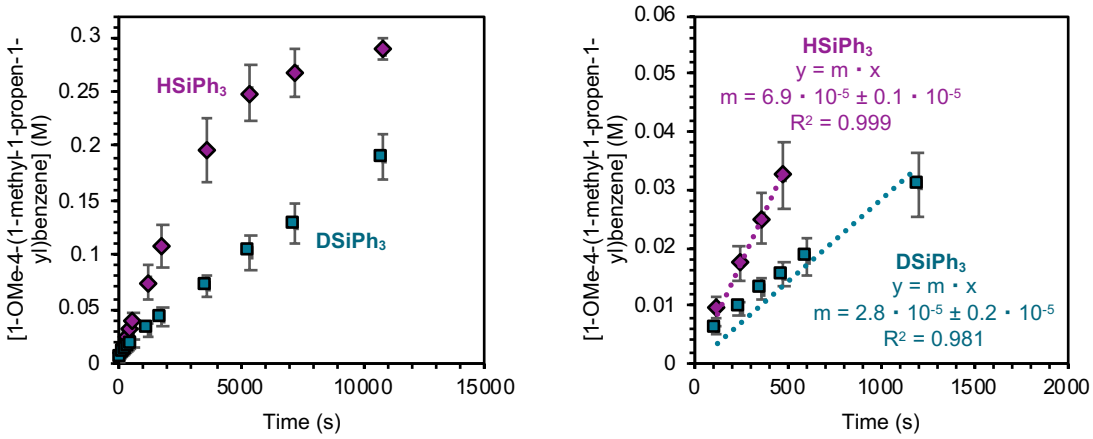

Figure B.18. H/D kinetic isotope effect for triphenylsilane. Trials were run in duplicate with durene as an internal standard.

c. Deuterium incorporation with DSiPh3

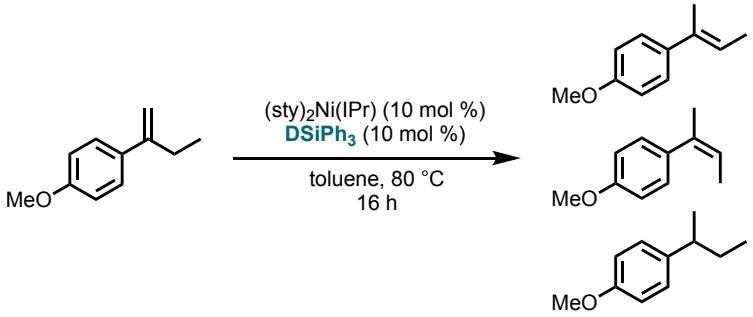

In a nitrogen-filled glovebox, $(sty)_2Ni(IPr)$ (32.8 mg, 0.050 mmol, 0.10 equiv) was weighed into 1-dram vials. Magnetic stir bars were added to each vial. A stock solution of silane (0.031 M) was prepared by weighing out $DSiPh_3$ and adding the appropriate volume of toluene. $DSiPh_3$ stock solution was distributed (1.6 mL, 0.050 mmol, 0.10 equiv) using two portions of a 1-mL disposable syringe. Vials were sealed with septum caps, removed from the glovebox, and placed on a preheated aluminum vial block at 80 °C. After 30 minutes, 4'-OMe-α-ethylstyrene (90 µL, 0.50 mmol, 1.0 equiv) was added using a 100-µL microliter syringe. After 16 h, the reactions were quenched by cooling with liquid N_2 and opening to air. Small aliquots were removed and filtered through Celite with hexanes directly into GC-MS vials for analysis by GC-MS and GC-FID. A summary of relative composition for the crude reaction is shown in **Table B.25.** Approximately half of the crude reaction mixture was then filtered through a short silica plug using hexanes, solvent was

removed under reduced pressure, and samples for NMR were prepared in solutions of $CHCl_3/CDCl_3$ (9:1). ^1H and ^2H NMR spectra were recorded, shown in **Figure B.19.**

Table B.25. Summary of crude reaction composition and analysis of mass spectra from GC-MS.

Component	Relative % composition	Predicted and observed mass fragmentation
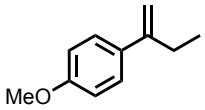	5%	Exact Mass: 162.1045 predicted: m/z: 162.1045 (100.0%), 163.1078 (11.9%) **observed:** **m/z: 162.1 (100%), 163.1 (16%)**
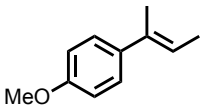	78%	Exact Mass: 162.1045 predicted: m/z: 162.1045 (100.0%), 163.1078 (11.9%) **observed:** **m/z: 162.1 (100%), 163.1 (15%)**
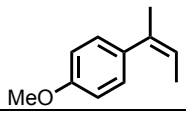	17%	
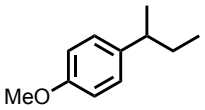	1%	Exact Mass: 162.1045 predicted: m/z: 162.1045 (100.0%), 163.1078 (11.9%) **observed:** **m/z: 162.1 (100%), 163.1 (15%)**

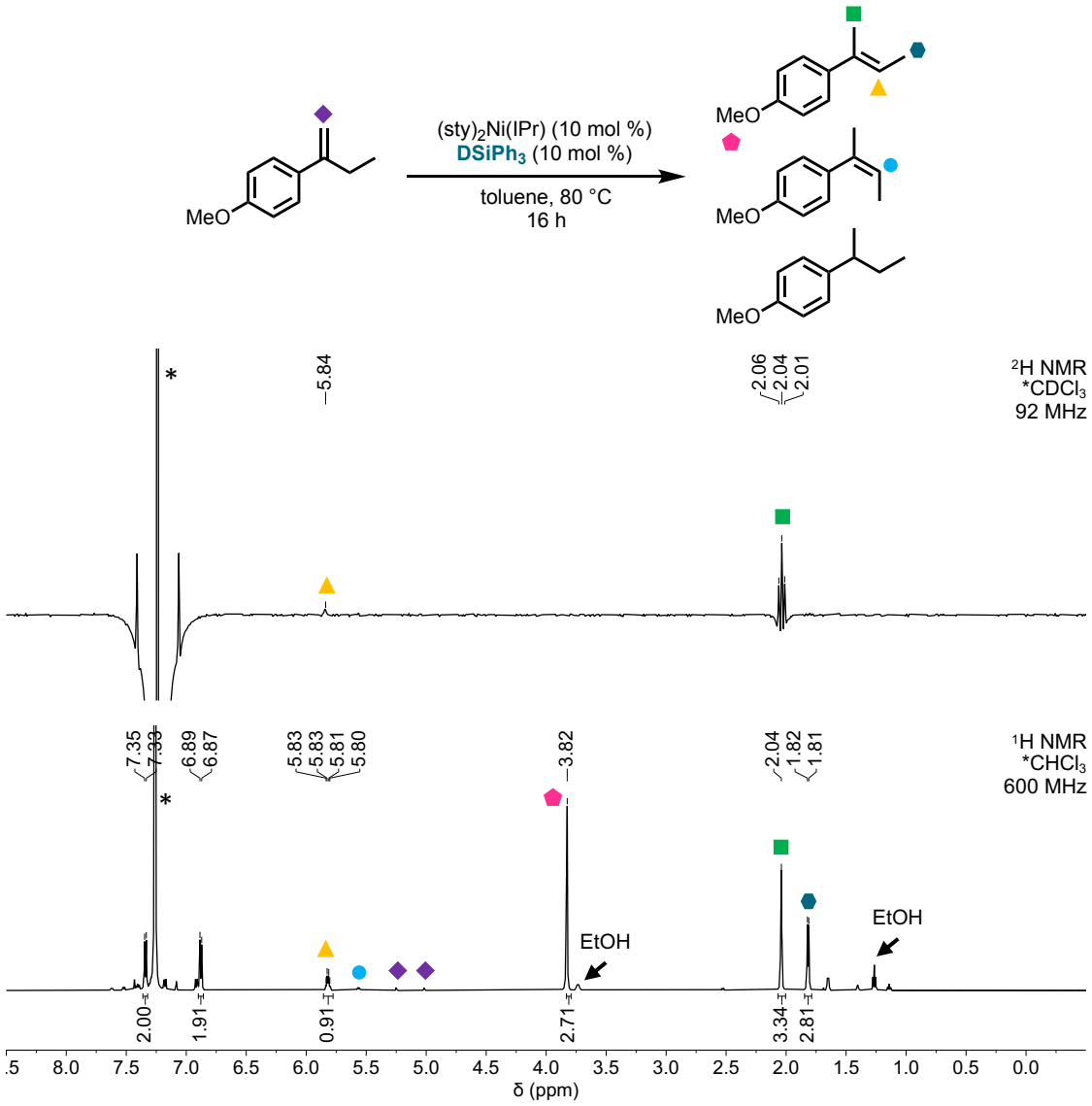

Figure B.19. NMR analysis of deuterium incorporation study with $DSiPh_3$. NMR spectra were recorded at 298 K. $CHCl_3$ was stabilized with EtOH (visible in the ^1H NMR spectrum).

d. Silane linear free energy relationship

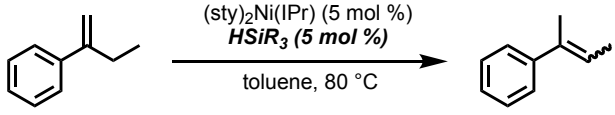

In a nitrogen-filled glovebox, $(sty)_2Ni(IPr)$ (8.2 mg, 0.013 mmol, 0.05 equiv) was weighed into 1-dram vials. Magnetic stir bars were added to each vial. $HSi(4\text{-}CF_3\text{-}C_6H_4)_3$ (5.8 mg, 0.013 mmol, 0.05 equiv), $HSi(4\text{-}NMe_2\text{-}C_6H_4)_3$ (4.9 mg, 0.013 mmol, 0.05 equiv), $HSi(3\text{-}F\text{-}C_6H_4)_3$ (3.9 mg, 0.013 mmol, 0.05 equiv), and $HSi(4\text{-}OMe\text{-}C_6H_4)_3$ (4.4 mg, 0.013

mmol, 0.05 equiv) were weighed into respective vials. A stock solution of $HSiPh_3$ (0.016 M) was prepared in a 2.0-mL volumetric flask by weighing out the reagent and adding the appropriate volume of toluene. $HSiPh_3$ stock solution was distributed (0.80 mL, 0.013 mmol, 0.05 equiv) using a 1-mL disposable syringe. Toluene (0.80 mL) was added to the other vials. Mesitylene (10 μL, 0.072 mmol, 0.29 equiv) was distributed using a 25-μL microliter syringe. Vials were sealed with septum caps, removed from the glovebox and placed on a pre-heated aluminum vial block at 80 °C. After 30 minutes of heating, α-ethylstyrene (36 μL, 0.25 mmol, 1.0 equiv) was added using a 100-μL microliter syringe. Throughout the course of the reaction, ~5 μL aliquots were removed from the reaction, filtered through Celite with hexanes directly into a GC and analyzed by GC-FID. The concentration of α,β-dimethylstyrene was found versus mesitylene as an internal standard based on an independent calibration curve prepared with commercial reagents.

Table B.26. Concentration of β-methylstyrene formed over time. Concentrations of β-methylstyrene were determined using GC-FID against mesitylene as an internal standard. Linear portion of kinetic curve values used to construct the Hammett plot are **bolded**.

Silane = $HSi(4\text{-}CF_3\text{-}C_6H_4)_3$	
Time (s)	**[α,β-dimethylstyrene] (M)**
30	**0.027 ± 0.001**
60	**0.050 ± 0.002**
90	**0.071 ± 0.003**
120	**0.089 ± 0.004**
150	0.104 ± 0.005
180	0.118 ± 0.005
210	0.131 ± 0.005
240	0.141 ± 0.005
270	0.151 ± 0.005
300	0.163 ± 0.004
360	0.176 ± 0.006
420	0.191 ± 0.004
480	0.202 ± 0.005
540	0.212 ± 0.005
600	0.218 ± 0.003
720	0.234 ± 0.003
840	0.244 ± 0.006
960	0.251 ± 0.005
1080	0.257 ± 0.005
1200	0.262 ± 0.005

Silane = $HSi(3\text{-}F\text{-}C_6H_4)_3$	
Time (s)	**[α,β-dimethylstyrene] (M)**
30	**0.018 ± 0.001**
60	**0.037 ± 0.002**
90	**0.056 ± 0.002**
120	**0.073 ± 0.002**
150	**0.088 ± 0.003**
180	0.104 ± 0.002
210	0.1171 ± 0.0001
240	0.1284 ± 0.0006
270	0.1400 ± 0.0006
300	0.1494 ± 0.0005
360	0.1694 ± 0.0005
420	0.1836 ± 0.0005
480	0.196 ± 0.001
540	0.2065 ± 0.0002
600	0.2162 ± 0.0009
720	0.2315 ± 0.0007
840	0.2414 ± 0.0005
960	0.251 ± 0.002
1080	0.258 ± 0.002
1200	0.263 ± 0.002

1560	0.269	±	0.002
2880	0.277	±	0.002
4080	0.2748	±	0.0002
7200	0.2787	±	0.0008
10800	0.278	±	0.002

1500	0.273	±	0.002
3000	0.284	±	0.004
4800	0.2849	±	0.0005
7200	0.282	±	0.002
10800	0.282	±	0.002
21600	0.281	±	0.002

Silane = $HSiPh_3$			
Time (s)	**[α,β-dimethylstyrene] (M)**		
120	**0.062**	**±**	**0.0002**
240	**0.107**	**±**	**0.0006**
360	**0.142**	**±**	**0.003**
480	**0.170**	**±**	**0.003**
600	0.193	±	0.004
780	0.218	±	0.002
960	0.238	±	0.001
1140	0.251	±	0.003
1380	0.2628	±	0.0009
1620	0.270	±	0.001
1860	0.276	±	0.001
2100	0.281	±	0.002
2400	0.283	±	0.002
3600	0.2866	±	0.0004
5400	0.2867	±	0.0001
7200	0.289	±	0.004
11700	0.285	±	0.003
18000	0.27	±	0.03

Silane = $HSi(4\text{-}OMe\text{-}C_6H_4)_3$			
Time (s)	**[α,β-dimethylstyrene] (M)**		
120	**0.055**	**±**	**0.002**
240	**0.094**	**±**	**0.001**
360	**0.122**	**±**	**0.003**
480	**0.145**	**±**	**0.003**
600	0.167	±	0.004
780	0.194	±	0.006
960	0.216	±	0.006
1140	0.232	±	0.006
1380	0.247	±	0.007
1620	0.260	±	0.005
1860	0.269	±	0.004
2100	0.275	±	0.004
2400	0.279	±	0.003
3600	0.286	±	0.002
5400	0.2849	±	0.0006
7200	0.2842	±	0.0007
11700	0.284	±	0.002
18000	0.285	±	0.002

Silane = $HSi(4\text{-}NMe_2\text{-}C_6H_4)_3$			
Time (s)	**[α,β-dimethylstyrene] (M)**		
120	**0.0412**	**±**	**0.0008**
240	**0.073**	**±**	**0.002**
360	**0.097**	**±**	**0.002**
480	**0.117**	**±**	**0.003**
600	0.135	±	0.003
780	0.158	±	0.004
960	0.178	±	0.003
1140	0.194	±	0.003
1380	0.213	±	0.004
1620	0.229	±	0.004
1860	0.242	±	0.003
2100	0.252	±	0.003
2400	0.262	±	0.002
3600	0.280	±	0.002

5400	0.284	±	0.001
7200	0.2846	±	0.0000
11700	0.2831	±	0.0001
18000	0.283	±	0.001
20400	0.2826	±	0.0004

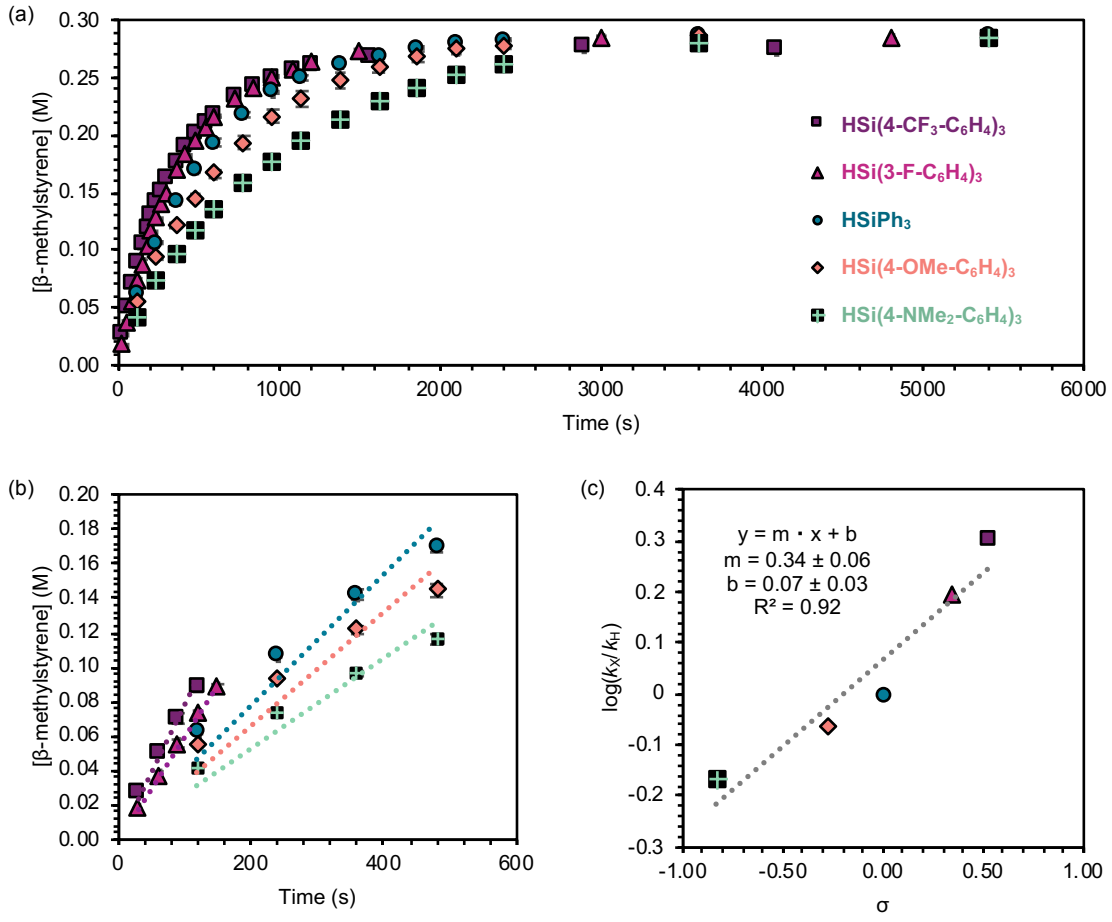

Figure B.20. Linear free energy relationship with substituted triaryl silanes. Trials were run in duplicate with mesitylene as an internal standard. (a) Full kinetic profiles, (b) linear fits (y = m · x) for each silane are as follows: HSi(4-CF_3-C_6H_4)$_3$: m = 7.7 · 10^{-4} ± 0.3 · 10^{-4}, R^2 = 0.997; HSi(3-F-C_6H_4)$_3$: m = 5.99 · 10^{-4} ± 0.07 · 10^{-4}, R^2 = 0.999; $HSiPh_3$: m = 3.8 · 10^{-4} ± 0.2 · 10^{-4}, R^2 = 0.989; HSi(4-OMe-C_6H_4)$_3$: m = 3.3 · 10^{-4} ± 0.1 · 10^{-4}, R^2 = 0.987; HSi(4-NMe_2-C_6H_4)$_3$: m = 2.6 · 10^{-4} ± 0.1 · 10^{-4}, R^2 = 0.990, and (c) Hammett plot.

e. Substrate-based kinetic isotope experiment

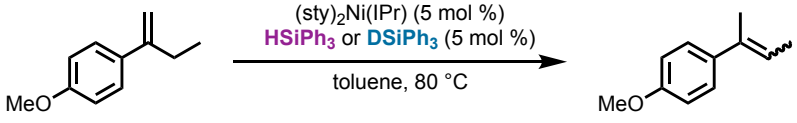

In a nitrogen-filled glovebox, $(sty)_2Ni(IPr)$ was weighed directly into 1-dram vials. Magnetic stir bars were added to each vial. A stock solution of $HSiPh_3$ (0.021 M) and durene (0.11 M) was prepared by weighing the reagents directly into a 10-mL volumetric flask and adding the appropriate volume of toluene. Silane/durene stock solution was distributed (0.60 mL, $HSiPh_3$: 0.013 mmol, 0.05 equiv; durene: 0.063 mmol, 0.25 equiv) to each vial using a 1-mL disposable syringe. To each vial was added an additional 0.19 mL toluene to bring the total volume to 0.84 mL after substrate addition. Vials were sealed with septum caps, removed from the glovebox, and placed on a preheated aluminum vial block at 80 °C. After 30 minutes, 4'-OMe-α-ethylstyrene (45 μL, 0.25 mmol, 1.0 equiv) or 4'-OMe-α-ethylstyrene-d_2 (45 μL, 0.25 mmol, 1.0 equiv) were distributed using a 100-μL microliter syringe. Throughout the course of the reaction, ~5 μL aliquots were removed from the reaction, filtered through Celite with hexanes directly into a GC and analyzed by GC-FID. The concentration of 4'-OMe-α,β-dimethylstyrene was found versus durene as an internal standard based on an independent calibration curve prepared with commercial reagents.

Table B.27. Concentration of 4'-OMe-α,β-dimethylstyrene formed over time. Concentrations of 4'-OMe-α,β-dimethylstyrene were determined using GC-FID against durene as an internal standard (based on starting material, 4'-OMe-α-ethylstyrene). Linear portion of kinetic curve values used to compare reaction rates are **bolded**.

4'-OMe-α-ethylstyrene		**4'-OMe-α-ethylstyrene-d_2**	
Time (s)	**[4'-OMe-α,β-dimethylstyrene] (M)**	**Time (s)**	**[4'-OMe-α,β-dimethylstyrene] (M)**
120	**0.023 ± 0.003**	**120**	**0.025 ± 0.003**
240	**0.044 ± 0.004**	**240**	**0.047 ± 0.001**
360	**0.068 ± 0.002**	**360**	**0.066 ± 0.000**
480	**0.086 ± 0.005**	**480**	**0.084 ± 0.003**
600	0.10 ± 0.01	600	0.097 ± 0.002
720	0.11 ± 0.01	720	0.112 ± 0.004
840	0.13 ± 0.02	840	0.120 ± 0.004
960	0.143 ± 0.009	960	0.128 ± 0.005
1080	0.15 ± 0.01	1080	0.132 ± 0.005
1200	0.168 ± 0.003	1200	0.150 ± 0.006
1500	0.19 ± 0.01	1500	0.167 ± 0.005
1800	0.202 ± 0.007	1800	0.187 ± 0.000
2400	0.230 ± 0.004	2400	0.22 ± 0.02
3000	0.24 ± 0.02	3000	0.23 ± 0.01
3600	0.26 ± 0.02	3600	0.24 ± 0.02

5400	0.26	±	0.01	5400	0.26 ± 0.01
7200	0.28	±	0.02	7200	0.26 ± 0.02
9000	0.271	±	0.003	9000	0.26 ± 0.02
10800	0.274	±	0.000	10800	0.27 ± 0.01
12600	0.269	±	0.002	12600	0.26 ± 0.02
14400	0.271	±	0.004	14400	0.27 ± 0.02
16200	0.272	±	0.004	16200	0.26 ± 0.02
18000	0.274	±	0.005	18000	0.271 ± 0.008

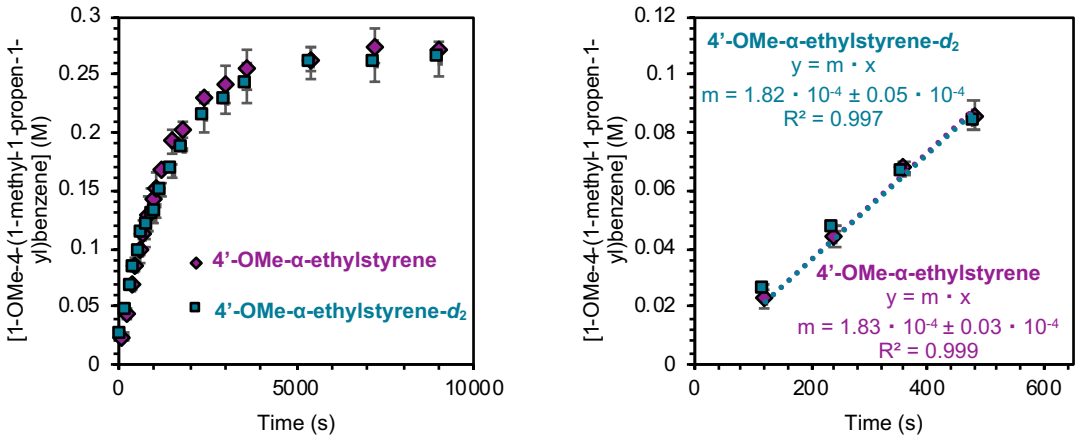

Figure B.21. H/D kinetic isotope effect for 4'-OMe-α-ethylstyrene. Trials were run in duplicate with durene as an internal standard.

B.1.6. NMR and IR Spectra

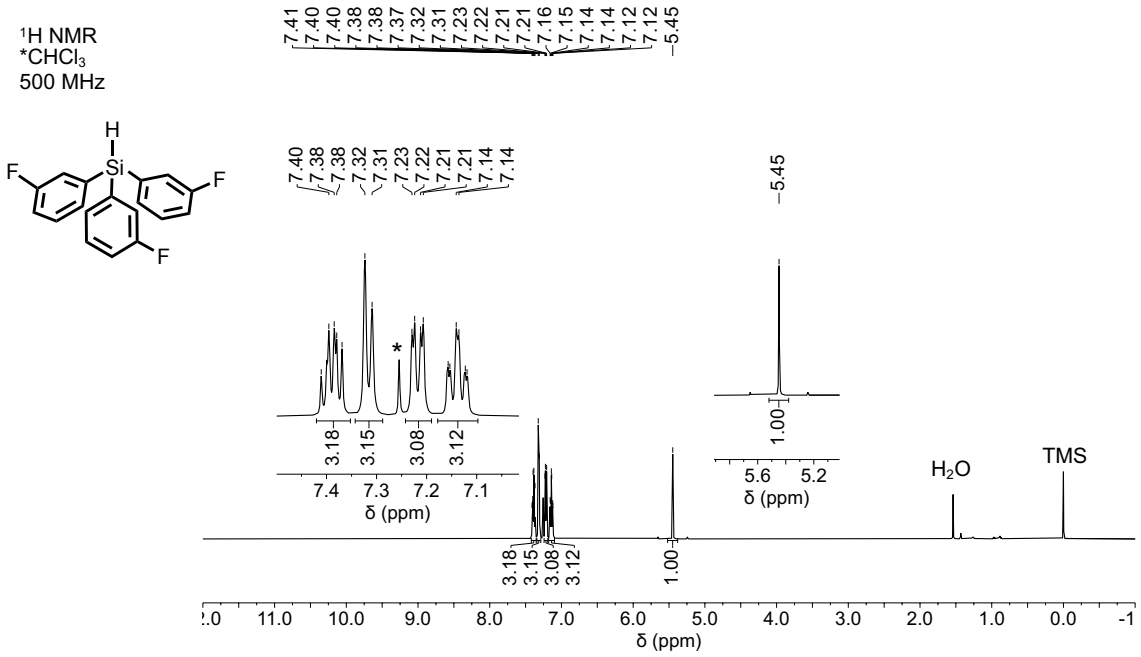

Figure B.22. ^{1}H NMR spectrum of tris(3-fluorophenyl)silane, $HSi(3\text{-}F\text{-}C_6H_4)_3$, recorded in $CDCl_3$ at 298 K.

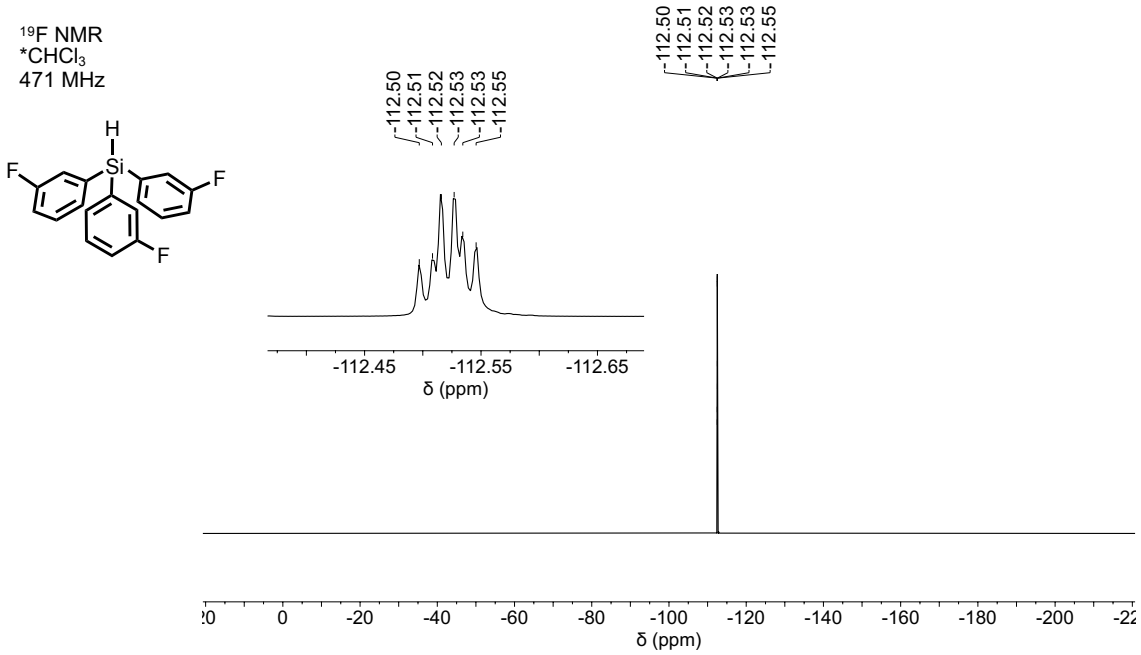

Figure B.23. ^{19}F NMR spectrum of tris(3-fluorophenyl)silane, $HSi(3\text{-}F\text{-}C_6H_4)_3$, recorded in $CDCl_3$ at 298 K.

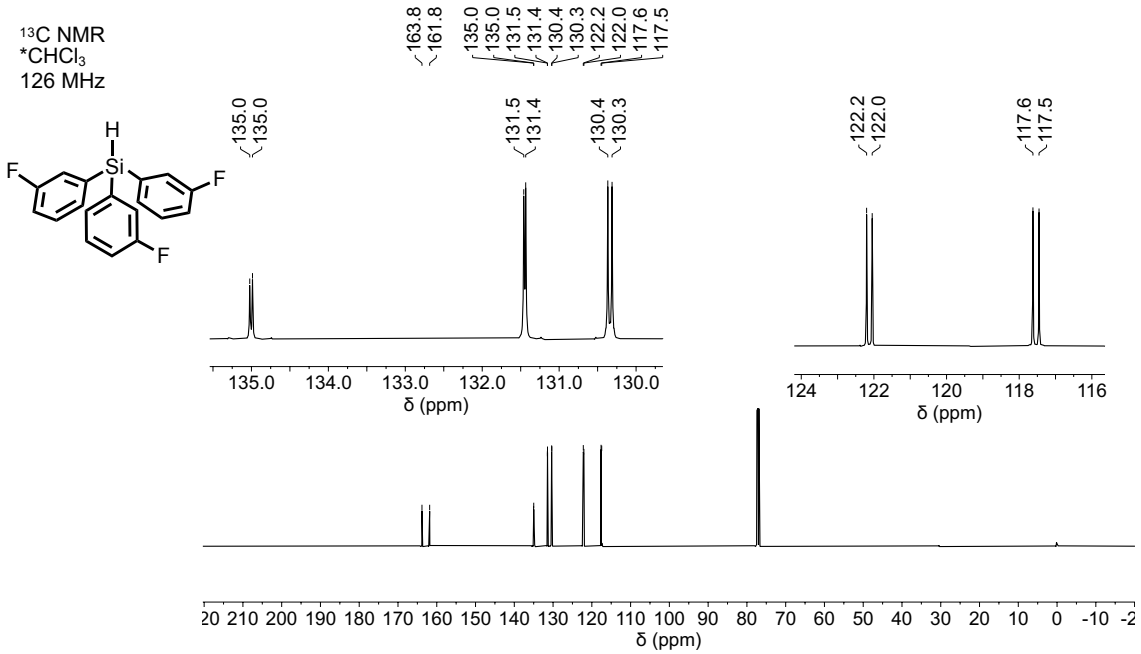

Figure B.24. ^{13}C NMR spectrum of tris(3-fluorophenyl)silane, $HSi(3\text{-}F\text{-}C_6H_4)_3$, recorded in $CDCl_3$ at 298 K.

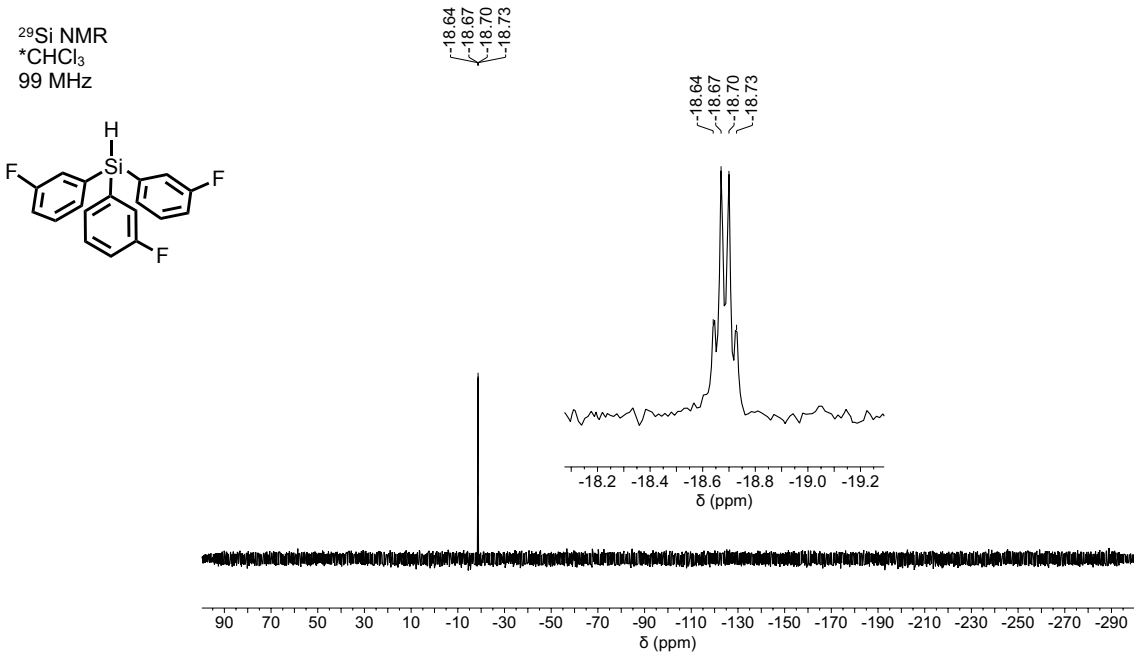

Figure B.25. ^{29}Si NMR spectrum of tris(3-fluorophenyl)silane, $HSi(3\text{-}F\text{-}C_6H_4)_3$, recorded in $CDCl_3$ at 298 K.

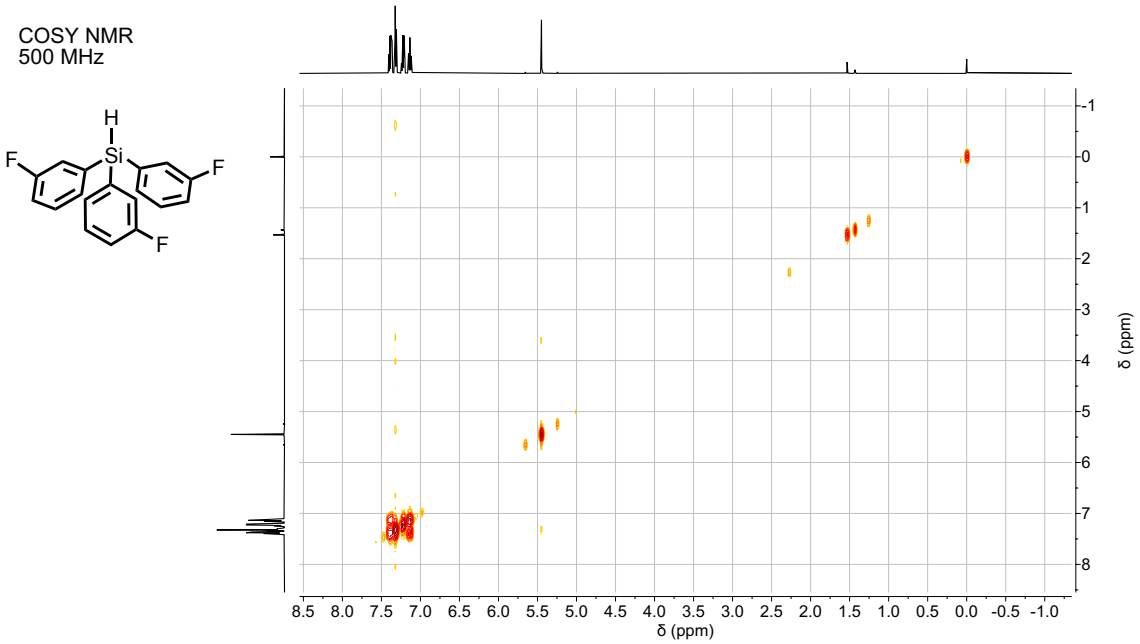

Figure B.26. COSY NMR spectrum of tris(3-fluorophenyl)silane, $HSi(3\text{-}F\text{-}C_6H_4)_3$, recorded in $CDCl_3$ at 298 K.

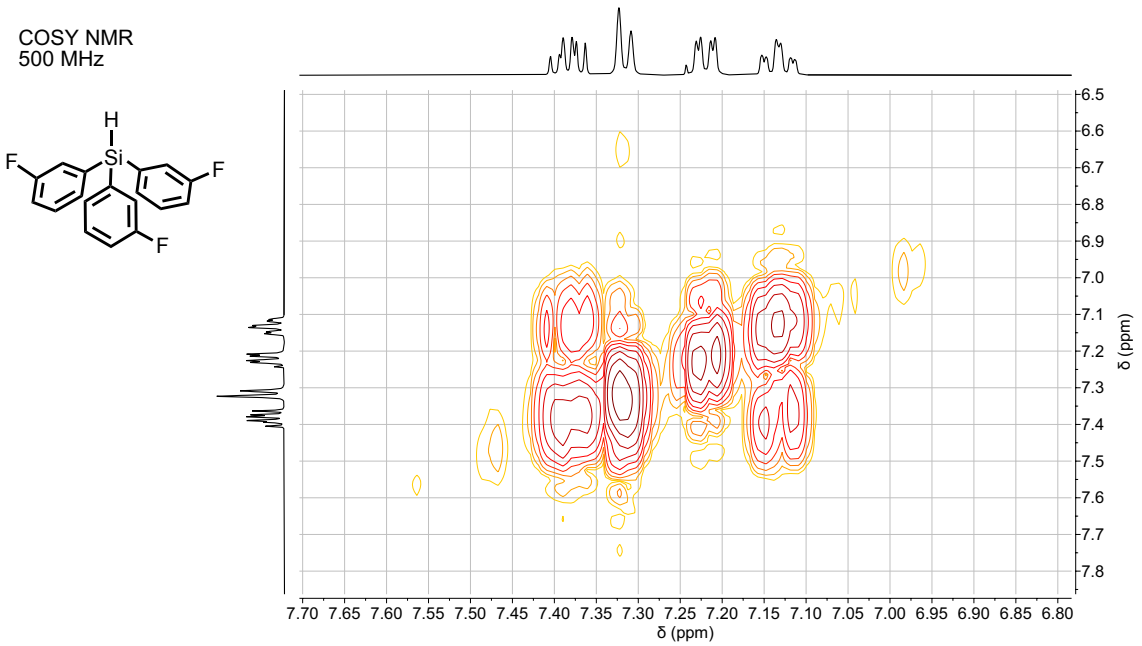

Figure B.27. Aryl region of COSY NMR spectrum of tris(3-fluorophenyl)silane, HSi(3-F-C_6H_4)$_3$, recorded in $CDCl_3$ at 298 K.

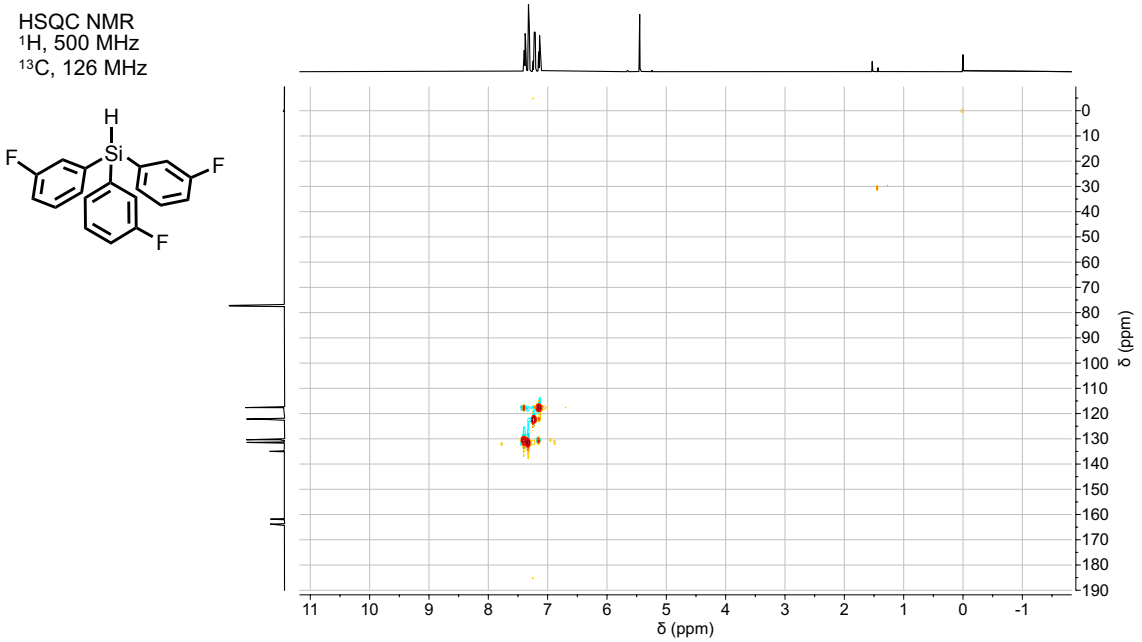

Figure B.28. HSQC NMR spectrum of tris(3-fluorophenyl)silane, HSi(3-F-C_6H_4)$_3$, recorded in $CDCl_3$ at 298 K.

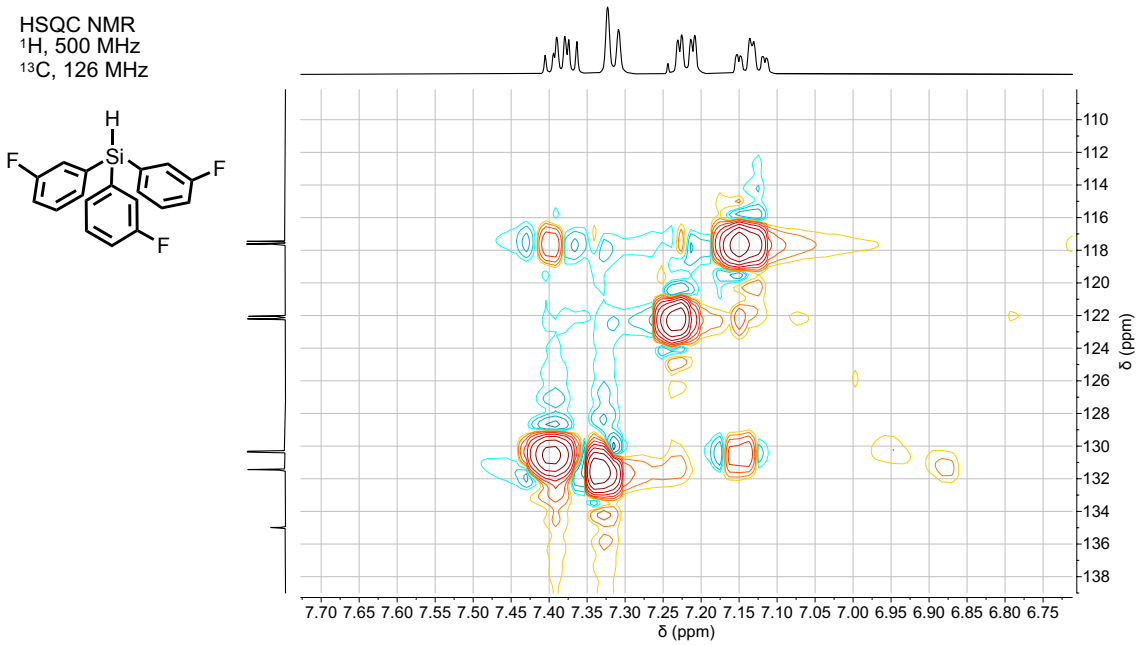

Figure B.29. Aryl region of HSQC NMR spectrum of tris(3-fluorophenyl)silane, $HSi(3\text{-}F\text{-}C_6H_4)_3$, recorded in $CDCl_3$ at 298 K.

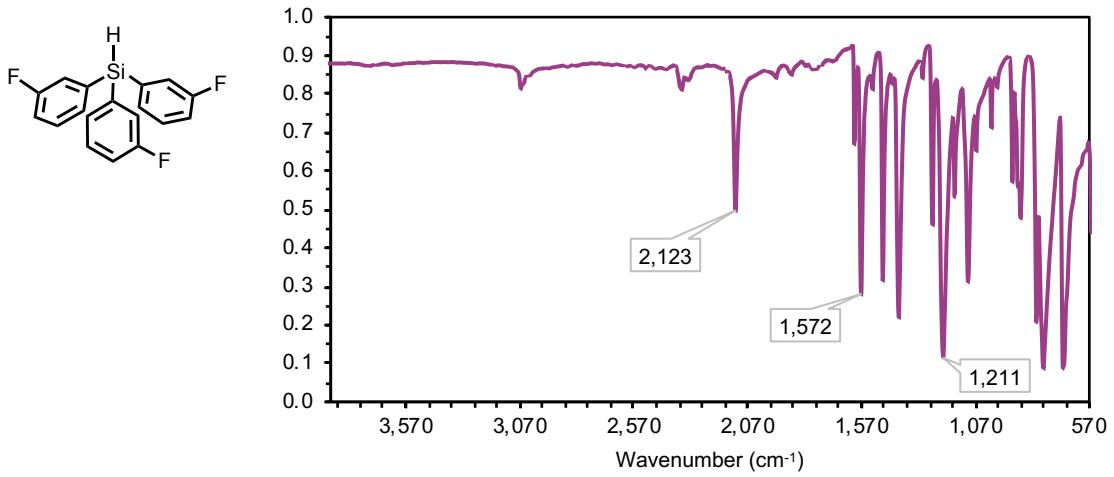

Figure B.30. IR spectrum of tris(3-fluorophenyl)silane, $HSi(3\text{-}F\text{-}C_6H_4)_3$, recorded neat at room temperature.

APPENDIX C

SUPPLEMENTARY CONTENT FOR CHAPTER IV

Experimental details

C.1.1. Materials and Methods

All syntheses and manipulations were carried out under nitrogen using standard Schlenk (vacuum 10^{-2} mbar) techniques or in a nitrogen-filled glovebox unless otherwise indicated. All reagents and solvents were used after drying and stored under nitrogen, unless otherwise indicated. Tetrahydrofuran (THF; Fisher Chemical; HPLC grade, unstabilized), hexanes (Fisher Chemical; HPLC grade), diethyl ether (Et_2O; B&J Brand; HPLC grade, unstabilized), dichloromethane (DCM; Oakwood Chemical; HPLC grade, unstabilized), dimethylformamide (DMF; Alfa Aesar; HPLC grade, unstabilized) and acetonitrile (MeCN; Fisher Chemical; HPLC grade) were dispensed under nitrogen from an LC Technology SP-1 solvent system. Benzene (ACS grade) and pentane (HPLC grade) were refluxed overnight with CaH_2 and distilled under nitrogen before use. The dried solvents were thereafter stored on activated 4Å molecular sieves under nitrogen. C_6D_6 and $CDCl_3$ were purchased from Cambridge Isotope Laboratories, degassed by freeze-pump-thaw, and thereafter stored on activated 4Å molecular sieves under nitrogen. All stock solutions were prepared by mass and were dispensed into reaction vessel by difference from syringe, as detailed in the procedure for each experiment.

C.1.2. General Experimental

Nuclear magnetic resonance (NMR) spectra were collected at room temperature (298 K) unless otherwise stated on a Bruker AV-III HD 600 NMR (600.13 MHz for ^{1}H; 150.90 MHz for ^{13}C; 564.69 MHz for ^{19}F; 119.23 MHz for ^{29}Si; 232.94 MHz for ^{31}P; 92.12 MHz for ^{2}H), Bruker Avance-III HD 500 NMR (499.90 MHz for ^{1}H; 126 MHz for ^{13}C; 471 MHz for ^{19}F; 99 MHz for ^{29}Si; 202.46 MHz for ^{31}P), or Varian Inova 500 NMR (499.90 MHz for ^{1}H; 126 MHz for ^{13}C; 471 MHz for ^{19}F; 99 MHz for ^{29}Si; 202.46 MHz for ^{31}P). ^{1}H and ^{13}C spectra were referenced to the residual solvent peak ($CDCl_3$: ^{1}H δ = 7.26 ppm,

^{13}C δ = 77.16 ppm; C_6D_6: ^{1}H δ = 7.16 ppm, ^{13}C δ = 128.06 ppm). Chemical shifts are reported in parts per million (ppm, δ) relative to tetramethylsilane at 0.00 ppm. Peaks are characterized as follows: s (singlet), d (doublet), t (triplet), q (quartet), pent (pentet), hept (heptet), m (multiplet), br (broad), app (apparent), and/or ms (multiple signals). Coupling constants, *J*, are reported in Hz. Electron paramagnetic resonance (EPR) spectra were collected at 77 K on a Bruker Elexsys E500 EPR X-band spectrometer. Infrared spectroscopy was performed on an Agilent Nicolet 6700 FT-IR, and peaks are reported in cm^{-1}. For catalytic reactions, yields were determined using Gas Chromatography-Mass Spectrometry (GCMS) or Gas Chromatography (GC) against an internal standard. GCMS was carried out on a Shimadzu GC-2010 Plus/GCMS-QP2010 SE using a Restek Rtx®-5 (Crossbond 5% diphenyl – 95% dimethyl polysiloxane; 15 m, 0.25 mm ID, 0.25 μm df) column. GC was carried out on a Thermo Fisher Trace 1300 Gas Chromatograph using a Restek Rtx®-5 (Crossbond 5% diphenyl – 95% dimethyl polysiloxane; 15 m, 0.25 mm ID, 0.25 μm df) column. High-resolution mass spectrometry (HRMS) was carried out on a Waters XEVO G2-XS TOF mass spectrometer.

C.1.3. Synthesis of Non-Commercial Reagents

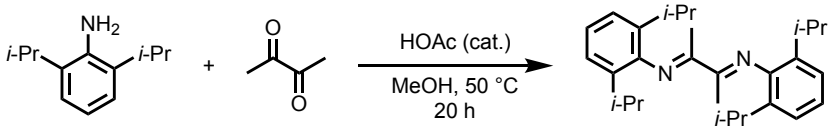

(2.0 equiv) (**S1**)

***N,N'*-Diisopropylphenyl-2,3-butanediimine (S1)** was synthesized via literature procedure:[246] Under ambient conditions, 2,6-diisopropylaniline (4.4 mL, 25 mmol, 2.0 equiv) was dissolved in MeOH (50 mL) in a RBF equipped with a magnetic stir bar. Acetic acid (catalytic) was added. A solution of 2,3-butanedione (1.1 mL, 13 mmol, 1.0 equiv) in MeOH (24 mL) was prepared and added slowly to the aniline solution. Upon addition of the 2,3-butanedione solution, the reaction turned yellow. The reaction was stirred at room temperature for 20 h before being concentrated under reduced pressure to an orange oil. The oil was redissolved in minimal MeOH and placed in the freezer to yield a yellow precipitate. Vacuum filtration was used to isolate the product as a yellow powder (3.21 g, 7.9 mmol, 64% yield). No further purification was required. NMR spectra match values previously reported.[246]

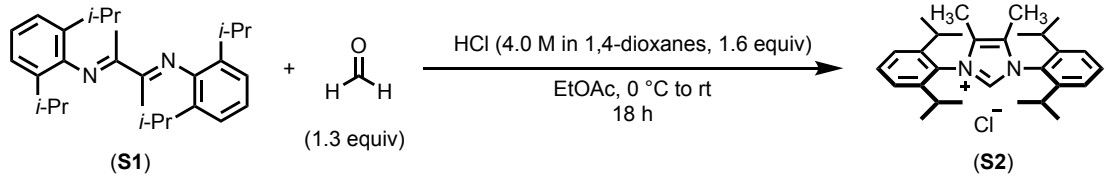

[1,3-Bis(2,6-diisopropylphenyl)-4,5-dimethyl]imidazolium chloride (S2) was synthesized via modified literature procedure:[247] Under ambient conditions, **S1** (0.697 g, 1.7 mmol, 1.0 equiv) was dissolved in EtOAc (4 mL) in a RBF equipped with a magnetic stir bar and the solution was cooled to 0 °C with an ice/water bath. In a scintillation vial, paraformaldehyde (69 mg, 2.2 mmol, 1.3 equiv) was dissolved in HCl (4.0 M in 1,4-dioxanes, 0.68 mL, 2.7 mmol, 1.6 equiv). After 10 min, the paraformaldehyde/HCl solution was added to the solution of **S1** causing the color to change from yellow to red. The reaction allowed to warm to room temperature overnight. Overnight, a precipitate formed, which was collected via vacuum filtration and washed with Et_2O. The beige solid was dissolved in minimal MeOH and layered with Et_2O to yield the product as a white solid collected by vacuum filtration (0.42 g, 0.93 mmol, 54% yield). No further purification was required. NMR spectra match values previously reported.[247]

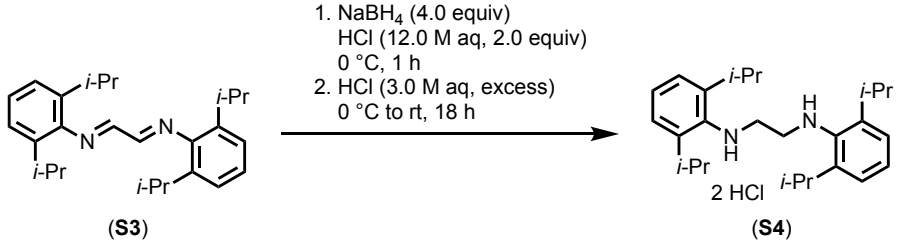

***N,N'*-Bis(2,6-diisopropylphenyl)ethylenediamine dihydrochloride (S4)** was synthesized via literature procedure:[248] Under ambient conditions, (1*E*,2*E*)-1,2-bis(2,6-diisopropylphenylimino)ethane (1.0 g, 2.7 mmol, 1.0 equiv) was dissolved in THF (14 mL) in a RBF equipped with a magnetic stir bar. NaBH4 (0.42 g, 11 mmol, 4.0 equiv) was added to the reaction and the solution was cooled to 0 °C with an ice/water bath. After reaction was cool, HCl (12 M, 0.46 mL, 5.3 mmol, 2.0 equiv) was added dropwise over 20 min. Addition of HCl led to gas formation and the reaction color slowly changed to red, then yellow and finally colorless upon full addition of HCl. The reaction was left to stir at 0 °C for 1 h before HCl (3 M, 6.0 mL, 18 mmol, 6.7 equiv) was added slowly. The resulting

solution was allowed to warm to room temperature and stirred overnight. The white precipitate was collected via vacuum filtration and washed with water, yielding the product as a white solid (1.00 g, 2.2 mmol, 82% yield). No further purification was required. NMR spectra match values previously reported.[248,249]

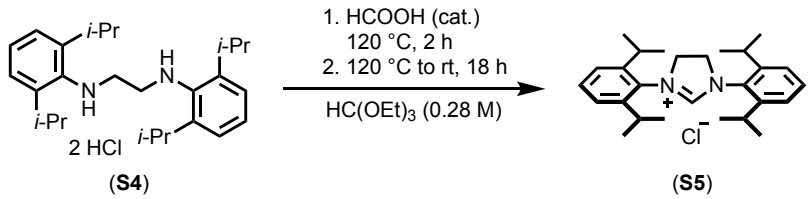

1,3-Bis(2,6-diisopropylphenyl)imidazolium chloride (S5) was synthesized via modified literature procedure:[249] Under ambient conditions, **S4** (0.75 g, 1.7 mmol, 1.0 equiv) was dissolved in triethyl orthoformate (6.0 mL, 36 mmol, 21 equiv) in a RBF equipped with a magnetic stir bar. Four drops of formic acid were added and the RBF was equipped with a distillation arm leading to a second RBF cooled with an ice/water bath (to collect EtOH formed during the course of the reaction). The solution of **S4** in triethyl orthoformate was heated to 120 °C for 2 h and approximately 2.0 mL of EtOH were collected in the distillation receiving RBF. After 2 h, the reaction was allowed to cool to room temperature and stirred overnight. A white precipitate formed and was collected via vacuum filtration and washed with Et_2O. The white solid was collected and carried forward without any further purification (0.70 g, 1.6 mmol, 96% yield). NMR spectra match values previously reported.[248,249]

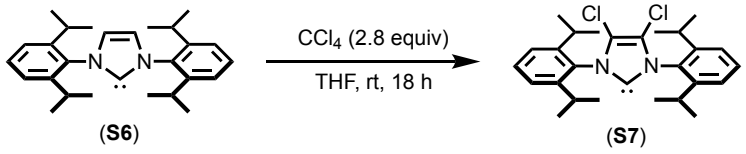

1,3-Bis(2,6-diisopropylphenyl)-4,5-dichloroimidazol-2-ylidene (S7) was synthesized via modified literature procedure:[249] In a Schlenk flask equipped with a magnetic stir bar in a N2-filled glovebox, **S6** (1.0 g, 2.6 mmol, 1.0 equiv) was dissolved in THF (2.0 mL). The flask was sealed and removed from the glovebox. Under Schlenk conditions, CCl_4 (0.7 mL, 7.2 mmol, 2.8 equiv) was added and the reaction was stirred overnight at room temperature. After 18 h, volatiles were removed under reduced pressure to yield the product

as a beige powder (0.94 g, 2.1 mmol, 79% yield). No further purification was required. NMR spectra match values previously reported.

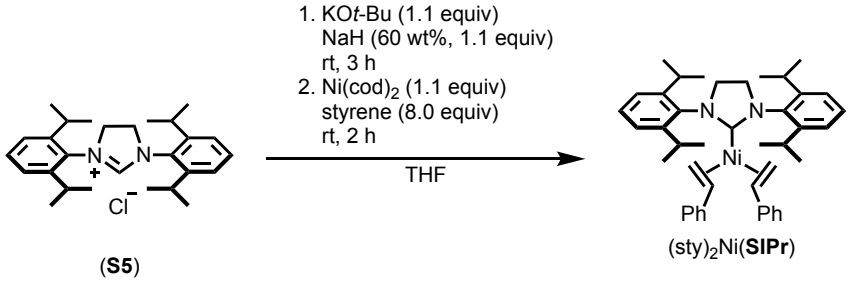

(**S5**) (sty)$_2$Ni(**SIPr**)

(styrene)$_2$Ni(SIPr) was synthesized via modified literature procedure:[136] To a 50 mL RBF equipped with a magnetic stir bar was added **S5** (0.22 g, 0.51 mmol, 1.0 equiv) and THF (12 mL). To this solution, KO*t*-Bu (62 mg, 0.55 mmol, 1.1 equiv) and NaH (60 wt%, 22 mg, 0.55 mmol, 1.1 equiv) were added and the reaction was stirred at room temperature for 3 h before being filtered through Celite to give a light golden solution. A separate solution of Ni(cod)$_2$ (0.15 g, 0.55 mmol, 1.1 equiv) and styrene (0.50 mL, 4.4 mmol, 8.0 equiv) in THF (2 mL). After stirring for 10 min, the Ni(cod)$_2$/styrene solution was added to the filtered solution of deprotonated **S5**. The reaction was stirred at room temperature for 2 h before being concentrated under reduced pressure. The resulting dark green/black goo was redissolved in minimal THF and filtered through Celite. The filtrate was concentrated to a green/yellow solid, which was washed with hexanes to yield the product as a green solid. NMR spectra match values previously reported.

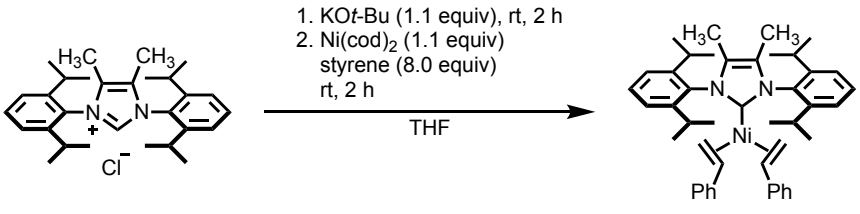

(**S2**) (sty)$_2$Ni(**^{Me}IPr**)

(styrene)$_2$Ni(^{Me}IPr) was synthesized via literature procedure:[136] To a 50 mL RBF equipped with a magnetic stir bar was added **S2** (0.17 g, 0.36 mmol, 1.0 equiv) and THF (10 mL). KO*t*-Bu (43 mg, 0.39 mmol, 1.1 equiv) was added to the solution and the reaction was stirred for 2 h before being filtered through Celite to give a light golden solution. A separate solution of Ni(cod)$_2$ (0.11 g, 0.39 mmol, 1.1 equiv) and styrene (0.40 mL, 3.8

mmol, 8.0 equiv) in THF (2 mL). After stirring for 10 min, the $Ni(cod)_2$/styrene solution was added to the filtered solution of deprotonated **S2**. The reaction was stirred at room temperature for 2 h before being concentrated under reduced pressure. The crude product was taken up in minimal THF and layered with hexanes before being placed in the freezer (-30 °C) overnight. The product was collected as a dark yellow powder via vacuum filtration. NMR spectra match values previously reported.[136]

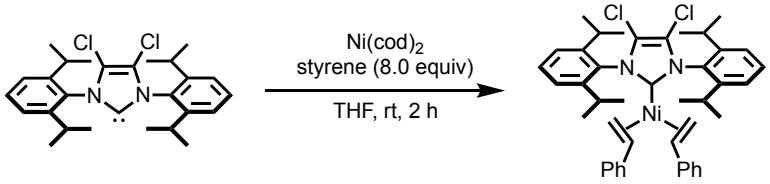

(**S7**) (sty)$_2$Ni(**^{Cl}IPr**)

(styrene)$_2$Ni(^{Cl}IPr) was synthesized via literature procedure:[136] To a 50 mL RBF equipped with a magnetic stir bar was added $Ni(cod)_2$ (0.15 g, 0.55 mmol, 1.0 equiv), styrene (0.5 mL, 4.4 mmol, 8.0 equiv) and THF (1 mL). A separate solution of **S7** (0.25 g, 0.55 mmol, 1.0 equiv) in THF (9 mL) was prepared. After stirring for 20 min, the deprotonated solution of **S7** was added to the $Ni(cod)_2$/styrene solution and the reaction was stirred at room temperature for 2 h. After 2 h, the reaction was dried under reduced pressure and the resulting crude product was taken up in minimal THF and layered with hexanes. After cooling to -30 °C overnight, the reaction was filtered over a glass frit to collect the precipitate, yield the product as an orange powder. NMR spectra match values previously reported.[136]

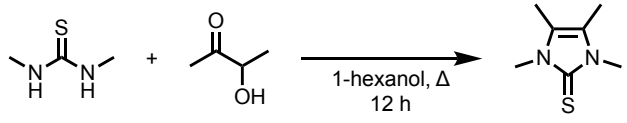

(**S8**)

1,3,4,5-tetramethylimidazole-2(3H)-thione (S8) was synthesized via literature procedure:[250] To a 250 mL Schlenk flask equipped with a magnetic stir bar was added *N,N'*-dimethylthiourea (4.17 g, 40.0 mmol, 1.0 equiv), acetoin (3.52 g, 40.0 mmol, 1.0 equiv) and 1-hexanol (100 mL). The reaction was heated to reflux for 12 h. After cooling the reaction to room temperature, the reaction mixture was concentrated before being

opened to air and washed with water (50 mL) and Et_2O (50 mL). The suspension was filtered through a glass frit to collect the product as an off white powder (3.86 g, 24.7 mmol, 62% yield). NMR spectra match values previously reported.[250]

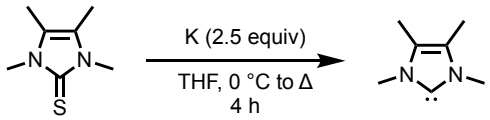

(**S8**) (**ITMe**)

1,3,4,5-tetramethylimidazol-2-ylidene (ITMe) was synthesized via literature procedure:[250] To a 100 mL Schlenk flask equipped with a magnetic stir bar was added **S8** (1.17 g, 7.5 mmol, 1.0 equiv) and THF (45 mL). The reaction was cooled to 0 °C before potassium chunks (0.73 g, 18.8 mmol, 2.5 equiv) were added. The reaction was warmed to room temperature and then heated to reflux for 4 h. After 4 h, the reaction was cooled to room temperature, filtered over a glass frit under air-free conditions, and the filtrate was concentrated to yield **ITMe** as a white powder (0.81 g, 6.4 mmol, 85% yield). NMR spectra match values previously reported.[250]

C.1.4. Complex Screening

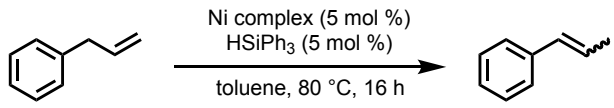

In a nitrogen-filled glovebox, stock solutions of the reagents (see **Table C.1.** for stock solution information) were prepared by weighing out the Ni complex into volumetric flasks and diluting with toluene to the appropriate volume. Disposable 1-mL syringes were used to distribute Ni stock solutions (0.20 mL, 0.004 mmol, 0.05 equiv) and a 250-µL microliter syringe was used to distribute $HSiPh_3$/durene stock solutions ($HSiPh_3$: 50 µL, 0.004 mmol, 0.05 equiv; durene: 50 µL, ~0.023 mmol, ~0.25 equiv) to 1-dram scintillation vials equipped with magnetic stir bars. The vials were sealed with septum caps, removed from the glovebox and heated for 30 min on a pre-heated aluminum vial block at 80 °C before allylbenzene (11 µL, 0.083 mmol, 1.0 equiv) was distributed with a 25-µL microliter syringe. The reactions were heated and stirred for 16 h before being quenched by cooling in a liquid N2 bath and opening to air. An aliquot was removed and filtered with hexanes

to assess the progress and selectivity of the reaction. Results from the screening of Ni complexes are summarized below in **Table C.2.**

Table C.1. Stock solutions used in the screening of Ni complexes for the isomerization of allylbenzene.

Entry	Reagent	Volume of flask	Mass of reagent added	[reagent]	Volume distributed
1	(styrene)$_2$Ni(^{Me}IPr)	1.0 mL	13.8 mg	0.020 M	0.20 mL
	$HSiPh_3$	5.0 mL	102.8 mg	0.079 M	50 µL
	Durene	5.0 mL	305.0 mg	0.45 M	50 µL
2	(styrene)$_2$Ni(SIPr)	1.0 mL	13.2 mg	0.020 M	0.20 mL
	$HSiPh_3$	5.0 mL	103.4 mg	0.079 M	50 µL
	Durene	5.0 mL	308.1 mg	0.46 M	50 µL
3	(styrene)$_2$Ni(IPr)	2.0 mL	26.2 mg	0.020 M	0.20 mL
	$HSiPh_3$	5.0 mL	103.4 mg	0.079 M	50 µL
	Durene	5.0 mL	308.1 mg	0.46 M	50 µL
4	(styrene)$_2$Ni(^{Cl}IPr)	1.0 mL	14.7 mg	0.020 M	0.20 mL
	$HSiPh_3$	5.0 mL	103.4 mg	0.079 M	50 µL
	Durene	5.0 mL	308.1 mg	0.46 M	50 µL

Table C.2. Results of Ni complex screening.

Entry	Ni complex	Trial	% conversion	*E/Z* ratio
1	(sty)$_2$Ni(SIPr)	1	95	8 : 1
2	(sty)$_2$Ni(SIPr)	2	92	8 : 1
		Average:	94 ± 2	7 ± 1 : 1
3	(sty)$_2$Ni(IPr)	1	99	21 : 1
4	(sty)$_2$Ni(IPr)	2	99	21 : 1
		Average:	99 ± 0	21 ± 1 : 1
5	(sty)$_2$Ni(^{Cl}IPr)	1	98	21 : 1
6	(sty)$_2$Ni(^{Cl}IPr)	2	98	21 : 1
		Average:	98 ± 0	21 ± 0 : 1
7	(sty)$_2$Ni(^{Me}IPr)	1	98	21 : 1
8	(sty)$_2$Ni(^{Me}IPr)	2	98	20 : 1
		Average:	98 ± 0	21 ± 1 : 1

C.1.5. Kinetic Studies

a. Monitoring the isomerization of allylbenzene at 80 °C: Varying the NHC

In a nitrogen-filled glovebox, Ni complexes were weighed directly into 1-dram vials equipped with magnetic stir bars ((sty)$_2$Ni(IPr): 8.3 mg, 0.013 mmol, 0.05 equiv; (sty)$_2$Ni(^{Cl}IPr): 9.7 mg, 0.013 mmol, 0.05 equiv; (sty)$_2$Ni(^{Me}IPr): 8.6 mg, 0.013 mmol, 0.05

equiv). A stock solution for $HSiPh_3$ (0.087 M) and durene (0.45 M) was prepared by weighing out the reagents and dissolving in the appropriate volume of toluene. The silane/durene stock solution was distributed (150 µL) with a 250-µL microliter syringe. Additional toluene (0.60 mL) was added to each vial with a 1-mL disposable syringe. Vials were sealed with septum caps, removed from the glovebox and placed on a pre-heated aluminum vial block at 80 °C. After 30 min of heating, allylbenzene (33 µL, 0.25 mmol, 1.0 equiv) was added to each vial in two portions using a 25-µL microliter syringe. Throughout the course of the reaction, 5 µL aliquots were removed and filtered through Celite with hexanes. The filtrate was analyzed by GC-FID to assess the progress and selectivity of the reaction. The product concentration was determined by relative integration (by GC) of the product peaks against durene, in accordance with calibration curves prepared independently using the commercial compounds.

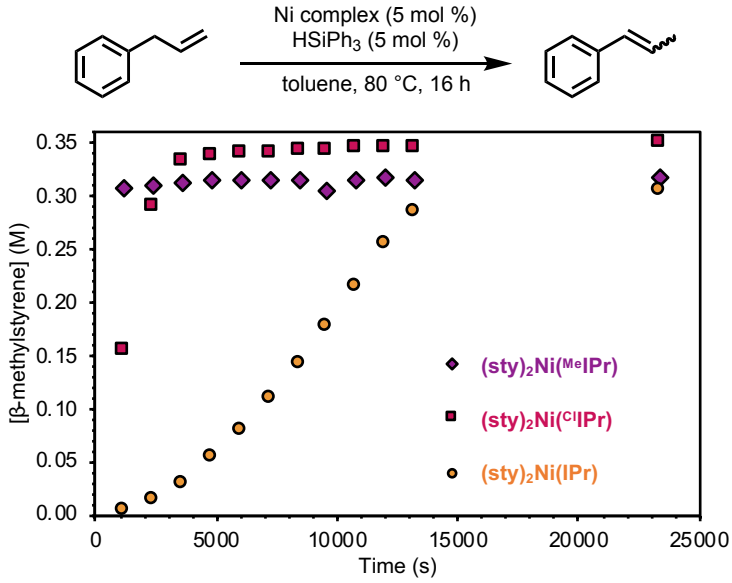

Figure C.1. Isomerization of allylbenzene to compare the reactivity of different Ni complexes with modified NHC ligands at 80 °C. Product concentration was calculated vs durene as an internal standard.

Table C.3. Formation of β-methylstyrene over time at 80 °C.

Ni complex	Time (s)	[β-methylstyrene] (M)	*E*	:	*Z*
$(sty)_2Ni(^{Me}IPr)$	1200	0.31	25	:	1
	2400	0.31	23	:	1
	3600	0.31	22	:	1

	4800	0.31	22 : 1
	6000	0.32	22 : 1
	7200	0.31	22 : 1
	8400	0.32	22 : 1
	9600	0.31	22 : 1
	10800	0.32	21 : 1
	12000	0.32	21 : 1
	13200	0.32	21 : 1
	23400	0.32	21 : 1
$(sty)_2Ni(^{Cl}IPr)$	1200	0.15	25 : 1
	2400	0.29	24 : 1
	3600	0.33	24 : 1
	4800	0.34	23 : 1
	6000	0.34	22 : 1
	7200	0.34	22 : 1
	8400	0.34	22 : 1
	9600	0.34	21 : 1
	10800	0.34	21 : 1
	12000	0.35	21 : 1
	13200	0.35	21 : 1
	23400	0.35	21 : 1
$(sty)_2Ni(IPr)$	1200	0.0038	1 : 0
	2400	0.015	26 : 1
	3600	0.030	29 : 1
	4800	0.053	32 : 1
	6000	0.080	33 : 1
	7200	0.11	34 : 1
	8400	0.14	33 : 1
	9600	0.18	33 : 1
	10800	0.21	32 : 1
	12000	0.25	30 : 1
	13200	0.29	27 : 1
	23400	0.31	21 : 1

b. Monitoring the isomerization of allylbenzene at 70 °C: Varying the NHC

In a nitrogen-filled glovebox, Ni complexes were weighed directly into 1-dram vials equipped with magnetic stir bars ($(sty)_2Ni(IPr)$: 8.5 mg, 0.013 mmol, 0.05 equiv; $(sty)_2Ni(^{Cl}IPr)$: 9.1 mg, 0.013 mmol, 0.05 equiv; $(sty)_2Ni(^{Me}IPr)$: 8.6 mg, 0.013 mmol, 0.05

equiv). A stock solution for $HSiPh_3$ (0.087 M) and durene (0.45 M) was prepared by weighing out the reagents and dissolving in the appropriate volume of toluene. The silane/durene stock solution was distributed (150 µL) with a 250-µL microliter syringe. Additional toluene (0.60 mL) was added to each vial with a 1-mL disposable syringe. Vials were sealed with septum caps, removed from the glovebox and placed on a pre-heated aluminum vial block at 80 °C. After 30 min of heating, allylbenzene (33 µL, 0.25 mmol, 1.0 equiv) was added to each vial in two portions using a 25-µL microliter syringe. Throughout the course of the reaction, 5 µL aliquots were removed and filtered through Celite with hexanes. The filtrate was analyzed by GC-FID to assess the progress and selectivity of the reaction. The product concentration was determined by relative integration (by GC) of the product peaks against durene, in accordance with calibration curves prepared independently using the commercial compounds.

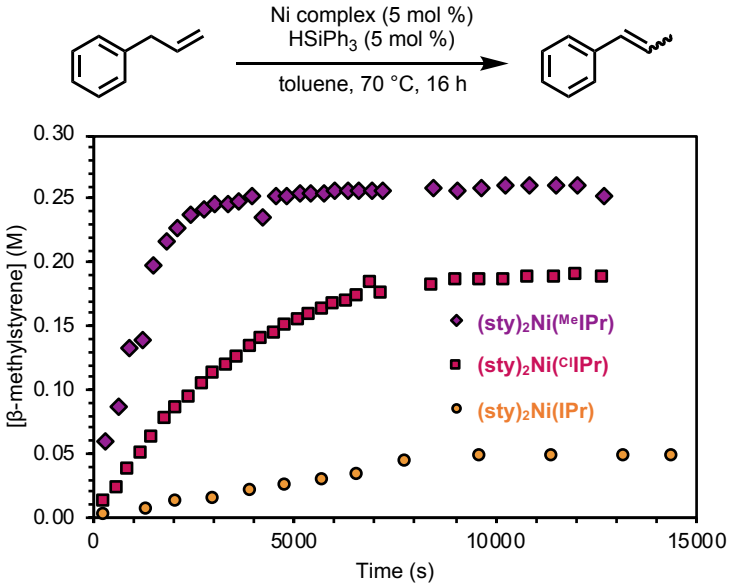

Figure C.2. Isomerization of allylbenzene to compare the reactivity of different Ni complexes with modified NHC ligands at 70 °C. Product concentration was calculated vs durene as an internal standard.

Table C.4. Formation of β-methylstyrene over time at 70 °C.

Ni complex	Time (s)	[β-methylstyrene] (M)	*E* : *Z*
$(sty)_2Ni(^{Me}IPr)$	300	0.060	34 : 1
	600	0.087	32 : 1
	900	0.13	33 : 1
	1200	0.14	28 : 1

	1500	0.20	34 : 1
	1800	0.22	33 : 1
	2100	0.23	33 : 1
	2400	0.24	32 : 1
	2700	0.24	32 : 1
	3000	0.25	32 : 1
	3300	0.25	32 : 1
	3600	0.25	31 : 1
	3900	0.25	31 : 1
	4200	0.24	30 : 1
	4500	0.25	31 : 1
	4800	0.25	31 : 1
	5100	0.26	30 : 1
	5400	0.26	30 : 1
	5700	0.26	30 : 1
	6000	0.26	30 : 1
	6300	0.26	30 : 1
	6600	0.26	30 : 1
	6900	0.26	30 : 1
	7200	0.26	30 : 1
	8400	0.26	29 : 1
	9000	0.26	29 : 1
	9600	0.26	29 : 1
	10200	0.26	29 : 1
	10800	0.26	29 : 1
	11460	0.26	29 : 1
	12000	0.26	28 : 1
	12660	0.25	28 : 1
$(sty)_2Ni(^{Cl}IPr)$	300	0.013	19 : 1
	600	0.0223	20 : 1
	900	0.038	21 : 1
	1200	0.051	21 : 1
	1500	0.063	22 : 1
	1800	0.077	22 : 1
	2100	0.085	22 : 1
	2400	0.095	22 : 1
	2700	0.10	22 : 1
	3000	0.11	22 : 1
	3300	0.12	23 : 1

	3600	0.13	23 : 1
	3900	0.13	23 : 1
	4200	0.14	24 : 1
	4500	0.15	24 : 1
	4800	0.15	24 : 1
	5100	0.15	24 : 1
	5400	0.16	25 : 1
	5700	0.16	25 : 1
	6000	0.17	25 : 1
	6300	0.17	25 : 1
	6600	0.17	25 : 1
	6900	0.18	26 : 1
	7200	0.18	25 : 1
	8400	0.18	26 : 1
	9000	0.19	26 : 1
	9600	0.19	26 : 1
	10200	0.19	26 : 1
	10800	0.19	26 : 1
	11460	0.19	26 : 1
	12000	0.19	26 : 1
	12660	0.19	26 : 1
$(sty)_2Ni(IPr)$	300	0.0017	1 : 1
	1320	0.0067	23 : 1
	2100	0.012	24 : 1
	3000	0.014	22 : 1
	3900	0.021	26 : 1
	4800	0.026	27 : 1
	5700	0.030	28 : 1
	6600	0.034	27 : 1
	7800	0.043	28 : 1
	9600	0.047	28 : 1
	11400	0.047	29 : 1
	13200	0.047	28 : 1
	14400	0.047	28 : 1

c. Monitoring the isomerization of allylbenzene at 70 °C: Varying the alkene

In a nitrogen-filled glovebox, Ni complexes were weighed directly into 1-dram vials equipped with magnetic stir bars. A stock solution of $HSiPh_3$ (0.015 M) and durene

(0.066 M) was prepared by weighing out the reagents and dissolving in the appropriate volume of hexanes. The silane/durene stock solution was distributed (0.80 mL) with a 1-mL disposable syringe. Vials were sealed with septum caps, removed from the glovebox and placed on a pre-heated aluminum vial block at 80 °C. After 30 min of heating, allylbenzene (33 µL, 0.25 mmol, 1.0 equiv) was added to each vial in two portions using a 25-µL microliter syringe. Throughout the course of the reaction, 5 µL aliquots were removed and filtered through Celite with hexanes. The filtrate was analyzed by GC-FID to assess the progress and selectivity of the reaction. The product concentration was determined by relative integration (by GC) of the product peaks against durene, in accordance with calibration curves prepared independently using the commercial compounds.

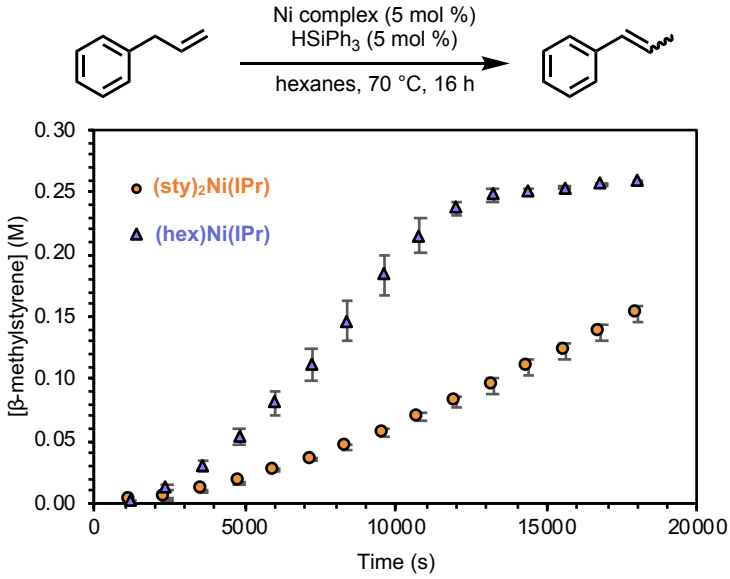

Figure C.3. Comparing the influence of stabilizing alkene ligands on catalyst activity. Trials were run in duplicate with durene as an internal standard.

Table C.5. Formation of β-methylstyrene over time at 70 °C.

Ni complex	Time (s)	[β-methylstyrene] (M)	*E* : *Z*
$(sty)_2Ni(IPr)$	1200	0.0021 ± 0.0001	25 : 1
	2400	0.0051 ± 0.0000	1 : 0
	3600	0.011 ± 0.000	33 : 1
	4800	0.018 ± 0.001	37 : 1
	6000	0.026 ± 0.001	40 : 1
	7200	0.035 ± 0.002	40 : 1

	8400	0.046	±	0.002	40	:	1
	9600	0.057	±	0.003	40	:	1
	10800	0.069	±	0.004	40	:	1
	12000	0.082	±	0.005	40	:	1
	13200	0.094	±	0.006	40	:	1
	14400	0.11	±	0.006	39	:	1
	15600	0.12	±	0.006	39	:	1
	16800	0.14	±	0.007	39	:	1
	18000	0.15	±	0.007	37	:	1
	1200	0.0030	±	0.0004	1	:	0
	2400	0.013	±	0.002	33	:	1
	3600	0.031	±	0.004	38	:	1
	4800	0.053	±	0.007	41	:	1
	6000	0.08	±	0.01	41	:	1
	7200	0.11	±	0.01	40	:	1
	8400	0.15	±	0.02	38	:	1
(hex)Ni(IPr)	9600	0.18	±	0.02	37	:	1
	10800	0.22	±	0.01	33	:	1
	12000	0.24	±	0.01	30	:	1
	13200	0.25	±	0.00	27	:	1
	14400	0.25	±	0.00	26	:	1
	15600	0.25	±	0.00	25	:	1
	16800	0.26	±	0.00	24	:	1
	18000	0.26	±	0.00	23	:	1

C.1.6. Development of an in situ catalyst formation approach

a. Screening free NHC ligands

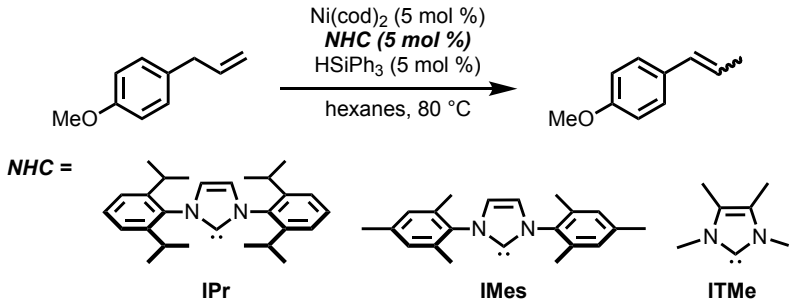

In a nitrogen-filled glovebox, $Ni(cod)_2$ (5.2 mg, 0.019 mmol, 0.06 equiv) and NHC (see **Table C.6.**) were weighed directly into 1-dram vials. Magnetic stir bars were added to each vial. A stock solution of $HSiPh_3$ (0.18 M) and durene (0.74 M) was prepared by

weighing the reagents into a 1-mL volumetric flask and adding the appropriate volume of hexanes. The stock solution (0.1 mL, $HSiPh_3$: 0.018 mmol, 0.06 equiv; durene: 0.074 mmol, 0.22 equiv) was distributed to each vial. An addition 1.1 mL of hexanes was added to each vial. The vials were sealed with septum caps and removed from the glovebox. 4-Allylanisole (50 µL, 0.33 mmol, 1.0 equiv) was added to each vial using a 100-µL microliter syringe. Throughout the course of the reaction, 5 µL aliquots were removed and filtered through Celite with hexanes. The filtrate was analyzed by GC-FID to assess the progress and selectivity of the reaction.

Table C.6. Reagents and amounts used for the screening of NHC ligands.

NHC ligand	Amount added	mmol added
IMes	5.6 mg	0.018 mmol
IPr	7.0 mg	0.018 mmol
ITMe	2.5 mg	0.020 mmol

Table C.7. Formation of 4-OMe-β-methylstyrene over time at 80 °C.

NHC ligand	Time (h)	Conversion
IMes	3	44 ± 8
	6	64 ± 15
	19	89 ± 7
IPr	3	96 ± 1
	6	97 ± 0
	19	96 ± 0
ITMe	3	3 ± 0
	6	3 ± 1
	19	3 ± 1

b. Determining effect of silane modification

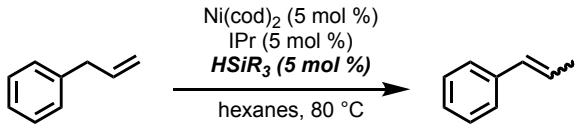

In a nitrogen-filled glovebox, $Ni(cod)_2$ (5.2 mg, 0.019 mmol, 0.05 equiv) and IPr (7.0 mg, 0.018 mmol, 0.06 equiv) were weighed into 1-dram vials. Stock solutions of $HSi(4\text{-}CF_3\text{-}C_6H_4)_3$ (0.048 M), $HSi(4\text{-}OMe\text{-}C_6H_4)_3$ (0.046 M), $HSiPh_3$ (0.046 M) and

durene (0.25 M) were prepared using volumetric flasks by weighing out the reagents and adding the appropriate volume of hexanes. Magnetic stir bars were added to each vial. Durene stock solution (0.30 mL, 0.075 mmol, 0.21 equiv) was distributed to each vial using a 1-mL disposable syringe. Silane stock solutions (0.40 mL, 0.018 mmol, 0.05 equiv) were distributed using a 1-mL disposable syringe. Hexanes (0.40 mL) was added to each vial using a 1-mL disposable syringe. Vials were sealed with septum caps and removed from the glovebox. Allylbenzene (48 μL, 0.36 mmol, 1.0 equiv) was distributed using a 100-μL microliter syringe and vials were placed on a vial block preheated to 80 °C. Throughout the course of the reaction, 5 μL aliquots were removed and filtered through Celite with hexanes. The filtrate was analyzed by GC-FID to assess the progress and selectivity of the reaction.

Table C.8. Formation of β-methylstyrene over time at 80 °C.

Silane	Time (s)	Conversion
$HSi(4\text{-}CF_3\text{-}C_6H_4)_3$	360	14 ± 1
	720	27 ± 1
	1080	35 ± 1
	1440	42 ± 1
	1800	47 ± 1
	3600	62 ± 0
	5400	70 ± 0
	7200	75 ± 0
	10800	80 ± 0
$HSiPh_3$	360	3 ± 0
	720	9 ± 1
	1080	17 ± 2
	1440	26 ± 3
	1800	37 ± 4
	3600	98 ± 1
	5400	99 ± 0
	7200	99 ± 0
	10800	99 ± 0
$HSi(4\text{-}OMe\text{-}C_6H_4)_3$	360	4 ± 0
	720	8 ± 1
	1080	13 ± 1
	1440	18 ± 1
	3600	68 ± 4
	5400	99 ± 0
	7200	98 ± 0

10800	99 ± 0	

c. NMR monitoring to observe resting state

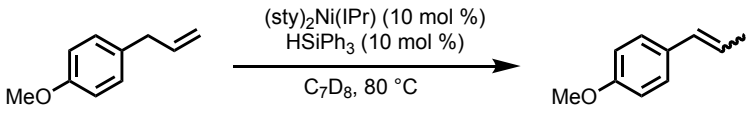

In a nitrogen-filled glovebox, $(sty)_2Ni(IPr)$ (16.2 mg, 0.025 mmol, 0.10 equiv) was weighed into a 1-dram vial. In a 1.0 mL volumetric flask was weighed $HSiPh_3$ (7.8 mg, 0.030 mmol, 0.030 M), durene (18.5 mg, 0.14 mmol, 0.14 M) and 4-allylanisole (45 mg, 0.30 mmol, 0.30 M) and the appropriate volume of C_7D_8 was added. To the weighed out $(sty)_2Ni(IPr)$ was added 0.83 mL of the stock solution ($HSiPh_3$: 0.025 mmol, 0.10 equiv; durene: 0.12 mmol, 0.46 equiv; 4-allylanisole: 0.25 mmol, 1.0 equiv). The solution was shaken until homogeneous and then transferred to a J-young NMR tube with a disposable pipet. The NMR tube was sealed and removed from the glovebox. A room temperature spectrum was recorded, and the sample was removed from the NMR. The instrument was warmed to 80 °C and allowed the sample was re-inserted into the instrument. 1H NMR spectra were recorded periodically up to 806 min. Select spectra are shown in **Figure C.4.** below.

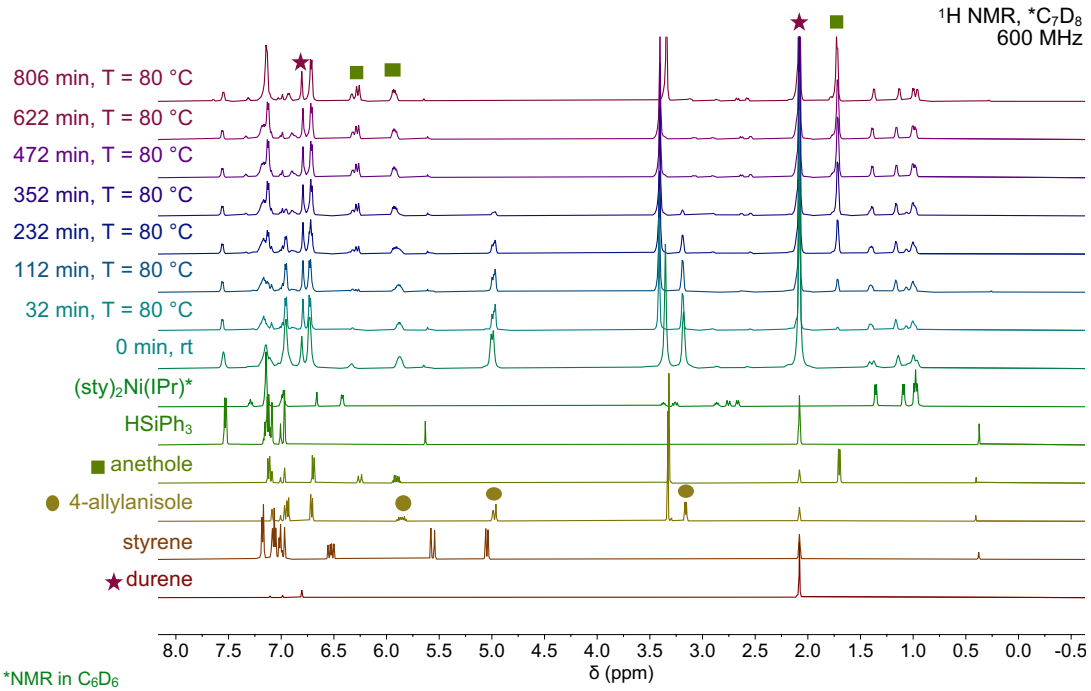

Figure C.4. ^{1}H NMR monitoring of the isomerization of 4-allylanisole with isolated $(sty)_2Ni(IPr)$.

C.1.7. NMR and IR Spectra

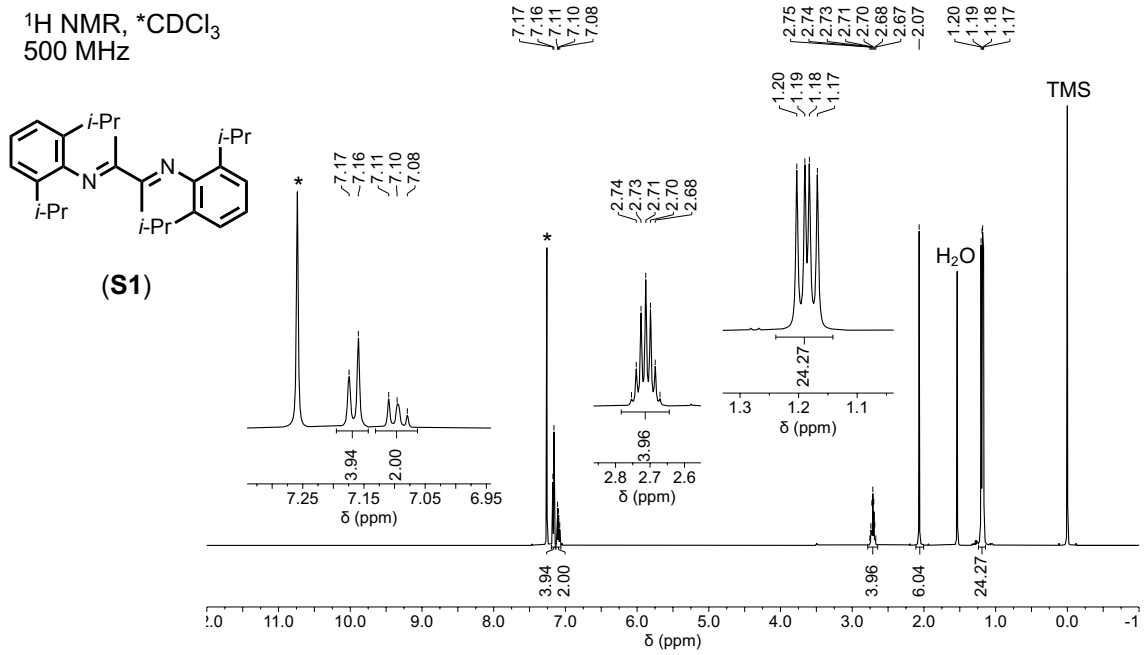

Figure C.5. ^{1}H NMR spectrum of *N,N'*-diisopropylphenyl-2,3-butanediimine (**S1**) recorded in $CDCl_3$ at 298 K.

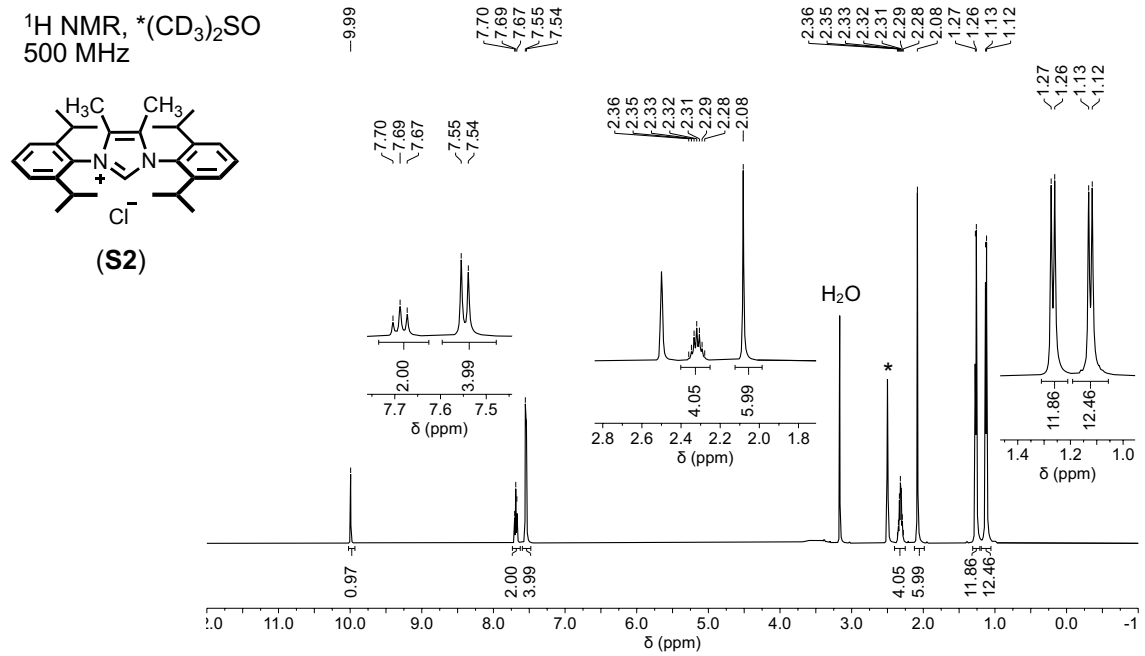

Figure C.6. ^{1}H NMR spectrum of [1,3-bis(2,6-diisopropylphenyl)-4,5-dimethyl]imidazolium chloride (**S2**) recorded in $(CD_3)_2SO$ at 298 K.

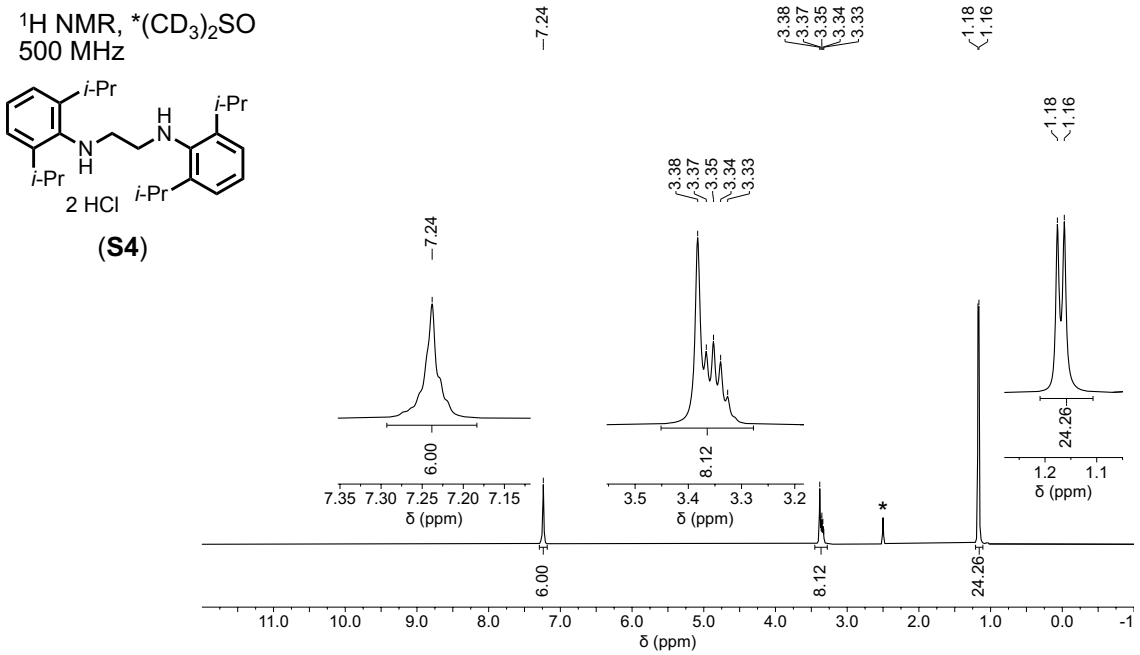

Figure C.7. ^{1}H NMR spectrum of *N,N'*-bis(2,6-diisopropylphenyl)ethylenediamine dihydrochloride (**S4**) recorded in $(CD_3)_2SO$ at 298 K.

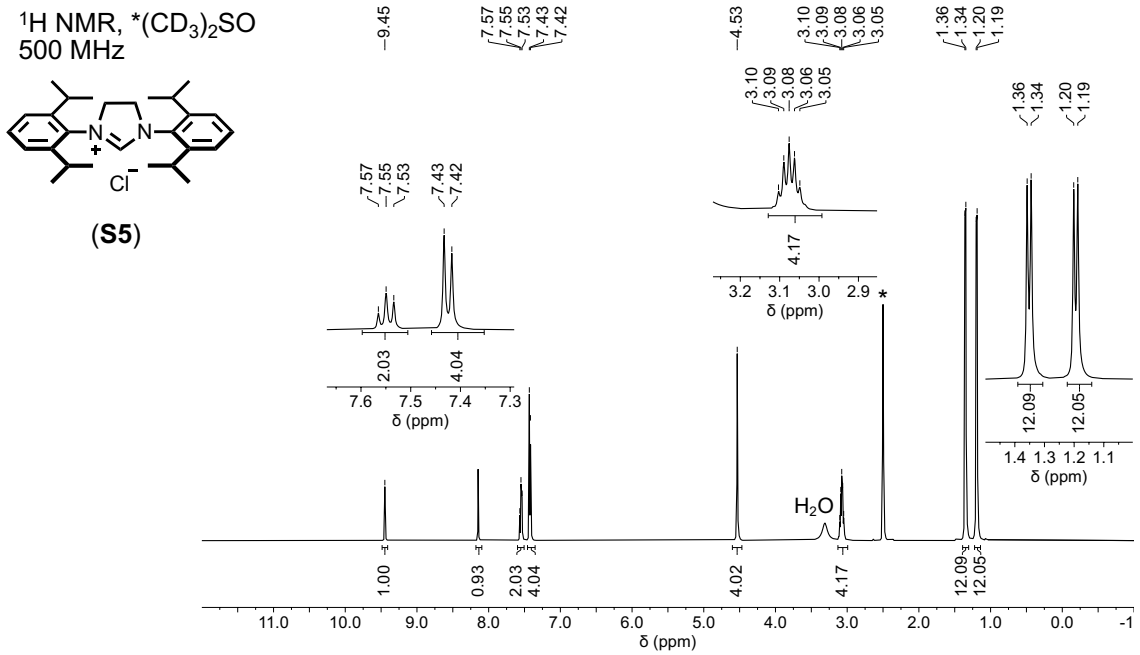

Figure C.8. ^{1}H NMR spectrum of 1,3-bis(2,6-diisopropylphenyl)imidazolium chloride (**S5**) recorded in $(CD_3)_2SO$ at 298 K.

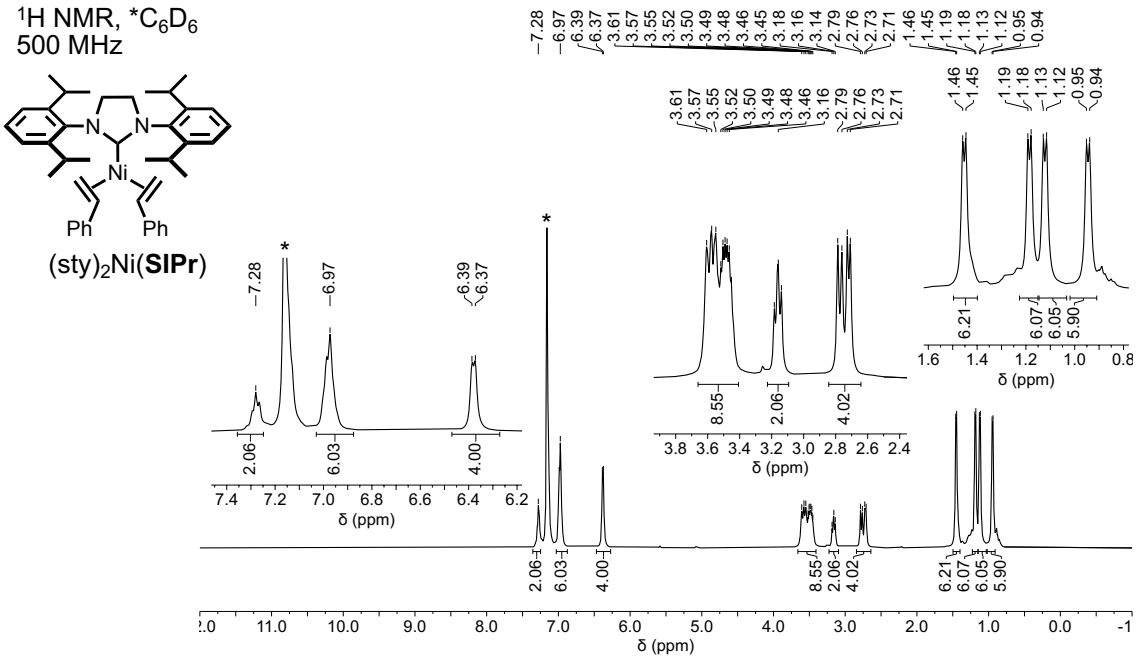

Figure C.9. ^{1}H NMR spectrum of (sty)$_2$Ni(**SIPr**) recorded in C_6D_6 at 298 K.

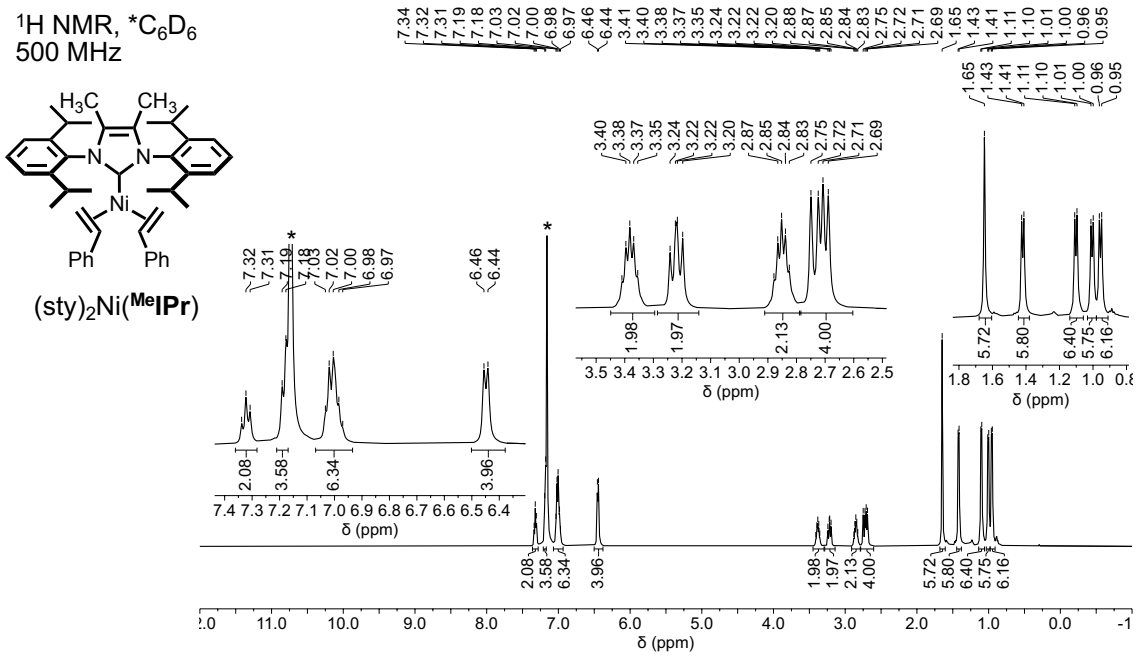

Figure C.10. ^{1}H NMR spectrum of (sty)$_2$Ni(**^{Me}IPr**) recorded in C_6D_6 at 298 K.

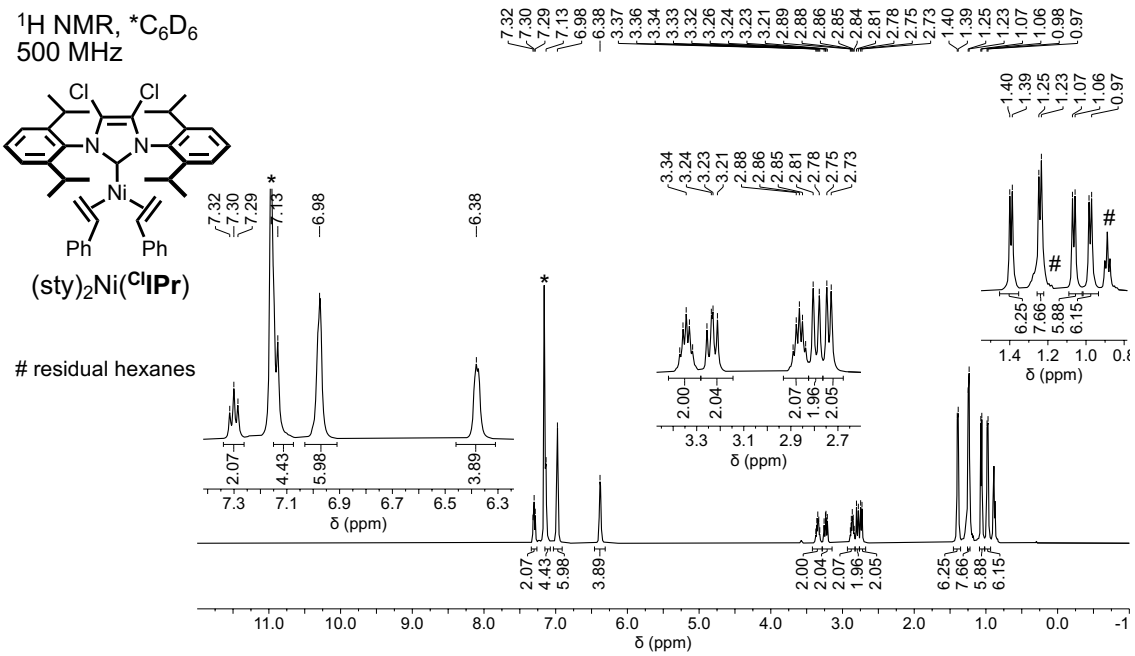

Figure C.11. ^{1}H NMR spectrum of (sty)$_2$Ni(**^{Cl}IPr**) recorded in C_6D_6 at 298 K.

APPENDIX D

SUPPLEMENTARY CONTENT FOR CHAPTER V

Experimental details

D.1.1. Materials and Methods

All syntheses and manipulations were carried out under nitrogen using standard Schlenk (vacuum 10^{-2} mbar) techniques or in a nitrogen-filled glovebox unless otherwise indicated. All reagents and solvents were used after drying and stored under nitrogen, unless otherwise indicated. Tetrahydrofuran (THF; Fisher Chemical; HPLC grade, unstabilized), hexanes (Fisher Chemical; HPLC grade), diethyl ether (Et_2O; B&J Brand; HPLC grade, unstabilized), dichloromethane (DCM; Oakwood Chemical; HPLC grade, unstabilized), dimethylformamide (DMF; Alfa Aesar; HPLC grade, unstabilized) and acetonitrile (MeCN; Fisher Chemical; HPLC grade) were dispensed under nitrogen from an LC Technology SP-1 solvent system. Benzene (ACS grade) and pentane (HPLC grade) were refluxed overnight with CaH_2 and distilled under nitrogen before use. The dried solvents were thereafter stored on activated 4Å molecular sieves under nitrogen. C_6D_6 and $CDCl_3$ were purchased from Cambridge Isotope Laboratories, degassed by freeze-pump-thaw, and thereafter stored on activated 4Å molecular sieves under nitrogen. All stock solutions were prepared by mass and were dispensed into reaction vessel by difference from syringe, as detailed in the procedure for each experiment.

D.1.2. General Experimental

Nuclear magnetic resonance (NMR) spectra were collected at room temperature (298 K) unless otherwise stated on a Bruker AV-III HD 600 NMR (600.13 MHz for ^{1}H; 150.90 MHz for ^{13}C; 564.69 MHz for ^{19}F; 119.23 MHz for ^{29}Si; 232.94 MHz for ^{31}P; 92.12 MHz for ^{2}H), Bruker Avance-III HD 500 NMR (499.90 MHz for ^{1}H; 126 MHz for ^{13}C; 471 MHz for ^{19}F; 99 MHz for ^{29}Si; 202.46 MHz for ^{31}P), or Varian Inova 500 NMR (499.90 MHz for ^{1}H; 126 MHz for ^{13}C; 471 MHz for ^{19}F; 99 MHz for ^{29}Si; 202.46 MHz for ^{31}P). ^{1}H and ^{13}C spectra were referenced to the residual solvent peak ($CDCl_3$: ^{1}H δ = 7.26 ppm,

^{13}C δ = 77.16 ppm; C_6D_6: ^{1}H δ = 7.16 ppm, ^{13}C δ = 128.06 ppm). Chemical shifts are reported in parts per million (ppm, δ) relative to tetramethylsilane at 0.00 ppm. Peaks are characterized as follows: s (singlet), d (doublet), t (triplet), q (quartet), pent (pentet), hept (heptet), m (multiplet), br (broad), app (apparent), and/or ms (multiple signals). Coupling constants, *J*, are reported in Hz. Electron paramagnetic resonance (EPR) spectra were collected at 77 K on a Bruker Elexsys E500 EPR X-band spectrometer. Infrared spectroscopy was performed on an Agilent Nicolet 6700 FT-IR, and peaks are reported in cm^{-1}. For catalytic reactions, yields were determined using Gas Chromatography-Mass Spectrometry (GCMS) or Gas Chromatography (GC) against an internal standard. GCMS was carried out on a Shimadzu GC-2010 Plus/GCMS-QP2010 SE using a Restek Rtx®-5 (Crossbond 5% diphenyl – 95% dimethyl polysiloxane; 15 m, 0.25 mm ID, 0.25 μm df) column. GC was carried out on a Thermo Fisher Trace 1300 Gas Chromatograph using a Restek Rtx®-5 (Crossbond 5% diphenyl – 95% dimethyl polysiloxane; 15 m, 0.25 mm ID, 0.25 μm df) column. High-resolution mass spectrometry (HRMS) was carried out on a Waters XEVO G2-XS TOF mass spectrometer.

D.1.3. Synthesis of Non-Commercial Reagents

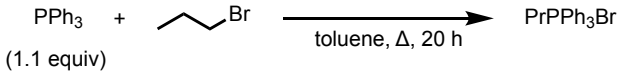

Propyltriphenylphosphonium bromide ($PrPPh_3Br$) was synthesized via literature procedure:[212] To a dried 3-neck RBF equipped with a magnetic stir bar was added toluene (65 mL). The toluene was sparged with N2 for 1 hour before PPh3 (24.4 g, 93 mmol, 1.1 equiv) and bromopropane (8.0 mL, 88 mmol, 1.0 equiv) were added. The reaction was equipped with a N2-flushed condenser and the reaction was placed in a preheated oil bath at 130 °C. The reaction was refluxed for 20 hour before being removed from the oil bath and being cooled to room temperature. Once the reaction was cool, the white precipitate was collected via filtration through a glass frit and the precipitate was washed with Et2O. The product was dried under reduced pressure and isolated as a white solid without further purification (22.0 g, 57 mmol, 65% yield). NMR spectra match values previously reported.[212]

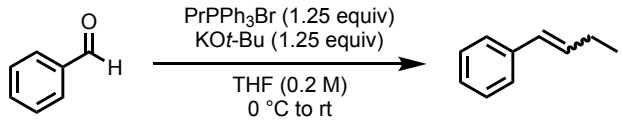

1-Phenyl-1-butene was synthesized via a modified literature procedure:[251] To a 200-mL oven dried Schlenk flask was added $PrPPh_3Br$ (10.0 g, 26 mmol, 1.3 equiv) and THF (140 mL). The reaction was cooled to 0 °C with an ice/water bath for 5 minutes before KO*t*-Bu (2.91 g, 26 mmol, 1.3 equiv) was added in one portion. The reaction was stirred for 30 minutes before benzaldehyde (2.1 mL, 21 mmol, 1.0 equiv) was added dropwise. The reaction was monitored via TLC for the disappearance of benzaldehyde. After 1 hour the reaction was complete and the reaction was opened to air and H_2O (80 mL) was added. The reaction was transferred to a separatory funnel and the aqueous layer was separated and extracted with Et_2O (3 x 80 mL). The combined organic layers were dried over Na_2SO_4, filtered and concentrated under reduced pressure. Triphenylphosphonium oxide was removed via filtration through a silica plug with hexanes. The clear solution was concentrated under reduced pressure to yield the product as a pale yellow liquid (2.19 g, 16.6 mmol, 80% yield). NMR spectra match values previously reported.[251]

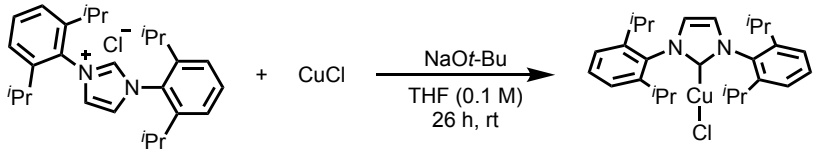

(IPr)CuCl was synthesized via literature procedure:[246] In a nitrogen-filled glovebox, IPr・HCl (0.42 g, 1.0 mmol, 1.0 equiv), CuCl (0.099 g, 1.0 mmol, 1.0 equiv) and NaO*t*-Bu (0.096 g, 1.0 mmol, 1.0 equiv) were weighed directly into a 5-dram vial equipped with a magnetic stir bar. THF (10 mL) was added to the vial and the reaction was stirred for 26 hours before being filtered through a pad of Celite and concentrated under reduced pressure. The product was collected as a white powder and did not require further purification (0.29 g, 0.58 mmol, 58% yield). NMR spectra match values previously reported.[252]

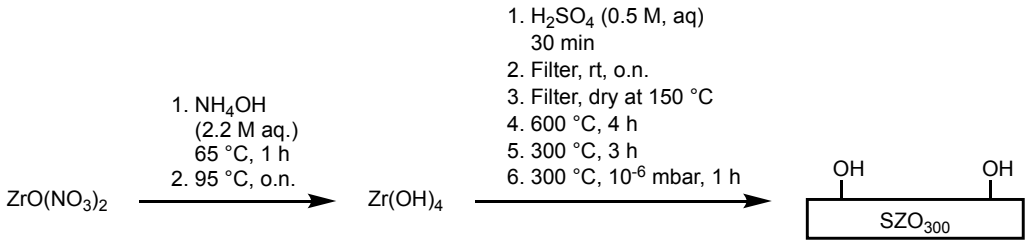

Sulfated zirconia (SZO) was prepared via literature procedure:[175] A solution of NH_4OH (2.2 M) was prepared using UltraPure water. To a 500-mL RBF equipped with a magnetic stir bar was added zirconyl nitrate (20.0 g, 87 mmol, 1.0 equiv) and H_2O (120 mL). The RBF was placed in a preheated oil bath at 65 °C and stirred until zirconyl nitrate was in solution. NH_4OH solution (80 mL, 176 mmol, 2.0 equiv) was added and the solution was stirred for 1 hour before the temperature was increased to 95 °C. After stirring overnight, the reaction was filtered while hot and the solid was washed with 500 mL UltraPure water. The $Zr(OH)_4$ was placed in an oven at 150 °C for 6 days. The collected $Zr(OH)_4$ was placed in a 250-mL RBF with 150 mL of H_2SO_4 (0.5 M, UltraPure water). The mixture was stirred for 30 minutes and the resulting mixture was decanted/filtered, and the solid was mixed overnight in UltraPure water. The SZO was then calcined at 600 °C for 4 hours, dehydroxylated at 300 °C for 3 hours, and activated at 300 °C under reduced pressure ($5 \cdot 10^{-6}$ mbar) for 1 hour before being taken into a nitrogen-filled glovebox and stored under inert conditions. The concentration of surface hydroxyl groups (0.16 mmol OH/g SZO) was determined via titration with dibenzyl magnesium and analyzed via ^1H NMR versus ferrocene as an internal standard.

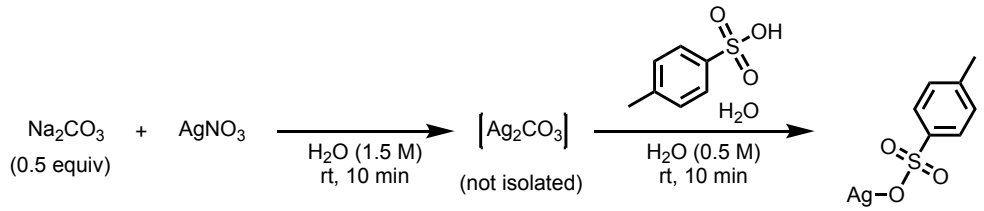

Silver tosylate, AgOTs was synthesized via literature procedure:[253] Solutions of Na_2CO_3 (1.06 g, 10.0 mmol, 0.5 equiv in 3.3 mL H_2O) and $AgNO_3$ (3.40 g, 20.0 mmol, 1.0 equiv in 7.0 mL H_2O) were prepared and stirred until reagents were fully dissolved. The $AgNO_3$ solution was added to the Na_2CO_3 solution and a pale yellow precipitate formed (presumably Ag_2CO_3). After 5 minutes, the precipitate was collected via filtration through

a glass frit. The precipitate was transferred to a RBF equipped with a magnetic stir bar and H_2O (40 mL) was added. P-toluenesulfonic acid monohydrate was added in three portions. The reaction was allowed to stir for 10 minutes before it was filtered through a glass frit. H_2O was removed under reduced pressure while heating at 60 °C. The product was isolated as a white powder and carried forward without further purification (4.71 g, 16.9 mmol, 84% yield).

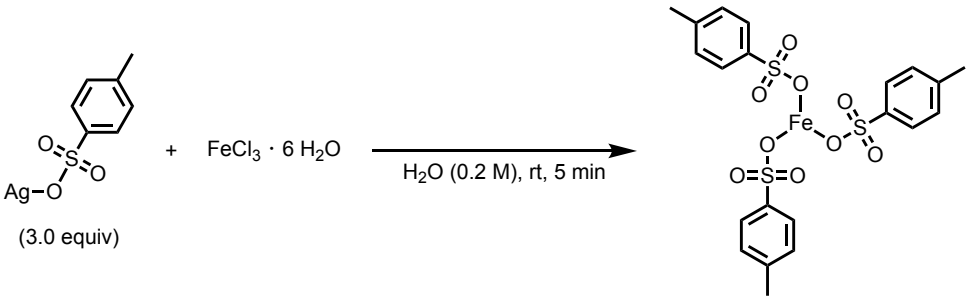

Iron tritosylate, $Fe(OTs)_3$ was synthesized via literature procedure:[254] Solutions of AgOTs (1.89 g, 6.8 mmol, 3.0 equiv in 22 mL H_2O) and $FeCl_3 \cdot 6\ H_2O$ (0.61 g, 2.3 mmol, 1.0 equiv in 8.0 mL H_2O) were prepared. The AgOTs solution was added to the $FeCl_3 \cdot 6\ H_2O$ solution and a white precipitate formed rapidly. The reaction was stirred for 5 minutes before being filtered through a frit to remove the precipitated AgCl. The orange filtrate was dried under reduced pressure to yield the hydrated product as a yellow orange solid. The product was further dehydrated under reduced pressure at 120 °C to yield the product as a red powder (0.75 g, 1.3 mmol, 57% yield).

D.1.4. Ni(0)/silane reactivity with β-methylstyrene

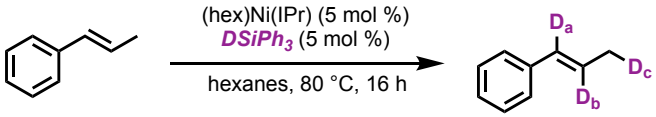

In a nitrogen-filled glovebox, (hex)Ni(IPr) was weighed directly into 1-dram vials. A stock solution of $DSiPh_3$ (0.016 M) and durene (0.070 M) was prepared by weighing out the reagent and adding the appropriate volume of hexanes. The $DSiPh_3$/durene stock solution was distributed (0.80 mL) using a 1-mL disposable syringe. The vials were sealed with septum caps, removed from the glovebox and placed on a preheated aluminum vial block at 80 °C. After 30 minutes, *trans*-β-methylstyrene (32 μL, 0.25 mmol, 1.0 equiv) was

distributed in two portions using a 25-μL microliter syringe. After 16 hours, the reactions were quenched by cooling in liquid N_2 and opening to air. The crude reaction mixtures were filtered through short silica plugs with hexanes and the hexanes was removed from the filtrate under reduced pressure. Samples for NMR analysis were prepared in $CHCl_3/CDCl_3$ (9:1).

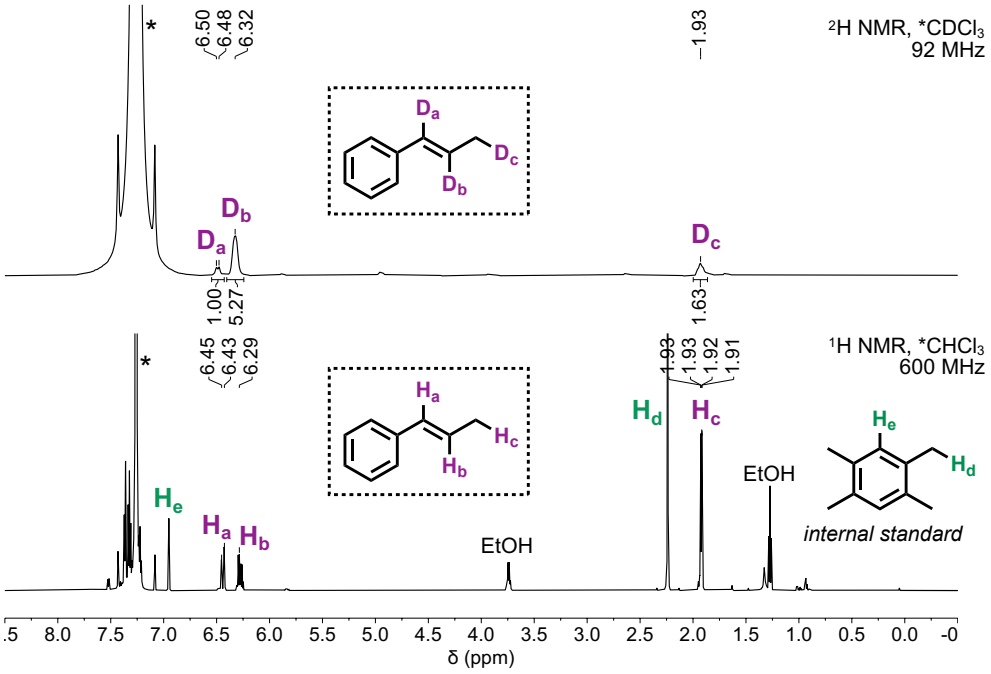

Figure D.1. NMR analysis of isolated *trans*-β-methylstyrene recorded in $CHCl_3/CDCl_3$ (9:1) at 298 K.

D.1.5. Screening of reactivity

a. Synthesis of 4,4,5,5-tetramethyl-2-(1-methyl-3-phenylpropyl)-1,3,2-dioxaborolane

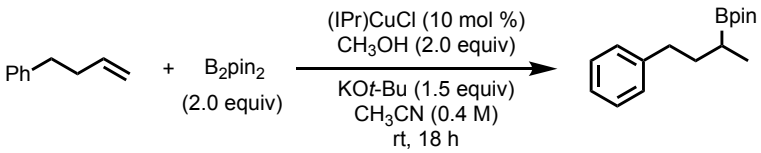

4,4,5,5-tetramethyl-2-(1-methyl-3-phenylpropyl)-1,3,2-dioxaborolane was prepared via literature procedure:[64] In a nitrogen-filled glovebox, (IPr)CuCl (48.8 mg, 0.10 mmol, 0.10 equiv) and KO*t*-Bu (170.1 mg, 1.5 mmol, 1.5 equiv) were weighed into a 1-

dram vial equipped with a magnetic stir bar. Acetonitrile (2.0 mL) was added using a 5-mL disposable syringe and the reaction was stirred for 5 minutes before B2pin2 (0.51 g, 2.0 mmol, 2.0 equiv) was added in one portion. The vial was sealed with a septum cap and removed from the glovebox. 4-Phenyl-1-butene (150 µL, 1.0 mmol, 1.0 equiv) was added in two portions using a 100-µL microliter syringe. DrySolv MeOH (80 µL, 2.0 mmol, 2.0 equiv) was added using a 100-µL microliter syringe. The reaction was stirred at room temperature for 18 hours. After 18 hours, the reaction was opened to air and filtered through a silica plug using a glass frit. Crude material was collected as a yellow oil after concentration under reduced pressure. Product formation was confirmed by ^{1}H NMR and mass spectroscopy.

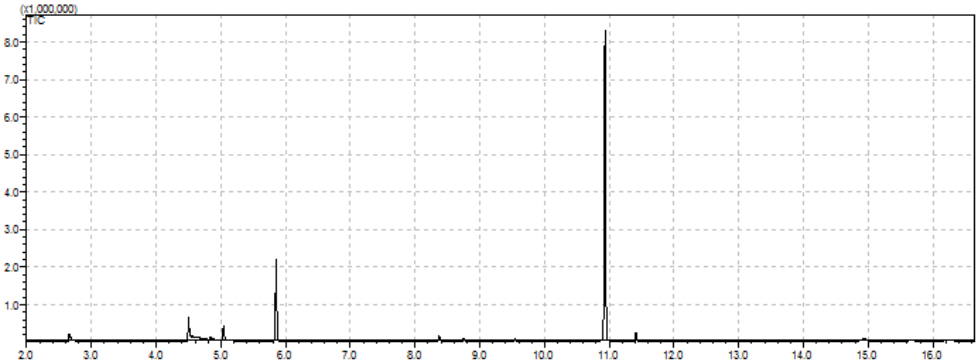

Figure D.2. GC-MS chromatograph for the isolated crude product with a retention time of 10.94 min.

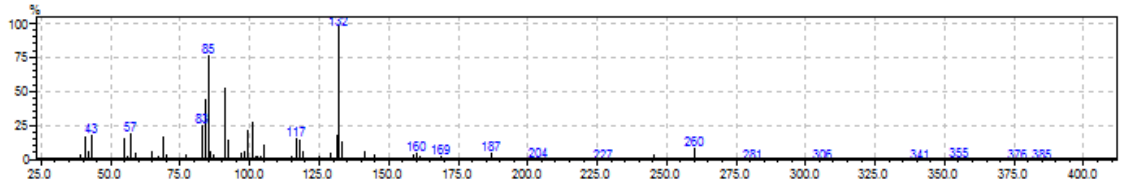

Figure D.3. Mass spectrum for the isolated crude product (retention time = 10.94 min).

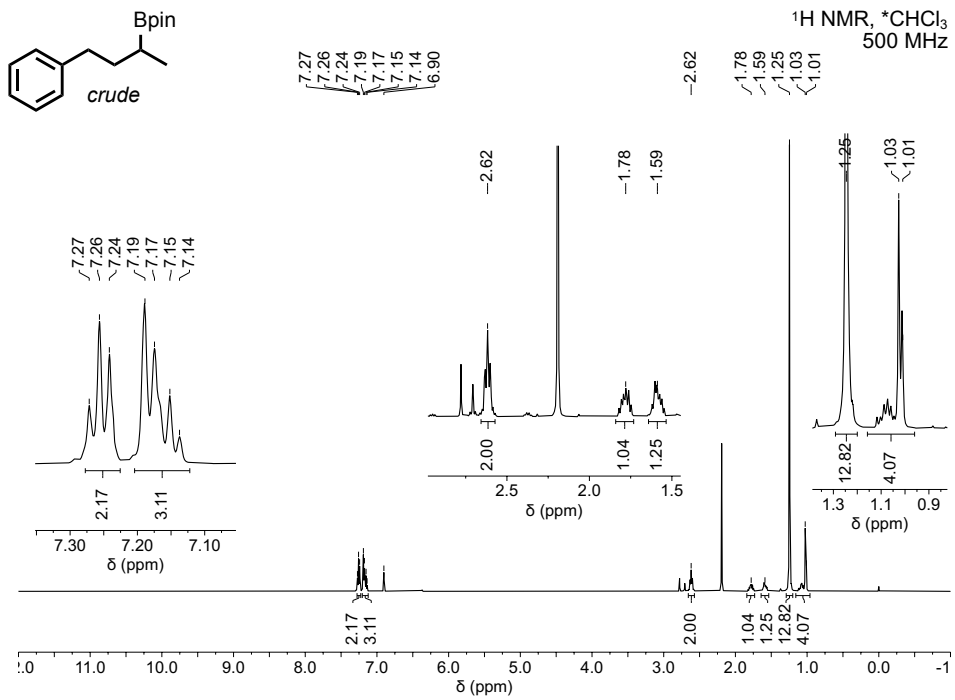

Figure D.4. ^{1}H NMR spectrum of isolated crude product recorded in $CDCl_3$ at 298 K.

b. General procedure for screening of reaction conditions

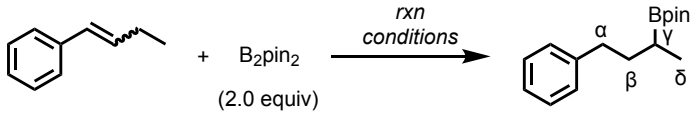

In a nitrogen-filled glovebox, solid reagents were weighed directly into 1-dram vials equipped with magnetic stir bars (see **Table D..** for specific amounts of each reagents for screening on a 0.15 mmol scale). After weighing out the solid reagents, solvent (1.5 mL) was added using two portions of a 1-mL disposable syringe. Cyclooctane (10 μL, 0.074 mmol, 0.49 equiv) was distributed to each vial using a 25-μL microliter syringe. Vials were sealed with septum caps and removed from the glovebox. For trials with HBF_4, a stock solution of HBF_4 was prepared using volumetric glassware. DrySolv MeOH was distributed to each vial using a 25-μL microliter syringe. 1-Phenyl-1-butene (22 μL, 0.15 mmol, 1.0 equiv) was distributed using a 50-μL microliter syringe. Vials were placed on a preheated aluminum vial block (temperature specified below). Reactions were stirred for 24 h before being removed from the vial block and opened to air. Analysis of the crude reaction mixtures was carried out with GC-MS after filtration of an aliquot through Celite, washing with DCM. Results of screening are summarized **Table D..**

Table D.1. Reagents and amounts used in catalytic screening reactions.

Reagent	Equiv	mmol	Amount
$(sty)_2Ni(IPr)$	0.05	0.008	4.9 mg
$HSiPh_3$	0.05	0.008	2.0 mg
$Ni[P(OEt)_3]_4$	0.05	0.008	5.4 mg
SZO (0.16 mmol OH/g)	0.05	0.008	46.9 mg
HBF_4 (50 wt%)	0.05	0.010	50 µL of 0.2 M stock solution
IPrCuCl	0.10	0.015	7.3 mg
KO*t*-Bu	1.5	0.23	25.3 mg
B_2pin_2	2.0	0.30	76.2 mg
MeOH	2.0	0.30	12 µL
IPr	0.15	0.023	8.7 mg
Ni(cod)2	0.05	0.008	2.1 mg
CuCl	0.10	0.015	1.5 mg

Table D.2. Results of catalyst and reaction condition screening.

Entry	Reaction conditions	Results
1	$(sty)_2Ni(IPr)$ (5 mol %) $HSiPh_3$ (5 mol %0 (IPr)CuCl (10 mol %) KO*t*-Bu (1.5 equiv) MeOH (2.0 equiv) acetonitrile (0.1 M) 40 °C, 24 h	No γ-product observed. Peak at 10.57 min with *m/z* of 260 likely corresponds to the α- or β-functionalized product.
2	$(sty)_2Ni(IPr)$ (5 mol %) $HSiPh_3$ (5 mol %0 (IPr)CuCl (10 mol %) KO*t*-Bu (1.5 equiv) MeOH (2.0 equiv) toluene (0.1 M) 80 °C, 24 h	No γ-product observed. Peak at 10.57 min with *m/z* of 260 likely corresponds to the α- or β-functionalized product.

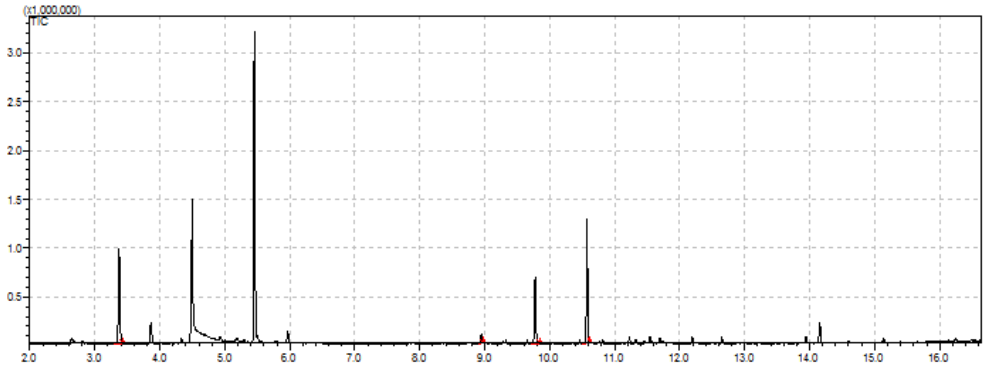

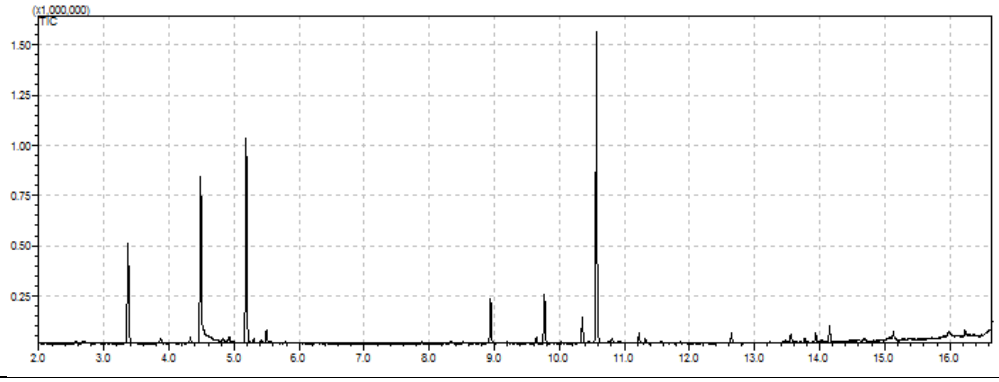

3	$Ni[P(OEt)_3]_4$ (5 mol %) SZO (5 mol %) (IPr)CuCl (10 mol %) KO*t*-Bu (1.5 equiv) MeOH (2.0 equiv) acetonitrile (0.1 M) 40 °C, 24 h	No γ-product observed. Peak at 10.57 min with *m/z* of 260 likely corresponds to the α- or β-functionalized product.

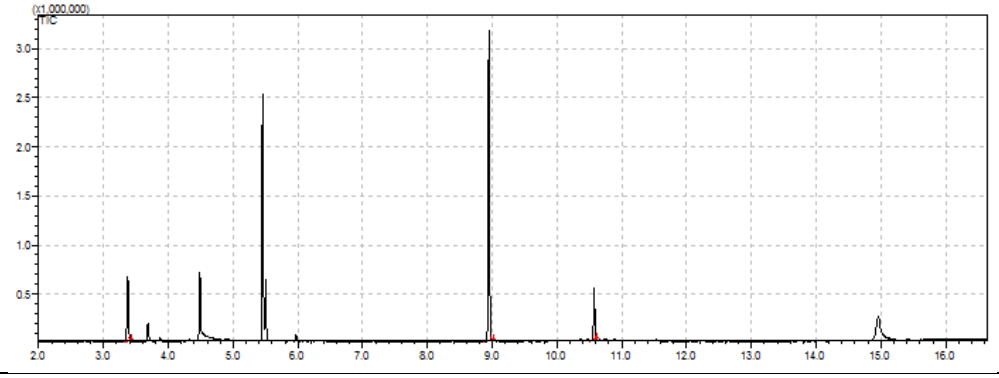

4	$Ni[P(OEt)_3]_4$ (5 mol %) HBF_4 (5 mol %) (IPr)CuCl (10 mol %) KO*t*-Bu (1.5 equiv) MeOH (2.0 equiv) acetonitrile (0.1 M) 40 °C, 24 h	No γ-product observed. Peak at 10.57 min with *m/z* of 260 likely corresponds to the α- or β-functionalized product.

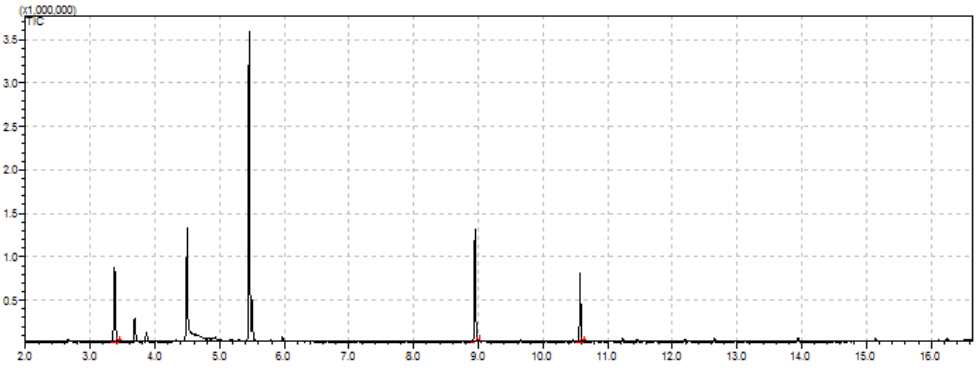

5	$Ni(cod)_2$ (5 mol %) $HSiPh_3$ (5 mol %) CuCl (10 mol %) IPr (15 mol %) toluene (0.1 M) 80 °C, 24 h	No γ-product observed. Peak at 10.57 min with *m/z* of 260 likely corresponds to the α- or β-functionalized product.

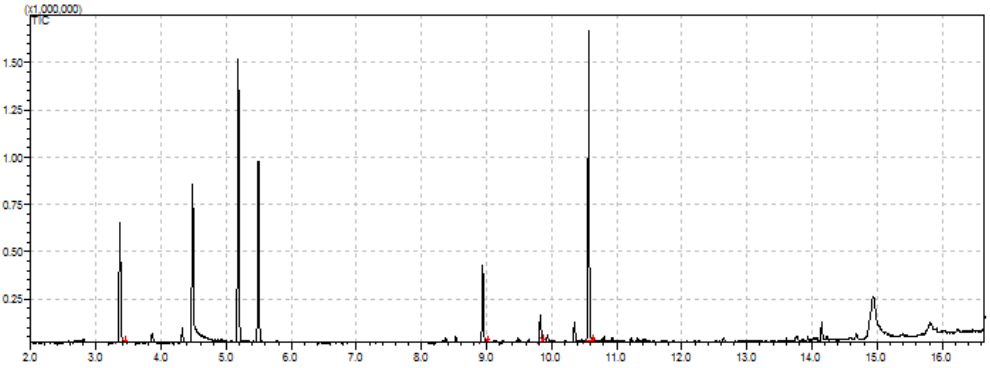

D.1.6. NMR and IR Spectra

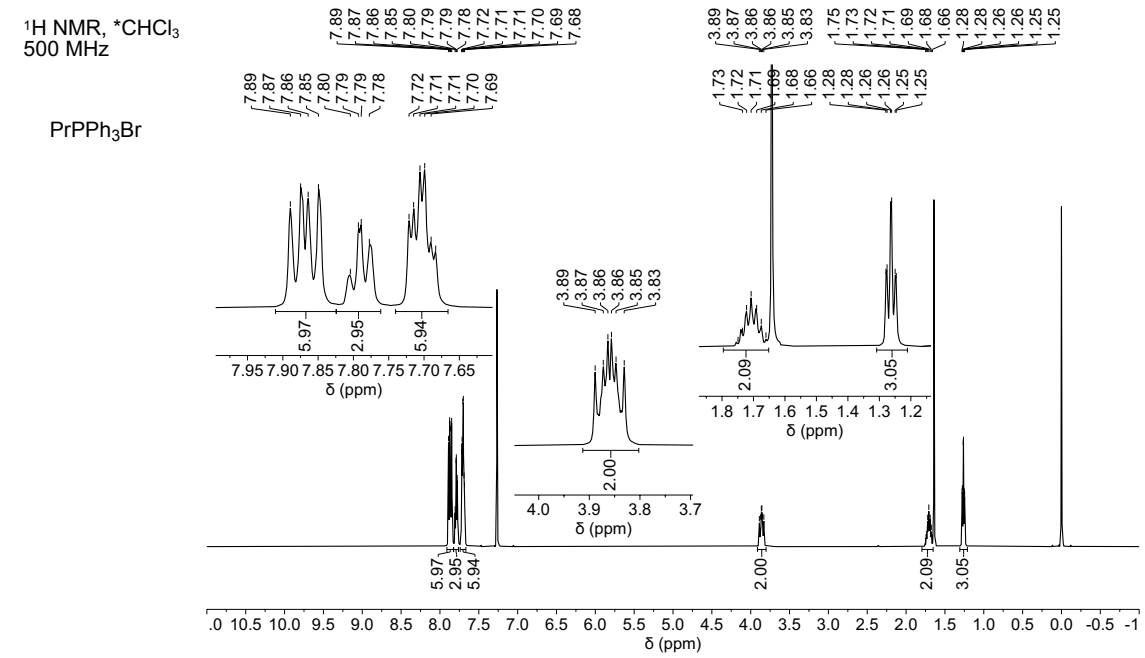

Figure D.5. ^{1}H NMR spectrum of **propyltriphenylphosphonium bromide ($PrPPh_3Br$)** recorded in $CDCl_3$ at 298 K.

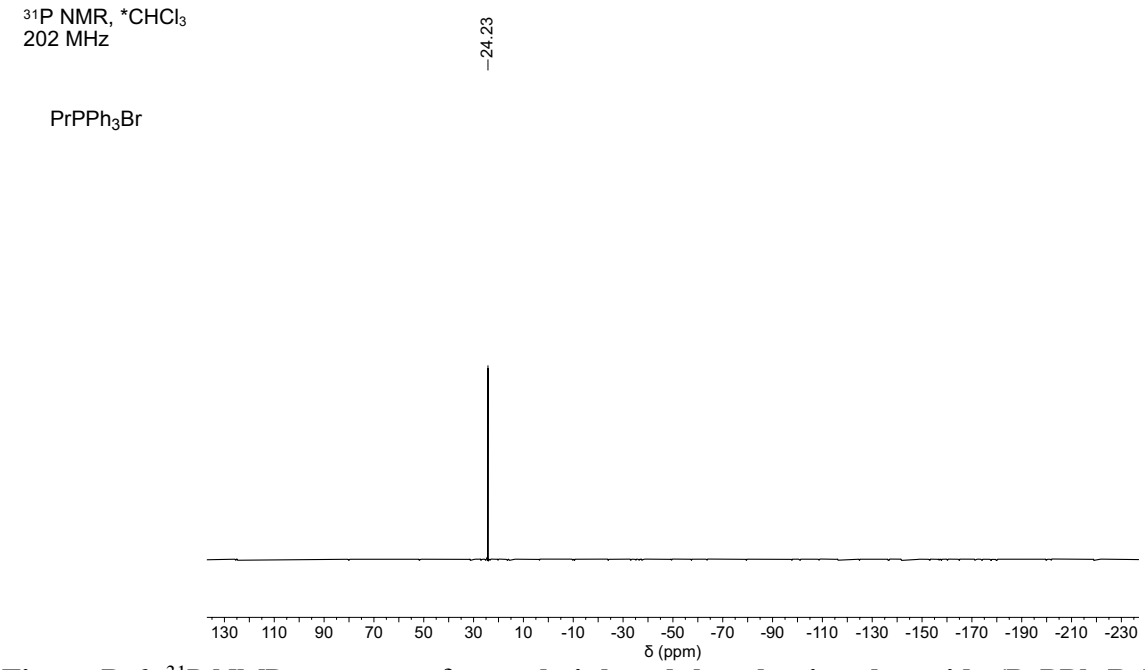

Figure D.6. ^{31}P NMR spectrum of **propyltriphenylphosphonium bromide ($PrPPh_3Br$)** recorded in $CDCl_3$ at 298 K.

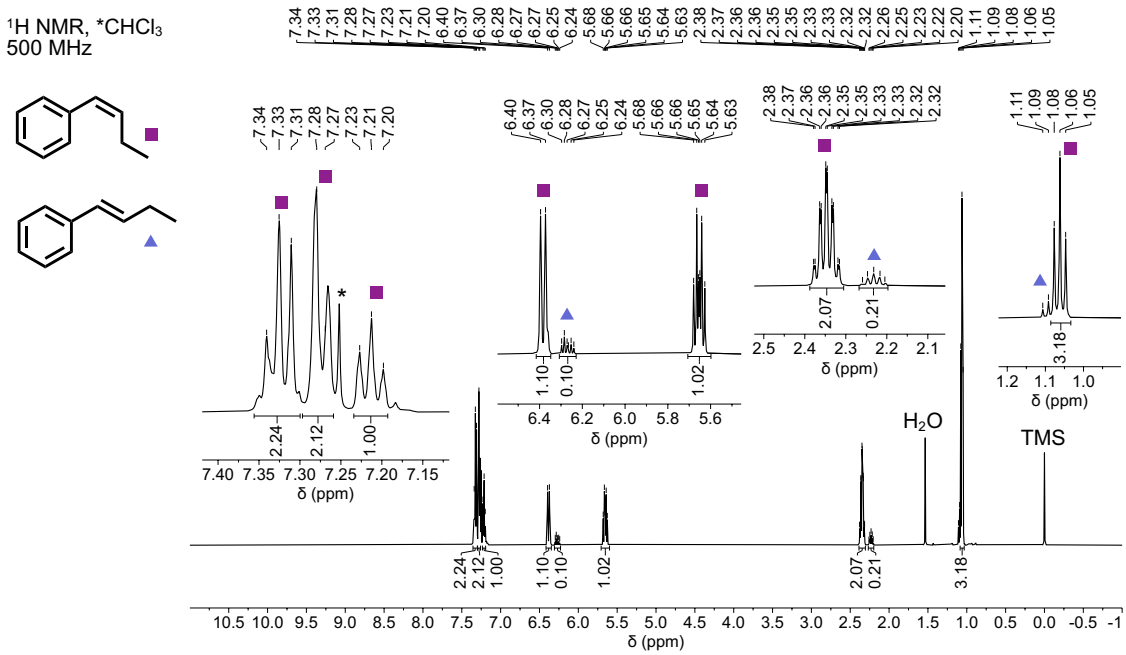

Figure D.7. ^{1}H NMR spectrum of 1-phenyl-1-butene recorded in $CDCl_3$ at 298 K.

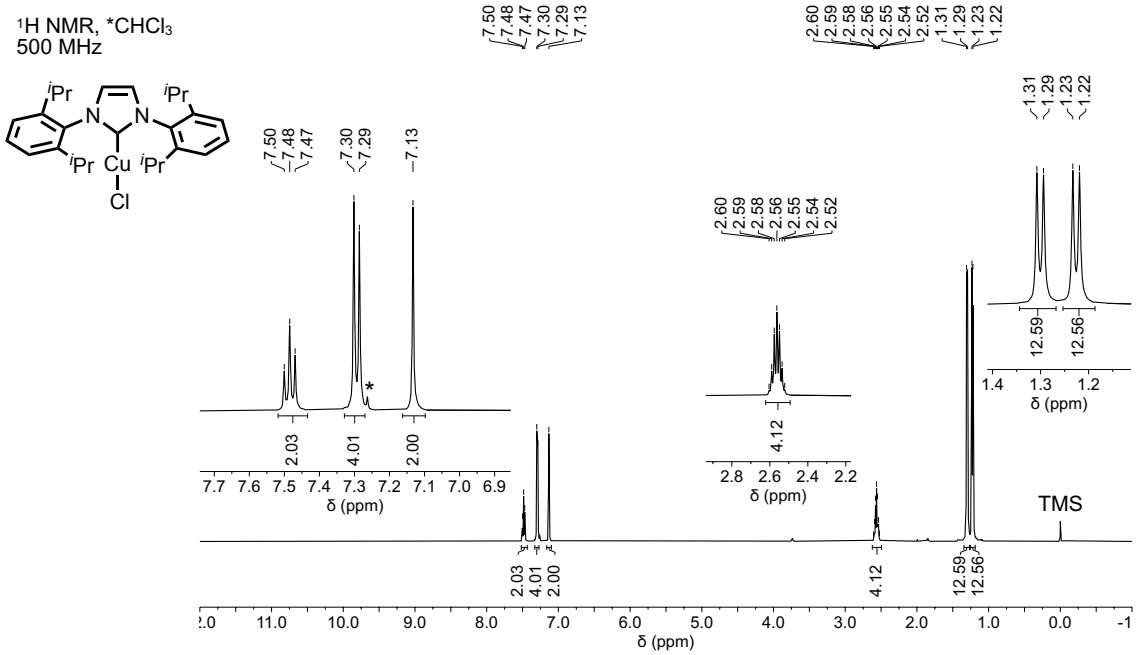

Figure D.8. ^{1}H NMR spectrum of (IPr)CuCl recorded in $CDCl_3$ at 298 K.

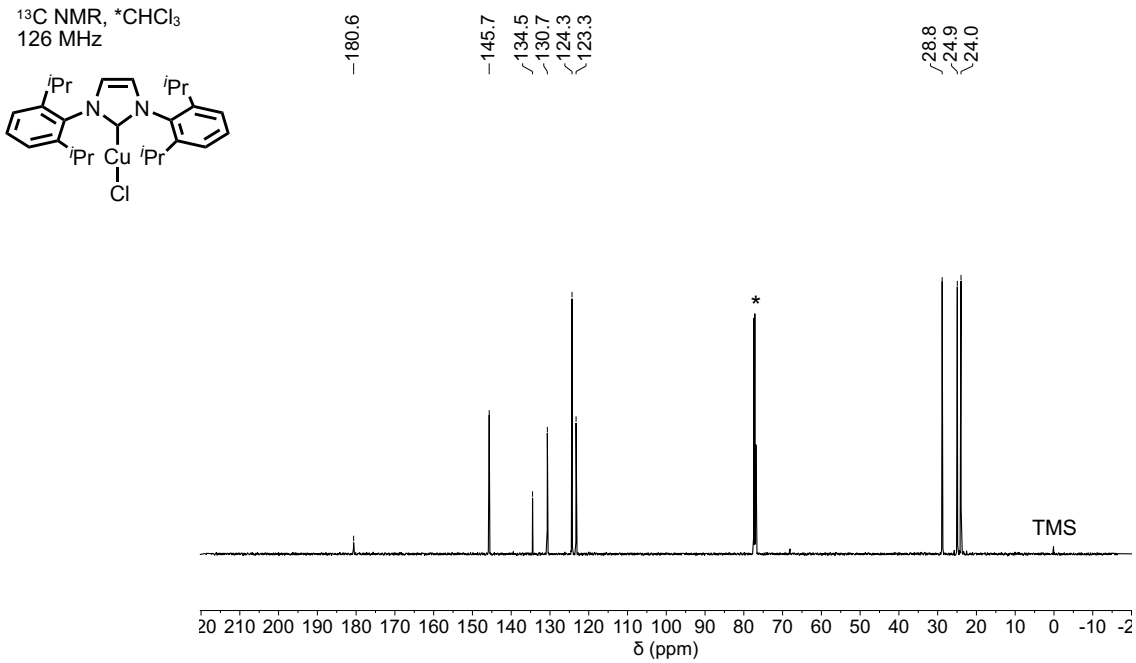

Figure D.9. ^{13}C NMR spectrum of (IPr)CuCl recorded in $CDCl_3$ at 298 K.

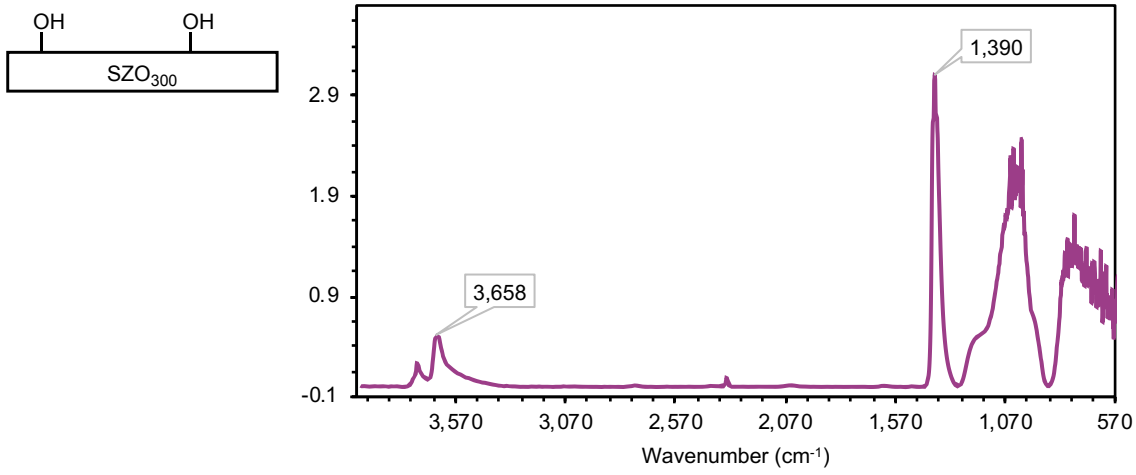

Figure D.10. IR spectrum of sulfated zirconia recorded at room temperature.

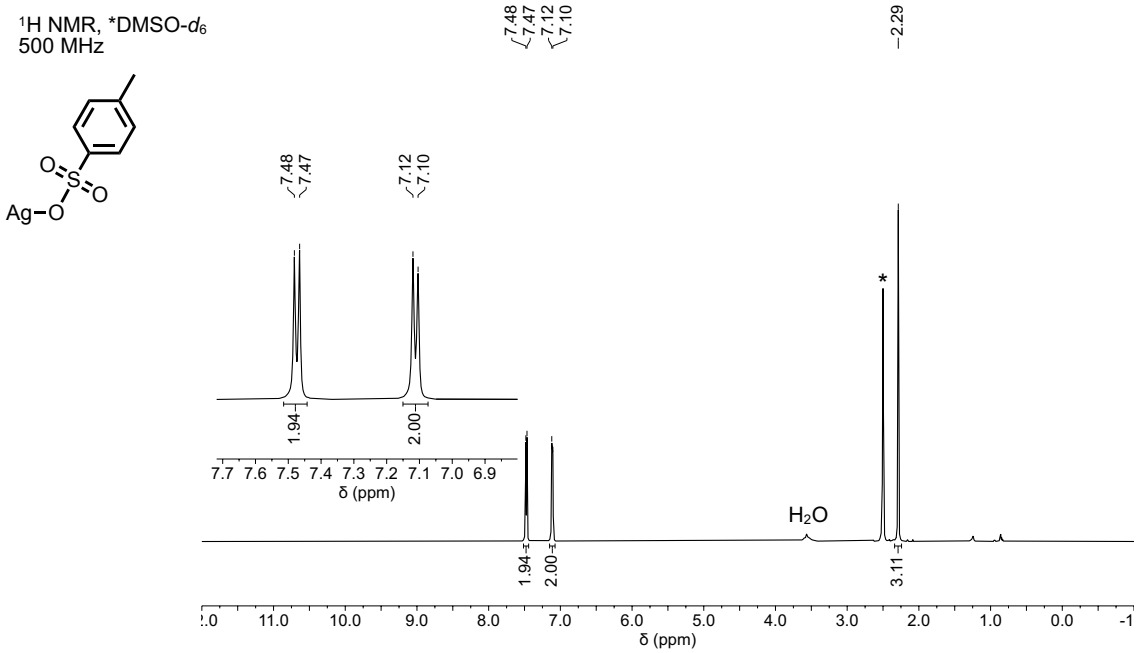

Figure D.11. [1]H NMR spectrum of AgOTs recorded in DMSO-d_6 at 298 K.

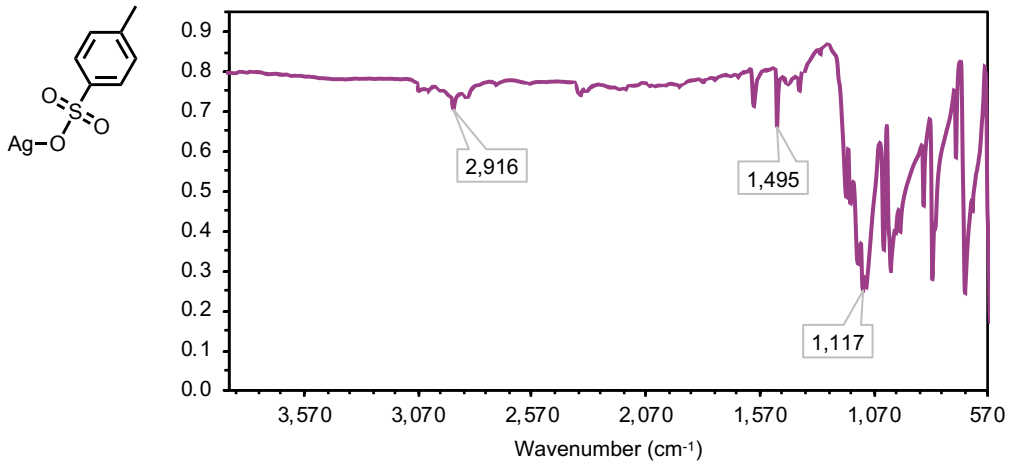

Figure D.12. IR spectrum of AgOTs recorded neat at room temperature.

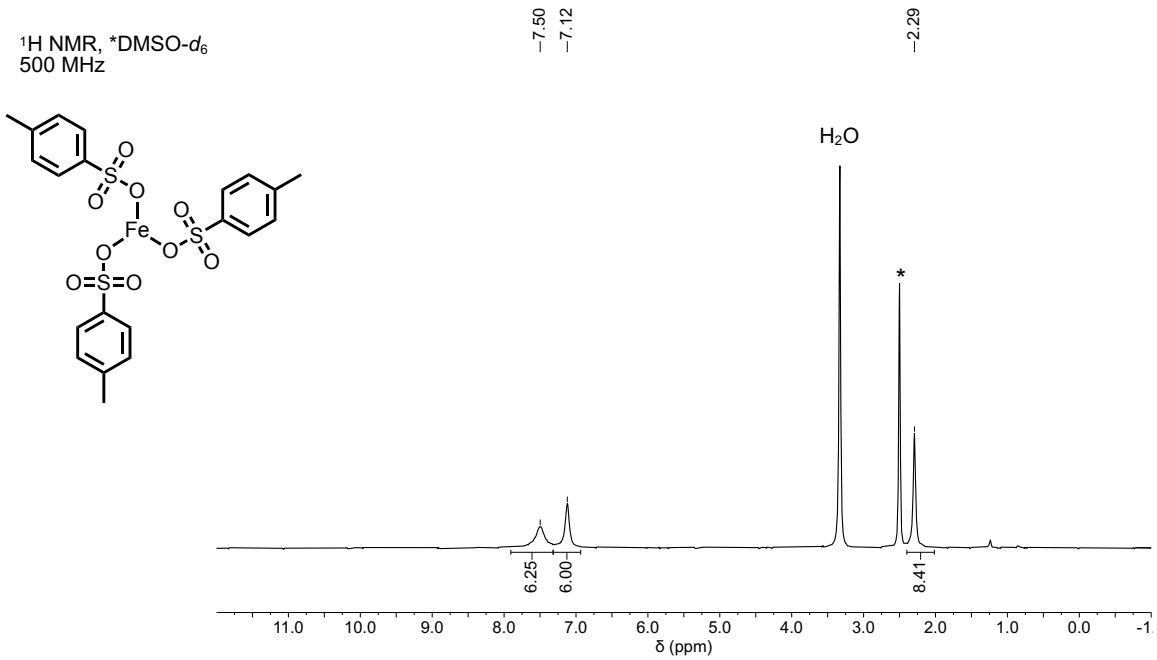

Figure D.13. ^{1}H NMR spectrum of $Fe(OTs)_3$ (partially hydrated) recorded in DMSO-d_6 at 298 K.

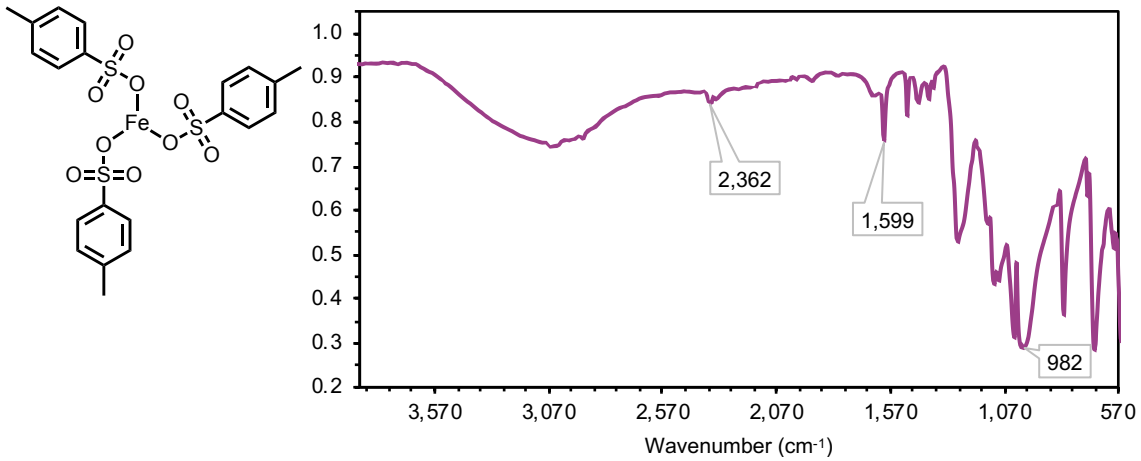

Figure D.14. IR spectrum of $Fe(OTs)_3$ (partially hydrated) recorded neat at room temperature.

REFERENCES CITED

(1) Molloy, J. J.; Morack, T.; Gilmour, R. Positional and Geometrical Isomerisation of Alkenes: The Pinnacle of Atom Economy. *Angew. Chem., Int. Ed.* **2019**, *58*, 13654–13664.

(2) Liu, X.; Li, B.; Liu, Q. Base-Metal-Catalyzed Olefin Isomerization Reactions. *Synth.* **2019**, *51*, 1293–1310. https://doi.org/10.1055/s-0037-1612014.

(3) Kolb, H. C.; VanNieuwenhze, M. S.; Sharpless, K. B. Catalytic Asymmetric Dihydroxylation. *Chem. Rev.* **1994**, *94*, 2483–2547.

(4) Su, S.; Wang, C. Catalytic Asymmetric Osmium-Free Dihydroxylation of Alkenes. *Synth.* **2021**, *53*, 1229–1236.

(5) Tanaka, S.; Kunisawa, T.; Yoshii, Y.; Hattori, T. Acylation of Alkenes with the Aid of AlCl3 and 2,6-Dibromopyridine. *Org. Lett.* **2019**, *21*, 8509–8513.

(6) Demming, R. M.; Hammer, S. C.; Nestl, B. M.; Gergel, S.; Fademrecht, S.; Pleiss, J.; Hauer, B. Asymmetric Enzymatic Hydration of Unactivated, Aliphatic Alkenes. *Angew. Chem., Int. Ed.* **2019**, *58*, 173–177.

(7) Hintermann, L. *Recent Developments in Metal-Catalyzed Additions of Oxygen Nucleophiles to Alkenes and Alkynes*; 2010; Vol. 31.

(8) Johnson, L. K.; Killian, C. M.; Brookhart, M. New Pd(II)- and Ni(II)-Based Catalysts for Polymerization of Ethylene and α-Olefins. *J. Am. Chem. Soc.* **1995**, *117*, 6414–6415.

(9) Svejda, S. A.; Brookhart, M. Ethylene Oligomerization and Propylene Dimerization Using Cationic (α-Diimine)Nickel(II) Catalysts. *Organometallics* **1999**, *18*, 65–74.

(10) Ma, S.; Xi, Y.; Fan, H.; Roediger, S.; Hartwig, J. F. Enantioselective Hydroamination of Unactivated Terminal Alkenes. *Chem* **2022**, *8*, 532–542.

(11) Obligacion, J. V.; Chirik, P. J. Earth-Abundant Transition Metal Catalysts for Alkene Hydrosilylation and Hydroboration. *Nat. Rev. Chem.* **2018**, *2*, 15–34.

(12) Gao, W.; Zhang, X.; Xie, X.; Ding, S. One Simple Ir/Hydrosilane Catalytic System for Chemoselective Isomerization of 2-Substituted Allylic Ethers. *Chem. Commun.* **2020**, *56*, 2012–2015.

(13) Weber, F.; Schmidt, A.; Röse, P.; Fischer, M.; Burghaus, O.; Hilt, G. Double-Bond Isomerization: Highly Reactive Nickel Catalyst Applied in the Synthesis of the Pheromone (9 Z,12 Z)-Tetradeca-9,12-Dienyl Acetate. *Org. Lett.* **2015**, *17*, 2952–2955.

(14) Zhang, S.; Bedi, D.; Cheng, L.; Unruh, D. K.; Li, G.; Findlater, M. Cobalt(II)-Catalyzed Stereoselective Olefin Isomerization: Facile Access to Acyclic Trisubstituted Alkenes. *J. Am. Chem. Soc.* **2020**, *142*, 8910–8917.

(15) Crossley, S. W. M.; Barabé, F.; Shenvi, R. A. Simple, Chemoselective, Catalytic Olefin Isomerization. *J. Am. Chem. Soc.* **2014**, *136*, 16788–16791.

(16) Janssen-Müller, D.; Sahoo, B.; Sun, S.; Martin, R. Tackling Remote Sp 3 C−H Functionalization via Ni-Catalyzed "Chain-walking" Reactions. *Isr. J. Chem.* **2019**, *60*, 195–206.

(17) Touney, E. E.; Van Hoveln, R.; Buttke, C. T.; Freidberg, M. D.; Guzei, I. A.; Schomaker, J. M. Heteroleptic Nickel Complexes for the Markovnikov-Selective Hydroboration of Styrenes. *Organometallics* **2016**, *35*, 3436–3439.

(18) Scheuermann, M. L.; Johnson, E. J.; Chirik, P. J. Alkene Isomerization-Hydroboration Promoted by Phosphine-Ligated Cobalt Catalysts. *Org. Lett.* **2015**, *17*, 2716–2719.

(19) Macnair, A. J.; Millet, C. R. P.; Nichol, G. S.; Ironmonger, A.; Thomas, S. P. Markovnikov-Selective, Activator-Free Iron-Catalyzed Vinylarene Hydroboration. *ACS Catal.* **2016**, *6*, 7217–7221.

(20) Zhang, G.; Zeng, H.; Wu, J.; Yin, Z.; Zheng, S.; Fettinger, J. C. Highly Selective Hydroboration of Alkenes, Ketones and Aldehydes Catalyzed by a Well-Defined Manganese Complex. *Angew. Chem., Int. Ed.* **2016**, *55*, 14369–14372.

(21) Jankins, T. C.; Martin-Montero, R.; Cooper, P.; Martin, R.; Engle, K. M. Low-Valent Tungsten Catalysis Enables Site-Selective Isomerization-Hydroboration of Unactivated Alkenes. *J. Am. Chem. Soc.* **2021**, *143*, 14981–14986.

(22) Kang, T.; Kim, N.; Cheng, P. T.; Zhang, H.; Foo, K.; Engle, K. M. Nickel-Catalyzed 1,2-Carboamination of Alkenyl Alcohols. *J. Am. Chem. Soc.* **2021**, *143*, 13962-13970.

(23) Nakajima, Y.; Shimada, S. Hydrosilylation Reaction of Olefins: Recent Advances and Perspectives. *RSC Adv.* **2015**, *5*, 20603–20616.

(24) Troegel, D.; Stohrer, J. Recent Advances and Actual Challenges in Late Transition Metal Catalyzed Hydrosilylation of Olefins from an Industrial Point of View. *Coord. Chem. Rev.* **2011**, *255*, 1440–1459.

(25) Burgess, K.; Ohlmeyer, M. J. Transition-Metal-Promoted Hydroborations of Alkenes, Emerging Methodology for Organic Transformations. *Chem. Rev.* **1991**, *91*, 1179–1191.

(26) Pakiam, R.; van der Walt, E. How Palladium Became a Really, Really Precious Metal. *The Washington Post*. 2021.

(27) Ritter, S. K. NIckel Shines as a Catalyst. *Chemical & Engineering News*. December 2015.

(28) Richmond, E.; Moran, J. Recent Advances in Nickel Catalysis Enabled by Stoichiometric Metallic Reducing Agents. *Synth.* **2018**, *50*, 499–513.

(29) Tolman, C. A. Chemistry of Tetrakis(Triethyl Phosphite)Nickel Hydride, HNi[P(OEt)3]4+. IV. Mechanism of Olefin Isomerization. *J. Am. Chem. Soc.* **1972**, *94*, 2994–2999.

(30) Kapat, A.; Sperger, T.; Guven, S.; Schoenebeck, F. E-Olefins through Intramolecular Radical Relocation. *Science.* **2019**, *363*, 391–396.

(31) Chen, F.; Chen, K.; Zhang, Y.; He, Y.; Wang, Y. M.; Zhu, S. Remote Migratory Cross-Electrophile Coupling and Olefin Hydroarylation Reactions Enabled by in Situ Generation of NiH. *J. Am. Chem. Soc.* **2017**, *139*, 13929–13935.

(32) Pappas, I.; Treacy, S.; Chirik, P. J. Alkene Hydrosilylation Using Tertiary Silanes with α-Diimine Nickel Catalysts. Redox-Active Ligands Promote a Distinct Mechanistic Pathway from Platinum Catalysts. *ACS Catal.* **2016**, *6*, 4105–4109.

(33) Buslov, I.; Becouse, J.; Mazza, S.; Montandon-Clerc, M.; Hu, X. Chemoselective Alkene Hydrosilylation Catalyzed by Nickel Pincer Complexes. *Angew. Chem., Int. Ed.* **2015**, *54*, 14523–14526.

(34) Du, X.; Huang, Z. Advances in Base-Metal-Catalyzed Alkene Hydrosilylation. *ACS Catal.* **2017**, *7*, 1227–1243.

(35) Obligacion, J. V; Chirik, P. J. Earth-Abundant Transition Metal Catalysts for Alkene Hydrosilylation and Hydroboration. *Nat. Rev. Chem.* **2018**, *2*, 15–34.

(36) Kocen, A. L.; Klimovica, K.; Brookhart, M.; Daugulis, O. Alkene Isomerization by "Sandwich" Diimine-Palladium Catalysts. *Organometallics* **2017**, *36*, 787–790.

(37) Bai, X. F.; Song, T.; Deng, W. H.; Wei, Y. L.; Li, L.; Xia, C. G.; Xu, L. W. (EtO)3SiH-Promoted Palladium-Catalyzed Isomerization of Olefins: Convenient Synthesis of Internal Alkenes from Terminal Alkenes. *Synlett* **2014**, *25*, 417–422.

(38) Iluc, V. M.; Hillhouse, G. L. Snapshots of the Oxidative-Addition Process of Silanes to Nickel(0). *Tetrahedron* **2006**, *62*, 7577–7582.

(39) Zell, T.; Schaub, T.; Radacki, K.; Radius, U. Si-H Activation of Hydrosilanes Leading to Hydrido Silyl and Bis(Silyl) Nickel Complexes. *Dalt. Trans.* **2011**, *40*, 1852–1854.

(40) Schmidt, D.; Zell, T.; Schaub, T.; Radius, U. Si-H Bond Activation at {(NHC)2Ni0} Leading to Hydrido Silyl and Bis(Silyl) Complexes: A Versatile Tool for Catalytic Si-H/D Exchange, Acceptorless Dehydrogenative Coupling of Hydrosilanes, and Hydrogenation of Disilanes to Hydrosilanes. *Dalt. Trans.* **2014**, *43*, 10816–10827.

(41) Rigo, P.; Bressan, M.; Basato, M. Nickel(0) Complexes with the Hybrid Bidentate Ligand l-(Thioethyl)-2-(Diphenylphosphino)Ethane. Synthesis and Catalytic Properties of the Related Nickel Hydride Derivative. *Inorg. Chem.* **1979**, *18*, 860–863.

(42) Kanai, H. Selective Cis-Isomerisation of but-1-Ene by Homogeneous Catalysis with Triphenylphosphinenickel Complexes. *J. Chem. Soc., Chem. Commun.* **1972**, 203–204.

(43) Zhang, J.; Gao, H.; Ke, Z.; Bao, F.; Zhu, F.; Wu, Q. Investigation of 1-Hexene Isomerization and Oligomerization Catalyzed with β-Diketiminato Ni(II) Bromide Complexes/Methylaluminoxane System. *J. Mol. Catal. A Chem.* **2005**, *231*, 27–34.

(44) Bartlett, S. A.; Badiola, K. A.; Arandiyan, H.; Masters, A. F.; Maschmeyer, T. The Autocatalytic Isomerization of Allylbenzene by Nickel(0) Tetrakis(Triethylphosphite). *Eur. J. Inorg. Chem.* **2018**, *2018*, 3384–3387.

(45) Kathe, P. M.; Caciuleanu, A.; Berkefeld, A.; Fleischer, I. Tandem Olefin Isomerization/Cyclization Catalyzed by Complex Nickel Hydride and Brønsted Acid. *J. Org. Chem.* **2020**, *85*, 15183–15196.

(46) Birdwhistell, K. R.; Lanza, J. Simple Synthesis and Use of a Nickel Alkene Isomerization Catalyst: An Advanced Lab in Inorganic/Organometallic Chemistry. *J. Chem. Educ.* **1997**, *74*, 579–581.

(47) Hwan, J. L.; Smith, C. R.; RajanBabu, T. V. Facile Pd(II)- and Ni(II)-Catalyzed Isomerization of Terminal Alkenes into 2-Alkenes. *J. Org. Chem.* **2009**, *74*, 4565–4572.

(48) Wang, L.; Liu, C.; Bai, R.; Pan, Y.; Lei, A. Easy Access to Enamides: A Mild Nickel-Catalysed Alkene Isomerization of Allylamides. *Chem. Commun.* **2013**, *49*, 7923–7925.

(49) Halli, J.; Kramer, P.; Bechthold, M.; Manolikakes, G. Nickel-Catalyzed Synthesis of Enamides and Enecarbamates via Isomerization of Allylamides and Allylcarbamates. *Adv. Synth. Catal.* **2015**, *357*, 3321–3324.

(50) Lee, W. C.; Wang, C. H.; Lin, Y. H.; Shih, W. C.; Ong, T. G. Tandem Isomerization and C-H Activation: Regioselective Hydroheteroarylation of Allylarenes. *Org. Lett.* **2013**, *15*, 5358–5361.

(51) Iwamoto, H.; Tsuruta, T.; Ogoshi, S. Development and Mechanistic Studies of (E)-Selective Isomerization/Tandem Hydroarylation Reactions of Alkenes with a Nickel(0)/Phosphine Catalyst. *ACS Catal.* **2021**, *11*, 6741–6749.

(52) Sommer, H.; Juliá-Hernández, F.; Martin, R.; Marek, I. Walking Metals for Remote Functionalization. *ACS Cent. Sci.* **2018**, *4*, 153–165.

(53) Juliá-Hernández, F.; Moragas, T.; Cornella, J.; Martin, R. Remote Carboxylation of Halogenated Aliphatic Hydrocarbons with Carbon Dioxide. *Nature* **2017**, *545*, 84–88.

(54) Zhang, Y.; Xu, X.; Zhu, S. Nickel-Catalysed Selective Migratory Hydrothiolation of Alkenes and Alkynes with Thiols. *Nat. Commun.* **2019**, *10*, 1–9.

(55) Xiao, J.; He, Y.; Ye, F.; Zhu, S. Remote Sp3 C–H Amination of Alkenes with Nitroarenes. *Chem* **2018**, *4*, 1645–1657.

(56) Zhou, F.; Zhu, J.; Zhang, Y.; Zhu, S. NiH-Catalyzed Reductive Relay Hydroalkylation: A Strategy for the Remote C(Sp3)−H Alkylation of Alkenes. *Angew. Chem., Int. Ed.* **2018**, *57*, 4058–4062.

(57) He, Y.; Cai, Y.; Zhu, S. Mild and Regioselective Benzylic C–H Functionalization: Ni-Catalyzed Reductive Arylation of Remote and Proximal Olefins. *J. Am. Chem. Soc.* **2017**, *139*, 1061–1064.

(58) He, Y.; Cai, Y.; Zhu, S. Addition to "Mild and Regioselective Benzylic C-H Functionalization: Ni-Catalyzed Reductive Arylation of Remote and Proximal Olefins." *J. Am. Chem. Soc.* **2017**, *139*, 2120.

(59) Fogg, D. E.; Dos Santos, E. N. Tandem Catalysis: A Taxonomy and Illustrative Review. *Coord. Chem. Rev.* **2004**, *248*, 2365–2379.

(60) Fiorito, D.; Scaringi, S.; Mazet, C. Transition Metal-Catalyzed Alkene Isomerization as an Enabling Technology in Tandem, Sequential and Domino Processes. *Chem. Soc. Rev.* **2021**, *50*, 1391–1406.

(61) Lohr, T. L.; Marks, T. J. Orthogonal Tandem Catalysis. *Nat. Chem.* **2015**, *7*, 477–482.

(62) Vasseur, A.; Bruffaerts, J.; Marek, I. Remote Functionalization through Alkene Isomerization. *Nat. Chem.* **2016**, *8*, 209–219.

(63) Chen, F.; Xu, X.; He, Y.; Huang, G.; Zhu, S. NiH-Catalyzed Migratory Defluorinative Olefin Cross-Coupling: Trifluoromethyl-Substituted Alkenes as Acceptor Olefins to Form Gem-Difluoroalkenes. *Angew. Chem., Int. Ed.* **2020**, *59*, 5398–5402.

(64) Kerchner, H. A.; Montgomery, J. Synthesis of Secondary and Tertiary Alkylboranes via Formal Hydroboration of Terminal and 1,1-Disubstituted Alkenes. *Org. Lett.* **2016**, *18*, 5760–5763.

(65) Iwamoto, H.; Kubota, K.; Ito, H. Highly Selective Markovnikov Hydroboration of Alkyl-Substituted Terminal Alkenes with a Phosphine-Copper(i) Catalyst. *Chem. Commun.* **2016**, *52*, 5916–5919.

(66) Cai, Y.; Yang, X. T.; Zhang, S. Q.; Li, F.; Li, Y. Q.; Ruan, L. X.; Hong, X.; Shi, S. L. Copper-Catalyzed Enantioselective Markovnikov Protoboration of α-Olefins Enabled by a Buttressed N-Heterocyclic Carbene Ligand. *Angew. Chemie - Int. Ed.* **2018**, *57*, 1376–1380.

(67) Smith, J. R.; Collins, B. S. L.; Hesse, M. J.; Graham, M. A.; Myers, E. L.; Aggarwal, V. K. Enantioselective Rhodium(III)-Catalyzed Markovnikov Hydroboration of Unactivated Terminal Alkenes. *J. Am. Chem. Soc.* **2017**, *139*, 9148–9151.

(68) Su, W.; Qiao, R. X.; Jiang, Y. Y.; Zhen, X. L.; Tian, X.; Han, J. R.; Fan, S. M.; Cheng, Q.; Liu, S. Ligand-Free Iron-Catalyzed Regioselectivity-Controlled Hydroboration of Aliphatic Terminal Alkenes. *ACS Catal.* **2020**, *10*, 11963–11970.

(69) Rodriguez, J.; Culver, D. B.; Conley, M. P. Generation of Phosphonium Sites on Sulfated Zirconium Oxide: Relationship to Brønsted Acid Strength of Surface -OH Sites. *J. Am. Chem. Soc.* **2019**, *141*, 1484–1488.

(70) Burker, A. J.; Marques, C. S.; Turner, N. J.; Hermann, G. J. Catalysis and Prerequisites for the Modern Pharmaceutical Industry Landscape. In *Active Pharmaceutical Ingredients in Synthesis*; Burke, A. J., Marques, C. S., Turner, N. J., Hermann, G. J., Eds.; Wiley-VCH, 2018; pp 1–30.

(71) McGrath, N. A.; Brichacek, M.; Njardarson, J. T. A Graphical Journey of Innovative Organic Architectures That Have Improved Our Lives. *J. Chem. Educ.* **2010**, *87*, 1348–1349.

(72) Hassam, M.; Taher, A.; Arnott, G. E.; Green, I. R.; Van Otterlo, W. A. L. Isomerization of Allylbenzenes. *Chem. Rev.* **2015**, *115*, 5462–5569.

(73) Zimmermann, H.; Walzl, R. Ethylene. In *Ullmann's Encyclopedia of Industrial Chemistry*; John Wiley & Sons, Ltd, 2009.

(74) James, D. H.; Castor, W. M. Styrene. In *Ullmann's Encyclopedia of Industrial Chemistry*; John Wiley & Sons, Ltd, 2011.

(75) Elias, H.-G. Plastics, General Survey. In *Ullmann's Encyclopedia of Industrial Chemistry*; John Wiley & Sons, Ltd, 2000.

(76) Tobita, H. Polymerization Processes, 1. Fundamentals. In *Ullmann's Encyclopedia of Industrial Chemistry*; John Wiley & Sons, Ltd, 2015; pp 1–50.

(77) Cornils, V.; Herrmann, W. A.; Beller, M.; Paciello, R. *Applied Homogeneous Catalysis with Organometallics Compounds*; 2018; Vol. 53.

(78) Byrne, P. A.; Gilheany, D. G. The Modern Interpretation of the Wittig Reaction Mechanism. *Chem. Soc. Rev.* **2013**, *42*, 6670–6696.

(79) Bisceglia, J. Á.; Orelli, L. R. Recent Progress in the Horner-Wadsworth-Emmons Reaction. **2015**, No. 1113, 744–775.

(80) Janicki, I.; Kiełbasiński, P. Still–Gennari Olefination and Its Applications in Organic Synthesis. *Adv. Synth. Catal.* **2020**, *362*, 2552–2596.

(81) Van Staden, L. F.; Gravestock, D.; Ager, D. J. New Developments in the Peterson Olefination Reaction. *Chem. Soc. Rev.* **2002**, *31*, 195–200.

(82) Montgomery, T. P.; Ahmed, T. S.; Grubbs, R. H. Stereoretentive Olefin Metathesis: An Avenue to Kinetic Selectivity. *Angew. Chem., Int. Ed.* **2017**, *56*, 11024–11036.

(83) Swamy, K. C. K.; Reddy, A. S.; Sandeep, K.; Kalyani, A. Advances in Chemoselective and/or Stereoselective Semihydrogenation of Alkynes. *Tetrahedron Lett.* **2018**, *59*, 419–429.

(84) Fürstner, A. Trans-Hydrogenation, Gem-Hydrogenation, and Trans-Hydrometalation of Alkynes: An Interim Report on an Unorthodox Reactivity Paradigm. *J. Am. Chem. Soc.* **2019**, *141*, 11–24.

(85) Larsen, C. R.; Grotjahn, D. B. The Value and Application of Transition Metal Catalyzed Alkene Isomerization in Industry. *Appl. Homog. Catal. with Organomet. Compd. A Compr. Handb. Three Vol.* **2012**, 1365–1378.

(86) Liu, X.; Li, B.; Liu, Q. Base-Metal-Catalyzed Olefin Isomerization Reactions. *Synth.* **2019**, *51*, 1293–1310.

(87) Larsen, C. R.; Grotjahn, D. B. Stereoselective Alkene Isomerization over One Position. *J. Am. Chem. Soc.* **2012**, *134*, 10357–10360.

(88) Gauthier, D.; Lindhardt, A. T.; Olsen, E. P. K.; Overgaard, J.; Skrydstrup, T. In Situ Generated Bulky Palladium Hydride Complexes as Catalysts for the Efficient Isomerization of Olefins. Selective Transformation of Terminal Alkenes to 2-Alkenes. *J. Am. Chem. Soc.* **2010**, *132*, 7998–8009.

(89) Murai, M.; Nishimura, K.; Takai, K. Palladium-Catalyzed Double-Bond Migration of Unsaturated Hydrocarbons Accelerated by Tantalum Chloride. *Chem. Commun.* **2019**, *55*, 2769–2772.

(90) Kundu, G.; Sperger, T.; Rissanen, K.; Schoenebeck, F. A Next-Generation Air-Stable Palladium(I) Dimer Enables Olefin Migration and Selective C−C Coupling in Air. *Angew. Chem., Int. Ed.* **2020**, *59*, 21930–21934.

(91) Yu, X.; Zhao, H.; Li, P.; Koh, M. J. Iron-Catalyzed Tunable and Site-Selective Olefin Transposition. *J. Am. Chem. Soc.* **2020**, *142*, 18223–18230.

(92) Woof, C. R.; Durand, D. J.; Fey, N.; Richards, E.; Webster, R. L. Iron Catalyzed Double Bond Isomerization: Evidence for an FeI/FeIII Catalytic Cycle. *Chem. - A Eur. J.* **2021**, *27*, 5972–5977.

(93) Li, G.; Kuo, J. L.; Han, A.; Abuyuan, J. M.; Young, L. C.; Norton, J. R.; Palmer, J. H. Radical Isomerization and Cycloisomerization Initiated by H• Transfer. *J. Am. Chem. Soc.* **2016**, *138*, 7698–7704.

(94) Liu, X.; Zhang, W.; Wang, Y.; Zhang, Z. X.; Jiao, L.; Liu, Q. Cobalt-Catalyzed Regioselective Olefin Isomerization under Kinetic Control. *J. Am. Chem. Soc.* **2018**, *140*, 6873–6882.

(95) Meng, Q. Y.; Schirmer, T. E.; Katou, K.; König, B. Controllable Isomerization of Alkenes by Dual Visible-Light-Cobalt Catalysis. *Angew. Chem., Int. Ed.* **2019**, *58*, 5723–5728.

(96) Bergamaschi, E.; Beltran, F.; Teskey, C. Visible-light Controlled Divergent Catalysis Using a Bench-stable Cobalt(I) Hydride Complex. *Chem. – A Eur. J.* **2020**, 5180–5184.

(97) Delgado, K. R.; Youmans, D. D.; Diver, S. T. Mild Isomerization of Conjugated Dienes Using Co-Mediated Hydrogen Atom Transfer. *Org. Lett.* **2020**, *22*, 750–754.

(98) Frauenrath, H.; Brethauer, D.; Reim, S.; Maurer, M.; Piv-Doz, G. R. Highly Enantioselective Isomerization of 4,7-Dihydro-1,3-Dioxepins Catalyzed by Me-DuPHOS-Modified Dihalogenonickel Complexes and Determination of the Absolute Configuration of the Isomerization Products. *Angew. Chem., Int. Ed.* **2001**, *40*, 177–179.

(99) Liu, C.-F.; Wang, H.; Martin, R. T.; Zhao, H.; Gutierrez, O.; Koh, M. J. Olefin Functionalization/Isomerization Enables Stereoselective Alkene Synthesis. *Nat. Catal.* **2021**, *4*, 674-683.

(100) Massad, I.; Marek, I. Alkene Isomerization through Allylmetals as a Strategic Tool in Stereoselective Synthesis. *ACS Catal.* **2020**, *10*, 5793–5804.

(101) Larionov, E.; Li, H.; Mazet, C. Well-Defined Transition Metal Hydrides in Catalytic Isomerizations. *Chem. Commun.* **2014**, *50*, 9816–9826.

(102) Wang, Z.; Yin, H.; Fu, G. C. Catalytic Enantioconvergent Coupling of Secondary and Tertiary Electrophiles with Olefins. *Nature* **2018**, *563*, 379–383.

(103) Sun, S. Z.; Börjesson, M.; Martin-Montero, R.; Martin, R. Site-Selective Ni-Catalyzed Reductive Coupling of α-Haloboranes with Unactivated Olefins. *J. Am. Chem. Soc.* **2018**, *140*, 12765–12769.

(104) Zhou, F.; Zhang, Y.; Xu, X.; Zhu, S. NiH-Catalyzed Remote Asymmetric Hydroalkylation of Alkenes with Racemic α-Bromo Amides. *Angew. Chem., Int. Ed.* **2019**, *58*, 1754–1758.

(105) Liu, B.; Hu, P.; Xu, F.; Cheng, L.; Tan, M.; Han, W. Nickel-Catalyzed Remote and Proximal Wacker-Type Oxidation. *Commun. Chem.* **2019**, *2*, 1–8.

(106) Yu, R.; Rajasekar, S.; Fang, X. Enantioselective Nickel-Catalyzed Migratory Hydrocyanation of Nonconjugated Dienes. *Angew. Chem., Int. Ed.* **2020**, *59*, 21436–21441.

(107) He, Y.; Liu, C.; Yu, L.; Zhu, S. Ligand-Enabled Nickel-Catalyzed Redox-Relay Migratory Hydroarylation of Alkenes with Arylborons. *Angew. Chem., Int. Ed.* **2020**, *59*, 9186–9191.

(108) Liu, J.; Gong, H.; Zhu, S. BH3 · Me2S: An Alternative Hydride Source for NiH-Catalyzed Reductive Migratory Hydroarylation and Hydroalkenylation of Alkenes. *Eur. J. Org. Chem.* **2021**, *2021*, 1543–1546.

(109) Liu, J.; Gong, H.; Zhu, S. Nickel-Catalyzed, Regio- and Enantioselective Benzylic Alkenylation of Olefins with Alkenyl Bromide. *Angew. Chem., Int. Ed.* **2021**, *60*, 4060–4064.

(110) Chen, J.; Zhu, S. Nickel-Catalyzed Multicomponent Coupling: Synthesis of α-Chiral Ketones by Reductive Hydrocarbonylation of Alkenes. *J. Am. Chem. Soc.* **2021**, *143*, 14089–14096.

(111) He, Y.; Han, B.; Zhu, S. Terminal-Selective C(Sp3)-H Arylation: NiH-Catalyzed Remote Hydroarylation of Unactivated Internal Olefins. *Organometallics* **2021**, *40*, 2253–2264.

(112) Jiang, X.; Han, B.; Xue, Y.; Duan, M.; Gui, Z.; Wang, Y.; Zhu, S. Nickel-Catalysed Migratory Hydroalkynylation and Enantioselective Hydroalkynylation of Olefins with Bromoalkynes. *Nat. Commun.* **2021**, *12*, 1–8.

(113) Gao, J.; Jiao, M.; Ni, J.; Yu, R.; Cheng, G. J.; Fang, X. Nickel-Catalyzed Migratory Hydrocyanation of Internal Alkenes: Unexpected Diastereomeric-Ligand-Controlled Regiodivergence. *Angew. Chem., Int. Ed.* **2021**, *60*, 1883–1890.

(114) Gaydou, M.; Moragas, T.; Juliá-Hernández, F.; Martin, R. Site-Selective Catalytic Carboxylation of Unsaturated Hydrocarbons with CO2 and Water. *J. Am. Chem. Soc.* **2017**, *139*, 12161–12164.

(115) Cramer, R.; Lindsey, R. V. The Mechanism of Isomerization of Olefins with Transition Metal Catalysts. *J. Am. Chem. Soc.* **1966**, *8*, 3534–3544.

(116) Lochow, C. F.; Miller, R. G. Nickel-Promoted Isomerizations of Alkenes Bearing Polar Functional Groups. *J. Org. Chem.* **1976**, *41*, 3020–3022.

(117) Malanga, C.; Urso, A.; Lardicci, L. Nickel Mediated Flash Isomerization: A New Approach to 1,4-but-1-Ene Diol Derivatives. *Tetrahedron Lett.* **1995**, *36*, 1133–1136.

(118) Breitenfeld, J.; Vechorkin, O.; Corminboeuf, C.; Scopelliti, R.; Hu, X. Why Are (NN2)Ni Pincer Complexes Active for Alkyl-Alkyl Coupling: β-H Elimination Is Kinetically Accessible but Thermodynamically Uphill. *Organometallics* **2010**, *29*, 3686–3689.

(119) Stavropoulos, P.; Muetterties, M. C.; Carrièe, M.; Holm, R. H. Structural and Reaction Chemistry of Nickel Complexes in Relation to Carbon Monoxide Dehydrogenase: A Reaction System Simulating Acetyl-Coenzyme A Synthase Activity. *J. Am. Chem. Soc.* **1991**, *113*, 8485–8492.

(120) Kuntz, E. G.; Godard, G.; Basset, J. M.; Vittori, O. M. Nickel(0)-TPPTS-Cyanide Complex in Water. An Efficient and Flexible Catalyst for the Isomerization of Olefinic Compounds at Room Temperature. *Oil Gas Sci. Technol.* **2007**, *62*, 781–785.

(121) Boro, B. J.; Duesler, E. N.; Goldberg, K. I.; Kemp, R. A. Synthesis, Characterization, and Reactivity of Nickel Hydride Complexes Containing 2,6-C 6H 3 (CH 2PR 2) 2 (R = TBu, CHex, and TPr) Pincer Ligands. *Inorg. Chem.* **2009**, *48*, 5081–5087.

(122) Chakraborty, S.; Krause, J. A.; Guan, H. Hydrosilylation of Aldehydes and Ketones Catalyzed by Nickel PCP-Píncer Hydride Complexes. *Organometallics* **2009**, *28*, 582–586.

(123) Frauenrath, H.; Reim, S.; Wiesner, A. Asymmetric Double-Bond Isomerization of Cyclic Allyl Acetals by Using Diop and Chiraphos Modified Nickel Complexes. *Tetrahedron: Asymmetry* **1998**, *9*, 1103–1106.

(124) Wille, A.; Tomm, S.; Frauenrath, H. A Highly Z-Selective Isomerization (Double-Bond Migration) Procedure for Allyl Acetals and Allyl Ethers Mediated by Nickel Complexes. *Synthesis (Stuttg).* **1998**, *3*, 305–308.

(125) Chen, X.; Wang, Z.; Zhou, J.; Liu, Y.; Jin, H.; Zhou, B. Nickel-Catalyzed Remote Hydrosilylation of Unconjugated Enones with Bulky Triphenylsilane. *Org. Biomol. Chem.* **2021**, *19*, 8021–8024.

(126) Mirza-Aghayan, M.; Boukherroub, R.; Bolourtchian, M.; Hoseini, M.; Tabar-Hydar, K. A Novel and Efficient Method for Double Bond Isomerization. *J. Organomet. Chem.* **2003**, *678*, 1–4.

(127) Mirza-Aghayan, M.; Boukherroub, R.; Bolourtchian, M. A Mild and Efficient Palladium-Triethylsilane System for Reduction of Olefins and Carbon-Carbon Double Bond Isomerization. *Appl. Organomet. Chem.* **2006**, *20*, 214–219.

(128) Ahn, H.; Son, I.; Lee, J.; Lim, H. J. Palladium−Hydride-Catalyzed Regiodivergent Isomerization of 1-Alkenes. *Asian J. Org. Chem.* **2017**, *6*, 335–341.

(129) Tsay, C.; Peters, J. C. Thermally Stable N2 and H2 Adducts of Cationic Nickel(II). *Chem. Sci.* **2012**, *3*, 1313–1318.

(130) Du, X.; Zhang, Y.; Peng, D.; Huang, Z. Base-Metal-Catalyzed Regiodivergent Alkene Hydrosilylations. *Angew. Chem., Int. Ed.* **2016**, *55*, 6671–6675.

(131) Chen, J.; Guo, J.; Lu, Z. Recent Advances in Hydrometallation of Alkenes and Alkynes via the First Row Transition Metal Catalysis. *Chin. J. Chem.* **2018**, *36*, 1075–1109.

(132) Benítez Junquera, L.; Puerta, M. C.; Valerga, P. R-Allyl Nickel(II) Complexes with Chelating N-Heterocyclic Carbenes: Synthesis, Structural Characterization, and Catalytic Activity. *Organometallics* **2012**, *31*, 2175–2183.

(133) Chaulagain, M. R.; Mahandru, G. M.; Montgomery, J. Alkyne Hydrosilylation Catalyzed by Nickel Complexes of N-Heterocyclic Carbenes. *Tetrahedron* **2006**, *62*, 7560-7566.

(134) Miller, Z. D.; Li, W.; Belderrain, T. R.; Montgomery, J. Regioselective Allene Hydrosilylation Catalyzed by N-Heterocyclic Carbene Complexes of Nickel and Palladium. *J. Am. Chem. Soc.* **2013**, *135*, 15282–15285.

(135) Miller, Z. D.; Dorel, R.; Montgomery, J. Regiodivergent and Stereoselective Hydrosilylation of 1,3-Disubstituted Allenes. *Angew. Chem., Int. Ed.* **2015**, *54*, 9088–9091.

(136) Felten, S.; Marshall, S. F.; Groom, A. J.; Vanderlinden, R. T.; Stolley, R. M.; Louie, J. Synthesis and Characterization of [(NHC)Ni(Styrene)2] Complexes: Isolation of Monocarbene Nickel Complexes and Benchmarking of %VBur in (NHC)Ni-π Systems. *Organometallics* **2018**, *37*, 3687–3697.

(137) Wu, J.; Faller, J. W.; Hazari, N.; Schmeier, T. J. Stoichiometric and Catalytic Reactions of Thermally Stable Nickel(0) NHC Complexes. *Organometallics* **2012**, *31*, 806–809.

(138) Nett, A. J.; Canellas, S.; Higuchi, Y.; Robo, M. T.; Kochkodan, J. M.; Haynes, M. T.; Kampf, J. W.; Montgomery, J. Stable, Well-Defined Nickel(0) Catalysts for Catalytic C-C and C-N Bond Formation. *ACS Catal.* **2018**, *8*, 6606–6611.

(139) Nattmann, L.; Saeb, R.; Nöthling, N.; Cornella, J. An Air-Stable Binary Ni(0)–Olefin Catalyst. *Nat. Catal.* **2019**, *3*, 6-13.

(140) Hurst, M. R.; Zakharov, L. N.; Cook, A. K. The Mechanism of Oxidative Addition of Pd(0) to Si–H Bonds: Electronic Effects, Reaction Mechanism, and Hydrosilylation. *Chem. Sci.* **2021**, *12*, 13045–13060.

(141) Akhani, R. K.; Moore, M. I.; Pribyl, J. G.; Wiskur, S. L. Linear Free-Energy Relationship and Rate Study on a Silylation-Based Kinetic Resolution: Mechanistic Insights. *J. Org. Chem.* **2014**, *79*, 2384–2396.

(142) Blackmond, D. G. Kinetic Profiling of Catalytic Organic Reactions as a Mechanistic Tool. *J. Am. Chem. Soc.* **2015**, *137*, 10852–10866.

(143) Cheng, L.; Li, M. M.; Xiao, L. J.; Xie, J. H.; Zhou, Q. L. Nickel(0)-Catalyzed Hydroalkylation of 1,3-Dienes with Simple Ketones. *J. Am. Chem. Soc.* **2018**, *140*, 11627–11630.

(144) Green, S. A.; Huffman, T. R.; McCourt, R. O.; Van Der Puyl, V.; Shenvi, R. A. Hydroalkylation of Olefins to Form Quaternary Carbons. *J. Am. Chem. Soc.* **2019**, *141*, 7709–7714.

(145) Bair, J. S.; Schramm, Y.; Sergeev, A. G.; Clot, E.; Eisenstein, O.; Hartwig, J. F. Linear-Selective Hydroarylation of Unactivated Terminal and Internal Olefins with Trifluoromethyl-Substituted Arenes. *J. Am. Chem. Soc.* **2014**, *136*, 13098–13101.

(146) Biswas, S. Mechanistic Understanding of Transition-Metal-Catalyzed Olefin Isomerization: Metal-Hydride Insertion-Elimination vs. π-Allyl Pathways. *Comments Inorg. Chem.* **2015**, *35*, 301–331.

(147) Wang, S. C.; Troast, D. M.; Conda-Sheridan, M.; Zuo, G.; Lagarde, D.; Louie, J.; Tantillo, D. J. Mechanism of the Ni(0)-Catalyzed Vinylcyclopropane-Cyclopentene Rearrangement. *J. Org. Chem* **2009**, *74*, 7822–7833.

(148) Green, S. A.; Crossley, S. W. M.; Matos, J. L. M.; Vásquez-Céspedes, S.; Shevick, S. L.; Shenvi, R. A. The High Chemofidelity of Metal-Catalyzed Hydrogen Atom Transfer. *Acc. Chem. Res.* **2018**, *51*, 2628–2640.

(149) Kawamura, K. E.; Chang, A. S.; Martin, D. J.; Smith, H. M.; Morris, P. T.; Cook, A. K. Modular Ni(0)/Silane Catalytic System for the Isomerization of Alkenes. *Organometallics* **2022**, *41*, 486–496.

(150) Trost, B. M.; Cregg, J. J.; Quach, N. Isomerization of N-Allyl Amides to Form Geometrically Defined Di-, Tri-, and Tetrasubstituted Enamides. *J. Am. Chem. Soc.* **2017**, *139*, 5133–5139.

(151) Krompiec, S.; Krompiec, M.; Penczek, R.; Ignasiak, H. Double Bond Migration in N-Allylic Systems Catalyzed by Transition Metal Complexes. *Coord. Chem. Rev.* **2008**, *252*, 1819–1841.

(152) Donohoe, T. J.; O'Riordan, T. J. C.; Rosa, C. P. Ruthenium-Catalyzed Isomerization of Terminal Olefins: Applications to Synthesis. *Angew. Chem., Int. Ed.* **2009**, *48*, 1014–1017.

(153) Schmidt, A.; Nödling, A. R.; Hilt, G. An Alternative Mechanism for the Cobalt-Catalyzed Isomerization of Terminal Alkenes to (Z)-2-Alkenes. *Angew. Chem., Int. Ed.* **2015**, *54*, 801–804.

(154) Legacy, C. J.; Hope, T. O.; Gagné, Y.; Greenaway, F. T.; Frenette, M.; Emmert, M. H. Mechanistic Insights into Fe Catalyzed α-C−H Oxidations of Tertiary Amines. *ChemCatChem* **2021**, *13*, 235–246.

(155) Nielsen, C. D. T.; Burés, J. Visual Kinetic Analysis. *Chem. Sci.* **2019**, *10*, 348–353.

(156) Martínez-Carrión, A.; Howlett, M. G.; Alamillo-Ferrer, C.; Clayton, A. D.; Bourne, R. A.; Codina, A.; Vidal-Ferran, A.; Adams, R. W.; Burés, J. Kinetic Treatments for Catalyst Activation and Deactivation Processes Based on Variable Time Normalization Analysis. *Angew. Chem., Int. Ed.* **2019**, *58*, 10189–10193.

(157) Gómez-Gallego, M.; Sierra, M. A. Kinetic Isotope Effects in the Study of Organometallic Reaction Mechanisms. *Chem. Rev.* **2011**, *111*, 4857–4963.

(158) Schultz, D.; Campeau, L. C. Harder, Better, Faster. *Nat. Chem.* **2020**, *12*, 661–664.

(159) Larsen, C. R.; Paulson, E. R.; Erdogan, G.; Grotjahn, D. B. A Facile, Convenient, and Green Route to (E)-Propenylbenzene Flavors and Fragrances by Alkene Isomerization. *Synlett* **2015**, *26*, 2462–2466.

(160) Wu, J.; Faller, J. W.; Hazari, N.; Schmeier, T. J. Stoichiometric and Catalytic Reactions of Thermally Stable Nickel(0) NHC Complexes. *Organometallics* **2012**, *31*, 806–809.

(161) Seayad, A.; Ahmed, M.; Klein, H.; Jackstell, R.; Gross, T.; Beller, M. Internal Olefins to Linear Amines. *Science.* **2002**, *297*, 1676–1678.

(162) Edwards, D. R.; Crudden, C. M.; Yam, K. One-Pot Carbon Monoxide-Free Hydroformylation of Internal Olefins to Terminal Aldehydes. *Adv. Synth. Catal.* **2005**, *347*, 50–54.

(163) Behr, A.; Obst, D.; Schulte, C.; Schosser, T. Highly Selective Tandem Isomerization-Hydroformylation Reaction of Trans-4-Octene to n-Nonanal with Rhodium-BIPHEPHOS Catalysis. *J. Mol. Catal. A Chem.* **2003**, *206*, 179–184.

(164) Obligacion, J. V.; Chirik, P. J. Bis(Imino)Pyridine Cobalt-Catalyzed Alkene Isomerization-Hydroboration: A Strategy for Remote Hydrofunctionalization with Terminal Selectivity. *J. Am. Chem. Soc.* **2013**, *135*, 19107–19110.

(165) Ruddy, A. J.; Sydora, O. L.; Small, B. L.; Stradiotto, M.; Turculet, L. (N-Phosphinoamidinate)Cobalt-Catalyzed Hydroboration: Alkene Isomerization Affords Terminal Selectivity. *Chem. - Eur. J.* **2014**, *20*, 13918–13922.

(166) Palmer, W. N.; Diao, T.; Pappas, I.; Chirik, P. J. High-Activity Cobalt Catalysts for Alkene Hydroboration with Electronically Responsive Terpyridine and α-Diimine Ligands. *ACS Catal.* **2015**, *5*, 622–626.

(167) Ogawa, T.; Ruddy, A. J.; Sydora, O. L.; Stradiotto, M.; Turculet, L. Cobalt- and Iron-Catalyzed Isomerization-Hydroboration of Branched Alkenes: Terminal Hydroboration with Pinacolborane and 1,3,2-Diazaborolanes. *Organometallics* **2017**, *36*, 417–423.

(168) Obligacion, J. V.; Chirik, P. J. Highly Selective Bis(Imino)Pyridine Iron-Catalyzed Alkene Hydroboration. *Org. Lett.* **2013**, *15*, 2680–2683.

(169) Xi, Y.; Hartwig, J. F. Diverse Asymmetric Hydrofunctionalization of Aliphatic Internal Alkenes through Catalytic Regioselective Hydroboration. *J. Am. Chem. Soc.* **2016**, *138*, 6703–6706.

(170) Miyaura, N.; Suzuki, A. Palladium-Catalyzed Cross-Coupling Reactions of Organoboron Compounds. *Chem. Rev.* **1995**, *95*, 2457–2483.

(171) Williams, L. A.; Guo, N.; Motta, A.; Delferro, M.; Fragalà, I. L.; Miller, J. T.; Marks, T. J. Surface Structural-Chemical Characterization of a Single-Site D0 Heterogeneous Arene Hydrogenation Catalyst Having 100% Active Sites. *Proc. Natl. Acad. Sci. U. S. A.* **2013**, *110*, 413–418.

(172) Gu, W.; Stalzer, M. M.; Nicholas, C. P.; Bhattacharyya, A.; Motta, A.; Gallagher, J. R.; Zhang, G.; Miller, J. T.; Kobayashi, T.; Pruski, M.; et al. Benzene Selectivity in Competitive Arene Hydrogenation: Effects of Single-Site Catalyst···acidic Oxide Surface Binding Geometry. *J. Am. Chem. Soc.* **2015**, *137*, 6770–6780.

(173) Stalzer, M. M.; Nicholas, C. P.; Bhattacharyya, A.; Motta, A.; Delferro, M.; Marks, T. J. Single-Face/All-Cis Arene Hydrogenation by a Supported Single-Site D0 Organozirconium Catalyst. *Angew. Chem., Int. Ed.* **2016**, *55*, 5263–5267.

(174) Stalzer, M. M.; Delferro, M.; Marks, T. J. Supported Single-Site Organometallic Catalysts for the Synthesis of High-Performance Polyolefins. *Catal. Lett.* **2015**, *145*, 3–14.

(175) Tafazolian, H.; Culver, D. B.; Conley, M. P. A Well-Defined Ni(II) α-Diimine Catalyst Supported on Sulfated Zirconia for Polymerization Catalysis. *Organometallics* **2017**, *36*, 2385–2388.

(176) Culver, D. B.; Tafazolian, H.; Conley, M. P. A Bulky Pd(II) α-Diimine Catalyst Supported on Sulfated Zirconia for the Polymerization of Ethylene and Copolymerization of Ethylene and Methyl Acrylate. *Organometallics* **2018**, *37*, 1001–1006.

(177) Culver, D. B.; Conley, M. P. Activation of C−F Bonds by Electrophilic Organosilicon Sites Supported on Sulfated Zirconia. *Angew. Chem., Int. Ed.* **2018**, *57*, 14902–14905.

(178) Hino, M.; Kobayashi, S.; Arata, K. Reactions of Butane and Isobutane Catalyzed by Zirconium Oxide Treated with Sulfate Ion. Solid Super Acid Catalyst. *J. Am. Chem. Soc.* **1979**, *101*, 6439–6441.

(179) Hino, M.; Arata, K. Synthesis of Solid Super Acid Catalyst with Acid Strength of H0 < -16.04. *J. Chem. Soc., Chem. Commun.* **1980**, 851–852.

(180) Hintermann, L. Expedient Syntheses of the N-Heterocyclic Carbene Precursor Imidazolium Salts IPr·HCl, IMes·HCl and IXy·HCl. *Beilstein J. Org. Chem.* **2007**, *3*, 1–5.

(181) Jafarpour, L.; Stevens, E. D.; Nolan, S. P. A Sterically Demanding Nucleophilic Carbene: Thermochemistry and Catalytic Application in Olefin Metathesis. *J. Organomet. Chem.* **2000**, *606*, 49–54.

(182) Bantreil, X.; Nolan, S. P. Synthesis of N-Heterocyclic Carbene Ligands and Derived Ruthenium Olefin Metathesis Catalysts. *Nat. Protoc.* **2011**, *6*, 69–77.

(183) Briggs, A. J. Improved Preparation of 1,3-Bis(2,6-Di-Iso-Propylphenyl)Imidazolium Tetrafluoroborate. *Synth. Commun.* **2013**, *43*, 3258–3261.

(184) Wu, J.; Hazari, N.; Incarvito, C. D. Synthesis, Properties, and Reactivity with Carbon Dioxide of (Allyl)2Ni(L) Complexes. *Organometallics* **2011**, *30*, 3142–3150.

(185) Iglesias, M. J.; Blandez, J. F.; Fructos, M. R.; Prieto, A.; Álvarez, E.; Belderrain, T. R.; Nicasio, M. C. Synthesis, Structural Characterization, and Catalytic Activity of IPrNi(Styrene)2 in the Amination of Aryl Tosylates. *Organometallics* **2012**, *31*, 6312–6316.

(186) Dible, B. R.; Sigman, M. S.; Arif, A. M. Oxygen-Induced Ligand Dehydrogenation of a Planar Bis-μ-Chloronickel(I) Dimer Featuring an NHC Ligand. *Inorg. Chem.* **2005**, *44*, 3774–3776.

(187) Doobary, S.; Sedikides, A. T.; Caldora, H. P.; Poole, D. L.; Lennox, A. J. J. Electrochemical Vicinal Difluorination of Alkenes: Scalable and Amenable to Electron-Rich Substrates. *Angew. Chem., Int. Ed.* **2020**, *59*, 1155–1160.

(188) Li, C.; Li, M.; Li, J.; Wu, W.; Jiang, H. Palladium-Catalyzed Oxidative Allylation of Bis[(Pinacolato)Boryl]Methane: Synthesis of Homoallylic Boronic Esters. *Chem. Commun.* **2017**, *54*, 66–69.

(189) De Carolis, M.; Protti, S.; Fagnoni, M.; Albini, A. Metal-Free Cross-Coupling Reactions of Aryl Sulfonates and Phosphates through Photoheterolysis of Aryl-Oxygen Bonds. *Angew. Chem., Int. Ed.* **2005**, *44*, 1232–1236.

(190) Mayer, M.; Czaplik, W. M.; Von Wangelin, A. J. Practical Iron-Catalyzed Allylations of Aryl Grignard Reagents. *Adv. Synth. Catal.* **2010**, *352*, 2147–2152.

(191) Bedford, R. B.; Brenner, P. B.; Carter, E.; Clifton, J.; Cogswell, P. M.; Gower, N. J.; Haddow, M. F.; Harvey, J. N.; Kehl, J. A.; Murphy, D. M.; et al. Iron Phosphine Catalyzed Cross-Coupling of Tetraorganoborates and Related Group 13 Nucleophiles with Alkyl Halides. *Organometallics* **2014**, *33*, 5767–5780.

(192) Yang, Y.; Zhou, Q.; Cai, J.; Xue, T.; Liu, Y.; Jiang, Y.; Su, Y.; Chung, L.; Vicic, D. A. Exploiting the Trifluoroethyl Group as a Precatalyst Ligand in Nickel-Catalyzed Suzuki-Type Alkylations. *Chem. Sci.* **2019**, *10*, 5275–5282.

(193) Lin, S.; Song, C. X.; Cai, G. X.; Wang, W. H.; Shi, Z. J. Intra/Intermolecular Direct Allylic Alkylation via Pd(II)-Catalyzed Allylic C-H Activation. *J. Am. Chem. Soc.* **2008**, *130*, 12901–12903.

(194) Gresser, M. J.; Wales, S. M.; Keller, P. A. The Attempted Stereoselective Synthesis of Chiral 2,2′-Biindoline. *Tetrahedron* **2010**, *66*, 6965–6976.

(195) Matcha, K.; Antonchick, A. P. Cascade Multicomponent Synthesis of Indoles, Pyrazoles, and Pyridazinones by Functionalization of Alkenes. *Angew. Chem., Int. Ed.* **2014**, *53*, 11960–11964.

(196) Xiong, T.; Li, Y.; Mao, L.; Zhang, Q.; Zhang, Q. Palladium-Catalyzed Allylic C–H Amination of Alkenes with N-Fluorodibenzenesulfonimide: Water Plays an Important Role. *Chem. Commun.* **2012**, *48*, 2246–2248.

(197) Brimble, M. A.; Flowers, C. L.; Trzoss, M.; Tsang, K. Y. A Facile Synthesis of Fused Aromatic Spiroacetals Based on the 3,4,3′,4′-Tetrahydro-2,2′-Spirobis(2H-1-Benzopyran) Skeleton. *Tetrahedron* **2006**, *62*, 5883–5896.

(198) Lühning, L. H.; Strehl, J.; Schmidtmann, M.; Doye, S. Hydroaminoalkylation of Allylsilanes and a One-Pot Procedure for the Synthesis of 1,5-Benzoazasilepines. *Chem. - Eur. J.* **2017**, *23*, 4197–4202.

(199) Li, Z.; Cao, X.; Lai, G.; Liu, J.; Ni, Y.; Wu, J.; Qiu, H. Controlled Introduction of Allylic Group to Chlorosilanes. *J. Organomet. Chem.* **2006**, *691*, 4740–4746.

(200) Peng, Y.; Li, D.; Fan, J.; Xu, W.; Xu, J.; Yu, H.; Lin, X.; Wu, Q. Enantiocomplementary C–H Bond Hydroxylation Combining Photo-Catalysis and Whole-Cell Biocatalysis in a One-Pot Cascade Process. *Eur. J. Org. Chem.* **2020**, *2020*, 821–825.

(201) Zhu, D.; Lv, L.; Li, C. C.; Ung, S.; Gao, J.; Li, C. J. Umpolung of Carbonyl Groups as Alkyl Organometallic Reagent Surrogates for Palladium-Catalyzed Allylic Alkylation. *Angew. Chem., Int. Ed.* **2018**, *57*, 16520–16524.

(202) Sweeney, J. B.; Ball, A. K.; Lawrence, P. A.; Sinclair, M. C.; Smith, L. J. A Simple, Broad-Scope Nickel(0) Precatalyst System for the Direct Amination of Allyl Alcohols. *Angew. Chem., Int. Ed.* **2018**, *57*, 10202–10206.

(203) Liu, G.; Wurst, J. M.; Tan, D. S. Stereoselective Synthesis of Benzannulated Spiroketals: Influence of the Aromatic Ring on Reactivity and Conformation. *Org. Lett.* **2009**, *11*, 3670–3673.

(204) Barluenga, J.; Fernández-Simón, J. L.; Concellón, J. M.; Yus, M. Chloromethyl-Lithium and 1-Chloro-2-Methylprop-1-Enyl-Lithium: Useful Intermediates in the Synthesis of Unsaturated and Bifunctionalized Compounds. *J. Chem. Soc. Perkin Trans.* **1988**, *12*, 3339–3343.

(205) Reid, W. B.; Watson, D. A. Synthesis of Trisubstituted Alkenyl Boronic Esters from Alkenes Using the Boryl-Heck Reaction. *Org. Lett.* **2018**, *20*, 6832–6835.

(206) Molloy, J. J.; Metternich, J. B.; Daniliuc, C. G.; Watson, A. J. B.; Gilmour, R. Contra-Thermodynamic, Photocatalytic E→Z Isomerization of Styrenyl Boron Species: Vectors to Facilitate Exploration of Two-Dimensional Chemical Space. *Angew. Chem., Int. Ed.* **2018**, *57*, 3168–3172.

(207) McIntyre, S.; Hörmann, E.; Menges, F.; Smidt, S. P.; Pfaltz, A. Iridium-Catalyzed Enantioselective Hydrogenation of Terminal Alkenes. *Adv. Synth. Catal.* **2005**, *347*, 282–288.

(208) Firmansjah, L.; Fu, G. C. Intramolecular Heck Reactions of Unactivated Alkyl Halides. *J. Am. Chem. Soc.* **2007**, *129*, 11340–11341.

(209) Rao Volla, C. M.; Dubbaka, S. R.; Vogel, P. Palladium-Catalyzed Desulfinylative C-C Allylation of Grignard Reagents and Enolates Using Allylsulfonyl Chlorides and Esters. *Tetrahedron* **2009**, *65*, 504–511.

(210) Zhao, J.; Cheng, B.; Chen, C.; Lu, Z. Cobalt-Catalyzed Migrational Isomerization of Styrenes. *Org. Lett.* **2020**, *22*, 837–841.

(211) Zavesky, B. P.; De Jesús Cruz, P.; Johnson, J. S. Progress toward a Convergent, Asymmetric Synthesis of Jervine. *Org. Lett.* **2020**, *22*, 3537–3541.

(212) Strauss, M. A.; Wegner, H. A. Exploring London Dispersion and Solvent Interactions at Alkyl–Alkyl Interfaces Using Azobenzene Switches. *Angew. Chem., Int. Ed.* **2019**, *58*, 18552–18556.

(213) Savela, R.; Zawartka, W.; Leino, R. Iron-Catalyzed Chlorination of Silanes. *Organometallics* **2012**, *31*, 3199–3206.

(214) Lee, G. S.; Kim, D.; Hong, S. H. Pd-Catalyzed Formal Mizoroki–Heck Coupling of Unactivated Alkyl Chlorides. *Nat. Commun.* **2021**, *12*, 1–12.

(215) Wu, Q.; Wang, L.; Jin, R.; Kang, C.; Bian, Z.; Du, Z.; Ma, X.; Guo, H.; Gao, L. Nickel-Catalyzed Allylic C(Sp2)–H Activation: Stereoselective Allyl Isomerization and Regiospecific Allyl Arylation of Allylarenes. *Eur. J. Org. Chem.* **2016**, *2016*, 5415–5422.

(216) Jolly, P. I.; Fleary-Roberts, N.; O'Sullivan, S.; Doni, E.; Zhou, S.; Murphy, J. A. Reactions of Triflate Esters and Triflamides with an Organic Neutral Super-Electron-Donor. *Org. Biomol. Chem.* **2012**, *10*, 5807–5810.

(217) Nakayama, K.; Maeta, N.; Horiguchi, G.; Kamiya, H.; Okada, Y. Radical Cation Diels-Alder Reactions by TiO 2 Photocatalysis. *Org. Lett.* **2019**, *21*, 2246–2250.

(218) Albright, H.; Vonesh, H. L.; Schindler, C. S. Superelectrophilic Fe(III)-Ion Pairs as Stronger Lewis Acid Catalysts for (E)-Selective Intermolecular Carbonyl-Olefin Metathesis. *Org. Lett.* **2020**, *22*, 3155–3160.

(219) Cook, A.; Prakash, S.; Zheng, Y. L.; Newman, S. G. Exhaustive Reduction of Esters Enabled by Nickel Catalysis. *J. Am. Chem. Soc.* **2020**, *142*, 8109–8115.

(220) Hogan, A.-M. L.; Tricotet, T.; Meek, A.; Khokhar, S. S.; O'Shea, D. F. Applications of Enantioselective Carbolithiation of Ortho-Substituted-b-Methylstyrenes. *J. Org. Chem.* **2008**, *73*, 6041–6044.

(221) Borate, H. B.; Gaikwad, S. H.; Kudale, A. S.; Chavan, S. P.; Pharande, S. G.; Wagh, V. D.; Sawant, V. S. One-Step Method for the Synthesis of Aryl Olefins from Aryl Aldehydes and Aliphatic Aldehydes. *Tetrahedron Lett.* **2013**, *54*, 1528–1530.

(222) Mahesh, M.; Murphy, J. A.; Wessel, H. P. Novel Deoxygenation Reaction of Epoxides by Indium. *J. Org. Chem.* **2005**, *70*, 4118–4123.

(223) de Haan, J. W.; Van de Ven, L. J. M. Configurations and Conformations in Acyclic, Unsaturated Hydrocarbons. A 13C NMR Study. *Org. Magn. Reson.* **1973**, *5*, 147–153.

(224) Belger, C.; Neisius, N. M.; Plietker, B. A Selective Ru-Catalyzed Semireduction of Alkynes to Z Olefins under Transfer-Hydrogenation Conditions. *Chem. - Eur. J.* **2010**, *16*, 12214–12220.

(225) Couperus, P. A.; Clague, A. D. H.; van Dongen, J. P. C. M. 13C Chemical Shifts of Some Model Olefins. *Org. Magn. Reson.* **1976**, *8*, 426–431.

(226) Ma, E.; Jiang, Y.; Chen, Y.; Qi, L.; Yan, X.; Li, Z. Salicylate-Directed C−O Bond Cleavage: Iron-Catalyzed Allylic Substitution with Grignard Reagents. *Asian J. Org. Chem.* **2018**, *7*, 914–917.

(227) Adam, W.; Stegmann, V. R. Unusual Temperature Dependence in the Cis/Trans-Oxetane Formation Discloses Competitive Syn versus Anti Attack for the Paternò-Büchi Reaction of Triplet-Excited Ketones with Cis- and Trans-Cyloоctenes. Conformational Control of Diastereoselectivity in The. *J. Am. Chem. Soc.* **2002**, *124*, 3600–3607.

(228) Anselmi, C.; Centini, M.; Fedeli, P.; Paoli, M. L.; Sega, A.; Scesa, C.; Pelosi, P. Unsaturated Hydrocarbons with Fruity and Floral Odors. *J. Agric. Food Chem.* **2000**, *48*, 1285–1289.

(229) Breit, B.; Demel, P.; Grauer, D.; Studte, C. Stereospecific and Stereodivergent Construction of Tertiary and Quaternary Carbon Centers through Switchable Directed/Nondirected Allylic Substitution. *Chem. - Asian J.* **2006**, *1*, 586–597.

(230) Chen, C.; Dugan, T. R.; Brennessel, W. W.; Weix, D. J.; Holland, P. L. Z -Selective Alkene Isomerization by High-Spin Cobalt(II) Complexes. *J. Am. Chem. Soc.* **2014**, *136*, 945–955.

(231) Gärtner, D.; Stein, A. L.; Grupe, S.; Arp, J.; Von Wangelin, A. J. Iron-Catalyzed Cross-Coupling of Alkenyl Acetates. *Angew. Chem., Int. Ed.* **2015**, *54*, 10545–10549.

(232) Pieterse, T.; Visser, M.; Marais, C.; Bezuidenhoudt, B. C. B. Al(OTf)3: An Efficient Lewis Acid Additive for Domino Addition-Elimination of Grignard Reagents to Activated Ketones. *Synlett* **2016**, *27*, 1541–1546.

(233) Wei, W.; Dai, X. J.; Wang, H.; Li, C.; Yang, X.; Li, C. J. Ruthenium(II)-Catalyzed Olefination: Via Carbonyl Reductive Cross-Coupling. *Chem. Sci.* **2017**, *8*, 8193–8197.

(234) Villaseñor, E.; Gutierrez-Gonzalez, R.; Carrillo-Hermosilla, F.; Fernández-Galán, R.; Lõpez-Solera, I.; Fernández-Pacheco, A. R.; Antiñolo, A. Neutral Dimethylzirconocene Complexes as Initiators for the Ring-Opening Polymerization of ε-Caprolactone. *Eur. J. Inorg. Chem.* **2013**, *7*, 1184–1196.

(235) Dalton, T.; Greßies, S.; Das, M.; Niehues, M.; Schrader, M. L.; Gutheil, C.; Ravoo, B. J.; Glorius, F. Silver-Catalysed Hydroarylation of Highly Substituted Styrenes. *Angew. Chem., Int. Ed.* **2021**, *60*, 8537–8541.

(236) Rodriguez, D.; Perez Sestelo, J.; Sarandeses, L. A. Palladium-Catalyzed Cross-Coupling Reactions of Allylic Halides and Acetates Wtih Indium Organometallics. *J. Org. Chem.* **2004**, *69*, 8136–8139.

(237) Bandari, R.; Höche, T.; Prager, A.; Dimberger, K.; Buchmeiser, M. R. Ring-Opening Metathesis Polymerization Based Pore-Size-Selective Functionalization of Glycidyl Methacrylate Based Monolithic Media: Access to Size-Stable Nanoparticles for Ligand-Free Metal Catalysis. *Chem. - Eur. J.* **2010**, *16*, 4650–4658.

(238) Lebel, H.; Davi, M.; Díez-González, S.; Nolan, S. P. Copper-Carbene Complexes as Catalysts in the Synthesis of Functionalized Styrenes and Aliphatic Alkenes. *J. Org. Chem.* **2007**, *72*, 144–149.

(239) Xu, L.; Li, B. J.; Wu, Z. H.; Lu, X. Y.; Guan, B. T.; Wang, B. Q.; Zhao, K. Q.; Shi, Z. J. Nickel-Catalyzed Efficient and Practical Suzuki-Miyaura Coupling of Alkenyl and Aryl Carbamates with Aryl Boroxines. *Org. Lett.* **2010**, *12*, 884–887.

(240) Liu, C. F.; Luo, X.; Wang, H.; Koh, M. J. Catalytic Regioselective Olefin Hydroarylation(Alkenylation) by Sequential Carbonickelation-Hydride Transfer. *J. Am. Chem. Soc.* **2021**, *143*, 9498–9506.

(241) Molander, G. A.; Argintaru, O. A. Stereospecific Ni-Catalyzed Cross-Coupling of Potassium Alkenyltrifluoroborates with Alkyl Halides. *Org. Lett.* **2014**, *16*, 1904–1907.

(242) Jang, H. Y.; Krische, M. J. Rhodium-Catalyzed Reductive Cyclization of 1,6-Diynes and 1,6-Enynes Mediated by Hydrogen: Catalytic C-C Bond Formation via Capture of Hydrogenation Intermediates. *J. Am. Chem. Soc.* **2004**, *126*, 7875–7880.

(243) Li, J.; Tian, H.; Jiang, M.; Yang, H.; Zhao, Y.; Fu, H. Consecutive Visible-Light Photoredox Decarboxylative Couplings of Adipic Acid Active Esters with Alkynyl Sulfones Leading to Cyclic Compounds. *Chem. Commun.* **2016**, *52*, 8862–8864.

(244) Han, P.; Wang, R.; Wang, D. Z. Electronic Polarizability-Based Stereochemical Model for Sharpless AD Reactions. *Tetrahedron* **2011**, *67*, 8873–8878.

(245) Gary, D. C.; Glassy, B. A.; Cossairt, B. M. Investigation of Indium Phosphide Quantum Dot Nucleation and Growth Utilizing Triarylsilylphosphine Precursors. *Chem. Mater.* **2014**, *26*, 1734–1744.

(246) Peppas, A.; Papadaki, E.; Schnakenburg, G.; Magrioti, V.; Philippopoulos, A. I. Heteroleptic Copper(I) Complexes Incorporating Sterically Demanding Diazabutadiene Ligands (DABs). Synthesis, Spectroscopic Characterization and Solid State Structural Analysis. *Polyhedron* **2019**, *171*, 412–422.

(247) Gaillard, S.; Bantreil, X.; Slawin, A. M. Z.; Nolan, S. P. Synthesis and Characterization of IPrMe-Containing Silver(I), Gold(I), and Gold(III) Complexes. *Dalt. Trans.* **2009**, *35*, 6903–6914.

(248) Hans, M.; Lorkowski, J.; Demonceau, A.; Delaude, L. Efficient Synthetic Protocols for the Preparation of Common N-Heterocyclic Carbene Precursors. *Beilstein J. Org. Chem.* **2015**, *11*, 2318–2325.

(249) Arduengo, A. J.; Krafczyk, R.; Schmutzler, R.; Craig, H. A.; Goerlich, J. R.; Marshall, W. J.; Unverzagt, M. Imidazolylidenes, Imidazolinylidenes and Imidazolidines. *Tetrahedron* **1999**, *55*, 14523–14534.

(250) Kuhn, N.; Kratz, T. Synthesis of Imidazol-2-Ylidenes by Reduction of Imidazole-2(3H)-Thiones. *Synth.* **1993**, *6*, 561–562.

(251) Tan, E. H. P.; Lloyd-Jones, G. C.; Harvey, J. N.; Lennox, A. J. J.; Mills, B. M. [(RCN)2PdCl2]-Catalyzed *E/Z* Isomerization of Alkenes: A Non-Hydride Binuclear Addition-Elimination Pathway. *Angew. Chem., Int. Ed.* **2011**, *50*, 9602–9606.

(252) Liu, J.; Zhang, R.; Wang, S.; Sun, W.; Xia, C. A General and Efficient Copper Catalyst for the Double Carbonylation Reaction. *Org. Lett.* **2009**, *11*, 1321–1324.

(253) Zhang, G.; Zhang, X.; Kong, L.; Wang, S.; Tian, Y.; Tao, X.; Yang, J. Anion-Controlled Dimer Distance Induced Unique Solid-State Fluorescence of Cyano Substituted Styrene Pyridinium. *Sci. Rep.* **2016**, *6*, 1–9.

(254) Haynes, J. S.; Sams, J. R.; Thompson, C.; Sams, R. Synthesis and Structural Studies of Iron (II) and Iron(III) Sulfonates. *Can. J. Chem.* **1981**, *59*, 669-678.